Studies On Anthracene Tagged Oligonucleotides

Jean-Louis Henry Alan Duprey

A thesis submitted to the University of Birmingham for the degree of Doctor of Philosophy

School of Chemistry
College of Engineering and Physical Sciences
The University of Birmingham
May 2010

Abstract

This project has principally involved the synthesis, characterisation and study of a range of oligonucleotides that were modified by the inclusion of a non-nucleosidic anthracene unit. An anthracene tagged oligonucleotide system designed in our group[1] was found to act as a potential fluorescent SNP sensor and this research has been focused on determining the scope and mode of this sensing.

This involved firstly the synthesis of different stereoisomers of a non-nucleosidic backbone attached to DNA via a short carbon chain linker. These monomers were then coupled to a number of short (15-mer) oligonucleotide chains using solid state DNA synthesis and purified using RP-HPLC.

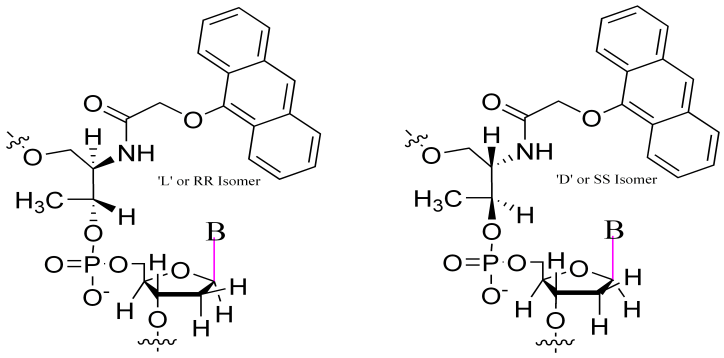

Two systems were studied, the first a duplex with anthracene functioning as a non-bonding base opposite of a natural nucleobase and the second as a wedge type system.

The probes were then examined by a variety of physical techniques that included variable temperature UV, fluorescence and CD spectroscopy in order to understand the effect of varying base pairs and introducing mismatches. A dependence on the stereoconfiguration of the Probe and the location of the mismatch was found, such that only a mismatch upstream of the probe on the *RR* isomer probe strand was found to sense mismatches.

Certain duplexes were then studied in greater depth using transient absorption spectroscopy, to probe the formation of electron transfer intermediates and by high field (900 MHz) NMR spectroscopy to look at the effect of intercalation between base pairs.

In order to aid explanation of the acquired data, molecular modelling studies were undertaken using AMBER and the University of Birmingham Bluebear cluster to produce solvated, molecular dynamics optimized structures.

Further studies were undertaken by synthesizing a full range of longer tether lengths and studying the effect of these changes on the properties of the duplex. The formation of excimers in bis-anthracene systems as potential precursors to photo-ligated DNA duplexes was also studied.

Acknowledgements

This work was a collaborative effort that involved a great many people and I would like to thank them for the help and time that they provided. For help and instruction with DNA synthesis and purification I would like to thank Dr Joe Vyle and his group at Queens University Belfast, particularly Jennifer and Leonie for their assistance whilst in Belfast. The fluorescence lifetime studies and quantum yields were undertaken with the guidance of Dr Dario Bassani at the University of Bordeaux 1 and I would like to thank him for his time and effort. I would also like to thank Guiallume Raffy who operated the laser to perform some of the lifetime studies.

For her assistance in interpreting the CD spectra I would like to thank Prof. Alison Rodger at Warwick University.

Dr Christian Ludwig at the Henry Wellcome NMR center carried out the DNA NMR experiments and Dr Eva Hyde helped with the interpretation.

At the University of Birmingham I would like to thank Dr John Wilkie for providing the resources and assistance in carrying out the molecular modelling studies. I would also like to thank his student, Andy Christofersson who gave me a lot of assistance in setting up the calculations. Thanks are also due to Dr Neil Spencer for carrying out NMR studies and interpretation, Graham Burns for assistance with HPLC and Peter Ashton for mass spectrometry.

I would like to thank the members of the Tucker group for their help, in particular Dr John Zhao for helping with DNA synthesis and Giorgio Mirri for help performing the cyclic voltammetry but everybody else helped in some way or the other. I would also like to acknowledge the assistance that my project

students, Emma and Sarah, provided in synthesising additional materials that I was able to benefit from.

Finally, I am very grateful to my supervisor Dr Jim Tucker for his assistance and guidance throughout the project.

I would also like to thank all my family and friends, you know who you are and what you did, I could not have done it without you.

Table of Contents

1.1 DNA **3**
1.1.1 The structure of DNA duplexes **5**
1.1.2 The structure of DNA chains **6**
1.2 Using DNA in a supramolecular system **7**
1.3 Modifying DNA **8**
1.4 Modifying DNA through sub-unit tagging **8**
1.3.1 Tagging the backbone terminals **8**
1.4.2 Tagging the sugar unit **10**
1.4.3 Tagging the nucleobase **11**
1.5 Modifying DNA through sub-unit deletion and replacement **13**
1.5.1 Removing DNA bases **13**
1.5.2 Replacing the nucleobases with organic groups **13**
1.5.3 Shape mimics of bases **14**
1.5.4 Replacing nucleosides with non-natural base pairs **14**
1.5.5 Replacing nucleobases with metal-binding ligands **16**
1.5.6 Non-nucleosidic backbones **16**
1.5.6.1 Peptide Nucleic Acids 17
1.5.6.2 Direct insertion of aromatic and organometallic groups into the DNA backbone 19
1.5.6.3 Alkyl based acyclic linkers as ribose mimics 20
1.6 Applying modified DNA to designing new systems **23**
1.6.1 DNA as a supramolecular scaffold **23**
1.6.2 Interstrand stacking helices containing modified DNA **24**
1.6.3 DNA-metal wire complexes using self assembly **25**
1.7 DNA sensors **26**
1.7.1 SNPs and their detection **27**
1.8 Electrochemical DNA sensors **28**
1.9 EPR DNA sensors **30**
1.10 Luminescent DNA sensors **31**
1.10.1 Metal complex luminescent DNA sensors **31**
1.10.2 Fluorescent methods of DNA analysis **32**
1.10.2.1 Taqman Probe 32
1.10.2.2 Molecular Beacons 33
1.10.2.3 Quencher free molecular beacons 34
1.10.2.4 Base Discriminating Fluorophores 35
1.10.2.5 Excimer fluorescence sensing 36
1.11 Anthracene as a fluorescent sensor **38**
1.11.1 Introduction **38**
1.11.1.1 Anthracene in sensing systems 38
1.11.2 Anthracene in DNA **40**
1.11.2.1 Anthracene as an intercalator 40
1.11.2.2 Covalently linked anthracene DNA systems 42
1.11.2.3 Anthracene tagged DNA-like oligomers 44
1.11.2.4 Photochemical dimerisation of anthracene-DNA conjugates 45

1.11.3 Attaching anthracene as a non-nucleosidic base 46
1.12 References 48
Chapter 2 Synthesis and Characterization 53
2.1 Introduction 53
2.2 Short chain anthracene non-nucleosidic linkers 54
2.2.1 Synthesis of the *n* = 1 linker 54
2.2.1.1 Non-nucleosidic base analogues 55
2.1.1.2 Synthetic route 55
2.1.1.3 Hydroxyl group protection 56
2.1.2 Phosphoramidite synthesis 59
2.2 DNA Synthesis 61
2.2.1 Introduction 61
2.2.2 Designing sequences to be synthesized 62
2.2.2.1 Primary sequence 62
2.2.2.2 Variation of the base opposite anthracene 63
2.2.2.3 Variation of the bases adjacent to anthracene 63
2.2.2.4 A modified complementary strand for interstrand stacking 64
2.2.2.5 SNP sensing strand 64
2.2.3 Procedure for DNA synthesis 64
2.2.3.1 Modified DNA synthetic procedure 64
2.2.3.2 Deprotection and removal from CPG 65
2.2.4 Purification 65
2.2.5 Characterization and quantification 66
2.2.5.1 Characterization by mass spectrometry 66
2.2.5.2 Quantification by UV spectroscopy 67
2.2.5.3 Determining the molar absorption coefficient 68
2.3 Longer Chain Syntheses 69
2.3.1 Synthetic route 69
2.3.2 ^{31}P NMR Spectroscopy 71
2.3.3 DNA synthesis of longer chains 72
2.3.3.1 Synthesized sequences 72
2.3.3.2 Methodology 72
2.3.4 HPLC 72
2.3.5 Purification and quantification 74
2.4 References 75
Chapter 3 Results and Techniques 76
3.1 Introduction 76
3.2 Photochemistry and fluorescence 78
3.2.1 Fluorescence quenching 79
3.2.2 Collisional quenching 80
3.2.3 Static quenching 81
3.3 Fluorescence results for single strand *n* = 1 system L and D isomer 82
3.3.1 Preliminary studies 82
3.3.2 Investigating DNA strands using fluorescence (single strand) 84
3.3.3 Quantum yield results 88

3.3.3.1 Unincorporated anthracene quantum yield 89
3.3.3.2 Anthracene tagged DNA single strand quantum yields 89
3.3.3.3 Discussion of quantum yields 90
3.3.3.4 G base quenching 91
3.3.4 Fluorescence lifetimes 92

3.4 Fluorescence monitoring of hybridisation of the probes in a base-opposite system 97
3.4.1 Base opposite anthracene system 97
3.4.1.1 Fluorescence results for different Probes of the L and D isomers 98
3.4.1.2 Varying the opposing bases (base opposite) 101
3.4.1.3 Downstream mismatches (base opposite) 102
3.4.1.3 Upstream mismatches (base opposite) 103
3.4.1.4 Double mismatches 104
3.4.2 Conclusions 105
3.4.3 Comparison with existing system 107

3.5 Deletion duplexes 107
3.5.1 Fluorescence quantum yields 107
3.5.2 Fluorescence monitoring of hybridisation for a deletion systems 109
3.5.3 Comparison of the two systems 110
3.5.4 Explaining the base sensing selectivity 111

3.6 Fluorescent lifetimes upon hybridisation 112
3.5.1 Fluorescence lifetimes of matching base opposite system for the L and D isomer Probes 112
3.6.2 Fluorescence lifetimes for different hybridised Probe systems 113
3.6.3 Fluorescence lifetimes of Probe A base opposite system mismatches for the D isomer Probes 114
3.6.4 Fluorescence lifetimes of base opposite system mismatches for the L isomer Probes 114
3.6.5 Fluorescence lifetimes for deletion duplexes 117
3.6.6 Discussion and conclusions on lifetimes 118
3.6.6.1 Importance of oxygen quenching 118
3.6.6.2 Assigning the lifetimes 119
3.6.6.3 Relative importance of each parameter on the overall quantum yield 120
3.6.6.4 Explaining the importance of τ 1 121

3.7 Rationalising the order of quenching through electron transfer 122
3.7.1 Electron migration in DNA 122
3.7.1.1 Introduction 122
3.7.1.2 Photoinduced Electron Transfer in DNA 123
3.7.2 Rehm-Weller equation 124
3.7.3 Cyclic Voltammetry 126
3.7.3.1 Cyclic Voltammetry of anthracene 127
3.7.3.2 Oxidation of anthracene 128
3.7.3.3 Reduction of anthracene 128
3.7.4 Applying cyclic voltammetry to anthracene modified DNA 129
3.7.5 Solvation and acid base effects on ΔG^{o}_{ET} 130
3.7.6 Applying protonation effects to mismatch sensing for the base opposite system 132
3.7.7 PrG as an exception to the pattern 135

3.8 Excitation spectra of hybridised DNA 135
3.8.1 Excitation spectra for Probe A D and L 135
3.8.2 Energy transfer bands in the excitation spectra 136

3.9 Absorption Studies **138**
3.9.1 Changes In the anthracene absorption spectrum **138**
3.9.2 Hypochromism **140**
3.10 Melting points **141**
3.10.1 Studies on unmodified DNA **143**
3.10.2 Studies on anthracene modified DNA – modifying the opposite base for L and D **144**
3.10.2.1 Melting point at 370 nm 145
3.10.2.2 Examining the ^1L_a anthracene absorption region at different temperatures 146
3.10.3 Melting points of different matching Probe duplexes **147**
3.10.4 Conclusions on the melting points of fully matched duplexes **150**
3.10.5 Mismatched duplexes melting temperatures **150**
3.10.5.1 Downstream mismatches 150
3.10.5.2 Upstream mismatches 151
3.10.5.3 Conclusions 151
3.10.6 Observing duplex melting using variable temperature fluorescence **153**
3.10.8 Melting points of deletion sequences **154**
3.10.8.1 Unmodified deletions sequences 154
3.10.8.2 Melting points of fully matching deletion sequences 155
3.10.8.3 Mismatch deletion sequences 157
3.11 Transient absorption spectroscopy **157**
3.11.1 Introduction **157**
3.11.2 Results **159**
3.12 Circular Dichroism **161**
3.12.1 Origin of the CD effect **161**
3.12.2 CD of anthracene in DNA **162**
3.13 CD of the single strand forms **162**
3.14 CD of the hybridized duplexes **164**
3.14.1 CD spectra of unmodified DNA **166**
3.14.2 CD spectra of fully matching base opposite duplexes **166**
3.14.2 Effect of changing bases opposite of the anthracene **167**
3.14.3 Deletion duplex CD spectra **168**
3.14.4 Effect of flanking bases on CD spectra **169**
3.14.5 Explaining the shoulder in the CD spectra **171**
3.14.5.1 CD signals arising from non-degenerate coupling 172
3.14.6 Effect of mismatches on the CD spectrum **172**
3.15 Induced CD spectra of anthracene modified duplexes **173**
3.15.1 Using ICD to interpret structure **173**
3.15.2 ICD of fully matching base opposite sequences **175**
3.15.3 ICD of upstream mismatches **176**
3.15.4 Deletion duplexes ICD studies **177**
3.16 Applying the work to real life SNPs **179**
3.16.1 Fluorescence results for SNP sensors **180**
3.16.2 Fluorescence lifetimes **181**
3.16.3 Melting points **181**
3.16.4 Conclusions **182**

3.17 Interstrand stacking duplexes 182
3.17.1 Anthracene excimers and dimers 183
3.17.2 Fluorescence Studies on Excimers 184
3.17.3 Fluorescence lifetime studies 185
3.17.4 Conclusions 186
3.18 Absorption Studies on interstrand duplexes 186
3.18.1 UV melting points of interstrand duplex 186
3.18.2 Melting point studies at 370 nm 186
3.18.3 UV-vis spectra at different temperatures 187
3.19 Circular Dichroism studies of interstrand duplexes 188
3.19.1 Exiton coupling of anthracenes 188
3.19.2 Analysing the exciton coupling in the LL system as a degenerate coupled-oscillator system 190
3.20 Dimerisation of interstrand duplexes 192
3.21 Conclusions 193
3.22 References 194
Chapter 4 Molecular modeling of anthracene duplexes 197
4.1 Introduction 197
4.1.1 Molecular Modeling 197
4.1.2 Model building 197
4.1.3 Using AMBER 198
4.2 Modeling unmodified DNA 199
4.3 Modeling modified DNA duplexes 200
4.4 Rationalization of experimental results for the L (*RR*) isomer matched duplexes 201
4.4.1 *n* = 1 L anthracene core structure 201
4.4.2 Fluorescence 202
4.4.3 Implications for the CD data 203
4.5 Comparison with matched duplexes of the D (*SS*) isomer 204
4.5.1 Fluorescence differences 204
4.5.2 Explanation of the differences in melting point between stereoisomers 205
4.5.3 CD data 206
4.5.3.1 CD data and modeling of different bases opposite the anthracene 206
4.6 Probe A vs. Probe G:Structures of more emissive duplexes 207
4.7 Refining the explanation of mismatch sensing 215
4.7.1 Evidence of structural differences between probes with CT/CC and CA mismatches 216
4.7.2 Expanding the analysis to other kinds of mismatch 219
4.7.3 Conclusions 221
4.7.4 Melting Temperature rationalisation 221
4.7.4.1 Explaining the low melting temperature of PrATarB1 221

4.8 Explaining differences in quantum yields on the basis of single strand structures **224**

4.9 Deletion Structures **226**
4.9.1 SS stereoisoemer system **226**
4.9.2 RR stereoisomer system **227**

4.10 Conclusion **228**

4.9 References **229**

Chapter 5 Longer anthracene tether lengths **230**

5.1 Introduction **230**

5.2 Fluorescence studies on the single strands **230**
5.2.1 Single strand spectra **230**
5.2.2 Single strand quantum yields **231**
5.2.3 Single strand fluorescence lifetimes **232**
5.2.4 Discussion **232**

5.3 Fluorescence studies on the duplexes (base opposite) **234**
5.3.1 Quantum yields for base opposite systems **234**
5.3.2 Fluorescence lifetimes for base opposite hybridized systems **235**
5.3.3 Sensing the base opposite **235**
5.3.3.1 Fluorescence hybridization titrations 236
5.3.3.2 Fluorescence lifetimes of hybridized duplexes 238
5.3.4 Mismatch sensing **240**
5.3.4.1 Downstream mismatches 240
5.3.4.2 Upstream mismatch 241

5.4 Fluorescence studies on the deletion systems **243**
5.4.1 Fluorescence titration studies **243**
5.4.2 Fluorescent lifetimes **243**

5.5 Melting points **244**

5.6 Circular Dichroism **246**
5.6.1 Longer chain length L isomer spectra **246**
5.6.2 Longer chain D isomer spectra **247**
5.6.2.1 *n* = 6 D spectrum 248

5.7 Molecular modelling of longer chain duplexes **248**
5.7.1 *n* = 3 ..... **248**
5.7.1.1 Explaining melting point differences for a longer chain (*n* = 3) 249
5.7.1.2 Explaining the fluorescence sensing 250
5.7.2 Extending the modelling to longer lengths **250**

5.8 Face to face bis-anthracene duplexes **253**
5.8.1 Fluorescence spectra of bisanthracene duplexes **254**
5.8.2 Melting Points of bisanthracene duplexes **255**
5.8.3 CD spectra of bisanthracene duplexes **256**
5.8.3.1 CD of matched and mismatched longer tether length bisanthracene duplexes 256

5.9 Stacking conformation duplexes **258**
5.9.1 Fluorescence studies of excimers in stacking duplexes **259**
5.9.2 Melting points **260**
5.10 Conclusions **260**
5.10 References **261**
Chapter 6 NMR Studies of an anthracene tagged duplex **262**
6.1 Introduction to NMR spectra of DNA **262**
6.1.1 Proton shifts of bases, nucleotides and nucleosides **262**
6.1.2 NMR experiments **263**
6.1.2.1 TOCSY experiments 263
6.1.2.2 NOESY experiments 264
6.1.3 Preparation of sample for NMR studies **264**
6.2 Analysis of the NMR spectrum of anthracene oligonucleotides **265**
6.2.1 Previous work in identifying anthracene in oligonucleotides **265**
6.2.2 NMR studies on anthracene tagged DNA duplexes **267**
6.2.3 Imino Protons 1D spectra **267**
6.2.4 2D NOESY spectrum of the imino region **270**
6.3 Analysis of the aromatic region of Probe A TarA2 ..... **273**
6.3.1 TOCSY **273**
6.3.2 1D spectrum of the DNA aromatic region **274**
6.4 Conclusions **275**
6.5 References **276**
Chapter 7 Experimental **277**
7.1 Synthesis and experimental details **277**
7.1.1 Reagents and chemicals **277**
7.1.2 DNA synthesis and purification **277**
7.1.3 DNA analysis **278**
7.1.3.1 UV Vis and CD 278
7.1.3.3 Fluorescence and photochemistry 278
7.1.3.4 Cyclic voltammetry 279
7.1.3.5 Transient Absorption spectroscopy 279
7.1.3.6 DNA NMR 280
7.2 Molecular modeling parameters **280**
7.3 *n* = 1 synthesis **281**
7.3.1 *n* = 1 Ester (2) **281**
7.3.2 *n* = 1 Acid (3) **282**
7.3.3 *n* = 1 L Diol (4L) **283**
7.3.4 *n* = 1 D Diol (4D) **284**
7.3.5 *n* = 1 DMT L (5L) **286**
7.3.6 *n* = 1 DMT D (5D) **287**
7.3.7 *n* = 1 L Phosphoramidite (6L) **289**
7.3.8 *n* = 1 D Phosphoramidite (6D) **290**

7.4 *n* = 3 synthesis **292**
7.4.1 *n* = 3 Ester (2b) **292**
7.4.2 *n* = 3 Acid (3b) **293**
7.4.3 *n* = 3 L Diol (4bL) **294**
7.4.4 *n* = 3 D Diol (4bD) **295**
7.4.5 *n* = 3 L DMT (5bL) **296**
7.4.6 *n* = 3 D DMT (5bD) **298**
7.4.7 *n* = 3 L Phosphoramidite (6bL) **299**
3.4.8 *n* = 3 D Phosphoramidite (6bD) **301**

7.5 *n* = 4 synthesis **303**
7.5.1 *n* = 4 ester (2c) **303**
7.5.2 *n* = 4 Acid (3c) **304**
7.5.3 *n* = 4 L Diol (4cL) **305**
7.5.4 *n* = 4 D Diol (4cD) **306**
7.5.5 *n* = 4 L DMT (5cL) **307**
7.5.6 *n* = 4 D DMT (5cD) **309**
7.5.7 *n* = 4 L Phosphoramidite (6cL) **310**
7.5.8 *n* = 4 D Phosphoramidite (6cD) **312**

7.6 *n* = 5 synthesis **314**
7.6.1 *n* = 5 Ester (2d) **314**
7.6.2 *n* = 5 Acid (3d) **315**
7.6.3 *n* = 5 L Diol (4dL) **316**
7.6.4 *n* = 5 D Diol (4dD) **317**
7.6.5 *n* = 5 L DMT (5dL) **318**
7.6.6 *n* = 5 D DMT (5dD) **320**
7.6.7 *n* = 5 L Phosphoramidite (6dL) **321**
7.6.8 *n* = 5 D Phosphoramidite (6dD) **323**

7.7 *n* = 6 synthesis **324**
7.7.1 n = 6 Ester (2e) **324**
7.7.2 *n* = 6 Acid (3e) **326**
7.7.3 *n* = 6 L Diol (4eL) **327**
7.7.3 *n* = 6 D Diol (4eD) **328**
7.7.5 *n* = 6 L DMT (5eL) **329**
7.7.6 *n* = 6 D DMT (5eD) **331**
7.7.7 *n* = 6 L Phosphoramidite (6eL) **332**
7.7.8 *n* = 6 D Phosphoramidite (6eD) **334**

7.8 References **336**

Appendix of Data

Abbreviations

General abbreviations:

aq.	aqueous
CH_3CN	acetonitrile
DCM	dichloromethane
DIEA	*N,N*-diisopropylethyleneamine
DIPC	*N,N'*-diisopropylcarbodiimide
DMAP	*N,N*-dimethylaminopyridine
DMF	*N,N*-dimethylformamide
DMSO	dimethyl sulphoxide
DNA	2'-deoxyribonucleic acid
Et	ethyl
ET	electron transfer
EtOAc	ethyl acetate
EtOH	ethanol
Hex	hexane
HBTU	O-Benzotriazole-*N,N,N',N'*-tetramethyl-uronium-hexafluoro-phosphate
HOBt	*1*-hydroxybenzotriazole hydrate
HPLC	high performance liquid chromatography
M	molar
Me	methyl
MeOH	Methanol
μM	micromolar

µmol	micromole
mmol	millimole
M.p.	melting point
nm	nanometer
ns	nanosecond
ODN	oligodeoxynucleotide
PET	photo-induced electron transfer
Ph	phenyl
PyBOP	benzotriazol-1-yl-oxytripyrrolidinophosphonium hexafluorophosphate
RNA	ribonucleic acid
room temp.	room temperature
soln.	Solution
TEA	triethylamine
Tlc	thin layer chromatography
T_m	melting temperature (DNA)

Spectroscopic terms:

CD	Circular Dichroism
IR	Infra-Red
NMR	Nuclear magnetic resonance
UV/Vis	Ultra-Violet/Visible
ES	electrospray
MALDI-TOF	Matrix Assisted Laser Desorption Ionization Time Of Flight

NMR terms:

$CDCl_3$	Deuterated chloroform
CD_3CN	Deuterated acetonitrile
COSY	Correlated Spectroscopy
DEPT	Distortionless Enhancement by Polarisation Transfer
D_2O	Deuterium Oxide
HSQC	Heteronuclear Single Quantum Correlation
HMBC	Heteronuclear Multiple Bond Correlation
TOCSY	Total Correlated Spectroscopy
δ	chemical shift
d	doublet
dd	doublet of doublets
MHz	Megahertz
ppm	parts per million
q	quartet
s	singlet
t	triplet

UV/Vis terms:

ε	extinction co-efficient
hν	light energy
λ	wavelength

Cyclic Voltammetry Terms:

SCE	Saturated Calomel Electrode
SHE	Standard Hydrogen Electrode

Fluorescence Terms:

λex	Wavelength of excitation
λem	Wavelength of emission

DNA terms:

CPG	controlled-pore glass
A	adenine
C	cytosine
G	guanine
T	thymine
U	uridine

Studies On Anthracene Tagged Oligonucleotides

Chapter 1 Introduction

1.1 DNA

DNA has been described as 'the blueprint of life' as it contains within its structure the information required for the propagation of life by all living beings. However, DNA is not just a carrier of genetic information; it is also a versatile supramolecular scaffold onto which smaller organic structures can be arranged into predesigned geometries and utilized in a wide variety of applications.[1]

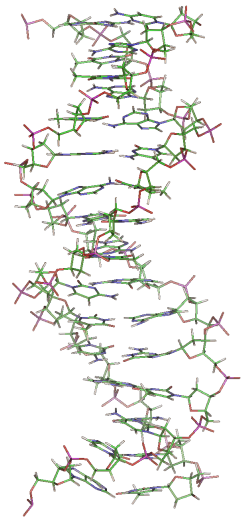

Fig. 1 15-mer DNA oligonucleotide double helix

The DNA double helix (Fig. 1) is a molecular assembly that consists of a set of four aromatic heterocycles (Fig. 2), two purines (Adenine (A), and Guanine (G)) and two pyrimidines (Cytosine (C) and Thymine (T)). These nucleobases form bonds with deoxyribose sugars, which are in turn held in place by a carbon-oxygen-phosphorus (phosphodiester) repeating scaffold that forms a polymer strand. This is described as having a direction and by convention this is defined

as the contiguous set of atoms starting at the oxygen atom attached to the 5' sugar carbon and going to the oxygen atom attached to the 3' sugar carbon.

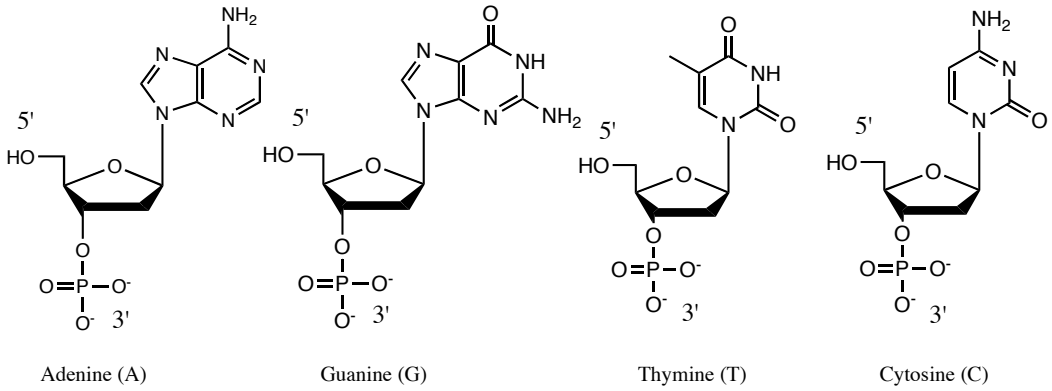

Fig. 2 Chemical structure of the four nucleotides that occur naturally in DNA

Hydrogen bonding between complementary GC and AT pairs helps hold the two strands together to form a double helix, with a GC pair being held together by three hydrogen bonds and an AT pair held together by two bonds (Fig. 3).

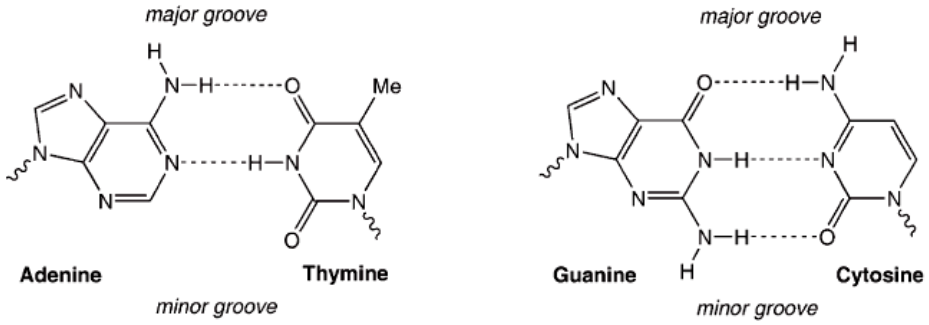

Fig. 3 Hydrogen bonding between Watson-Crick base pairs

The resulting system is sufficiently flexible that it can be remoulded during replication and transcription processes, yet rigid enough to act as a straight molecule on a scale of several nanometres, thus preventing conformational changes that could affect biological function until such changes are initiated by the appropriate protein.

1.1.1 The structure of DNA duplexes

The DNA backbone has evolved to hold the flat aromatic bases in a well-organized fashion. In the double helical structure these nucleobases are nearly perpendicular to the backbone and they stack on top of one another much like a roll of coins. The helical twist offsets these stacked bases, which thus have to rotate in order to stay in direct π-π van der Waals contact. As a result the planes of the bases are separated by ca. 3.4 Å, which corresponds to the thickness of the π system in an aromatic ring.

The stability of DNA is largely dominated by the stacking interactions between the aromatic purine or pyrimidine rings.[2] Although clearly important to the stability of DNA it has proved difficult to fully understand the roles that they play in this process, although a great deal of study has been devoted to this.[3, 4] These interactions encompass a number of factors that contribute to enhanced stability such as the hydrophobicity (represented by the log P of octanol and water), the polarisability of the bases, the overall dipole moment and the stacking area. A recent study has shown that it is likely that the degree of overlap between bases is the most important factor.[5]

The measure of the stability of a DNA duplex is the melting point or $T_{m.}$ This value is usually determined by variable temperature UV spectroscopy and is the temperature at which the DNA duplex is 50% dissociated. It varies greatly with a number of factors:

- Sequence length: The more base pairs there are the greater the amount of stacking interactions and hydrogen bonds.
- GC content: There are three hydrogen bonds in a GC base pair compared to two for an AT base pair.

- Salt content: The negatively charged phosphate groups on the backbone of DNA repel each other and require positive counterions (usually Na^+ but also Mg^{2+}) in order to balance the charge and to overcome this repulsion.

Although hydrogen bonding has been shown to play only a minor role in stabilizing the formation of the DNA duplex in terms of energetics,[2]it is nonetheless extremely important in terms of selectivity. Mismatched DNA sequences undergo large decreases in their melting points not as a result of loss of hydrogen bonding but most likely as a consequence of the structural distortion that occurs when hydrogen bonds are formed between mismatched base pairs. This can lead to twisting of the backbone and to distortion of the structure of the duplex.[2]

There are a number of different possible conformations of the double helix that can be adopted but the three most common are 'A', 'B' and 'Z'. The conformations differ in terms of the direction of helical sense and tightness, with the A form having the tightest twist and a right-handed helical sense, the B form having a moderate and right handed twist and the Z form being the least compact and having a left-handed twist.[6]

1.1.2 The structure of DNA chains

In the single strand form DNA is considerably more flexible, with a substantial degree of bond rotation that can occur in the phosphodiester backbone. Nevertheless, a significant amount of ordered structure remains, mostly as a result of the energetically favourable stacking of base pairs on top of each other.[7]

1.2 Using DNA in a supramolecular system

Since the 1980s there have been a number of advances in the field of chemical DNA synthesis[8] that have culminated in the design and manufacture of DNA synthesizers, allowing the routine synthesis of DNA at reasonable cost. Currently, it is possible to synthesize oligonucleotides up to 100 base pairs in length using the phosphoramidite technique.[8] The ease of access to structurally specific DNA strands has led to the use of DNA in a number of different fields of science and technology. For instance, DNA has been successfully used to perform computational calculations,[9] build nano-wires,[10] construct and manipulate molecular machines.[11-13]

An understanding of the binding and structure of DNA has allowed the design of artificial self assembling DNA structures of which the DNA tetrahedron (Fig. 4) by Turberfield is one of the best known.[14] Such structures, which may be manipulated on a molecular scale, have potential applications in the area of therapeutic drug delivery.

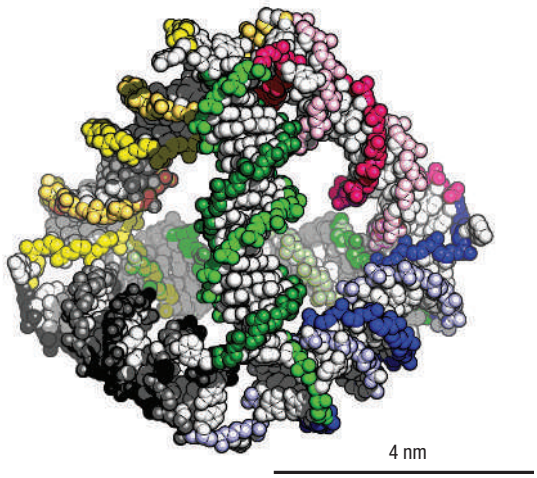

Fig. 4 Self assembled DNA Tetrahedron[15]

1.3 Modifying DNA

As the field of DNA technology expands it requires more and more utility from DNA. As superior functionality is desired, the natural limit of four nucleobases becomes a hindrance. No matter how much the sequence is optimized there is a limit to the performance that can be extracted if we limit ourselves to these four nucleobases. Therefore, in order to access functions that are beyond the capability of nature, the use of non-natural molecules is required that can fulfil these functions by being incorporated into DNA. As described in the following sections, such demand has led to a number of methods and techniques for the placement of modifications into DNA.[16, 17]

1.4 Modifying DNA through sub-unit tagging

1.3.1 Tagging the backbone terminals

One of the simplest modifications to DNA is the simple addition of a molecule to one end of the chain, either the 3' end or more commonly, the 5' end. This can be performed as a post synthetic modification and various luminescent groups have been tethered to the end of DNA, including, for instance metal complexes containing ruthenium and osmium used by Faulkner and co-workers as 5' and 3' tags for different but complementary DNA strands (Fig. 5).

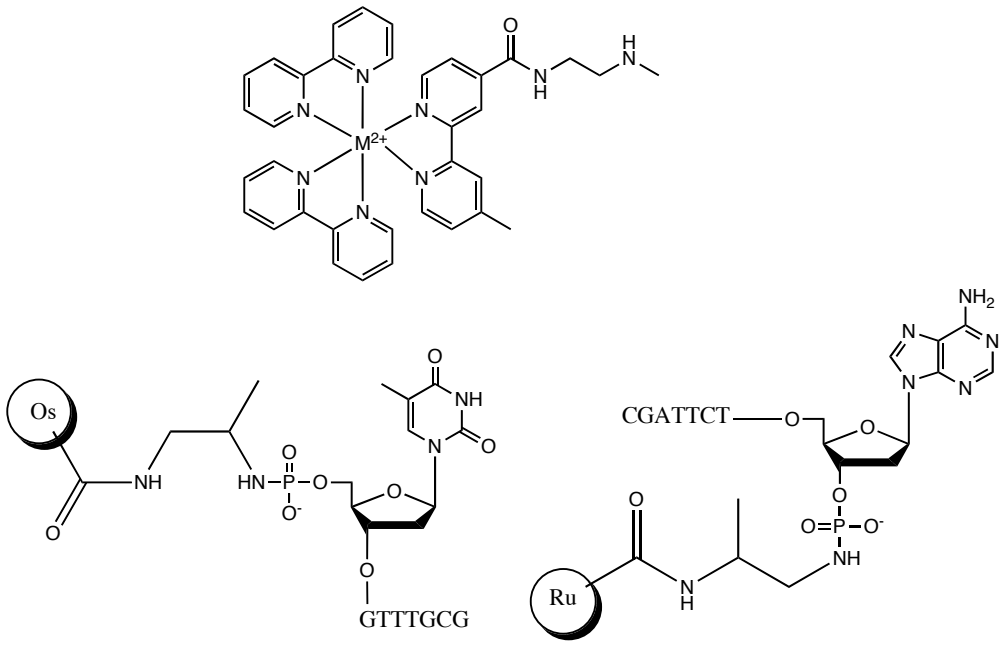

Fig. 5 Metal complexes attached to the ends of the DNA phosphate backbone

Visible metal to ligand charge transfer (MLCT) excitation of the $[Ru(II)(bpy)_3]^{2+}$ unit leads to resonance energy transfer to the MLCT state of the $[Os(II)\text{-}(bpy)_3]^{2+}$ moiety, with the energy transfer efficiency depending on the degree of hybridization.[18]

This has also been achieved with various photoactive moieties such as azo-benzene and anthracene with the aim of creating photoswitchable oligonucleotide systems.[19-21]

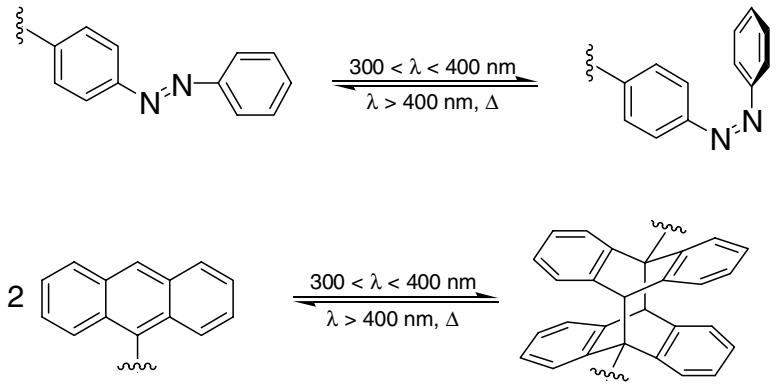

Fig. 6 Photoswitchable molecules attached to the phosphate chain backbone of DNA

1.4.2 Tagging the sugar unit

This is typically accomplished at the 2' position of the ribose ring (Fig. 7).

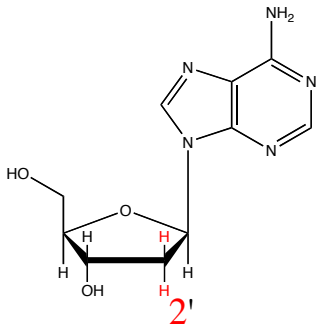

Fig. 7 2' site for modification on the ribose ring

A variety of different groups have been used in this manner to label DNA. Yu and co workers have attached metallocene groups such as ferrocene (Fig. 8) to DNA that act as redox reporter groups. The incorporation of the modified nucleoside allows electrochemical sensing of DNA mismatches.[22]

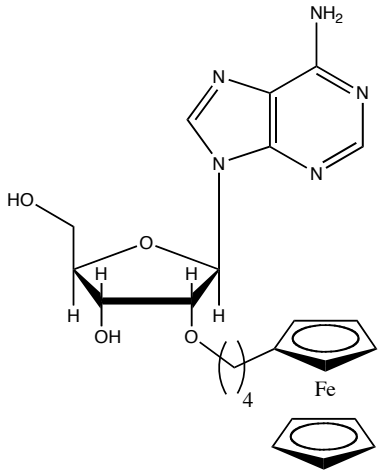

Fig. 8 Ferrocene covalently bound to the ribose ring

The previous modifications, whilst adding functionality to DNA that is not naturally present, are limited in their ability to probe the core of the duplex where the nucleobases reside. As these are the carriers of the information stored in DNA, the ability to detect and interact with them is an imperative for a highly sensitive DNA sensor.

One of the problems associated with incorporation into the interior of DNA is the resulting disruption of the local structure, which can significantly reduce the stability of the duplex and in some cases, reduce the sequence sensitivity. Solutions to this problem include the functionalisation of natural nucleosides or their replacement by non-natural nucleobases.

1.4.3 Tagging the nucleobase

The most common starting point for the modification of the nucleobase is 5-iodo-2'-deoxyuridine. The iodine group allows relatively simple functionalisation using various palladium-catalyzed cross coupling reactions. A simple example of this is the work of Kraatz who attached ferrocene to uracil via a Stille coupling (Fig. 9 left).[23] Another example is the work of Houlton and co-workers who have carried out similar work with cytosine (Fig. 9 right).[24]

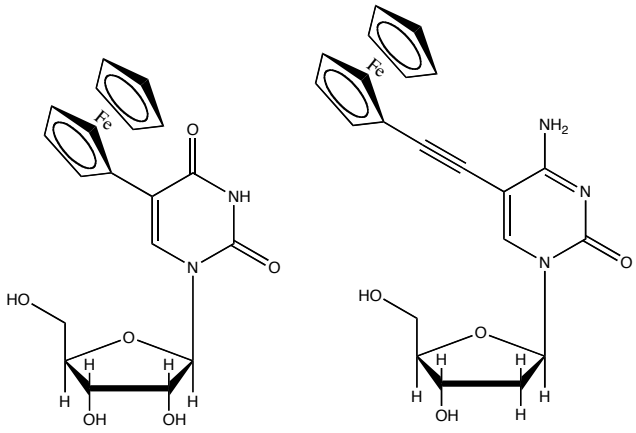

Fig. 9 Ferrocene attached to a uracil (left) and cytosine (right) nucleoside via palladium cross-coupling

Aromatic molecules are popular targets for attachment to nucleobases as demonstrated by the work of Saito and co-workers who have attached pyrenes to 7-deaza-2'-deoxyadenosine (Fig. 10) and incorporated the modified nucleoside into DNA.[25]

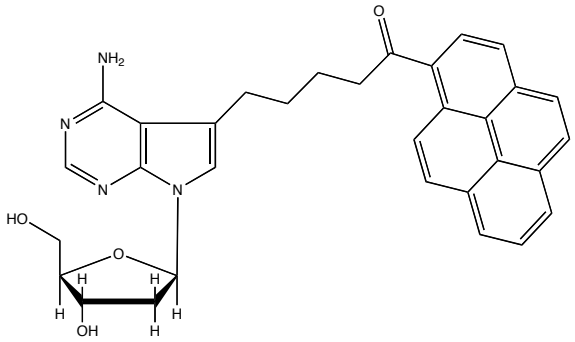

Fig. 10 Pyrene tagged adenosine DNA nucleoside

Similarly, Tor and co-workers have coupled phenanthroline to a nucleobase for the purpose of hybridization sensing (Fig. 11).[26]

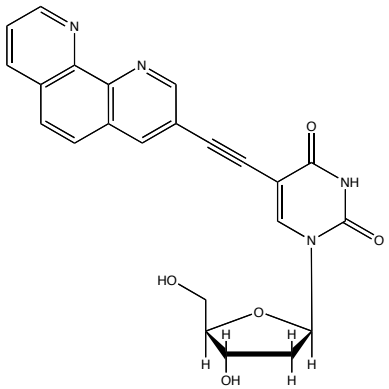

Fig. 11 Phenanthroline covalently bonded to a nucleobase

Unfortunately, there are a number of problems with this approach. The individual synthesis of all four (A, C, T and G) modified phosphoramidites is time consuming. Indeed, most modifications have been performed on thymidine due to the fact that this monomer does not need any base protection – the other free nucleotides require the amino groups to be protected. There are also a great many limitations in terms of the location of tagging on a base. Many positions that are available on natural bases cause the resulting duplexes to be highly destabilized by virtue of projecting the attached group into a region of the duplex with many steric interactions. Therefore many groups have concentrated on replacing natural nucleobases with completely artificial ones.

1.5 Modifying DNA through sub-unit deletion and replacement

1.5.1 Removing DNA bases

One of the simplest modifications is the so-called 'null replacement', where a DNA base is missing from the sugar unit. Such groups (called 'abasic') can simply be used as linkers or spacers, or also as biological probes of DNA damage and repair.[27, 28] Kool *et al*. have reported molecules that can be paired in such sites[29] and can furthermore be replicated into DNA efficiently by polymerase enzymes.[30] This can be considered a form of synthetic biology, with the expansion of the DNA 'alphabet' as one of its goals.

1.5.2 Replacing the nucleobases with organic groups

Among the first replacements for natural DNA bases were simple hydrocarbons and heterocycles. Benzene, the simplest aromatic hydrocarbon was substituted into DNA over twenty years ago (Fig. 12 left). It was designed to act as a nonselective pairing base but was found to be very destabilizing in the DNA duplex.[27]

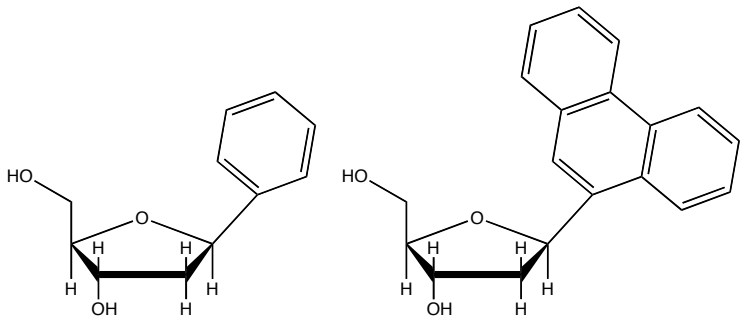

Fig. 12 Simple hydrocarbon base replacements benzene (left) and phenanthrene (right)

Subsequent efforts have involved the incorporation of a wide range of different aromatic hydrocarbons ranging from small units such as naphthalene,

phenanthrene (Fig. 12 right), to large tethered stillbene units. Various simple heterocycles (e.g. 3-nitropyrrole[31] and 5-nitroindole[32]) have been used as base replacements, usually with the aim of finding molecules that can base pair with natural DNA bases.

1.5.3 Shape mimics of bases

A number of shape mimics of natural bases have been synthesized in order to aid the study of hydrogen bonding in DNA duplexes. These structures are the closest possible steric mimics for the natural nucleobases that lack hydrogen bonding functionality.[33] For instance difluorotoluene isotere (dF) (Fig. 13) is a nearly perfect mimic of thymidine in the crystalline form and in solution.[34]

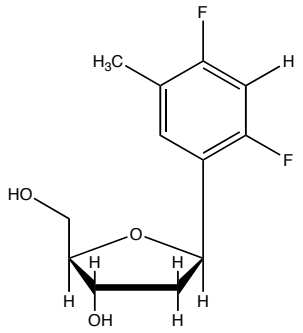

dF

Fig. 13 Difluorotoluene isotere a thymine shape mimic

1.5.4 Replacing nucleosides with non-natural base pairs

A growing field of research is the design and synthesis of bases that will pair with other non-natural bases. The aim of this research is to discover new pairs for hybridization and for polymerase enzyme replication. One of the earliest examples was the isoC-isoG pair (Fig. 14) studied by Benner, in which the hydrogen bonding groups were rearranged to give a different pairing selectivity.[35]

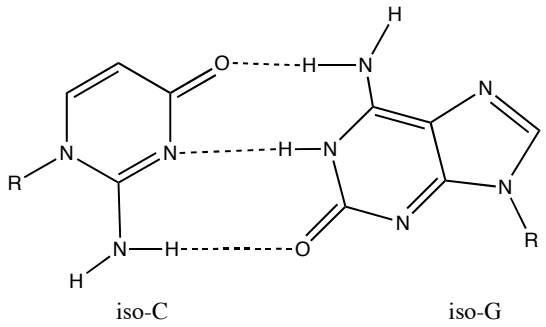

Fig. 14 DNA base replacements designed to form stable pairs

Work by Kool has demonstrated that non-hydrogen bonding bases can selectively pair up due to the destabilizing effect of being paired opposite to a natural base (see 1.3.2.2).[36]

Further development has resulted in pairing between molecules that do not resemble natural bases. These are based on the idea that hydrogen bonds are not needed to make stable pairs as long as the components can stack strongly. The Schultz, Romesberg and Ishikawa laboratories have all developed systems capable of forming stable self- and cross pairs (e.g. Fig. 15).[37, 38]

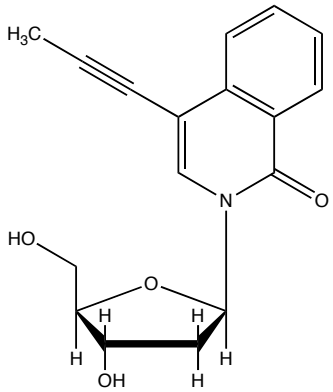

Fig. 15 7-propynyl isocarbostyril nucleoside capable of self pairing

1.5.5 Replacing nucleobases with metal-binding ligands

A novel design strategy involves replacing DNA bases with metal-binding ligands. In some cases, the molecules are designed to be assembled into base pairs by the metal, whilst in others the pairing is meant to be part of a larger non-natural supramolecular architecture. [39-41] Such ligands, referred to by Tor as 'ligandosides',[42] include pyridines, bipyridines, anilines and porphyrins (Fig. 16).

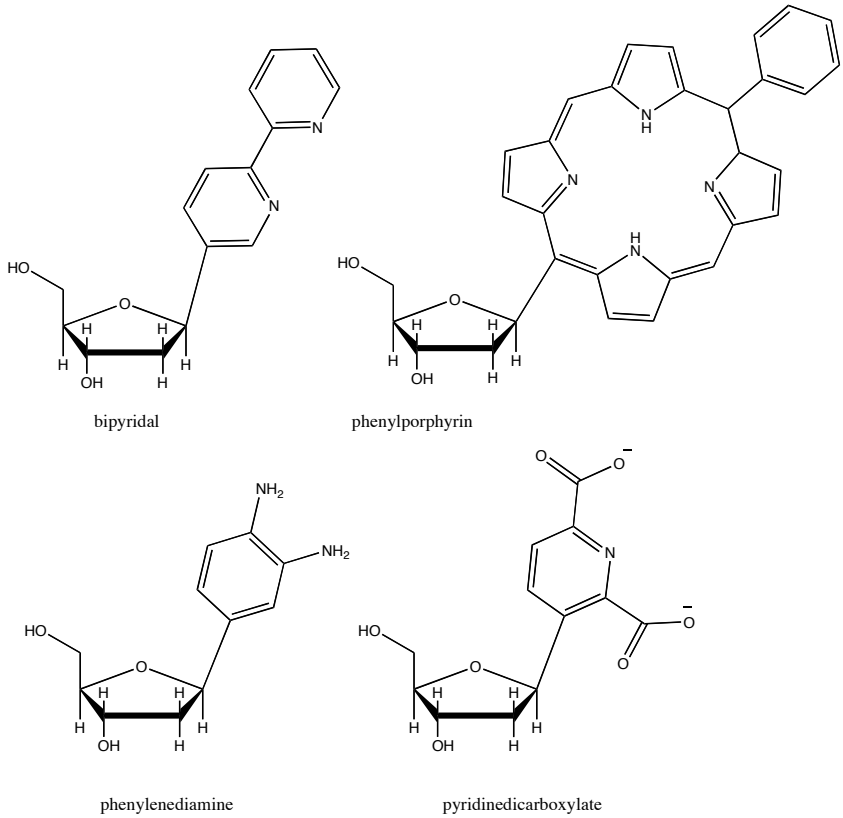

Fig. 16 Nucleosides modified with metal-binding ligands

1.5.6 Non-nucleosidic backbones

Compared to the tagging or replacement of nucleobases, the use of a non-nucleosidic backbone is a considerably simpler and more versatile approach in terms of synthesis. There are two different strategies that can be considered in terms of the modifications to DNA that can be performed:

- Backbone replacement:

  Replacing the sugar-phosphate backbone with a non-natural linker, for example a peptide in the case of Peptide Nucleic Acids (PNAs), whilst keeping the nucleobase.

- Partial backbone replacement:

  This involves replacing the sugar unit with a non-natural linker, but keeping the phosphate group. The linker might or might not contain a connection to a nucleobase.

1.5.6.1 Peptide Nucleic Acids

PNAs are functional analogues of DNA where the sugar-phosphate backbone has been replaced by a N-(2-aminoethyl)glycine unit (Fig. 17).[43] Despite the increased flexibility of the linker unit, PNA has been shown to hybridize similarly to DNA or RNA and follow the same Watson-Crick base pairing rules. Furthermore, PNA-DNA complexes were found to be more stable than the corresponding DNA duplex, and the thermal stability more strongly affected by mismatching PNA-DNA duplexes than DNA-DNA duplexes. This is attributed to the lack of negative charge on the PNA backbone which avoids the electrostatic repulsion of natural oligonucleotide duplexes.[44] However, there is a significant drawback insofar that a lack of charged phosphate groups significantly decreases the water solubility of the duplexes. Indeed, a PNA composed of more than 60% purines will be water insoluble.

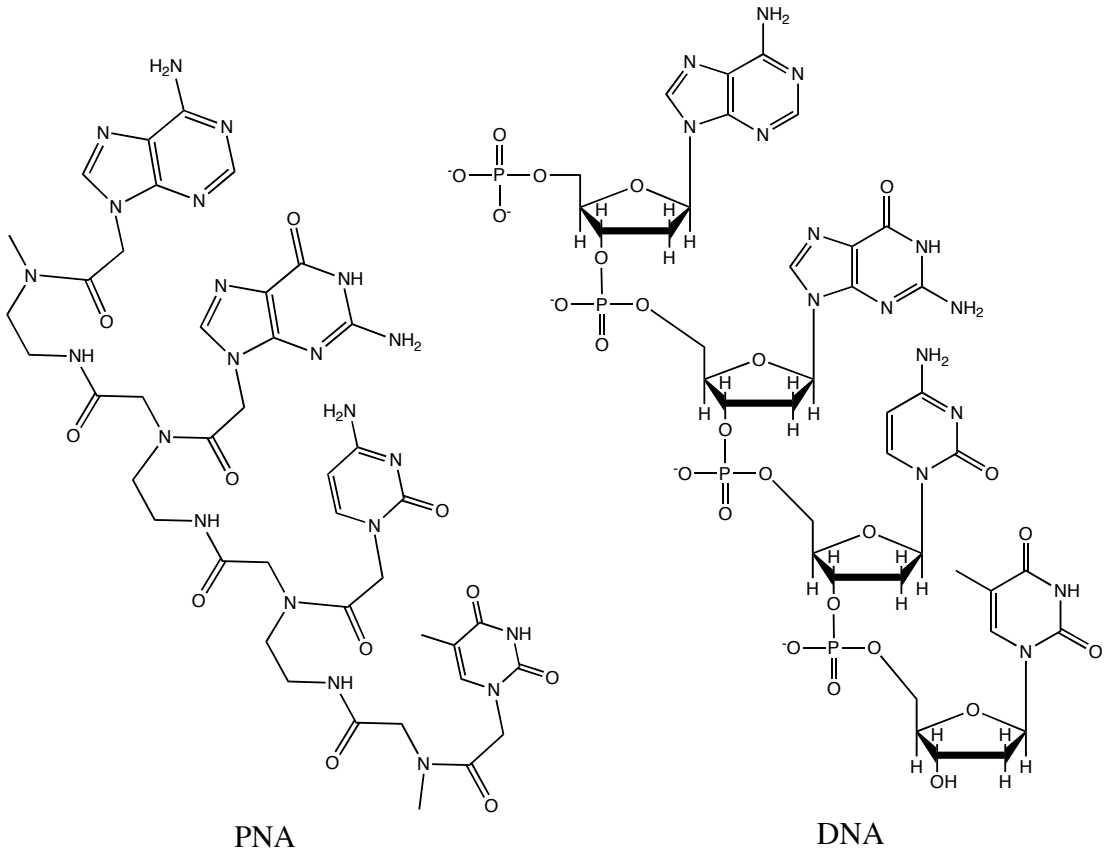

Fig. 17 Comparison of the backbone chain of PNA and DNA

The enhanced stability and recognition of PNAs has caused tremendous interest in the fields of diagnostics. PNAs are stable to strong acids and bases which allows for a wide variety of protecting groups to be used on the terminal nitrogen. This makes PNAs more chemically compatible with various tagging or co-synthesis techniques. Lastly, PNAs are not susceptible to enzymatic degradation by proteases and are stable both *in vivo* and in cell extracts. One of the major hurdles in further development is the lack of cellular permeability, however this has been partially overcome by the use or arginine residues instead of glycine which have been shown to be effectively internalized by cells leading to the repression of *m*RNA transcription.[45]

1.5.6.2 Direct insertion of aromatic and organometallic groups into the DNA backbone

A number of different molecules have been directly incorporated into a DNA backbone including napthalene[46], ferrocene,[47] pyrene,[48] phenanthrene,[49] phenanthroline[50] and anthraquinone.[51] Typically such molecules are designed to make use of favourable stacking interactions by aligning themselves parallel to the plane of the DNA bases and stabilizing the duplex through van der Waals π-π interactions. For instance, incorporation of a phenanthrene residues into the centre of subsequently hybridized DNA oligonucleotides (Fig. 18) confers an increase in the melting temperature of the DNA of 0.3 °C.[49] This is significant in that many similar modifications give rise to a decrease in the melting temperature.

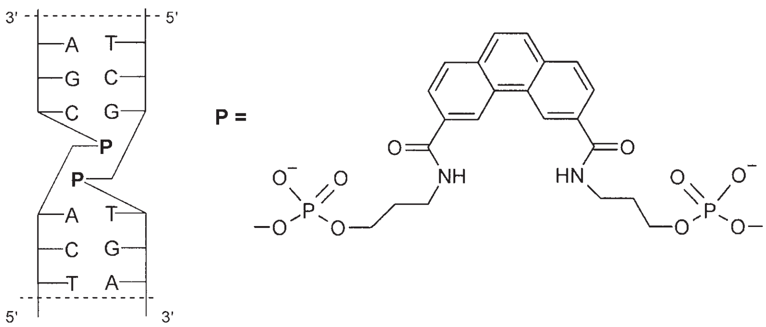

Fig. 18 Duplex containing non-nucleosidic interstrand stacker phenanthrene[49]

On the other hand, the napthalenecarboxamide modified strands synthesized by Lewis and co-workers (Fig. 19) are believed to adopt a face to face orientation that places them perpendicular to the plane of the DNA bases.[46]

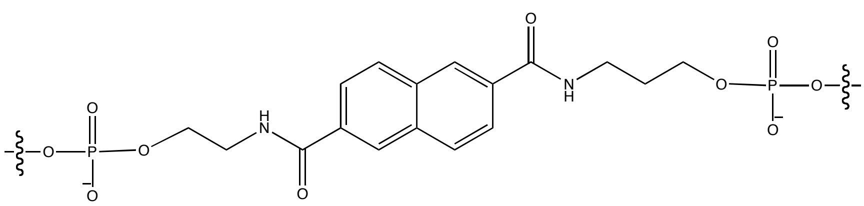

Fig. 19 Napthalenecarboxamide nucleoside for insertion into DNA

1.5.6.3 Alkyl based acyclic linkers as ribose mimics

Such simple acyclic systems hold a number of advantages when tethering molecules other than natural nucleobases [52]:

1. Any molecule can be attached at any point in the sequence, and four different monomers do not need to be synthesized.
2. The synthetic procedure is much simpler compared to modifying a nucleoside: starting from the tagged diol only four steps are necessary to introduce the group into DNA.
3. Non-nucleosidic bases allow a number of different sequence types: Wedge type/deletion where there is nothing opposite the modification, pairing with a natural base or even pairing with itself or another modified nucleoside.

A number of groups have used such linkers to attach molecules for the purpose of modification of RNA/DNA:

Saito and co-workers have developed amino acid linker groups attached to a diethanolamine backbone for the purpose of tethering two pyrene molecules to the DNA backbone. The use of different amino acids enables the stereochemistry of the linker to be controlled and easily varied (Fig. 20).[53]

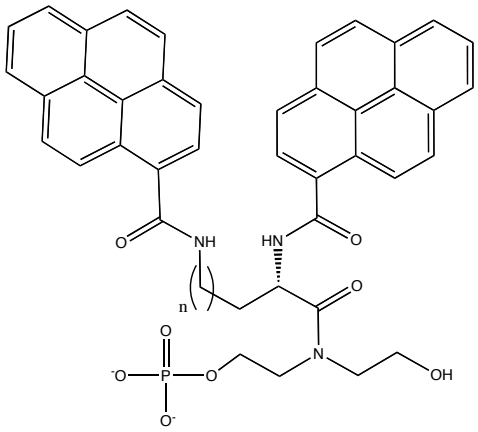

Fig. 20 Pyrene linked to an L-amino acid for incorporation into DNA n = 3, 2, 1 for lysine, ornithrine and α,γ-diamino butyric acid respectively

Of the available acyclic linkers, ethylene glycol (abbreviated as C2 due to the fact that there are two carbon atoms between the two phosphodiesters) and derivatives of 1,3 propane diol (abbreviated as C3) are the most frequently used due to their structural similarity to natural D-ribose (Fig. 21).

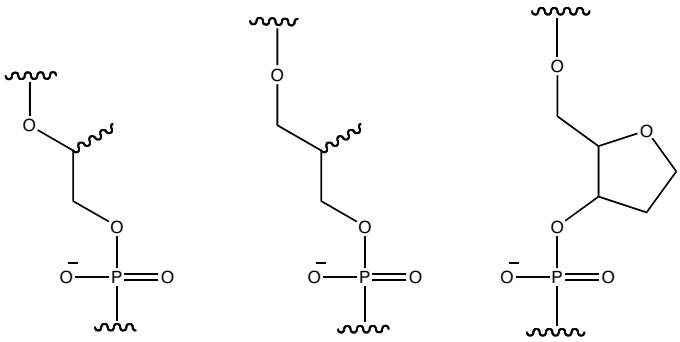

Fig. 21 Acyclic scaffolds based on ethylene glycol (left) and propane-1,3-diol (centre) compared to ribose sugar ring (right)

In synthesizing an ethidium nucleoside analogue, Wagenknecht and co-workers used an ethylene glycol analogue (Fig. 22).[54]

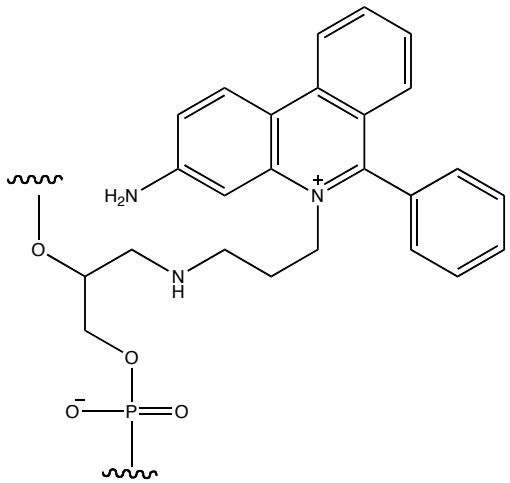

Fig. 22 Artificial phenanthridium base using ethylene glycol scaffold

A serinol linker was used by Bashkin and co-workers to tether a terpyridine metal-coordinating site to RNA to study copper-mediated RNA cleavage (Fig. 23).[55]

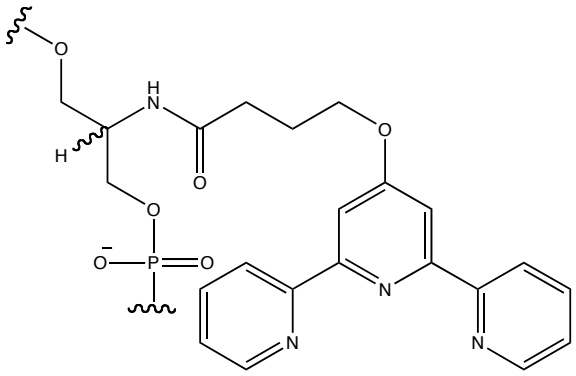

Fig. 23 Serinol tethered terpyridine – an impure mixture of the different stereoisomers of serinol was used in the synthesis to give a diastereomeric mixture of oligonucleotides[56]

In the past our research group has used the serinol linker to tether anthracene to DNA.[57] However, with serinol being a prochiral C3 scaffold, this approach results in the production of a mixture of stereoisomers upon incorporation into an oligonucleotide.[56] As a result of this Reynolds *et al* used the 2-aminobutane-1,3-diol (or threoninol) linker as an enantiomerically pure C3 scaffold.[58] Threoninol, which can be synthesized from the amino acid threonine, is commercially

available in both the L (*RR*) and D (*SS*) stereoisomers. Fukui *et al*. used the L form to conjugate acridine to DNA oligonucleotides (Fig. 24).[59]

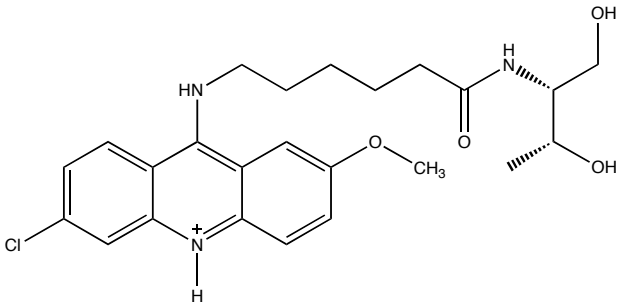

Fig. 24 Acridine conjugated to an L-threoninol backbone

Interestingly, Komiyama and Asanuma have utilized the D and L forms of threoninol to tether azobenzenes and acridine to DNA. In so doing they claim superior thermodynamic stability of the diastereoisomers derived from the D form over the L.[21, 60] This is ascribed to the different winding characteristics of the two forms: D threoninol prefers clockwise winding whereas the L form prefers anticlockwise winding. Since DNA naturally forms a right-handed duplex whose winding is clockwise, it is believed that the introduction of planar, stacking molecules via the D form causes less distortion to the duplex and hence confers greater stability.

1.6 Applying modified DNA to designing new systems

1.6.1 DNA as a supramolecular scaffold

DNA can be used as a scaffold onto which modifications can be attached with the aim of creating supramolecular systems. A recent example of this is the work of Stulz and co-workers who have used deoxyuridine modified with porphyrins to create DNA-porphyrin arrays on a nanometre scale.[61-63]

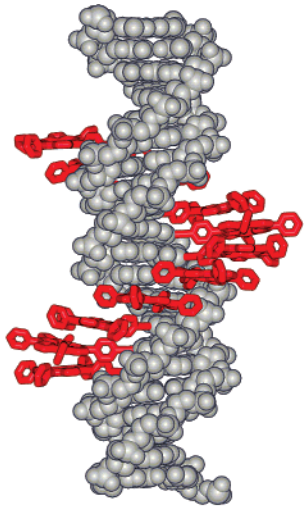

Fig. 25 Force-field minimized structures of the double strand form of porphyrin modified DNA[61]

This approach allows close contact and ordering of the porphyrin rings along with the possibility of combining the porphyrins with a variety of different metal centres. Such systems have the potential to function as photonic or electronic wires.

1.6.2 Interstrand stacking helices containing modified DNA

The ability to insert unnatural base pairs (section 1.3.4.2) has been extended to form DNA helices containing sections of completely modified DNA. Haner and co-workers have constructed DNA mimics based on interstacking phenanthrene,[49] pyrene[48] and phenanthroline[50] residues. They have found that low numbers of modifications can stabilize the duplex irrespective of the building block but adding more residues caused destabilization in the case of phenanthrene[64] but stabilization when pyrene is used.[48] Circular Dichroism studies revealed that the duplexes adopted the most common B form configuration (Fig. 26).[49]

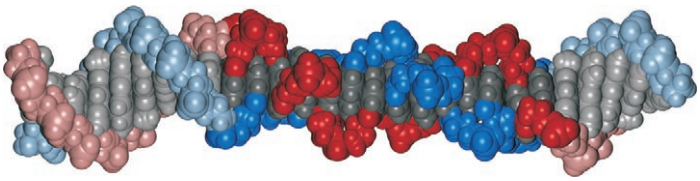

Fig. 26 AMBER model of interstrand stacking pyrenes in a DNA framework (pyrenes in dark grey, phosphate backbone in red and blue)

Further work in this group has also shown that the selectivity of the stacking can be controlled and monitored by synthesizing structurally related but electronically disparate hybrid oligonucleotides. In particular the synthesis of pyrene (S)/phenanthrene (P) hybrid strands allows the determination of the duplex structure through the monitoring of pyrene excimer formation. Therefore of the two possible structural outcomes shown in Fig. 27 it was possible to assign the structure to the model containing pyrene-pyrene stacking (Fig. 27 right).[65]

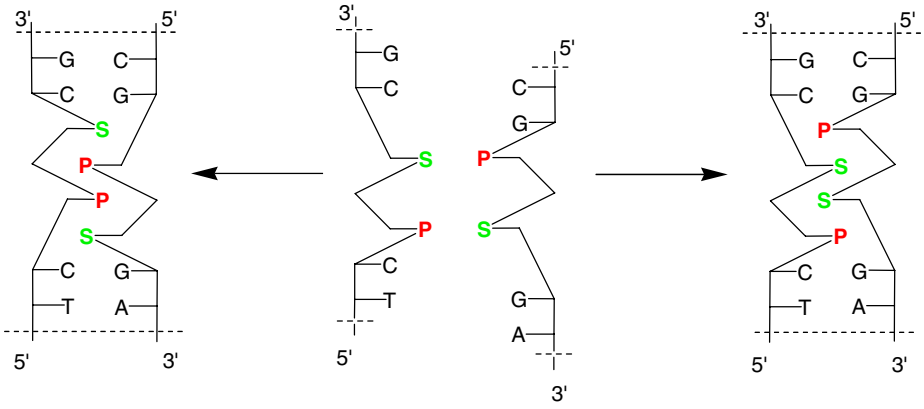

Fig. 27 Heterogeneous modified DNA with different possible conformations[65]

1.6.3 DNA-metal wire complexes using self assembly

Shionoya and co-workers have used the self assembling abilities of DNA to direct the complexation of different metal ions in matrices under precise control with regard to element, number and composition.[66]

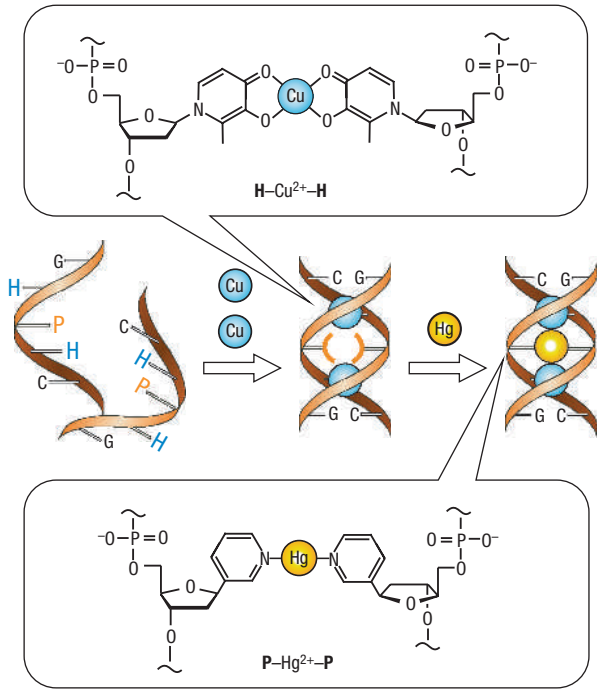

Fig. 28 Formation of heterogeneous metallo DNA chains[66]

By using different and selective metal binding groups they were able to construct heterogeneous metal chains inside of modified DNA (Fig. 28). This work has potential applications in the construction of DNA based charge conducting wires, potentially an important tool in the field of DNA nanotechnology.

1.7 DNA sensors

Due to its ubiquity in nature and biological systems, one of the most useful applications of modified DNA has been in the field of biological sensing. As our understanding of the importance of the genetic code has increased, so has the imperative to probe said code down to the base level. The ability to 'read' DNA has the potential to unlock many therapeutic possibilities both in terms of prevention and of cure.

A study on the global variations in the human genome revealed that around 12% of it contains many forms of genetic variation such as deletions, insertions, duplications, copies of multi-site variants and mutations – including at the single nucleotide level (Single Nucleotide Polymorphisms or SNPs).[67]

1.7.1 SNPs and their detection

One of the aims of the research within the Tucker group is the detection of SNPs using anthracene fluorescence. Single Nucleotide Polymorphisms (SNPs) are single nucleotides that share identical flanking sequences and vary between individuals; they occur with great frequency throughout the human genome and as a result provide an accessible route to the study of genetic variation. A single Watson-Crick base pair is replaced by any one of the other three base pairs in mutant DNA. Although a seemingly innocuous change, when an SNP site is located in a region of DNA responsible for protein encoding, the amino acid sequence of the resulting protein may be altered. Furthermore, SNPs in a promoter region may modulate the transcriptional efficiency of proteins encoded downstream.[68] The consequence of this is that a small difference in the DNA sequence can result in a much larger difference in the phenotype of each individual.

Since mutation during replication is rare, SNPs are mostly bi-allelic (i.e. there are only two possible alleles) and because people have two copies of each chromosome, one from the father and one from the mother, an SNP analysis will result in one of three possible diplotypes (Fig. 29):

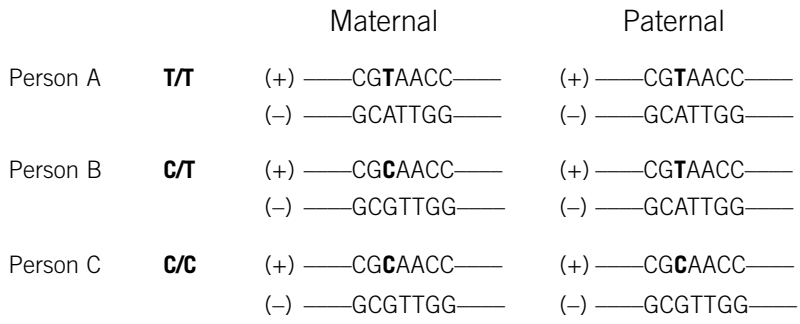

Fig. 29 Potential offspring from two heterozygous parents, Persons A and C are homozygous for T or C respectively whilst person B is heterozygous, carrying both T and C[69]

The emergence of SNPs as a useful diagnostic tool for disease has led to many efforts to develop SNP sensing systems in order to increase throughput and accuracy. This has resulted in a great deal of modifications to DNA in pursuit of these goals. A selection of modifications will be detailed in the following sections.

1.8 Electrochemical DNA sensors

Electrochemical sensing of DNA is a growing area with considerable scope for study due to the relative ease of device fabrication and the potential for immobilization of a device onto an electrode surface. As outlined below, both redox active tags and intercalators have been used in the construction of such devices.

Examples mentioned earlier include the work of Yu and co-workers who have covalently attached ferrocene to the 2' sugar position in order to probe base pair mismatches in DNA (Section 1.3.1.2).[22] In continuation of this work they then added electron donating groups to the ferrocene cyclopentadienyl ring in order to modify the redox properties and obtain two different electrochemical probes (Fig. 30).[70]

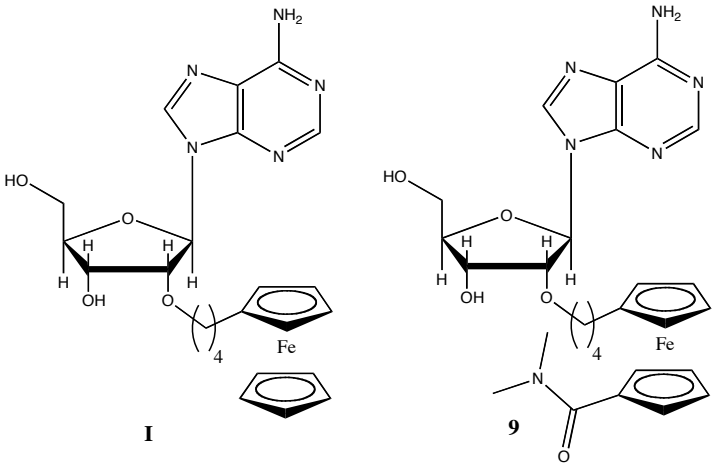

Fig. 30 Ferrocene modified monomers for incorporation into DNA

This enabled them to develop DNA nucleic acid detection chips that use differences in electrochemical output to identify mismatches (Fig. 31).

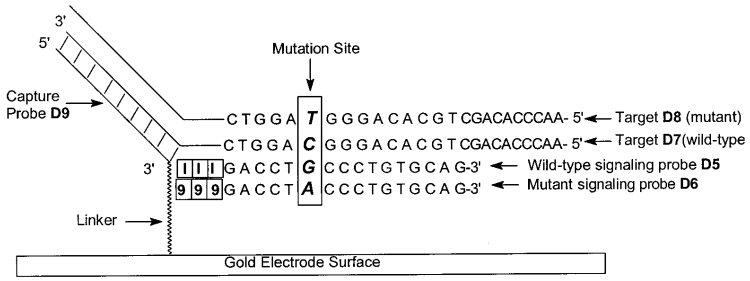

Fig. 31 Oligonucleotide mismatch detection using ferrocene modified DNA[70]

Plaxco and co-workers have designed a linear tagged electrochemical probe bound to an electrode surface that is capable of detecting specific DNA sequences through structural changes induced during hybridization (Fig. 32).[71]

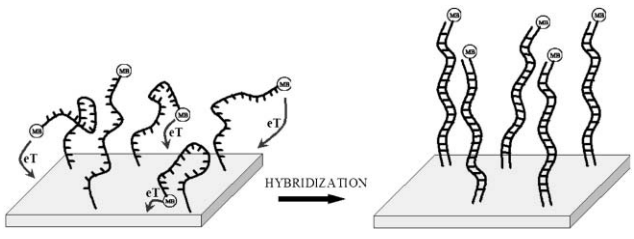

Fig. 32 Linear redox modified DNA Probe[71]

Another redox active group that has been extensively used is anthraquinone. It has been incorporated into DNA and tethered to a gold surface by Yamana and co-workers, who have then used it to sense mismatches in the duplex *via* a variable electrochemical response (Fig. 33).[72]

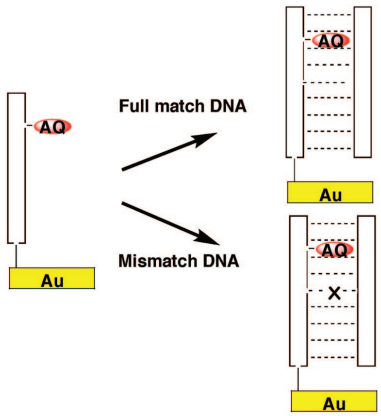

Fig. 33 Anthraquinone as an electrochemical mismatch sensor[72]

1.9 EPR DNA sensors

One particularly interesting approach to DNA sensing is the use of EPR (Electron Paramagnetic Resonance) spectroscopy. This technique gives information about unpaired electrons and has been successfully used to gain information on the structure dependent differences of the mobility of nucleic acids. Of particular relevance to the field of DNA sensing is the work of Sigurdsson, who has attached a nitroxide group to a modified cytosine nucleoside (Fig. 34).[73]

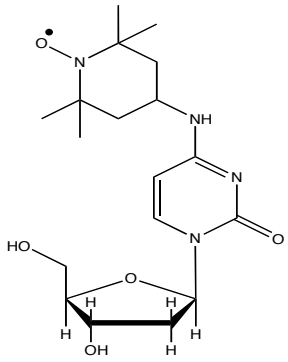

Fig. 34 (^{T}C) Spin labelled nucleoside for EPR DNA sensing

This spin labelled base, upon incorporation into DNA, is able to identify a mismatch in DNA. Furthermore, through differences in the EPR spectra of the mismatches the system is capable of differentiating one type of mismatch from another and thus the modified nucleoside can identify which base it is paired with.

1.10 Luminescent DNA sensors

A potential disadvantage of electrochemical sensing, for instance can be the relatively high concentration of sensor that is required for a sensing signal to be detected as well as the equipment required for this. Using luminescence sensors offers a solution to both of these potential problems as they can be used at very low concentrations and in certain situations the output can be measured visually.

1.10.1 Metal complex luminescent DNA sensors

Metal complexes have been used as luminescent DNA sensors by a number of groups including that of Mesmaeker whereby the a ruthenium metal centre is tagged onto DNA and where the luminescence is quenched via photo-induced electron transfer (PET) from the guanine bases on the target DNA strand (Fig. 35).[74]

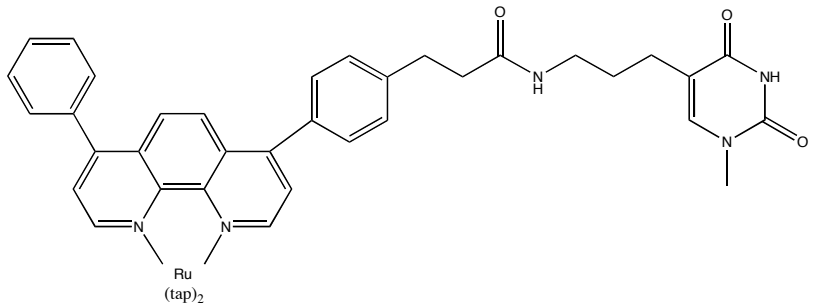

Fig. 35 Rutheium tagged nucleoside for luminescent sensing of DNA

1.10.2 Fluorescent methods of DNA analysis

Fluorescence is an important technique in the field of sensing and has been used to detect an extremely wide range of targets ranging from single atom ions to multi-cellular systems. There are a large number of molecules that can be made to fluoresce, and this means that a wide variety of probes can be constructed. Fluorescence can be detected using relatively simple equipment and functions effectively as a reporting mechanism down to low concentrations (< μM). A number of systems have already been successfully commercialized and an even greater number of systems have been designed, a selection of which are discussed in the sections that follow.

1.10.2.1 Taqman Probe

Currently genotyping assays are the most commonly used commercial technique to study polymorphisms. An example of this is Applied Biosystems' Taqman® SNP Genotyping Assay (Fig. 36). This uses probe and primer chemistry to discriminate between bases via differences in fluorescence.

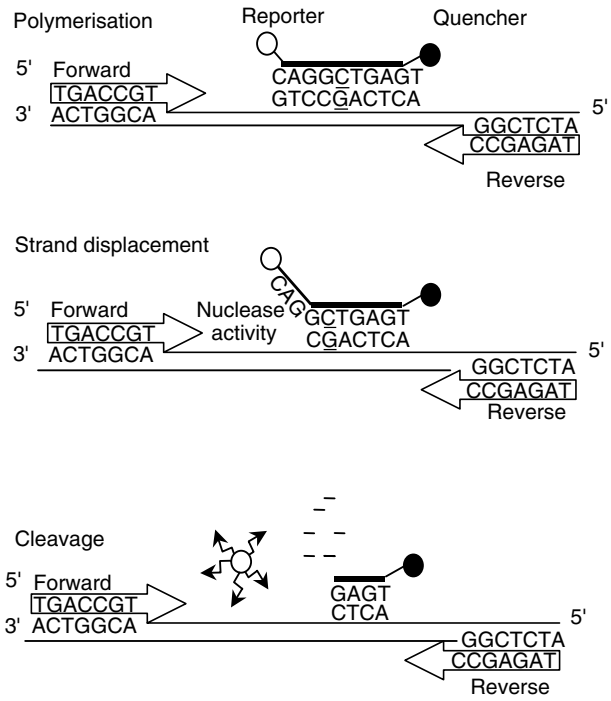

Fig. 36 Single Nucleotide Polymorphism detection using a Taqman probe system[69]

The system functions as follows:

1. The allele specific probe is annealed to the area of interest containing the SNP using a different fluorescent reporter tags for the different probes
2. During polymerase chain reaction the reporter tag is cleaved from the Probe
3. At the end point the genotype is determined according to the ratio of fluorescence originating from each different fluorophore.[69]

1.10.2.2 Molecular Beacons

One of the most common techniques in fluorescent DNA analysis is the use of molecular beacons. A molecular beacon (MB) is a fluorescent DNA/RNA probe consisting of a single strand of DNA, the ends of which are complementary and

give rise to a hairpin stem. Molecular beacons were first developed by Kramer and co-workers.[75, 76]

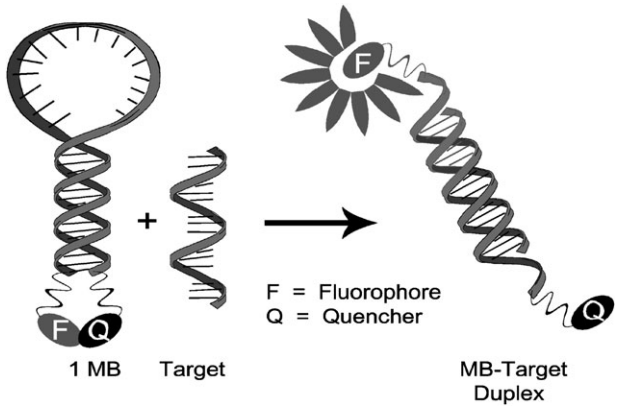

Fig. 37 Illustration of a molecular beacon (MB)[77]

At the 5' end is an attached fluorophore, whilst at the 3' end is a quencher. The hairpin structure keeps the two ends in close proximity, allowing fluorescence quenching (*via* photo-induced electron transfer (PET) or fluorescence resonance energy transfer (FRET)), and so the fluorescence intensity is low. When a target oligonucleotide with a complementary sequence is introduced to hybridize to the MB, the hairpin is opened and the fluorophore and quencher are separated. The fluorescence emission intensity increases and hence the target strand has been sensed (Fig. 37).

1.10.2.3 Quencher free molecular beacons

It has been shown by Kim and co-workers that fluorescent hairpin oligonucleotides can function as molecular beacons without the attachment of a quenching unit. Such probes have been called 'quencher-free molecular beacons' (QFMBs) and rely on either nucleobase quenching or changes in the microenvironment of the fluorophore.[77] The former is well known to occur[78] and

a number of studies have shown that PET between nucleobase and fluorophore is possible.[79] Consideration of the redox potentials can be used to influence selectivity in sensing and increase the specificity of the probe.[77]

Microenvironment changes can occur as a result of a change in the solvent polarity, hydrophobicity or pH of the media, intercalation of the fluorophore and nucleobase-pair degeneracy.[77] Kim designed a fluorene labelled nucleoside that can sense single base pair mismatches *via* a decrease in fluorescence emission and fully matching sequences *via* an increase in emission (Fig. 38).[80]

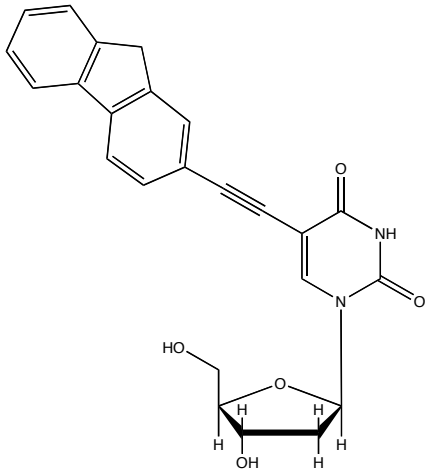

Fig. 38 Fluorene tagged nucleoside for use in quencher free molecular beacons

The work of Saito and co-workers has also introduced a quencher free molecular beacon based on the pyrrolocytidine moiety which is capable of forming Watson-Crick base pairs with guanidine.[81]

1.10.2.4 Base Discriminating Fluorophores

Apart from use in a molecular beacon device, the previously described system can also be used as a straightforward intercalative sensor whereby the fluorene tagged nucleoside is inserted into the centre of a DNA oligonucleotide.

Hybridization gives rise to an increase in fluorescence when the duplex is fully matching but a decrease upon intercalation with a mismatch to the modified T nucleobase. Variation of the opposite nucleobase gives rise to slightly different emission intensities and different red shifts of the emission band.[80]

The use of size-expanded fluorescent nucleotides has been investigated by Saito and co-workers to distinguish purines on the complementary strand. The fluorescence behaviour of the benzopyridopyrimidine (BPP) (Fig. 39) probe is strongly dependent on the purine base opposite.

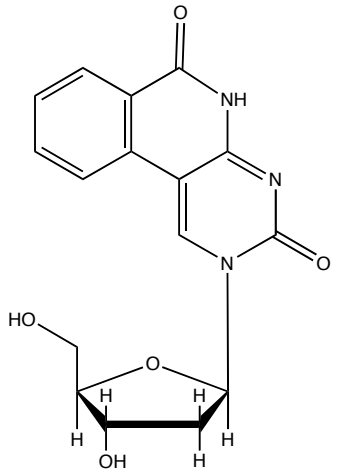

Fig. 39 BPP size-expanded base discriminating fluorescent nucleoside

BPP forms a stable Watson-Crick base pair with G and a relatively stable wobble base pair with A. However, base pairing with G gives rise to an extremely rapid quenching process that results in strong quenching compared to the BPP/A base pair.[82]

1.10.2.5 Excimer fluorescence sensing

It can be desirable in solution base sensing for the hybridization event to be accompanied not just by an increase or decrease in fluorescence emission, but by

a change in fluorescence wavelength to give a more definitive detection signal. The formation of excimers between two pyrene units will cause a change in fluorescence emission wavelength and this has been exploited by Masuko in the Excimer-forming two-probe nucleic acid hybridization (ETPH) method and by Saito as an insertion/deletion polymorphism detection system (Fig. 20).[53]

An excimer is a bimolecular complex between two identical molecules, one in its excited state and one in the ground state (for more details see section 3.15).

The ETPH method involves two oligonucleotide probes which are both complementary to half of the target sequence. One of the probes is labelled with pyrene at the 3' end whilst the other is labelled at the 5' end. Upon hybridization to the target strand, the two pyrenes are held close enough to each other to form an excimer (Fig. 40).[83]

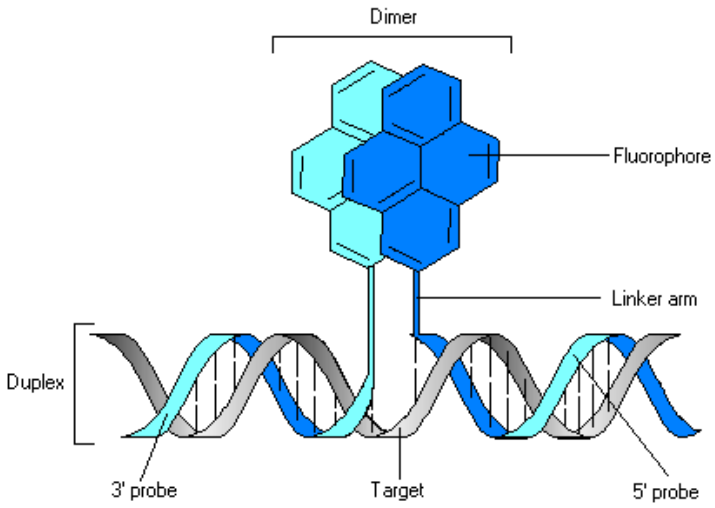

Fig. 40 Pyrene ETPH system

Masuko showed that the hybridization of the 3' and 5' oligonucleotides induced a colour change in the emission spectrum from blue (pyrene monomer) to green-white (excimer).

1.11 Anthracene as a fluorescent sensor

1.11.1 Introduction

Anthracene is a polyaromatic molecule found as a component of coal tar and was first discovered in 1832 by Dumas and Laurent. It was soon discovered that anthracene fluoresces when irradiated with ultra-violet light of a sufficiently high energy. This property has made anthracene an attractive component of many fluorescence sensing systems and indeed anthracene has been used as a sensor for various species.

1.11.1.1 Anthracene in sensing systems

A very simple sensing system using PET to anthracene can be used as a pH sensor (Fig. 41). The anthracene diethylamine moiety is essentially non-fluorescent at pH values >9 due to PET from the diethylamino groups. On lowering the pH to <5 a strong blue fluorescence is emitted due to disruption of PET by protonation of the nitrogen lone pairs.[84] The system allows for the visualization of acidic compartments inside living cells.

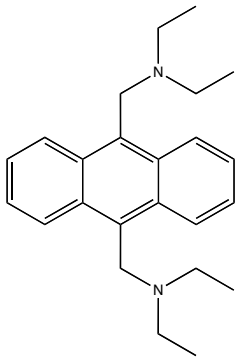

Fig. 41 Anthracene PET pH sensor

The photochemical properties of anthracene have also been used in sensing of simple metal cations. Anthracene is capable of undergoing a photoinduced 4π-4π

cycloaddition when irradiated at circa 360 nm, the efficiency of which is dependent on the relative orientation of the anthracene moieties.[85] Tucker and co-workers have used a photoactive bisanthracene crown ether that photocyclizes to form a cryptand (Fig. 42), whose efficiency of dimerisation and dimer stability is affected by the presence of different cations.[86]

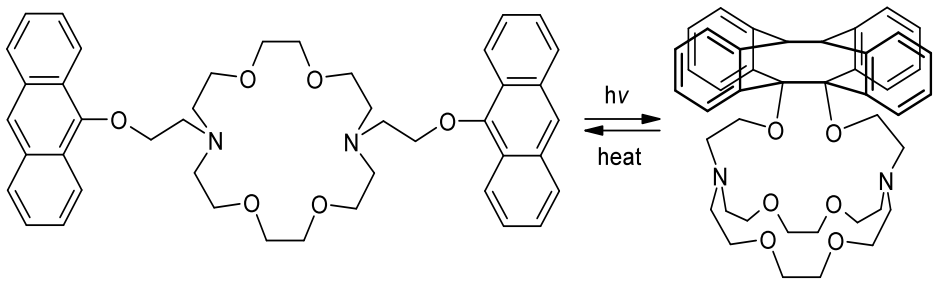

Fig. 42 Photocontrolled cryptand formation

Photodimerisation is more favourable when the smaller Rb^+ cation is complexed compared to the Cs^+ cation due to steric hindrance.

A similar system has been further developed to sense the binding of organic guest molecules using a Hamilton type receptor for barbital (Fig. 43).

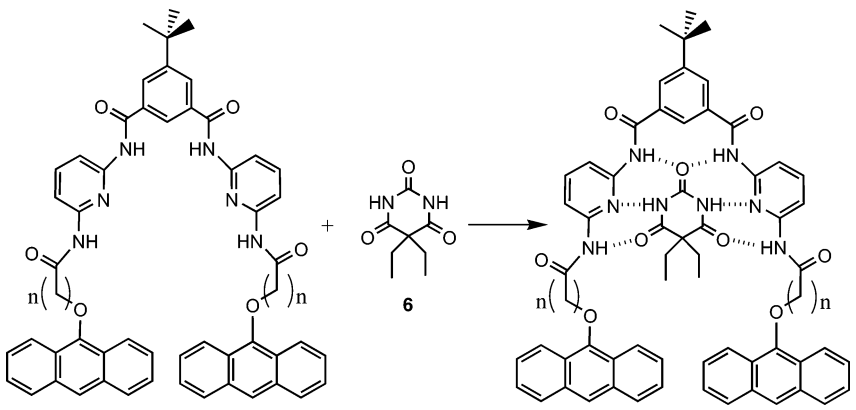

Fig. 43 Photocontrol of guest binding[87]

Variation of the methylene linker (n) has a profound influence on the photochemical and photophysical properties of the anthracene chromophores and dimerisation significantly affects the binding of the barbital molecule.[87]

1.11.2 Anthracene in DNA

A number of groups have designed DNA systems with the aim of exploiting the many useful properties of anthracene. These include fluorescence behaviour, the ability to intercalate, the formation of excimers and the ability to dimerise itself.

1.11.2.1 Anthracene as an intercalator

One of the simplest ways to study the effect of anthracene-DNA interactions is to add anthracene moieties to a solution of unmodified DNA oligonucleotides and to observe any changes in the photophysical properties. A great deal of work looking into the intercalative properties of anthracene has been undertaken by Kumar and co-workers who have extensively reported the results of the intercalation of anthracene derivatives (Fig. 44) into ct-DNA as monitored by a number of techniques such as fluorescence, UV-Vis, Circular Dichroism (CD) and IsoThermal Calorimetry (ITC).[88, 89]

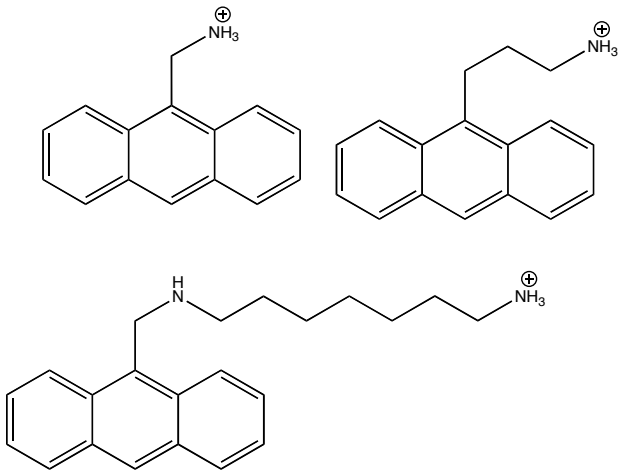

Fig. 44 AMAC (top left), APAC (top right) AODA (bottom)

Rodger and co-workers have extensively studied the interactions with DNA of an anthracene tagged spermine derivative (Fig. 45), principally via CD (Circular Dichroism) and LD (Linear Dichroism) spectroscopy.[90-92]

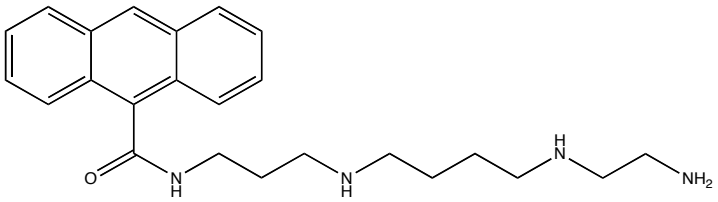

Fig. 45 Anthracene-9-carnonyl *N*1-spermine

They determined a number of different binding modes that were then calculated using molecular modelling.

The group of Teulade-Fichou designed a bisanthracene macrocycle that was found to bind to matched and mismatched base pairs in DNA by distinct binding modes that can be differentiated by UV/Vis and CD spectroscopy (Fig. 46).[93]

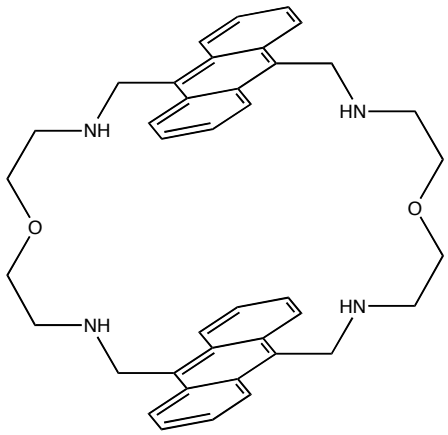

Fig. 46 Fluorescent bisanthracene macrocycle

Of particular interest is the fact that when the mismatched base is thymine, binding of the probe is almost completely quenched. As a result the probe is able to signal the presence of a single mismatched thymine residue in a duplex that contains 16 other GC and AT pairs. The selective recognition of T containing mismatches is important in SNP detection as T is involved in 49% of point mutations in the human genome, with a C-T transition representing about 33% of all substitutions.[94, 95]

1.11.2.2 Covalently linked anthracene DNA systems

In order to introduce specificity into the sensing it is advantageous to attach the reporting group to DNA, as we have seen in many previous examples. The same is true for anthracene and this has been accomplished via a number of techniques and using a variety of different attachment points. Yamana attached anthracene to the 2' position of the ribose moiety, where an increase in duplex stability was observed due to anthracene intercalation into the duplex (Fig. 47).[96] Similarly, Coleman attached anthracene to the 2' position in place of a nucleobase.[97]

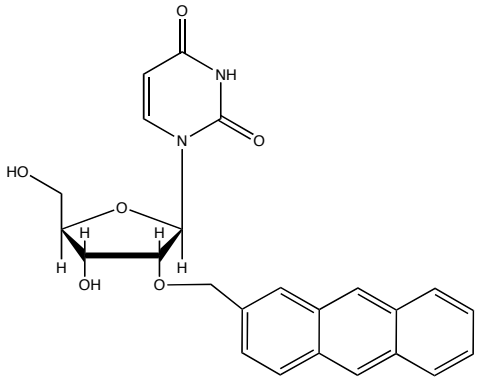

Fig. 47 Anthracene covalently attached to the 2' position of the sugar residue

Both Brown and Saito have made use of anthracene modified bases as Base-Discriminating Fluorescent nucleosides (BDFs). Brown and co-workers synthesized a thymine (dT*) substituted with anthracene attached either via a single (AeT) or double (AeeT) ethynyl linker group at the 9 position (Fig. 48).[98]

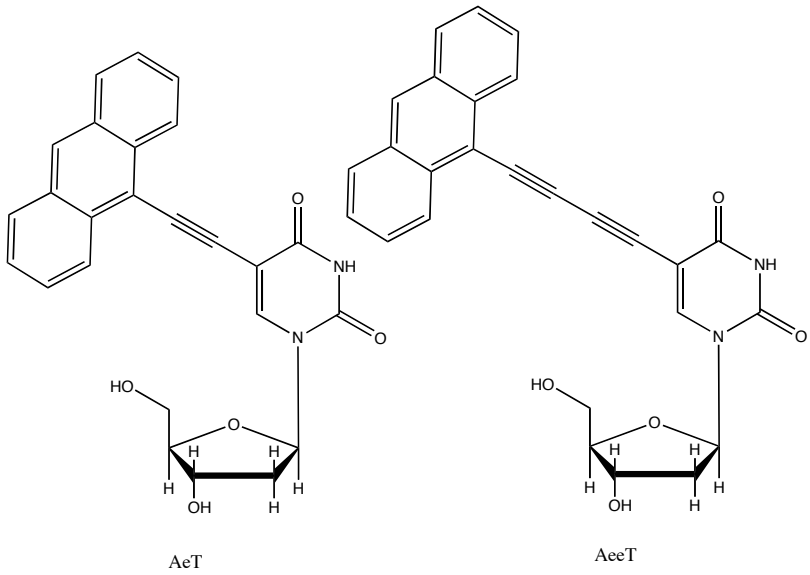

Fig. 48 Anthracene modified dT nucleosides synthesized by Tom Brown and co-workers

They reported destabilization of the duplex as a result of anthracene incorporation along with an approximately five-fold increase in fluorescence emission upon hybridization. It was found that the thermal stability, as reflected in the melting point, of the duplex was enhanced by the presence of a mismatch

between the dT* nucleoside and a C base compared to the fully matching strand by between 1.5 and 2.2 °C depending on the linker length. On the other hand, when hybridized with a G base opposite the anthracene a selective decrease in fluorescence emission is observed.

Saito and co-workers devised a similar system but with variation of the anthracene linking position.[99] They synthesized 2- and 9-anthracene labelled 2'deoxyuridines (Fig. 49) and incorporated them into DNA.

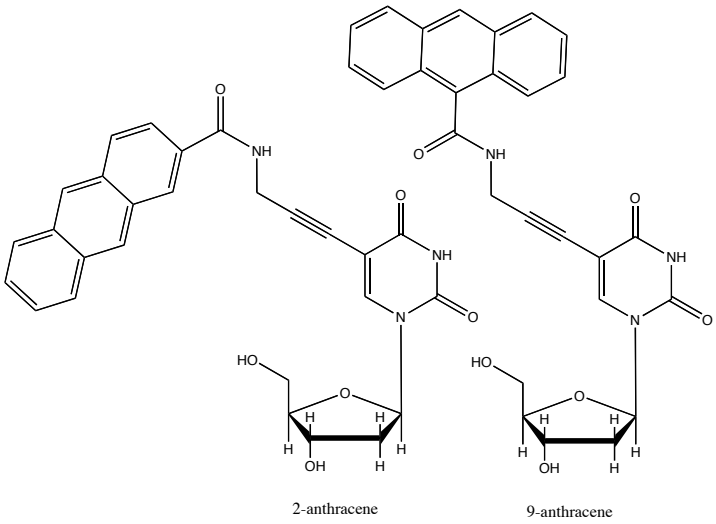

Fig. 49 Anthracene tagged deoxyuridine BDF probes synthesized by Saito and co-workers

In both cases the fluorescence emission was observed to increase upon hybridization with an A base opposite to the modified dU base.

1.11.2.3 Anthracene tagged DNA-like oligomers

The use of multiple anthracene modified nucleosides in forming fluorescent DNA oligomers has been reported by Inouye and co-workers. This was achieved via the stereoselective synthesis of alkynyl C-2 deoxy-β-**D**-ribofuranosides[100] followed by a Sonogashira coupling to attach the anthracene unit (Fig. 50).

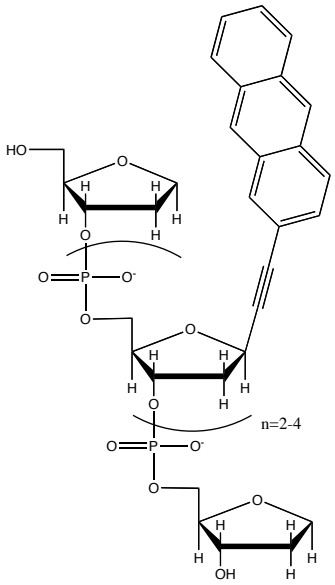

Fig. 50 Structure of DNA-like fluorescent oligomers

The resulting strands were examined using fluorescence techniques to probe the interactions between adjacent fluorophores, including the formation of anthracene excimers.[101]However, it was found that due to the relatively narrow plane of the anthracene rings, anthracene to anthracene excimer formation was very weak.

1.11.2.4 Photochemical dimerisation of anthracene-DNA conjugates

The photodimerisation properties of anthracene can also be harnessed for DNA signalling. Pioneering work in this field has been done by Ihara, who initially attached anthracene to the terminal positions of DNA oligonucleotides and successfully detected the formation of the duplex via an ETPH type dimer formation. Subsequent work achieved the photochemical ligation of anthracene DNA conjugates (Fig. 51).[19]

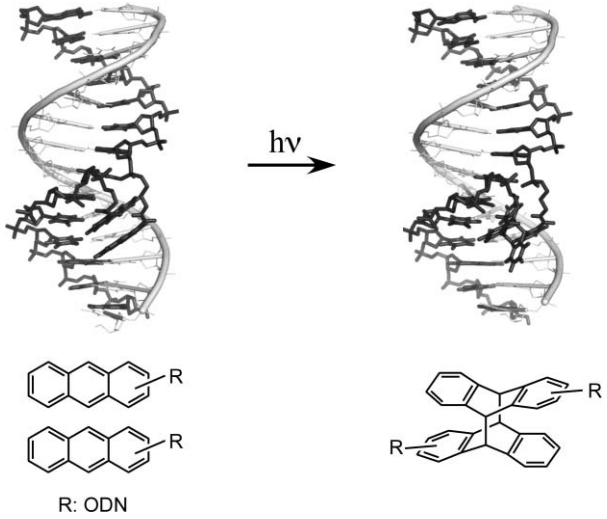

Fig. 51 Photodimerisation of anthracene using a DNA template[102]

Further work has refined the ligation yield through variation of the anthracene structure and different DNA conjugation points[102] and the resulting system has been tested as a potential route to SNP detection.[103]

1.11.3 Attaching anthracene as a non-nucleosidic base

Previous work in our group has involved the attachment of anthracene to a serinol (1,3-propanediol) non-nucleosidic backbone.[104] This was phosphytilated to give an anthracene phosphoramidite in a mixture of diastereomers.

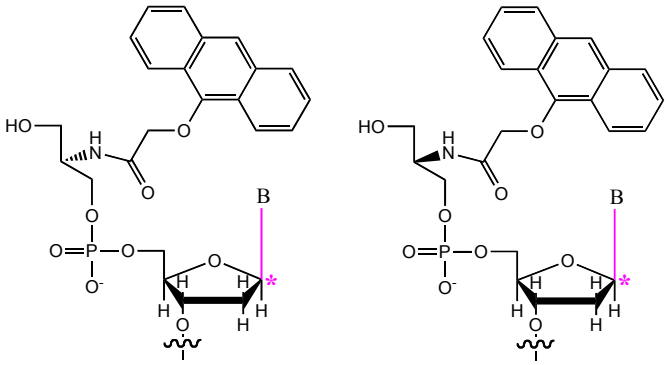

Fig. 52 Diastereomers of anthracene tagged non-nucleosidic DNA using a serinol linker

This molecule was then incorporated into DNA using solid-state DNA synthesis techniques to give a diastereomeric mixture of DNA oligonucleotides (Fig. 52). These were successfully purified and separated using chiral RP-HPLC.

Fluorescence studies were then carried out on this system in order to test its ability to act as an SNP sensor.[57]

The primary aim of this research is the covalent attachment of anthracene to a non-nucleosidic scaffold based on threoninol and subsequent incorporation of the resulting diasteriomerically pure phospharamidites into DNA oligonucleotides using solid state DNA synthesis. Once synthesized, purified and characterized, these anthracene tagged strands will be used to probe DNA via changes in fluorescence emission upon hybridization with a view to the development of sensors for SNP detection.

The mode of action of these compounds will be studied through the use of fluorescence spectroscopy (including determination of quantum yields, excitation and emission spectroscopy and fluorescence lifetimes), and UV-vis spectroscopy (including variable temperature UV).

The structure of the oligonucleotides will be established through the use of circular dichroism (CD), computational molecular modelling and high field NMR spectroscopy.

Finally, the potential application of photocontrol to anthracene in DNA will be explored with the aim of using light to control DNA binding.

1.12 References

1. Kool, E. T., *Acc. Chem. Res.* **2002,** *35* (11), 936-943.
2. Kool, E. T.; Morales, J. C.; Guckian, K. M., *Angew. Chem. Int. Ed.* **2000,** *39* (6), 990-1009.
3. Pang, Y. P.; Miller, J. L.; Kollman, P. A., *J. Am. Chem. Soc.* **1999,** *121* (8), 1717-1725.
4. Smithrud, D. B.; Wyman, T. B.; Diederich, F., *J. Am. Chem. Soc.* **1991,** *113* (14), 5420-5426.
5. Guckian, K. M.; Schweitzer, B. A.; Ren, R. X. F.; Sheils, C. J.; Tahmassebi, D. C.; Kool, E. T., *J. Am. Chem. Soc.* **2000,** *122* (10), 2213-2222.
6. Nakamoto, K. Tsuboi, M. and Strahan, G., *Drug-DNA Interactions*. Wiley: **2008**. Chapter 1.
7. Vesnaver, G.; Breslauer, K. J., *Proc. Natl. Acad. Sci. U. S. A.* **1991,** *88* (9), 3569-3573.
8. Beaucage, S. L.; Caruthers, M. H., *Tetrahedron Lett.* **1981,** *22* (20), 1859-1862.
9. Sakamoto, K.; Gouzu, H.; Komiya, K.; Kiga, D.; Yokoyama, S.; Yokomori, T.; Hagiya, M., *Science* **2000,** *288* (5469), 1223-1226.
10. Murphy, C. J.; Arkin, M. R.; Jenkins, Y.; Ghatlia, N. D.; Bossmann, S. H.; Turro, N. J.; Barton, J. K., *Science* **1993,** *262* (5136), 1025-1029.
11. Simmel, F. C.; Yurke, B., *Biophys. J.* **2001,** *80* (1), 178A-178A.
12. Simmel, F. C.; Yurke, B., *Smart Structures and Materials 2001: Industrial and Commercial Applications of Smart Structures Technologies* **2001,** *4332*, 419-428
13. Simmel, F. C.; Yurke, B., *Physical Review E* **2001,** *6304* (4), -.
14. Goodman, R. P.; Heilemann, M.; Doose, S.; Erben, C. M.; Kapanidis, A. N.; Turberfield, A. J., *Nature Nanotechnol.* **2008,** *3* (2), 93-96.
15. Bath, J.; Turberfield, A. J., *Nature Nanotechnol.* **2007,** *2* (5), 275-284.
16. Malinovskii, V. L.; Wenger, D.; Haner, R., *Chem. Soc. Rev.* **2010,** *39* (2), 410-422.
17. Weisbrod, S. H.; Marx, A., *Chem. Commun.* **2008,** (44), 5675-5685.
18. Bichenkova, E. V.; Yu, X.; Bhadra, P.; Heissigerova, H.; Pope, S. J. A.; Coe, B. J.; Faulkner, S.; Douglas, K. T., *Inorg. Chem.* **2005,** *44* (12), 4112-4114.
19. Ihara, T.; Fujii, T.; Mukae, M.; Kitamura, Y.; Jyo, A., *J. Am. Chem. Soc.* **2004,** *126* (29), 8880-8881.
20. Smith, E. E.; McClean, J. N.; Cooke, L. A.; Duprey, J. L.; McCourt, M.; Fabani, M. M.; Tucker, J. H. R.; Vyle, J. S., *Tetrahedron Lett.* **2007,** *48* (37), 6569-6572.
21. Asanuma, H.; Takarada, T.; Yoshida, T.; Tamaru, D.; Liang, X. G.; Komiyama, M., *Angew. Chem. Int. Ed.* **2001,** *40* (14), 2671-2673.
22. Umek, R. M.; Lin, S. W.; Vielmetter, J.; Terbrueggen, R. H.; Irvine, B.; Yu, C. J.; Kayyem, J. F.; Yowanto, H.; Blackburn, G. F.; Farkas, D. H.; Chen, Y. P., *J. Mol. Diagnostics* **2001,** *3* (2), 74-84.
23. Song, H. F.; Li, X. H.; Long, Y. T.; Schatte, G.; Kraatz, H. B., *Dalton Trans.* **2006,** (39), 4696-4701.
24. Pike, A. R.; Ryder, L. C.; Horrocks, B. R.; Clegg, W.; Connolly, B. A.; Houlton, A., *Chem. Eur. J.* **2004,** *11* (1), 344-353.

25. Saito, Y.; Miyauchi, Y.; Okamoto, A.; Saito, I., *Chem. Commun.* **2004,** (15), 1704-1705.
26. Hurley, D. J.; Seaman, S. E.; Mazura, J. C.; Tor, Y., *Org. Lett.* **2002,** *4* (14), 2305-2308.
27. Millican, T. A.; Mock, G. A.; Chauncey, M. A.; Patel, T. P.; Eaton, M. A. W.; Gunning, J.; Cutbush, S. D.; Neidle, S.; Mann, J., *Nucleic Acids Res.* **1984,** *12* (19), 7435-7453.
28. Takeshita, M.; Chang, C. N.; Johnson, F.; Will, S.; Grollman, A. P., *J. Biol. Chem.* **1987,** *262* (21), 10171-10179.
29. Matray, T. J.; Kool, E. T., *J. Am. Chem. Soc.* **1998,** *120* (24), 6191-6192.
30. Matray, T. J.; Kool, E. T., *Nature* **1999,** *399* (6737), 704-708.
31. Nichols, R.; Andrews, P. C.; Zhang, P.; Bergstrom, D. E., *Nature* **1994,** *369* (6480), 492-493.
32. Loakes, D.; Brown, D. M., *Nucleic Acids Res.* **1994,** *22* (20), 4039-4043.
33. Schweitzer, B. A.; Kool, E. T., *J. Org. Chem.* **1994,** *59* (24), 7238-7242.
34. Guckian, K. M.; Kool, E. T., *Angew. Chem. Int. Ed.* **1997,** *36* (24), 2825-2828.
35. Piccirilli, J. A.; Krauch, T.; Moroney, S. E.; Benner, S. A., *Nature* **1990,** *343* (6253), 33-37.
36. Schweitzer, B. A.; Kool, E. T., *J. Am. Chem. Soc.* **1995,** *117* (7), 1863-1872.
37. McMinn, D. L.; Ogawa, A. K.; Wu, Y. Q.; Liu, J. Q.; Schultz, P. G.; Romesberg, F. E., *J. Am. Chem. Soc.* **1999,** *121* (49), 11585-11586.
38. Ishikawa, M.; Hirao, I.; Yokoyama, S., *Tetrahedron Lett.* **2000,** *41* (20), 3931-3934.
39. Tanaka, K.; Shionoya, M., *J. Org. Chem.* **1999,** *64* (14), 5002-5003.
40. Meggers, E.; Holland, P. L.; Tolman, W. B.; Romesberg, F. E.; Schultz, P. G., *J. Am. Chem. Soc.* **2000,** *122* (43), 10714-10715.
41. Brotschi, C.; Haberli, A.; Leumann, C. J., *Angew. Chem. Int. Ed.* **2001,** *40* (16), 3012-3014.
42. Weizman, H.; Tor, Y., *J. Am. Chem. Soc.* **2001,** *123* (14), 3375-3376.
43. Egholm, M.; Buchardt, O.; Christensen, L.; Behrens, C.; Freier, S. M.; Driver, D. A.; Berg, R. H.; Kim, S. K.; Norden, B.; Nielsen, P. E., *Nature* **1993,** *365* (6446), 566-568.
44. Pianowski, Z. L.; Winssinger, N., *Chem. Soc. Rev.* **2008,** *37* (7), 1330-1336.
45. Dragulescu-Andrasi, A.; Rapireddy, S.; He, G. F.; Bhattacharya, B.; Hyldig-Nielsen, J. J.; Zon, G.; Ly, D. H., *J. Am. Chem. Soc.* **2006,** *128* (50), 16104-16112.
46. Lewis, F. D.; Zhang, Y. F.; Liu, X. Y.; Xu, N.; Letsinger, R. L., *J. Phys. Chem. B* **1999,** *103* (13), 2570-2578.
47. Navarro, A. E.; Spinelli, N.; Chaix, C.; Moustrou, C.; Mandrand, B.; Brisset, H., *Bioorg. Med. Chem. Lett.* **2004,** *14* (10), 2439-2441.
48. Malinovskii, V. L.; Samain, F.; Haner, R., *Angew. Chem. Int. Ed.* **2007,** *46* (24), 4464-4467.
49. Langenegger, S. M.; Haner, R. H., *Chembiochem* **2005,** *6* (12), 2149-2152.
50. Langenegger, S. M.; Haner, R., *Chembiochem* **2005,** *6* (5), 848-+.
51. Bouquin, N.; Malinovskii, V. L.; Haner, R., *Eur. J. Chem.* **2008,** (13), 2213-2219.
52. Kashida, H.; Liang, X. G.; Asanuma, H., *Curr. Org. Chem.* **2009,** *13* (11), 1065-1084.

53. Okamoto, A.; Ichiba, T.; Saito, I., *J. Am. Chem. Soc.* **2004,** *126* (27), 8364-8365.
54. Huber, R.; Amann, N.; Wagenknecht, H. A., *J. Org. Chem.* **2004,** *69* (3), 744-751.
55. Trawick, B. N.; Osiek, T. A.; Bashkin, J. K., *Bioconjug. Chem.* **2001,** *12* (6), 900-905.
56. Daniher, A. T.; Bashkin, J. K., *Chem. Commun.* **1998,** (10), 1077-1078.
57. Moran, N.; Bassani, D. M.; Desvergne, J. P.; Keiper, S.; Lowden, P. A. S.; Vyle, J. S.; Tucker, J. H. R., *Chem. Commun.* **2006,** (48), 5003-5005.
58. Reynolds, M. A.; Beck, T. A.; Hogrefe, R. I.; Mccaffrey, A.; Arnold, L. J.; Vaghefi, M. M., *Bioconjug. Chem.* **1992,** *3* (5), 366-374.
59. Fukui, K.; Iwane, K.; Shimidzu, T.; Tanaka, K., *Tetrahedron Lett.* **1996,** *37* (28), 4983-4986.
60. Shi, Y.; Machida, K.; Kuzuya, A.; Komiyama, M., *Bioconjug. Chem.* **2005,** *16* (2), 306-311.
61. Fendt, L. A.; Bouamaied, I.; Thoni, S.; Amiot, N.; Stulz, E., *J. Am. Chem. Soc.* **2007,** *129* (49), 15319-15329.
62. Bouamaied, I.; Fendt, L. A.; Haussinger, D.; Wiesner, M.; Thoni, S.; Amiot, N.; Stulz, E., *Nucleosides Nucleotides Nucleic Acids* **2007,** *26* (10-12), 1533-1538.
63. Bouamaied, I.; Nguyen, T.; Ruhl, T.; Stulz, E., *Org. & Biomol. Chem.* **2008,** *6* (21), 3888-3891.
64. Langenegger, S. M.; Haner, R., *Chembiochem* **2005,** *6* (12), 2149-2152.
65. Langenegger, S. M.; Haner, R., *Bioorg. Med. Chem. Lett.* **2006,** *16* (19), 5062-5065.
66. Tanaka, K.; Clever, G. H.; Takezawa, Y.; Yamada, Y.; Kaul, C.; Shionoya, M.; Carell, T., *Nature Nanotechnol.* **2006,** *1* (3), 190-U5.
67. Redon, R.; Ishikawa, S.; Fitch, K. R.; Feuk, L.; Perry, G. H.; Andrews, T. D.; Fiegler, H.; Shapero, M. H.; Carson, A. R.; Chen, W. W.; Cho, E. K.; Dallaire, S.; Freeman, J. L.; Gonzalez, J. R.; Gratacos, M.; Huang, J.; Kalaitzopoulos, D.; Komura, D.; MacDonald, J. R.; Marshall, C. R.; Mei, R.; Montgomery, L.; Nishimura, K.; Okamura, K.; Shen, F.; Somerville, M. J.; Tchinda, J.; Valsesia, A.; Woodwark, C.; Yang, F. T.; Zhang, J. J.; Zerjal, T.; Zhang, J.; Armengol, L.; Conrad, D. F.; Estivill, X.; Tyler-Smith, C.; Carter, N. P.; Aburatani, H.; Lee, C.; Jones, K. W.; Scherer, S. W.; Hurles, M. E., *Nature* **2006,** *444* (7118), 444-454.
68. Nakatani, K., *Chembiochem* **2004,** *5* (12), 1623-1633.
69. McGuigan, F. E. A.; Ralston, S. H., *Psychiatr. Genet.* **2002,** *12* (3), 133-136.
70. Yu, C. J.; Wan, Y. J.; Yowanto, H.; Li, J.; Tao, C. L.; James, M. D.; Tan, C. L.; Blackburn, G. F.; Meade, T. J., *J. Am. Chem. Soc.* **2001,** *123* (45), 11155-11161.
71. Ricci, F.; Lai, R. Y.; Plaxco, K. W., *Chem. Commun.* **2007,** (36), 3768-3770.
72. Kumamoto, S.; Watanabe, M.; Kawakami, N.; Nakamura, M.; Yamana, K., *Bioconj. Chem.* **2008,** *19* (1), 65-69.
73. Cekan, P.; Sigurdsson, S. T., *J. Am. Chem. Soc.* **2009,** *131* (50), 18054-+.
74. Ortmans, I.; Content, S.; Boutonnet, N.; Kirsch-De Mesmaeker, A.; Bannwarth, W.; Constant, J. F.; Defrancq, E.; Lhomme, J., *Chem. Eur. J.* **1999,** *5* (9), 2712-2721.
75. Tyagi, S.; Kramer, F. R., *Nat. Biotechnol.* **1996,** *14* (3), 303-308.

76. Kostrikis, L. G.; Tyagi, S.; Mhlanga, M. M.; Ho, D. D.; Kramer, F. R., *Science* **1998,** *279* (5354), 1228-1229.
77. Venkatesan, N.; Seo, Y. J.; Kim, B. H., *Chem. Soc. Rev.* **2008,** *37* (4), 648-663.
78. Maruyama, T.; Shinohara, T.; Hosogi, T.; Ichinose, H.; Kamiya, N.; Goto, M., *Anal. Biochem.* **2006,** *354* (1), 8-14.
79. Seidel, C. A. M.; Schulz, A.; Sauer, M. H. M., *J. Phys. Chem.* **1996,** *100* (13), 5541-5553.
80. Hwang, G. T.; Seo, Y. J.; Kim, B. H., *J. Am. Chem. Soc.* **2004,** *126* (21), 6528-6529.
81. Saito, Y. S., Y.; Bag, S.; Takeuchi, Y.; Matsumoto, K. and Saito, I. , *Nucleic Acids Symposium Series* **2008,** *52*, 361-362.
82. Okamoto, A.; Saito, Y.; Saito, I., *J. Photochem. Photobiol. C-Photochem. Rev.* **2005,** *6* (2-3), 108-122.
83. Masuko, M.; Ohtani, H.; Ebata, K.; Shimadzu, A., *Nucleic Acids Res.,* **1998,** *26* (23), 5409 - 5416.
84. Desilva, A. P.; Rupasinghe, R. A. D. D., *J. Chem. Soc., Chem. Commun.* **1985,** (23), 1669-1670.
85. Bouas-Laurent, H.; Castellan, A.; Desvergne, J.-P.; Lapouyade, R., *Chem. Soc. Rev.,* **2000,** *29*, 43 - 55.
86. McSkimming, G.; Tucker, J. H. R.; Bouas-Laurent, H.; Desvergne, J.-P.; Coles, S. J.; Hursthouse, M. B.; Light, M. E., *Chem. Eur. J.,* **2002,** *8* (15), 3331 - 3342.
87. Molard, Y.; Bassani, D. M.; Desvergne, J. P.; Moran, N.; Tucker, J. H. R., *J. Org. Chem.* **2006,** *71* (22), 8523-8531.
88. Modukuru, N. K.; Snow, K. J.; Perrin, B. S.; Thota, J.; Kumar, C. V., *J. Phys. Chem. B* **2005,** *109* (23), 11810-11818.
89. Kumar, C. V.; Asuncion, E. H., *J. Chem. Soc., Chem. Commun.* **1992,** (6), 470-472.
90. Rodger, A.; Blagbrough, I. S.; Adlam, G.; Carpenter, M. L., *Biopolymers* **1994,** *34* (12), 1583-1593.
91. Adlam, G.; Blagbrough, I. S.; Taylor, S.; Latham, H. C.; Haworth, I. S.; Rodger, A., *Bioorg. & Med. Chem. Lett.* **1994,** *4* (20), 2435-2440.
92. Rodger, A.; Taylor, S.; Adlam, G.; Blagbrough, I. S.; Haworth, I. S., *Bioorg. & Med. Chem.* **1995,** *3* (6), 861-872.
93. Granzhan, A.; Teulade-Fichou, M. P., *Chem. Eur. J.* **2009,** *15* (6), 1314-1318.
94. Zhang, F. K.; Zhao, Z. M., *Genomics* **2004,** *84* (5), 785-795.
95. Guo, Y. J.; Jamison, D. C., *BMC Genomics* **2005,** *6*, -.
96. Yamana, K.; Aota, R.; Nakano, H., *Tetrahedron Lett.* **1995,** *36* (46), 8427 - 8430.
97. Coleman, R. S.; Mortensen, M. A., *Tetrahedron Lett.* **2003,** *44*, 1215 - 1219.
98. Xiao, Q.; Ranasinghe, R. T.; Tang, A. M. P.; Brown, T., *Tetrahedron* **2007,** *63* (17), 3483-3490.
99. Saito, Y.; Motegi, K.; Bag, S. S.; Saito, I., *Bioorg. Med. Chem.* **2008,** *16* (1), 107-113.
100. Takase, M.; Morikawa, T.; Abe, H.; Inouye, M., *Org. Lett.* **2003,** *5* (5), 625-628.
101. Chiba, J.; Takeshima, S.; Mishima, K.; Maeda, H.; Nanai, Y.; Mizuno, K.; Inouye, M., *Chem. Eur. J.* **2007,** *13* (29), 8124-8130.

102. Mukae, M.; Ihara, T.; Tabara, M.; Jyo, A., *Org. Biomol. Chem.* **2009,** *7* (7), 1349-1354.
103. Mukae, M.; Ihara, T.; Tabara, M.; Arslan, P.; Jyo, A., *Supramol. Chem.* **2009,** *21* (3-4), 292-295.
104. Moran, N. Novel Anthracene-Tagged DNA Sensors. University of Exeter, **2006**.

Chapter 2 Synthesis and Characterization

2.1 Introduction

The focus of the synthetic part of this project was the preparation and characterization of a range of anthracene probes that could be utilized in solid-phase DNA synthesis to create anthracene-tagged oligonucleotide sensors. The methodology was an extension of previous work carried out in the group that led to the synthesis of a diastereomeric mixture of two non-nucleosidic amidites.[1] As described in Chapter 1, the key aim of the work was to create enantiomerically pure starting phosphoramidite monomers to ensure that the resulting oligonucleotides contained anthracene in a single environment.[2] The steps used were based on previous work in the group performed by N. Moran.[3] However, a few modifications were undertaken over the course of the syntheses, mainly to improve the overall yield.

The overall scheme used for all of the syntheses is depicted in the following scheme (Scheme 1).

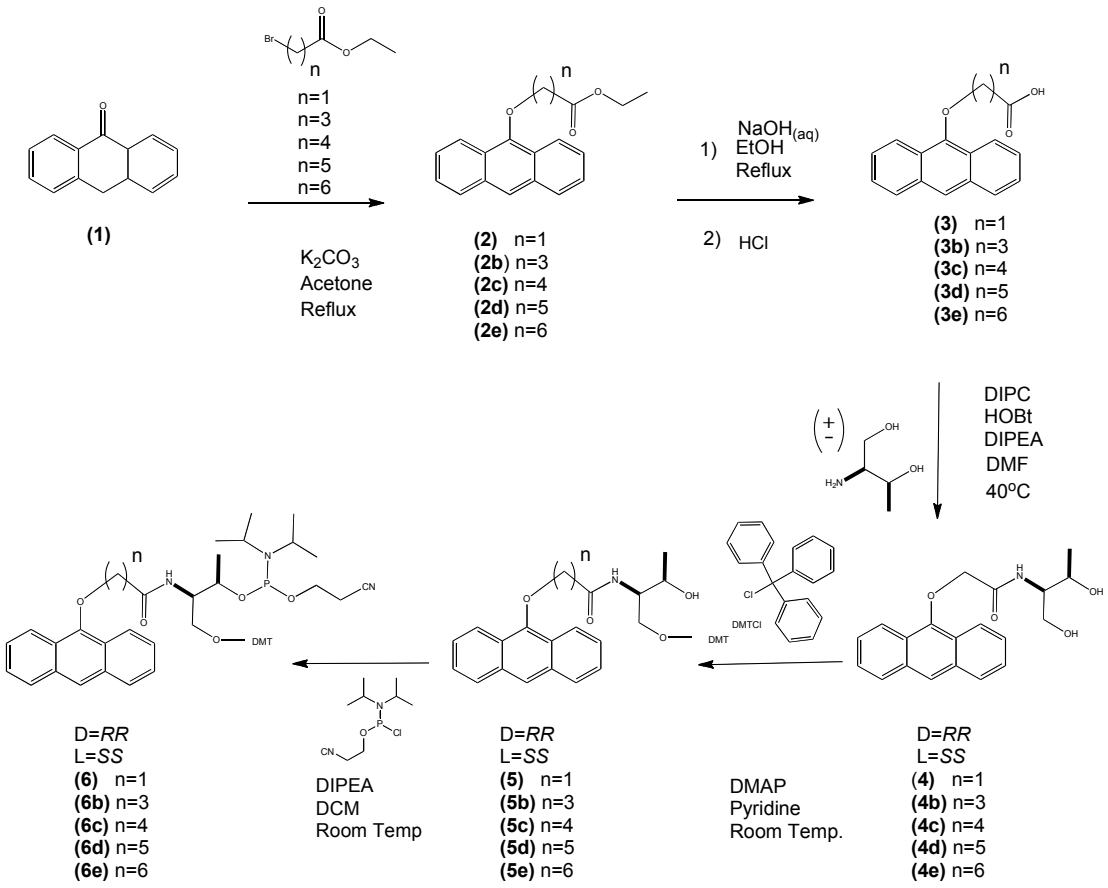

Scheme 1 Overall synthetic strategy used for the synthesis of the anthracene non-nucleosidic phosphoramidites

2.2 Short chain anthracene non-nucleosidic linkers

2.2.1 Synthesis of the *n* = 1 linker

It was first decided to synthesise the L and D *n* = 1 monomers, where *n* denotes the number of carbons between the carbonyl group and the ether oxygen. This involves a common carboxylic acid intermediary derived from the anthracene alkoxy ester and is based on the method used by Hamilton and co-workers.[4] Starting from anthrone **(1)** and ethyl bromo acetate, a base-induced nucleophilic substitution gave the anthracene-O-alkoxy ester **(2)** in 33% yield. Subsequent saponification with aqueous sodium hydroxide in ethanol followed by precipitation with HCl gave the acid **(3)** in quantitative yield (Scheme 2).

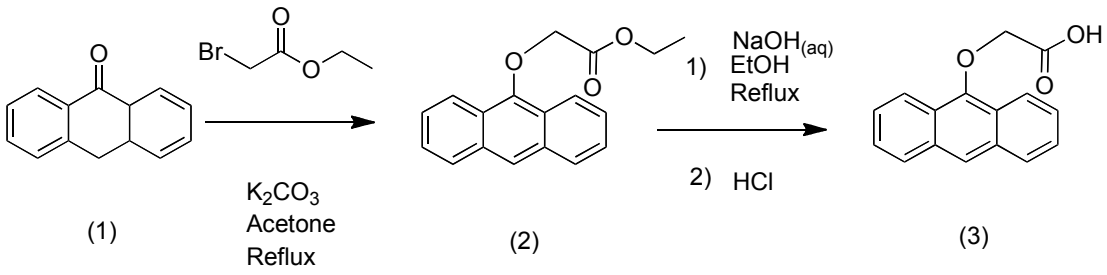

Scheme 2 Synthesis of *n* = 1 anthracene carboxylic acid from anthrone

2.2.1.1 Non-nucleosidic base analogues

Threoninol (2-amino-1,3-butanediol) is a reduced form of threonine (derived from the methyl ester) and contains primary and secondary hydroxyl moieties analogous to the *5'*- and *3 '*-OH groups on a standard nucleoside. The presence of a methyl group adjacent to one of the alcohol groups creates two stereogenic centres and as a result of this, and regioselective protection of one alcohol, it is possible to synthesize diastereomerically pure phosphoramidites.

2.1.1.2 Synthetic route

The carboxylic acid was coupled to either commercially purchased D or L threoninol using DIPC and HOBt as the coupling agents to give **(4)D** and **(4)L** as the *SS* and *RR* stereoisomers respectively (Scheme 3). In order to simplify nonclamenture, all compounds that have the *RR* or *SS* stereoconfiguration, being synthesised from the L or D form of threoninol respectively will be referred to as L or D in recognition of the threoninol compound they were synthesised from. This designation should not be held to mean that they are in fact D and L enantiomers of each other.

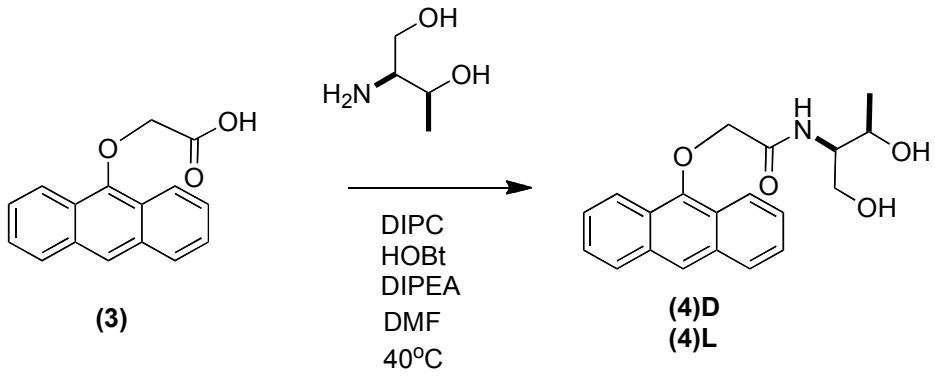

Scheme 3 Amide bond forming step

Silica gel chromatography on methanol in DCM (1 to 10% gradient) gave the products in a first time yield of 61 and 29%[a] yield for the *SS* and *RR* stereoisomers respectively.

2.1.1.3 Hydroxyl group protection

For DNA synthesis using the standard Caruthers methodology[5] the 5'-alcohol group is protected using an acid labile protecting group. The most common protecting group chosen for this is DiMethoxyTrityl (DMT). The attachment of this group is well documented in the literature and in line with previous work in the group the procedure used by Hulton *et al*. was followed[6] to give compounds **(5)D** in 54% yield and **(5)L** in 44% yield as the *SS* and the *RR* stereoisomers respectively (Scheme 4). DMAP is added to catalyze the selective tritylation of primary alcohols in the presence of secondary alcohol groups.

[a] subsequent repetition of this reaction gave a higher yield of 53%

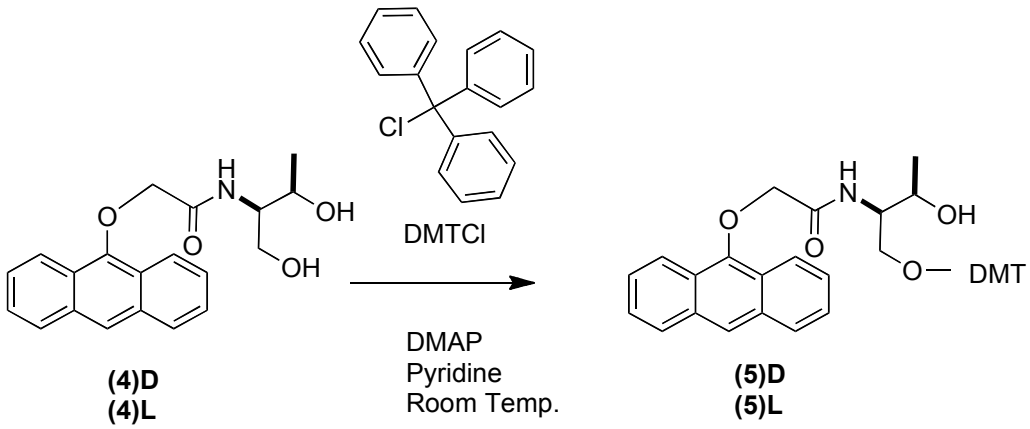

Scheme 4 Tritylation of the anthracene diol

Deuterated acetonitrile was used as the solvent for NMR spectroscopy in characterizing the product due to the fact that $CDCl_3$ is known to be acidic by virtue of generating DCl and therefore caused decomposition of the compound.

A full NMR assignment was undertaken in order to confirm that the DMT was attached to the primary alcohol. The proposed structure of the *RR* structure of the DMT protected compound is shown in Fig. 53 below:

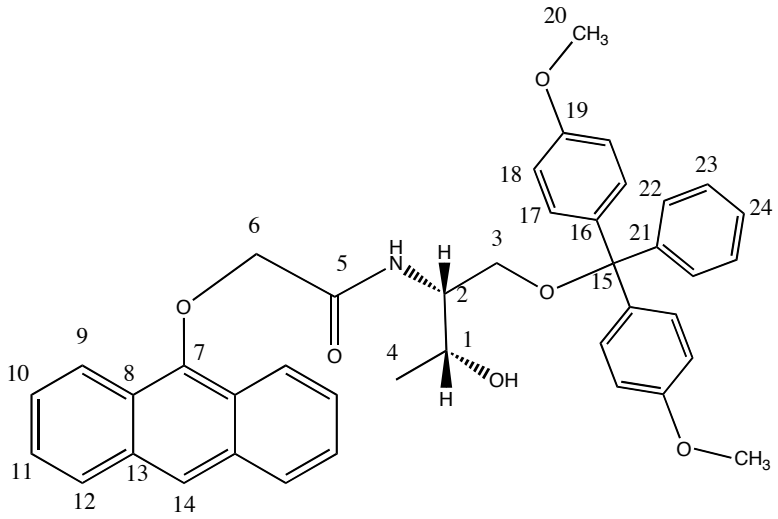

Fig. 53 Carbon/proton numerical assignment for the DMT protected n = 1 diol (5) *RR* Isomer

The primary issue is whether the DMT group is bonded to C*3*OH or C*1*OH. ^{1}H and ^{1}H decoupled ^{13}C NMR spectroscopy experiments were performed on the sample

followed by COSY, HMBC and HSQC. The proton NMR spectrum of compound **(5)L** is shown below (Fig. 54).

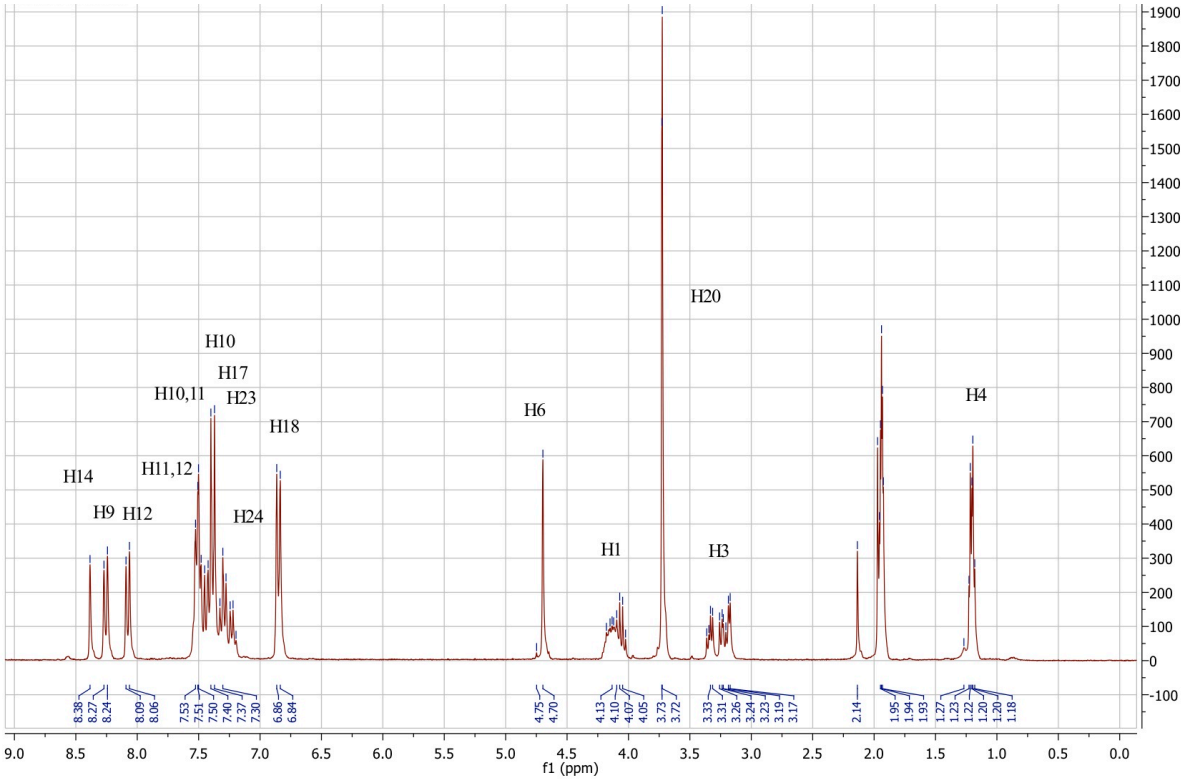

Fig. 54 300 MHz ^{1}H NMR spectrum of (5) L in CD_3CN at 25 °C

The assignment of H*4* (Me) is clear as it shows HMBC to C*1* (^{2}J) and C*2* (^{3}J), which can be differentiated on the basis that C*1* will have the highest frequency as it is bonded to oxygen. C*1* and C*2* are both CHs on the basis of DEPT13 signals. The protons H*1* and H*2* can be assigned from HSQC, since C*1* and C*2* have been identified. Furthermore, H*2* shows HMBC to C*5* (^{3}J) whereas H*1* would be ^{4}J coupling and therefore does not show coupling. To further clarify the spectrum C*5* can be used to assign the two H*6*s via HMBC, which then gives C*6* from the HSQC coupling. The H*6* protons can then be used to identify C*7* (quaternary) via HMBC. This leaves C*3* as the remaining CH_2 signal in DEPT 13. It can then be used to assign the two H*3* protons via HSQC. Having assigned all of the carbons and

hydrogens in the threoninol backbone, the key interaction is that of the C*15* trityl quaternary. This shows ^{3}J coupling in the HMBC spectrum to 2 x H*3* (blue Fig. 55), indicating that the protecting group is in the correctly assigned position. In confirmation, there is no evidence of coupling between H*1* and C*15* (red Fig. 55).

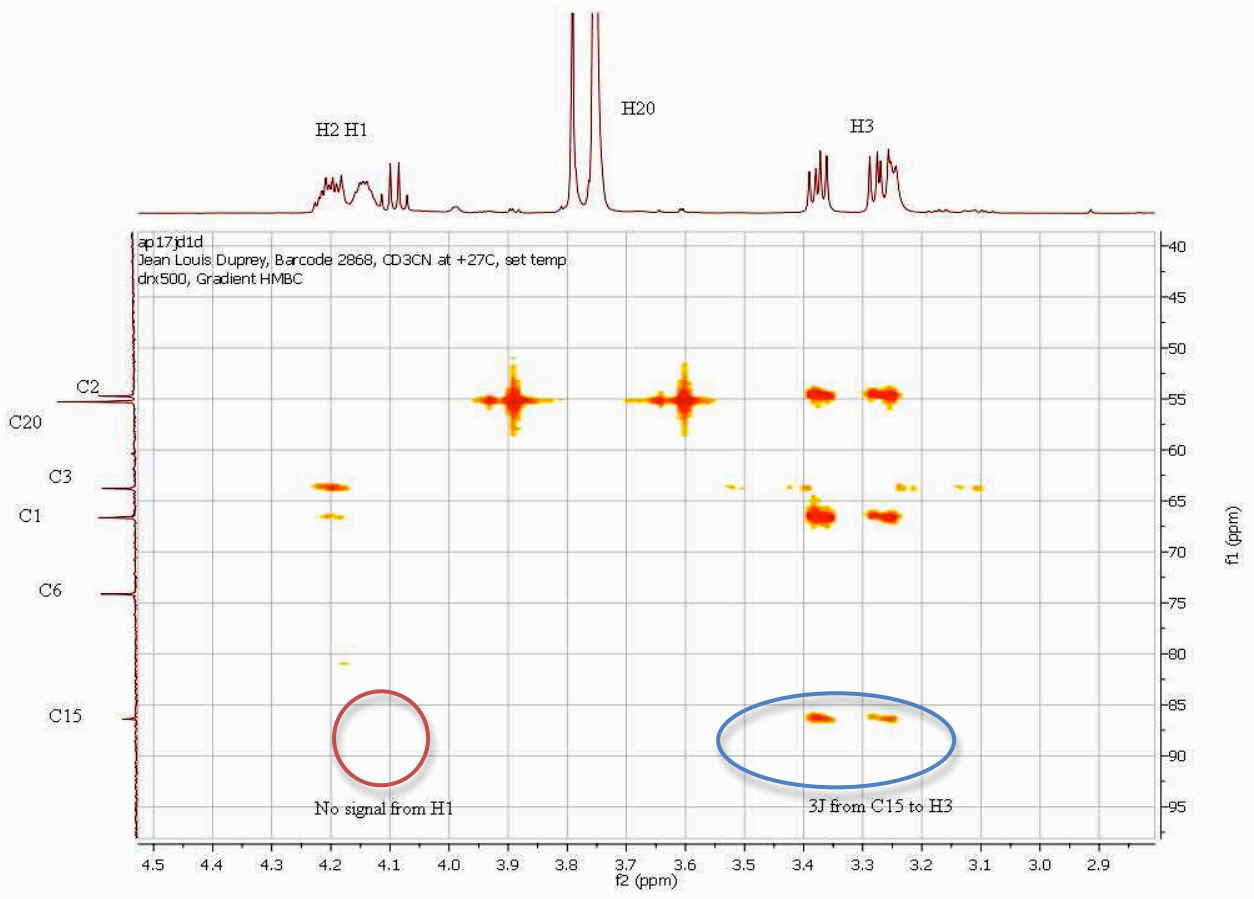

Fig. 55 500 MHz HMBC NMR spectrum of (5) D in the aliphatic threoninol area 27°C[b]

2.1.2 Phosphoramidite synthesis

Phosphoramidite derivatives were synthesized from the mono-DMT protected diols **(5)** using 2-cyanoethyl *N,N*-diisopropylchlorophosphoramidite and DIPEA in dry DCM under argon (Scheme 5).

[b] The cross peaks at 3.55 ppm and 3.85 ppm in the HMBC spectrum (f1 axis) are due to unsuppressed $^{1}J_{CH}$ couplings in the OMe group of the DMT functionality, those at 64 ppm (f1 axis) are due to unsuppressed $^{1}J_{CH}$ coupling on the C3 carbon.

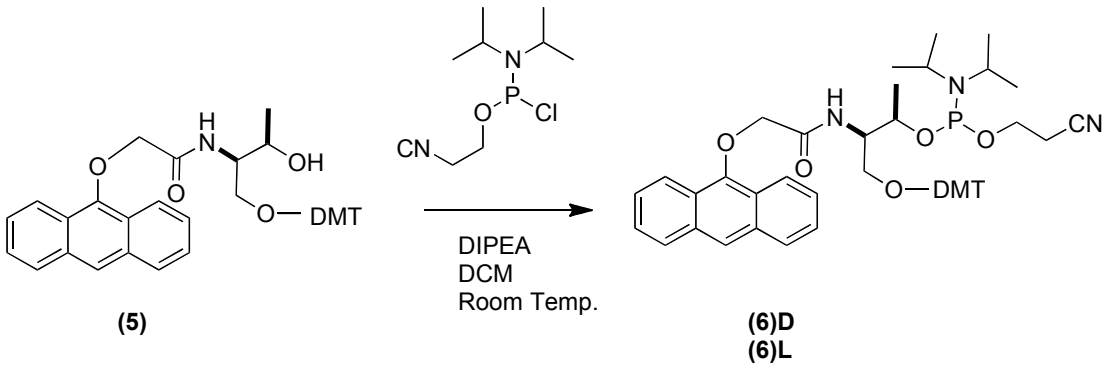

(5) (6)D (6)L

Scheme 5 Phosphitylation of *n*=1 DMT protected diol

TLC in 50:49:1 Hex:EtOAc:TEA on silica pre-eluted with TEA after one hour showed the emergence of two very close fluorescent spots on the plate that were believed to be the two P(III) diastereomers. The reaction was quenched using polymer bound benzyl alcohol,[7] and the mixture stirred in the reaction flask for 30 minutes. The solvent was removed and the compound re-dissolved in EtOAc and washed with saturated sodium hydrogen carbonate and brine. Once the solvent was dried and removed using a rotary evaporator the compound was re-dissolved in 50:49:1 Hex:EtOAc:TEA. An Ellman's test indicated the presence of some H-phosphonate (HPO_3^{2-}), therefore the solution was passed through activated basic alumina in order to remove it. The solvent was then evaporated again using a rotary evaporator after dry acetonitrile was added as a co-solvent to remove TEA and this gave a pale yellow fluffy solid in 27 and 78% yield for the D and L isomer respectively.

The phosphoramidite monomer was characterized via high resolution positive electrospray mass spectrometry followed by ^{31}P and ^{1}H NMR spectroscopy. The ^{31}P NMR spectrum showed two peaks at 147.0 and 147.7 corresponding to the expected region for diastereomeric phosphoramidites.

2.2 DNA Synthesis

2.2.1 Introduction

Synthesis of both the modified and unmodified oligonucleotides was performed on a Beckmann 1000M automated DNA synthesizer which incorporates the "phosphoramidite" DNA synthesis method. The method uses a solid support, Controlled Pore Glass (CPG), to which a 5' protected deoxynucleoside (A ,C, T or G) is attached at the 3' terminus by a succinimide linker. During the synthesis cycle the DNA phosphoramidites are coupled sequentially to the support via the route detailed below (Fig. 56).

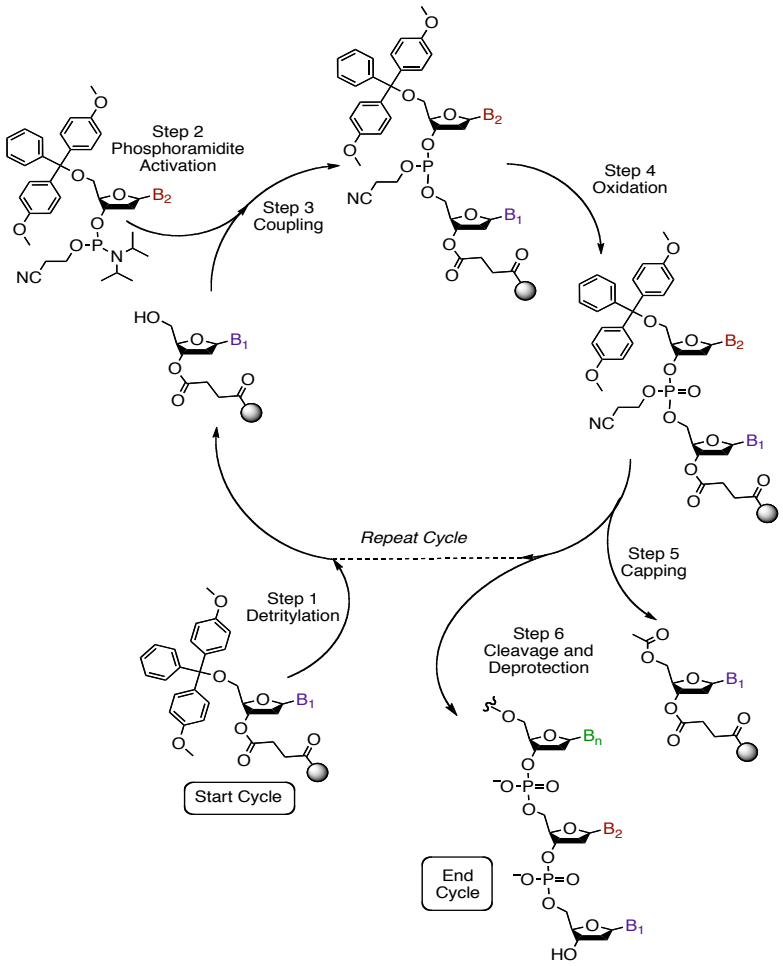

Fig. 56 DNA synthesis cycle[8]

There are six primary steps involved in the synthesis cycle:

1. Detritylation of the solid bound base– this involves acid initiated removal of the DMT 5' protecting group. This step is accompanied by a vivid red colour due to the presence of the DMT^+ cation and quantification of this colour or conductivity measurements enable the effectiveness of the synthesis to be monitored.
2. Activation of the phosphoramidite in solution: This is achieved using either benzotriazole (BTT) or benzylmercaptoterazole (BMT).
3. Addition of the activated phosphoramidite to the deprotected hydroxyl on the support.
4. Capping of any unreacted chains with acetyl groups.
5. Oxidation of the intermediate phosphite ester to the phosphatetriester using iodine and water.

Steps 1 to 5 are repeated for as long an oligonucleotide sequence as desired.

2.2.2 Designing sequences to be synthesized

2.2.2.1 Primary sequence

The first sequence chosen for modified oligonucleotides is shown below, which was the same sequence as synthesized previously[1] which would allow direct comparison between the results.

Probe A: 5'-TGGACTC(X)CTCAATG -3'

X= D or L anthracene tagged nucleotide

It is a 15-mer with 3 A residues, 4 C, 3G and 4T. As an unmodified duplex, together with its matching strand it has a melting point of 55 °C, making it essentially 100% as the duplex form at room temperature. Although the

anthracene is likely to change this slightly [2, 9, 10] it was thought that this should not affect the room temperature stability significantly.

The complementary strand that was synthesized for Probe A, as in the original work, contains an adenine residue opposite the anthracene. This sequence, containing 15 base pairs was denoted "Target A1". Further unmodified and modified strands were synthesized as detailed below, with all data presented in Appendix 1.

2.2.2.2 Variation of the base opposite anthracene

In order to investigate the effect of varying the base opposite the anthracene three further complementary strands were synthesized with T, C and G opposite the anthracene. These were termed Targets A3, A4 and A5 respectively. It was also decided to investigate the sensing of deletion polymorphisms by synthesizing a 14-mer with no base opposite the anthracene. This oligonucleotide was termed Target A2.

2.2.2.3 Variation of the bases adjacent to anthracene

A systematic variation of the bases surrounding anthracene was undertaken with Probes B, C and D having the base downstream of the anthracene varied, whilst Probes E, F and G had the upstream base varied. All Probes then had the fully matching strand synthesized with both an A opposite the anthracene (denoted Target X1 with X denoting Probe B-G, the complementary strand) and no base opposite (denoted Target X2).

2.2.2.4 A modified complementary strand for interstrand stacking

A complementary strand to Probe A, denoted Probe M was synthesized using both isomers of the anthracene linkers in order to study the effects of the interaction between two anthracenes in DNA with both matched and mismatched stereochemistry.

2.2.2.5 SNP sensing strand

A strand containing a SNP in a DNA sequence relevant to the onset of diabetes was synthesized with the *n* = 1 L isomer for the purpose of determining the applicability of the system for real-life SNP sensing.

2.2.3 Procedure for DNA synthesis

All unmodified sequences were synthesized using the normal settings for a 1 μM load synthesis. The strands were synthesized as DMT-ON and were purified in the same manner as the modified oligonucleotides as described subsequently. Data on the sequence composition is presented in Appendix 1.

2.2.3.1 Modified DNA synthetic procedure

The phosphoramidites were dissolved in dry acetonitrile at a concentration of 0.1 M. This was slightly higher than the usual concentration but was considered necessary to maximize the coupling yield due to the decomposition of the phosphoramidite. With that in mind it was decided to perform a manual off column coupling. Therefore, the first seven bases of the oligonucleotide were synthesized as per the standard procedure for a 1 μM synthesis then the process was interrupted with the DMT group removed. A mixture of benzotriazole (0.3M) in acetonitrile and the anthracene phosphoramidite was manually

pumped over the CPG twice with a total coupling time of fourteen minutes. Washing, capping and deblocking for that step were performed on the synthesizer manually. Once a successful coupling was confirmed at the deblocking step the synthesis was continued on as normal.

2.2.3.2 Deprotection and removal from CPG

Upon completion of the synthesis the oligonucleotide was manually deprotected using $MeNH_2$ at 65°C for 1 hour, spin filtered to remove the CPG support, evaporated down to remove the $MeNH_2$ and re-dissolved in water.

2.2.4 Purification

Purification of the *n* = 1 DMT ON oligonucleotides was performed firstly *via* preparative reversed phase C18 HPLC using aqueous 0.1 M triethylammnonium acetate (TEAAc) buffer with an increasing acetonitrile gradient. The retention times of the oligonucleotides was consistently around 21 minutes as would be expected given that the DMT group dominates the hydrophobic interaction. The eluted buffer mixture was then removed under vacuum and the oligonucleotides were redissolved in 80% acetic acid. The DMT protecting group was removed by allowing this mixture to stand at room temperature for 30 minutes. The acetic acid was removed *in vacuo* using ethanol in the role of a co-solvent. Finally, the oligonucleotides were dissolved in 1M TEAAc and de-salted using a Waters C18 Sep-Pak with 60% methanol as the eluent.

The Probes were re-examined for purity using analytical HPLC where it was apparent that the different stereoisomers had different retention times suggesting two different environments for the anthracene (Fig. 57).

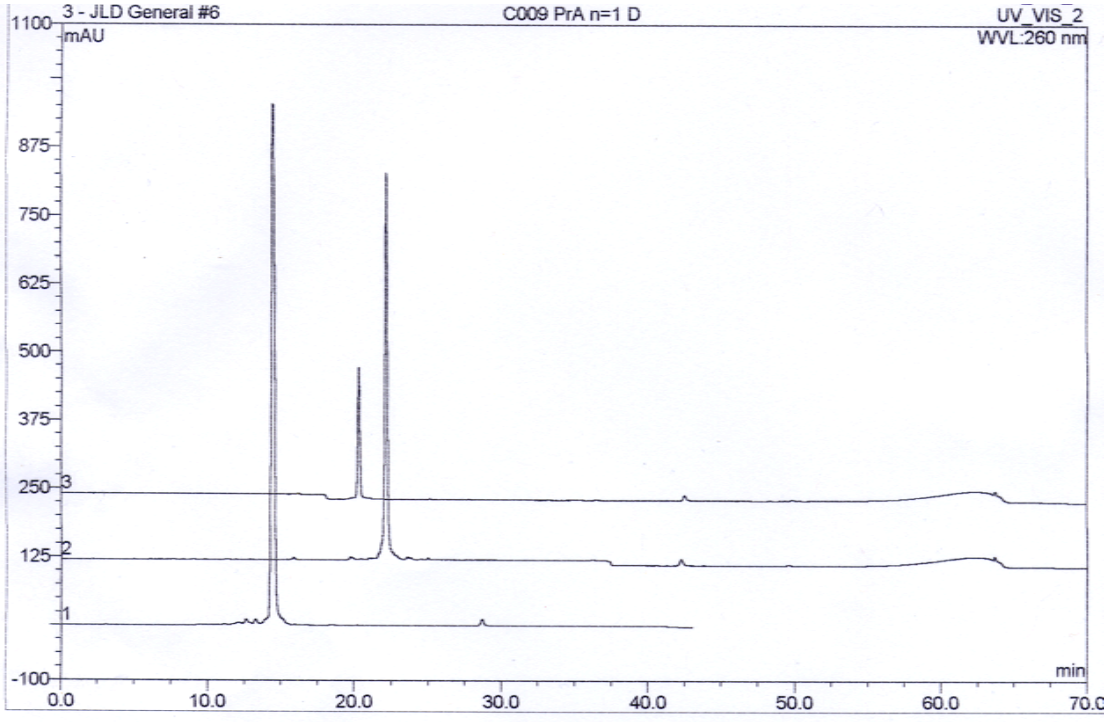

Fig. 57 HPLC chromatograms showing the retention time (min) for unmodified DNA (left) n = 1 D Probe (centre) and n = 1 L (right)

The D oligonucleotide has a retention time that is approximately 5 minutes longer than the unmodified DNA but 2 minutes shorter than the L oligonucleotide. This suggests that in the single stranded form the anthracene moiety is more shielded from external interaction in the L oligonucleotide than the D.

2.2.5 Characterization and quantification

The characterization of DNA was performed by both UV spectroscopy and mass spectrometry techniques.

2.2.5.1 Characterization by mass spectrometry

Characterization of the *n* = 1 strands was performed by MALDI TOF mass spectrometry and/or electrospray mass spectrometry. The predicted and

observed mass values for all synthesized strands are presented in Appendix 1 together with sequence composition, HPLC information and ε values.

2.2.5.2 Quantification by UV spectroscopy

DNA oligonucleotides absorb between 200 and 280 nm in the UV region of the electromagnetic spectrum with a maximum absorption at 260 nm. This is due to the π to π* transitions within purines and pyrimidines. It is important to note that anthracene also contributes to absorption in this area *via* a high energy band between 248 and 254 nm.

In order to confirm that the purification was successful the DNA was scanned between 200 and 450 nm. The presence of a large band at 260 nm showed that the DNA had been successfully recovered and much smaller bands between 350 and 400 nm corresponding to the anthracene low energy transitions suggested successful incorporation of the anthracene amidite (Fig. 58).

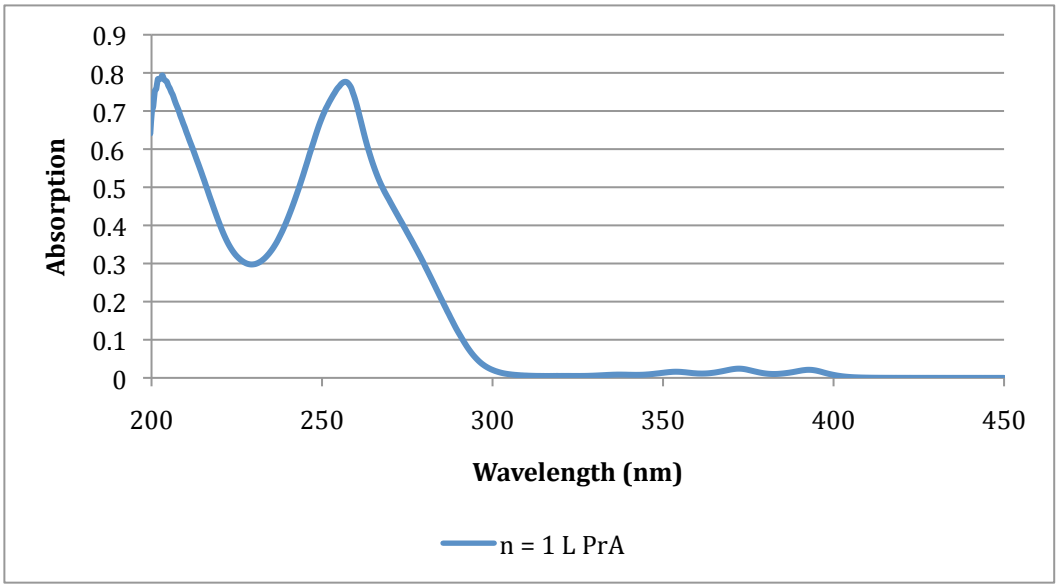

Fig. 58 UV spectrum of single strand n = 1 L Probe A anthracene modified DNA in water 10mM pH 7 phosphate buffer 100 mM NaCl

The concentrations of the oligonucleotide stock solutions were then determined from these scans. The UV absorbance of a known volume of solution allows the concentration to be determined using the Beer-Lambert law (Equation 1) once the unknown value of ε is determined, as described in the following section.

$$A = \varepsilon c l$$

Equation 1 Beer-Lambert law

2.2.5.3 Determining the molar absorption coefficient

ε is the molar absorption coefficient ($M^{-1}cm^{-1}$) and is calculated in two stages. Firstly, the ε value of unmodified DNA is calculated using an online DNA absorption program which takes into account the different ε values of the different bases. For the sequence below the calculated value was 129.9×10^{-3} $M^{-1}cm^{-1}$.

$$5'-TGGACTC-CTCCATG-3'$$

The next step is the determination of the ε value of anthracene absorption at 260 nm. This was achieved by taking a known concentration of the anthracene monomer (**4)L** (Fig. 59) in water with 5% MeCN and measuring the absorption at 260 nm (Fig. 60).

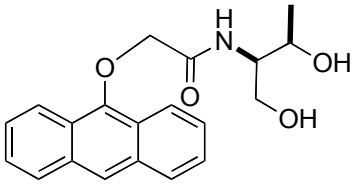

(4)D
(4)L

Fig. 59 Structure of anthracene diol 4

By rearranging Equation 1 the value of ε can be calculated for the monomer (51444 $M^{-1}cm^{-1}$), which is then added to that of the DNA strand to give an overall

value for each strand. The ε values for the synthesized strands are given in Appendix 1 together with the calculated yield for each synthesis.

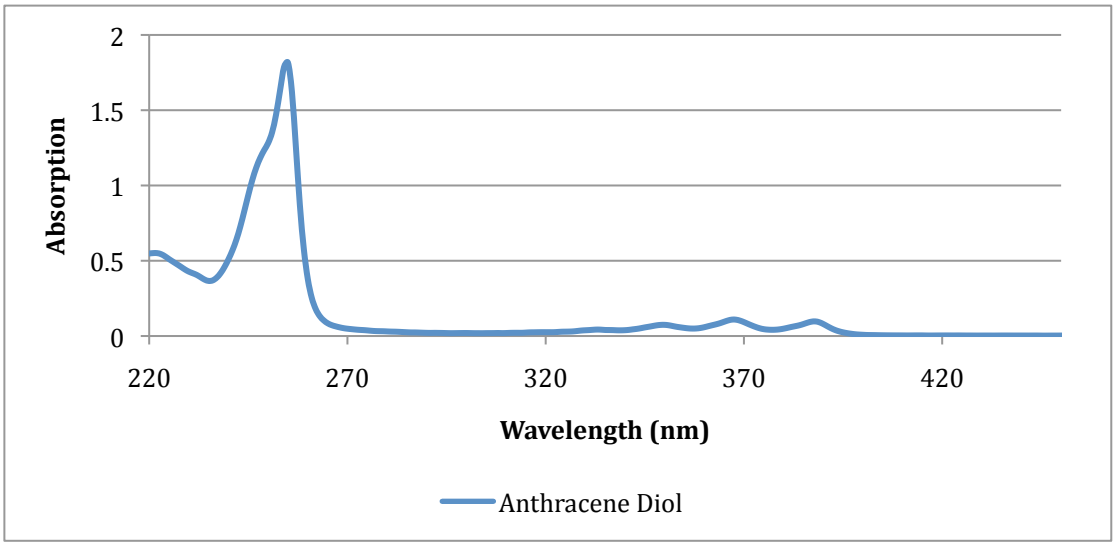

Fig. 60 UV spectrum of the n=1 anthracene diol (4)L in water 5% acetonitrile

2.3 Longer Chain Syntheses

2.3.1 Synthetic route

One of the primary advantages of the chosen synthetic scheme is the ease with which it can be modified to create longer length alkyl chain lengths between the anthracene and the threoninol sections. This is achieved by simply changing the bromo ester starting material. In this manner anthracene carboxylic acids of chain lengths of 3, 4, 5 and 6 carbons could be synthesized (Scheme 6). The synthesis of the *n* = 2 linker was not attempted due to numerous unsuccessful attempts previously in the group[3] where it was observed that upon saponification, a faster, competing elimination reaction gives anthraquinone instead of the desired anthracene carboxylic acid.

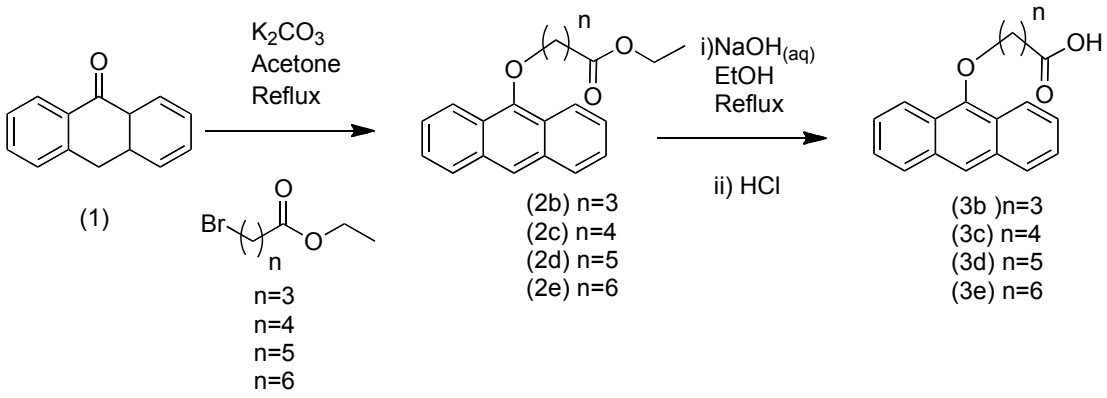

Scheme 6 Formation of anthracene carboxylic acids from anthrone

The procedure was modified in response to problems with the supply of HOBt and PyBOP was used as the coupling agent instead. However, purification of the diol proved difficult with a side product from the coupling reaction present in the product after flash column chromatography. The side product, identified by NMR spectroscopy and mass spectrometry as $(C_2H_4N)_3PO^-$ was not removed and the DMT reaction was performed on the impure mixture. Further coupling reactions used HBTU as the coupling agent, the by-products of which were easier to remove.

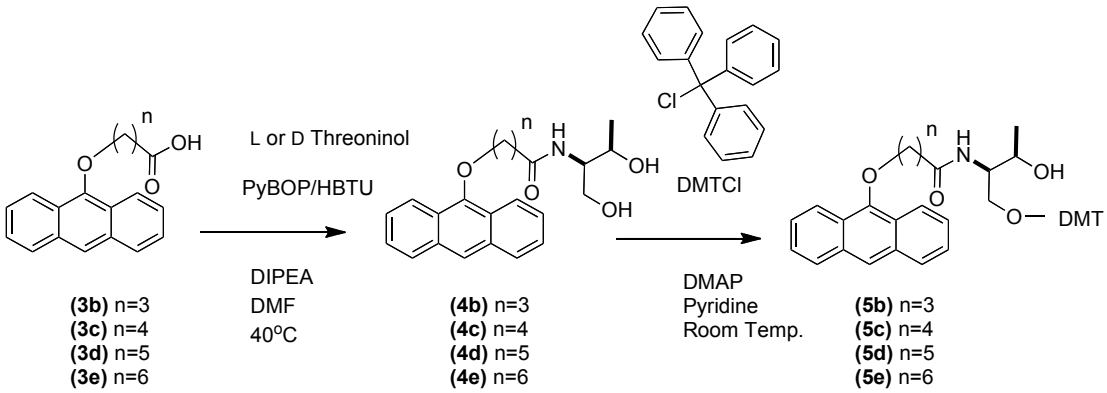

Scheme 7 Amide bond coupling followed by DMT alcohol protection for longer chain monomers

The phosphitylation reactions were carried out under the same conditions as for the *n* = 1 strand (Scheme 8).

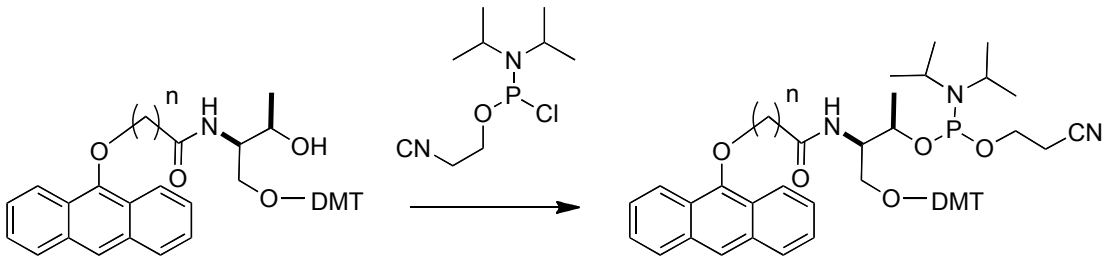

(5b) n=3
(5c) n=4
(5d) n=5
(5e) n=6

(6b) n=3
(6c) n=4
(6d) n=5
(6e) n=6

Scheme 8 Phosphitylation reactions for the longer chain monomers

2.3.2 ^{31}P NMR Spectroscopy

Comparison of the ^{31}P Spectra of the phosphoramidites of different lengths, with the exception of the *n* = 1 linker, show that they are very similar (Table 1).

Table 1 ^{31}P δ (ppm) in CD_3CN

Carbon Linker Length	δ ^{31}P
1	148.4, 146.0
3	147.7, 147.0
4	147.6, 147.0
5	147.7, 147.0
6	147.6, 146.9

Clearly the nuclear environment surrounding the phosphorus atom is different with a short chain, perhaps as a result of the phosphorus atom being held close to the aromatic rings of the DMT group. The shift would therefore be different depending on the orientation of the ring to the phosphorus. If the phosphorus atom was held directly above or below an aromatic ring it would feel a slightly different magnetic field to if it was located in the same plane as the ring.

2.3.3 DNA synthesis of longer chains

2.3.3.1 Synthesized sequences

The same sequences as for the *n* = 1 linker were synthesized as discussed previously (section 2.2.2), details are presented in Appendix 1. Additional strands synthesized were complementary probe strands with the anthracene unit displaced from the centre of the 15-mer. These were synthesized for the *n* = 6 linker with the aim of probing excimer formation between strands (see 5.6.2)

2.3.3.2 Methodology

As a result of changes in equipment a slightly different methodology was used for the synthesis of longer chain oligonucleotides. No manual coupling was performed due to the improved solubility of the phosphoramidites; instead the coupling of the modified bases was performed on an ABI 394 DNA synthesizer with an extended coupling time of 5 minutes. The oligonucleotide strands were synthesized as DMT-OFF, the strands were cleaved from the CPG support on the machine using NH_3 solution and the deprotection of the bases was accomplished by heating the samples for 6 hours at 50 °C. The ammonium solution was then removed under vacuum and the oligonucleotides were purified using RP-HPLC as before.

2.3.4 HPLC

Degassed water with 0.1 M TEAAc and 5% acetonitrile on an increasing gradient was again used for purification of the oligonucleotides (Fig. 61).

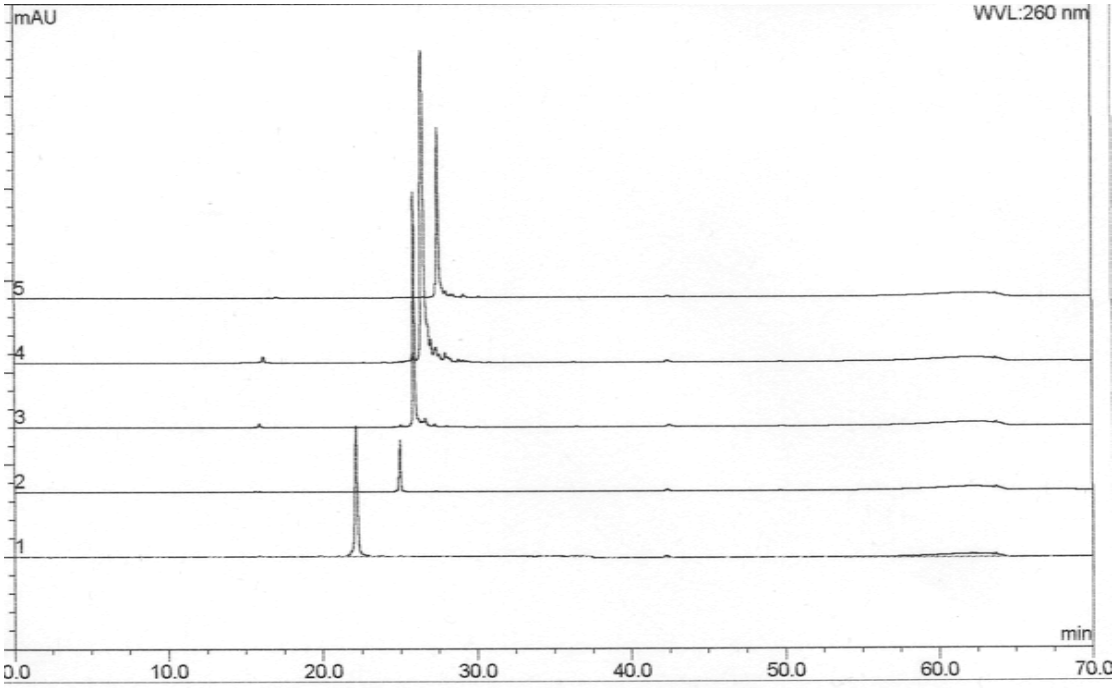

Fig. 61 Overlaid HPLC chromatograms for the different sequence lengths of the L isomer linker from bottom n = 1, n = 3, n = 4, n = 5, n = 6

As expected, the increasing chain length gives rise to a longer retention time on the column, although the effect of increasing the chain length beyond three carbons has a relatively small effect on the retention time and a change in the stereoisomer for the longer chain lengths has almost no effect (Fig. 62).

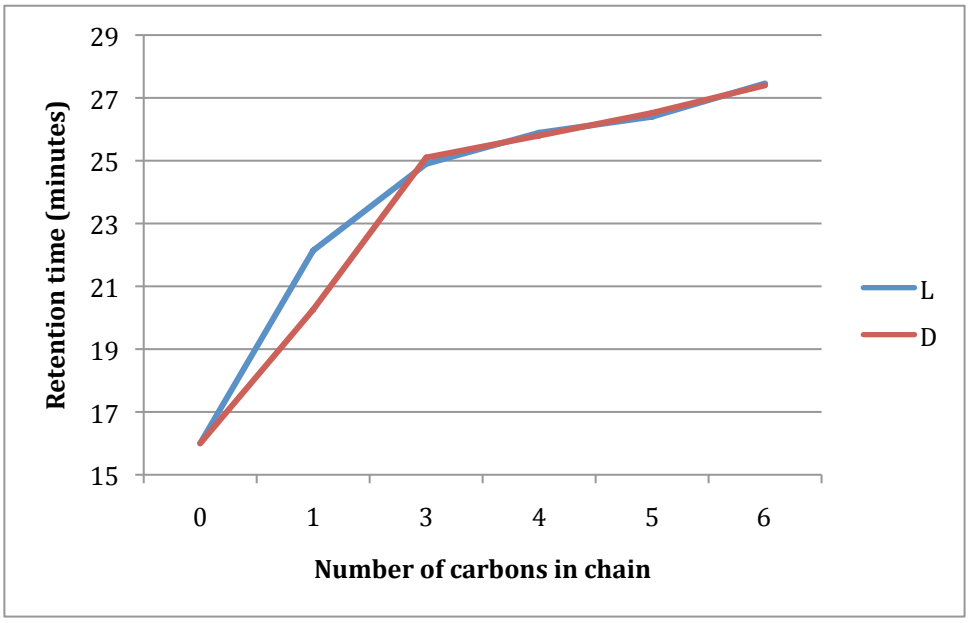

Fig. 62 Graph of HPLC retention time against carbon chain linker length

2.3.5 Purification and quantification

The oligonucleotide strands were desalted by size exclusion chromatography using NAP-10 columns from GE Healthcare. Quantification was performed using the same procedure as for the n = 1 strands.

2.4 References

1. Moran, N.; Bassani, D. M.; Desvergne, J. P.; Keiper, S.; Lowden, P. A. S.; Vyle, J. S.; Tucker, J. H. R., *Chem. Commun.* **2006,** (48), 5003-5005.
2. Kashida, H.; Liang, X. G.; Asanuma, H., *Curr. Org. Chem.* **2009,** *13* (11), 1065-1084.
3. Moran, N. Novel Anthracene-Tagged DNA Sensors. University of Exeter, 2006.
4. Chang, S. K.; Vanengen, D.; Fan, E.; Hamilton, A. D., *J. Am. Chem. Soc.* **1991,** *113* (20), 7640-7645.
5. Beaucage, S. L.; Caruthers, M. H., *Tetrahedron Lett.* **1981,** *22* (20), 1859-1862.
6. Pike, A. R.; Ryder, L. C.; Horrocks, B. R.; Clegg, W.; Elsegood, M. R. J.; Connolly, B. A.; Houlton, A., *Chem. Eur. J.,* **2002,** *8* (13), 2891 - 2899.
7. Battaggia, S.; Vyle, J. S., *Tetrahedron Lett.* **2003,** *44* (4), 861 - 863.
8. Greco, N. J.; Tor, Y. Z., *Nat. Prot.* **2007,** *2* (2), 305-316.
9. Fukui, K.; Tanaka, K., *Nucleic Acids Res.* **1996,** *24* (20), 3962-3967.
10. Fukui, K.; Iwane, K.; Shimidzu, T.; Tanaka, K., *Tetrahedron Letters* **1996,** *37* (28), 4983-4986.

Chapter 3 Results and Techniques

3.1 Introduction

Previous work in the group successfully demonstrated that fluorescent sensing of SNPs using anthracene tagged non-nucleosidic bases was possible.[1] However, further understanding of the structure and mechanism of the probe was limited by the formation of two stereoisomers (*R* and *S*) of the DMT protected anthracene diol when using a serinol linker. Subsequent phosphitylation of this compound and incorporation of the resulting phosphoramidite into DNA oligonucleotides using solid state DNA synthesis techniques gave a mixture of two different anthracene tagged oligonucleotide probes.

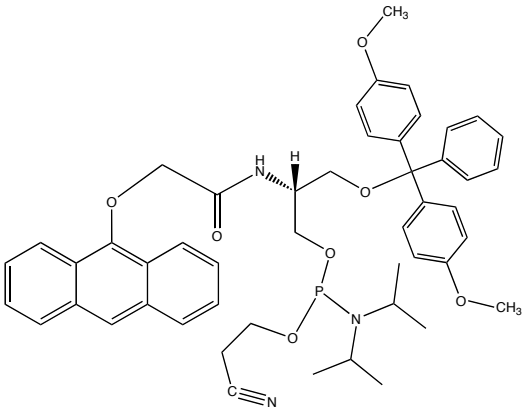

Fig. 63 DMT protected and phosphytilated anthracene containing a non-nucleosidic serinol backbone (*R* stereoisomer shown)

Although these were successfully separated and purified using chiral HPLC, it was not possible to assign the stereochemistry of each chiral centre. The two probes, denoted fast and slow relative to their retention times, were characterised *via* MALDI mass spectrometry and their interactions with unmodified DNA were probed using fluorescence spectroscopy, variable temperature UV spectroscopy and Circular Dichroism (CD) spectroscopy. The

different stereoisomers had different fluorescent sensing capabilities and different melting points.

One of the rationales for the replacement of the serinol linker with either the D or L form of threoninol was that the stereochemistry of the linker could be defined before incorporation into DNA and thus the previous results could be rationalised in light of data acquired from systems with known stereochemistry. This approach has been used successfully by a number of different groups with different attached molecules.[2, 3]

Therefore, as described in Chapter 2, a series of anthracene tagged oligonucleotides with a threoninol backbone were synthesised. It was decided to vary the bases around the anthracene to allow further exploration of the effect of changing the environment around the modified nucleotide and greater understanding of the mode of sensing. The synthesis of a number of different target oligonucleotides allows for the more specific investigation of the selectivity of the sensing mechanism. The original probe showed the ability to sense a C to A mismatch upstream of an anthracene probe flanked by two C bases. The creation of a library of probes and targets allowed for a thorough and systematic analysis of different base combinations and mismatches. Therefore, as described in this Chapter, a wide number of combinations of probes and targets could be investigated using a number of different techniques.

3.2 Photochemistry and fluorescence

The field of photochemistry is concerned with the interaction between light (any form of electromagnetic radiation – but usually in the UV and visible region) and matter and the physical processes that take place at the molecular level following the absorption of radiation.[4]

The initial process is illustrated (Equation 2) below as a molecule (*M*) absorbs a photon of light which causes an electron to be promoted to a higher energy level and the species becomes electronically excited (*M**).

$$M + h\nu \rightarrow M^*$$

Equation 2

A number of different photophysical or photochemical processes can occur following this event and they are illustrated in a Jablonski diagram (Fig. 64), where S_0, S_1 and T_1 are the singlet ground state, first singlet excited state and first triplet excited state respectively.

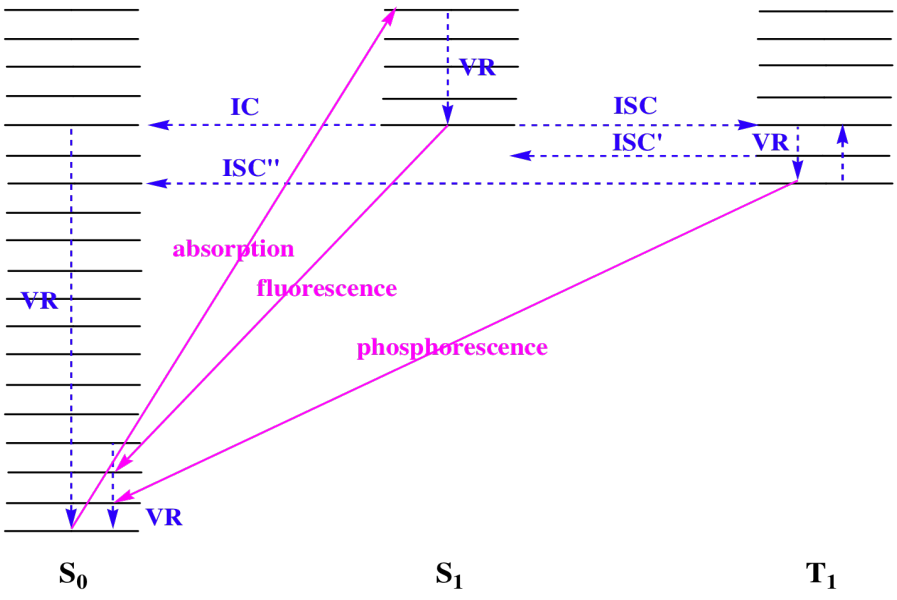

Fig. 64 Jablonski Diagram

As the excited molecule is intrinsically unstable it seeks to lose excess energy and has a number of routes open to do this. Of most relevant to the field of sensing are the luminescence processes, fluorescence and phosphorescence (as depicted in Fig. 64), where the excited molecule loses energy via emission of a photon to reach either the ground state or a lower energy excited state. Fluorescence is a short-lived, spin allowed (e.g. S_1 to S_0) downward transition whereas phosphorescence is a much longer-lived phenomenon that involves Inter System Crossing (ISC) to a triplet state and subsequent emission as the electron transits from a state of different spin multiplicity from the ground state (e.g. T_1 to S_0).

Fluorescence is a very useful property for a sensing system to possess as it can be readily detected at quite low concentrations and requires relatively inexpensive equipment. Additionally, fluorescence is both highly sensitive to and easily modified by the surrounding environment.

3.2.1 Fluorescence quenching

There are a number of processes that can lead to a reduction in fluorescence intensity and these are termed quenching processes. These processes can occur either during the excited state lifetime e.g. collisional quenching, energy transfer, charge transfer reactions or photochemistry or due to the formation of complexes in the ground state. In this work the principal focus will be on the most common processes namely collisional (dynamic) quenching and static (complex forming) quenching.

3.2.2 Collisional quenching

Collisional quenching can occur when the fluorophore is in its excited state and it experiences contact with an atom or molecule that can facilitate non-radiative transitions to the ground state. Common quenchers in this category include O_2, I^-, acrylamide and many solvents. When quenching is purely collisional it is also known as dynamic quenching. In this case, the change in fluorescence is proportional to the concentration of the quencher as can be seen from the Stern-Volmer equation (Equation 3):

$$\frac{F_o}{F} = 1 + K_{sv}[Q]$$

Equation 3

F_0 and F are the fluorescent intensities observed in the absence and presence, respectively of quencher, [Q] is the concentration of quencher and K_{sv} is the Stern-Volmer quenching constant. The result is a straight line graph of F_0/F vs [Q] with a gradient equal to K_{sv}. This is illustrated below for the case of fluorescin quenched by the iodide anion (Fig. 65).[5]

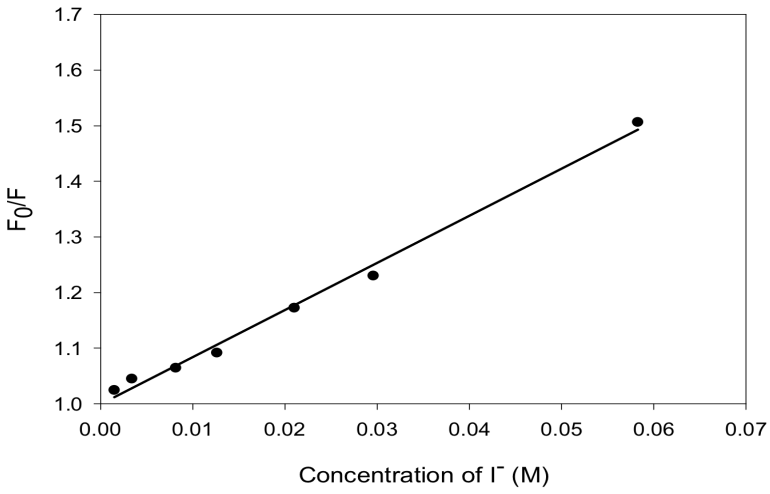

Fig. 65 Graph illustrating collisional quenching of fluorescin (1 µM) by iodide anions[5]

3.2.3 Static quenching

In this scenario the fluorophore forms a stable complex with another molecule in the ground state. If this ground state is non-fluorescent then it can be said that the fluorophore has been statically quenched. The dependence of the fluorescence as a function of quencher concentration then follows the following equation (Equation 4):

$$\frac{F_o}{F} = 1 + K_a[Q]$$

Equation 4

K_a is the association constant of the complex and the other parameters are described by Equation 3. When static quenching occurs, the lifetime of the sample will not change since those fluorophores that are not complexed, and therefore not quenched, will have a normal emission decay. However overall, the fluorescence of the sample is reduced since the number of emitting fluorophores is reduced.

If both static and collisional quenching are occurring then the following relationship can be applied (Equation 5):

$$\frac{F_o}{F} = (1 - k_q\tau[Q])(1 + K_a[Q])$$

Equation 5

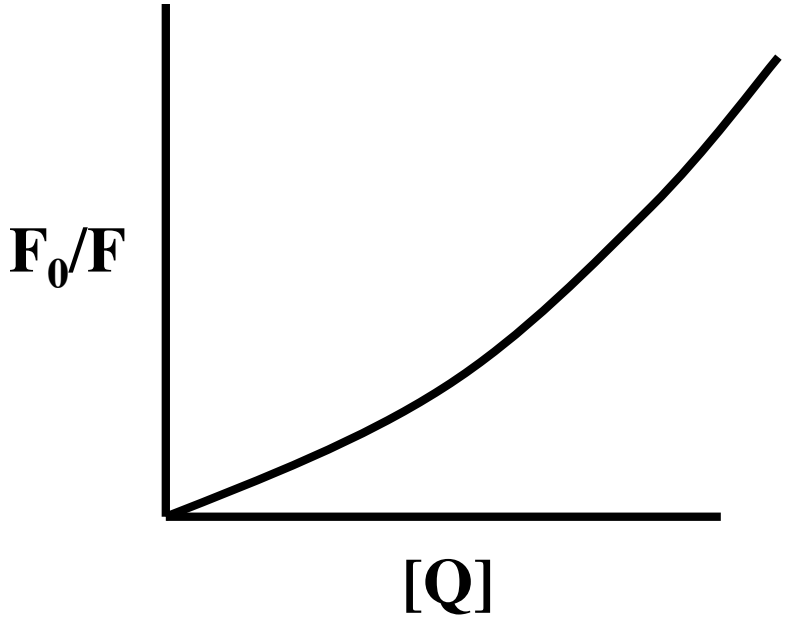

Fig. 66 Example graph of a dynamically and statically quenched system

In this case a plot of F_0/F vs. [Q] gives an upward curving plot (Fig. 66).

3.3 Fluorescence results for single strand *n* = 1 system L and D isomer

The following sections detail the fluorescence emission studies performed on the anthracene tagged oligonucleotide Probes, starting with the single stranded Probes. All data is presented together in Appendix 1 and selected results are presented when appropriate in the context of the systems being discussed.

3.3.1 Preliminary studies

Since fluorescence relies on light absorption at a particular wavelength, the first step was to scan the absorption spectrum of the compound to be analysed. The UV spectrum of the anthracene monomer (Fig. 67) before incorporation into DNA is shown in Fig. 68.

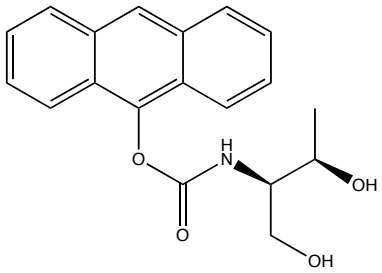

Fig. 67 Uncoupled anthracene diol monomer (4)L

It can be seen that the spectrum consists of two components: a low energy (300-400 nm) band (^1L_a) and a higher energy (250-270 nm) band that corresponds to the second electronic transition of anthracene (^1B_b).[6] The assignment of these bands is based on the Perimeter Free Electron Model (PFEO) and can be used as a theoretical classification of the π-electronic excited states of aromatic hydrocarbons, where the π-orbitals are treated as orbitals of free electrons travelling in a one-dimensional loop around the molecular perimeter. The superscript 1 indicates a singlet excited state, and the subscripts a and b refer to the alternative positions for the nodes relative to the molecule.[7]

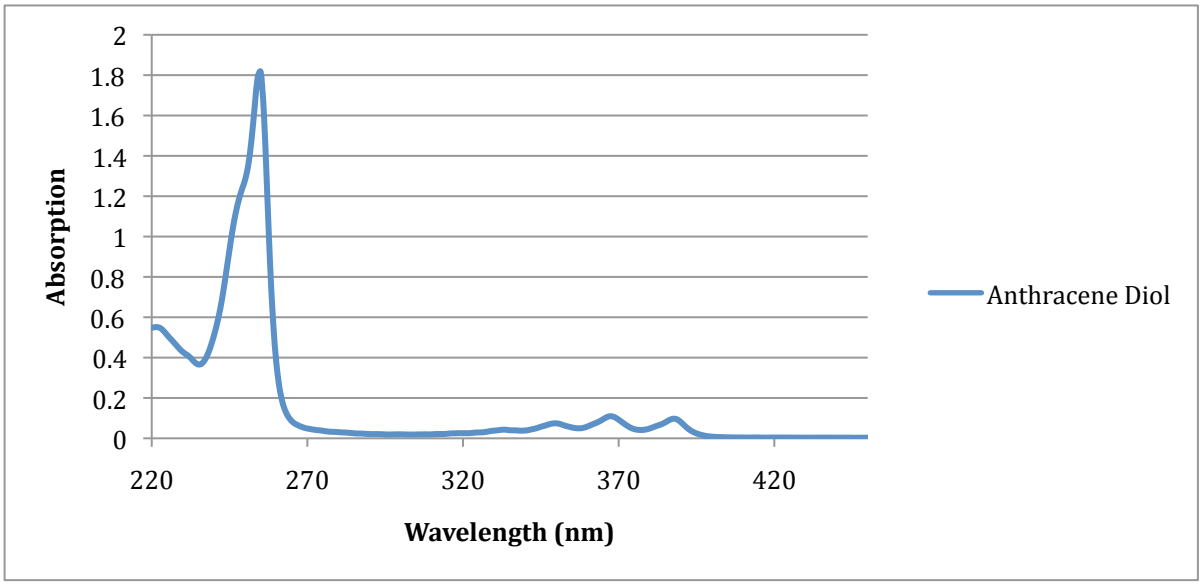

Fig. 68 UV Spectrum of the pre-DMT anthracene diol in water (5% MeCN)50uM room temp

In order to avoid irradiation of the DNA it was decided to irradiate in the anthracene finger region between 320 and 420 nm where the transitions correspond to the S_0 to S_1 transition. DNA has no absorption in this region and hence potential alternative photo-processes and reactions can be avoided.

3.3.2 Investigating DNA strands using fluorescence (single strand)

Having chosen the area to irradiate, the excitation and emission spectra of the unincorporated anthracene and the original starting sequence in 100 mM NaCl and 10 mM pH 7 phosphate buffer. The emission was monitored from a λ_{ex} of 350 nm and the excitation spectrum was taken at 424.4 nm.

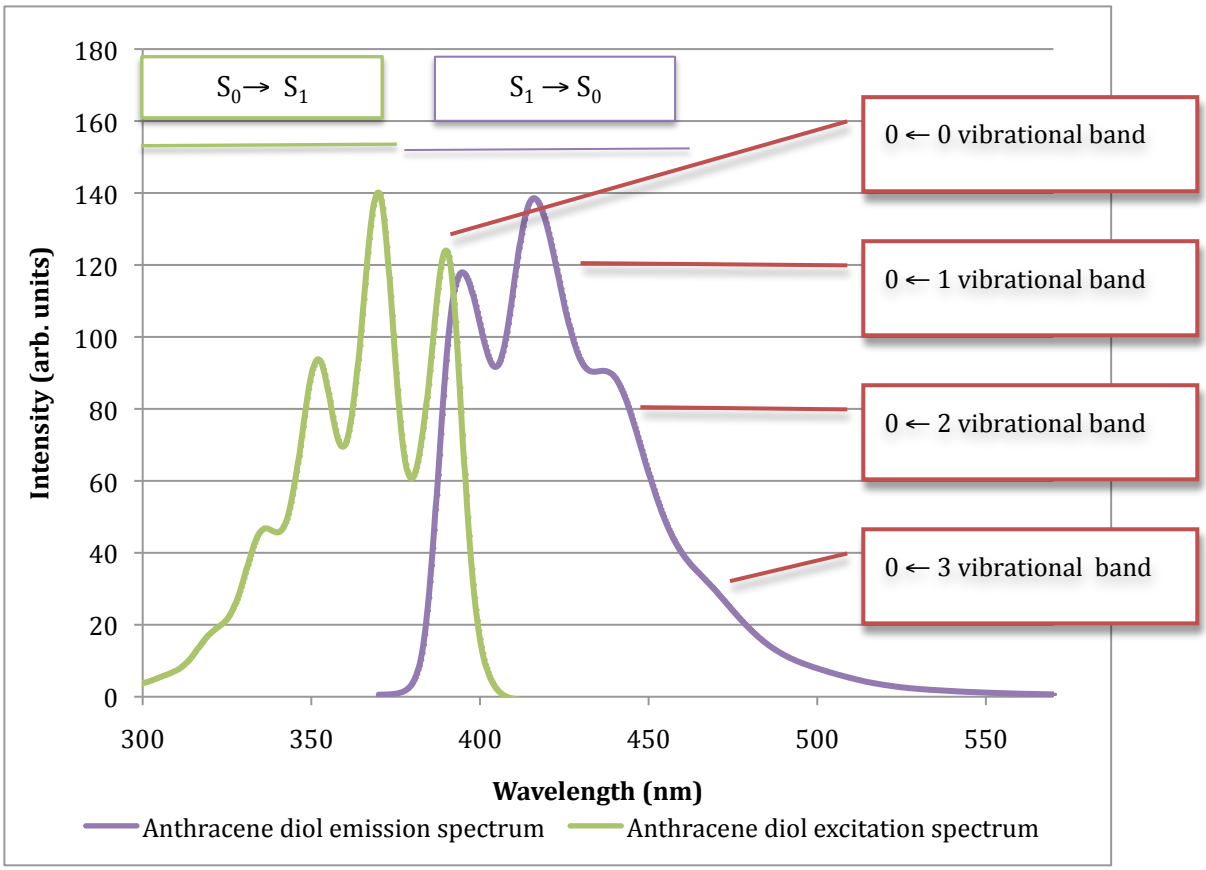

Fig. 69 Excitation and emission spectra of unincorporated anthracene diol (4) in water sat. solution pH 7 10 mM phosphate buffer 100 mM NaCl

Inspection of the emission and excitation spectra of the anthracene compounds (Fig. 69 and Fig. 70) indicated that they were very similar to those of literature

known compounds 9,10-dimethoxy anthracene[8] and 9-anthracenemethylamine hydrochloride, although the 0 → 3 vibrational band was too broadened in the emission spectrum to be visible. The two spectra for the diol (Fig. 69) match relatively closely and the 0 → 0 vibrational bands closely overlap, showing that the energy is absorbed and emitted by the same chromophore as would be expected.

When comparing the oligonucleotide anthracene spectra (Fig. 70) and the diol spectra, the spectra look very similar; suggesting that in the single strand form the shape of the spectrum of the lower energy band (^1L_a) is not greatly affected by being attached to an oligonucleotide. There is however a slight decrease in the overall intensity of the emission compared to the absorption and the 0 → 2 band is broader in the oligonucleotide anthracene. The major difference is the red shift on going from unattached anthracene (maxima at 414 nm) and DNA incorporated anthracene (maxima at 422 nm). Often, such shifts occur when the dipole moment of the excited state is greater than that of the ground state. In this case, rearrangement of solvent molecules in the microenvironment can lower the energy of the excited state prior to emission, resulting in a red shift of the emission maxima.[9]

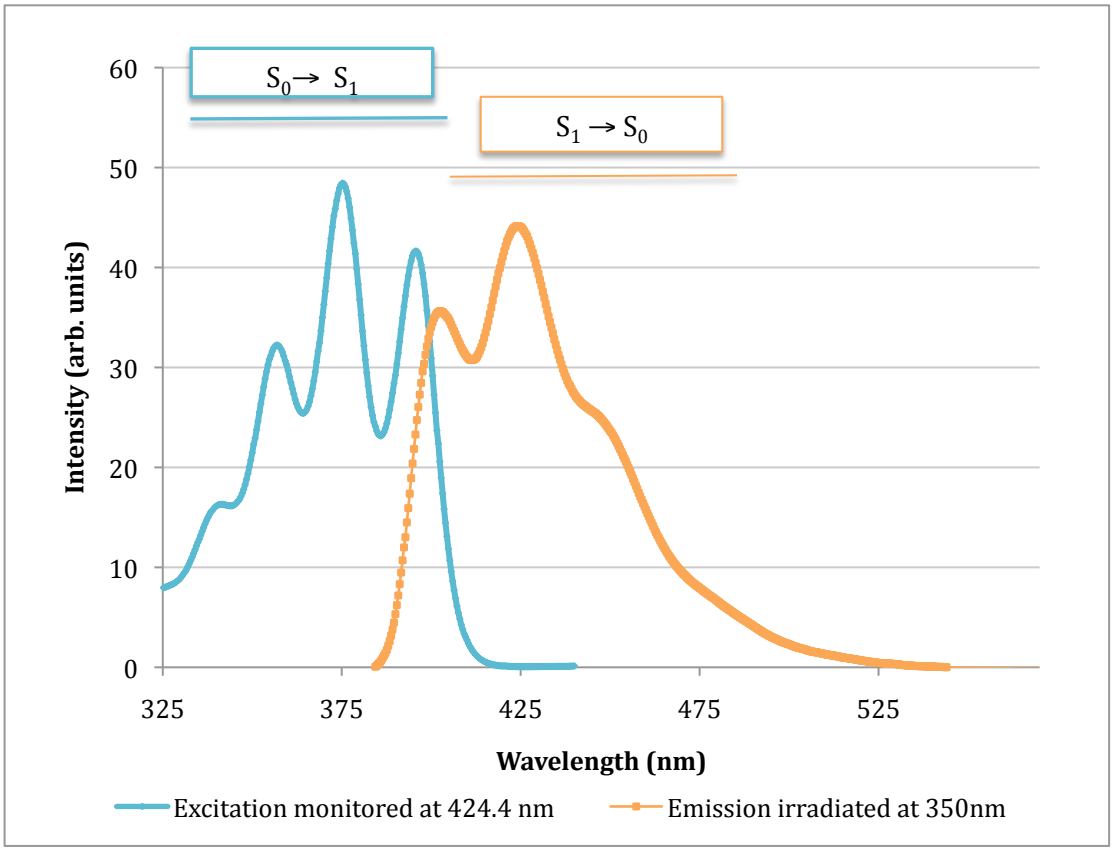

Fig. 70 Excitation and emission spectra of Probe A L in water 1 µM pH 7 10 mM phosphate buffer 100 mM NaCl

The use of low concentrations of oligonucleotide is important due to the possibility of energy migration. This is a phenomenon that can occur radiatively where there is an overlap of absorption and emission spectra and therefore preferential reabsorption of the light at these wavelengths. Such effects are manifested by a change in the fluorescence emission spectrum in the region where said spectra overlap, but can be mitigated by the use of very dilute solutions.[10]

However, a comparison of the emission spectra of the two isomers (Fig. 71) shows that the spectra are red shifted (a bathochromic shift) by different amounts and the structure of the 0 → 2 vibrational band is less distinct, showing

that the anthracenes interact differently with their environments with the excited state of the L isomer perhaps interacting more with water solvent molecules leading to greater spectral broadening and a greater red shift.

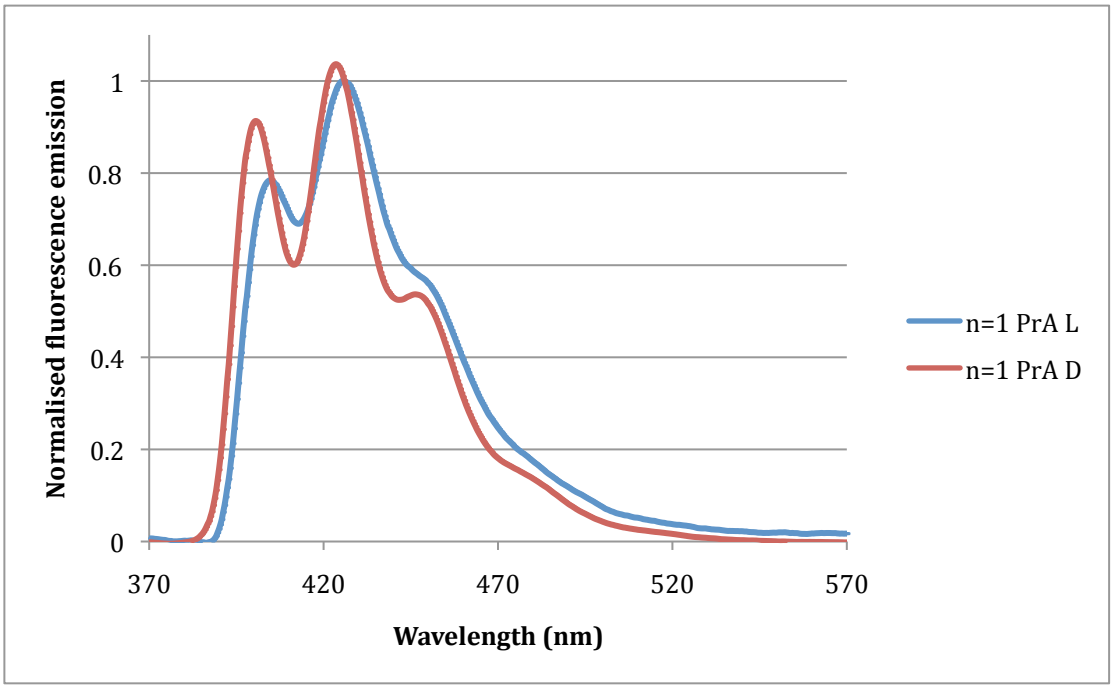

Fig. 71 Normalised fluorescence spectra of Probe A L and D isomers single strand in water 1 μM pH 7 10 mM phosphate buffer 100 mM NaCl

Four principal experiment techniques were then undertaken as listed below.

1. quantum yield determination
2. fluorescence lifetime determination
3. fluorescence emission hybridisation titrations
4. fluorescence excitation spectra studies

As described in the following sections, quantum yields were used to quantify the different emissive properties of the different probes in their single stranded and double stranded duplex forms. The fluorescent lifetime data was useful for rationalising differences in the quantum yield and also the results from fluorescence hybridisation titrations (see 3.4), which were used to convey sensing through changes in fluorescence intensity at a particular wavelength

upon duplex formation. Studies on the excitation spectra were utilised to look into energy transfer from the DNA bases to the anthracene.

3.3.3 Quantum yield results

If we consider that an excited state decays by a first order process we can assume that the number of molecules losing a quantum of energy in time *dt* will be proportional to the number of molecules *N* in the excited state (Equation 6).

$$\frac{-dN(t)}{dt} = N(t)k$$

Equation 6

where *k* is the constant of proportionality and the probability that the molecule will lose a quantum through all processes in time dt. By rearranging and integrating we get Equation 7.

$$N(t) = N(0)e^{-kt}$$

Equation 7

Therefore the lifetime τ is defined as the time it takes for *N(0)* molecules to decay to $N(t) = \frac{N(0)}{e}$

This occurs at time $t = \frac{1}{k} = \tau$

This lifetime is measurable because the emitted light at time t, *I(t)* is proportional to the number of molecules in the excited state at that time *N(t).* The lifetime is defined as simply the time it takes for the maximum intensity to decrease by $\frac{1}{e}$

If *k* = A, the Einstein coefficient, this represents the situation where all the quanta of energy are lost through spontaneous fluorescence and τ =1/A. This

special lifetime, when all competing processes can be ignored, is called the intrinsic lifetime τ_o. Therefore, A is proportional to the number of molecules giving off photons through spontaneous fluorescence and *k* is proportional to the number of molecules losing quanta of energy through all processes.

The quantum yield (Equation 8) is defined as the ratio of these two values[11]:

$$q = \frac{A}{k} = \frac{\tau}{\tau_o}$$

Equation 8 Definition of the quantum yield

The difficulty in accurately measuring quantum yields means that they are commonly measured relative to a standard that absorbs at a similar wavelength. In this case quinine sulphate in H_2SO_4 is used as it has a broad emission band in the same region as anthracene centred at 470 nm.

3.3.3.1 Unincorporated anthracene quantum yield

As a reference, the QY of the anthracene diol (4) was determined in methanol/water 10:90 and found to be 0.08 (see Fig. 69 for a spectrum).

3.3.3.2 Anthracene tagged DNA single strand quantum yields

The calculated quantum yields are presented in Appendix 2.1 for all synthesised probes. These values were calculated at room temperature with 1 μM concentration of probe, 10 mM phosphate buffer pH 7 and 100 mM NaCl in Millipore pure water. Selected results will be presented throughout the chapter at the relevant time.

Calculation of the QY for the different single strand probes gives the following results (Table 2).

Table 2 Quantum Yields of single strand Probes recorded at room temperature λex 350 nm λem 426 nm 1 μM oligonucleotide concentration 10 mM pH 7 phosphate buffer 100 mM NaCl

Probe	Core Sequence	QY
***n*=1 L Pr A**	**5' CLC**	**0.0181**
***n*=1 L Pr B**	**5' CLG**	**0.0149**
***n*=1 L Pr C**	**5' CLA**	**0.0152**
***n*=1 L Pr D**	**5' CLT**	**0.0206**
***n*=1 L Pr E**	**5' GLC**	**0.0227**
***n*=1 L Pr F**	**5' ALC**	**0.0259**
***n*=1 L Pr G**	**5' TLC**	**0.0294**
***n*=1 D Pr A**	**5' CDC**	**0.0527**
***n*=1 D Pr B**	**5' CDG**	**0.0066**
***n*=1 D Pr C**	**5' CDA**	**0.0416**
***n*=1 D Pr D**	**5' CDT**	**0.1106**
***n*=1 D Pr E**	**5' GDC**	**0.0456**
***n*=1 D Pr F**	**5' ADC**	**0.0682**
***n*=1 D Pr G**	**5' TDC**	**0.0237**

3.3.3.3 Discussion of quantum yields

It is immediately apparent that the quantum yield of the probe is primarily affected by the stereochemistry of the probe. The L isomer probes have a quantum yield that is consistently around 0.02. This contrasts strongly with the D isomer probes, which vary from 0.006 to 0.11. The difference between the two probes suggests quite different environments for the anthracene probe that can be affected by changing the flanking bases for the D isomer but not for the L isomer (Fig. 72).

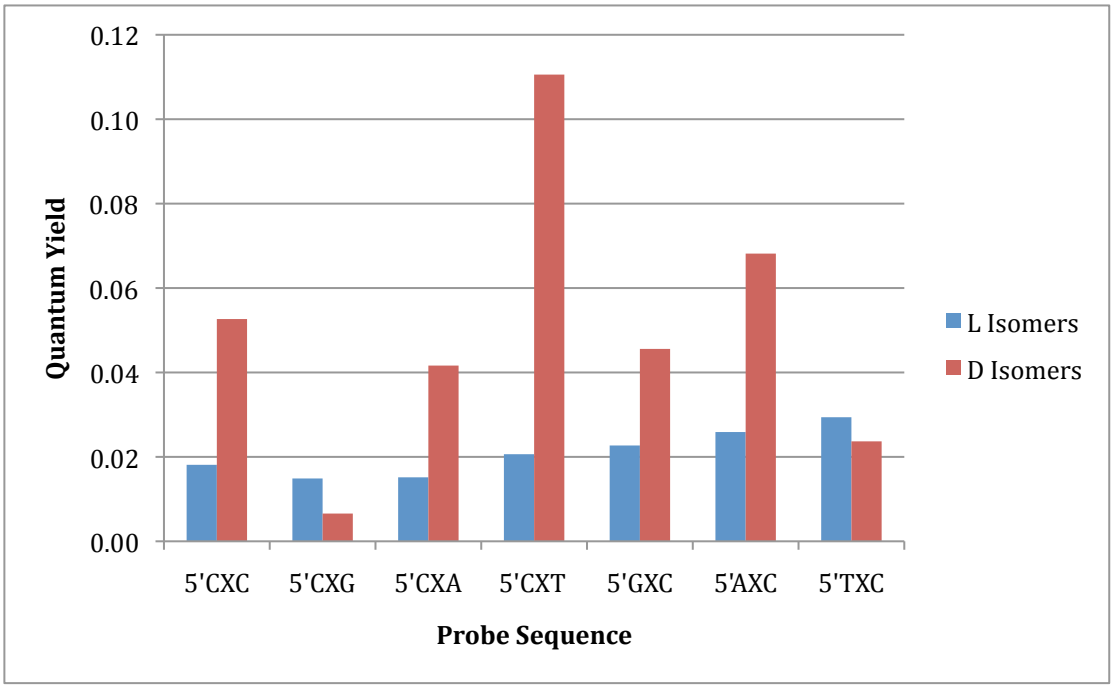

Fig. 72 Graph of Quantum yields of different single strand probes *n* = 1 L vs. D λex 350 nm λem 426 nm 1 μM oligonucleotide concentration 10 mM pH 7 phosphate buffer 100 mM NaCl

3.3.3.4 G base quenching

One of the most obvious factors that would be expected to affect the quantum yield is the nature of the base flanking the anthracene. Much has been written in the literature of the role of G in the quenching of excited states due to its relative ease of oxidation.[12, 13] The ability of G bases to conduct electrons is the subject of vigorous scientific debate with a great deal of effort devoted to examining the phenomenon.[14] If this was the dominant factor in affecting the fluorescence of anthracene we would expect to see much lower quantum yields for strands with G bases adjacent to the anthracene. The graph above shows that this is not the case, with only 1 out of 4 combinations that fit this description demonstrating a noticeably low quantum yield.

Furthermore, a matching strand for Probe A, denoted Probe M, with a core sequence of GXG also does not have a very low quantum yield (Table 3).

Table 3 Quantum yields of matching Probes M L and D hybridized with a target equivalent to Probe A recorded at room temperature λex 350 nm λem 426 nm 1 μM oligonucleotide concentration 10 mM pH 7 phosphate buffer 100 mM NaCl

Probe	Quantum Yield
***n* = 1 Probe M L**	**0.12**
***n* = 1 Probe M D**	**0.013**

Although the disparity in yield between isomers is in keeping with the results seen previously, the very high quantum yield for Probe M (L), higher than for any other combination investigated, strongly suggests that quenching by electron transfer from G to anthracene is not certainly more important than other anthracene-base interactions. This means that alternative explanations for the different levels of emission from the probes need to be found, as described in detail in this chapter (*vide infra*).

3.3.4 Fluorescence lifetimes

For each populated excited state that emits after a flash of radiation, there will be a different lifetime that is associated with it.[4] These lifetimes can be measured using radiation in the form of a very short intense pulse that lasts for a length of time that is shorter than the length of time of the emission that is being studied. This is known as flash photolysis and generates a high concentration of the molecule in its excited state M* and the decay of these molecules is recorded by observing the fluorescence. The concentration of molecules in the excited state will decay to zero at a rate k_f that takes into account all the different pathways by which the extinction can be removed.[4]

$$[M*] = [M*]_0 e^{-kt}$$

Equation 9

Therefore the fluorescent lifetime τ_f is given by

$$\tau_f = \frac{1}{k_f}$$

Equation 10

The probability that an emitted photon will be detected within a specific time interval decreases exponentially with increasing time interval.

As a consequence of this the emission intensity, directly related to [M*], is a measure of the probability of observing an emitted photon within a given time interval. The result is a decay profile such as the ones shown below (Fig. 73). These can give a very precise estimate of both the length and number of radiative lifetimes. In the case of one single emitting state then the data can be fitted by a mono-exponential decay profile, two state by bi-exponential and so on. Of the illustrated examples the first two (Fig. 73 top and middle) represent tri-exponential decay profiles with differing lifetime weightings. The bottom decay profile is of a bi-exponential decay profile. A good statistical fit is indicated by the value of the reduced chi-squared statistical parameter χ^2 being close to one and the Durbin Watson parameter being close to 0.3.[15]

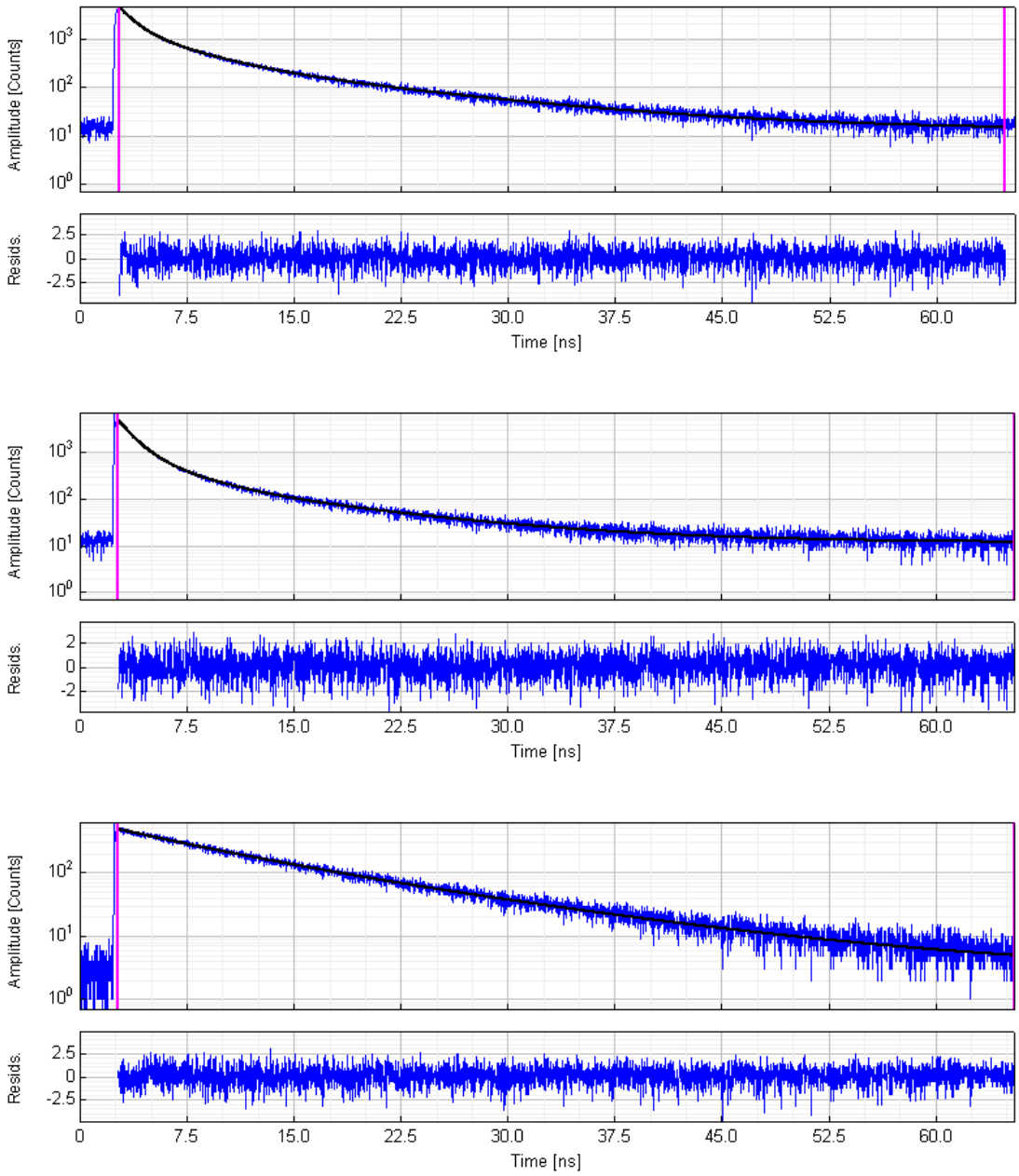

Fig. 73 Fluorescent decay profile of Probe A L single strand (top) Probe A L TarA1 (middle) Probe A L TarF1 (bottom) λex 375 nm λem 426 nm 1 µM oligonucleotide concentration 10 mM pH 7 phosphate buffer 100 mM NaCl

Studies were performed in Bordeaux on the individual probes at 1 µM concentration. The oligonucleotides were excited at 371 or 375 nm using either a pulsed LED or a laser and the fluorescent decay was detected using either a single photon counter or photodiode array. The final data was compiled by collecting for 10,000 counts and fitting the decay using a multiexponential decay.

As for the quantum yield, the fluorescence decay of the uncoupled anthracene diol (Fig. 67) was analysed and the decay found to be monoexponential.

Table 4 Fluorescence lifetime of unincorporated anthracene diol (4)in MeOH

	τ 1 (ns)	τ 1 Weighted (%)	χ^2
n **= 1 diol**	**4.24**	**100**	**1.24**

The complete results for the DNA strands are presented in Appendix 2.3 and as with the quantum yields selected results are reproduced in the text that follows. The average lifetime results for the single strands are presented below in Table 5. The trend in the average lifetime follows that of the quantum yield.

Table 5 Average fluorescent lifetimes for single strand probes recorded at room temperature λex 375 nm λem 426 nm 1 μM oligonucleotide concentration 10 mM pH 7 phosphate buffer 100 mM NaCl

Probe	Core Sequence	Average Lifetimes (ns)
***n*=1 L Pr A**	**5' CLC**	**6.21**
***n*=1 L Pr B**	**5' CLG**	**5.77**
***n*=1 L Pr C**	**5' CLA**	**6.27**
***n*=1 L Pr D**	**5' CLT**	**5.48**
***n*=1 L Pr E**	**5' GLC**	**7.25**
***n*=1 L Pr F**	**5' ALC**	**7.02**
***n*=1 L Pr G**	**5' TLC**	**7.56**
***n*=1 L Pr A**	**5' CDC**	**11.05**
***n*=1 D Pr B**	**5' CDG**	**6.30**
***n*=1 D Pr C**	**5' CDA**	**9.00**
***n*=1 D Pr D**	**5' CDT**	**14.05**
***n*=1 D Pr E**	**5' GDC**	**9.55**
***n*=1 D Pr F**	**5' ADC**	**11.07**
***n*=1 D Pr G**	**5' TDC**	**10.75**

Compared to dimethoxymethyl anthracene (DMEOA), which has a single lifetime of 14.6 ns in ethanol,[8] and the anthracene diol, which has a single lifetime of 4.24 ns in methanol, the anthracene unit in an oligonucleotide is much more quenched. The short lifetimes of the L isomer anthracene probes explain in part their lack of variation for the quantum yields; because the anthracene has a short lifetime, additional quenching mechanisms will not compete for the excited state

unless they are extremely efficient.[16] In the case of the D series, the longer lifetimes will mean that the anthracene is more sensitive to environmental effects or other quenching channels.

A more detailed analysis of the lifetime data shows that the emission of all the anthracene probes is tri-exponential, with each one having a short, medium and long component to the average lifetime (Table 6). For the purposes of our work we have assigned the lifetimes in the following manner:

τ 1 is the lifetime between 0.5 and 2 ns, τ 2 between 2.5 and 6 and τ 3 is greater than 8 ns.

Table 6 Lifetimes of single strand form oligonucleotides recorded at room temperature λex 375 nm λem 426 nm 1 μM oligonucleotide concentration 10 mM pH 7 phosphate buffer 100 mM NaCl

SS Oligo		τ 1 (ns)	τ1 Weighted (%)	τ 2 (ns)	τ2 Weighted (%)	τ 3 (ns)	τ3 Weighted (%)	χ^2
n=1 L Pr A	5' CLC	0.92	11	3.50	33	11.95	56	1.021
n=1 L Pr B	5' CLG	0.80	18	3.41	35	9.34	47	1.086
n=1 L Pr C	5' CLA	0.93	10	3.86	36	8.81	54	0.99
n=1 L Pr D	5' CLT	0.68	20	2.77	37	10.11	43	0.981
n=1 L Pr E	5' GLC	1.39	13	5.08	53	12.84	34	1.022
n=1 L Pr F	5' ALC	1.50	12	5.40	58	12.55	29	0.997
n=1 L Pr G	5' TLC	0.88	12	3.57	33	11.56	54	1.005
n=1 L Pr A	5' CDC	1.19	8	4.47	20	13.87	73	0.98
n=1 D Pr B	5' CDG	0.92	16	3.73	33	9.57	51	0.999
n=1 D Pr C	5' CDA	1.27	8	5.06	47	14.58	45	0.957
n=1 D Pr D	5' CDT	0.94	5	4.06	15	16.69	80	1.01
n=1 D Pr E	5' GDC	1.06	6	5.23	38	13.42	56	1.028
n=1 D Pr F	5' ADC	1.58	5	5.68	41	16.13	54	1.036
n=1 D Pr G	5' TDC	0.99	9	4.28	34	16.21	57	0.96

This implies that there are at least three different environments for the anthracene and/or quenching processes. Given the similarity between the lifetime of the anthracene monomer (Table 4) and the second lifetime, τ_2 of the oligonucleotides it would appear that it is the first and third lifetimes that arise from incorporation of the duplex. It should also be noted that there could be shorter lifetimes that are faster than can be detected by the equipment.

3.4 Fluorescence monitoring of hybridisation of the probes in a base-opposite system

As well as measuring quantum yields and lifetimes, bulk changes in emission intensity were monitored for all the systems and titrations were undertaken where hybridisation led to noticeable changes in fluorescence emission intensity. The results of these titrations, presented as the percentage change in fluorescence emission at 426 nm are presented in Appendix 2.2.

Two different systems were studied, which we have previously designated base opposite systems and deletion systems (see 2.2.2). In the following section the experiments undertaken on the base opposite system will be detailed.

3.4.1 Base opposite anthracene system

In the base opposite system there is a non-binding base opposite the anthracene, this allows the DNA to maintain a more natural structure as the anthracene has space to insert itself opposite. For all of the probes adenine was chosen as the primary opposite base,[13] so that a comparison of results could be made with the previously published serinol system.

In all experiments the Probe was made up to 1 μM at pH 7 in 10 mM phosphate buffer with 100 mM NaCl. Aliquots of 0.5 equivalents of target oligonucleotide were then titrated into the solution and the emission values again taken. Up to 2 equivalents of target were added in this manner. Quantum yields were taken upon addition of 1 equivalent of Target.

3.4.1.1 Fluorescence results for different Probes of the L and D isomers

Despite their differing quantum yields, both probes experience a similar degree of quenching for this system (Table 7).

Table 7 Quantum Yields of single strand and double strand D and L isomers with matching sequence for the base opposite system recorded at room temperature λex 350 nm λem 426 nm 1 μM oligonucleotide concentration 10 mM pH 7 phosphate buffer 100 mM NaCl

Probe		SS Quantum Yield	DS 3'GAG
n = 1 L Pr A	5' CLC	0.018	**0.007**
n = 1 D Pr A	5' CDC	0.053	**0.021**

From the quantum yield results both probes are quenched to the same degree – approximately 75%. The decrease in fluorescence was expected based on the serinol system, and the degree of quenching was approximately similar. A representative example is show in Fig. 74.

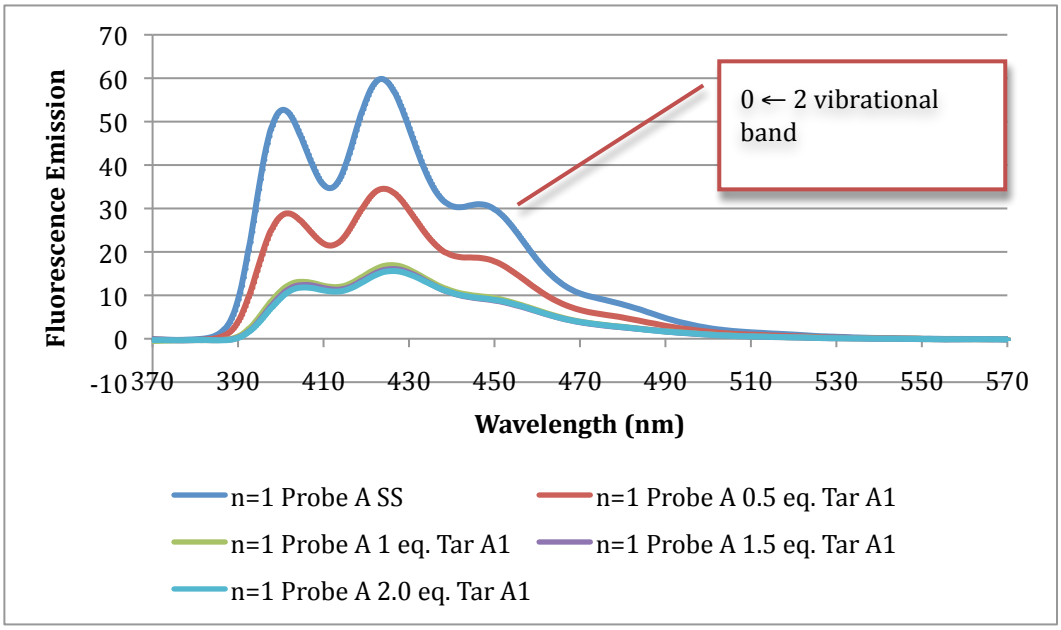

Fig. 74 Fluorescence spectra of Probe A D upon addition of 0.5 equivalent aliquots of Target A1 recorded at room temperature λex 350 nm 1 μM oligonucleotide concentration 10 mM pH 7 phosphate buffer 100 mM NaCl

Observation of the spectra corresponding to the titrations reveals that while the single strand form has a relatively well-defined structure, the duplex form is broader and less well defined. In particular, the 0 ← 2 vibrational band of the $S_1 \rightarrow S_0$ emission spectrum becomes more diffuse.

A look at the variation between the quantum yields of the different probes with their matching bases shows that there is now some variation between the different L isomer probes in the base opposite system compared to the single strand but that this is mostly confined to the bases where there is an upstream (towards the 5' side) modification (Fig. 75).

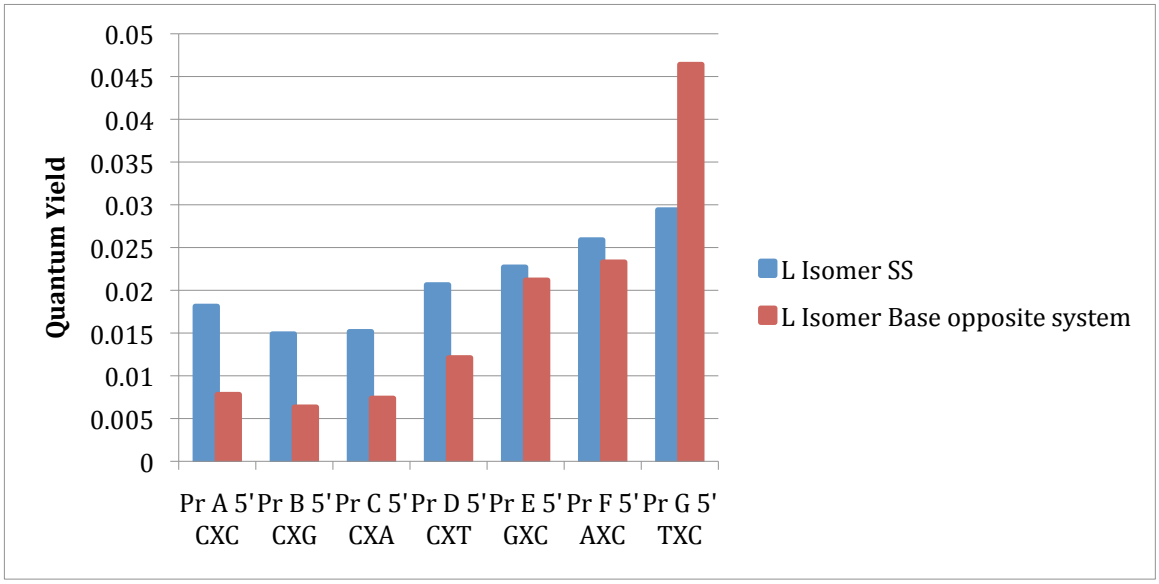

Fig. 75 Comparison of QY for base opposite matched duplexes and single strand form Probes (L isomer Probes) λex 350 nm 1 µM oligonucleotide concentration 10 mM pH 7 phosphate buffer 100 mM NaCl

Conversely, while the D isomer shows considerable variation in quantum yield in the single strand form, there is substantially less in the duplex form(Fig. 76).

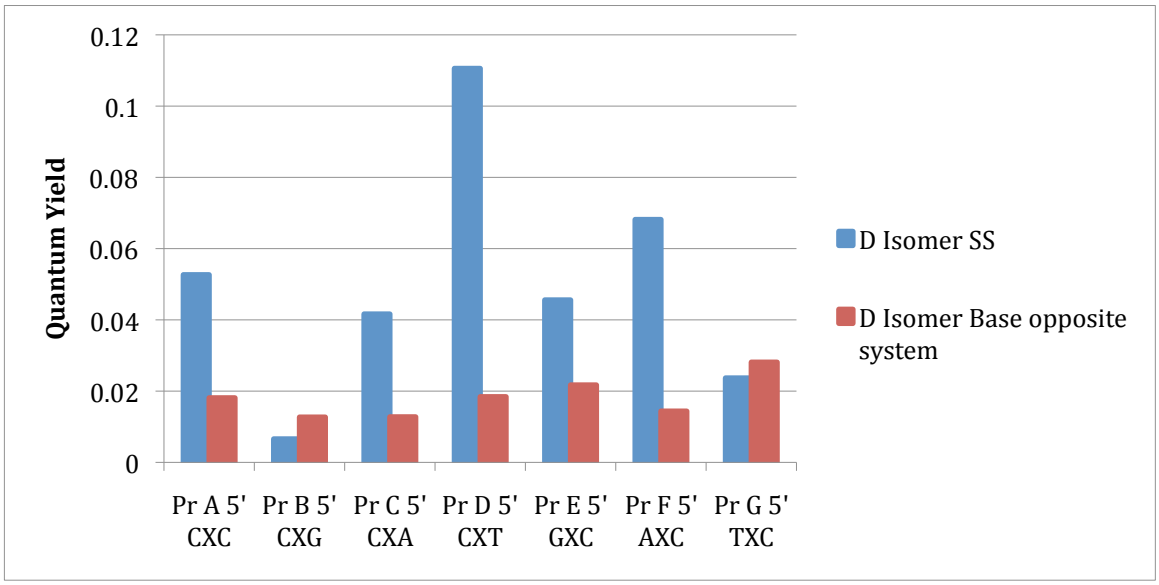

Fig. 76 Comparison of QY for base opposite matched duplexes with single strand Probes (D Isomer Probes) λex 350 nm 1 µM oligonucleotide concentration 10 mM pH 7 phosphate buffer 100 mM NaCl

The most striking results are that the duplexes formed from Probe G and its base opposite target show an increase in fluorescence QY upon hybridisation for both

the L and D isomers while the D isomer of Probe B does the same. This phenomenon is difficult to explain, particularly as for Probe B (D) it is as a result of very low single strand fluorescence QY, but for Probe G it is as a result of unusually high duplex fluorescence.

Nevertheless, what is apparent is that, unlike the single strand forms, the duplex forms of the probes follow a similar trend for both isomers (Fig. 77), particularly the L. This is not surprising given the greater rigidity of the duplex structure versus the single strand form.

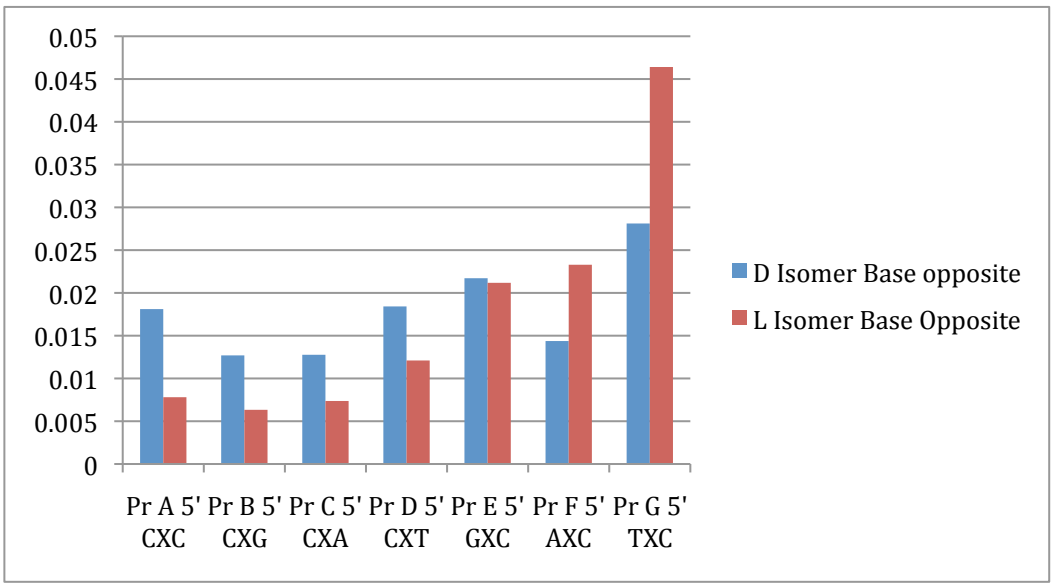

Fig. 77 Comparison of QY for base opposite matched duplexes (L and D Isomer Probe) λex 350 nm 1 μM oligonucleotide concentration 10 mM pH 7 phosphate buffer 100 mM NaCl

3.4.1.2 Varying the opposing bases (base opposite)

In order to investigate whether the probes have any selectivity for the opposite base, target strands were synthesised with C, G and T opposite the probe. The results show that there is no fluorescent selectivity for any particular base (Table 8).

Table 8 PrA percentage change in fluorescence at 426 nm of matched duplexes with different bases opposite anthracene recorded at room temperature λex 350 nm λem 426 nm 1 μM oligonucleotide concentration 10 mM pH 7 phosphate buffer 100 mM NaCl

Probe	Target	3'GAG	GTG	GCG	GGG
		A1	A3	A4	A5
n = 1 L Pr A	5' CLC	**-75**	**-76**	**-75**	**-78**
n = 1 D Pr A	5' CDC	**-72**	**-86**	**-81**	**-79**

This suggests that location of the anthracene is away from the opposite base, which plays no role in quenching. Based on the quantum yield variation of the Probes it could be supposed that the anthracene interacts more strongly with one side of the duplex, the upstream, than the other. Later in this chapter experiments will be described that further investigate these trends.

In order to investigate the utility of this system as an SNP probe a number of mismatched targets were synthesised with single mismatches adjacent to the probe both upstream and downstream of the anthracene. The mismatches consisted of both transitions (changing a purine for a purine and pyrimidine for a pyrimidine) and transversions (changing a purine to a pyrimidine and vice versa). Fluorescent titrations were performed for all of these systems and the percentage change in fluorescence upon hybridisation calculated. Based on the serinol system an increase in fluorescence was expected upon hybridisation to a mismatch.

3.4.1.3 Downstream mismatches (base opposite)

The first mismatches to be investigated were downstream mismatches whereby the base downstream of the probe was paired with the incorrect Watson-Crick hydrogen bonding base. The results showed no sensing of the mismatch and no

selectivity for different mismatch combinations, for instance between transversions and transitions (Table 9).

Table 9 PrA percentage fluorescence change upon hybridization with downstream mismatches recorded at room temperature λex 350 nm λem 426 nm 1 μM oligonucleotide concentration 10 mM pH 7 phosphate buffer 100 mM NaCl

Probe	Target	GAC	GAT	GAA
		B1	C1	D1
n = 1 L Pr A	5' CLC	**-75**	**-75**	**-55**
n = 1 D Pr A	5' CDC	**-54**	**-73**	**-56**

Again, the result implies that variation of the downstream environment does not influence the environment of the anthracene.

3.4.1.3 Upstream mismatches (base opposite)

The equivalent upstream mismatches were then investigated for both probes. In this case, mismatches were detected *via* an increase in fluorescence for one isomer (L) only (Table 10).

Table 10 PrA percentage fluorescence change upon hybridization with upstream mismatches recorded at room temperature λex 350 nm λem 426 nm 1 μM oligonucleotide concentration 10 mM pH 7 phosphate buffer 100 mM NaCl

Probe	Target	CAG	TAG	AAG
		E1	F1	G1
n = 1 L PrA	5' CLC	**86**	**45**	**70**
n = 1 D PrA	5' CDC	**-68**	**-52**	**-61**

The L isomer probe therefore shows an OFF-ON fluorescent sensing ability for mismatches that occur upstream of the probe, along with a limited ability to discriminate between them on the basis of the amount of increase (Fig. 78).

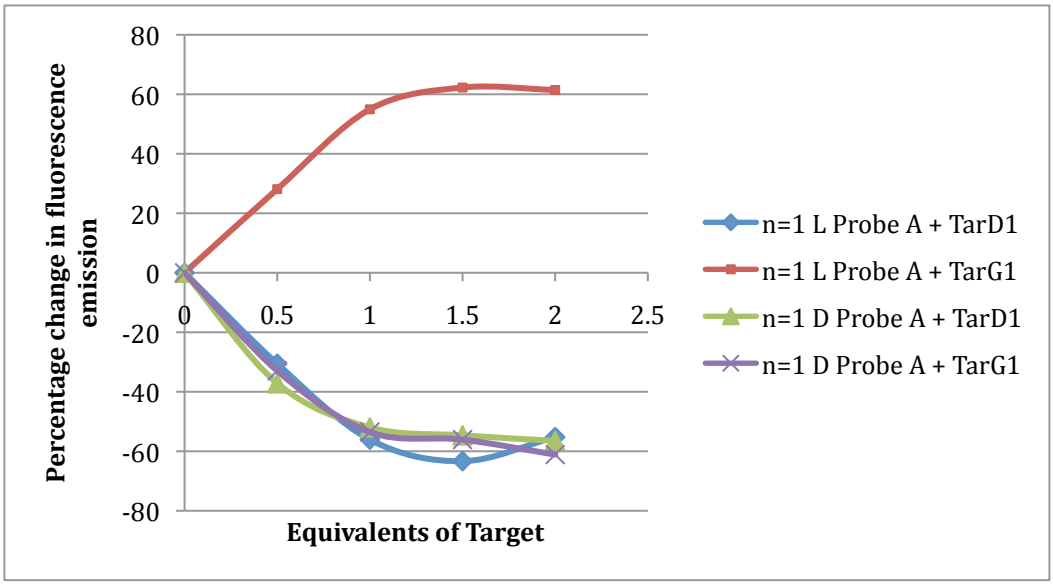

Fig. 78 Titrations showing the percentage change in emission upon hybridisation of anthracene Probes with Targets recorded at room temperature λex 350 nm λem 426 nm 1 μM solution 10 mM pH 7 phosphate buffer 100 mM NaCl.

Plotting of the fluorescence titrations shows a curve with an end-point at one equivalent of target as would be expected of a system with a very high binding constant. The published results for the serinol system showed similar trends.

3.4.1.4 Double mismatches

The ability of the probes to detect a second mismatch was also investigated, primarily by hybridisation with Target 2MM which introduces an A-A mismatch further upstream of the anthracene. For Probes A, E and F this gives two mismatches upstream of the Probe. The degree of quenching is comparable to the single mismatches in magnitude but is surprisingly not greater. Hybridisation of Tar 2MM with Probes B, C and D gave triple mismatches that were observed to give a greater increase in fluorescence than a double mismatch.

Table 11 n = 1 Probe percentage fluorescence change upon hybridization with multiple mismatches recorded at room temperature λex 350 nm λem 426 nm 1 μM oligonucleotide concentration 10 mM pH 7 phosphate buffer 100 mM NaCl

	Target	2MM GAAT	
	Isomer	L	D
n=1 Pr A	5' CXC	**61**	**-24**
n=1 Pr B	5' CXG	**143**	**82**
n=1 Pr C	5' CXA	**124**	**-18**
n=1 Pr D	5' CXT	**172**	**-51**
n=1 Pr E	5' GXC	**72**	**25**
n=1 Pr F	5' AXC	**13**	**-31**
n=1 Pr G	5' TXC	**29**	**28**

Further mismatches were generated by hybridising Probes A, E and F with a target containing a second upstream mismatch or by hybridising Probes B, C and D with target strands E1/2 to G1/2 and Probes E, F and G with Targets B1/2 to D1/2. Values of the percentage of fluorescence change for these duplexes are presented in the table in Appendix 2.

Generally the fluorescence emission increased substantially with two mismatches in an unpredictable manner for the L isomer. In the case of the D isomer probes the fluorescence change was more variable and more difficult to explain. Due to the difficulty in rationalising very complex systems further work was restricted to the study of single mismatches.

3.4.2 Conclusions

The stereochemical configuration of the probe backbone appears to play a critical role in the effectiveness of the anthracene as an SNP sensor. It also allows it to discriminate between upstream and downstream mismatches. This could be due to the orientation of the anthracene appendage in the *SS* (D) form away from

the centre of the helix, whereas the *RR* (L) form promotes incorporation of the anthracene into the duplex.[3] The upstream vs. downstream selectivity of the Probe can be rationalised as a first approximation by considering the distance between the threoninol and the natural nucleotide, the space between the two being the likely location of the anthracene (Fig. 79).

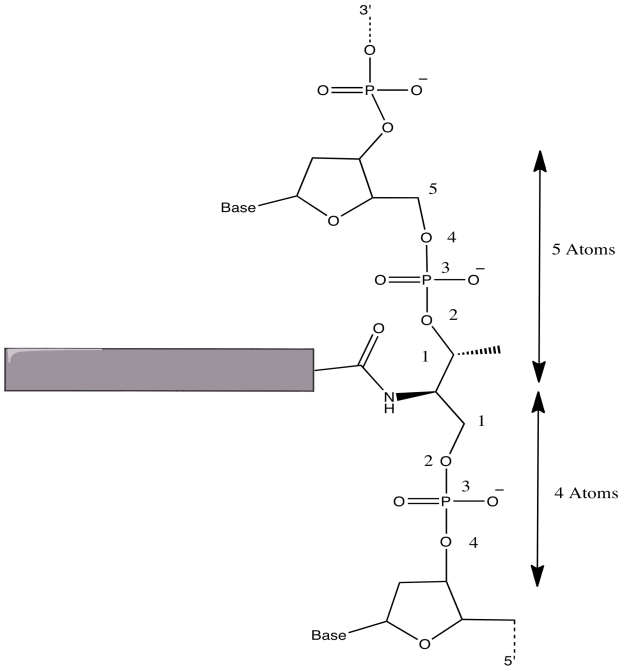

Fig. 79 Diagram showing the number of carbon atoms between the anthracene (grey) and the upstream and downstream bases

Therefore it can be seen that the number of atoms from the anthracene to the nearest five membered ring of the sugar backbone is five on the downstream side and four on the upstream side. Although this 2D representation is an oversimplification, given the complex angles and dihedrals in DNA, by thinking of the relative placement of the anthracene we can begin to rationalise the results using more complex modelling techniques (see Chapter 4).

3.4.3 Comparison with existing system

As a full range of mismatch titrations were not performed with the serinol probe[1] it is difficult to compare the two systems. However, it appears that the stereochemistry of the published probe is of the *RR* form, as the *SS* form appears unable to detect any mismatches.

These results suggested that the system had the potential to detect mismatches in oligonucleotide sequences with an unpaired base opposite of the anthracene. As a comparison it was decided to investigate the effect of removing this base from the system.

3.5 Deletion duplexes

This type of non-nucleosidic system can be classified as a wedge type system (schematic diagram shown in Fig. 80). Previous work in this field by Saito[17] (with pyrenes) and Tanaka[18] (L threoninol with acridine), Asanuma[19] and Komiyama[2, 20, 21] (both with D and L threoninol with azobenzenes) have given varied and differing results.

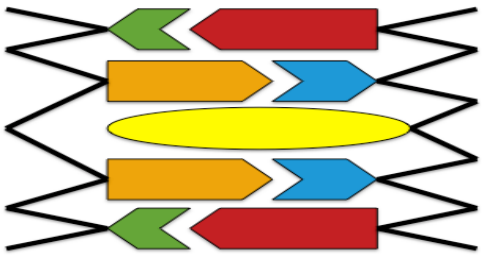

Fig. 80 Schematic diagram of a wedge type system

3.5.1 Fluorescence quantum yields

As with the base opposite system the quantum yields of the deletion system duplexes were measured and compared to the single strand form. Both the L

isomer duplex (Fig. 81) and the D isomer (Fig. 82) duplex quantum yields showed similar patterns to the base opposite system (Fig. 75 and Fig. 76) respectively.

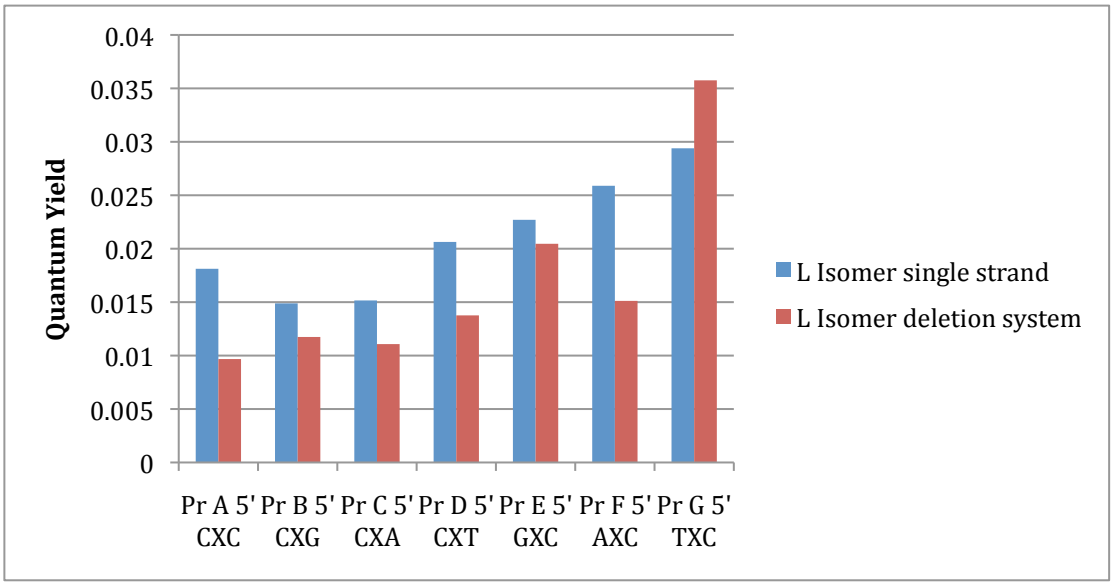

Fig. 81 Comparison of QY for deletion matched duplexes (L isomer Probe) λex 350 nm 1 μM oligonucleotide concentration 10 mM pH 7 phosphate buffer 100 mM NaCl

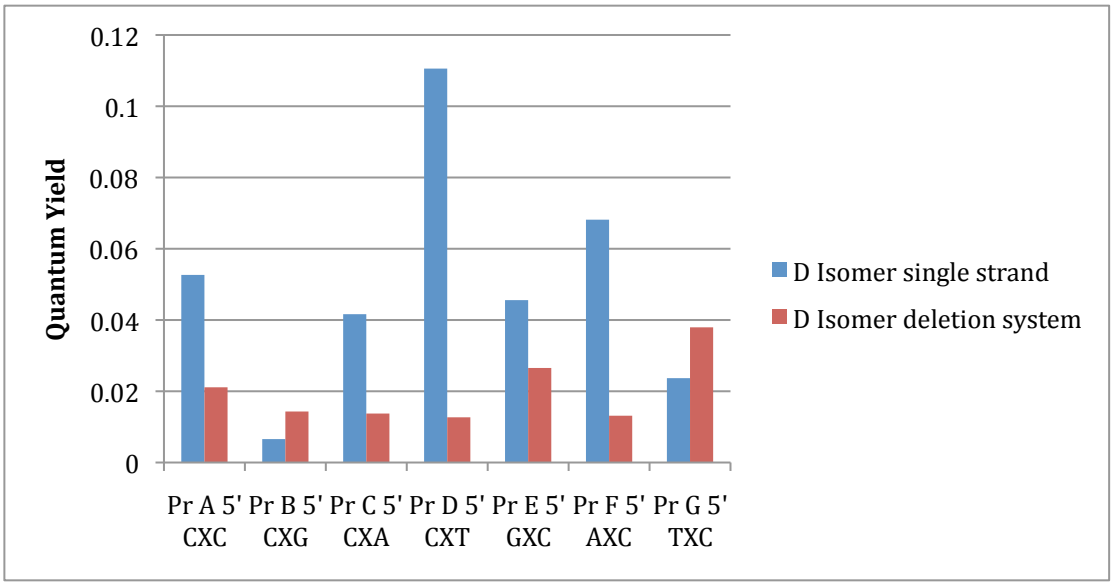

Fig. 82 Comparison of QY for matched deletion duplexes (D isomer Probe) λex 350 nm 1 μM oligonucleotide concentration 10 mM pH 7 phosphate buffer 100 mM NaCl

The lower quantum yield values compared to the base opposite system may be as a result of the more compact structure of the deletion system.[22]

3.5.2 Fluorescence monitoring of hybridisation for a deletion systems

A similar range of titrations was performed as with the base opposite system to give the following results (Table 12).

Table 12 Probe A percentage fluorescence change upon hybridization with fully matching deletion duplexes recorded at room temperature λex 350 nm λem 426 nm 1 μM oligonucleotide concentration 10 mM pH 7 phosphate buffer 100 mM NaCl

Probe	Target	3' G_G
		A2
n = 1 L Pr A	5' CLC	**-50**
n = 1 D Pr A	5' CDC	**-77**

We again see a decrease in the fluorescence emission upon hybridisation, although it is slightly less than before with the base opposite system. Further mismatch titrations as before give a substantively different range of results. In this case the D isomer again shows no sensing but the L isomer is demonstrating an ability to discriminate not only the location of a mismatch but also the type of mismatch, in this case a C to A mismatch (Table 13).

Table 13 PrA percentage fluorescence change upon hybridization with upstream and downstream mismatches for the deletion system recorded at room temperature λex 350 nm λem 440 nm 1 μM oligonucleotide concentration 10 mM pH 7 phosphate buffer 100 mM NaCl

Probe	Target	3' G_C	G_T	G_A	C_G	T_G	A_G
		B2	C2	D2	E2	F2	G2
n = 1 L Pr A	5' CLC	**-98**	**-74**	**-72**	**-52**	**0**	**25**
n = 1 D Pr A	5' CDC	**-91**	**-82**	**-57**	**-66**	**-40**	**-6**

The quenching of the fluorescence in the presence of downstream mismatches is concurrent with the previous studies (Table 9) however, the quenching that occurs with some upstream mismatches with the L isomer was not seen before.

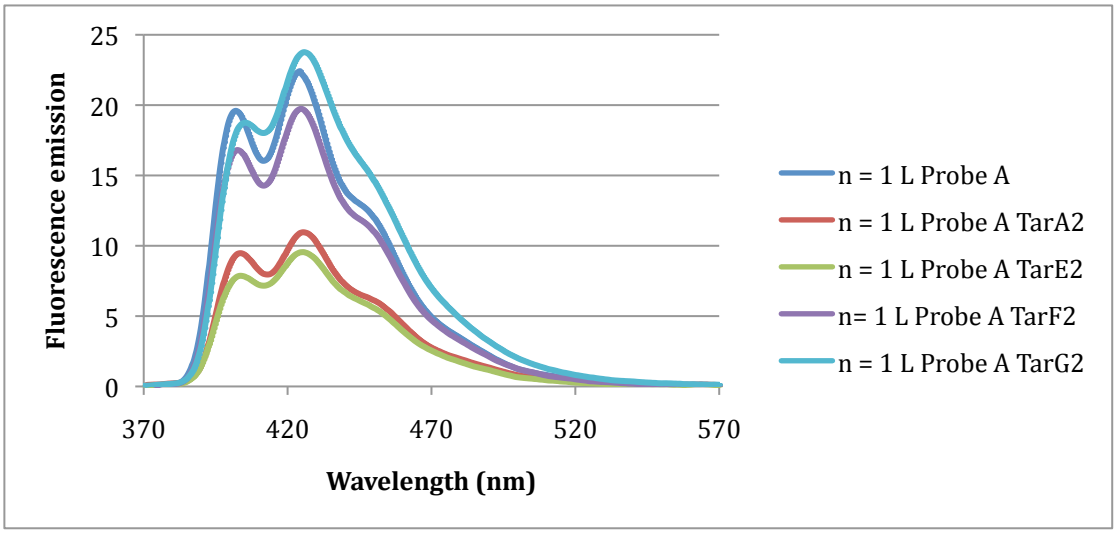

Fig. 83 Graphs of fluorescent titrations of Probe A L with upstream mismatch for the deletion system λex 350 nm λem 426 nm 1 μM oligonucleotide concentration 10 mM pH 7 phosphate buffer 100 mM NaCl

Now we have an order of anthracene quenching of C > T > A, which will be shown later to be able to be explained in terms of properties of the bases. Furthermore, the selective increase in fluorescence upon hybridisation of the L isomer Probe with a C-A mismatch now means that a specific mutation can be differentiated from the others by OFF-ON sensing (Fig. 83). Of the many fluorescent-tagged nucleobases that have been reported, generally they are limited in their ability to differentiate between all of the possible base-pairing partners.[23-26] A modified nucleobase that can discriminate between the four DNA bases through differences in fluorescence emission has been reported,[27] however the sensing is via different decreases in emission with the single strand form being more emissive than any of the duplexes.

3.5.3 Comparison of the two systems

The two systems both show selectivity in sensing mismatches although, as stated above, with different selectivities: The base opposite system is able to detect

single base mismatches upstream of the anthracene, whilst the deletion is able to detect a single C to A mismatch upstream of the anthracene. The greater selectivity of the deletion system may be due to the more compact structure of the duplex (alluded to as a result of higher T_ms, see 3.10.8.2) in holding the anthracene closer to the quenching base and magnifying the different quenching properties of the bases.

3.5.4 Explaining the base sensing selectivity

Previously, we have attempted to rationalise our findings in structural terms – in particular the orientation of the anthracene relative to other bases in the duplex. Whilst this may still be important, in trying to rationalise the selectivity of sensing it becomes necessary to consider the quenching ability of the different nucleotides. This appears to be particularly true for the deletion system as was demonstrated previously. Work in this area has been undertaken by a number of groups[28-33], including that of Netzel[33], Seidel[29] and more recently Wagenknecht[34] and Kool[32] who have attempted to rationalise the emission quenching ability of the different bases towards fluorescent dyes by considering their ease of oxidation and of reduction. For instance, in his work Netzel has suggested an order of pyrene base quenching ability for the different bases of A < G < C ≈ T.

These results are calculated on the basis of the ΔG^0 values for electron transfer between the bases considering not only the ease of oxidisation of the nucleobase but also how easily the oxidised form is reduced. Although this analysis ignores any electronic coupling and Frank-Condon factors, by considering that the related donors and acceptors are held in similar electrostatic and hydrophobic

environments is assumes that the electron transfer rates will be proportional to ΔG^0.

When one considers the different emission profiles for the mismatched bases of the deletion probe system we can see that they might be related to this pattern if the order of quenching for anthracene can be predicted.

Thus this analysis might be used to rationalise some of the data (see section 3.7) but first a more in-depth study of the hybridised systems will be undertaken using the fluorescent lifetimes.

3.6 Fluorescent lifetimes upon hybridisation

The lifetimes of the *n* = 1 D and L Probe systems were studied and compared, both to each other and to the single strand form. In particular, the effect of mismatches on the number, length and value of the lifetimes was studied. The lifetimes were assigned in the same way as for the single strand Probes (see 3.3.4).

3.5.1 Fluorescence lifetimes of matching base opposite system for the L and D isomer Probes

Upon hybridisation to a matching strand, for the base opposite system, the fluorescence decreases, the average lifetime decreases, the weighting of the τ1 component increases and the weighting of τ3 decreases (Table 14).

Table 14 Fluorescence lifetimes of Probe A single- and double-stranded matching recorded at room temperature λex 350 nm λem 426 nm 1 μM oligonucleotide concentration 10 mM pH 7 phosphate buffer 100 mM NaCl

n	Probe	Isomer	Target	τ 1 (ns)	τ 1 Weighted (%)	τ 2 (ns)	τ 2 Weighted (%)	τ 3 (ns)	τ 3 Weighted (%)	χ^2
1	A	L	SS	0.92	11	3.5	33	11.95	56	1.021
1	A	D	SS	1.19	8	4.47	20	13.87	73	0.98
1	A	L	A1	1.05	38	4.28	36	12.4	26	1.044
1	A	D	A1	1.5	33	3.68	41	9.08	25	0.999

The changes in the lifetimes and weightings show that anthracene in a duplex environment is much more quenched, and by different ratios of quenching pathways compared to the single strand, which supports the fluorescence hybridisation studies and quantum yield results. This is most likely because of the much more rigid structure of bases in the duplex form where the aromatic groups are held together in face to face contact, facilitating static quenching through ground state complexes. This is likely to be the reason for the increase in weighting of τ1.

3.6.2 Fluorescence lifetimes for different hybridised Probe systems

Table 15 Fluorescence lifetimes of different Probes for matching duplexes recorded at room temperature λex 350 nm λem 426 nm 1 μM oligonucleotide concentration 10 mM pH 7 phosphate buffer 100 mM NaCl

N	Probe	Isomer	Target	τ1 (ns)	τ1 Weighted (%)	τ 2 (ns)	τ2 Weighted (%)	τ 3 (ns)	τ 3 Weighted (%)	χ^2
1	A	L	A1	1.05	38	4.28	36	12.4	26	1.044
1	A	D	A1	1.5	33	3.68	41	9.08	25	0.999
1	B	L	B1	1.1	29	4.76	45	11.8	25	0.987
1	C	L	C1	0.833	23	4.39	51	10.2	26	1.024
1	D	L	D1	0.731	35	3.52	34	10.7	31	1.002
1	E	L	E1	1.45	21	6	59	14.6	20	0.994
1	F	L	F1	1.44	14	5.6	63	12.9	23	0.992
1	G	L	G1	0	0	3.21	8	13.6	92	1.006

Varying the bases surrounding the anthracene causes clear changes in the lifetimes and weightings of these lifetimes (Table 15). As with the single strands

this demonstrates clearly the effect that different nucleobases have on the emission processes.

3.6.3 Fluorescence lifetimes of Probe A base opposite system mismatches for the D isomer Probes

Further studies were undertaken to look at the effect on lifetimes of having mismatched targets both downstream of the anthracene (Tar B1 to D1) and upstream (Tar E1 to G1). The first result for the *n* = 1 D isomer is that the lifetimes are all still triexponential, as would be expected from the fluorescent hybridization studies which indicated that the fluorescence is quenched irrespective of the target strand sequence. Hence Targets B1 and D1 and E1 and G1, which are downstream and upstream mismatches respectively, all have the same decay profile (Table 16).

Table 16 Fluorescence lifetimes of Probe A D isomer matched duplexes recorded at room temperature λex 371 nm λem 426 nm 5 μM oligonucleotide concentration 10 mM pH 7 phosphate buffer 100 mM NaCl

Isomer	Probe	Target	τ 1 (ns)	τ 1 Weighted (%)	τ 2 (ns)	τ 2 Weighted (%)	τ 3 (ns)	τ 3 Weighted (%)	χ2
D	A	A1	1.5	33	3.68	41	9.08	25	0.999
D	A	B1	1.47	9	5.93	55	12.6	35	1.056
D	A	D1	1.41	11	5.57	55	12.1	34	1.15
D	A	E1	1.23	10	5.14	42	12.6	47	1.11
D	A	G1	1.02	12	4.53	48	13.3	40	1.037

3.6.4 Fluorescence lifetimes of base opposite system mismatches for the L isomer Probes

A similar set of studies were undertaken for the L isomer with different target strands hybridized to Probe A. A comparative selection of these results is presented in Table 17.

Table 17 Fluorescence lifetimes of Probe A L in single strand form and with matched and mismatched duplexes for the base opposite system recorded at room temperature λex 375 nm λem 426 nm 1 μM oligonucleotide concentration 10 mM pH 7 phosphate buffer 100 mM NaCl

Probe	τ 1 (ns)	τ 1 Weighted (%)	τ 2 (ns)	τ 2 Weighted (%)	τ 3 (ns)	τ 3 Weighted (%)	χ^2	Fluorescence Change %
L Pr A SS	0.92	11	3.5	33	11.95	56	1.02	
L PrATarA1	1.05	38	4.28	36	12.4	36	0.98	-75
L PrATarB1	0.78	39	3.9	33	12.9	37	1.018	-75
L PrATarD1	0.94	32	4.08	40	12,9	28	1.011	-55
L PrATarE1		0	5.13	20	13.27	80	1.02	86
L PrATarF1		0	5.91	29	13.45	71	0.97	45
L PrATarG1	0.88	2	4.6	21	14.41	77	0.97	70

An important factor appears to be the loss of one of the lifetimes in situations where the fluorescence increases and thus the appearance of a bi-exponential decay. In the cases of Targets E1 and F1 we observe the loss of the shortest lifetime τ**1**, possibly as the result of the loss of one of the quenching pathways. Although Target G1 is still fitted as tri-exponential, a breakdown of the data into weighted lifetimes demonstrates that τ **1** is very much a minor component and that Target G1 can essentially be considered as bi-exponential.

Conversely, Probe A Target B1 and D1, which are duplexes with a downstream mismatch, have triexponential decay profiles and give a decrease in fluorescence emission upon hybridisation. This shows that for Probe A (base opposite system), the loss of a lifetime correlated with an increase in fluorescence upon hybridisation rather than the presence or absence of mismatches in the sequence.

Further studies whereby the target was fixed and the Probe varied further validates this hypothesis. The following (Table 18) shows how Target E1 when

hybridised with all of the L probes creates a duplex that only has a tri-exponential decay form when the fluorescence emission decreases.

Table 18 Fluorescence lifetimes of different L isomer Probes with a fixed Target (TarE1) recorded at room temperature λex 350 nm λem 426 nm 1 μM oligonucleotide concentration 10 mM pH 7 phosphate buffer 100 mM NaCl

Probe	τ 1 (ns)	τ 1 Weighted (%)	τ 2 (ns)	τ 2 Weighted (%)	τ 3 (ns)	τ 3 Weighted (%)	χ^2	Fluorescent Change %
L PrATarE1		0	5.13	20	13.27	80	1.02	86
L PrBTarE1		0	2.86	16	16.63	84	1.02	131
L PrCTarE1		0	3.024	5	16.81	95	0.97	255
L PrDTarE1		0	2.31	9	14.95	91	1.04	144
L PrETarE1	1.45	21	6	59	14.6	20	0.99	-21
L PrFTarE1		0	2.86	16	12.12	84	1.05	13
L PrGTarE1		0	2.94	17	10.54	83	0.96	0

Thus, only the matching sequence PrE TarE1 has a tri-exponential decay profile and all other combinations, which give a fluorescence increase upon hybridisation, have bi-exponential profiles. The final evidence that the decay form (i.e. bi-or tri-exponential) is related to the fluorescence increases upon hybridisation for a base opposite system and not upon the matching or mismatching of any base pairs, is that PrG TarG1, a matched duplex for which the fluorescence emission increases upon hybridisation, has a bi-exponential profile (Table 19).

Table 19 Fluorescence lifetimes of PrG L TarG1 with matching strand for the base opposite system recorded at room temperature λex 350 nm λem 426 nm 1 μM oligonucleotide concentration 10 mM pH 7 phosphate buffer 100 mM NaCl

Probe	τ 1 (ns)	τ 1 Weighted (%)	τ 2 (ns)	τ 2 Weighted (%)	τ 3 (ns)	τ 3 Weighted (%)	χ^2
PrG L TarG1	0	0	3.21	8	13.61	92	1.006

This duplex is the only matching duplex for the L isomer that results in an increase in fluorescence upon hybridisation (Fig. 75) and also has a biexponential decay profile.

3.6.5 Fluorescence lifetimes for deletion duplexes

For deletion duplexes, the situation for the base opposite system where duplexes with decreased fluorescence emission have tri-exponential lifetimes and those that show a fluorescence increase have bi-exponential is not observed. The data indicates that all of the Probe A matching and mismatching fluorescence decay profiles are tri-exponential (Table 20).

Table 20 Fluorescence lifetimes of PrA L and D with matches and mismatches for the deletion system recorded at room temperature λex 375 nm λem 426 nm 5 μM oligonucleotide concentration 10 mM pH 7 phosphate buffer 100 mM NaCl

n	Isomer	Probe	Target	τ 1	τ 1 Weighted (%)	τ 2	τ 2 Weighted (%)	τ 3	τ 3 Weighted (%)	χ^2
1	L	A	A2	1.46	65	3.42	22	12.21	13	0.993
1	L	A	D2	0.84	40	4.19	32	13.1	27	0.999
1	L	A	G2	0.97	10	4.06	27	9.94	62	0.982
1	D	A	A2	1.19	27	2.1	66	11.9	7	1.034
1	D	A	D2	0.98	17	4.75	63	9.87	20	1.049
1	D	A	G2	0.623	10	4.47	31	13.87	59	1.094

This may be due to the deletion duplexes adopting a more compressed structure, meaning that the anthracene is held closer to the adjacent bases, making static quenching more likely. This can be seen in the fact that the τ1 weighting factor is always greater in the deletion form (Tar X2) compared to the base opposite form (Tar X1). However, the duplex that is more emissive than the single strand form (PrA L TarG2) does have a small τ1 weighting factor that suggests that the deletion and base opposite systems follow similar patterns.

3.6.6 Discussion and conclusions on lifetimes

Previous work in the field has established that the shortest lifetimes in such systems can be attributed to the intrahelical conformation where the fluorophore is quenched by direct face-to-face contact with the neighbouring upstream residue. It could be considered that the quenching is as a result of direct electron transfer between the anthracene and the nearest base or in other words static quenching. Indeed, it has been shown that photo-induced electron transfer (PET) between donors and acceptors or good intercalators is both possible and dependent on changes in the π-π stacking or orientation of the molecules.[16]

Conversely, longer lifetimes can be ascribed to an extrahelical conformation or at least a loose microenvironment of the anthracene whereby the quenching is dominated by collisional or dynamic quenching, in this case by water or by oxygen.[13] The lifetime of the unincorporated anthracene (Fig. 67), 4.24 ns (Table 4) being in the range of the second lifetime would also seem to corroborate this hypothesis.

3.6.6.1 Importance of oxygen quenching

In order to determine whether one of the lifetimes arises due to dynamic quenching as a result of dissolved oxygen, the lifetimes of some degassed samples were measured. If dynamic quenching by oxygen were responsible in full or in part for one of the quenching processes we would expect to see a significant change in either the lifetime or the weighting. Given that the lifetime for oxygen quenching processes is of the order of 2-5 ns, a change in the values for $\tau 2$ would be expected.

The samples were made up as before but were purged by bubbling nitrogen gas through the solution for 20 minutes prior to the lifetime being taken. They were then compared to the lifetimes of the sample that was not degassed. However, no dependence on dynamic quenching by oxygen in the decay process was observed (see Appendix 2).

3.6.6.2 Assigning the lifetimes

A breakdown of selected lifetime data below highlights trends in the calculated lifetimes and weightings that can be used to assign the processes taking place during quenching (Table 21).

Table 21 Fluorescence lifetimes of selected PrA L duplexes recorded at room temperature λex 375 nm λem 426 nm 1 μM oligonucleotide concentration 10 mM pH 7 phosphate buffer 100 mM NaCl

Probe	τ 1 (ns)	τ 1 Weighted (%)	τ 2 (ns)	τ 2 Weighted (%)	τ 3 (ns)	τ 3 Weighted (%)
L PrA	0.92	11	3.5	33	11.95	56
L PrATarA1	1.05	38	4.28	36	12.41	26
L PrATarA2	1.46	65	3.42	22	12.21	13
L PrATarE1			5.13	20	13.45	80
L PrATarG1			4.6	21	14.40	77

The single strand form in solution is expected to be more weakly structured than the matching duplex and more capable of forming hydrophobic pockets. As a result one would expect the longer lifetime components to dominate the overall emission and indeed this is what is seen – in the single strand form long lifetimes account for 31 % of the total lifetime whereas for the matching double strand it is only 26 %. Furthermore, the deletion system PrA (L) TarA2, in which we can suppose that the anthracene is even more tightly held (based on melting point data – see 3.10.8.2), has an even lower ratio of long to short lifetime (22% long lifetime to 65% short lifetime).

The presence of all three lifetimes show that the anthracene does not rest permanently intercalated into the duplex but that the system is in dynamic equilibrium with the relative ratios of the different lifetimes fluctuating as a result of changes in the anthracene microenvironment.

The lifetimes are therefore assigned in the following manner:

1. The shortest lifetime ($\tau 1$) arises from the anthracene being in an environment where it is closely held adjacent to a nucleobase that quenches fluorescence through static quenching.
2. The intermediate lifetime ($\tau 2$) is assigned to the anthracene being in an environment that exposes it to water where it is dynamically quenched.
3. The longest lifetime ($\tau 3$) is a consequence of anthracene being held in a hydrophobic environment but where it cannot be statically quenched by any neighbouring nucleobases.

3.6.6.3 Relative importance of each parameter on the overall quantum yield

As the quantum yield is an absolute measurement of the fluorescence emission, it is possible to see how much each factor (lifetime and weighting) contributes to the quantum yield by observing how changes in these factors correlate with change in the quantum yield for the different types of duplex. To do this the factor in question is simply plotted against the quantum yield and a correlation is looked for. When applied to all of the n = 1 stands two of the three weighting factors are seen to give a correlation (Fig. 84).

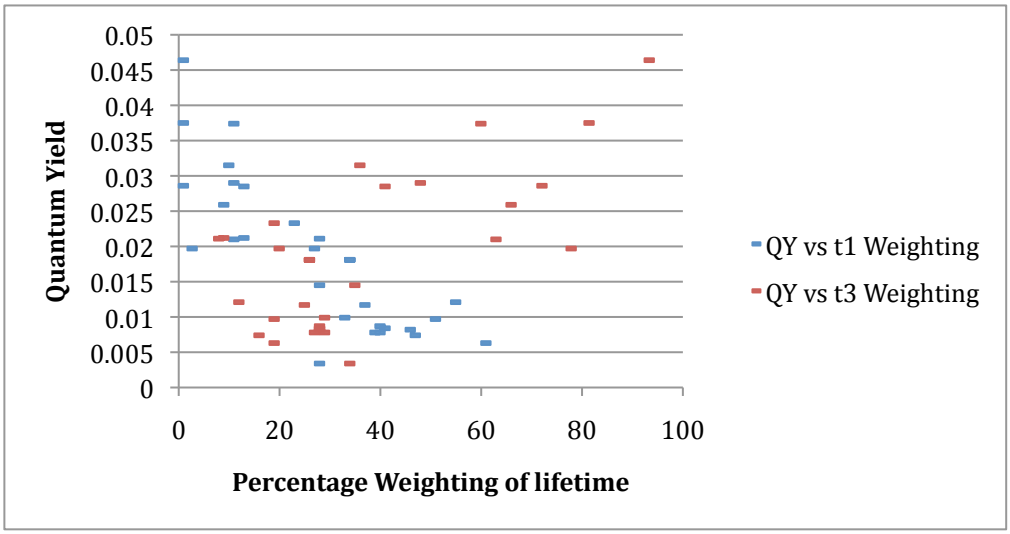

Fig. 84 Scatter graph of quantum yield of fluorescence against lifetime weighting percentage

The above chart implies that the most important factors that influence the quantum yield are the weighting of the first and third lifetimes. This most likely reflects the effect of changing the quenching efficiency of the base adjacent to the anthracene. When there is an efficient quencher in this position it means that the first quenching pathway dominates and as it is the most effective and as a result the overall quantum yield decreases. When the anthracene finds itself in a hydrophobic environment the quenching of this base is not strong, and hence the third lifetime dominates – this would explain the positive and negative correlations for these two factors.

3.6.6.4 Explaining the importance of τ 1

The above conclusions, if applied, can be used to rationalise some of the previous results. If the assumption, as stated above, that the shortest lifetime τ1 results from static quenching between the anthracene and the adjacent base is correct and, as concluded previously on the basis of fluorescence yields, that the L probe is sensitive to the upstream base then we might be able to see evidence relating τ1 to the order of quenching proposed by Netzel (Table 22).[33]

Table 22 τ1 values (ns) for different upstream bases for single strand L Probes

Probe	Sequence	Upstream Base	τ 1
n=1 L Pr A	5' CLC	C	0.92
n=1 L Pr B	5' CLG	C	0.8
n=1 L Pr C	5' CLA	C	0.93
n=1 L Pr D	5' CLT	C	0.68
n=1 L Pr E	5' GLC	G	1.39
n=1 L Pr F	5' ALC	A	1.5
n=1 L Pr G	5' TLC	T	0.88

If we consider the upstream C (Probes A - D) to have an average τ1 lifetime of 0.83 ns then this produces the order A < G < C ~ T for the quenching ability, which is the same order as proposed by Netzel. This would seem to suggest that the quenching process for the shortest lifetime involves electron transfer, a concept that will be explored further in the following section.

3.7 Rationalising the order of quenching through electron transfer

Various patterns in the results have been related to an order of quenching suggested by Netzel[33] and others. However, up to this point in the thesis an in-depth analysis has not been performed on the theory behind it.

3.7.1 Electron migration in DNA

3.7.1.1 Introduction

It was suggested as early as the 1960s, by Eley and Spivey, that DNA is potentially suitable for charge migration.[35] In the early 1990s there was a highly controversial dispute about the question of DNA acting as a molecular wire as a result of the work published by Barton and co-workers.[36] Although it is still a matter of debate as to how far charge can actually be transferred through DNA,

especially through metallated DNA, the controversy has mostly been solved by the description of different charge transfer mechanisms and their elucidation through experiment.[37]

Charge transfer in DNA is mostly studied in a photoinduced fashion. This allows for a clearly defined starting time of the electron transfer and the photoexcitation pumps a significant amount of energy as a driving force into the system and shifts the endergonic process towards an exergonic situation.

3.7.1.2 Photoinduced Electron Transfer in DNA

Photochemically induced, DNA-mediated charge transfer processes have been categorised into oxidative processes (also called hole transfer, hole transport or hole migration)[38] and reductive processes (also called excess electron transport, electron transport or electron migration).[39] During oxidative hole transfer an electron is transferred from the DNA to the photoexcited charge donor in a HOMO–controlled process. In the case of reductive electron transfer the photoexcited electron of the donor is injected into the DNA in a LUMO-controlled fashion.[38]

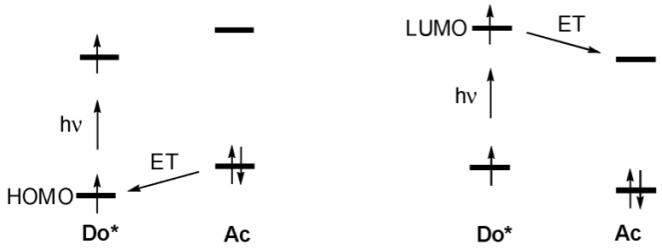

Fig. 85 Comparison of photo induced oxidative process (left) and reductive process (right)[38]

As anthracene has well studied photochemistry and is easily photoexcitable, it is possible to apply charge transfer theories to the system.

3.7.2 Rehm-Weller equation

If we consider that the quenching of anthracene is heavily influenced by electron transfer both to and from the molecule, then it is possible to estimate an order for the dependence of quenching upon the base by considering the free energy of electron transfer $\Delta G^{o}(ET)$ for the formation of solvent-separated radical ion pairs (SSIP) using the Rehm-Weller equation.[40] This evaluates the quenching reaction for a fluorescent molecule (A) being quenched by a nucleobase (N) via an encounter complex according to the following reaction:

$$A^{*} + N \rightarrow \left(A - N\right)^{*} \rightarrow A^{\bullet(+/-)} + N^{\bullet(+/-)}$$

Equation 11

Encounter complex **Solvated Ion Pairs**

The classification of the complex as encounter or exiplex can be considered as a matter of definition, but kinetic analysis work by Rehm and Weller[41] on the quenching of polynuclear aromatics by electron donors have shown that reactions that follow the above scheme produce results that are incompatible with electron transfer within an exiplex. Therefore, as the definition of an encounter complex implies an ill defined mutual orientation of the components which requires little more than orbital overlap somewhere in the complex,[10] it can be said to be more applicable in these circumstances.

Since it is not known whether the excited anthracene acts as an electron donor and the nucleobase as an electron acceptor (Equation 12) or vice versa (Equation 13), both possibilities need to be considered.

Nucleobase reduction:

$$\Delta G^{\circ}_{ET} = E^{\circ}(An^{\bullet+}/An) - E^{\circ}(N/N^{\bullet-}) - E_{\infty}(An) + \Delta G^{\circ}_{(\varepsilon)}$$

Equation 12

Nucleobase oxidation:

$$\Delta G^{\circ}_{ET} = E^{\circ}(N^{\bullet+}/N) - E^{\circ}(An/An^{\bullet-}) - E_{\infty}(An) + \Delta G^{\circ}_{(\varepsilon)}$$

Equation 13

$E_{o,o}$ (An) is the excited state energy of the anthracene tagged oligonucleotide obtained from the crossing point wavelength of the absorption and emission spectra, in this case at 400 nm (see Fig. 70).

$\Delta G^{o}_{(\varepsilon)}$ is a coulombic interaction term between the oxidised donor and the reduced acceptor. Defined below,[42] it contains two correction terms based on the Born equation. Firstly, the interaction energy of radical ions with radius r_{ion} in a complex with a centre-to-centre distance a_{EC} and secondly the difference of ion solvation between a solvent of interest, in this case water with a dielectric constant E_w = 78 and an organic solvent E_o.

If the standard parameters r_{ion} = 3 Å and a_{EC} = 7 Å are used then for a quenching reaction in water a value of -0.1eV can be estimated using Equation 14.[29]

$$\Delta G^{\circ}(\varepsilon) = \frac{e^2}{4\pi\varepsilon_0}\left[\left(\frac{1}{r_{ion}} - \frac{1}{a_{EC}}\right)\frac{1}{\varepsilon_W} - \frac{1}{r_{ion}\varepsilon_0}\right]$$

Equation 14

Whilst this analysis does not give a quantitative value for the rate of electron transfer, by ignoring the Franck Condon factors we can assume that the trend of ΔG_{ET} is an accurate reflection of the rate of transfer and therefore quenching.

3.7.3 Cyclic Voltammetry

In an effort to quantify the ΔG_{ET} values as accurately as possible cyclic voltammetry experiments were performed on the DMT protected anthracene. Of the numerous dynamic electrochemical methods, cyclic voltammetry has arguably become the most popular. Its applications range from the study of simple redox processes to the characterisation of multi-electron-transfer processes in bio- and macromolecular chemistry.[43] This is because of the wealth of information that can be obtained: thermodynamic parameters such as the redox potential, insights into the kinetics of electrode reactions and the determination of reactive intermediates.

A CV experiment (see example below) consists of the application of a repetitive linear scan over a fixed potential range at a stationary electrode and the continuous monitoring of the current that results. The primary experimental parameter, the rate at which the potential is scanned, provides a direct means to study the electrode processes.[44]

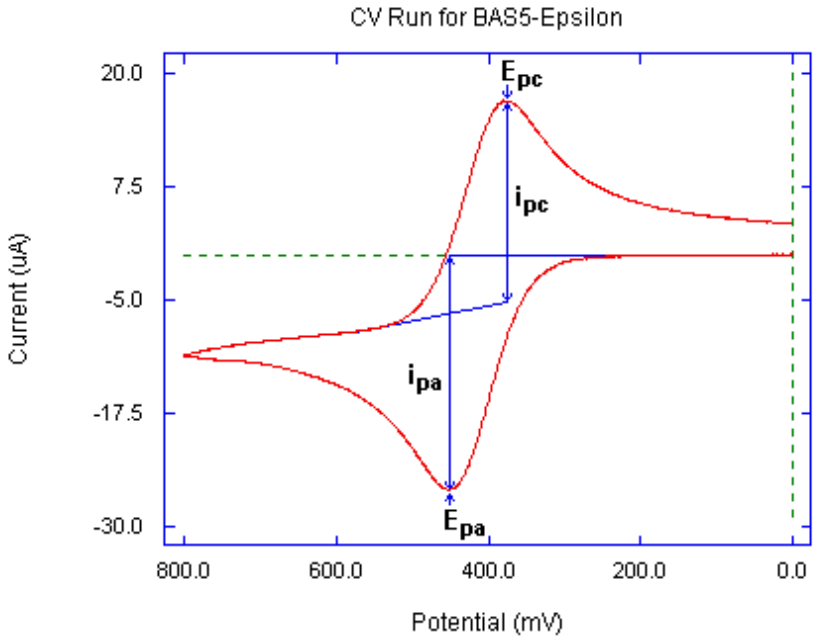

Fig. 86 Example of a reversible voltammogram

3.7.3.1 Cyclic Voltammetry of anthracene

The electrochemistry of anthracene has been studied in great detail and is known to react as below.

$$An \rightarrow An^{+\bullet} + e^{-} \quad E^{o}_{Ox} = 1.1V$$
$$An + e^{-} \rightarrow An^{-\bullet} \quad E^{o}_{Red} = -2.17V$$

Equation 15 Redox potentials of anthracene at a scanning rate of 1000Vs^{-1} [45]

However, the redox potentials can be significantly altered by the presence of substituents on the 9-position of anthracene, with electron donating groups leading to more negative potentials and electron withdrawing groups to more positive ones.[45]

Therefore, it was decided to scan one of the anthracene monomers over a similar range as anthracene. The scans were performed in dry acetonitrile and 0.1M tetrabutylammonium hexafluorophospahte buffer using $Ag/AgCl_{2(aq)}$ as the reference (Fig. 87).

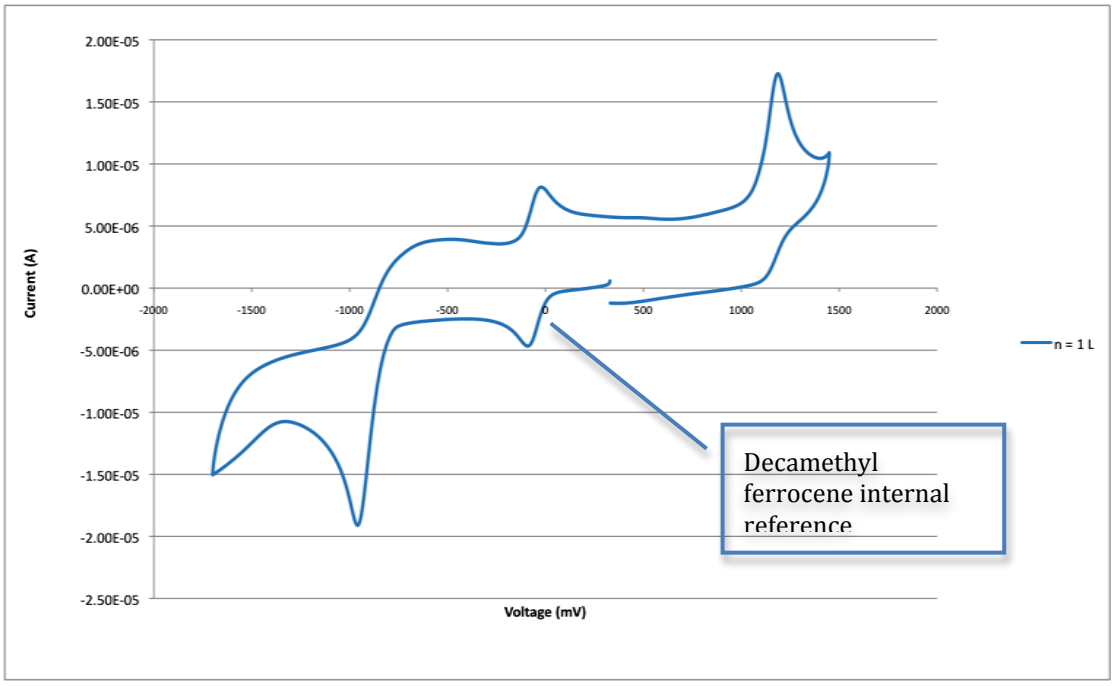

Fig. 87 Cyclic Voltammogram of n = 1 L anthracene monomer in dry acetonitrile with 0.1 M $TBAPF_6$ as the electrolyte and $Ag/AgCl_{2(aq)}$ as the reference, scan speed 1000 mV/s

3.7.3.2 Oxidation of anthracene

A peak was observed in the voltammogram at + 1.2 V (vs. $Ag/AgCl_{2(aq)}$ converted to 1.21 vs. SCE) and this was believed to be the due to the one-electron oxidation of anthracene as no equivalent peaks were observed in the solvent CV and the intensity was observed to increase as more anthracene monomer was added, both in the DMT protected form and in the unprotected diol. This value is in reasonably close agreement with literature values for similar compounds.[45]

3.7.3.3 Reduction of anthracene

A second peak was observed at -0.95 V (-1.14 V vs. SCE), which could correspond to the reduction of anthracene but could not be conclusively assigned. The peak is located in the region where the reduction of water in acetonitrile would be expected, however, upon addition of molecular sieves the peak was not seen to diminish and upon further addition of monomer the peak was seen to increase in

proportion to the oxidation peak. Examination of the literature shows that measuring this value is difficult due to the fact that it undergoes rapid dimerisation upon oxidation.[46, 47] A literature search of similar compounds shows that the reduction peak is expected to be at a lower voltage, around -2.2 V (-2.28 vs SHE).

It was decided to use the literature value for methoxy anthracene and applying these values to ΔG calculations.

3.7.4 Applying cyclic voltammetry to anthracene modified DNA

Much consideration was given to which values of electrode potentials for the nucleobases to use. This is a highly complicated and continuously evolving field in which a great variety of techniques have been applied to solve the problem but at the same time, generating wide range of results. Recent literature in the field takes data from the work of Seidel[29] or Steeken.[48, 49] Further theoretical work has been undertaken by Crespo-Hernandez and co-workers.[31] Although none of the values agree in an absolute sense for a number of reasons,[50] the order is consistent throughout. Therefore the values of Steenken were used for the calculations (a worked example is shown in Appendix 4).

Table 23 ΔG^{o}_{ET} values for anthracene-nucleobase complexes

Nucleobase	ΔG^{o}_{ET}(eV)	Effect Of ET On Base
Guanine	0.0085	Oxidation
Adenine	1.36	Oxidation
Cytosine	-0.45	Reduction
Thymine	-0.45	Reduction

Application of the Rehm-Weller equation therefore gives an order of ΔG^{o}_{ET} of T ~ C > G >> A (Table 23) where C and T are reduced whilst G and A are oxidised (Fig. 88).

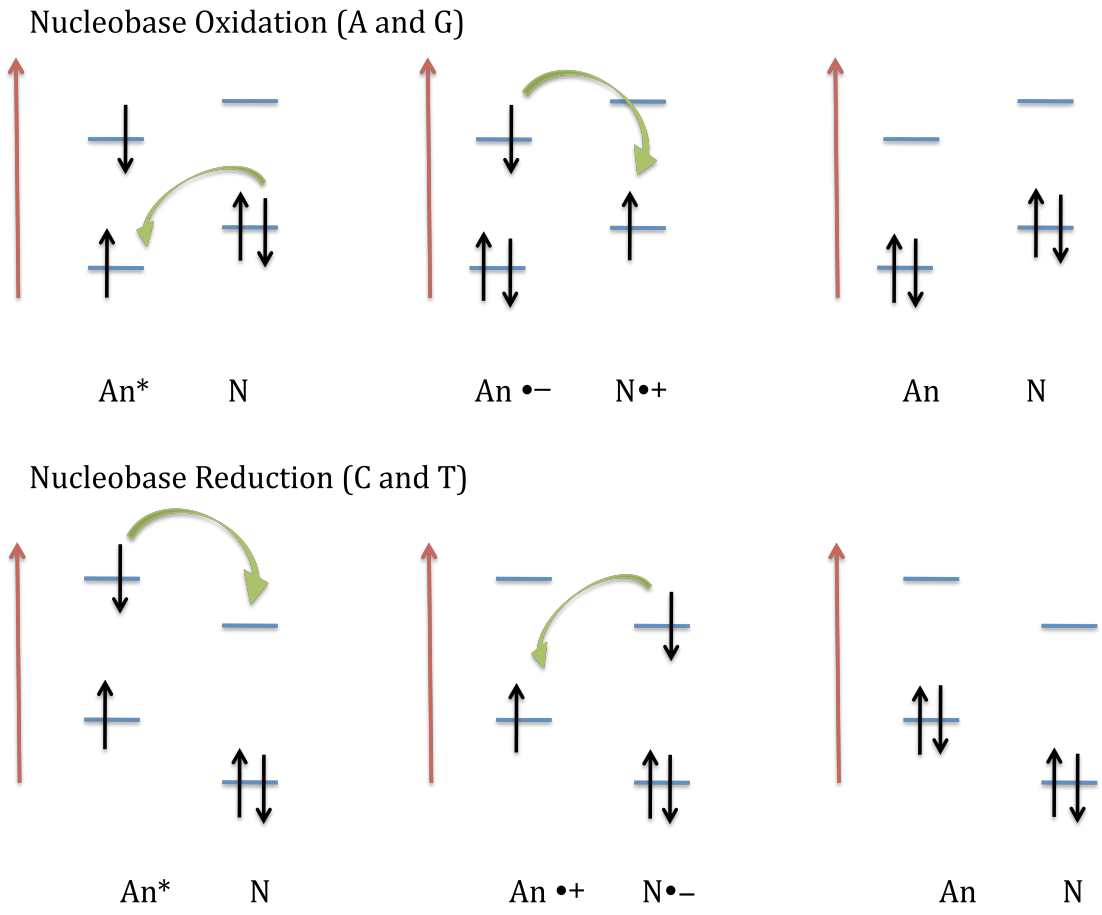

Fig. 88 Schematic representation of electron transfer processes between anthracene and adjacent nucleobases An* is the excited state of anthracene, N is the nucleobase being oxidised or reduced

However, this does not offer an explanation of the order of quenching observed in our anthracene mismatch sensing systems (base opposite or deletion). This suggests that further factors need to be considered.

3.7.5 Solvation and acid base effects on ΔG°_{ET}

Although the equation predicts the reduction of T to be as favourable as C due to the similar reduction potentials, it does not consider the potential effect of protonation of the electron adduct of cytosine. The subject has been extensively looked at by Steenken and co-workers[48] and the important concept is that the electron adduct of C is protonated (probably at N3), even up to pH 13.

It can be shown that the tendency for $C^{\bullet -}$ to be protonated by G in DNA is larger by a factor of $10^{4.5}$ compared to water and greater by more than 10 orders of magnitude than T being protonated by A. This is due to the differences in p*K*a between the different base pairs when a pyrimidine is reduced which show that G, with a p*K*a of 9.5 is a relatively strong acid and $C^{\bullet -}$ is a strong base (pKa >13) giving a ΔpKa (G/C(H)$^{\bullet}$) < -3.5. This means that in DNA the N1 proton of guanine will be pulled over to the N3 of cytosine as shown below (Fig. 89):

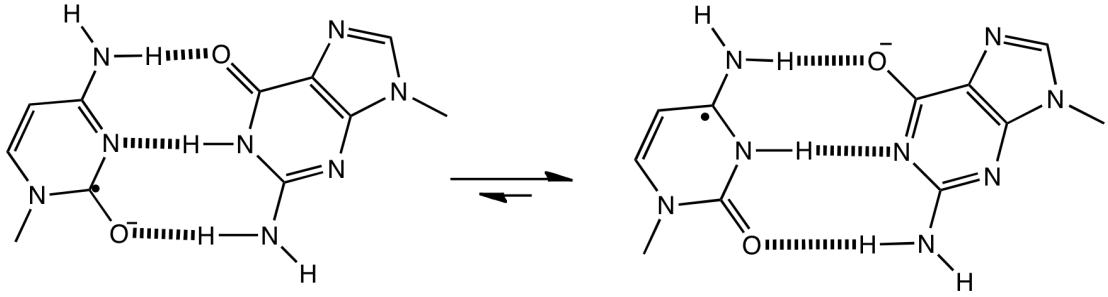

Fig. 89 Protonation equilibrium for C•-G

In contrast, with the AT pair the situation is very different as $T^{\bullet -}$ is a weak base (pKa (T(H)$^{\bullet}$=6.9) and A is a very weak acid (pKa > 13.75) giving a ΔpKa (A/T(H$^{\bullet}$) > 6.85 and therefore the following equilibrium(Fig. 90):

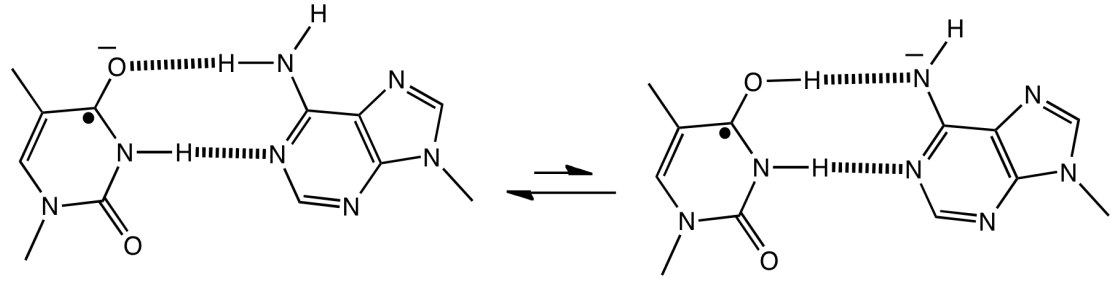

Fig. 90 Protonation equilibrium for T• -A

Although these p*K*a values do refer to aqueous solution and therefore include the free energies of hydration for the proton exchange species, since all reactions are

in the same environment these cancel out and we can assume that the Δp*K*a values quantitatively reflect the proton transfer equilibria under non-aqueous conditions.

The ΔΔp*K*a result of 10.45 can be considered as a 0.59V driving force for the protonation of $C^{\bullet -}$ compared to $T^{\bullet -}$ in their Watson – Crick base pairs. As a consequence of the increased driving force for protonation of $C^{\bullet -}$ there is an increase in the reduction potential of C relative to T. As a result C becomes the most easily reduced base and hence, as has been discussed above, is the best quencher. This is could be due to the fact that the protonated radical GC pair G-CH• is a poor conductor of electrons.[51] Indeed this result is observed for pyrene in the work carried out by Netzel.[33]

3.7.6 Applying protonation effects to mismatch sensing for the base opposite system

Understanding of the role of proton transfer in affecting the reduction potential can lead to an explanation for the difference in fluorescent emission for the mismatch sensing (Table 24). The fluorescent emission varies upstream of the probe as illustrated below with a decrease for a C to G matching pair, a large increase for a C to C mismatch, a comparable increase for a C to A mismatch and a slightly smaller increase for a C to T mismatch.

However, this order cannot yet be fully rationalised by considering the order of quenching that we have proposed that takes into account protonation effects.

Table 24 L Isomer PrA upstream variation

		3'GAG	CAG	TAG	AAG
		A1	E1	F1	G1
n = 1 L Pr A	5' CLC	**-75**	**86**	**45**	**70**

However, if one considers that when a mismatch occurs there is no longer a ready source of protons (from G) then according to the ΔG^{o}_{ET} values C is no longer a good quencher. If it can be proven that the anthracene is closely located near to the upstream base, and this what we have inferred previously and is supported later with modelling (Chapter 4), then one can assume that a sudden decrease in the ability of C to accept electrons will lead to slower/no electron transfer[16, 52] and hence less quenching of the excited anthracene (Fig. 91). An alternative view is that the absence of the G-CH• base pair no longer acts as an electron trap.

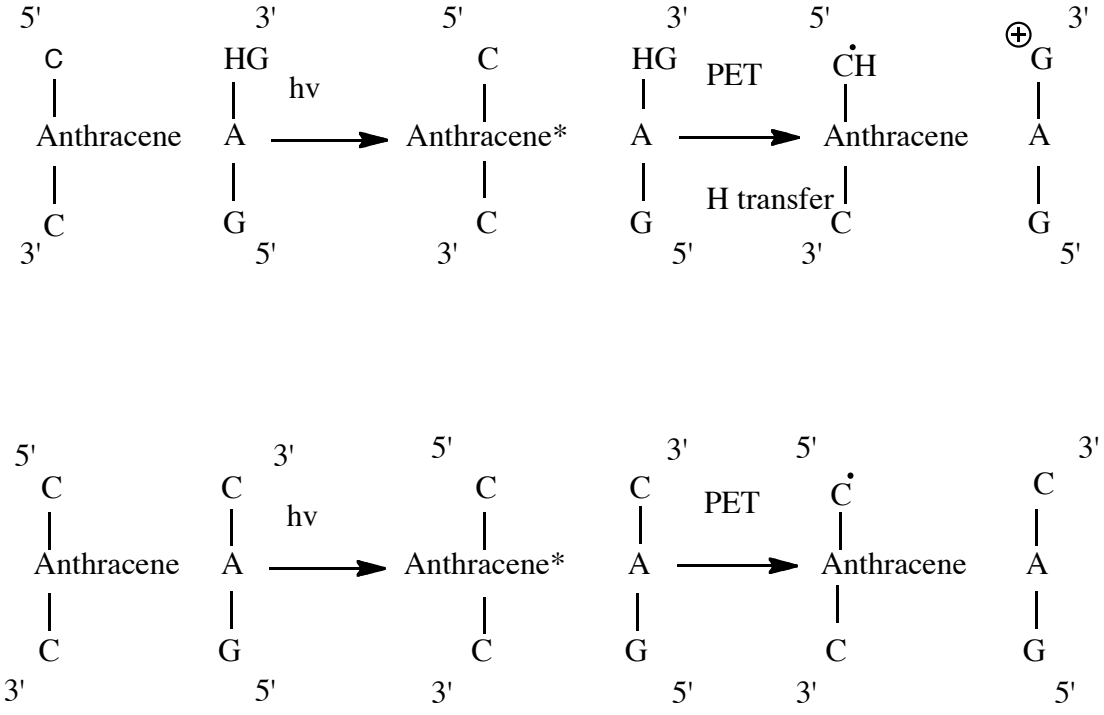

Fig. 91 Representation of the differences in quenching processes between C-G base pairs (top) and C-C mismatches (bottom)

Secondly, this allows us to consider the quenching ability of the new adjacent base. The same argument for poor quenching can be applied to the Target strand C (Target E1) and the ΔG^{o}_{ET} values show A (TarG1) to be a poor quencher, hence we can rationalise these combinations to be more emissive than that of T (TargetF1), which in the absence of a rapid proton source is thermodynamically the best electron acceptor and hence quencher. However, the greater proximity of a poorly quenching C is the dominant factor leading to the overall increase in emission.

In addition it should be noted that in the absence of a G to donate a proton, one of the protons may come from water. It has been shown by Geacintov and co-workers that quenching by C and T in water is still relatively efficient due to proton transfer from water compared to a polar organic solvent such as DMSO.[50] However, in the double strand form there will be considerably less water molecules available compared to the single strand form, due to the hydrophobic core of the duplex, so this could further inhibit the quenching of C. This would help explain why the quantum yield is greater in the mismatched double strand form than in the single strand form where there is also an absence of G but more available water molecules.

Finally, this hypothesis would also seem to correlate with the lifetime data discussed earlier which shows tri-exponential decay in the fully matching strand but only bi-exponential decay in the mismatched strand. The lifetime found to be no longer present was the shortest one which was attributed to rapid electron transfer between the anthracene and the neighbouring base i.e. static quenching.

If the previous arguments are correct then the most rapid pathway is no longer available and quenching has to take place utilizing electron transfer from the opposite base, which would be much slower, or dynamic quenching via the solvent.

3.7.7 PrG as an exception to the pattern

The noticeable exception to the trend of fluorescence is Probe G (5'TXC) with its matching targets. For this particular probe, hybridisation results in an increase in fluorescence for both isomers. This is the opposite of the trend observed for all of the other probes with matching targets. Furthermore, it is difficult to explain in terms of electron transfer, as T should be a good quencher. One of the other differences is that mismatches that result in an increase in emission for the other probes give a decrease with Probe G, again directly opposite to the general trends. It is possible that we are observing a structural effect as a consequence of anthracene being adjacent to a T base in the duplex, however further modelling studies will be required to fully examine this.

3.8 Excitation spectra of hybridised DNA

3.8.1 Excitation spectra for Probe A D and L

By scanning over the same range as for the UV spectra and monitoring at a wavelength in the emission spectrum, an excitation spectrum was produced for the two different stereoisomers of the duplex (Fig. 92) and compared with that of the anthracene monomeric unit **4** (green– not to scale) without DNA. The bathochromic shift from the unbound monomer to the duplex is clear, which

appears for reasons discussed later. There is also a substantial difference in the emission intensity at 260 nm between the D and the L isomers, with the D form excitation band being three times greater. This is in agreement with the quantum yield results discussed earlier (see 3.4.1.1).

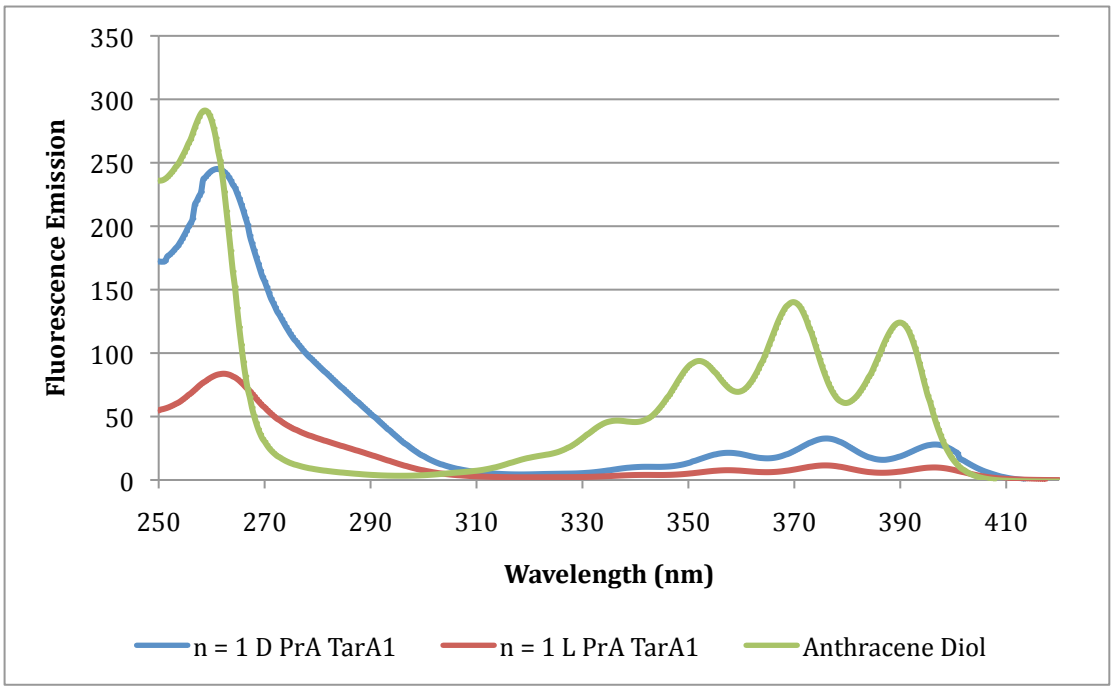

Fig. 92 Excitation spectra of anthracene in the monomeric and DNA bound forms monitored at 426 nm DNA at 1 μM oligonucleotide concentration 10 mM pH 7 phosphate buffer 100 mM NaCl monomer form at sat. concentration

The presence of a broad shoulder between 280 and 290 nm could be due to either a significant broadening of the anthracene ^1B_b band or energy transfer from the DNA to the anthracene.

3.8.2 Energy transfer bands in the excitation spectra

Kumar and co-workers have reported finding bands in the excitation spectra of DNA intercalated anthracene that have been assigned to the transfer of energy between DNA bases and the anthracene moiety. In particular they found that this band only appeared when the anthracene was bound to poly [dA-dT] sequences.[53]

Spectra were taken of the L isomer of Probe A (with CG base pairs on either side of the anthracene) and compared with the matching duplex of Probes F and G (both have an upstream A-T base pair). Examination of the spectra do not show a correspondingly well defined peak at 285 nm as seen by Kumar, however there is a pronounced shoulder in the correct area of the normalized spectra compared to the monomer anthracene (blue) (Fig. 93).

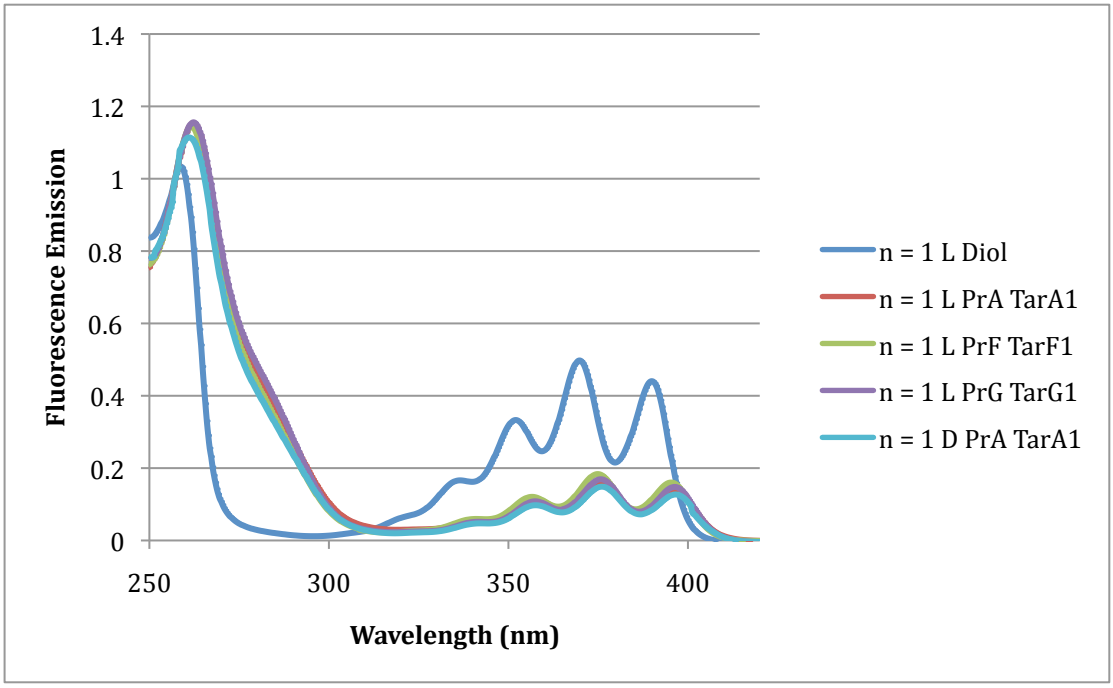

Fig. 93 Normalised excitation spectra of the L isomer 1 µM oligonucleotide concentration 10 mM pH 7 phosphate buffer 100 mM NaCl

Normalisation of the spectra and comparison of Probes of the different isomers and with different bases adjacent to the anthracene have shown no variation in this shoulder, contrary to Kumar's findings.

The most likely explanation is that energy transfer in such a system as Kumar's will go via a non-radiative dipole-dipole interaction or Forster mechanism,[6] which requires the correct orientation of the species to each other but means

that the donating base pair does not need to be adjacent to the anthracene. In Poly dA dT the system has a large potential number of donors (AT base pairs), hence there is a high probability that one with the correct orientation will be found. In our sequence there are far fewer base pairs that can overlap and hence it is much more unlikely that the energy transfer will occur.

3.9 Absorption Studies

3.9.1 Changes In the anthracene absorption spectrum

The incorporation of anthracene into DNA causes a number of changes in the absorption spectra much as it does with the emission spectra. Incorporation of an anthracene-o-alkoxy subunit (blue - peaks at 350, 367 and 388 nm) into DNA leads (green line) to a bathochromic (red) shift of 3 nm with the anthracene modified DNA displaying peaks at 353, 370 and 391 nm.

Duplex formation (red line) gives rise to hypochromicity (absorbance decrease) upon incorporation into DNA and a further bathochromic shift of the same amount (Fig. 94).

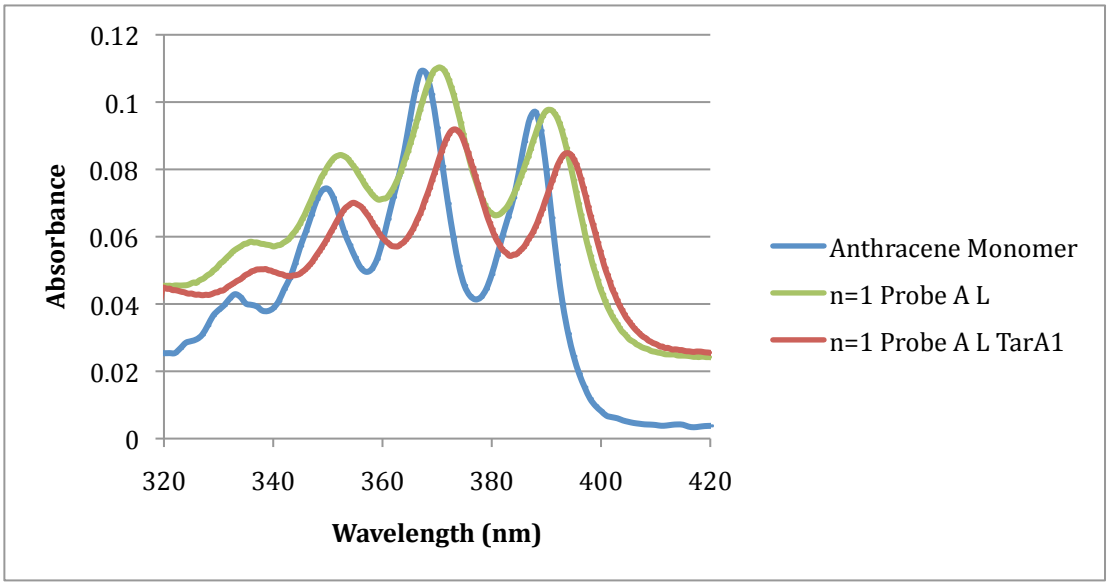

Fig. 94 Comparison of unincorporated single strand and anthracene tagged DNA 5 µM oligonucleotide concentration 10 mM pH 7 phosphate buffer 100 mM NaCl monomer 56 µM in water

The bathochromic shift is consistent with work by other groups that have studied a number of systems whereby aromatic molecules were incorporated into DNA.[32, 54-56] In particular Kumar has studied the interaction of the anthracene derivative of 1,8-octyldiamine (AODA) with ct-DNA and the effect the binding has on the spectroscopic properties of the anthracene and has observed comparable shifts, although a greater degree of hypochromicity.[56]

The groups have not completely ascribed the same explanation to the observed phenomena. Sarkar and co-workers have explained the shift in terms of a change of the local polarity around the chromophore, which affects the stabilization of its different energy levels. With a decrease of the local polarity as a consequence of interaction with base pairs compared to the bulk water solvent, the energy gap between the highest occupied molecular orbital (HOMO) and the lowest-unoccupied molecular orbital (LUMO) of the chromophore is decreased. This in turn leads to the shift towards absorption at longer wavelengths.[55]

The work of Kumar shows that the binding of anthracene to DNA, observed by Isothermal Titration Calorimetry (ITC), is exothermic and stabilizes the HOMO of the incorporated anthracene relative to the free species. The red shift in the absorption spectrum therefore implies that the binding to DNA stabilizes the first excited state of the Probe to a greater extent than the ground state (Fig. 95).

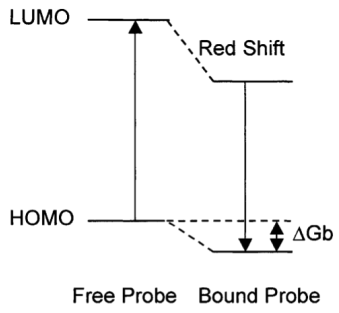

Fig. 95 Energy level diagram for the electronic transitions of the free and bound probe

However, the work of Asanuma[54] suggests that exiton coupling of natural nucleobases with intercalated chromophores can also contribute to the red shifting of the spectrum.

Kool and co-workers observed a slightly stronger red shift with neighbouring purines compared to pyrimidines. This effect is also apparent with the anthracene probes (see below) and can be explained by more favourable stacking between the anthracene and the larger aromatic systems of the purines and consequent greater hydrophobicity when forming ground state complexes.[16]

3.9.2 Hypochromism

Based on the UV absorption measurements the degree of hypochromism can be calculated and expressed as a percent hypochromism (%H). It was calculated according to the following equations.

$$A = \int \varepsilon(v) \partial v$$

Equation 16

$$H\% = \left(1 - \frac{A_{ds}}{A_{ss}}\right) 100$$

Equation 17

Where ε is the extinction coefficient of anthracene at a defined wavenumber. The calculation was performed in the region of 320-415 nm responsible for the S_0 to S_1 transition.

Table 25 Hypochromicity of PrA L duplexes 20 µM 10 mM pH 7 Phosphate buffer 100 mM NaCl

Sequence	Hypochromicity %
***n* = 1 L PrATarA1**	**9**
***n* = 1 L PrATarA2**	**20**
***n* = 1 L PrATarD1**	**15**
***n* = 1 L PrATarG1**	**21**
***n* = 1 L PrATarG2**	**4**

Generally, it appears that the hypochromicity is greater for purines than pyrimidines, which can be explained by considering the greater aromaticity of purines versus pyrimidines.

The greater hypochromism of the matching deletion strand (PrATarA2) compared to the base opposite matching sequence (PrATarA1) may be a consequence of the anthracene being more tightly held in the duplex.

3.10 Melting points

UV melting point experiments involve studying the UV absorption of DNA under heating and cooling conditions. The midpoint temperature for melting DNA, T_m, is the temperature at which half of the DNA present in solution is denatured upon heating (see 1.1.1 for a discussion of the factors that affect the T_m). It is

usually higher than the annealing temperature, T_a, reflecting the differences in the structure and mechanism of half-melted and half-renatured DNA. Although the melting of DNA is thought of as the breaking of hydrogen bonds, it is in fact the loss of base-stacking that can be used to monitor the process using absorption spectroscopy to detect the hyperchromicity effect of denaturing. As the DNA maximum of absorption is at 260 nm, this is where the DNA absorption is measured over changing temperature – this has the additional benefit of overlapping with the anthracene ^1B_b band giving a stronger signal. An example is given below (Fig. 96) where the blue curve is the T_m and the red curve the T_a:

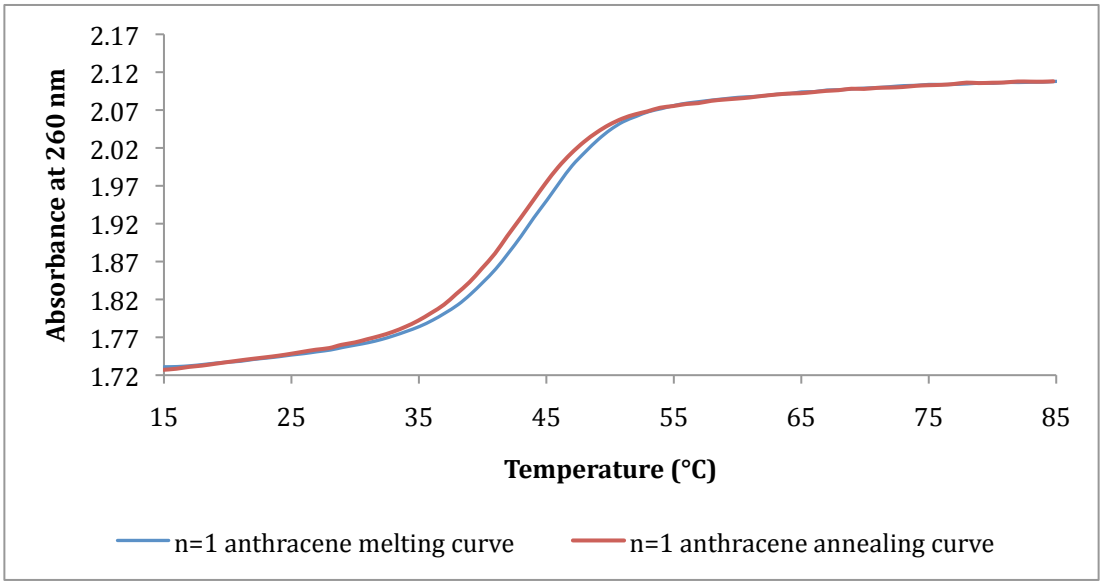

Fig. 96 Example of a DNA UV variable temperature experiment to determine the melting temperature of the DNA strand Probe A Tar G1. Strand concentration is 5 µM with 10 mM pH 7 phosphate buffer and 100 mM NaCl in water

Melting point studies were performed on a selection of oligonucleotides, in particular matching strands and mismatches of Probe A in order to determine whether there was a correlation between a change in the melting point and any changes in fluorescence emission. All results are presented together in Appendix

3. Selected data is presented throughout the subsequent sections in order to illustrate the findings.

Firstly, melting point temperatures were obtained for unmodified DNA (Table 26) in order to determine the effect on duplex stability of covalently attaching an anthracene moiety.

3.10.1 Studies on unmodified DNA

Table 26 Melting points of unmodified DNA oligonucleotides (°C) 5 μM with 10 mM pH 7 phosphate buffer and 100 mM NaCl

Target Strand	A1	B1	C1	D1	E1	F1	G1
	3'GAG	GAC	GAT	GAA	CAG	TAG	AAG
Tar MT 5'CTC	**55**	**36**	**41**	**42.5**	**41.5**	**42.5**	**42**
Tar MA 5'CAC	**54**	**34.5**	**41**	**40.5**	**40**	**41.5**	**46**

Two different duplex types were investigated. Firstly, the fully matching duplex (native strand) was examined – TarMTTarA1- in order to establish a value for unmodified fully binding DNA. Since anthracene cannot hydrogen bond one might expect this value to be higher than can be achieved with any of our probes, although much recent research has cast doubt on the importance of hydrogen bonding in duplex stability.[57] Secondly, a strand with an adenine instead of the anthracene (Tar MA) was tested in order to determine whether anthracene offers more stabilisation via π-stacking (unmodified strand). As would be expected, the duplexes with a central A-A mismatch (TarMATarA1) have a lower melting point than the fully matching duplex (TarMTTarA1) due to the loss of hydrogen bonding between the central A-T base pair, but the difference is not very significant.

The effects of mismatching unmodified DNA under the same conditions as our L and D isomer modified duplexes were also investigated.

The relative order of stability of mismatches (Table 26) can be considered in terms of a number of factors. For instance, a C to C mismatch (with Target E1) is the least stable mismatch because there is poor stacking stabilisation due to the presence of two pyrimidines and only one hydrogen bond.[58]

Although there is little literature comparing CC, CT and CA mismatches, the difference in stability between CT and CA mismatches is well studied and the CT mismatch is known to be the most destabilising of the two as a result of poor stacking from two pyrimidines.[59]

3.10.2 Studies on anthracene modified DNA – modifying the opposite base for L and D

The next sequences to be examined were the matching sequences with the base opposite the anthracene varied (Table 27).

Table 27 Melting points of Probe A (°C) with varied opposing bases 5 μM with 10 mM pH 7 phosphate buffer and 100 mM NaCl

Target Strand	A1	A3	A4	A5
	3'GAG	GTG	GCG	GGG
Tm *n* = 1 Pr A L	**54**	**55**	**55**	**55**
Tm *n* = 1 Pr A D	**48**	**48**	**46**	**48**

These results provide us with a number of interesting observations. Firstly, it would appear that varying the base opposite the anthracene has no major effect on the melting point in much the same way as there is no effect upon fluorescent emission.

Secondly, on average, the L isomer probe (Table 27) has a melting point that closely approximates that of unmodified DNA (Table 26) indicating that anthracene can, presumably via π-π-stacking, provide a greater or equal degree of stabilisation compared to a normal base in a mismatch situation. This would suggest that the anthracene is intercalating into the duplex – a phenomenon that is well documented in the literature.[56, 60] The reasons for this will be discussed later in section 3.10.5.3. Conversely, the D isomer appears to destabilise the duplex, which strongly suggests that not only is the anthracene not intercalating, but that it may be interfering with the normal base pairing interactions, perhaps by inserting itself into one of the DNA grooves.

3.10.2.1 Melting point at 370 nm

The Probe A (L) TarA1 duplex was also examined at the anthracene ^1L_a absorption band at 370 nm (Fig. 97) and a melting point was calculated from the data.

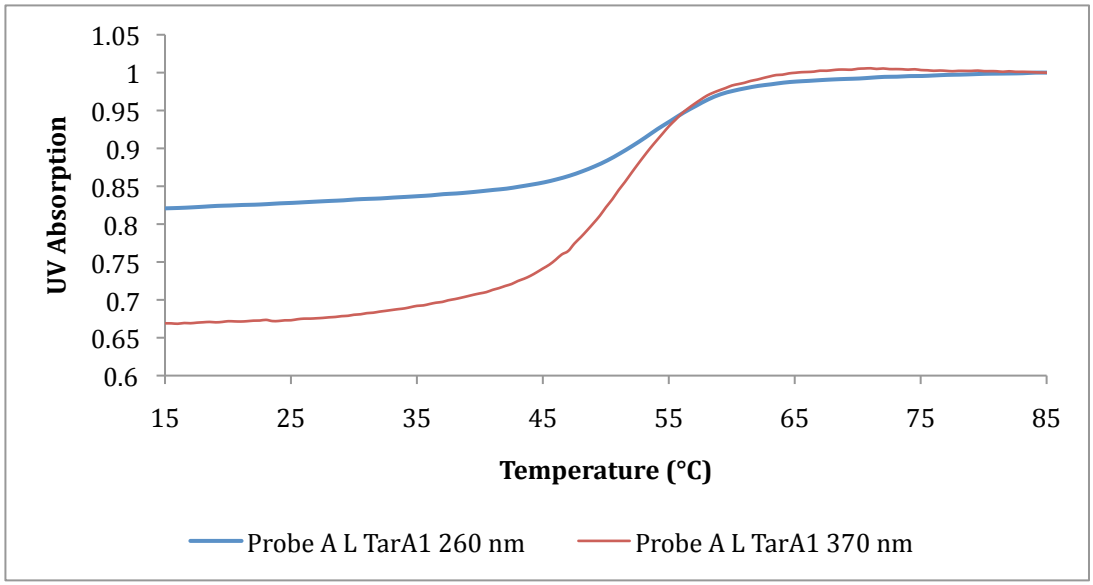

Fig. 97 Melting point curves for Probe A L TarA1 at 370 nm and 260 nm 20 µM and 5 µM respectively with 10 mM pH 7 phosphate buffer and 100 mM NaCl

The thermodynamic behaviour at 370 nm, giving a melting point of 51 ˚C can be seen to be very similar to the behaviour at 260 nm. The difference in calculated T_m values (~ 3 °C) implies that anthracene de-intercalation is one of the first steps in the denaturisation of the duplex. Nonetheless, overall the data suggests that double strand formation/breakup and anthracene incorporation into/disassociation from the duplex are cooperative. Further investigations were performed upon the L duplex in order to better understand the absorption photophysics of attaching an anthracene to an oligonucleotide.

3.10.2.2 Examining the ^1L_a anthracene absorption region at different temperatures

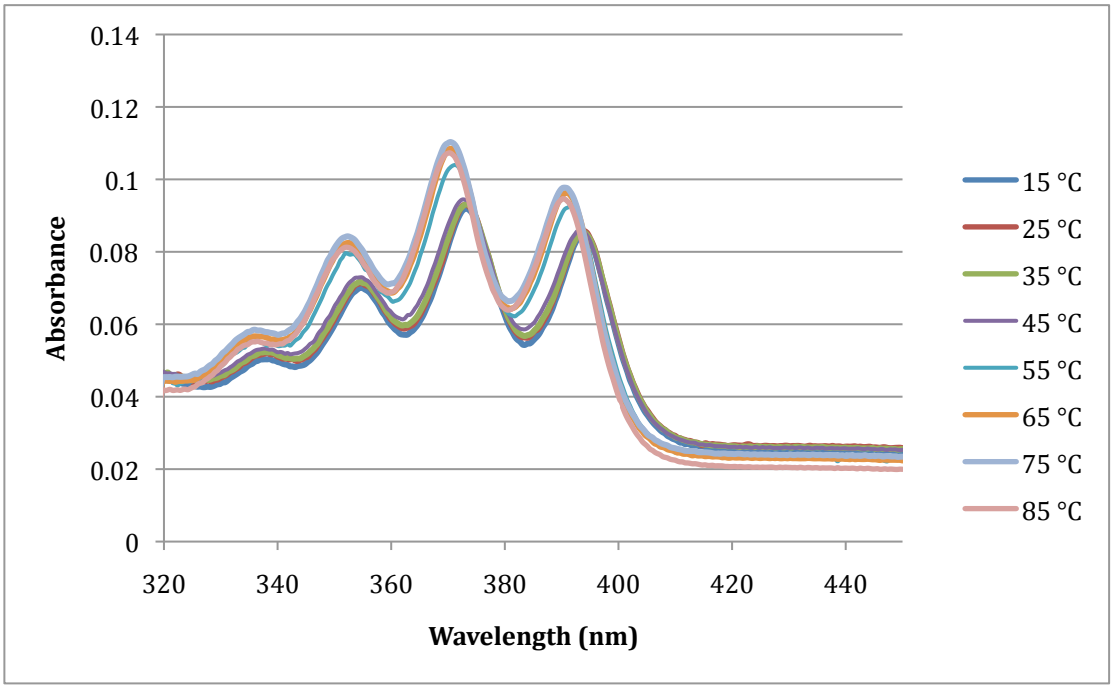

Fig. 98 Probe A L Target A1 duplex UV spectrum at different temperatures 5 µM with 10 mM pH 7 phosphate buffer and 100 mM NaCl

The above chart (Fig. 98) depicts the effect of increasing temperature on the modified DNA duplex. It suggests that the transition from double to single stranded form begins at between 35 and 45 ˚C and is complete between 55 and 65 ˚C. This is in keeping with the recorded melting point of 54 ˚C.

3.10.3 Melting points of different matching Probe duplexes

Following this the scope of the investigation was extended to all of the *n* = 1 chain probes and the melting points at 260 nm are displayed below in graphical form (Fig. 99).

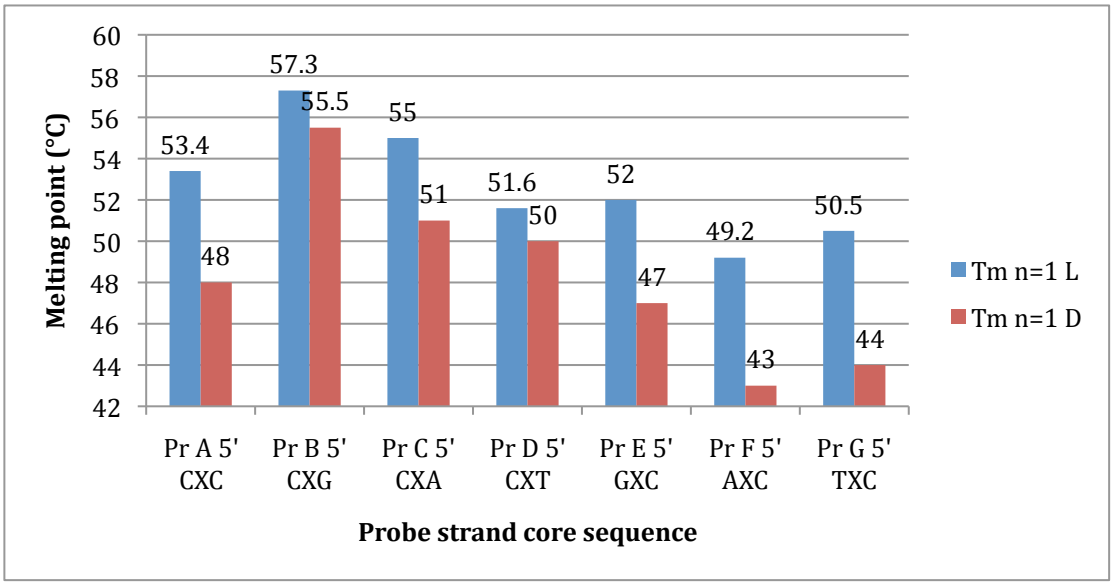

Fig. 99 Comparison of the melting points of *n* = 1 D and L Probes base opposite system 5 µM with 10 mM pH 7 phosphate buffer and 100 mM NaCl

It is apparent that the observation above that the L isomer stabilises the duplex relative to the D isomer still holds true even if the bases surrounding the anthracene are varied. The overall trend also appears to be related to whether the flanking bases are GC or AT pairs. However, another important factor appears to be whether the anthracene is flanked by a purine or a pyrimidine. In the situations where the downstream base is varied we can see that this is a more important factor than the number of hydrogen bonds (Table 28).

Table 28 Melting points of matching duplexes (°C) of different Probes with modified downstream base 5 µM with 10 mM pH 7 phosphate buffer and 100 mM NaCl

Pr A 5' CLC	**53.4**	Pr A 5' CDC	**48**
Pr B 5' CLG	**57.5**	Pr B 5' CDG	**55.5**
Pr C 5' CLA	**55**	Pr C 5' CDA	**51**
Pr D 5' CLT	**51.5**	Pr D 5' CDT	**50**

Where the downstream base flanking the anthracene is a G or A (in Probes B and C), in other words a purine, the melting point is higher. This is contrary to what would be expected by solely considering the number of hydrogen bonds where Probes containing more C and G bases (Probes A and B) should have the highest melting point.

There are a number of factors that affect the strength of the stacking interaction with planar attached aromatic molecules and these have been compiled and studied by Kool and co-workers who measured the stacking energy of a number of natural and non-natural bases upon duplex formation.[61] They studied the following factors:

1. Hydrophobicity (represented by the log P (octanol-water))
2. Polarizability ($Å^3$)
3. Dipole moment (debye)
4. Stacking area (measured in $Å^2$ and estimated from modelling studies)

These factors were all plotted against the ΔG° of stacking and examined for signs of correlation. Both hydrophobicity and dipole moment show no real relationship. The polarizability shows a suggestive link with the stacking energy but the trends are inconclusive. However, there was shown to be a good correlation with the stacking surface area. Small molecules that are likely to have the smallest overlap (e.g. pyrrole) stack the least strongly while pyrene, with a large area of overlap, stacks the most strongly.

If this is applied to the downstream base variation then the order is seen to follow that of base area with the purines stacking more strongly than the pyrimidines.

Table 29 Estimated stacking areas for nucleobases with non natural aromatic base[61]

Base	Stacking Area
Thymine	95 Å^2
Adenine	128 Å^2
Cytosine	102 Å^2
Guanine	139 Å^2

The above (Table 29) gives the stacking areas for the bases with pyrene. Whilst the absolute values for anthracene are expected to be different, the same trend should apply. Thus, it appears that the differences in melting point are as a result of the different stacking areas of the bases.

Analysis of the upstream variations of the bases does not show the same variation with a consistent variation of C / G > T / A adjacent to the anthracene that would be broadly expected based on the strength of hydrogen bonding (Table 30).

Table 30 Melting points of matching duplexes (°C) of different Probes with modified upstream base 5 µM with 10 mM pH 7 phosphate buffer and 100 mM NaCl

Pr A 5' CLC	**53.5**	Pr A 5' CDC	**48**
Pr E 5' GLC	**52**	Pr E 5' GDC	**47**
Pr F 5' ALC	**49**	Pr F 5' ADC	**43**
Pr G 5' TLC	**50.5**	Pr G 5' TDC	**44**

This would suggest that these bases interact differently with the anthracene to the downstream bases, something that is seen in the fluorescence results.

3.10.4 Conclusions on the melting points of fully matched duplexes

It was noted earlier that the anthracene L isomer can significantly stabilise a duplex. The analysis above shows that the different melting points of the Probes are a consequence of both different stacking areas and amount of hydrogen bonds.

3.10.5 Mismatched duplexes melting temperatures

Mismatched duplexes were created as before using Probe A and different target strands.

3.10.5.1 Downstream mismatches

The first to be investigated were downstream mismatches that, in absolute terms, gave a similar pattern to the fully matching strands, namely that the L isomer was approximately 5 °C more stable than the D isomer. Furthermore, compared to the A to A mismatched unmodified oligonucleotides (Table 26) the presence of anthracene appears to be stabilising in the L isomer but destabilising in the case of the D isomer by approximately 4 °C and 2 °C respectively (Table 31).

Table 31 Melting points of downstream mismatches (°C) of Probe A 5 μM with 10 mM pH 7 phosphate buffer and 100 mM NaCl

Target Strand	B1	C1	D1
	GAC	GAT	GAA
Tm n=1 Pr A L	**39.8**	**44.4**	**44.6**
Tm n=1 Pr A D	**35.5**	**39.5**	**37.5**

However, there is a noticeable decrease in the melting point for duplexes with the GAC strand for the L isomer. This may be a structural feature as the decrease is approximately equal to the loss of one hydrogen bonding base pair. The variation in the D isomer duplexes may be due to non Watson-Crick hydrogen bonds being formed that stabilise some mismatches more than others.

3.10.5.2 Upstream mismatches

Analysis of the upstream mismatches shows them to have considerably less variation than the downstream mismatches which would be expected as the amount of hydrogen bonding should be identical (Table 32).

Table 32 Melting points of upstream mismatches (°C) of Probe A 5 µM with 10 mM pH 7 phosphate buffer and 100 mM NaCl

Target Strand	E1	F1	G1
	CAG	TAG	AAG
Tm *n* = 1 Pr A L	**44.3**	**44.6**	**46**
Tm *n* = 1 Pr A D	**36.5**	**35**	**35**

3.10.5.3 Conclusions

There are two other main issues to consider when evaluating all of the data together. Firstly, there is the issue of whether the melting point results inform us of any stability changes as a result of attaching an anthracene moiety to the duplex. The second point is how the melting points relate to the changes in fluorescence. The table below (Table 33) compares the change in fluorescence upon hybridisation to the difference in melting point between the anthracene modified DNA and the unmodified DNA with adenine substituted for the anthracene (From Table 26). Thus, solely the effect of having a non-nucleosidic anthracene base instead of an adenine residue is observed.

Table 33 Change in fluorescence compared to change in melting point (°C) for Probe A L base opposite duplexes 5 µM with 10 mM pH 7 phosphate buffer and 100 mM NaCl

		A1	B1	C1	D1	E1	F1	G1
		3'GAG	GAC	GAT	GAA	CAG	TAG	AAG
Δ Fluorescence (%)	PrA 5' CLC	**-75**	**-75**	**-75**	**-55**	**86**	**45**	**70**
Δ Tm (Anthracene mod.-unmod.)	PrA 5' CLC	**-0.6**	**5.3**	**3.3**	**4.1**	**4.3**	**3.1**	**0**
Δ Fluorescence (%)	PrA 5' CDC	**-72**	**-54**	**-73**	**-56**	**-68**	**-52**	**-61**
Δ Tm	PrA 5' CDC	**-6**	**1**	**-1.5**	**-3**	**-3.5**	**-6.5**	**-11**

What we see from the table above are a number of effects:

1. The L isomer destabilises the duplex relative to an A to A mismatch to a much lesser extent than the D isomer. This suggests that anthracene attached to the L isomer is as effective a stabilizer as a non hydrogen bonding adenine, probably due to the similarly large surface areas.
2. The L isomer downstream mismatches do not stabilise the duplex relative to unmodified DNA more than the upstream mismatches. Conversely, for the D isomer the upstream mismatches appear to destabilise the duplex more than the downstream ones. These effects would seem to run contrary to the assumption that when the fluorescence is quenched it is as a result of the anthracene π-stacking more with the duplex as this should lead to greater stabilisation and a resultant higher melting point. Clearly the DNA structure is not the most important factor in affecting the fluorescence, further lending weight to the argument that it is the redox potentials of the bases that is important.

3. Anthracene stabilises the weakest mismatches more than stronger ones for both isomers. This can be seen in the order of stabilisation (ΔT_m) of C-C > C-T > C-A for all isomers and mismatches.

The work of Kool and co-workers shows that the overall stabilisation from aromatic molecules can be primarily attributed to solvent driven hydrophobic effects.[61] These arise from energetically unfavourable solvation of the flat aromatic surface undergoing stacking during helix formation. This tends to cause the system to minimise its contact with water by forming a duplex. However, the results above show that different structures (isomers, mismatches and flanking base combinations) allow different factors, such as base surface area and number of hydrogen bonds to determine the trends in melting points.

3.10.6 Observing duplex melting using variable temperature fluorescence

It is also possible to observe the effect of hybridization on fluorescence by heating the duplex up whilst irradiating (Fig. 100). This allows the effect of melting the duplex on quenching to be observed; in particular unlike UV melting the shape of the melting curve will depend on the fluorescent response of the Probe to being melted. As a result experiments using emission increasing (n = 1 Probe A Target G1) and emission decreasing (n = 1 Probe A Tar A1) duplexes were performed.

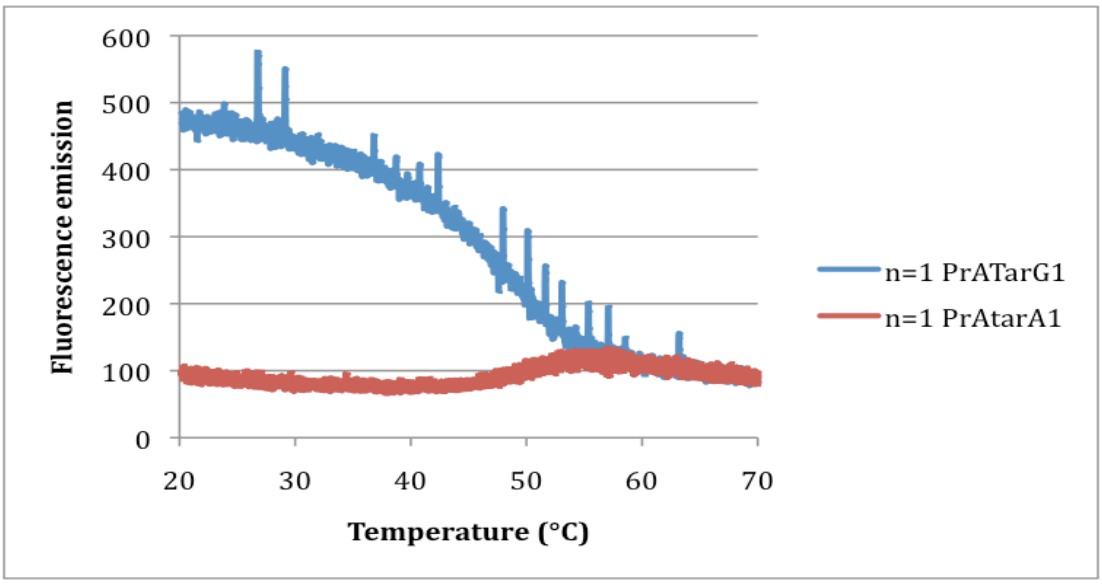

Fig. 100 Fluorescence emission at varying temperature λex 350 nm λem 426 nm 1 μM oligonucleotide concentration 10 mM pH 7 phosphate buffer 100 mM NaCl

Although the emission profile decreases slightly over time, probably as a result of photobleaching, it clearly shows a difference in the melting points between the matching (orange) and mismatching strands (red) where the mismatch has a lower melting point than the fully matching strand. The experiment also shows that the original fluorescence of the single strand Probe is restored upon melting.

3.10.8 Melting points of deletion sequences

Melting point experiments were again performed first with unmodified DNA with anthracene being replace by adenine as before however, in this case there was no base opposite which resulted in a wedge-type deletion structure.

3.10.8.1 Unmodified deletions sequences

As expected, given the loss of a hydrogen bonding pair and more importantly, base stacking interactions, the melting points were lower than in the previous experiments (with the exception of B2 vs. B1 – which appears to be abnormally low). The decrease was in agreement with the work of Bertrand et al.[62]

Table 34 Melting points (°C) Deletion system unmodified DNA (top) and base opposite sequence (bottom) 5 μM with 10 mM pH 7 phosphate buffer and 100 mM NaCl

Target Strand	A2	B2	C2	D2	E2	F2	G2
	3'G_G	G_C	G_T	G_A	C_G	T_G	A_G
Tar MA 5'CAC	**49.5**	**33**	**33.5**	**36.5**	**35.5**	**34.5**	**38**

Target Strand	A1	B1	C1	D1	E1	F1	G1
	3'GAG	GAC	GAT	GAA	CAG	TAG	AAG
Tar MT 5'CTC	**55**	**36**	**41**	**42.5**	**41.5**	**42.5**	**42**
Tar MA 5'CAC	**54**	**34.5**	**41**	**40.5**	**40**	**41.5**	**46**

Melting point experiments were run as before on the target sequences and compared with the base opposite equivalents both modified and non modified.

3.10.8.2 Melting points of fully matching deletion sequences

The results below show that the matching deletion sequences have a higher melting point than both native DNA and the base opposite sequences. In particular the L isomer has a melting point greater than that of a sequence with an extra hydrogen bonding pair which suggests a great deal of stabilisation results from the anthracene. This is a well studied phenomenon that was studied extensively by Tanaka and co-workers.[13] It has been explained in terms of π-π stacking energies that are not lost upon formation of the duplex, and consideration should also be given to the idea that there is now more room in the cavity for the anthracene and as such can engage in more π stacking with the adjacent bases.

Table 35 Melting points (°C) for modified DNA compared to unmodified for base opposite (1) and deletion systems (2) 5 µM with 10 mM pH 7 phosphate buffer and 100 mM NaCl

	A1	A2
	3'GAG	3'G_G
Pr A 5' CLC	**53.4**	**61**
Pr A 5' CDC	**48**	**53.5**
Tar MA	**54**	**49.5**
Tar MT	**55**	**n/a**

The enhanced stability of the deletion structure is a consistent feature throughout the different probes. The chart below (Fig. 101) shows that, with the exception of D isomer Probes B and D, the deletion form provides a significant enhancement to the melting point of the duplex of between 5 and 8 °C compared to the base opposite system.

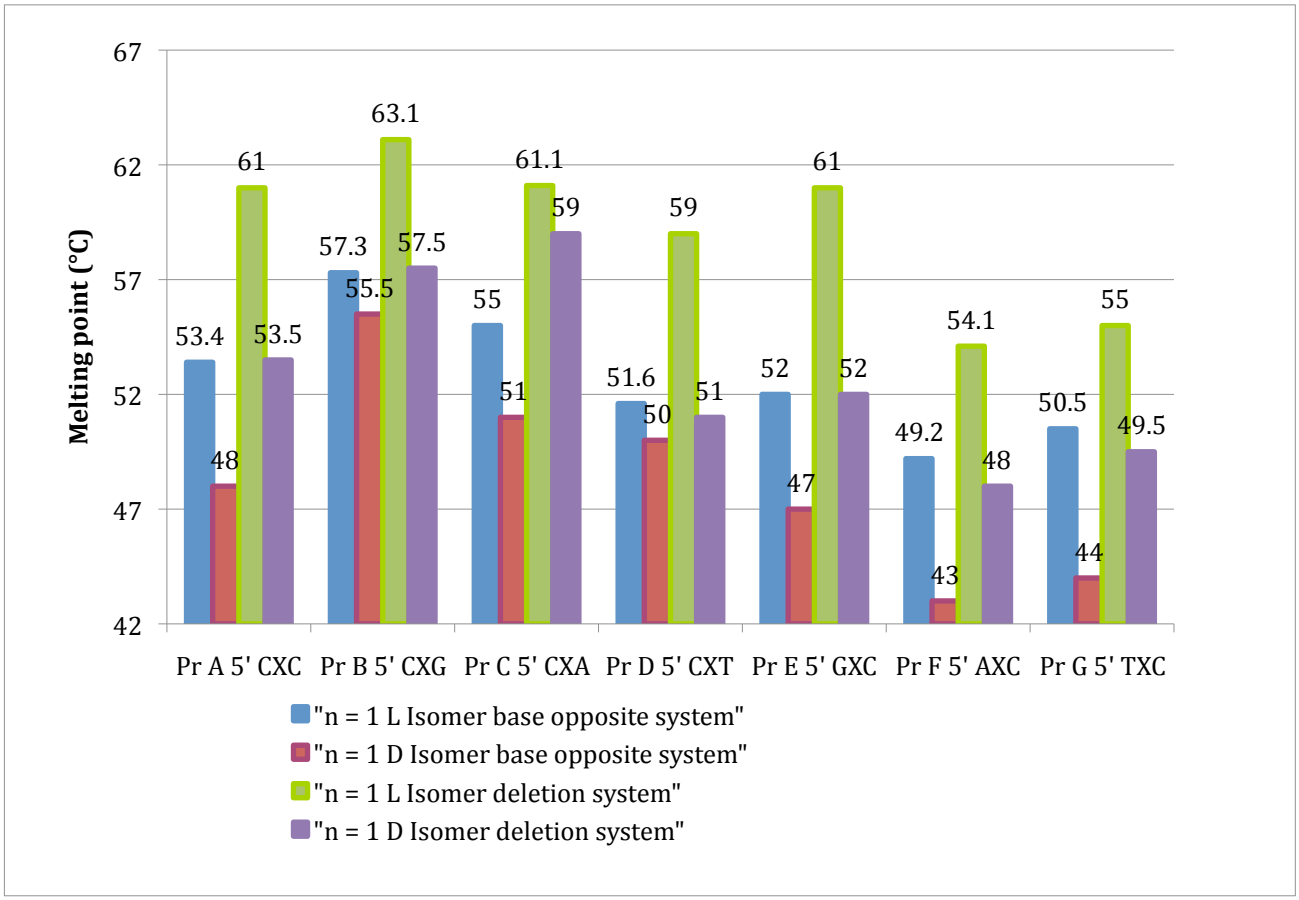

Fig. 101 Comparison of base opposite and deletion duplex melting points 5 µM with 10 mM pH 7 phosphate buffer and 100 mM NaCl

3.10.8.3 Mismatch deletion sequences

Further analysis of potential mismatch combinations with Probe A gave the following results.

Table 36 Melting points (°C) of deletion duplexes of PrA L 5 µM with 10 mM pH 7 phosphate buffer and 100 mM NaCl

Target Strand	A2	B2	C2	D2	E2	F2	G2
	3'G_G	G_C	G_T	G_A	C_G	T_G	A_G
Tm *n* = 1 Pr A **L**	**61**	**52**	**49.1**	**46.2**	**45.7**	**46**	**46.7**
Tm *n* = 1 Pr A **D**	**53.5**	**43**	**44.5**	**43.5**	**39**	**38.5**	**39.5**
ΔTm PrA **L** - unmodified MA	**11.5**	**19**	**15.6**	**9.7**	**10.2**	**11.5**	**8.7**
ΔTm PrA **D** - unmodified MA	**4**	**8**	**11**	**7**	**3.5**	**4**	**1.5**

Compared to a wedge structure of unmodified DNA the enhancement of stability is much greater (Table 36). Of further note is that the melting points of the upstream mismatches are lower for the D isomer than the corresponding downstream mismatches. This may be because, in its *RR* configuration the anthracene loses π-π stacking when upstream mismatches occur, leading to a less stable duplex.

3.11 Transient absorption spectroscopy

3.11.1 Introduction

If electron transfer is involved in the quenching process then it may be possible to observe evidence of the charged anthracene species using transient absorption spectroscopy. In this technique, a fraction of the molecules are promoted to an electronically excited state by means of an excitation (or pump) pulse. This is followed by a weak probe pulse that is sent through the sample

with a delay t. This probe pulse must be of low enough intensity that multiphoton/multistep processes are avoided. A difference spectrum, of the absorbance spectrum of the excited state minus the ground state absorbance spectrum (ΔA) is then calculated. By changing the time delay t between the pump and the probe and recording a ΔA spectrum every time, a profile of ΔA against t and λ is obtained (ΔA (λ,t)).

ΔA (λ,t) contains information on the dynamic processes that occur in photoactive systems such as energy migration, electron or proton transfers and intersystem crossing.

Generally, a ΔA spectrum contains contributions from four processes:

1. Ground state bleach: Due to the fact that a fraction of the molecules has been promoted to the excited state, the number of molecules in the ground state has been decreased and as a result the ground state absorption in the excited sample is less than the excited sample. The result is a negative signal observed in the wavelength region of the ground state absorption.
2. Stimulated emission: This appears only for optically allowed transitions and has a profile that follows the fluorescence spectrum of the excited chromophore. As stimulated emission results in an increase of light intensity on the detector, it gives a negative ΔA signal.
3. Excited state absorbance: Upon excitation by the pump pulse, optically allowed transitions from the excited state of a chromophore to higher excited states may occur and absorption of the probe pulse will occur at these wavelengths. This results in a positive signal in the ΔA spectrum.

4. Product absorption: After excitation of a photochemical system, reactions can occur that give rise to transient or long-lived molecular species such as triplet states, charge separated states and isomerised states. The absorption of such a product will appear as a positive signal in the ΔA spectrum.[63]

3.11.2 Results

In the anthracene-DNA system we would expect to see a signal for the Sn ← S1 excited state. If, as postulated earlier, electron transfer is involved in the quenching process, then we would expect to also see a signal corresponding to either the anthracene radical cation or the radical anion.

Work by Mataga and co-workers on 9-methyl anthracene have shown that the peak at 570 nm corresponds to the Sn ←S1 absorption of the locally excited (LE) anthracene. They also detected bands at 690 nm and 750 nm that were identified as the cation radical and anion radical of 9-methyl anthracene respectively.[64]

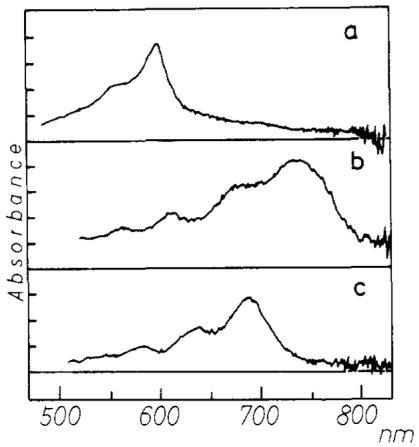

Fig. 102 Transient absorption spectra of the S1 state and the radical ions of 9-methyl anthracene (a) absorption spectrum of the Sn ←S1 spectrum in ethyl acetate (b) absorption spectrum of the anion radical in MeCN (c) absorption spectrum of the cation radical in MeCN[64]

The obtained spectrum of Probe A L TarA1 anthracene duplex showed the beginnings of a peak in the spectral wavelength area that would correspond to a radical ion (Fig. 103), suggesting the existence of a charged anthracene species and therefore of charge transfer in the system. Unfortunately, the equipment lacked the capability of monitoring the spectrum at higher wavelengths and as such the peak cannot be assigned to either the radical cation or anion.

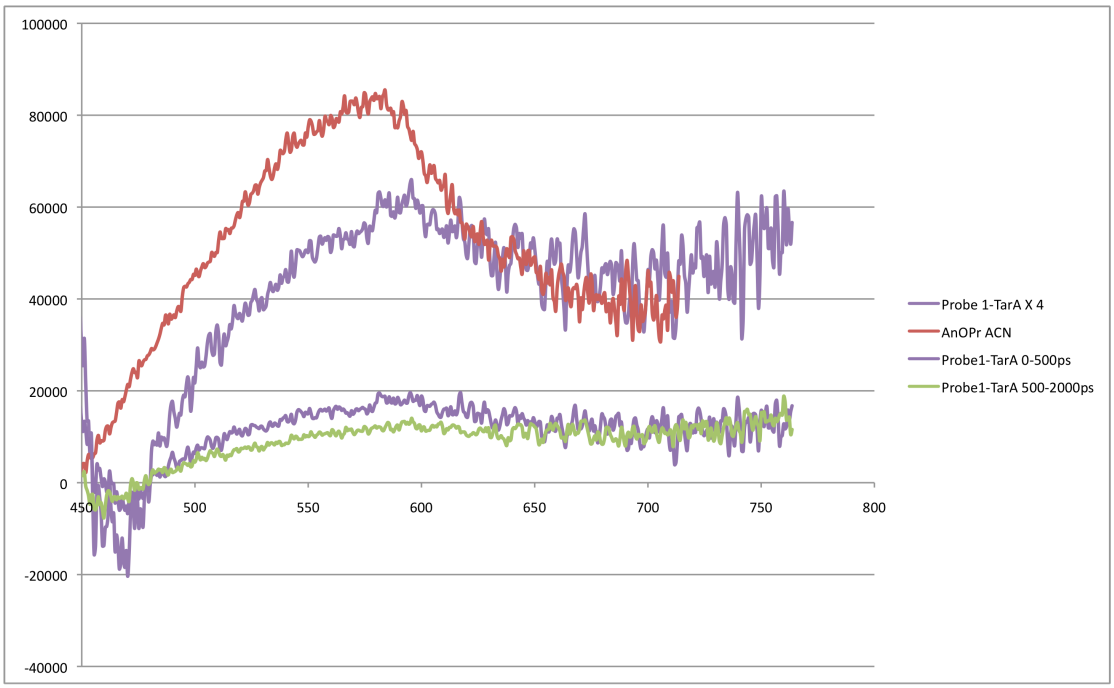

Fig. 103 Transient Absorption Spectra of Probe A L Tar A1 at 400 µM with 10 mM pH 7 phosphate buffer and 100 mM NaCl

Further studies are currently ongoing in order to expand the spectral window.

3.12 Circular Dichroism

3.12.1 Origin of the CD effect

Plane polarized light can be viewed as being made up of two circularly polarized components of equal magnitude, one rotating counter-clockwise (left handed, L) and the other clockwise (right handed, R). Circular dichroism refers to the difference in absorption of these two components. If plane polarized light is passed through a sample and the L and R components are not absorbed, or are absorbed equally, then upon recombination the light would be polarized in the original plane. However, if they are absorbed differently then the resulting recombined light is said to be elliptically polarized. A CD signal will be observed when a chromophore is chiral for one of three reasons:

1. It is intrinsically chiral because of its structure e.g. a C atom with four different substituents.
2. It is covalently linked to a stereogenic centre of the molecule.
3. It is placed in an asymmetric environment by virtue of the three dimensional structure adopted by the molecule.

A CD machine or spectropolarimeter measures the difference in absorption between the L and R circularly polarized components ($\Delta A = A_L - A_R$), but the resulting data is reported in terms of the ellipticity (θ) in degrees. The relationship between ΔA and ellipticity is $\theta = 32.98\ \Delta A$. A CD spectrum is measured as a function of wavelength.[65]

3.12.2 CD of anthracene in DNA

There are a number of advantages to studying the interaction of anthracene with DNA. Anthracene intercalation is predicted to give rise to signals in the CD spectrum that are reflective of the orientation of the anthracene relative to the base pair dyad axis.[60, 66] These signals can aid in explaining the observed emission and absorption results and in assigning the structure of the system. Intercalation is also known to cause unwinding of the helix, and DNA CD at 280 nm is known to be sensitive to this phenomenon. Since anthracene probes do not have any absorption in the 270-310 nm region one would expect no interference with the DNA CD at 280 nm.

3.13 CD of the single strand forms

Nucleic acids contain chiral nucleosides in the single strand form as a result of the C1' carbon on the sugar ring. Combined with the presence of a chiral threoninol unit this means this that a CD spectrum can be taken of the unhybridised strand. Given that the anthracene tagged oligonucleotides are expected to intercalate into the duplex,[1] it is reasonable to expect changes in the CD spectrum and indeed this is the case (Fig. 104).

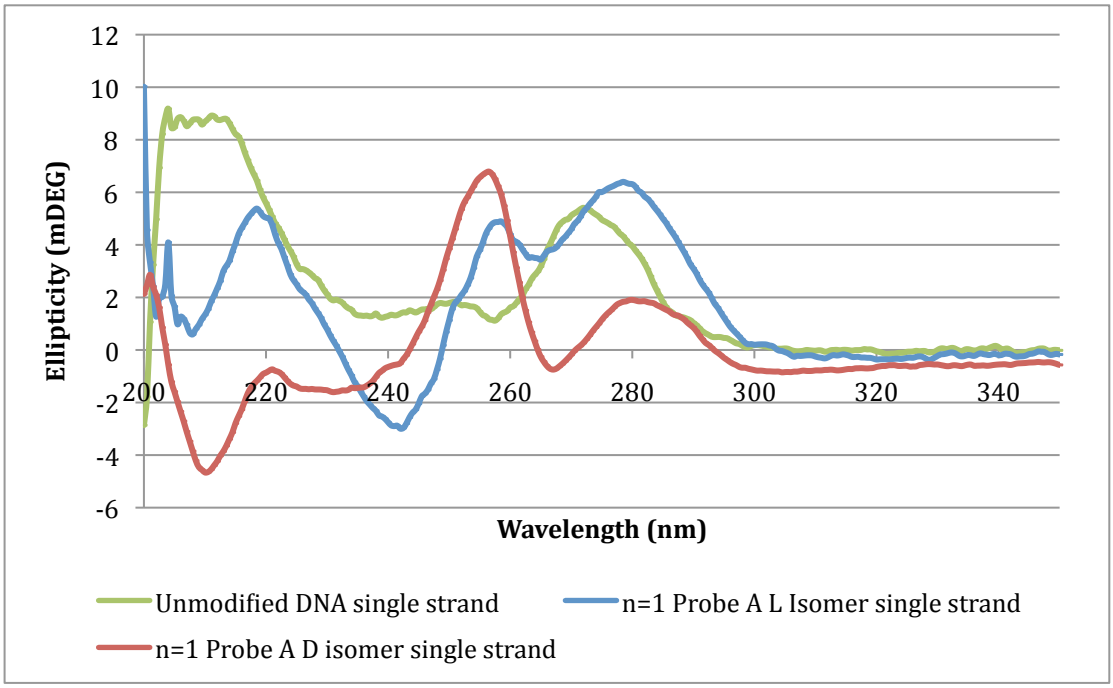

Fig. 104 CD spectra of single strand Probe A L and D 5µM with 10 mM pH 7 phosphate buffer and 100 mM NaCl

It is noticeable how, for the two different isomers, two very different spectra result. The key features of note are the difference in ΔA between 270 and 300 nm and between 240 and 270 nm for the two. The slight shift of the shoulder at 254 nm, which corresponds to the ^1B_b band of anthracene may be indicative of different pi-pi stacking environments between the anthracene and neighbouring nucleobases. Examination of the spectra in the ^1L_a region between 320 and 450 nm show opposite CD signal for the two different isomers (Fig. 105).

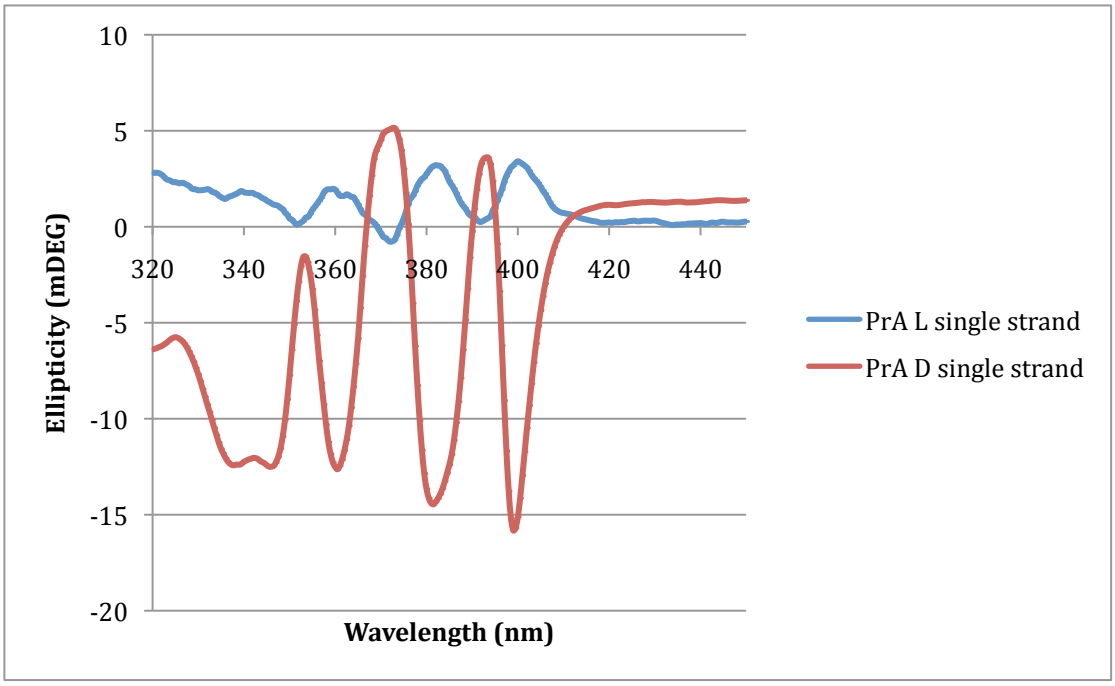

Fig. 105 CD spectra of single strand Probe A L and D 700 and 950 µM respectively with 10 mM pH 7 phosphate buffer and 100 mM NaCl

Comparison of the CD spectra of other single strand Probes also show considerable differences in the single strand form. This could be attributed to the anthracene taking different orientations in the strand. This would seem to reinforce the earlier results of the quantum yields where the D and L strands are very different.

3.14 CD of the hybridized duplexes

One of the primary applications of this technique regarding DNA strands is to determine the form of DNA that the oligonucleotides adopt. This is because there are three major possible structural forms that DNA can take:

- B-form: The most common (90%) structure, characterized by a right handed twist.
- A-form: Partially dehydrated form. Right handed twist but with a tighter helical twist.

- Z-form: Contains a left handed twist and is a much more stretched structure.

The structures are displayed below (Fig. 106).

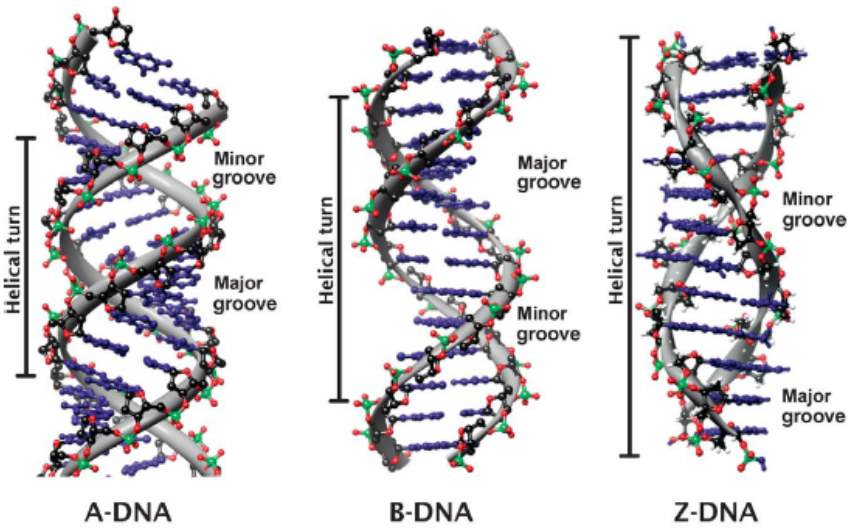

Fig. 106 Depiction of the different forms that duplex DNA can take[67]

Each different form has a different spectral profile and as such the different forms are visually relatively easy to distinguish (Fig. 107).

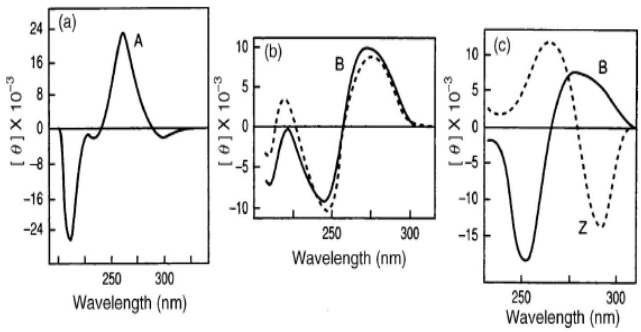

Fig. 107 CD spectra for the different DNA conformations[68]

Initially CD spectra were taken of unmodified DNA with mismatches in the same position as with the anthracene modified

3.14.1 CD spectra of unmodified DNA

As a result of studies on unmodified DNA it was found that the presence of single and double mismatches for the base opposite system did not alter the CD spectrum.

3.14.2 CD spectra of fully matching base opposite duplexes

CD was used to determine which form is adopted by our oligonucleotides by examining a modified duplex. Spectra of anthracene tagged base opposite oligonucleotides are shown below (Fig. 108).

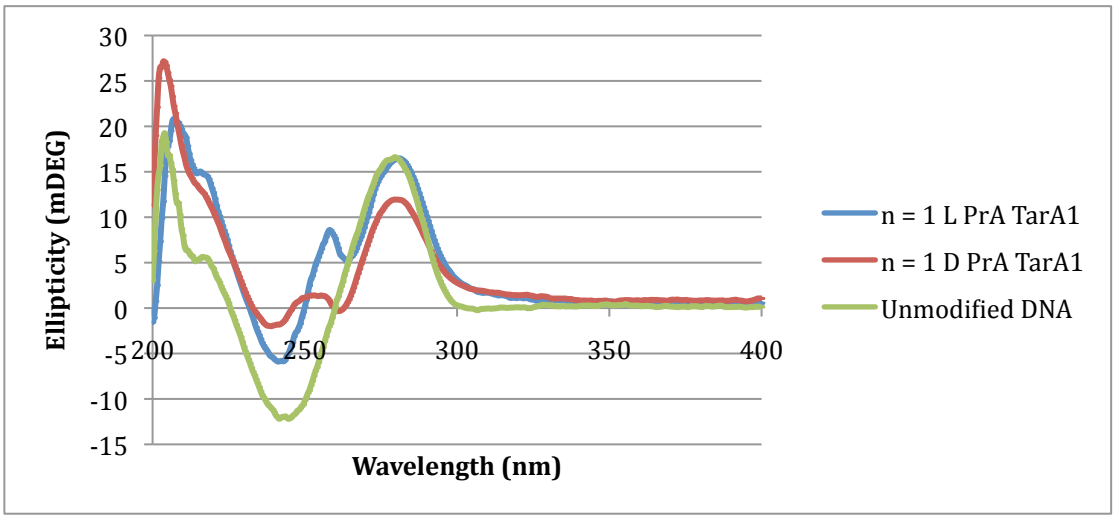

Fig. 108 CD spectra of Probe A (D and L) base opposite system 5µM with 10 mM pH 7 phosphate buffer and 100 mM NaCl

On inspection, the shape of the spectra (Fig. 108) indicates that the duplex is in the B form but there is also again a shoulder peak appearing at 254 nm that does not appear in unmodified DNA and is therefore believed to be due to the anthracene nucleotide, as observed in the absorption spectra (Fig. 109).

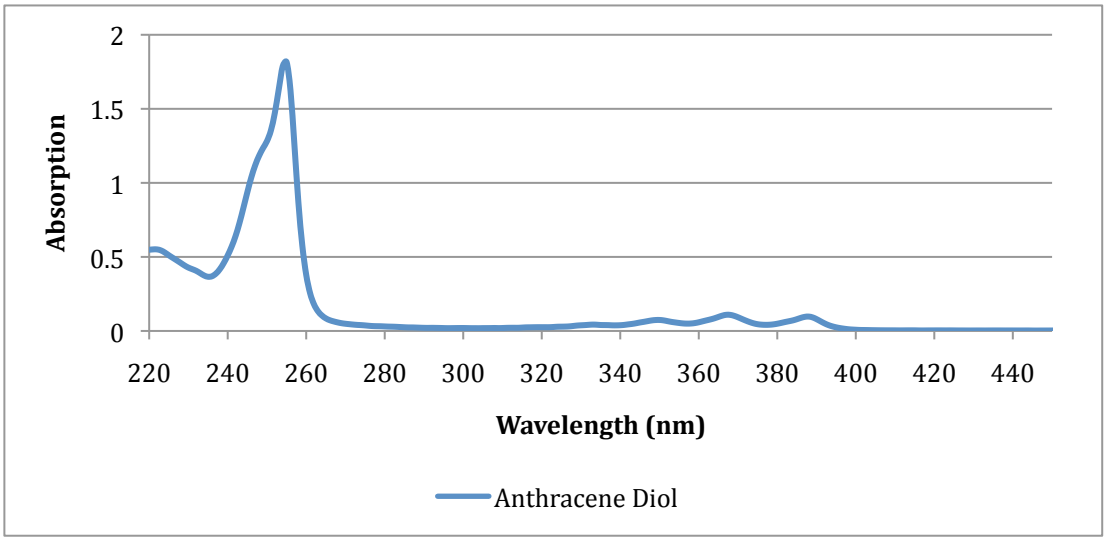

Fig. 109 UV Spectrum of the pre-DMT anthracene diol in water 50uM room temp

Spectra of both the unhybridised strands also show a peak in the same area, as do both forms of the D isomer. Of significance is that the band at 254 nm appears to have strongly positive CD for the L isomer but is less positive for the D isomer. Although the significance of this shoulder will be discussed in more detail later, it is noticeable that the intensity of the DNA CD band at 280 nm is less for the D isomer compared to the L. This implies changes in the winding of the duplex that could be explained by differences between the two configurations of threoninol (see section 1.3.4.3).

3.14.2 Effect of changing bases opposite of the anthracene

Consistent with fluorescence and melting point experiments, there is no change in the CD spectrum when the base opposite the anthracene is varied for the L isomer. However, this is not the case for the D isomer spectra that show that the band at 254 nm is higher for the other bases (C, G, T) than for A (Fig. 110).

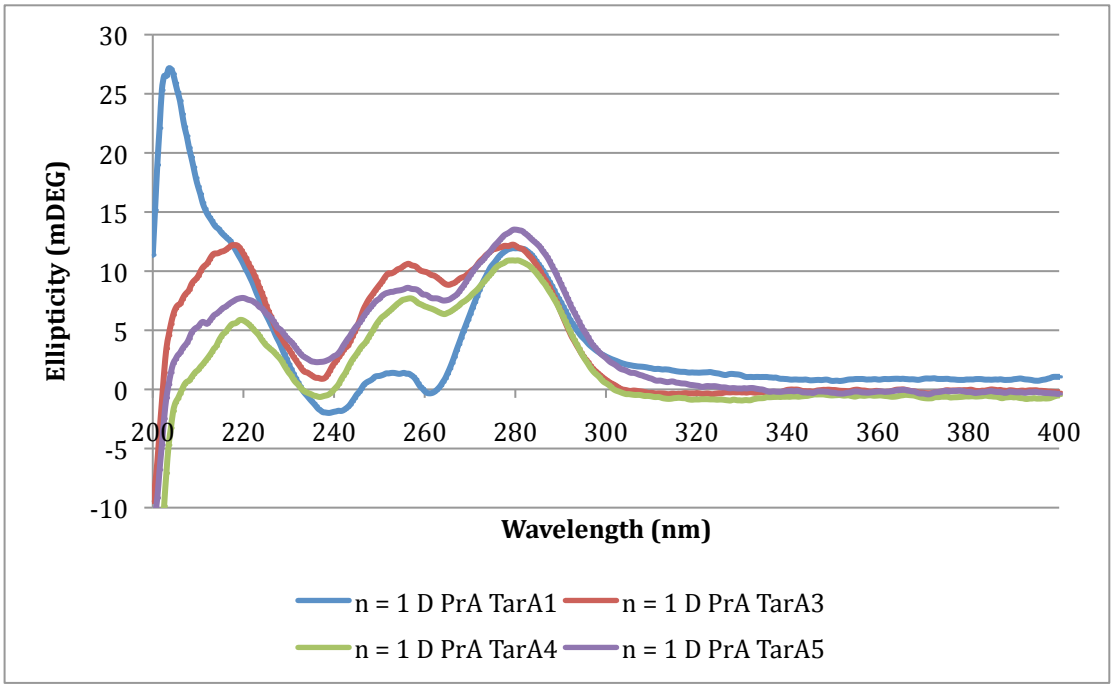

Fig. 110 CD spectra of Probe A (D) with different bases opposite the anthracene 5µM with 10 mM pH 7 phosphate buffer and 100 mM NaCl

Although the band is relatively broad, indicating considerable interaction with base pairs, the bands for the T, C and G bases indicate that the alignment of the anthracene with the base pairs is clearly different.

3.14.3 Deletion duplex CD spectra

In order to see if the presence of the shoulder was related to the particular base opposite structure, a CD spectrum was taken of the deletion system that showed a very similar shoulder (Fig. 111).

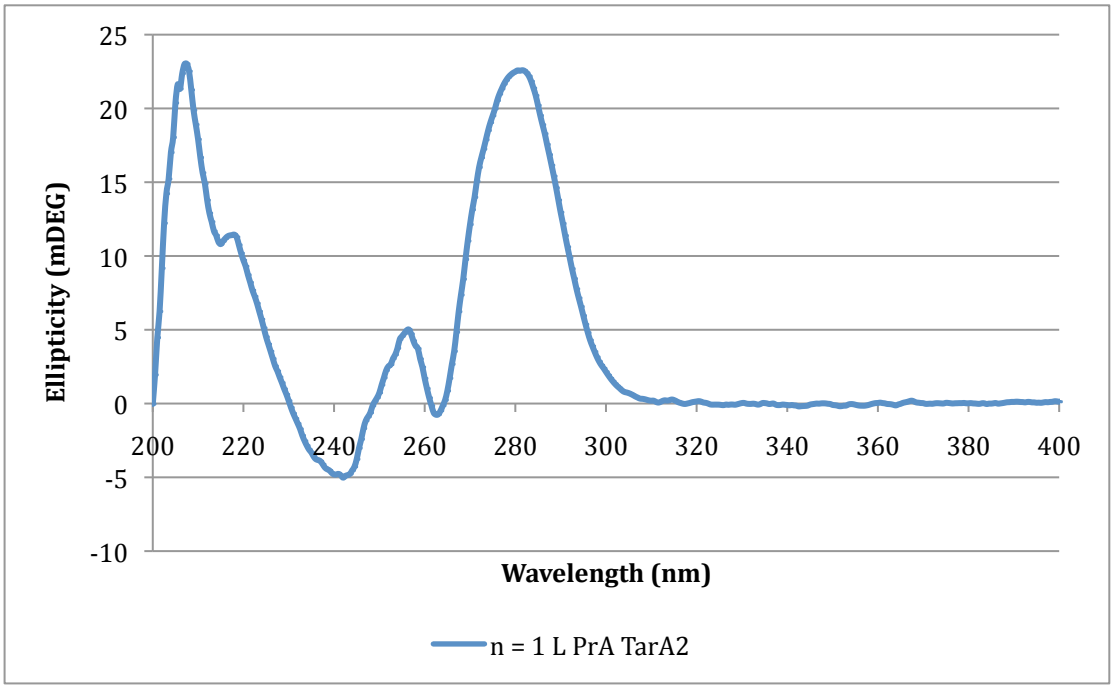

Fig. 111 CD spectrum of n = 1 PrA L TarA2 5µM with 10 mM pH 7 phosphate buffer and 100 mM NaCl

This shows that the presence of a base opposite of the anthracene in not important in giving rise to the coupling signal at 254 nm in the CD spectrum. This further confirms that the anthracene is not coupling with this base in the base opposite system. Also of note is the greater intensity of the DNA band at 280 nm, most likely as a result of greater winding of the duplex.

3.14.4 Effect of flanking bases on CD spectra

Of considerable interest is that the CD spectrum of the opposite strand to Probe A L (red), Probe M L (green), shows no such shoulder signal at 254 nm (Fig. 112). Indeed Probe M L has a CD signal that is very similar to unmodified DNA (blue). This could be due to the greater π-stacking ability of purines (such as G) causing a shift in the shoulder to higher wavelengths and thus the shoulder is absorbed into the positive B-DNA band between 260 and 300 nm.

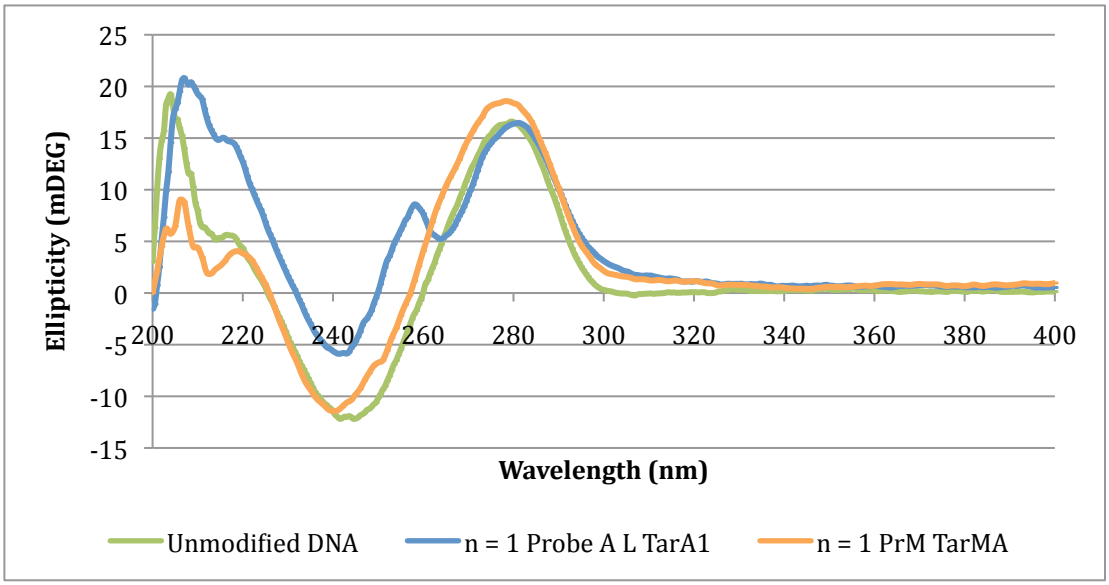

Fig. 112 CD spectra of hybridized C flanked anthracene modified DNA with hybridized G flanked DNA 5µM with 10 mM pH 7 phosphate buffer and 100 mM NaCl

However, when CD spectra of different *n* = 1 Probes are compared, they can be seen to have a characteristic shoulder but of varying intensity (Fig. 113).

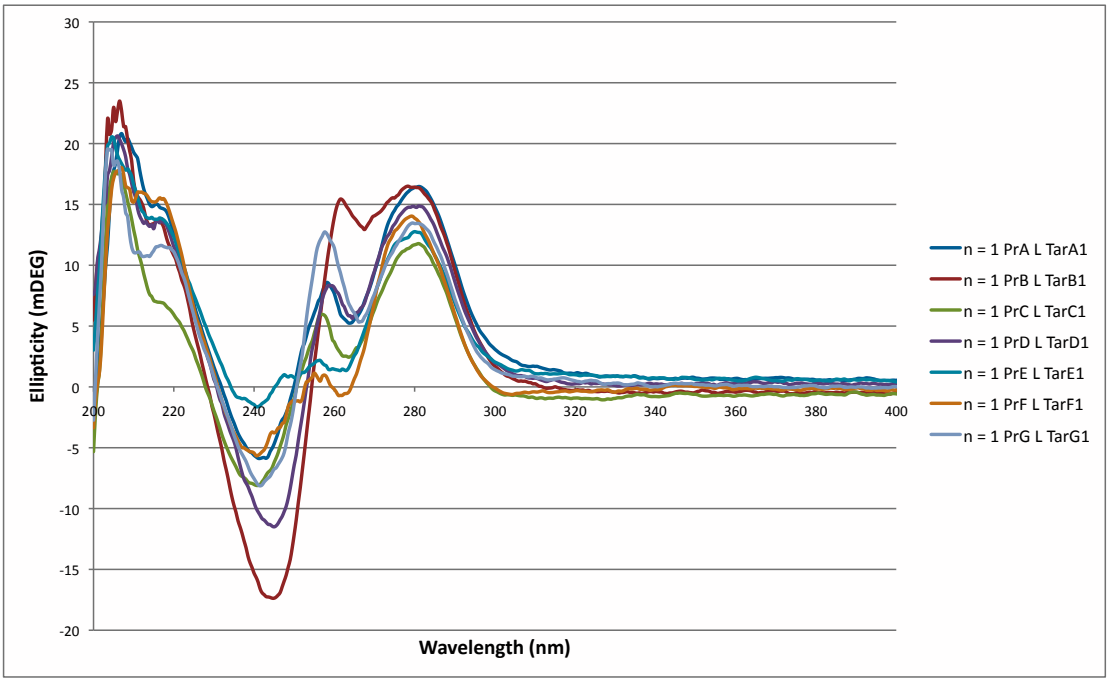

Fig. 113 CD spectra of fully matching duplexes of different probes base opposite system 5µM with 10 mM pH 7 phosphate buffer and 100 mM NaCl

The intensity of the peak height appears to be unrelated to any of the physical properties of the duplexes, nor their base pair composition, however the presence of a C base flanking the anthracene appears to be partially responsible.

3.14.5 Explaining the shoulder in the CD spectra

Work by Rodger and co-workers has shown that the intercalative binding of anthracene-9-carbonyl-*N*-spermine to poly[d(G-C)] gives rise to an induced CD signal with a band at 260nm.[69] An Induced CD spectrum is essentially a CD spectrum of the DNA-ligand complex with the uncomplexed DNA signal subtracted leaving only the signals resulting from the binding of the achiral ligand to the DNA. These signals have been attributed to the non-degenerate coupling of ligand and DNA transitions (Fig. 114).

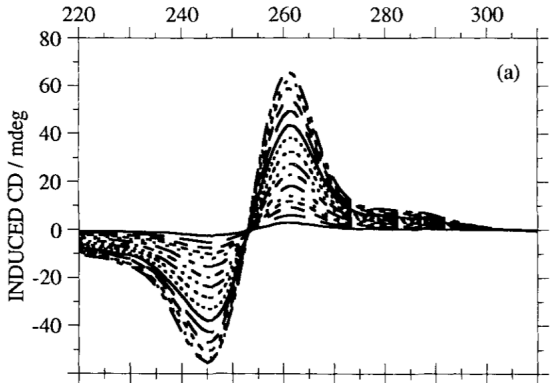

Fig. 114 Induced CD spectrum of anthracene-9-carbonyl-N-spermine to poly[d(G-C)][69]

Furthermore, the CD spectra of poly [d(A-T) and anthracene-9-carbonyl-N-spermine look similar to that of poly [d(G-C)] at low concentration. Therefore, the coupling of our anthracene unit with the adjacent bases may be responsible for generating the shoulder. The lack of base specificity for this effect is reflected in the presence of a similar shoulder in the CD spectra of other anthracene modified oligonucleotide Probes (Fig. 113).

3.14.5.1 CD signals arising from non-degenerate coupling

CD signals can also arise in non-chiral systems as a result of transitions that are electric dipole allowed (eda) and magnetic dipole forbidden (mdf). The inherent complexity of calculating the coupling between non-identical multiple chromophores (in this case anthracene and DNA bases) precludes any easy mathematical analysis, however some simple approximations have been applied in section 3.15 in order to understand the observed CD spectra.[70]

3.14.6 Effect of mismatches on the CD spectrum

The CD spectra of Probe A L with mismatches were taken and show a disappearance of the shoulder at 254 nm for the upstream mismatches (with the exception of TarG1, a C to A mismatch) but the retention of the shoulder for a downstream mismatch (PrATarB1)(Fig. 115).

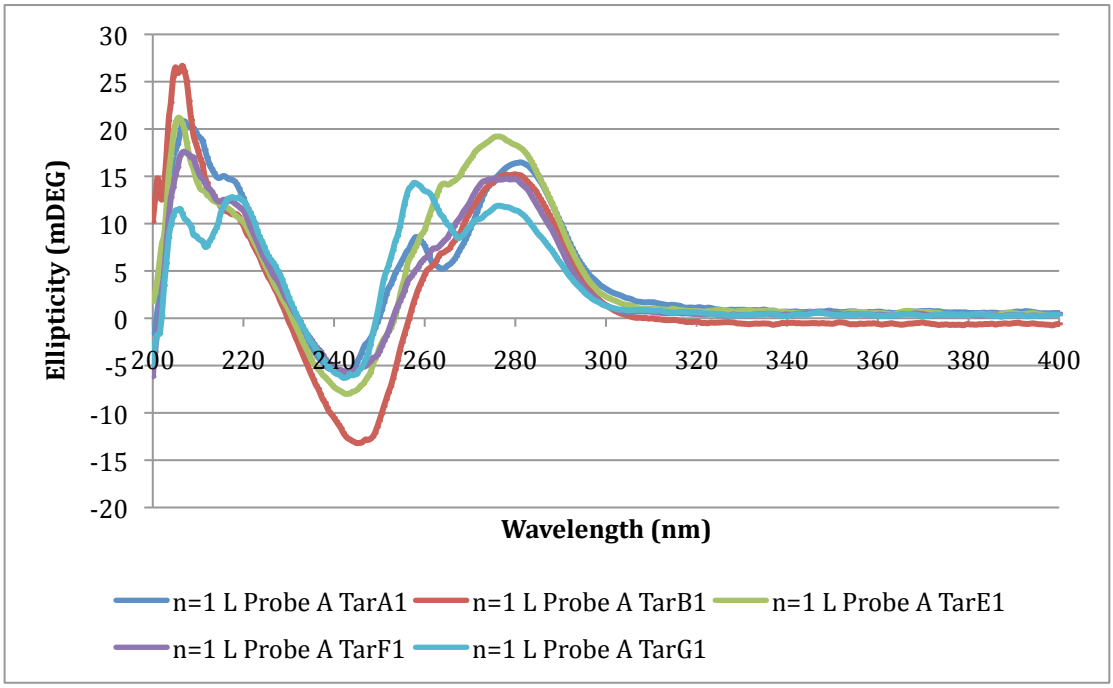

Fig. 115 CD spectra of n=1 Probe A with different mismatched strands 5μM with 10 mM pH 7 phosphate buffer and 100 mM NaCl

It is possible that these trends are related to the different degrees of stacking of the anthracene and bases as observed in the melting point experiments. The implications of the different spectra for the structure of our oligonucleotides will be discussed in the following section and in chapter 4.

3.15 Induced CD spectra of anthracene modified duplexes

The above spectra show that in order to be able to extract more data from the spectra it becomes necessary to remove the signals originating purely from DNA. The spectrum then becomes an ICD spectrum as discussed earlier, but it will still contain the signal from the inherent chirality of the anthracene linker.

3.15.1 Using ICD to interpret structure

The ICD of a chromophore intercalated into DNA allows the orientation relative to the base pair long (or dyad) axis to be probed. As mentioned before, the complexity of coupling between non-identical chromophores makes a mathematical description beyond the scope of this work – it is however possible by considering the bases to be stacked vertically with their planes perpendicular to the vector between their origins.[70] Instead the system will be analysed more simply in terms of the assumptions made below.

Anthracene has a weak short axis polarized transition at ~360 nm and a strong long axis one at ~ 252 nm (Fig. 116 Polarizations of anthracene).

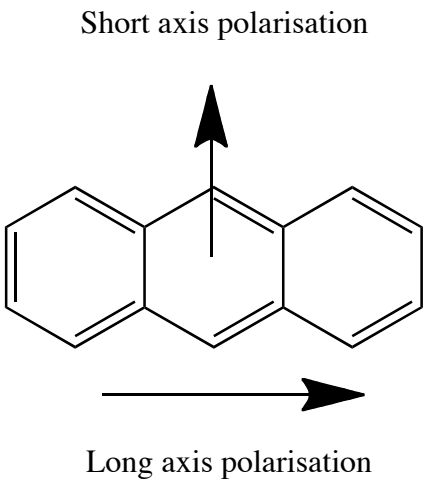

Fig. 116 Polarizations of anthracene

Therefore, for the interaction of a system such as ours with DNA it can be said that if the long axis polarized transition moment of the intercalator is orientated at an angle τ (Fig. 117) to the base pair long axis *y* (as defined below in Fig. 118) then a maximum CD signal is observed at 45°.[66, 70]

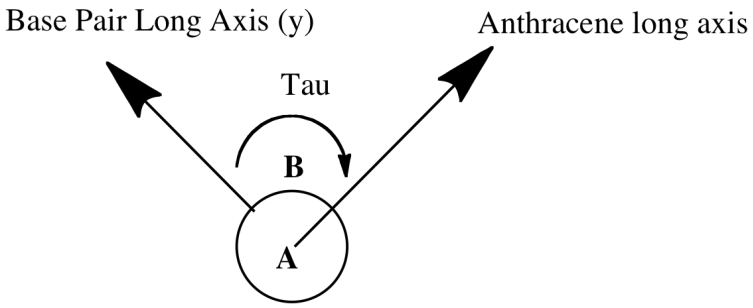

Fig. 117

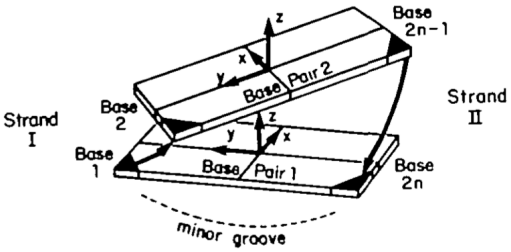

Fig. 118 Illustration of the definitions of DNA axes[71]

The intensity of the signal varies as a function of a number of variables:

1. The strength of the transitions in the chromophores
2. Their orientations relative to each other - τ (maximum intensity at 45° and minimum at 0 and 90°.
3. The distance between them (proportional to R_{AB}^{-2})

Further examination of such a system can show that the CD signal strength depends on the specific base pair sequence (i.e. C-G is different to G-C). This has been used to identify binding sites of intercalating molecules[72] and explains the different intensities of the signal at 254 nm observed with the different probes (Fig. 113 see also 3.14.5 discussion).

3.15.2 ICD of fully matching base opposite sequences

Fig. 119 Shows an ICD spectrum of Probe A (L) with its matching target strand, showing a broad positive peak between 254 and 257 nm. The spectrum was produced by subtracting an unmodified B DNA CD spectrum (the duplex with adenine instead of anthracene) from an anthracene modified one.

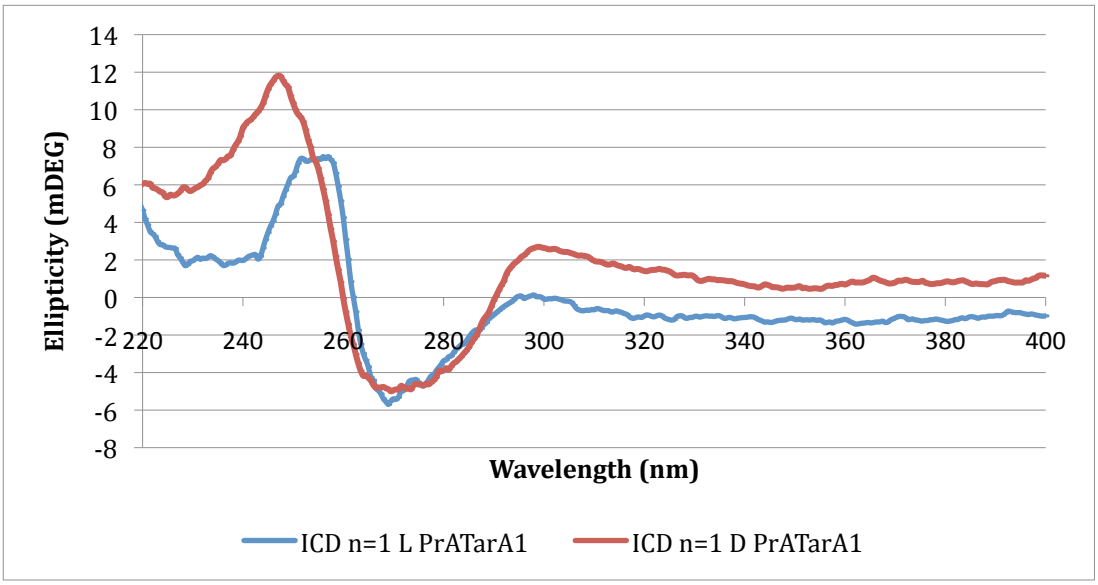

Fig. 119 ICD spectra of Probe A Target A1 5 µM with 10 mM pH 7 phosphate buffer and 100 mM NaCl subtracted using TarMATarA1

The ICD spectrum of the duplex with Probe A D is also shown and both spectra suggest that the anthracene magnetic moment, in this case synonymous with the anthracene long axis, is orientated relative to the base pair axis to a different extent for the two isomers. It would appear that either the D isomer duplex has the anthracene magnetic moment crossing the base magnetic moment closer to 45° than the L isomer or the L isomer anthracene is further from the base pairs that it couples to.

3.15.3 ICD of upstream mismatches

The graph below (Fig. 120) shows the ICD for the *n* = 1 L upstream mismatches, unlike the in previous graph (Fig. 115), it shows that there is still a signal from the anthracene in all of the mismatch strands but that the intensity is considerably reduced for the mismatches with smaller base mismatches (C-C Probe A TarE1 and C-T Probe A TarF1) compared to the bulkier C-A mismatch (Probe A TarG1).

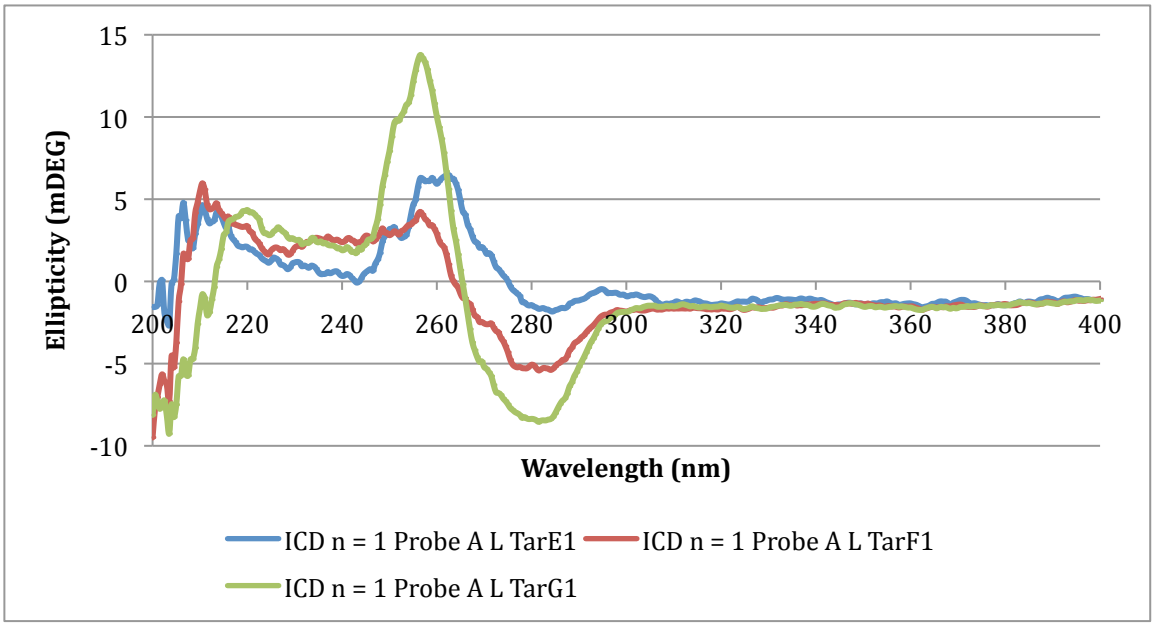

Fig. 120 ICD spectrum of mismatched sequences of Probe A 5 µM with 10 mM pH 7 phosphate buffer and 100 mM NaCl

It is noticeable that the most intense band most closely resembles the ^1B_b band of anthracene with the distinctive shoulder at 252 nm.

The increasing positive nature of the ICD signal at around 254 nm would appear to suggest an shift of the anthracene to a closer location to stacking bases and an orientation to a position where the anthracene long axis is aligned at 45° to the base pair long axis (see 4.7.1).

3.15.4 Deletion duplexes ICD studies

Displaying the CD spectra of the deletion strands in the ICD form can be quite informative as seen in Fig. 121, which show a positive band at 254 nm. This clearly shows that the anthracene is aligned quite similarly in all cases, both matched and mismatched. However, the fully matched strand (A2) appears to increase the winding of the duplex, whilst the mismatches cause unwinding as seen in the positive and negative bands respectively at 280 nm. The differences in fluorescent emission seen earlier are not reflected by differences in the ICD spectra.

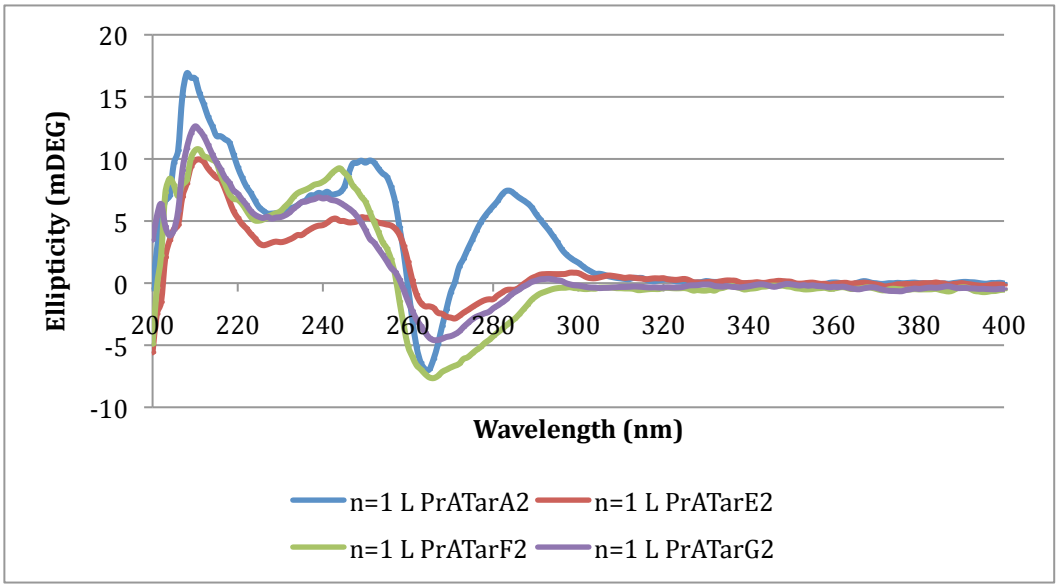

Fig. 121 ICD spectra of *n*=1 PrA with matched (blue) and mismatched target strands 5 μM with 10 mM pH 7 phosphate buffer and 100 mM NaCl

The ICD spectra can be combined with high concentration CD studies to deduce the structure of the intercalated structure by looking at the sign of the anthracene finger region (Fig. 122).

Examination of the spectra in the ^1L_a region between 320 and 450 nm shows that unlike in the single strand form, where the CD signals were of opposite sign, they are now negative overall for both isomers in the duplex form. However, the spectrum of the D isomer appears to be considerably more intense and complicated than the L. The former may be due to the cancelling out of the inherent chiral CD signal from the induced CD signal for the L isomer thus overall the signal is weaker. The more complicated D spectrum may arise due to multiple sources, the inherent chirality and the induced CD signal.

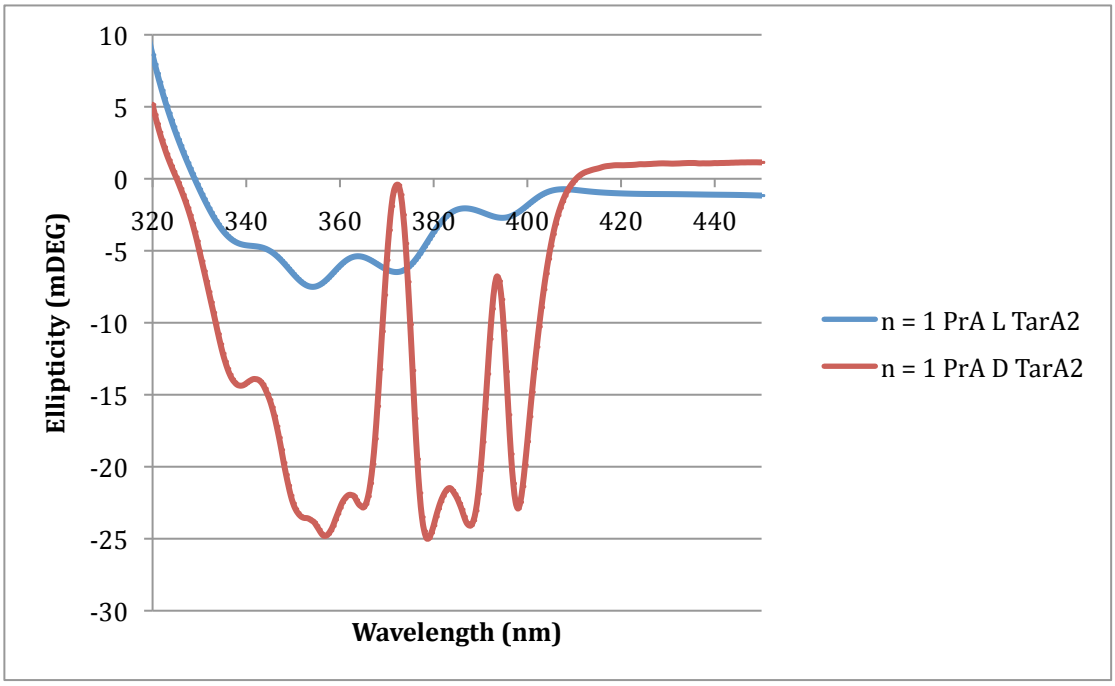

Fig. 122 CD spectrum of *n* = 1 PrA L and D TarA2 900 µM with 10 mM pH 7 phosphate buffer and 100 mM NaCl

The interpretation of the overall negative CD signal is that the anthracene is aligned along the base pair axis,[66] supporting an interpretation of the anthracene intercalating between base pairs.

3.16 Applying the work to real life SNPs

The following SNP is a real example of a disease causing variation in the genetic structure. It is believed to be partly responsible for the onset of type I diabetes. It was chosen due to the similarity of the central environment to our previously studied systems. It was decided to create a probe using the abasic structural motif in the hope that one polymorphism would give a stronger sensing effect than the other. The selection and design of the target/probe system was performed based on the previously reported results and represented an attempt to utilise the aforementioned studies to design systems and predict what the fluorescence response would be.

SNP Tar T 5' T A A C T A G A A G G T G C 3'

SNP Tar G 5' T A A C T A G C A G G T G C 3'

Hence, two probes were synthesised to investigate the fluorescent response to hybridisation with an anthracene probe.

SNP Probe T 3' A T T G A T C X T T C C A C G 5'

SNP Probe G 3' A T T G A T C X G T C C A C G 5'

Based on previous studies the predicted result is for an increase in the emission of SNP Probe T upon hybridisation and for a decrease with Probe G. This is using n = 1 L Probe G as the reference for SNP Probe T and n = 1 L Probe E as the reference for SNP Probe G.

3.16.1 Fluorescence results for SNP sensors

As can be seen from the graph of the fluorescence titration plot (Fig. 123) this is indeed the result obtained. SNP Probe T gives a 200% increase in emission upon hybridisation whilst Probe G gives a 20% decrease with the mismatches giving small increases.

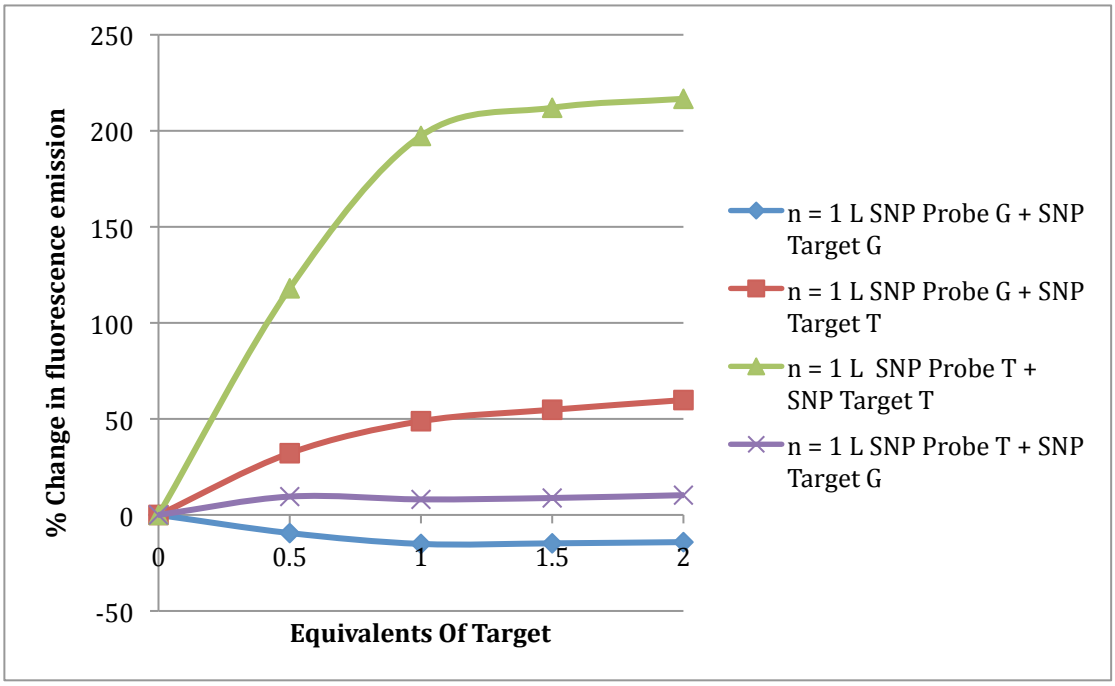

Fig. 123 SNP sensing fluorescence titrations 1 µM with 10 mM pH 7 phosphate buffer and 100 mM NaCl

3.16.2 Fluorescence lifetimes

The lifetimes of each Probe with its matching Target were taken and the results are displayed below in Table 37.

Table 37 Fluorescence lifetimes of SNP Probes with matching targets 5 µM with 10 mM pH 7 phosphate buffer and 100 mM NaCl

		τ 1 (ns)	τ 1 weighting (%)	τ 2 (ns)	τ 2 weighting (%)	τ 3 (ns)	τ 3 Weighting (%)	χ^2
SNP Probe G	SNP Tar G	2.37	7	5.04	68	8.88	28	1.047
SNP Probe T	SNP TarT	2.11	9	8.85	70	15.7	20	1.005

3.16.3 Melting points

Melting point studies were also performed and correlate with the base sequences and observed fluorescence results in that SNP PrGTarG with more C-G base pairs has a higher T_m than SNP PrTTarT, which both have higher T_ms than

the mismatches due to the loss of base pairing. The fact that the more emissive duplexes have lower T_ms (Table 38) also suggest that some structural distortion may take place in order to accommodate the anthracene in a more emissive environment.

Table 38 Melting points in °C for SNP duplexes 5 μM with 10 mM pH 7 phosphate buffer and 100 mM NaCl

SNP	TarG	TarT
PrG	55	34
PrT	37.5	41

3.16.4 Conclusions

The results show that we can differentiate between the two target strands using SNP Probe T, which will give a large fluorescence increase upon hybridisation with SNP Tar T but only a small one with SNP Tar G.

3.17 Interstrand stacking duplexes

In a continuation of previous work the effects of placing anthracene nucleotides on opposite strands of a duplex facing each other were studied. A number of groups have studied the interactions of adjacent groups in the structure of DNA and the coupling interactions between them.[32, 54] In this case the overall goal was the formation of an anthracene eximer and subsequent dimerisation reaction (Fig. 124).

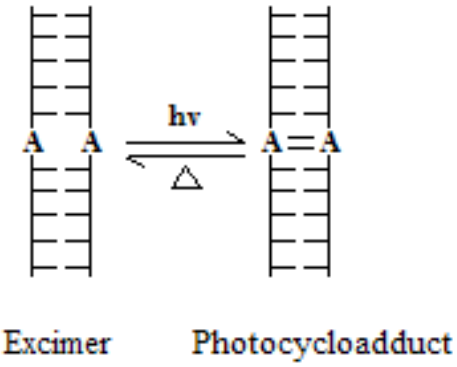

Fig. 124 Diagram of interstrand dimerisation

3.17.1 Anthracene excimers and dimers

The mechanism of photodimerisation occurs via a singlet arene excimer.[73] The term arises from 'excited dimer' since an excimer is a 1:1 complex formed between a molecule in the ground state and another identical molecule in the excited state. As the excimer lies at a lower energy than the first excited singlet the formation is favourable and is observable in the fluorescent emission spectrum. Although the presence of an excimer is a prerequisite for dimerisation it does not necessarily mean that dimerisation will follow as there are a number of decay paths open to the excimer (Fig. 125).

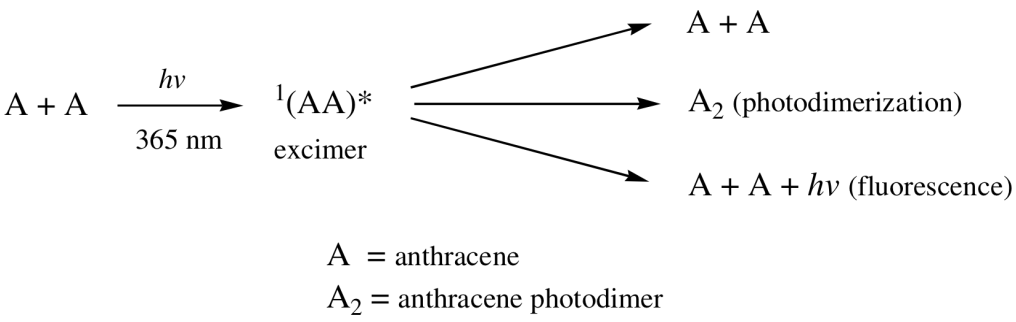

Fig. 125 Diagram of different decay processes for anthracene

The dimerisation of anthracene, via a 4π+4π photoactivated cycloddition has been extensively studied and is well understood.[73, 74] It is initiated by irradiation

of light greater than 365nm and is a reversible reaction, the reverse reaction being initiated by shorter wavelength light or heat (Fig. 126).

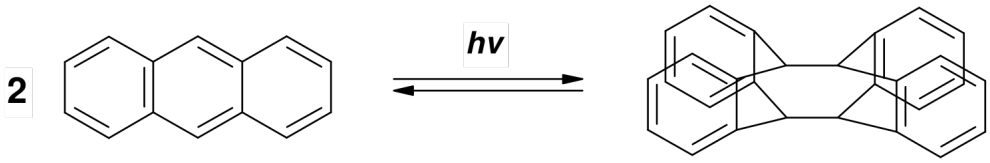

Fig. 126 Dimersation of anthracene

3.17.2 Fluorescence Studies on Excimers

The first evidence of the potential for dimerisation can be found in the presence of an excimer in the fluorescent emission spectrum. Excimers typically present as a broad, red-shifted structureless band between 450 and 520 nm.

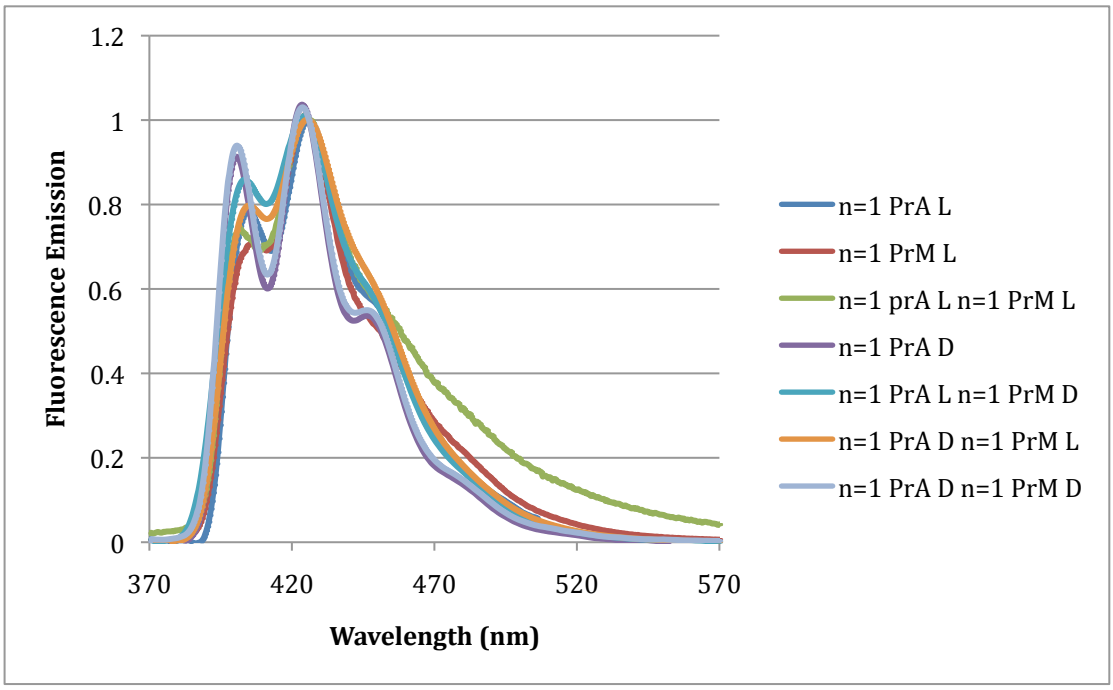

Fig. 127 Normalised fluorescence spectra of *n* = 1 PrA and PrM single strands and different duplex combinations of isomer 1 µM with 10 mM pH 7 phosphate buffer and 100 mM NaCl

The normalized fluorescence emission spectra above, showing the individual single strands compared to the bis-anthracene duplex, show few indications of

excimer presence (Fig. 127) The presence of a slight broadness between 470 and 550 nm for the LL duplex may be indicative of weak excimer formation, however there are no signs of any excimer formations in any of the other combinations.

3.17.3 Fluorescence lifetime studies

In association with the emission spectra, fluorescent lifetime studies were carried out on the LL and LD bis-anthracene duplexes in order to search for any sign of the longer-lived eximer. The decay profiles were recorded at 405 and 500 nm, corresponding to the predicted monomer and excimer contributions respectively. If an excimer is present we would expect to the presence of a long lifetime component of 15-25 ns at 500 nm and not at 405 nm.[75]

Table 39 Fluorescence lifetimes of single strand and bis-anthracene duplexes 1 μM with 10 mM pH 7 phosphate buffer and 100 mM NaCl

Probe	Wavelength (nm)	τ 1 (ns)	τ 1 Weighted (%)	τ 2 (ns)	τ 2 Weighted (%)	τ 3 (ns)	τ 3 Weighted (%)	τ Av(ns)	χ2
n =1 L PrM	405	1.54	12	7.06	27	20.05	61	18.08	1.02
	500	2.01	15	8.54	24	20.82	62	18.83	0.95
n =1 L PrA	405	0.98	59	3.33	32	11.85	9	6.10	0.90
	500	0.94	62	3.39	30	11.98	8	6.13	1.01
n =1 L PrA PrM	405	0.64	51	3.12	36	11.74	13	7.30	0.97
	500	0.51	64	2.28	28	8.78	8	4.68	1.03
n=1 D PrA	405	1.16	38	4.41	29	13.79	34	11.07	1.02
	500	1.18	48	4.88	29	14.03	23	10.12	1.02
n=1 D PrA L PrM	405	0.76	67	3.26	25	10.96	8	5.80	0.98
	500	0.51	64	2.28	28	8.78	8	4.68	1.03

As with the single anthracene systems the emission decay is well fitter by a tri-exponential decay function. However, there is no evidence of any long-lived species, and indeed, the fluorescent emission of the bis-anthracene duplex has a shorter lifetime than one of the single strands. In view of the proposed electron transfer quenching mechanism discussed earlier this is perhaps a consequence of the quenching processes of the duplex dominating (see top process Fig. 125).

3.17.4 Conclusions

As the formation of these excimers is reliant on the right orientation and distance between the two fluorophores, namely that they are parallel to each other, have a co-facial orientation and have an interplanar distance of 3-4 Å, the lack of excimer formation suggests a different arrangement within the duplex.

3.18 Absorption Studies on interstrand duplexes

3.18.1 UV melting points of interstrand duplex

Table 40 Melting points (°C) 5 μM with 10 mM pH 7 phosphate buffer and 100 mM NaCl

	PrM	
PrA	*n* = 1 L	*n* = 1 D
n = 1 L	56	49.5
n = 1 D	52.5	52

Comparison of the different combinations of isomers clearly shows that the LL duplex is considerably more stable than any other combination. This may be due to the maximization of potential base stacking interactions and avoidance of any steric clash between the two anthracenes.

3.18.2 Melting point studies at 370 nm

Inspection of the thermal melting curve at 370 nm shows no evidence of non-simultaneous de-intercalation of the anthracene from the duplex and gives a value that is very similar to that at 260 nm.

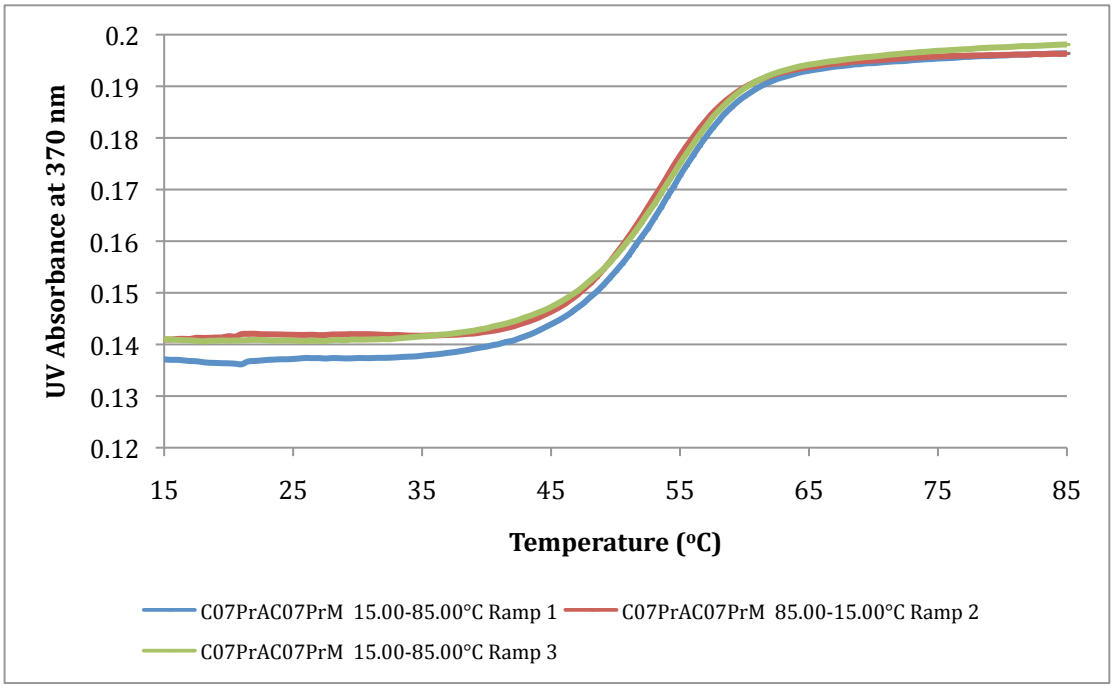

Fig. 128 Melting Point curve for bisanthracene duplexes 5 µM with 10 mM pH 7 phosphate buffer and 100 mM NaCl

3.18.3 UV-vis spectra at different temperatures

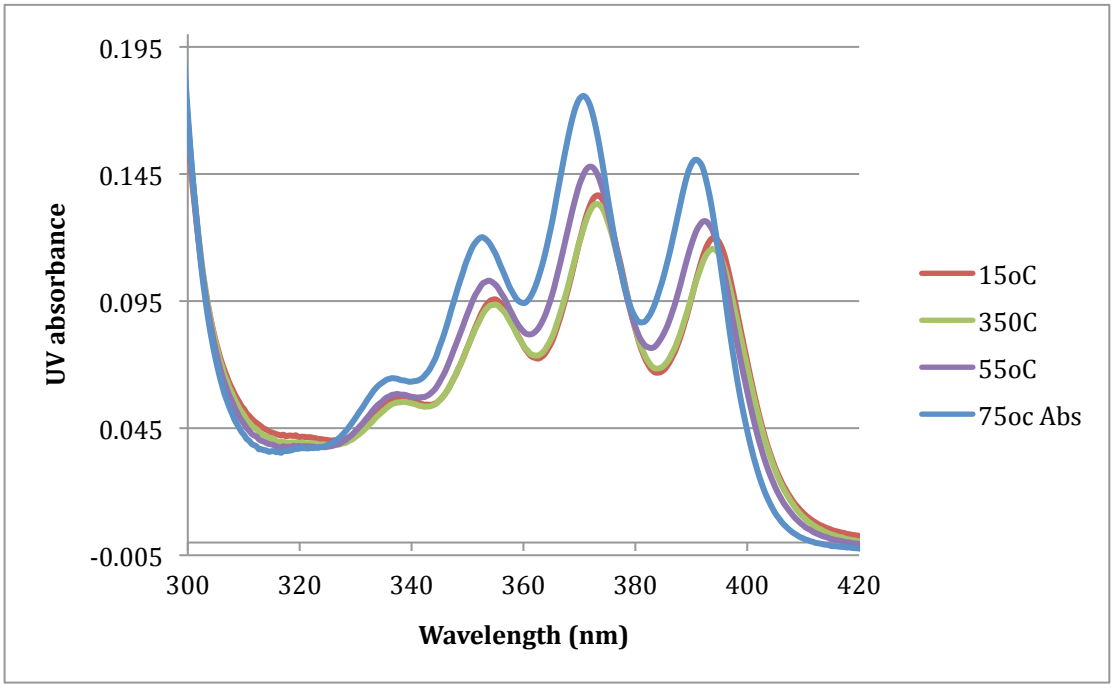

Fig. 129 UV spectra of n=1 PrA and PrM LL 20µM with 10 mM pH 7 phosphate buffer and 100 mM NaCl

The bathochromic shift for two anthracenes is unchanged from a single anthracene nucleoside at 3 nm and the T_m at 370 nm is the same.

3.19 Circular Dichroism studies of interstrand duplexes

3.19.1 Exiton coupling of anthracenes

The first strands to be studied were the matching strands Probe A and M for the L isomer. Unlike the situation where there is only one anthracene present in the duplex (purple) there is no positive shoulder at 258 nm but instead a strong negative band at 260 nm followed by a positive band at 245 nm (blue), neither of which is seen in any single anthracene combination (Fig. 130). Studies of mismatched strand combinations (red and green) were also performed.

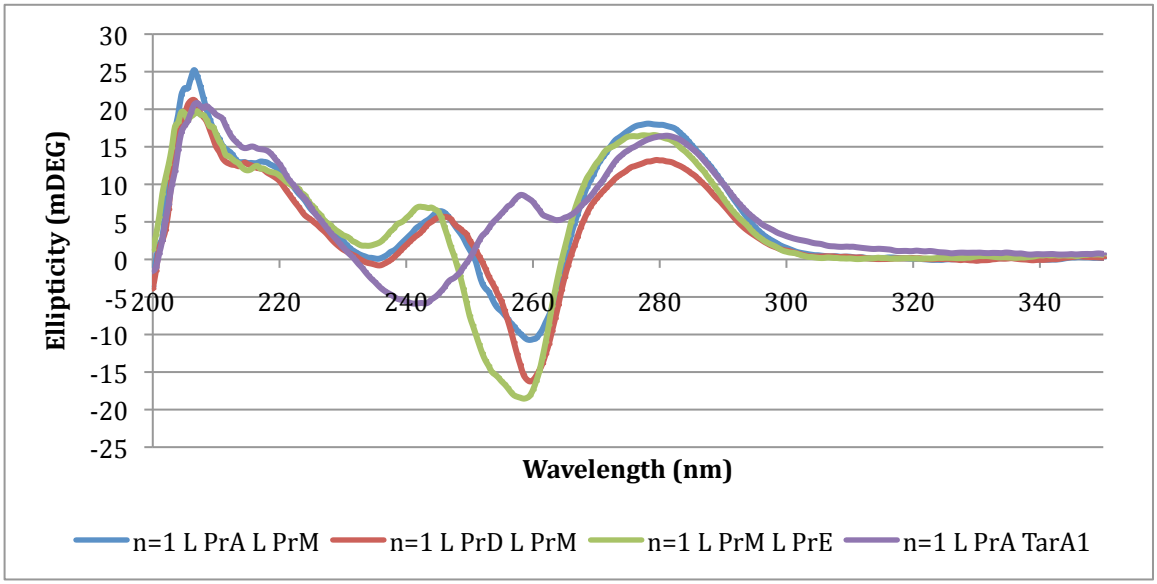

Fig. 130 CD spectra of bisanthracene duplexes matching and mismatching 5 μM with 10 mM pH 7 phosphate buffer and 100 mM NaCl

These bands have been theorized to be evidence of exiton coupling between the two anthracenes and as the different plots show, are not significantly affected by the presence of mismatches either downstream or upstream (red and green respectively). However, further studies whereby different stereoisomers were combined show that the coupling is unique to the combination of isomers with neither the LD nor the DD combination producing a similar spectrum (Fig. 131).

This is reflected in the melting points – with the LL combination giving the highest melting point, probably as a result of the strongest pi-stacking interactions (Table 40).

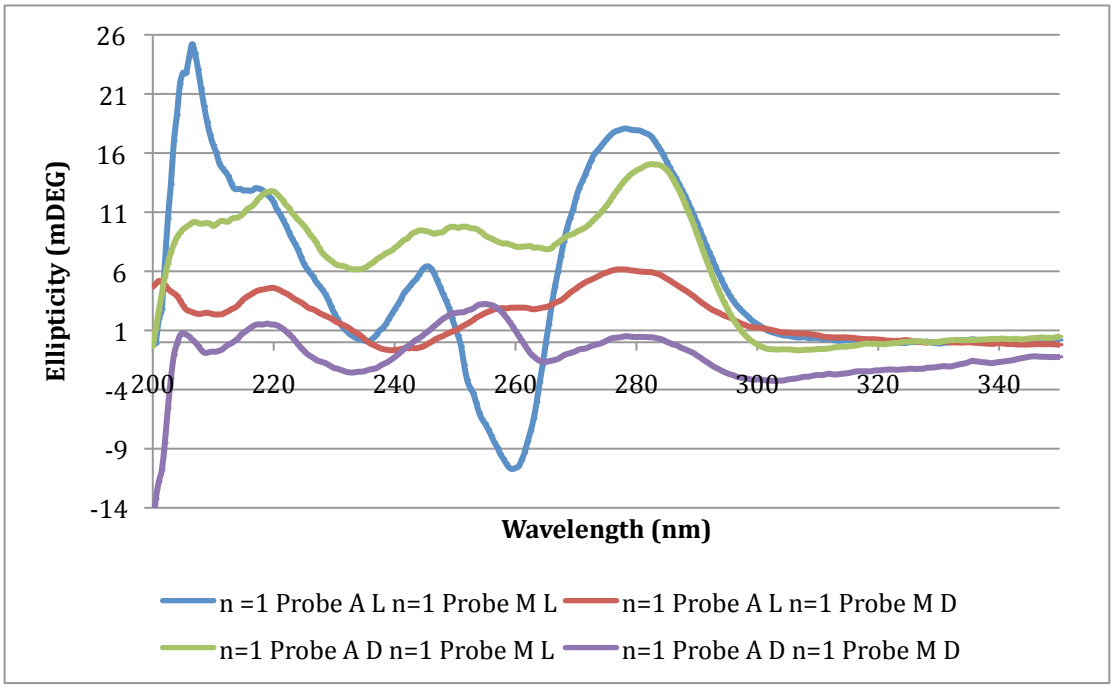

Fig. 131 CD spectra of *n* = 1 interstrand stacking duplexes 5 µM with 10 mM pH 7 phosphate buffer and 100 mM NaCl

Indeed the overall signal for the DD combination appears to be greatly reduced, perhaps as a result of positive and negative bands coinciding and cancelling each other out.

Assignment of the bands as coming from exciton coupling between anthracenes is aided by work from Rodgers and co-workers who have assigned a peak at in the binding of anthracene-9-carbonyl-*N*-spermine to poly [d(A-T)] at high concentrations as being indicative of exciton coupling between anthracenes.[76]

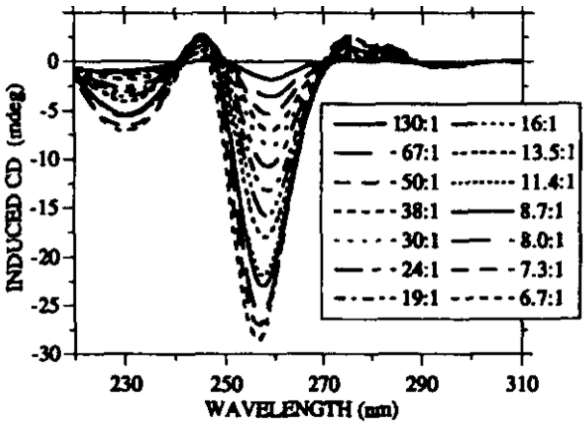

Fig. 132 ICD spectrum of anthracene-9-carbonyl-N-spermine binding to poly [d(A-T)] at high ligand to base ratios[76]

The positive band at 245 nm and negative band at 260 nm in their spectra correspond with the structure of the CD spectrum of the proposed exiton coupling of the *n* = 1 L interstrand duplex. Molecular modelling of their anthracene intercalator gave a proposed structure for the anthracene complex with a major groove binding site (see Chapter 4).

3.19.2 Analysing the exciton coupling in the LL system as a degenerate coupled-oscillator system

Unlike the coupling between anthracene and DNA bases, the exciton coupling between two anthracenes can be predicted by treating the system as a degenerate coupled oscillator with the following geometry and coordinates.

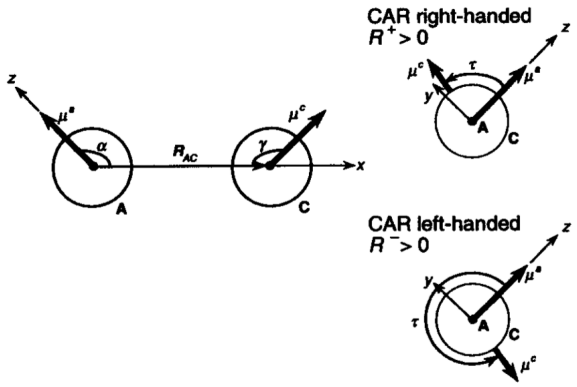

Fig. 133 Vectors and axes for the study of coupled oscillators[70]

To simplify the calculation we can treat the transitions as polarized either parallel or perpendicular to the line connecting the chromophore origins (R_{AC}) such that $\alpha = \gamma = 90°$. This gives a system as illustrated in Fig. 134.

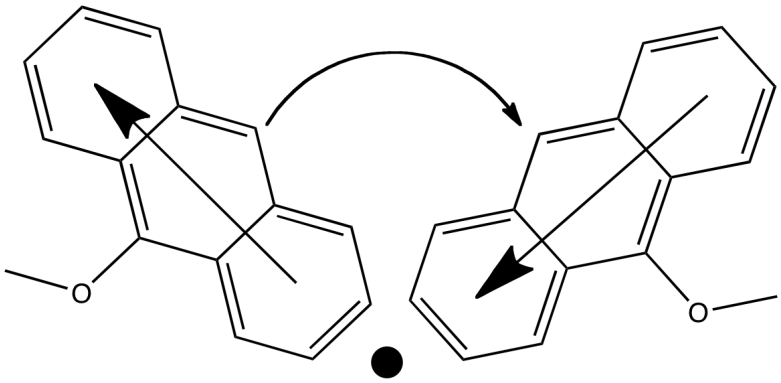

Fig. 134 Representation of the transitions in a bis anthracene exciton coupling system

This is predicted to give two bands in the CD spectrum of opposite sign that occur at energies slightly above and below the transition energies of the isolated chromophores. The spectra will adopt a particular shape depending on the value of τ.

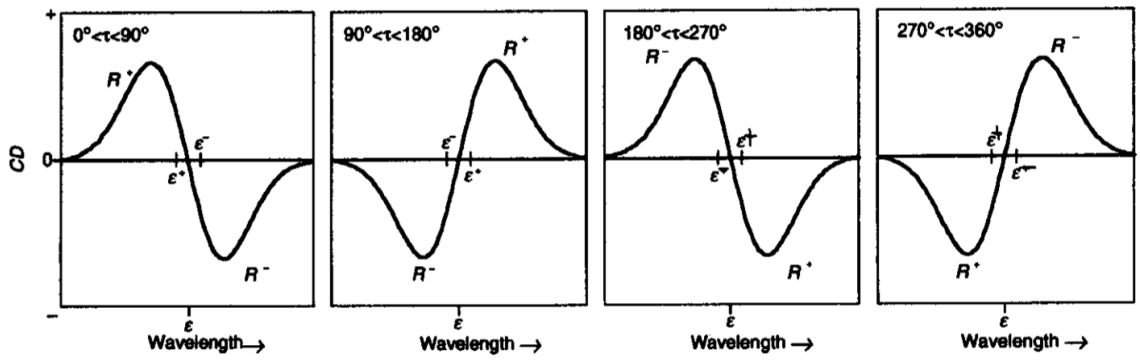

Fig. 135 Possible exciton coupling signals with respect to the angle between the polarization vectors

From observation of the spectrum, whereby the lowest energy/highest wavelength peak has negative CD and vice versa we can deduce that the value of τ will be between 0 and 90°.

3.20 Dimerisation of interstrand duplexes

The dimerisation of anthracene was attempted using a mercury vapour lamp using a lead nitrate filter. Irradiation was carried out for 15 minutes on a degassed 5 μM sample in 100 mM NaCl and 10 mM pH 7 phosphate buffer solution. A change in the UV absorption spectrum was observed after irradiation as shown below (Fig. 136).

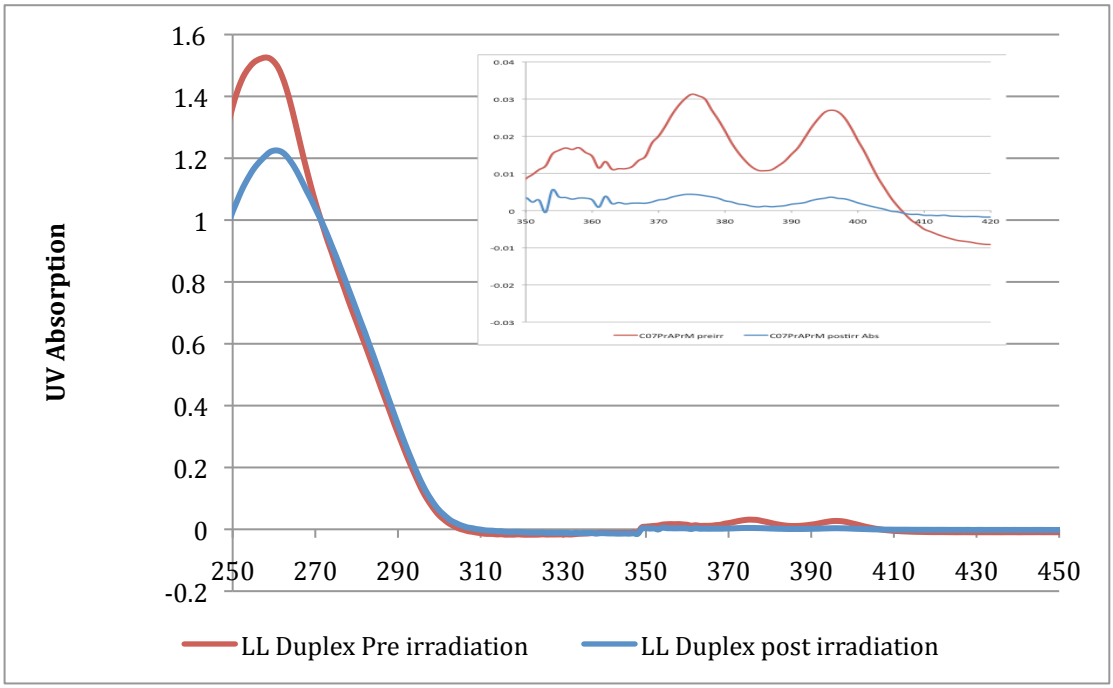

Fig. 136 UV spectrum of bisanthracene duplex Pre (red) and post (blue) irradiation 5 μM with 10 mM pH 7 phosphate buffer and 100 mM NaCl

However, subsequent mass spectrometry did not show the desired duplex dimer and instead suggested cleaving of the single strand at the site of the anthracene nucleoside. This was related to previous work in the group where it was observed that a similar system also cleaved upon irradiation. The loss of anthracene peaks in the $^{1}L_{a}$ region could be as a result of the formation of anthraquinone which forms readily in the presence of water and oxygen – although the sample was degassed it is likely that some oxygen remained.

Alternatively a Norrish Type I cleavage reaction has been shown to produce anthraquinone even in the absence of oxygen.

3.21 Conclusions

Analysis of the fluorescence results has shown a difference in the local environment of the anthracene for the two different stereoisomers in both the single and the double strand form. This in turn leads to a difference in the sensing ability of the two different stereoisomers: The anthracene *SS* stereoisomer probe, derived from D threoninol, is quenched irrespective of the target strand upon hybridisation whereas the *RR* stereoisomer probe, derived from L threoninol, shows an increase in fluorescence when hybridised to a target strand that contains a mismatched base pair located on the upstream side of the anthracene containing nucleoside. A sensing effect is apparent, although different, for both the base opposite and deletion systems. This sensing effect can be correlated with changes to the three anthracene fluorescence decay lifetimes.

Variable temperature UV spectroscopy and CD spectroscopy show that the anthracene in L duplex adopts a position whereby it intercalates into the duplex whilst the D duplex causes the anthracene to adopt a more destabilising orientation. This is indicated by both a higher melting point and the appearance of strong non-degenerate coupling signals in the CD spectrum for the L isomer.

Application of the same techniques to face to face bisanthracene duplexes have shown that the LL duplex is more stable than the other possible duplexes and also shows evidence of exciton coupling between the anthracenes.

3.22 References

1. Moran, N.; Bassani, D. M.; Desvergne, J. P.; Keiper, S.; Lowden, P. A. S.; Vyle, J. S.; Tucker, J. H. R., *Chem. Commun.* **2006,** (48), 5003-5005.
2. Asanuma, H.; Takarada, T.; Yoshida, T.; Tamaru, D.; Liang, X. G.; Komiyama, M., *Angew. Chem. Int. Ed.* **2001,** *40* (14), 2671-2673.
3. Shi, Y.; Machida, K.; Kuzuya, A.; Komiyama, M., *Bioconjug. Chem.* **2005,** *16* (2), 306-311.
4. Wayne, C. E.; Wayne, R. P., *Photochemistry, OUP,* **1996**.
5. Watt, R. M. V. E. W., *J. Biol. Chem* **1979,** *254* (5), 1684-1690.
6. Turro, N. J. R., V. and Scaiano, J. C., *Principles of Molecular Photochemistry*. University Science Books: **2009**.
7. Birks, J. B., *Photophysics of Aromatic molecules*. J. Wiley & Sons: **1970**.
8. Hirayama, S.; Yasuda, H.; Okamoto, M.; Tanaka, F., *J. Phys. Chem.* **1991,** *95* (8), 2971-2975.
9. Mataga, N.; Kaifu, Y.; Koizumi, M., *Bull. Chem. Soc. Jpn* **1956,** *29* (4), 465-470.
10. Barltrop, J. A., Coyle J.D., *Excited States In Organic Chemistry*. 1975.
11. van Holde, K. E. J., W. C. and Ho, P.S., *Principles Of Physical Biochemistry*. Prentice Hall: 1998.
12. Venkatesan, N.; Seo, Y. J.; Kim, B. H., *Chem. Soc. Rev.* **2008,** *37* (4), 648-663.
13. Fukui, K.; Tanaka, K.; Fujitsuka, M.; Watanabe, A.; Ito, O., *J. Photochem. Photobiol. B-Biology* **1999,** *50* (1), 18-27.
14. Wagenknecht, H. A., *Charge Transfer in DNA*. Wiley: **2005**.
15. Sauer, M.; Drexhage, K. H.; Lieberwirth, U.; Muller, R.; Nord, S.; Zander, C., *Chem. Phys. Lett.,* **1998,** *284*, 153 - 163.
16. Heinlein, T.; Knemeyer, J. P.; Piestert, O.; Sauer, M., *J. Phys. Chem. B* **2003,** *107* (31), 7957-7964.
17. Saito, Y.; Miyauchi, Y.; Okamoto, A.; Saito, I., *Chem. Commun.* **2004,** (15), 1704-1705.
18. Fukui, K.; Iwane, K.; Shimidzu, T.; Tanaka, K., *Tetrahedron Lett.* **1996,** *37* (28), 4983-4986.
19. Kashida, H.; Liang, X. G.; Asanuma, H., *Curr. Org. Chem.* **2009,** *13* (11), 1065-1084.
20. Kuzuya, A.; Machida, K.; Komiyama, M., *Tetrahedron Lett.* **2002,** *43* (46), 8249-8252.
21. Kashida, H.; Asanuma, H.; Komiyama, M., *Chem. Commun.* **2006,** (26), 2768-2770.
22. Fukui, K.; Tanaka, K., *Nucleic Acids Res.* **1996,** *24* (20), 3962-3967.
23. Hwang, G. T.; Seo, Y. J.; Kim, B. H., *J. Am. Chem. Soc.* **2004,** *126* (21), 6528-6529.
24. Hurley, D. J.; Seaman, S. E.; Mazura, J. C.; Tor, Y., *Org. Lett.* **2002,** *4* (14), 2305-2308.
25. Okamoto, A.; Tainaka, K.; Saito, I., *J. Am. Chem. Soc.* **2003,** *125* (17), 4972-4973.
26. Okamoto, A.; Kanatani, K.; Saito, I., *J. Am. Chem. Soc.* **2004,** *126* (15), 4820-4827.
27. Cekan, P.; Sigurdsson, S. T., *Chem. Commun.* **2008,** (29), 3393-3395.

28. Torimura, M.; Kurata, S.; Yamada, K.; Yokomaku, T.; Kamagata, Y.; Kanagawa, T.; Kurane, R., *Anal. Sci,* **2001,** *17* (1), 155-160.
29. Seidel, C. A. M.; Schulz, A.; Sauer, M. H. M., *J. Phys. Chem.* **1996,** *100* (13), 5541-5553.
30. Balon, M.; Munoz, M. A.; Carmona, C.; Guardado, P.; Galan, M., *Biophys. Chem.* **1999,** *80* (1), 41-52.
31. Crespo-Hernandez, C. E.; Close, D. M.; Gorb, L.; Leszczynski, J., *J. Phys. Chem. B* **2007,** *111* (19), 5386-5395.
32. Wilson, J. N.; Cho, Y. J.; Tan, S.; Cuppoletti, A.; Kool, E. T., *Chembiochem* **2008,** *9* (2), 279-285.
33. Manoharan, M.; Tivel, K. L.; Zhao, M.; Nafisi, K.; Netzel, T. L., *J. Phys. Chem.* **1995,** *99* (48), 17461-17472.
34. Prunkl, C.; Berndl, S.; Wanninger-Weiss, C.; Barbaric, J.; Wagenknecht, H. A., *Phys. Chem. Chem. Phys.* **2010,** *12* (1), 32-43.
35. Eley, D. D.; Spivey, D. I., *Trans. Faraday Soc.* **1962,** *58* (470), 411-&.
36. Boon, E. M.; Barton, J. K., *Curr. Opin. Struct. Biol.* **2002,** *12* (3), 320-329.
37. Jortner, J.; Bixon, M.; Langenbacher, T.; Michel-Beyerle, M. E., *Proc. Nat. Ac. Sci. USA* **1998,** *95* (22), 12759-12765.
38. Giese, B., *Annu. Rev. Biochem.* **2002,** *71*, 51-70.
39. Wagenknecht, H. A., *Angew. Chem. Int. Ed.* **2003,** *42* (22), 2454-2460.
40. Rehm, D.; Weller, A., *Isr. J. Chem.* **1970,** *8* (2), 259-&.
41. Weller, A., Rehm, D., *Ber. Bunsenges* **1969,** *73* (834).
42. Weller, *Z. Phys. Chem. N. F.* **1982,** *8*, 93-98
43. Heinze, J., *Angew. Chem. Int. Ed.* **1984,** *23* (11), 831-918.
44. Baldwin, R. P.; Ravichandran, K.; Johnson, R. K., *J. Chem. Ed.* **1984,** *61* (9), 820-823.
45. Okazaki, S.; Oyama, M.; Nomura, S., *Electroanalysis* **1997,** *9* (16), 1242-1246.
46. Hammerich, O.; Parker, V. D., *Acta Chem. Scand. Ser. B* **1982,** *36* (8), 519-527.
47. Nozaki, K.; Oyama, M.; Hatano, H.; Okazaki, S., *J. Electroanal. Chem.* **1989,** *270* (1-2), 191-204.
48. Steenken, S.; Telo, J. P.; Novais, H. M.; Candeias, L. P., *J. Am. Chem. Soc.* **1992,** *114* (12), 4701-4709.
49. Steenken, S.; Jovanovic, S. V., *J. Am. Chem. Soc.* **1997,** *119* (3), 617-618.
50. Shafirovich, V. Y.; Courtney, S. H.; Ya, N. Q.; Geacintov, N. E., *J. Am. Chem. Soc.* **1995,** *117* (17), 4920-4929.
51. Chen, H. Y.; Kao, C. L.; Hsu, S. C. N., *J. Am. Chem. Soc.* **2009,** *131* (43), 15930-15938.
52. Kelley, S. O.; Barton, J. K., *Science* **1999,** *283* (5400), 375-381.
53. Kumar, C. V.; Asuncion, E. H., *J. Chem. Soc., Chem. Commun.* **1992,** (6), 470-472.
54. Fujii, T.; Kashida, H.; Asanuma, H., *Chem. Eur. J.* **2009,** *15* (39), 10092-10102.
55. Sarkar, D.; Das, P.; Basak, S.; Chattopadhyay, N., *J. Phys. Chem. B* **2008,** *112* (30), 9243-9249.
56. Modukuru, N. K.; Snow, K. J.; Perrin, B. S.; Thota, J.; Kumar, C. V., *J. Phys. Chem. B* **2005,** *109* (23), 11810-11818.

57. Kool, E. T.; Morales, J. C.; Guckian, K. M., *Angew. Chem. Int. Ed.* **2000,** *39* (6), 990-1009.
58. Peyret, N.; Seneviratne, P. A.; Allawi, H. T.; SantaLucia, J., *Biochemistry* **1999,** *38* (12), 3468-3477.
59. SantaLucia, J.; Allawi, H. T.; Seneviratne, A., *Biochemistry* **1996,** *35* (11), 3555-3562.
60. Kumar, C. V.; Punzalan, E. H. A.; Tan, W. B., *Tetrahedron* **2000,** *56* (36), 7027-7040.
61. Guckian, K. M.; Schweitzer, B. A.; Ren, R. X. F.; Sheils, C. J.; Tahmassebi, D. C.; Kool, E. T., *J. Am. Chem. Soc.* **2000,** *122* (10), 2213-2222.
62. Bertrand, J. R.; Vasseur, J. J.; Rayner, B.; Imbach, J. L.; Paoletti, J.; Paoletti, C.; Malvy, C., *Nucleic Acids Res.* **1989,** *17* (24), 10307-10319.
63. Berera, R.; van Grondelle, R.; Kennis, J. T. M., *Photosynth. Res.* **2009,** *101* (2-3), 105-118.
64. Yao, H.; Okada, T.; Mataga, N., *J. Phys. Chem.* **1989,** *93* (21), 7388-7394.
65. Kelly, S. M.; Jess, T. J.; Price, N. C., *Biochim. Biophys. Acta, Proteins Proteomics* **2005,** *1751* (2), 119-139.
66. Norden, B. B., H.;, *J. Am. Chem. Soc.* **1999,** *121*, 11947-11952.
67. Nakamoto, K. T., M. and Strahan, G., *Drug-DNA Interactions*. Wiley: **2008**.
68. Pohl, F. M.; Jovin, T. M., *J. Mol. Biol.* **1972,** *67* (3), 375-&.
69. Rodger, A.; Blagbrough, I. S.; Adlam, G.; Carpenter, M. L., *Biopolymers* **1994,** *34* (12), 1583-1593.
70. Rodger, A. N., B., *Circular Dichroism and Linear Dichroism*. Oxford University Press: 1997.
71. Dickerson, R. E., *Nucleic Acids Res.* **1989,** *17* (5), 1797-1803.
72. Lyng, R.; Rodger, A.; Norden, B., *Biopolymers* **1992,** *32* (9), 1201-1214.
73. Becker, H.-C., *Chem. Rev.,* **1993,** *93*, 145 - 172.
74. Bouas-Laurent, H.; Castellan, A.; Desvergne, J.-P.; Lapouyade, R., *Chem. Soc. Rev.,* **2000,** *29*, 43 - 55.
75. McSkimming, G.; Tucker, J. H. R.; Bouas-Laurent, H.; Desvergne, J.-P.; Coles, S. J.; Hursthouse, M. B.; Light, M. E., *Chem. Eur. J.,* **2002,** *8* (15), 3331 - 3342.
76. Rodger, A.; Taylor, S.; Adlam, G.; Blagbrough, I. S.; Haworth, I. S., *Bioorg. & Med. Chem.* **1995,** *3* (6), 861-872.

Chapter 4 Molecular modelling of anthracene duplexes

4.1 Introduction

4.1.1 Molecular Modelling

Molecular modelling is a collective term referring to the many different theoretical and computational approaches used to calculate a molecular structure, perform molecular dynamics and calculate molecular properties such as reaction intermediates and thermodynamic analyses. All the methods used in modelling rely on a set of equations and a large set of parameters that when combined comprise a *semiempirical forcefield*. These equations are a mathematical description of molecular motion and atomic interaction energies. The parameter set describes the specific characteristics of all the different atoms and their bonds and the parameter values are derived from a combination of quantum mechanical calculations and experimental studies.[1]

4.1.2 Model building

The construction of a model usually consists of three steps:

Firstly the distance geometry must be defined in order to construct energetically reasonable structures. This is accomplished by considering atoms as rigid sphere-potentials (i.e. solid balls) and determining their relative three-dimensional positions in a molecule by using bond connectivity information combined with experimentally derived NOE interproton distances.

Secondly, the structure is subjected to *energy minimization* which will remove any structural anomalies and produce a lowest energy structure.

Lastly, the movement of a molecule can be simulated using a process called *molecular dynamics* (MD). This is often used to mould an initial structure into a more experimentally realistic one and is accomplished by a process called *simulated annealing*. This involves heating up the structure to increase the kinetic energy of the atoms (usually to 400-600 K) and then after a short period of time, slowly lowering it back to 275 K where it is allowed to equilibrate. This energy increase allows the molecule to explore more conformations and as the kinetic energy decreases, the potential energy surface of the molecule guides it to a more realistic structure with a relatively lower total energy. The time of the simulation needs to be considered, as well as the initial velocities, all of which can affect the validity of the final output model.

4.1.3 Using AMBER

Models of the different oligonucleotide probes, both single-and double stranded, were constructed using the Insight II modelling program biopolymer function. They were then modified by constructing the anthracene subunit and integrating it into the oligonucleotide using the ANTECHAMBER module of the AMBER 8 software program. The resulting structure was then immersed in a water box of radius 15Å using the TIP3P function in the LEAP module of AMBER. Additionally, some water molecules were replaced by sodium cations to neutralize the negative charge of the phosphate groups on the DNA backbone. The resultant structure contained approximately 4000 atoms including 800 DNA atoms, 30 counterions and 3200 water molecules. Energy minimization was then performed using the SANDER program. The resultant structure was then run in the AMBER force field under molecular dynamic conditions with three different

starting velocity parameters to produce a structure with a simulation time of 1 ns. The output parameters were re-entered into AMBER to produce a simulation run-time of up to 10ns.

4.2 Modelling unmodified DNA

Initially, unmodified DNA was modelled as a reference to compare to the later modification. The sequence chosen was the same as that used for the modified modelling except for being fully matched with respect to all of the bases. The model shows characteristic features of DNA such as propeller twist and kinking of the strand (Fig. 137).

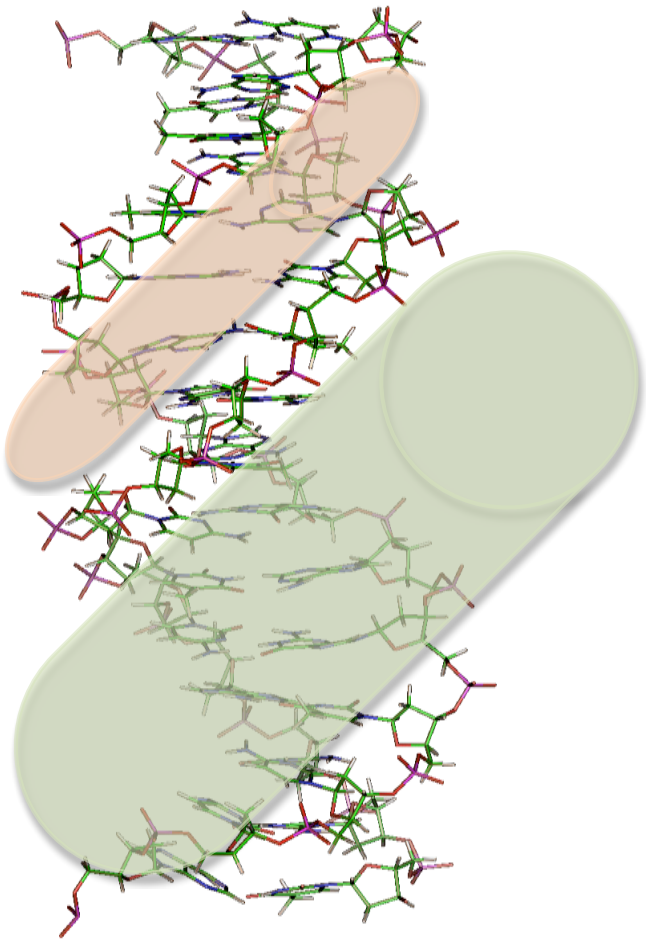

Fig. 137 AMBER model of unmodified DNA showing the major groove (green cylinder) and the minor groove (red cylinder)

Also clearly visible are the major and minor grooves. This model was used as the basis for the modified DNA duplexes by removing a single base and then manually constructing the anthracene nucleotide.

4.3 Modelling modified DNA duplexes

The first modified structures to be modelled were of the *n* = 1 oligonucleotides. The fully matching duplexes were modelled starting with Probe A Tar A1 L (*RR*) and D (*SS*). The structures are shown below (Fig. 138).

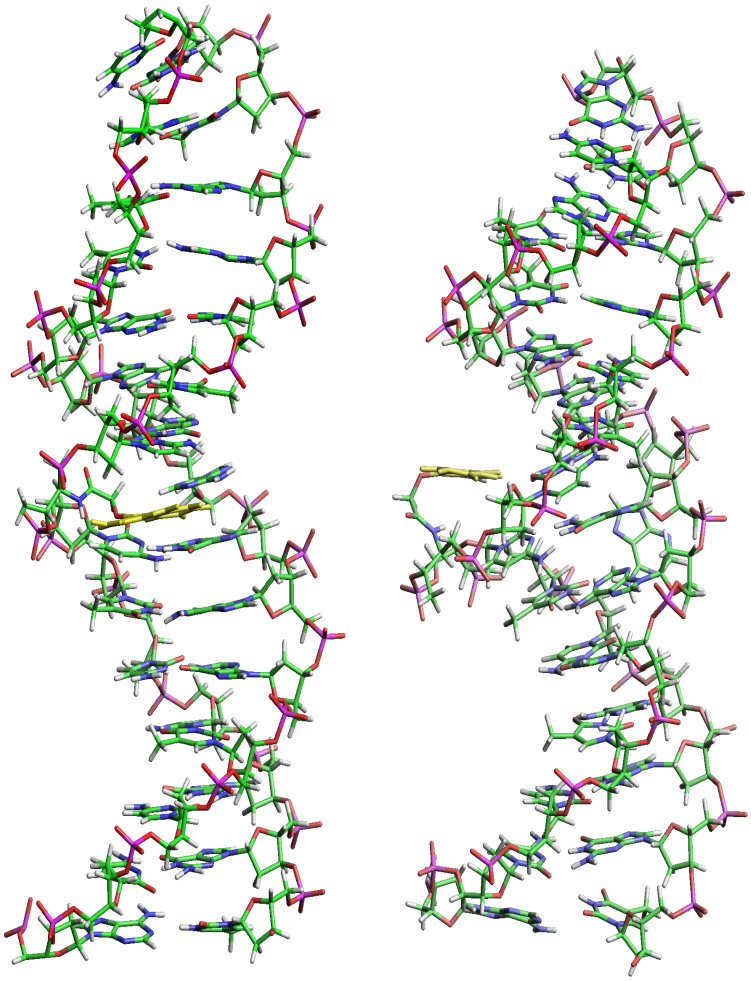

Fig. 138 AMBER models of anthracene (yellow) tagged DNA with L threoninol (left 5ns run time) and D threoninol (right 5ns run time) backbones

Initial inspection of the resulting structures show how the isomers adopt quite different orientations that are constrained by the stereochemistry of the pseudo-sugar backbone. The L threoninol directs the anthracene towards the major groove of DNA whilst the D threoninol directs the anthracene towards the minor groove (see Fig. 137).

4.4 Rationalization of experimental results for the L (*RR*) isomer matched duplexes

4.4.1 *n* = 1 L anthracene core structure

For the *RR* Probe A, a single 1ns molecular dynamics run produced a structure where the anthracene is stacked directly underneath the upstream C base in the major groove. Further modelling time (up to 5ns) or varied starting velocities did not show any difference in the final position adopted by the anthracene. This backs up the conclusions from the fluorescence studies outlined in the previous chapter that the anthracene signal is affected by the identity of the upstream base pair of the probe strand. The area of interest is displayed below in CPK form (Fig. 139), the anthracene (yellow) is situated closer to, and overlapping better with, the upstream bases (red) than the downstream (blue).

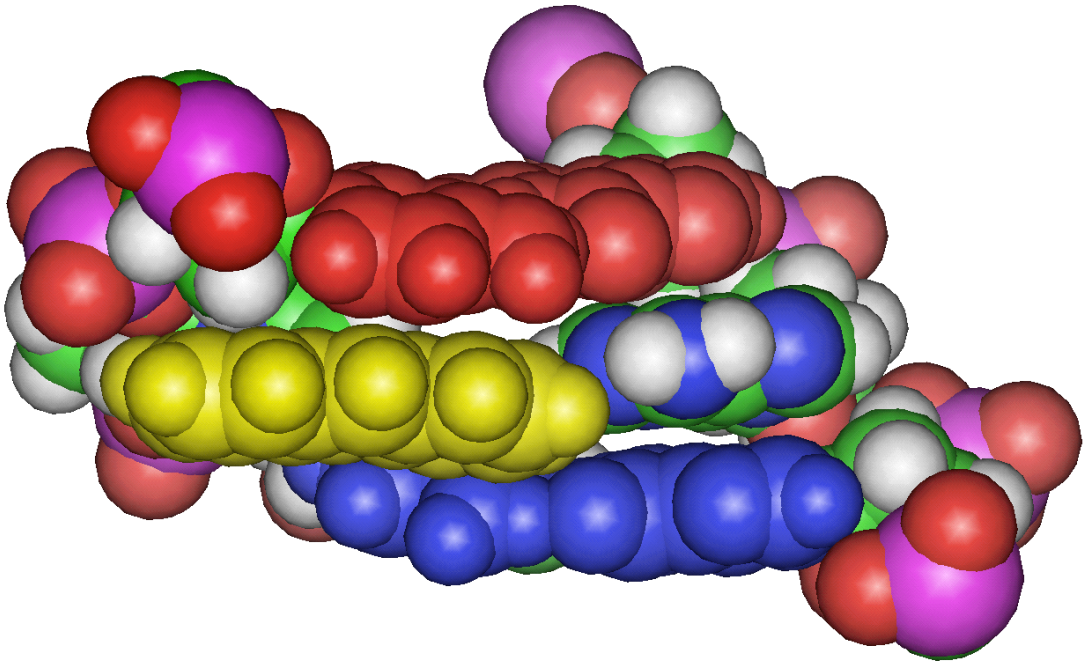

Fig. 139 CPK model of the core section of Probe A (L) Tar A1 view along xy plane

4.4.2 Fluorescence

The close stacking of the base would also seem to be consistent with the assumption that the formation of an encounter complex followed by electron transfer is important in quenching. The winding of the helix causes the downstream bases to be twisted away from the vertical axis of the anthracene and which can explain why variation of these bases has no effect on the fluorescence signal. This is demonstrated in the image below showing a view down the vertical z-axis of the duplex (Fig. 140) where it can be seen that the downstream bases (blue) are unable to associate with the anthracene.

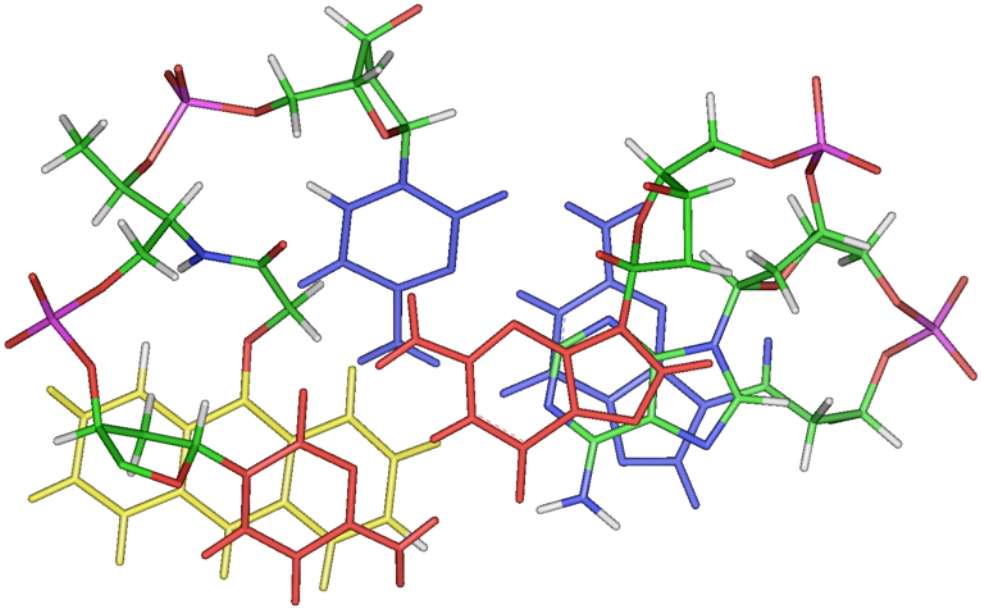

Fig. 140 Stick model of Probe A (L) Tar A1 view along z axis

The location of the anthracene, with no orbital overlap or close contact with the base directly opposite, is consistent with the experimental results which show there to be no change in fluorescence upon variation of this base. Subsequent modelling of the strands with different bases (C, G and T) in this position shows a very similar structure in all cases.

4.4.3 Implications for the CD data

The model suggests that the anthracene is located with its long axis inclined at an angle to the base pair long axis (Fig. 140). This agrees with the CD data (Fig. 141 blue), which suggests that the peak at 254 nm arises from the anthracene long axis transition moment being located close to and aligned towards the base pair long axis at an angle that approaches 45° (see 3.14).[2]

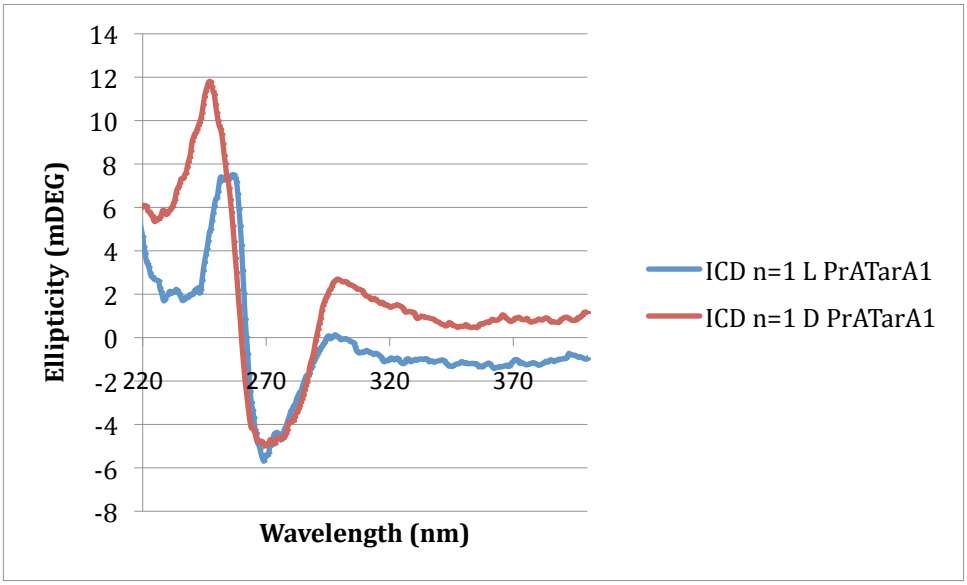

Fig. 141 ICD spectra of Probe A Target A1 5µM with 10 mM pH 7 phosphate buffer and 100 mM NaCl subtracted using TarMATarA1

4.5 Comparison with matched duplexes of the D (*SS*) isomer

4.5.1 Fluorescence differences

Due to the stereochemical constraints imposed by the threoninol backbone the D or *SS* isomer strand has the anthracene orientated into the minor groove. The location of the anthracene in the minor groove (Fig. 138 Fig. 143) would seem to explain why the D isomer lacks the ability to detect mismatches; it is no longer close enough to any of the bases to be affected by any changes.

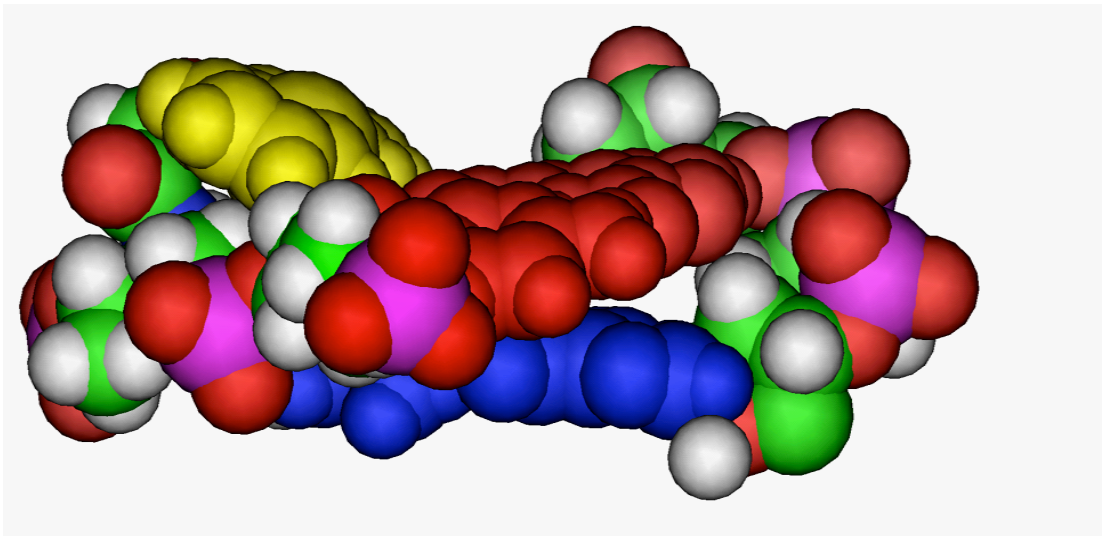

Fig. 142 CPK model of the core section of Probe A (D) Tar A1 view along xy plane

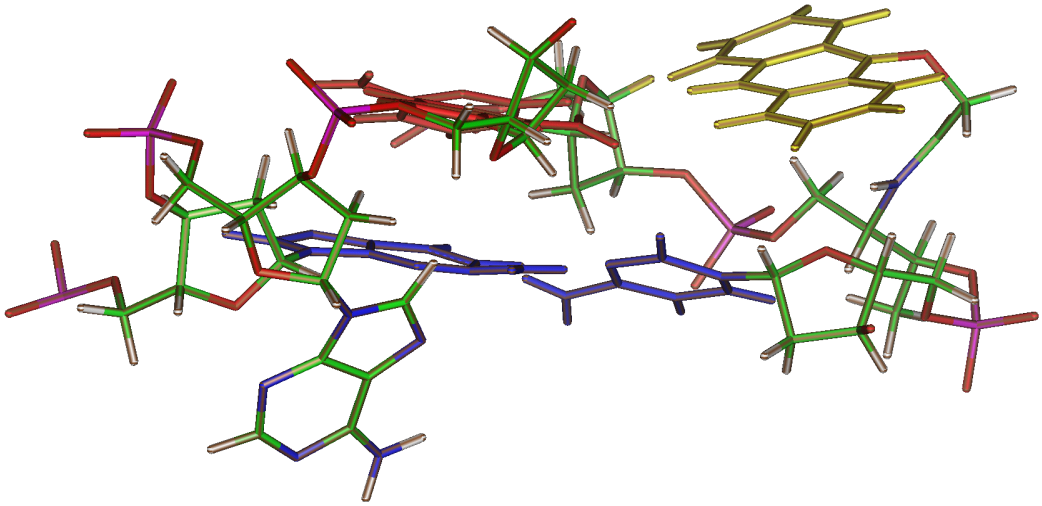

Fig. 143 Stick view of the core section of Probe A (D) Tar A1 view along xy axis

4.5.2 Explanation of the differences in melting point between stereoisomers

In section 1.3.4.3 it was discussed that in the work of Asanuma and Komiyama involving the intercalation of azo-benzenes into DNA, a comparison of the D and the L forms showed a very strong difference between the thermal stability of the different duplexes as seen by melting point studies. This was ascribed to the difference in winding tendencies with the D isomer favouring a more natural winding. As a result it would be expected to see a similar result with anthracene, but an inspection of the T_m data (Table 41) shows this not to be the case: for the *n* = 1 linker the L isomer strands always have a higher melting point (3.9).

Table 41 Melting points of Probe A (°C) D and L isomer matching strand 5μM with 10 mM pH 7 phosphate buffer and 100 mM NaCl

Target Strand	A1
	3'GAG
n = 1 Pr A L	**54**
n = 1 Pr A D	**48**

This can be explained by looking at the models (Fig. 138) that show that the insertion of the anthracene linked to the D isomer causes kinking of the helix.

This could impart a degree of strain in the structure and facilitate the break up of the two strands, leading to a lower melting point.

Initially, it was believed that the kicking out of the adenine base also contributed to the decrease in melting point. However, subsequent molecular modelling of the other base opposite duplexes (with C, G and T opposite of the anthracene) have shown that in these duplexes the opposite base is not kicked out.

4.5.3 CD data

The anthracene axis is aligned perpendicular to the base pair axes in the duplex. As mentioned previously this would be expected to give an induced CD signal at 254 nm, and that is in fact what is observed in the ICD spectrum (Fig. 141).

4.5.3.1 CD data and modelling of different bases opposite the anthracene

CD spectra of the D isomer Probe with different bases opposite of the adenine showed different peak intensities for the bases C, T and G (Fig. 144).

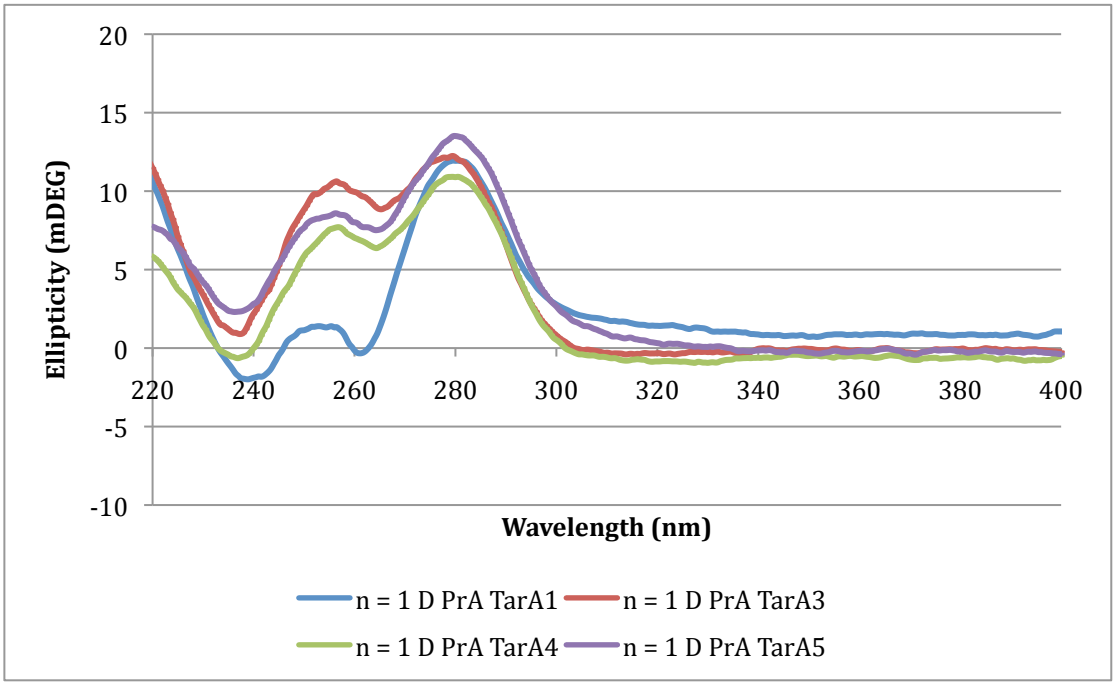

Fig. 144 CD spectra of Probe A (D) with different bases opposite the anthracene 5µM with 10 mM pH 7 phosphate buffer and 100 mM NaCl

Inspection of the duplex models shows that the anthracene in the PrA D TarA1 duplex adopts a different orientation relative to the base pair axes compared to the A3, 4 and 5 duplexes, this is as a result of the greater compression of the minor groove where the anthracene sits, as in the A1 duplex the adenine is twisted out of the duplex causing an increase in the compression of the minor groove (Fig. 145 far left).

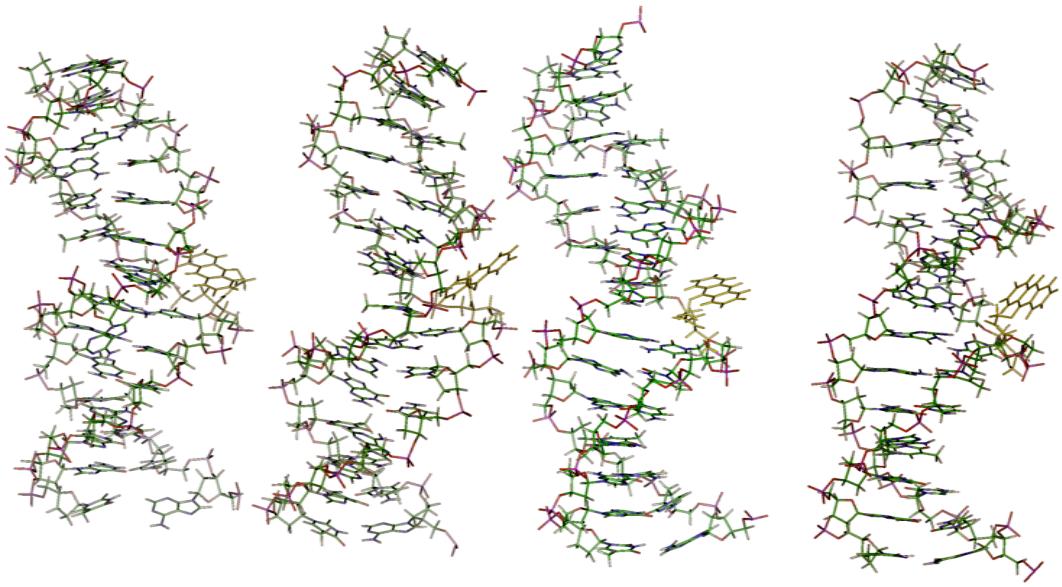

Fig. 145 AMBER models of base opposite duplexes PrA D Targets A1,A3,A4 and A5 (from left to right) representing an Adenine, Thymine, Cytosine and Guanine opposite the anthracene

The resulting difference in the size of the minor groove appears to cause the anthracene to insert into the duplex with the oxygen closer to the centre of the duplex for the TarA1 duplex and further away from the centre in the other three duplexes. This may also explain the different CD spectra.

4.6 Probe A vs. Probe G: Structures of more emissive duplexes

Although a number of changes in fluorescence can be explained by changes in redox potentials, some appear to depend on structural factors, i.e. the location of

the anthracene as determined by the base sequence. An example is that upon the formation of a duplex of Probe G L (5' TLC) with a matching target strand, the fluorescence emission increases by 67%. This is the only probe strand for which this occurs for both isomers and given the relatively high reduction potential of the T base does not appear to be related to redox processes.

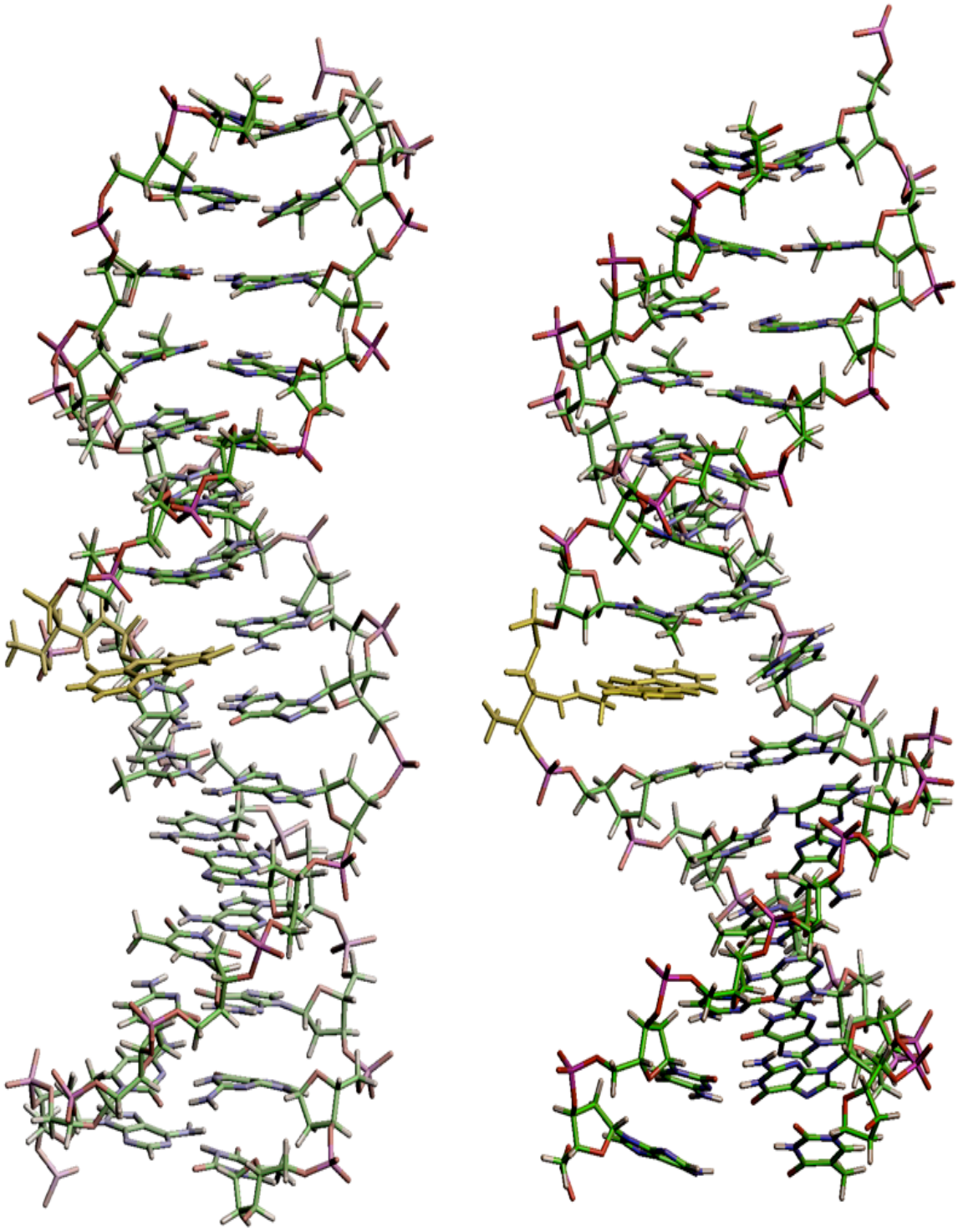

Fig. 146 AMBER models 4ns of PrA L TarA1 (left) and PrG L TaGA1 (right)

However, inspection of the models simulated for this duplex (Fig. 146 right) compared to Probe A TarA1 (Fig. 146 left), our standard, show that the anthracene (yellow) moiety is inserted into the duplex to a much greater extent in Probe G compared to Probe A. This is possible due to the opposite A base

being forced out of the duplex creating space for the anthracene to fully intercalate between the flanking bases. This can be better observed in the following magnified CPK model (Fig. 147red circle).

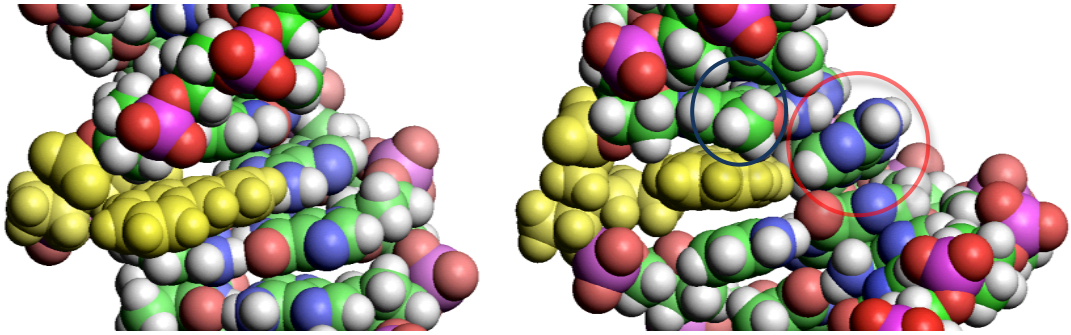

Fig. 147 Close up CPK view of PrATarA1 (left) and PrGTarG1 (right) showing the T methyl group (blue circle) and kicked out adenine (red circle)

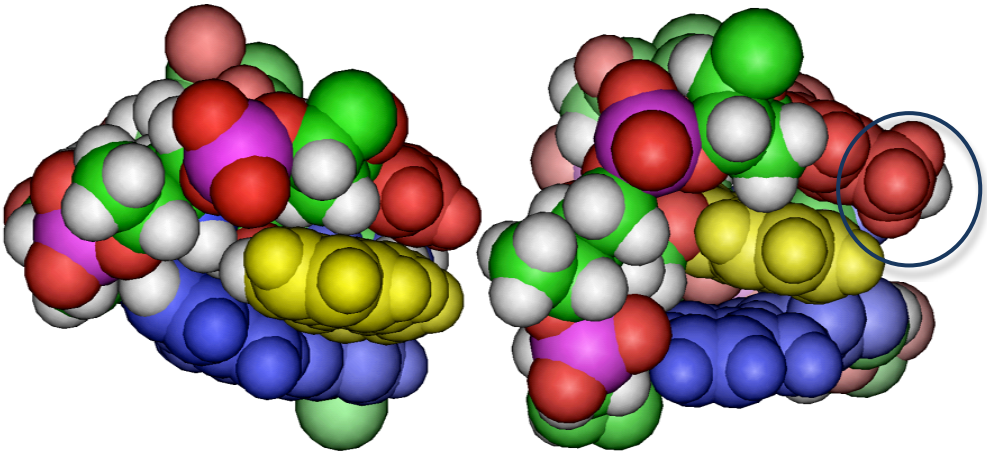

Fig. 148 Close up CPK view of PrATarA1 (left) and PrGTarG1 (right) showing the T methyl group (blue circle)

The driving force for this may be due to the steric clash between the methyl group on the upstream T base (Fig. 148 blue circle) and the anthracene that would prevent the anthracene from adopting the same conformation as in other duplexes. Given that T is the only non planar base this could be the reason for the unusual emission. Usually nucleobases are in direct π-π van der Waals contact throughout the stack, and so the bases are separated by a distance of ca. 3.4 Å.[3]

The diameter of a methyl group is ca 1.8 Å, and as a result could cause steric clashes between the anthracene and the T base. This would then lead to the bases to adopt a greater degree of separation from the anthracene. Since the strength of aromatic π-π interactions are inversely proportional to cube of the distance between the DNA base and the chromophore,[4] a significant increase in distance could greatly alter the emission properties of anthracene. This could explain the fact that there are only two fluorescence lifetimes observed in the duplex form (see 3.6.4 Table 17).

There is also further evidence that the position of the anthracene in the PrG (L) TarG1 duplex is different from that in other duplexes in the CD spectra of the standard matching sequence (PrA (L) TarA1). As shown in Fig. 149, it is noticeable that the shoulder at 254 nm is more intense for Probe G than it is for Probe A. If the intensity of this signal is a reflection of the angle between the long axis of the anthracene and the base pair long axis[5] then the different sizes of these signals would appear to back up the assumption of a different position of the anthracene relative to the z-axis.

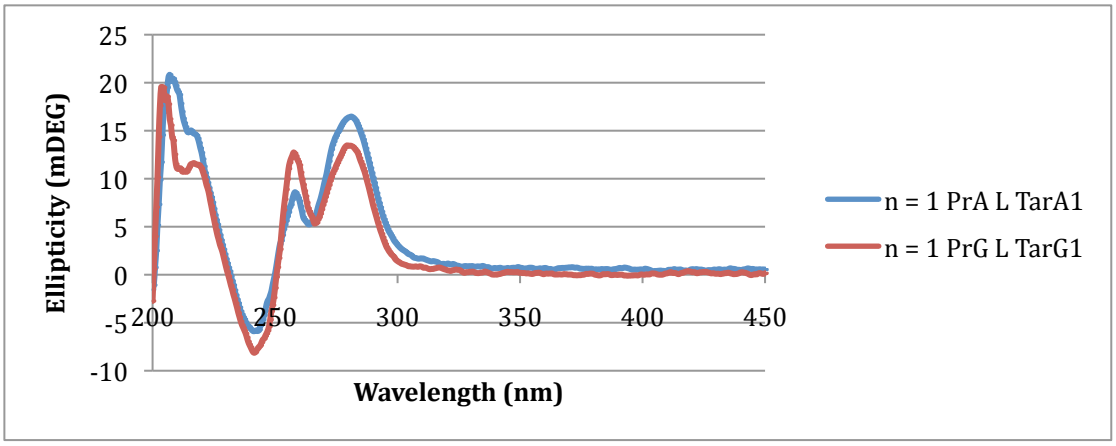

Fig. 149 CD spectra of Probe A and G with matching strands 5µM 10mM pH 7 phosphate buffer 100mM NaCl

If this reasoning is continued then it might be possible to explain the unusual reversal of trends that occur with Probe G L, namely that all upstream mismatches cause a decrease in emission (Table 42). This is a complete reversal of the trend for all of the other Probes, which show an increase in emission for upstream mismatches.

Table 42 Percentage change in fluorescent emission at 426 nm comparing Probe A (L) with Probe G (L) 1μM 10mM pH 7 phosphate buffer 100mM NaCl

	Target	A1	A3	A4	A5	E1	F1	G1	G2
Probe		3'GAG	GTG	GCG	GGG	CAG	TAG	AAG	A_G
n=1 Pr A	5' CLC	**-75**	**-76**	**-75**	**-78**	**86**	**45**	**70**	**25**
n=1 Pr G	5' TLC	**-65**	**-81**	**-80**	**-75**	**0**	**-38**	**58**	**18**

The explanation may be that the presence of a mismatch reduces the structural rigidity of the duplex and allows the anthracene to revert to a less sterically hindered location which is better placed for quenching.

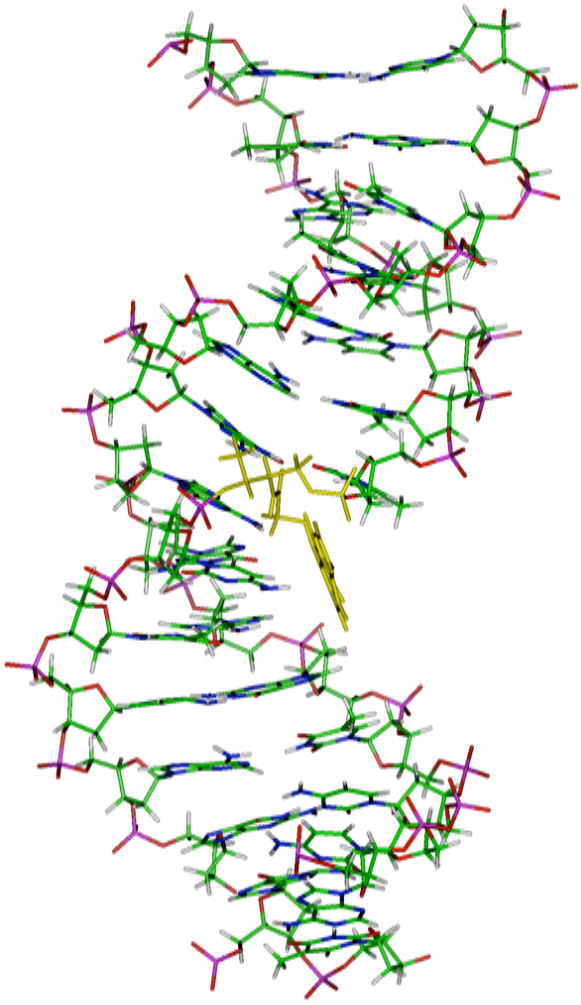

Fig. 150 AMBER model of Probe G L TarA1

The model of PrG (L) TarA1 (Fig. 150) illustrates how this is possible, with the anthracene now adopting a position where it is potentially more exposed to solvent quenching. This could explain the decrease in fluorescence emission. If we now consider Probe A L TarA1 (which is quenched upon hybridization [top left Fig. 151 and Fig. 152]), Probe G L TarG1 (which is more emissive upon hybridization [top right Fig. 151 and Fig. 152]) and Probe G L TarA1 (which is quenched upon hybridization [bottom Fig. 151 and Fig. 152) we can see that the first and last aforementioned duplexes have the most similar anthracene alignment.

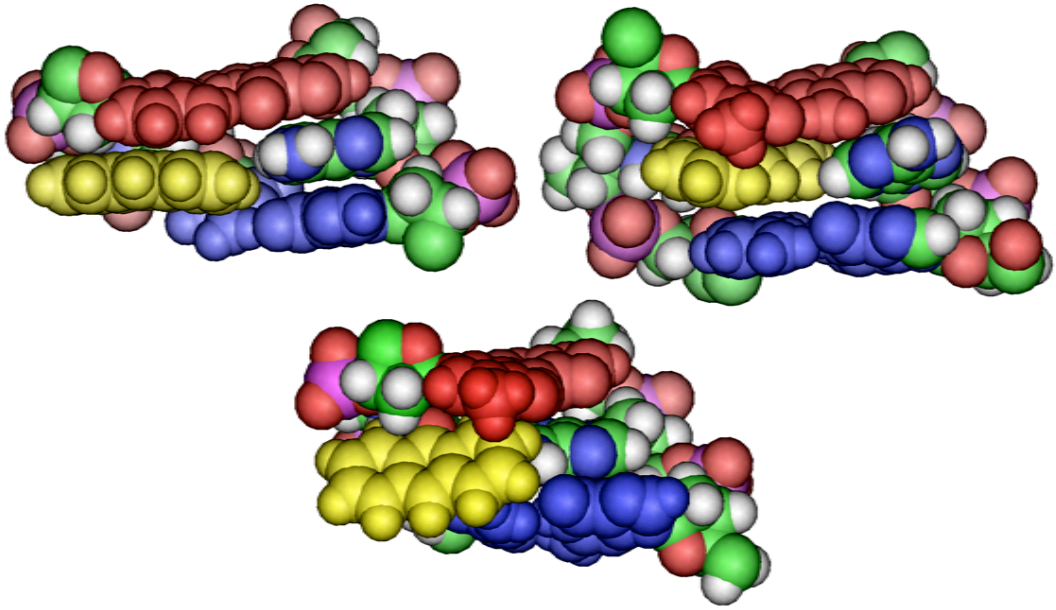

Fig. 151 AMBER CPK rendered models of Probe A TarA1 (top left) Probe G TarG1 (top right) and Probe G TarA1 (bottom) view along xy axis

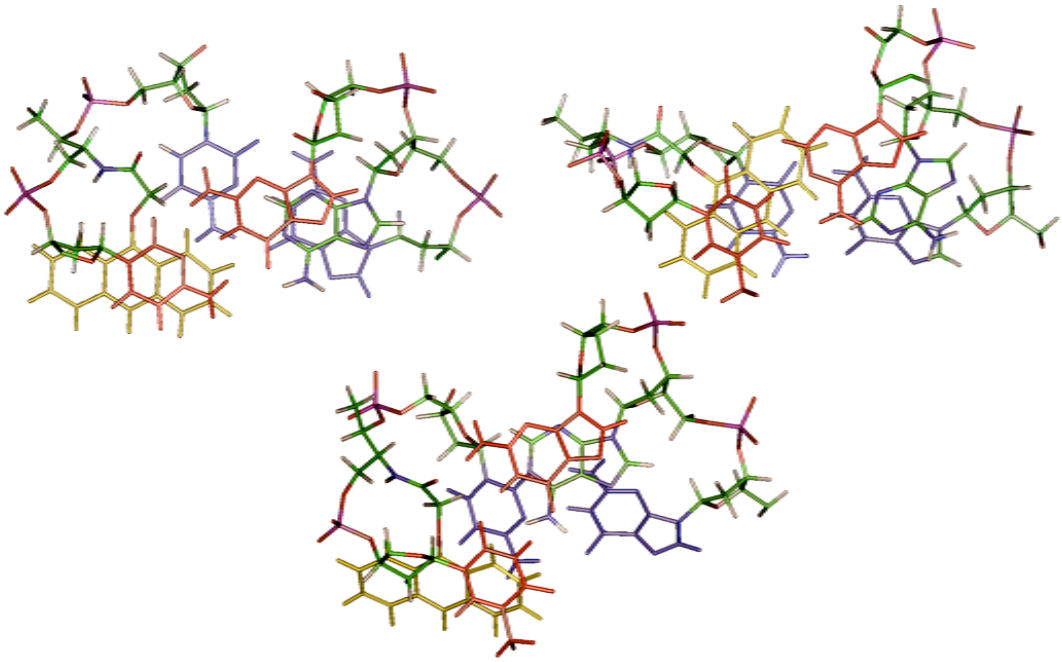

Fig. 152 AMBER models of Probe A TarA1 (top left) Probe G TarG1 (top right) and Probe G TarA1 (bottom) view along z axis

4.7 Refining the explanation of mismatch sensing

Analysis of mismatched duplexes of Probe A also shows how structural factors may be also partially responsible for increases in emission intensity. For instance, the L isomer duplex PrATarG1 (Fig. 153 right), which has an increase in fluorescent emission of 70%, shows a similar distortion of the duplex as described above:

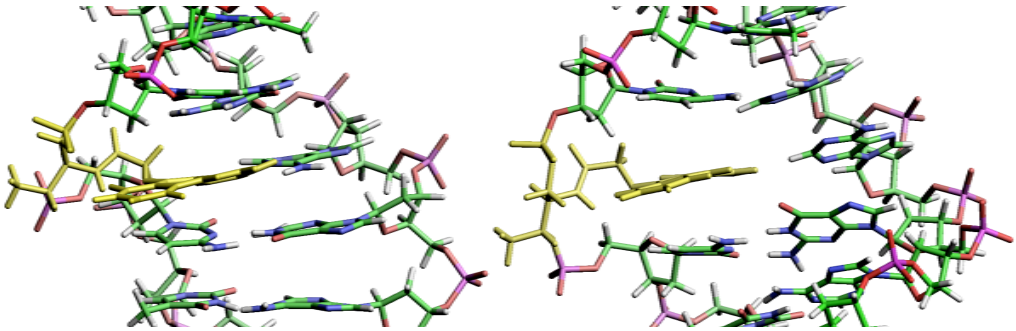

Fig. 153 Stick representation of the core Probe A TarA1 and Probe A TarG1 view along xy axis

This is significant in that we can explain the increase in fluorescent emission due to the absence of proton transfer from the upstream G-C base pair that prevents the C upstream of the anthracene from quenching via electron transfer as efficiently as before. However, to explain the different levels of emission increase requires us to look at secondary structural effects.

Table 43 PrA percentage fluorescence change upon hybridization with upstream mismatches recorded at room temperature λex 350 nm λem 426 nm 1 μM oligonucleotide concentration 10 mM pH 7 phosphate buffer 100 mM NaCl

		CAG	TAG	AAG
		E1	F1	G1
n = 1 Pr A	5' CLC	**86**	**45**	**70**

If it was considered that the loss of proton transfer to C was the only factor driving the increase in fluorescence emission then the increase in emission should be the same for all three different mismatches. Clearly, this is not the case and given that the base opposite the anthracene has not changed then there are two possible explanations

1. That the emission is affected by the single base opposite and upstream of the mismatch
2. The structure is altered by different mismatches to different extents and as a result the anthracene ends up in an environment that can be influenced by external quenchers, e.g. water, ions, to a greater or a lesser extent.

If 1. were wholly responsible then we would predict that the CT mismatch would rise the least (because T is a good quencher), CC somewhere in the middle (as C on its own is a worse quencher than T but better than A) and for the CA mismatch we would see the largest increase (A being the worst quencher).

Clearly this is not what is observed (Table 43). This leads to the conclusion that there are some structural factors that influence the degree of quenching.

4.7.1 Evidence of structural differences between probes with CT/CC and CA mismatches

Analysis of the ICD spectra confirm a structural difference for the C to A mismatch as evidenced by the presence of a shoulder at 254 nm that is stronger than in the other mismatch spectra (Fig. 154).

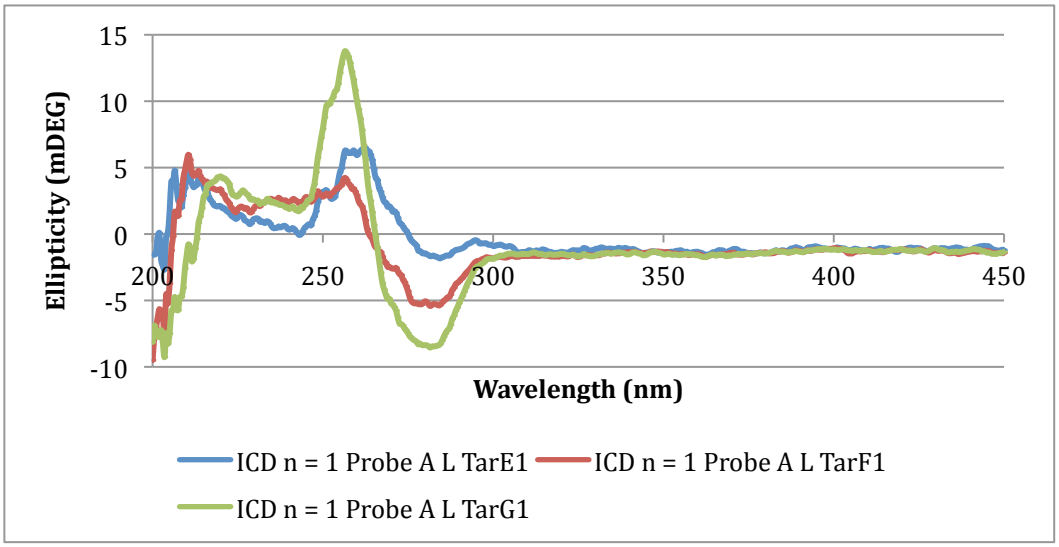

Fig. 154 ICD spectra of PrA L with base opposite mismatches 5 µM oligonucleotide concentration 10 mM pH 7 phosphate buffer 100 mM NaCl

In section 3.15.2 this was ascribed to the closer alignment of the anthracene magnetic moment, and hence the long axis, to 45°. Subsequent molecular modelling of the mismatched strands has shown that the CD data is in close agreement with the molecular modelling which shows a closer location, good overlap and closeness of the anthracene to a 45° alignment with the base pair long axis of the C to A mismatch (PrATarG1) compared to the C to T and C to C mismatches (PrA TarE1 and F1 Fig. 155 and Fig. 156). This structural difference may arise due to the greater space available in the C to A mismatch due to the bulkier adenine base.

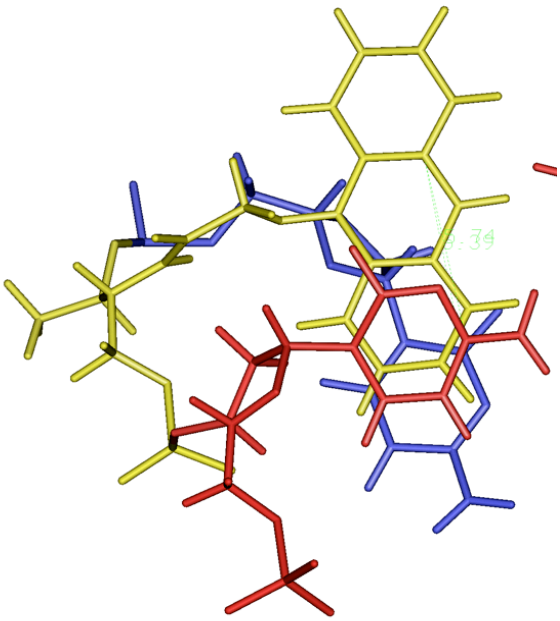

Fig. 155 Close up view of the core of the *n* = 1 PrA TarE1 duplex (upstream base in red, downstream in blue and anthracene in yellow)

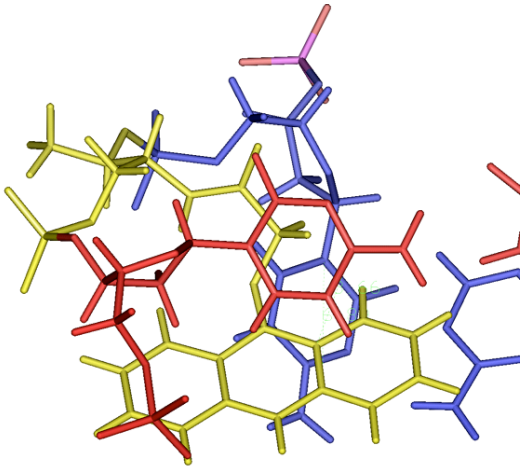

Fig. 156 Close up view of the core of the *n* = 1 PrA TarF1 duplex (upstream base in red, downstream in blue and anthracene in yellow)

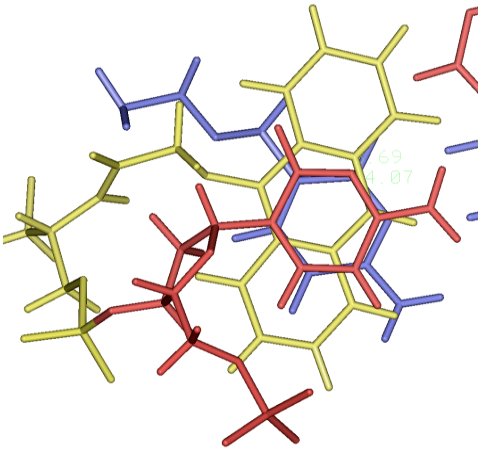

Fig. 157 Close up view of the core of the *n* = 1 PrA TarG1 duplex (upstream base in red, downstream in blue and anthracene in yellow)

The above figures demonstrate that the anthracene in the Probe A TarG1 mismatch (Fig. 157) has the best overlap with the up and downstream bases in the duplex. Furthermore, measurement of the base to anthracene distances in the models suggests that the PrA TarG1 duplex has the smallest average distance (approximately 3½ Å compared to 5½ Å for E1 and F1).

4.7.2 Expanding the analysis to other kinds of mismatch

Indeed, if then there are indications that the presence of mismatches gives rise to the importance of more distant structural effects then a more in-depth examination of fluorescence shows that even the base opposite the anthracene, previously considered of no importance can begin to influence the emission of anthracene (Table 44).

Table 44 Percentage change in fluorescence emission at 426 nm for 1uM solution room temp 10mM pH 7 phosphate buffer 100mM NaCl

		A1	A3	A4	A5
		3'GAG	GTG	GCG	GGG
n = 1 L PrE	5' GLC	**123**	**64**	**70**	**125**
n = 1 L PrF	5' ALC	**57**	**13**	**64**	**64**
n = 1 L PrG	5' TLC	**-65**	**-81**	**-80**	**-75**

Examination of the data shows that the presence of A and G bases opposite the anthracene generally give rise to a greater fluorescence emission than for T and C, a trend predicted by the ΔG_o calculations (see section 3.7.2). It is interesting to note that there is no such variation when the downstream base is mismatched.

The unusual decrease for the Probe G Target AX (upstream mismatches) structures could be the consequence of an unusual distorted structure seen previously (Fig. 158). In particular, the inclination of the anthracene with respect to the base pair xy plane may allow some sensing of the base directly opposite.

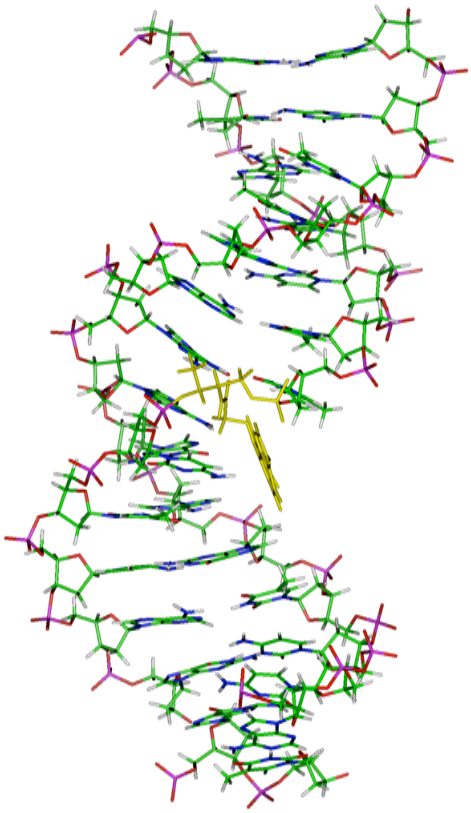

Fig. 158 AMBER model of *n* = 1 PrG TarA1 2ns

4.7.3 Conclusions

In trying to explain the trends in fluorescence changes that occur upon hybridization of *n* = 1 duplexes, it is apparent that although the degree of quenching is heavily affected by electron transfer processes, the structure of the duplex also plays a role. This is either by influencing the rate of electron transfer or by changing the influence of water quenching of the fluorescence emission.

4.7.4 Melting Temperature rationalisation

4.7.4.1 Explaining the low melting temperature of PrATarB1

The Probe A to Target B mismatch for the *n* = 1 L system (a C to C mismatch) displays an unusually low melting temperature (approx 5 °C lower than the other similar mismatches (Fig. 159).

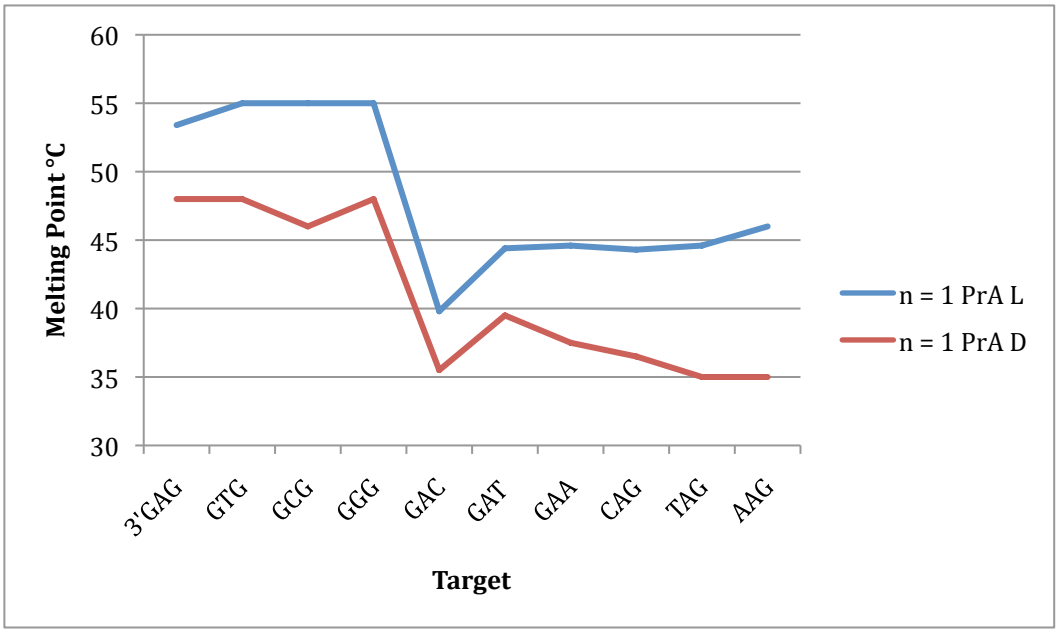

Fig. 159 Melting Points of PrA D and L isomers with base opposite target strands 5 µM solution room temp 10mM pH 7 phosphate buffer 100mM NaCl

This could be due to the formation of an extremely distorted structure proposed by molecular modelling (Fig. 160).°

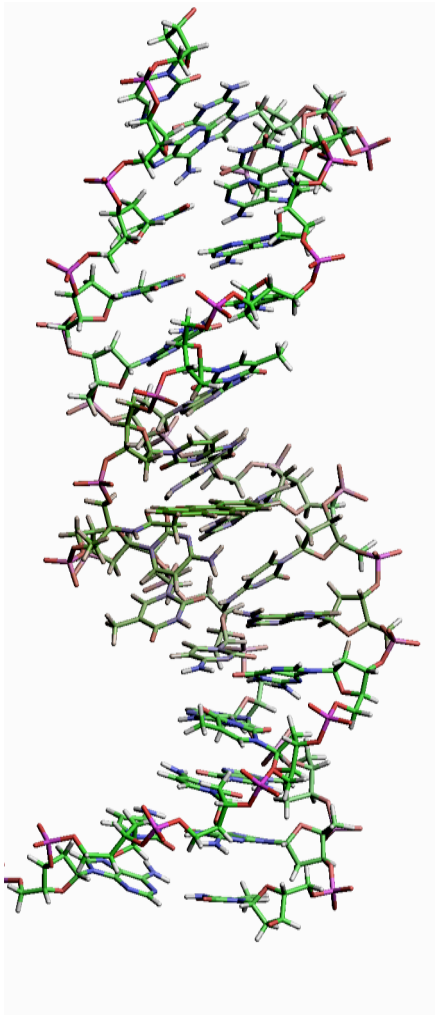

Fig. 160 AMBER model of n=1 L Probe A TarB1 (a C to C downstream mismatch)

A closer look at the central core highlights how the hydrogen bonding between two base pairs is broken, instead of the one that would be predicted by simple modelling of the system.

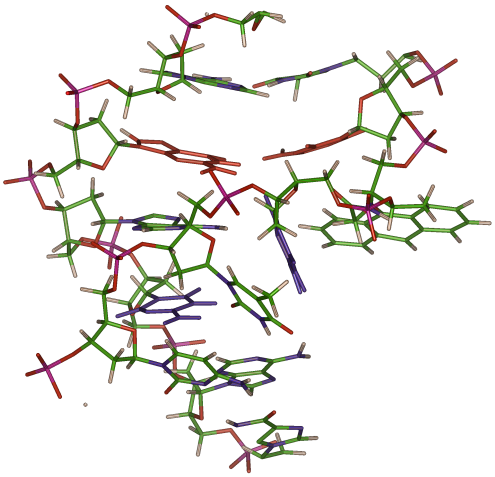

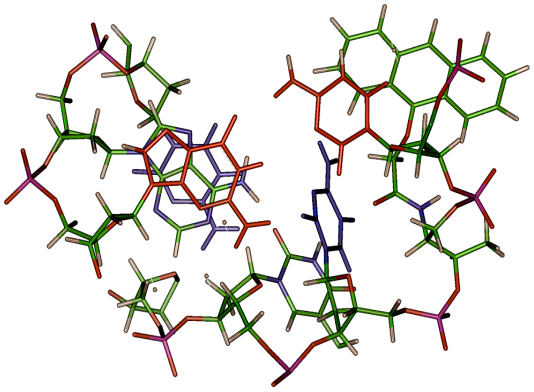

Fig. 161 PrA LTarB1 side view **PrA L TarB1 top view**

Further modelling of the analogous mismatches, C to A and C to T, do not show the same level of structural distortion, which is in keeping with their higher melting points.

This could arise as a result of the weakness of the C-C mismatch[6] (see 3.10.1).

4.8 Explaining differences in quantum yields on the basis of single strand structures

Since the single strand form of the oligonucleotide is less rigidly held than the duplex, more conformations are possible thus raising questions about the accuracy of the models. It is however, well documented that the single strand forms will attempt to maximize base stacking interactions and these are indeed the structures observed. Furthermore, with the n = 1 linker it seems likely that due to the inflexibility of the linkage the large difference in conformation will remain. Therefore if we consider the variation of the quantum yield of the single strand form (Table 45) between the different isomers of Probe A we can potentially explain the difference through different structures (Fig. 162).

Table 45 Quantum Yields of *n* = 1 Probes in single strand form

***n* = 1 L PrA**	**5' CLC**	**0.018**
***n* = 1 D PrA**	**5' CDC**	**0.053**

We can observe from the models that in the single strand form of Probe A L isomer the probability of forming an encounter complex is much greater than in the D isomer due to the relative orientation of the anthracene compared to the bases.

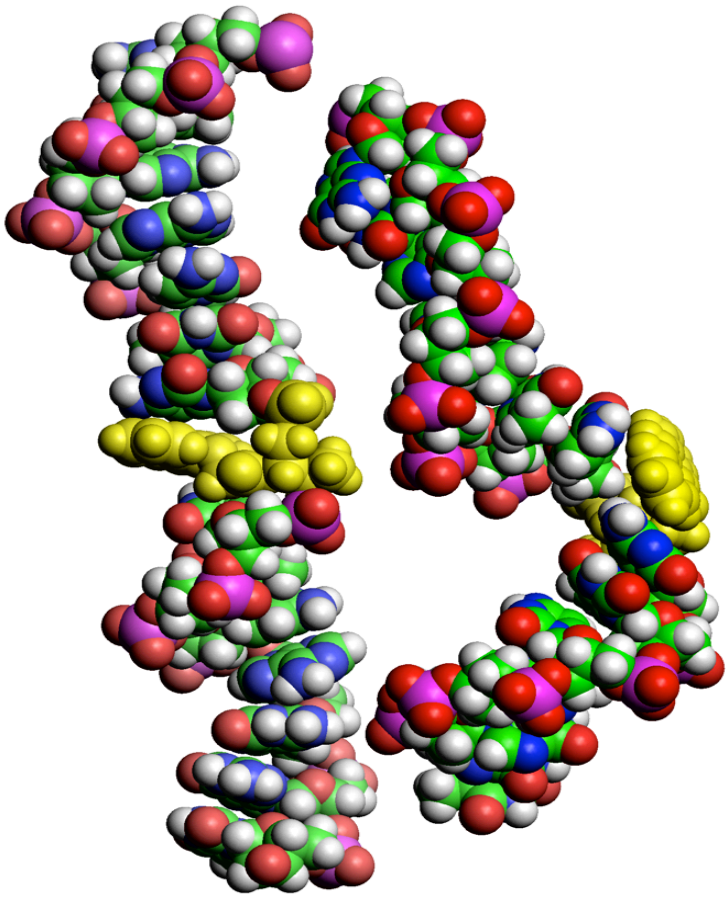

Fig. 162 AMBER models of Probe A L isomer (left) and D (right) in single strand form

In the L isomer (left), the anthracene stacks parallel to both of the adjacent nucleobases and has good orbital overlap with one of the bases. This makes the formation of an encounter complex relatively favourable and consequent quenching via electron transfer is presumably fast. In contrast, the D isomer is

orientated perpendicular to one of the bases and has poor orbital overlap with the other base.

4.9 Deletion Structures

4.9.1 SS stereoisomer system

Further modelling work was undertaken in order to model the deletion system. The D isomer structure is shown below and it is immediately obvious that the structure is quite similar to that of the base opposite system, although the anthracene is inserted more completely into the minor groove. This location is more suited to stabilizing the duplex and also results in less kinking of the duplex. This is reflected in the greater stability of the deletion compared to the base-opposite system and the consequent higher T_m of the former.

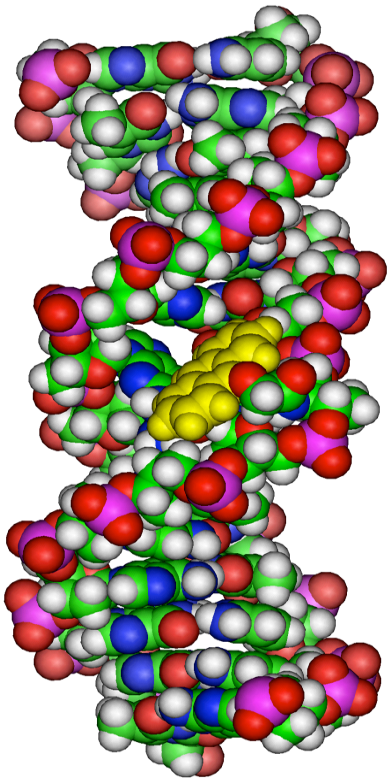

Fig. 163 AMBER models of Probe A D Target A2 anthracene moiety coloured yellow

4.9.2 RR stereoisomer system

The L isomer structure proved a more complicated system to simulate due to a considerable number of dihedral angles that had to be changed in order to accommodate the anthracene nucleobase into DNA. In particular the degree of twisting in the anthracene tagged strand is reduced in order to maintain the face to face orientation hydrogen bonding orientation of the bases. However, the final structure (Fig. 164) shows that the anthracene is intercalated into the core of the duplex, directly between the adjacent cytosine bases.

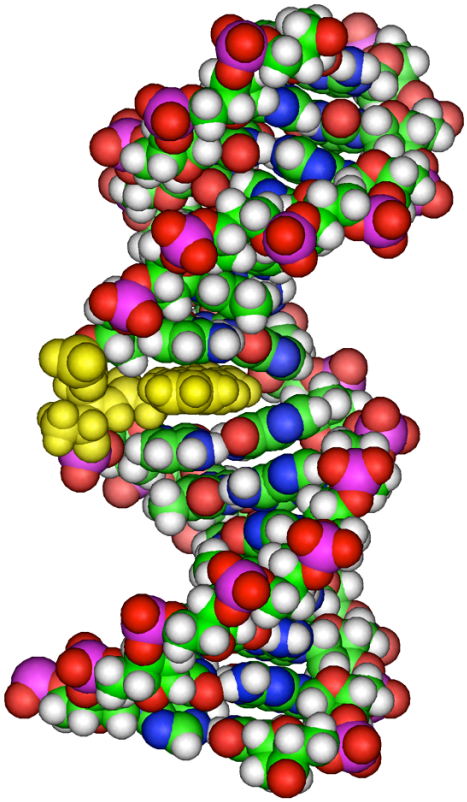

Fig. 164 AMBER models of Probe A L Target A2 anthracene and non nucleosidic backbone coloured yellow

It is also possible to observe the angling of the two guanine bases opposite of the anthracene that is required in order to allow the anthracene to fit into the duplex. This type of base angling in order to accommodate an intercalator is

known in the literature and similar systems to ours have been described through NMR studies and molecular modeling.[7]

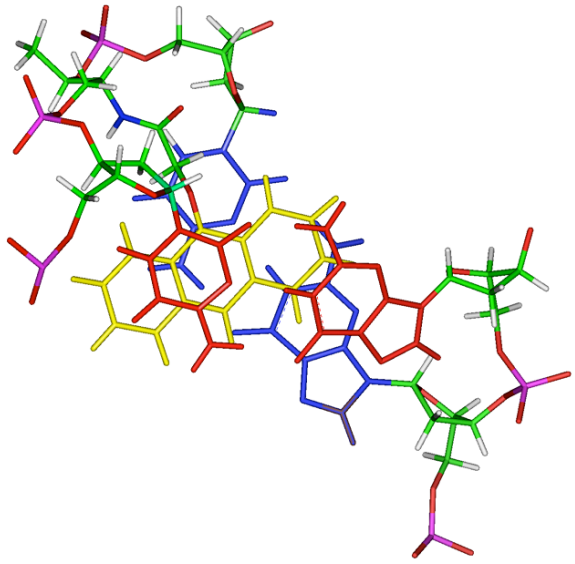

Fig. 165 AMBER models of Probe A L Target A2 top-down view

The location of the anthracene within the duplex, closer to and overlapping better with the upstream bases may also be responsible for the upstream selectivity of the mismatch sensing effect (Fig. 165).

4.10 Conclusion

The preceding work has demonstrated that molecular modelling is a powerful tool both to accurately visualise the systems that have been synthesised but also to rationalise the observed experimental results. In particular some of the differences in quantum yields (*RR* vs. *SS*), fluorescence sensing (upstream vs. downstream sensing) and variation in melting points (the decrease for the PrA Tar B1 system) can only be explained through an understanding of the conformation and structure of the oligonucleotides.

4.11 References

1. van Holde, K. E. J., W. C. and Ho, P.S., *Principles Of Physical Biochemistry*. Prentice Hall: 1998.
2. Rodger, A. N., B., *Circular Dichroism and Linear Dichroism*. Oxford University Press: 1997.
3. Kool, E. T., *Acc. Chem. Res.* **2002,** *35* (11), 936-943.
4. Long, E. C.; Barton, J. K., *Acc. Chem. Res.* **1990,** *23* (9), 271-273.
5. Kumar, C. V.; Punzalan, E. H. A.; Tan, W. B., *Tetrahedron* **2000,** *56* (36), 7027-7040.
6. Peyret, N.; Seneviratne, P. A.; Allawi, H. T.; SantaLucia, J., *Biochemistry* **1999,** *38* (12), 3468-3477.
7. Liang, X. G.; Asanuma, H.; Kashida, H.; Takasu, A.; Sakamoto, T.; Kawai, G.; Komiyama, M., *J. Am. Chem. Soc.* **2003,** *125* (52), 16408-16415.

Chapter 5 Longer anthracene tether lengths

5.1 Introduction

The successful synthesis of the *n* = 1 linker lengths, coupled to their usefulness as DNA probes led to the synthesis of further probes with longer linker lengths in order to both potentially improve the sensing and to better understand the mechanisms involved. As was shown earlier in chapter 2, by varying the number of carbons in the alkylbromo ester starting material it is possible to create identical probes with longer, more hydrophobic tethers.

5.2 Fluorescence studies on the single strands

5.2.1 Single strand spectra

The normalized single strand spectra of the probes show clearly that the spectra are less distinct in the longer chain forms (Fig. 166).

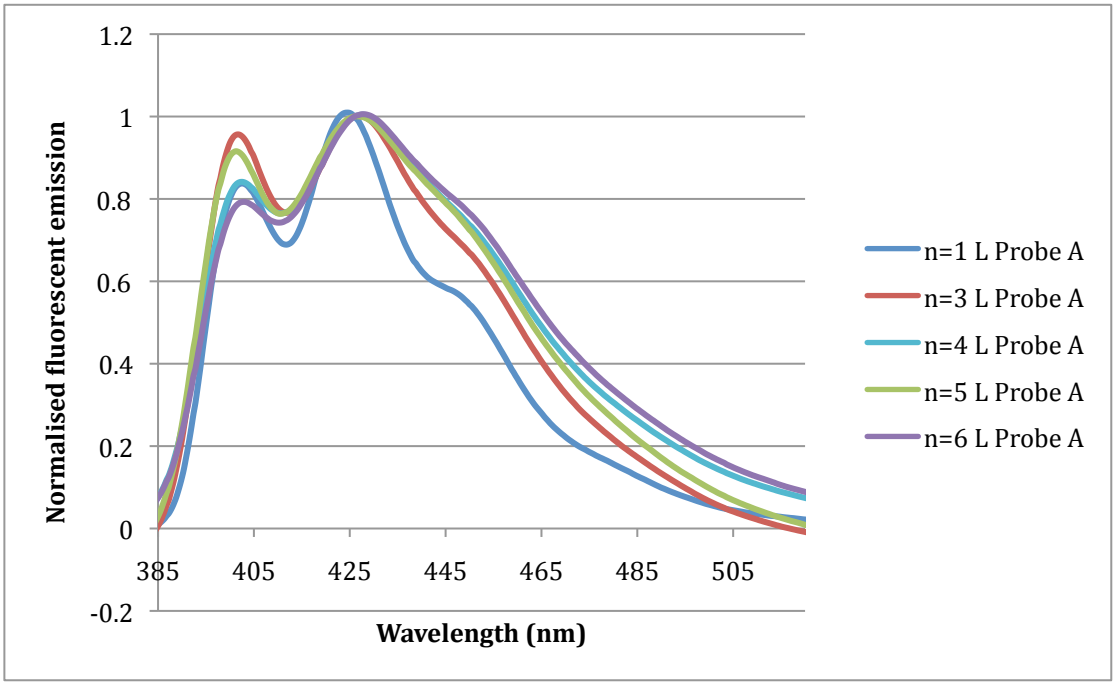

Fig. 166 Fluorescence emission spectra for L isomer strands of different carbon chain lengths normalized spectra 1uM DNA 10 mM pH 7 phosphate buffer 100mM NaCl

It is also noticeable that the longer linker lengths have a greater bathochromic shift than the *n* = 1 chain length. The greater bathochromic shift is comparable to those reported in the literature for similar aromatic probes with longer linker lengths.[1]

5.2.2 Single strand quantum yields

The effect of the longer linker length upon the quantum yields of the single strand oligonucleotide was investigated (Fig. 167 see Appendix 2 for actual values). For comparison purposes the core sequence (Probe A) was studied to enable direct comparison.

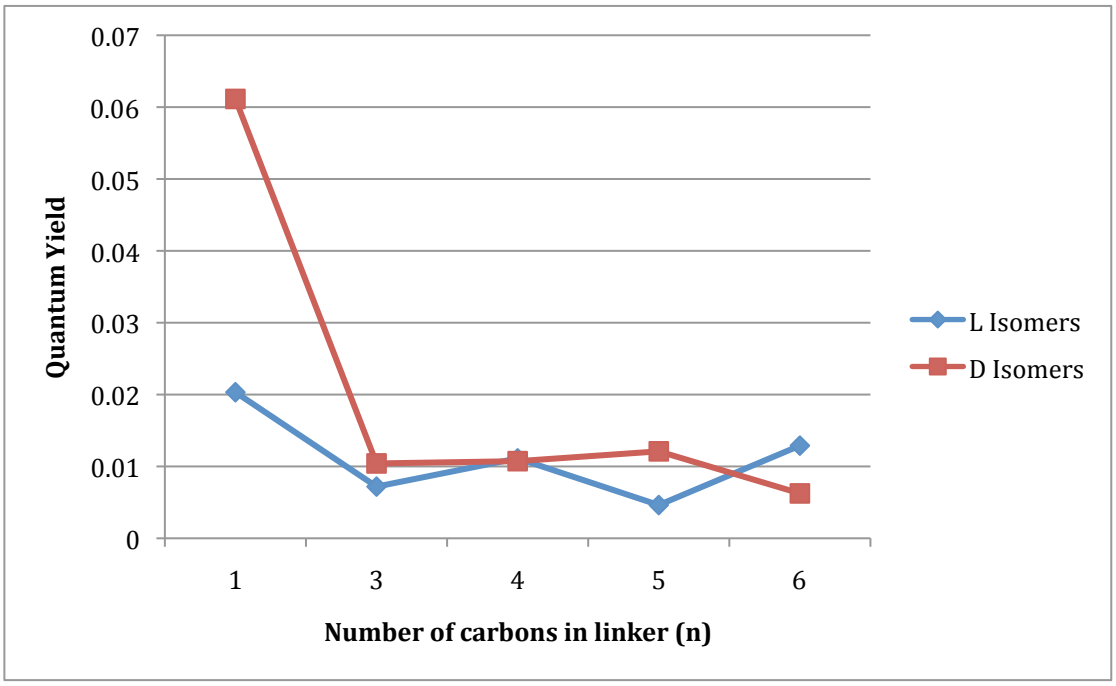

Fig. 167 Comparison of QY for different carbon chain lengths 1uM 10 mM pH 7 phosphate buffer 100mM NaCl room temp

The QY values are much lower for the longer linker lengths, particularly so for the D linker systems, and in general the QYs are more similar for longer linker lengths than they are for the *n* = 1 system. Since the base sequence is the same for all Probes, this implies that the longer linker anthracenes experience a more

quenching environment than the *n* = 1 strands. This is either as a consequence of the amount of exposure to a specific quenching pathway (static quenching) or due to the degree of effectiveness of one of the dynamic quenching pathways.

5.2.3 Single strand fluorescence lifetimes

Fluorescence lifetime studies were performed on the single strand oligonucleotides. The probes were irradiated at 370 nm and the fluorescence decay was monitored at 426 nm. The resulting decay profile was fitted using a multi exponential function.

Table 46 Fluorescence lifetimes of single stranded anthracene modified oligonucleotides of differing chain lengths λex 375 nm λem 426 nm 1 μM oligonucleotide concentration 10 mM pH 7 phosphate buffer 100 mM NaCl

n	Probe	Isomer	τ 1	τ 1 Weighted (%)	τ 2	τ 2 Weighted (%)	τ 3	τ 3 Weighted (%)	χ^2
1	A	L	0.92	11	3.5	33	11.95	56	1.021
1	A	D	1.19	8	4.47	20	13.87	73	0.98
3	A	L	0.589	37	2.96	40	9.76	23	1.05
3	A	D	0.795	34	3	41	9.33	26	1.021
4	A	L	0.532	31	2.52	44	8.35	25	1.04
4	A	D	0.621	35	2.56	42	8.26	24	0.97
5	A	L	0.559	31	2.59	42	9.04	27	1.011
5	A	D	0.760	42	3.23	37	10.0	21	1.10
6	A	L	0.706	32	2.82	40	8.65	28	0.987
6	A	D	0.567	28	2.61	41	8.29	31	0.95

5.2.4 Discussion

The most obvious information that can be drawn from these results is that increasing the chain length dramatically decreases the quantum yield and therefore fluorescence lifetime of the attached anthracene. This applies to both the L and the D isomers, the D isomer showing very similar QY and lifetimes to the L, unlike in the *n* = 1 probe. However, there is some small variation in the quantum yield of the *n* = 5 and 6 probes implying that small but significant

changes in the binding pocket of anthracene may be caused by making changes to the stereochemistry.

Also of interest is the slight increase in QY of the *n* = 4 linker relative to the *n* = 3 and *n* = 5 L isomer probes. Although not a big increase it repeats a pattern observed in previous work, albeit using acridine.[2] This could potentially be useful in affirming the conclusions drawn by Tanaka and co-workers to explain their results and in addition provide viable hypotheses for our results.

Although there is relatively little difference in the lifetimes for the longer strands, comparing the longer strand lifetimes to the *n* = 1 strands can allow us to explain general differences in emission trends.

The main observations are:

1. As the chain length increases, the percentage weighting of the shortest lifetimes (τ1 and τ2) increases and τ1 and τ2 decrease.
2. The weighting for τ3 decreases in the long chain form as τ3 itself is smaller

Interpreting the lifetimes data using the same assignment for the different lifetimes as for the *n* = 1 (see 3.5.6.2) suggests that increasing the tether length from one carbon to three or more puts the anthracene in an environment where it is more readily quenched, both by dynamic quenching via water and static quenching via electron transfer to an adjacent base, the degree of which is determined via the redox properties of said base. This could be due to the anthracene being forced out of a hydrophobic environment by the longer linker. The increasing HPLC retention times for the increasing linker length (2.3.4) suggest that the anthracene is pushed further into the surrounding solvent and

the result of this could be the inability to find a hydrophobic pocket. The presence of the anthracene in an environment where it is exposed to base quenching and solvent quenching could be responsible for the reduced quantum yield.

5.3 Fluorescence studies on the duplexes (base opposite)

As with the *n* = 1 linker, studies were undertaken on the longer chain Probes using the same targets in order to investigate the effect of hybridization on the fluorescence properties of the anthracene.

5.3.1 Quantum yields for base opposite systems

A study of the QY of the different probes with an adenine base opposite shows an interesting trend as a function of linker length with an as-yet unexplained change in the pattern of the quantum yield for the *n* = 6 linker(Fig. 168).

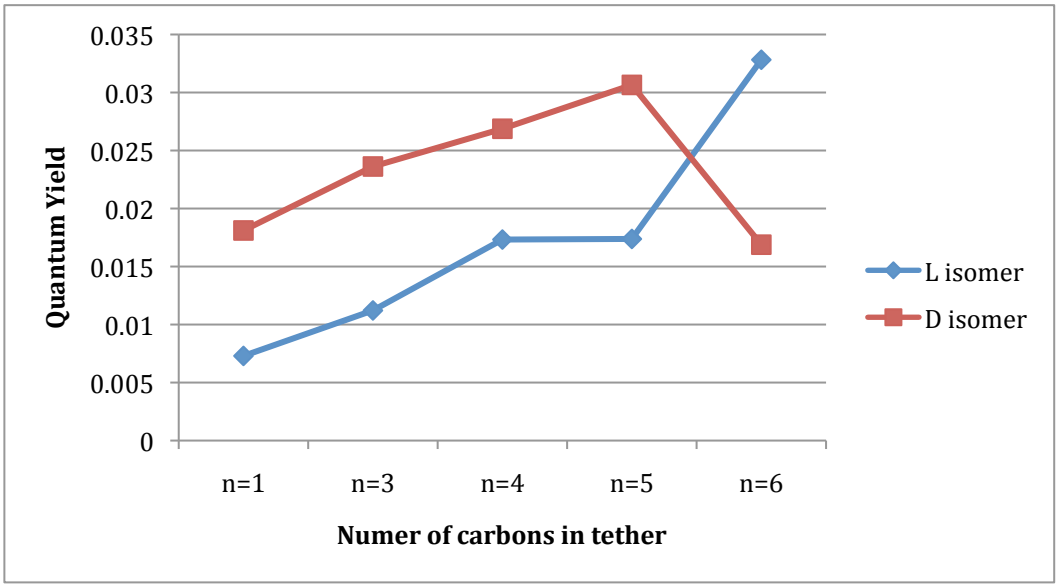

Fig. 168 Quantum yields for the fully matching hybridized duplexes for different carbon chain lengths

The results show a trend of an increase in the QY as the linker length increases. This implies the anthracene is either in an increasingly hydrophobic environment or further away from the adjacent C bases which could quench the fluorescence via electron transfer.

5.3.2 Fluorescence lifetimes for base opposite hybridized systems

Table 47 Lifetimes of PrA L and D duplexes recorded at room temperature λex 375 nm λem 426 nm 5 μM oligonucleotide concentration 10 mM pH 7 phosphate buffer 100 mM NaCl

n		Probe	Target	τ 1 (ns)	τ 1 Weighted (%)	τ 2 (ns)	τ 2 Weighted (%)	τ 3 (ns)	τ 3 Weighted (%)	χ^2
1	L	A	A1	1.05	38	4.28	36	12.4	26	1.044
1	D	A	A1	1.5	33	3.68	41	9.08	25	0.999
3	L	A	A1	0.817	13	3.97	54	8.76	33	1.053
3	D	A	A1	0.987	14	4.43	31	7.67	55	1.037
4	D	A	A1	1.27	10	4.44	34	7.2	55	1.007
5	L	A	A1	1.29	9	8.42	60	19.2	31	1.086
5	D	A	A1	1.31	15	3.48	39	7.9	45	0.946
6	L	A	A1	1.51	13	4.89	30	8.2	57	1.027
6	D	A	A1	1.49	16	5.75	58	9.75	26	1.017

A comparison of the lifetime data with the quantum yield results (Fig. 168) shows how no one decay pathway or process is fully responsible for the resulting quantum yield. This is represented in the data for the *n* = 6 D isomer Probe system where the quantum yield is the same as for the *n* = 1 D isomer, but the longer lifetimes are different and the weighting of τ1 is different.

5.3.3 Sensing the base opposite

The possibility that the longer chain anthracenes might reside in a different part of the duplex to the *n* = 1 strands made sensing the base directly opposite the anthracene a possible function of the longer probes, making them potential base-discriminating fluorophores via OFF-ON sensing. Many fluorescent-tagged nucleobases have been reported, but generally they are limited in their ability to differentiate between all of the possible base-pairing partners.[3-6] A modified

nucleobase that can discriminate between the four DNA bases has been reported[7], however the sensing is via different decreases in emission with the single strand form being more emissive than any of the duplexes, making it effectively an ON-OFF sensor.

5.3.3.1 Fluorescence hybridization titrations

Table 48 Percentage of fluorescence change upon hybridization, recorded at room temperature λex 350 nm λem 426 nm 1 μM oligonucleotide concentration 10 mM pH 7 phosphate buffer 100 mM NaCl

		A1	A3	A4	A5
		3'GAG	3'GTG	3'GCG	3'GGG
Pr A n=1 L	5' CLC	**-75**	**-76**	**-75**	**-78**
Pr A n=1 D	5' CDC	**-72**	**-86**	**-81**	**-79**
Pr A n=3 L	5' CLC	**52**	**-52**	**-43**	**10**
Pr A n=3 D	5' CDC	**166**	**-53**	**-27**	**43**
Pr A n=4 L	5' CLC	**70**	**-57**	**-26**	**29**
Pr A n=4 D	5' CDC	**161**	**-43**	**22**	**98**
Pr A n=5 L	5' CLC	**230**	**-25**	**-10**	**130**
Pr A n=5 D	5' CDC	**205**	**-35**	**20**	**107**
Pr A n=6 L	5' CDC	**139**	**-34**	**35**	**88**
Pr A n=6 D	5' CDC	**170**	**-41**	**31**	**111**

Unlike the *n* = 1 strands which are quenched, and by the same amount, the longer probes show differing emission profiles depending on the opposing base. The results suggest that the location of the anthracene allows it to interact with the base opposite in a way that is not possible for the shorter tether lengths. Furthermore, the emission increases more for purines than for pyrimidines. Interestingly, the order of quenching appears to be T < C < G < A which is again in keeping with the rate of electron transfer from base sequence (and ΔG_{ET}) as determined by the Rhem-Weller equation[8-10] [11](Fig. 169).

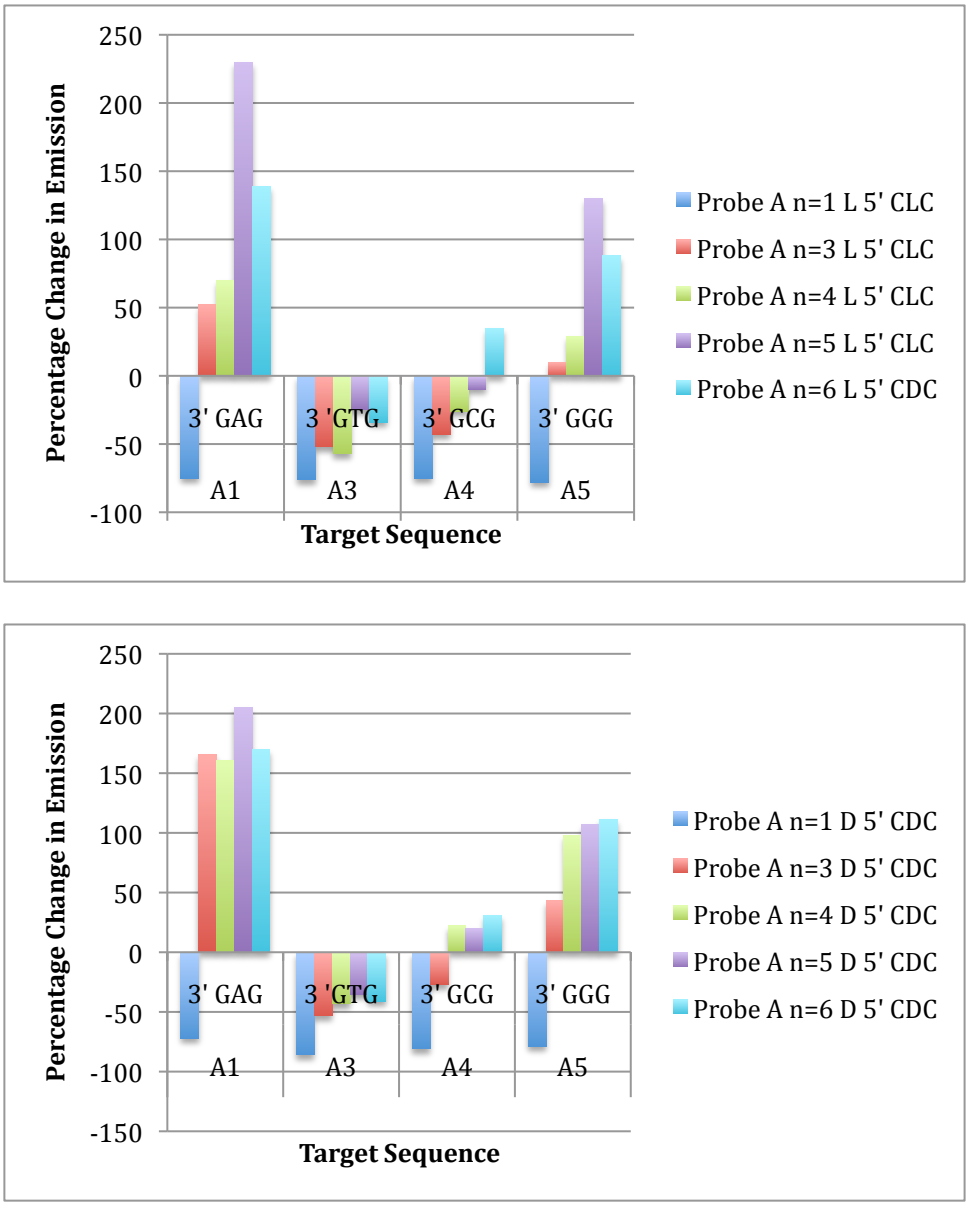

Fig. 169 Comparison of percentage change in fluorescence at 426 nm upon hybridization L isomer (top) and D isomer (bottom)

The graph clearly shows that for the n > 1, strands the anthracene is sensing the base opposite, to do this it must be relatively close to the opposite base for this effect to be observed.

The graph also shows how the D isomer appears to be more sensitive to the change in base than the L isomer, with the D strands showing greater differentiation between bases at shorter linker lengths reflected in the larger gradient of the line.

These results also highlight the importance of proton transfer from G to C in quenching the fluorescence of anthracene, showing how, by considering the bases individually, they obey the order of quenching proposed by the Rehm-Weller equation (see 3.7.5). This is in contrast to when they are bound together by hydrogen bonding, where proton transfer effects change the order of quenching.

5.3.3.2 Fluorescence lifetimes of hybridized duplexes

The fluorescence lifetimes were determined for the two isomers of the *n* = 3 and 6 systems with the base opposite of the anthracene varied. The complete data is presented in Appendix A2.3.4.2. A series of scatter graphs show that for longer carbon chain lengths there is a correlation between the change in fluorescence and the weighting of τ1 (Fig. 170) and the value of τ2.

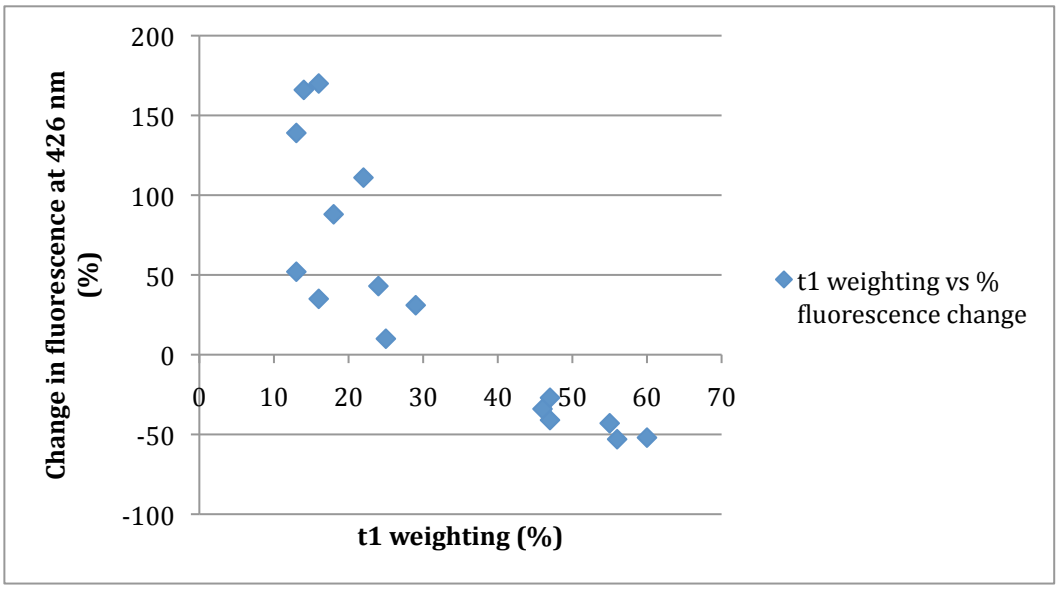

Fig. 170 Scatter plot of τ lifetime weighting for base opposite system n=3 and 5 L and D plotted against percentage change in fluorescence at 426nm

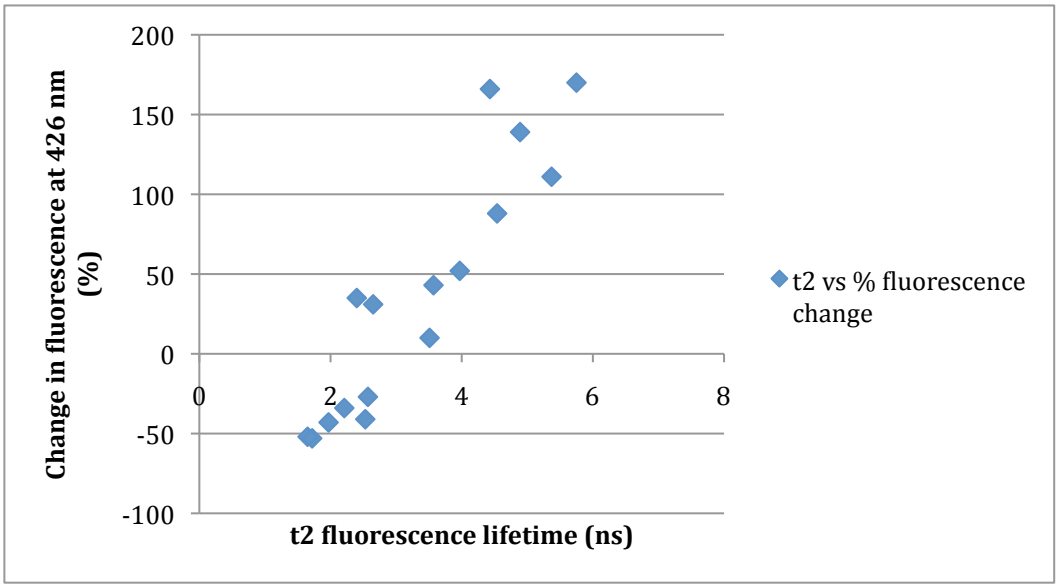

Fig. 171 Scatter plot of τ2 lifetime for base opposite system n=3 and 5 L and D plotted against percentage change in fluorescence at 426nm.

This is slightly different to the results observed when the bases were modified around the anthracene for the *n* = 1 linker (see section 3.5.6.3). This appears to suggest that varying the base opposite when a longer linker is present affects the degree of hydrophobicity of the anthracene lifetime. This makes sense by considering that in the short strand the anthracene and opposite base do not appear to interact significantly.

The observed trends in the preceding graphs suggests that the overall fluorescence change is most strongly dependent on the quenching mechanism that occurs for the shortest lifetimes, the first of which has been assigned to static quenching by electron transfer and the second to dynamic quenching by water (see 3.5.6.2). The association between τ1 and fluorescence emission in particular correlates well with the previously observed relationship (5.3.2.1) between the different bases opposite anthracene and the fluorescence change and also with quenching results of the *n* = 1 strands.

5.3.4 Mismatch sensing

Detailed fluorescence hybridization studies have been performed on the various mismatches possible with a base opposite the anthracene as per the *n* = 1 strands. As with the facing bases, they show what appears to be a different sensing mechanism to the short strands. Both the L and the D isomer show similar trends and will therefore be dealt with at the same time. By keeping the opposite base the same (A) and varying both the upstream and downstream bases it can be seen that some clear trends emerge.

5.3.4.1 Downstream mismatches

Actual values are presented in Appendix 2 and the data is represented below in graphical form.

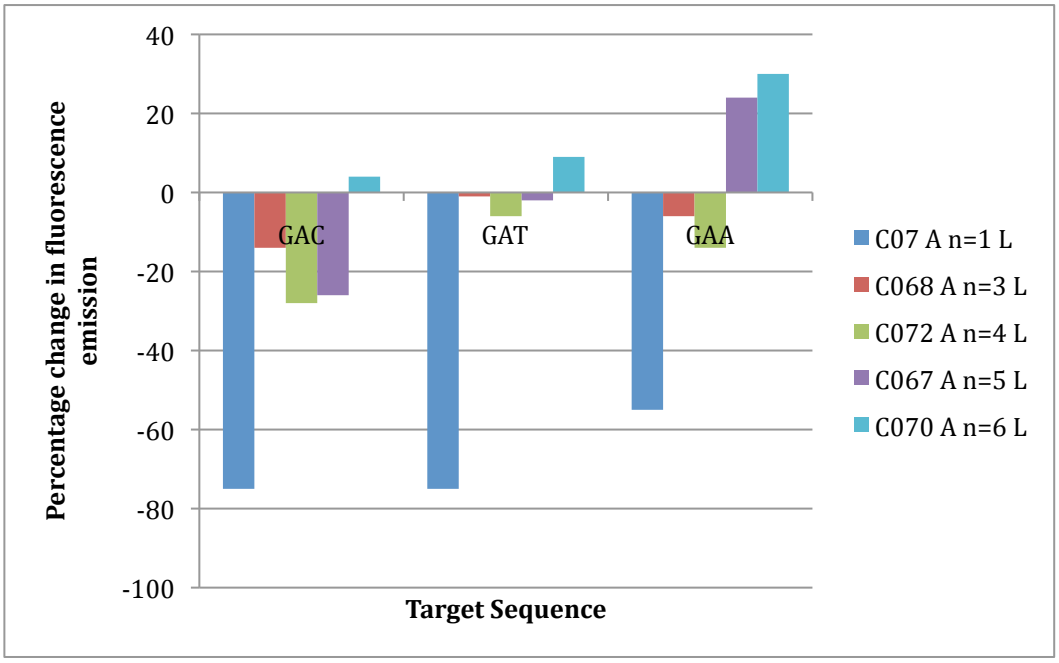

Fig. 172 Graph showing the percentage change in fluorescence emission at 426 nm for different downstream mismatches for different L isomer linker lengths.

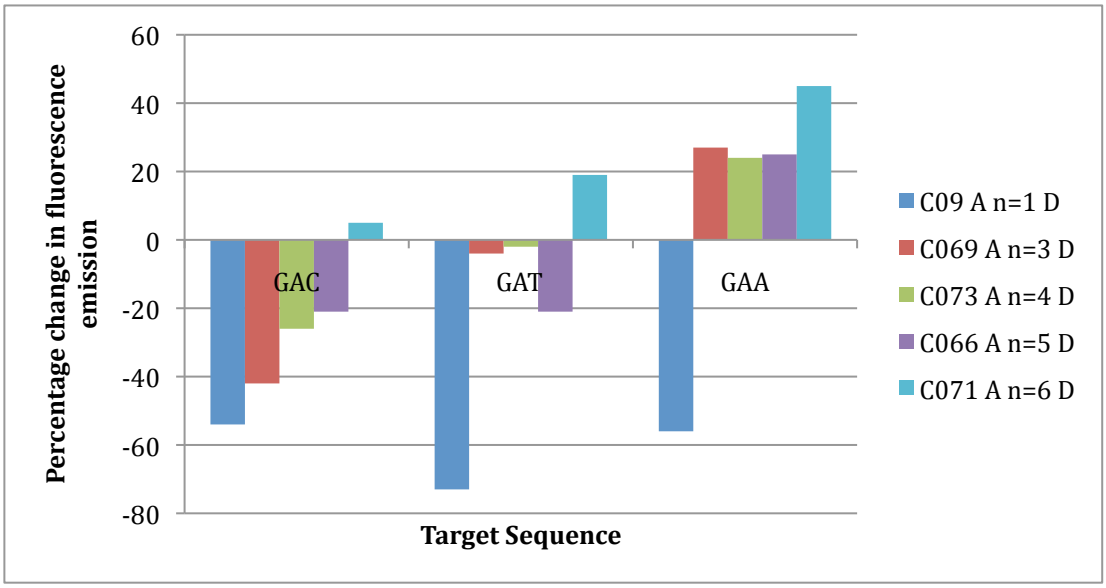

Fig. 173 Graph showing the percentage change in fluorescence emission at 426 nm for different downstream mismatches for different D isomer linker lengths.

Both graphs show a general trend towards greater emission as the mismatching base goes from C to T to A, reflecting the order of quenching previously proposed although the fact that the greatest quenching comes from C and not T is slightly surprising. There appears to be very little selectivity as regards linker length and isomer.

5.3.4.2 Upstream mismatch

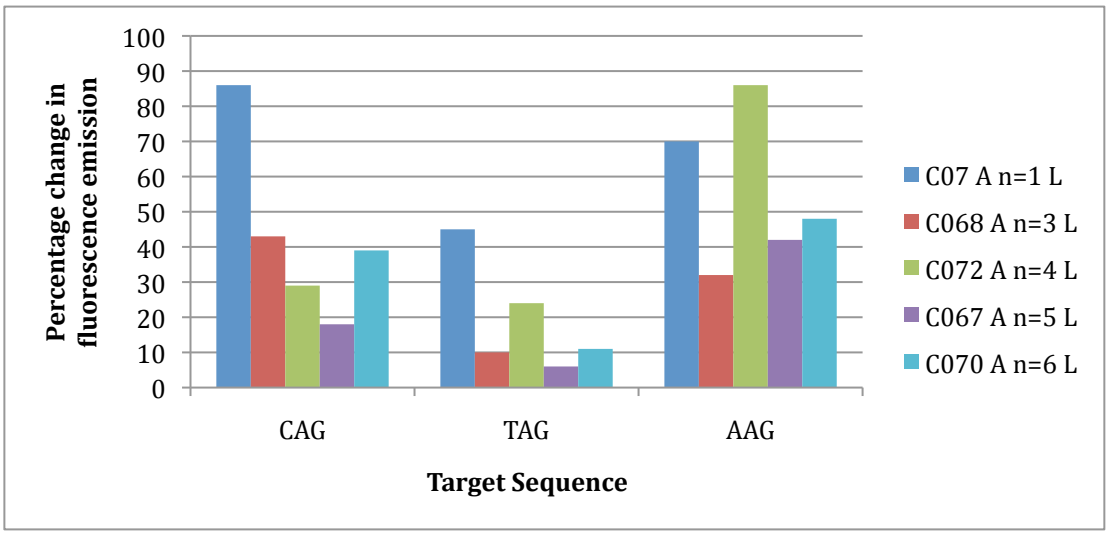

Fig. 174 Graph showing the percentage change in fluorescence emission at 426 nm for different upstream mismatches for different L isomer linker lengths.

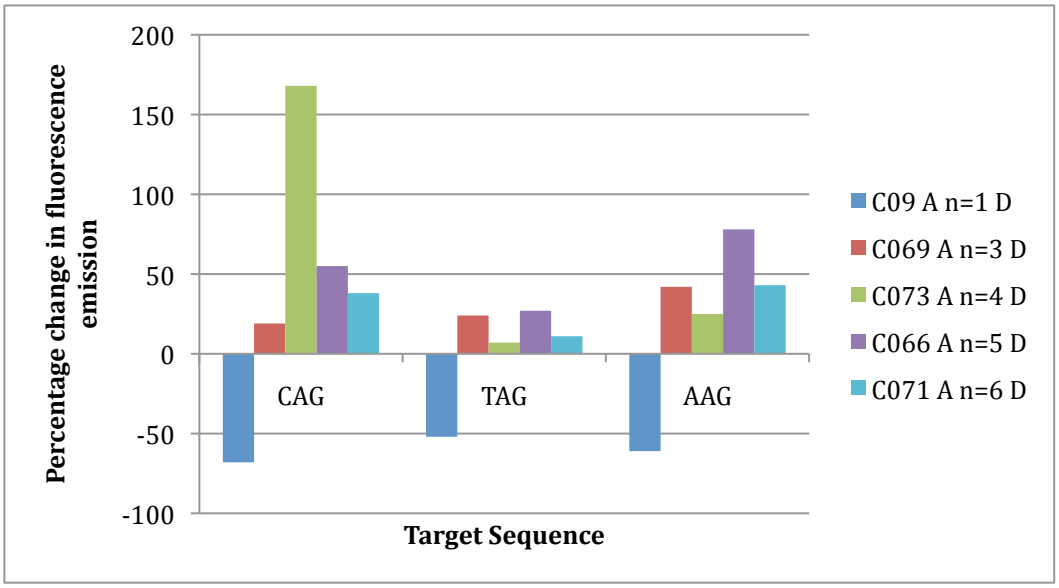

Fig. 175 Graph showing the percentage change in fluorescence emission at 426 nm for different upstream mismatches for different D isomer linker lengths

The patterns appear to be clearer upon looking at the upstream mismatches. For $n > 1$ the fluorescence increases upon hybridization for all of the mismatches, irrespective of the linker length. Furthermore, although the degree of emission enhancement varies, the probes generally follow a trend of quenching of T > C > A. This is what we would expect based on the previous work. Overall however, the ability of the longer chain probes to distinguish and sense mismatches is quite limited. This could be due to the greater flexibility afforded by the chain, allowing the anthracene to orientate itself favourably with respect to the reducing its interactions with water.

5.4 Fluorescence studies on the deletion systems

5.4.1 Fluorescence titration studies

Table 49 PrA percentage fluorescence change upon hybridization with deletion matching strands recorded at room temperature λex 350 nm λem 426 nm 1 μM oligonucleotide concentration 10 mM pH 7 phosphate buffer 100 mM NaCl

		A2
		3'G_G
Probe A n=1 L	5' CLC	**-50**
Probe A n=1 D	5' CDC	**-77**
Probe A n=3 L	5' CLC	**-68**
Probe A n=3 D	5' CDC	**-37**
Probe A n=4 L	5' CLC	**-54**
Probe A n=4 D	5' CDC	**24**
Probe A n=5 L	5' CLC	**-26**
Probe A n=5 D	5' CDC	**-20**
Probe A n=6 L	5' CDC	**-10**
Probe A n=6 D	5' CDC	**-37**

The deletion duplexes are generally quenched, as can be seen from the table above. Interestingly, the *n* = 4 D duplex shows an increase in fluorescence emission. This is unusual for the deletion system and, given that the probes have the same nucleobase environment, means that the most likely explanation is that this duplex adopts a unique structure as a consequence of a combination of stereochemistry and linker length.

5.4.2 Fluorescent lifetimes

The increase in fluorescence emission of *n* = 4 Probe A D TarA2 may be as a result of a longer first lifetime (**τ1**) that is approximately 50% greater than that seen for the other duplexes. **τ1** has been shown to be an important factor in the degree of quenching and related to the rate of electron transfer.

Table 50 Lifetimes of selected PrA matching deletion duplexes recorded at room temperature λex 375 nm λem 426 nm 5 μM oligonucleotide concentration 10 mM pH 7 phosphate buffer 100 mM NaCl

n		Probe	Target	τ 1	τ 1 Weighted (%)	τ 2	τ 2 Weighted (%)	τ 3	τ 3 Weighted (%)	χ^2
1	L	A	A2	1.14	50	2.79	32	11.3	18	0.993
1	D	A	A2	1.19	27	2.1	66	11.9	7	1.034
3	L	A	A2	0.525	64	2.26	19	10.1	17	0.985
3	D	A	A2	0.783	65	1.77	30	9.55	4	0.969
4	D	A	A2	1.6	58	2.4	39	9.53	4	1.011
5	D	A	A2	0.907	56	2.16	34	8.81	11	1.016
6	L	A	A2	1.02	45	2.11	46	8.15	9	0.992
6	D	A	A2	0.9	46	2.22	43	9.24	11	0.996

5.5 Melting points

Melting point studies were carried out as before to look at the effect of increasing the tether length on the stability of the duplex. The full data is presented in Appendix 3 with a brief summary below.

Analysis of the melting points of the matching base opposite duplexes do not show any clear patterns, although a plot of the melting point temperature against the linker length shows an overall gradual decrease for the L isomer in contrast to an overall increase for the D isomer (Fig. 176).

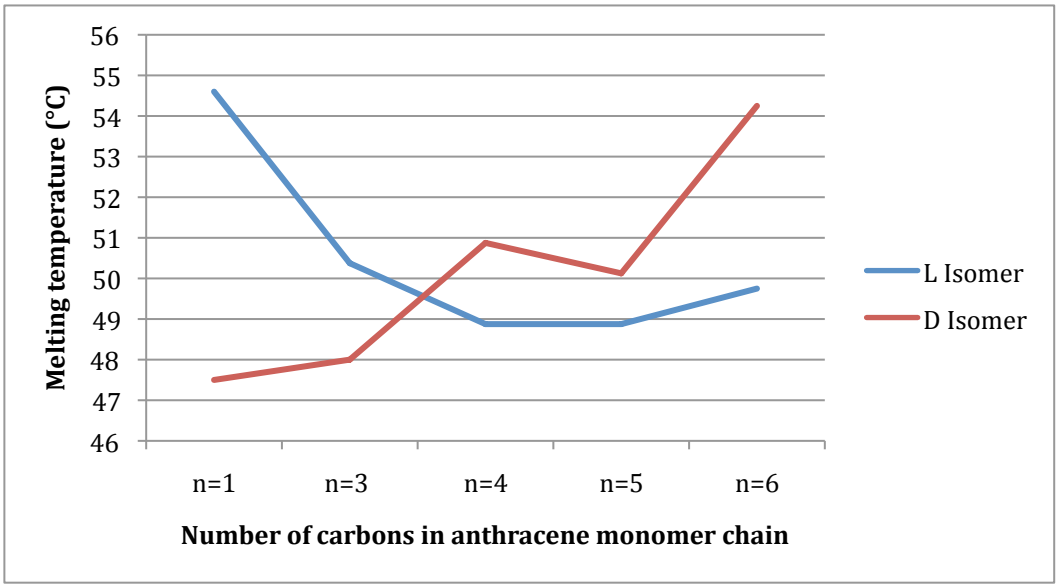

Fig. 176 Comparison of the melting point for matching oligonucleotides with a base opposite of different carbon chain lengths 5μM concentration of oligo 10mM pH 7 phosphate buffer 100mM NaCl

The crossover in relative stabilities for the L and D isomers, with the D isomer being more stable at longer chain lengths helps to understand the observations by Komiyama and Asanuma who found that D isomer duplexes are generally more stable in the face of initially conflicting results for our *n* = 1 linkers (section 3.9).[12-15] Clearly, the stability depends on the distance between the intercalator and the linker, something that was not studied in their work.

There is a slightly greater melting point for the *n* = 4 linker compared to the 3 and 5 lengths, in this case for the D isomer. This is also seen in the work of Tanaka[2] and implies that the specific conformation of the *n* = 4 linker that makes it more stable than would otherwise be expected.

The *n* = 4 PrA D TarA2 duplex, which displays an unusual fluorescence increase, also has a slightly higher temperature than might be expected by the overall trend (Table 51).

Table 51 Melting points (°C) of matching deletion duplexes of different carbon chain lengths 5μM concentration of oligo 10mM pH 7 phosphate buffer 100mM NaCl

Probe		A2
		3'G_G
Probe A n=1 L	5' CLC	**61**
Probe A n=1 D	5' CDC	**53.5**
Probe A n=3 L	5' CLC	**57**
Probe A n=3 D	5' CDC	**57**
Probe A n=4 L	5' CLC	**52**
Probe A n=4 D	5' CDC	**57**
Probe A n=5 L	5' CLC	**51**
Probe A n=5 D	5' CDC	**54**
Probe A n=6 L	5' CLC	**53.5**
Probe A n=6 D	5' CDC	**58.5**

A complete compendium of melting point results is presented in Appendix 3. The trends observed are similar to those for the *n* = 1 linker as regards the effects of mismatches

5.6 Circular Dichroism

Spectra were taken of the core matching sequence (PrA (CXC)) for linkers of different lengths and compared to the *n* = 1 strand for the two different isomers.

5.6.1 Longer chain length L isomer spectra

Inspection of the spectra for the L isomer (Fig. 177) shows that only the *n* = 1 duplex has a shoulder at 254 nm.

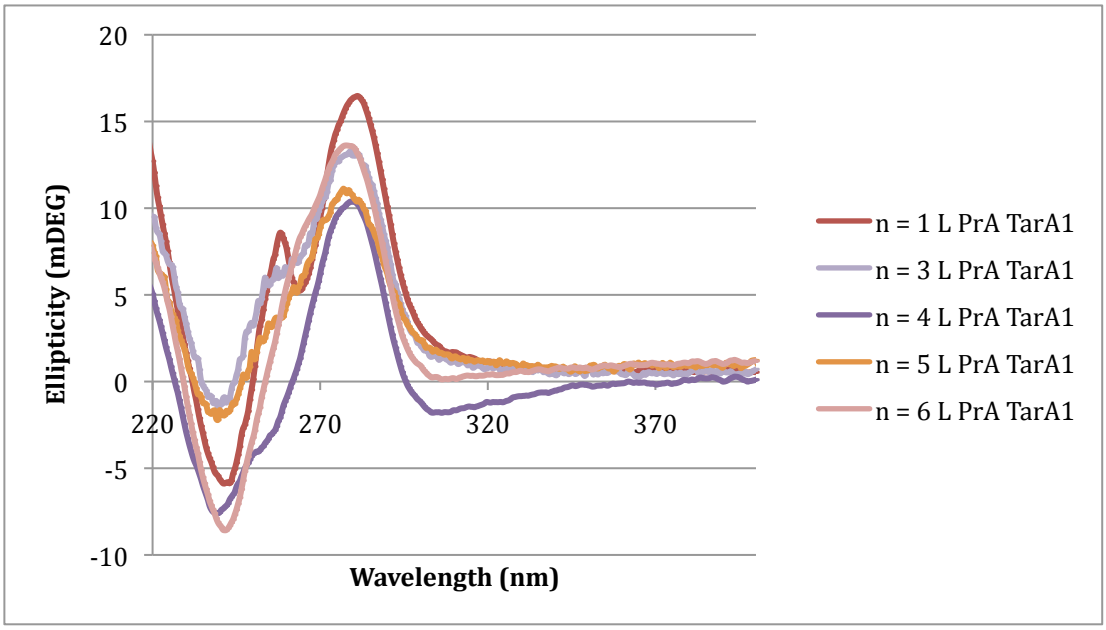

Fig. 177 CD spectra of base opposite system duplexes L isomers 5µM concentration of oligo 10mM pH 7 phosphate buffer 100mM NaCl

5.6.2 Longer chain D isomer spectra

The D isomer spectra (Fig. 178), by contrast, show similarities between the *n* = 3 and *n* = 1 spectra.

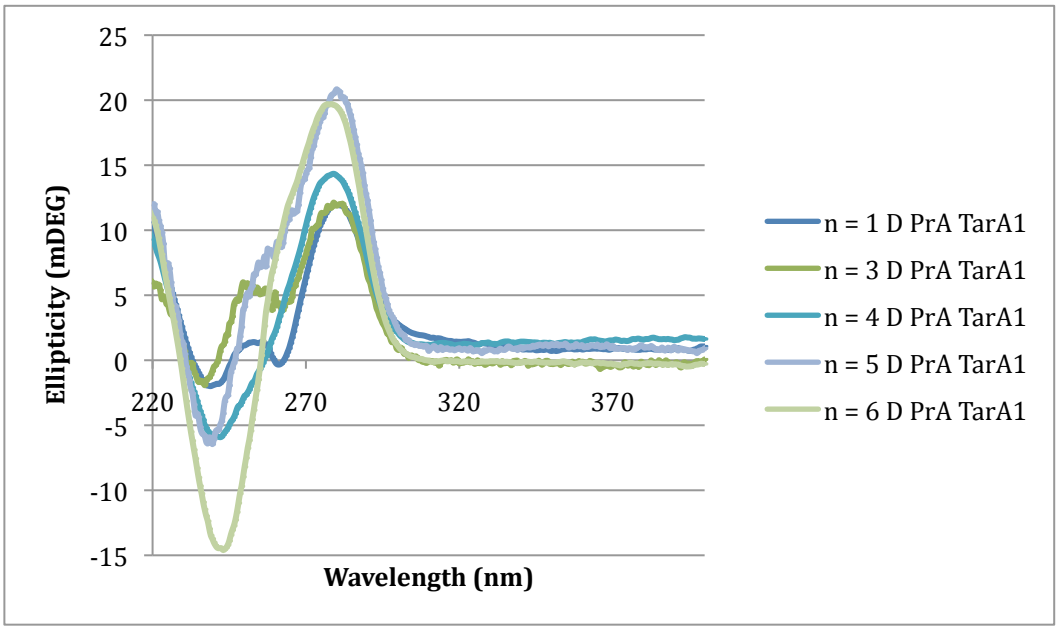

Fig. 178 CD spectra of base opposite system duplexes D isomers 5µM concentration of oligo 10mM pH 7 phosphate buffer 100mM NaCl

Analysis of the CD spectra suggest that as the linker length gets longer, the anthracene shoulder becomes less well defined until eventually it merges into the B DNA band. This could be due to the anthracene aromatic unit being less securely held or alternately that the anthracene intercalates in a different way, either at a different site or at a different orientation.

5.6.2.1 *n* = 6 D spectrum

A spectrum that stands out though is that of the *n* = 6 D anthracene duplex which has a particularly strong negative CD peak at 240 nm. This might be the result of particularly strong coupling between the bases and the anthracene due to a particularly stable anthracene intercalating site. This would explain the unusually high melting point (Fig. 176) and the drop in quantum yield (Fig. 168) of the duplex that is not in keeping with the general trend for the rest of the chain lengths.

5.7 Molecular modelling of longer chain duplexes

5.7.1 *n* = 3

As with the *n* = 1 strands (Chapter 4), modelling studies were performed on the anthracene duplexes in order to better understand the structure and mode of sensing. The first structures to be modelled were the *n* = 3 Adenine base opposite duplexes.

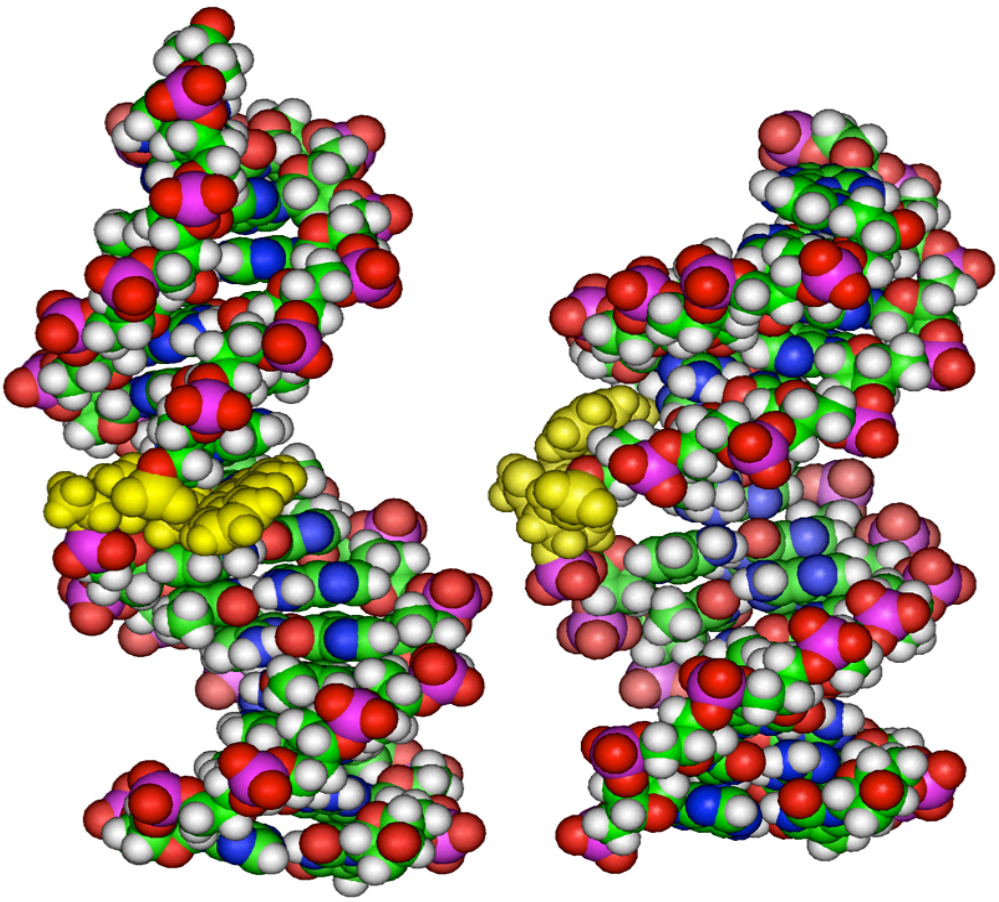

Fig. 179 AMBER models of *n* = 3 L PraTarA1 (left) and *n* = 3 D PrATarA1 (right) the anthracene modified non-nucleosidic base is coloured yellow

5.7.1.1 Explaining melting point differences for a longer chain (*n* = 3)

The modelling provides for an interesting comparison between the D and L isomers regarding how the melting point may be affected by the structure. The location of the anthracene in the D system is reminiscent of the *n* = 1 strand (see Chapter 4), with the anthracene projecting into the minor groove. This is reinforced by the similarities of the CD spectra (Fig. 178). However, the minor groove appears to have been enlarged in the *n* = 3 D duplex to accommodate the extra methylene groups. Compared to the structure of the *n* = 3 L duplex, where the anthracene sits underneath the upstream base with little steric interference it would suggest that the difference in T_m values is down to the different amounts

to which the anthracene linkers cause disruption to their respective structures. In view of the difference in T_m between the n = 1 L and n = 3 L, and n = 1 D and n = 3 D, this is most likely explained by the differences in rigidity between the two linker chains. In the n = 1 L it is the rigidity of the linker that gives the stabilization as it forces a strong stacking interaction with the upstream base pair (See Chapter 4). The loss of this rigidity leads to the formation of a weaker π-π stacking structure. Conversely, the n = 1 D anthracene projects into the minor groove and forces kinking of the DNA strand, which causes substantial destabilization of the duplex and a resulting low T_m value. The n = 3 D anthracene is not so rigidly held and hence less kinking of the duplex results.

5.7.1.2 Explaining the fluorescence sensing

The modelling shows that the anthracene is inclined at angle to the base opposite, something that was also seen with Probe G TarAX (X = 1, 3, 4, or 5) sensing (see section 4.7.2). This may have an affect on the ability of the anthracene to sense the base opposite insofar that inclination of the anthracene allows some interaction with the base opposite that cannot occur when they are aligned parallel to each other in the same plane

5.7.2 Extending the modelling to longer lengths

Further modelling of different linker lengths ($n \geq 4$) showed that extending the length of the carbon chain for the L isomer causes the anthracene to lie further away from centre of the helix and project further into the major groove compared to the n = 3 and n = 1 systems. Conversely, increasing the length of the D isomer anthracene chain eventually appears to allow it to intercalate better into the duplex compared to the shorter chain systems (Fig. 181). The point at

which this appears to occur is upon extending the chain length from the *n* = 4 system to the *n* = 5.

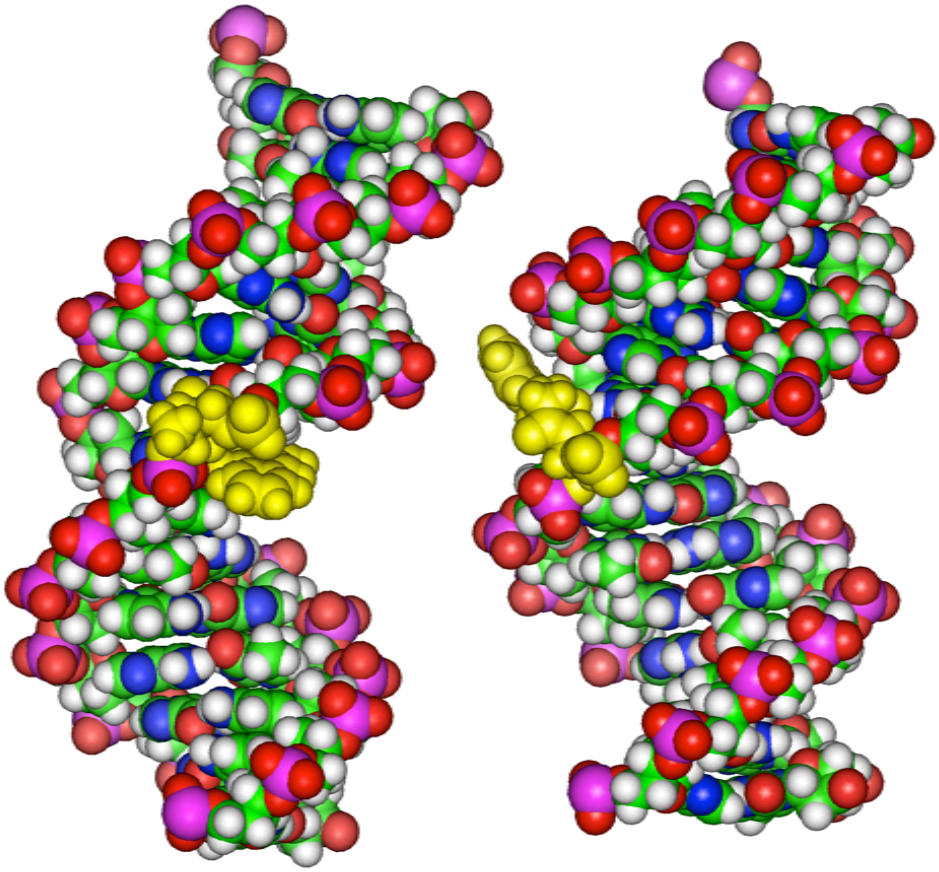

Fig. 180 AMBER models of *n* = 4 L PraTarA1 (left) and *n* = 4 D PrATarA1 (right) the anthracene tagged non-nucleosidic base is coloured yellow

In the *n* = 4 system the anthracene in the D system is still incapable of inserting itself into the duplex due to an insufficiently long carbon tether. As a result it appears to align itself into the minor groove (Fig. 180 right), which provides some stabilization. The extra methylene linker appears to allow the anthracene to adopt a position that causes less kinking of the duplex compared to the *n* = 3 D duplex. In the case of the L isomer, the anthracene is beginning to project outside of the duplex (Fig. 180 left).

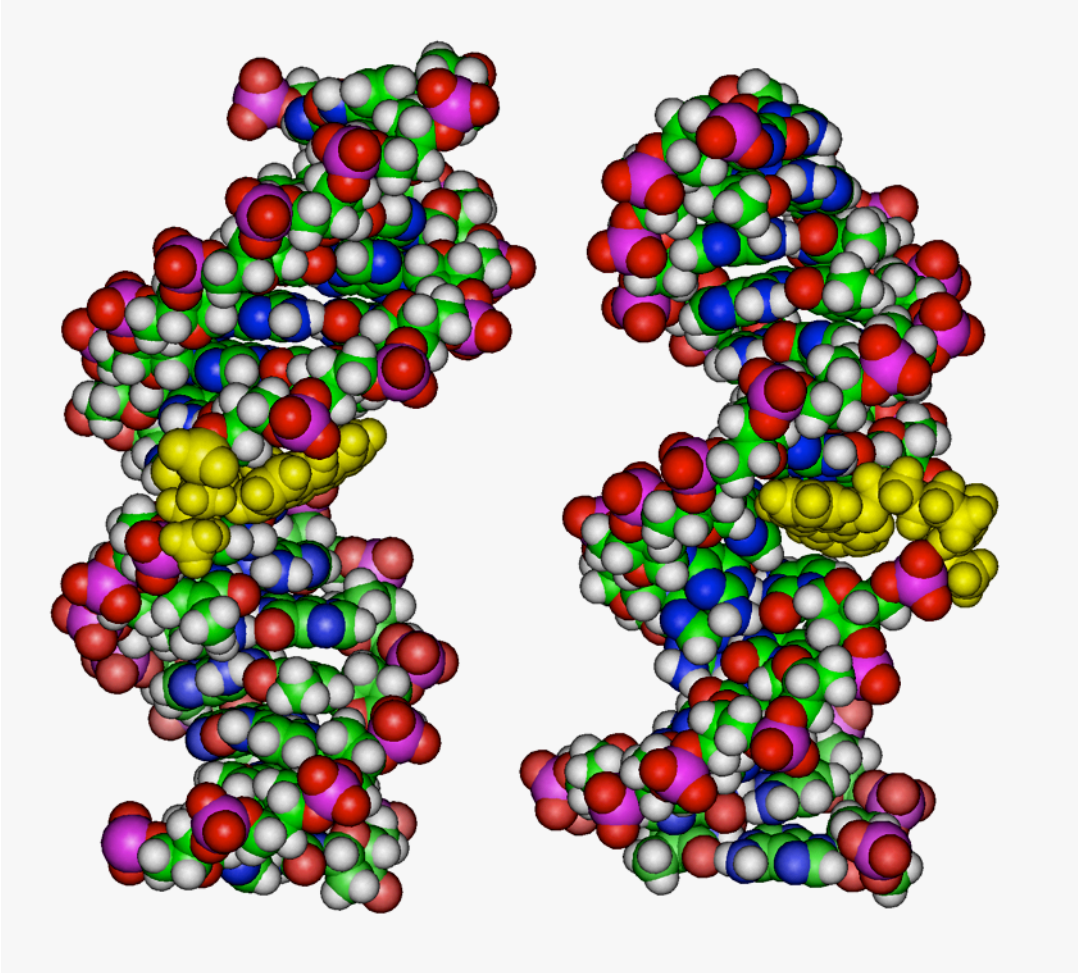

Fig. 181 AMBER models of *n* = 5 L PraTarA1 (left) and *n* = 5 D PrATarA1 (right) the anthracene tagged non-nucleosidic base is coloured yellow

This reasoning can be applied in order to explain the general trend in the melting point as the linker length changes (Fig. 176). This trend, whereby the melting point decreases for the L isomer with increasing linker length can be explained by considering how the anthracene moiety is pushed increasingly further out of the duplex. Thus stabilization through π-π stacking becomes more difficult and the anthracene will project further into the surrounding water (Fig. 182).

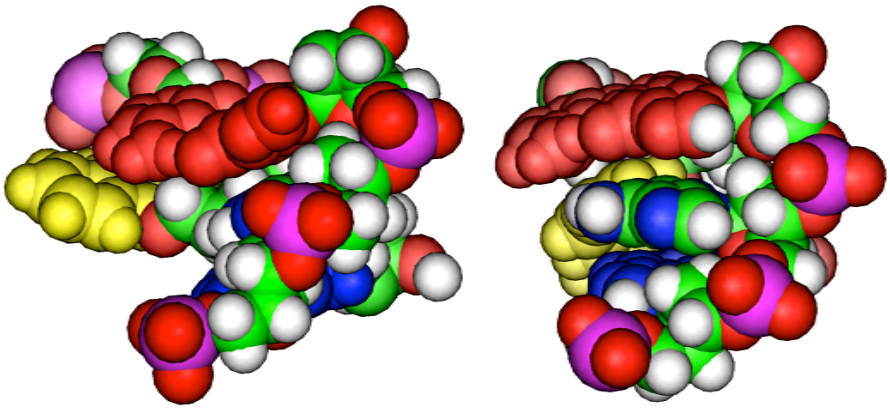

Fig. 182 Side view of an AMBER model of *n* = 5 PrA L TarA1 (left) and *n* = 3 PrA L TarA1 (right) the anthracene moiety is coloured yellow, the upstream bases red and the downstream bases blue

By contrast, the increasing tether length on the D isomer linkage confers much greater flexibility and allows the anthracene to insert itself further into the duplex as illustrated by the *n* = 5 linker anthracene (Fig. 183 left).

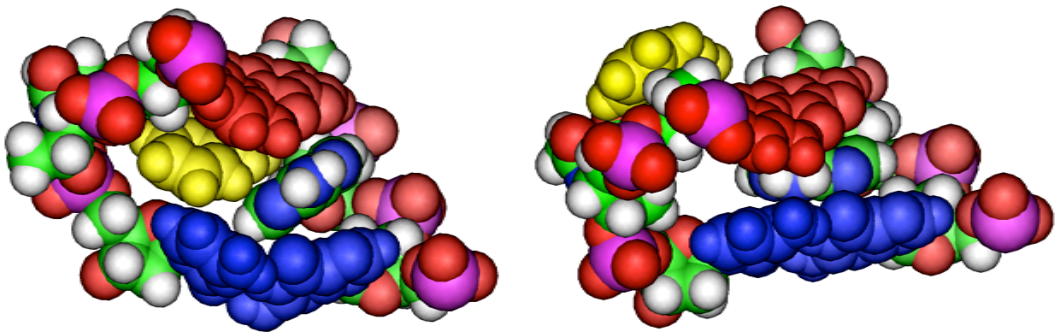

Fig. 183 Side view of an AMBER model of *n* = 5 PrA D TarA1 (left) and *n* = 3 PrA D TarA1 (right) the anthracene moiety is coloured yellow, the upstream bases red and the downstream bases blue

5.8 Face to face bis-anthracene duplexes

With a lack of success in dimerising the *n* = 1 strands it was decided to attempt to do similar studies on the longer chain duplexes. Initial work cantered on looking at the emission spectra and melting points in order to identify potentially stable combinations. This work is a continuation of earlier work on the *n* = 1 strands (see 3.17).

Molecular modelling studies on the *n* = 1 strands (Chapter 4) show that overlap of the anthracene moiety is likely to be difficult from a structural point of view, based on the degree of flexibility of the amide linkage, and hence formation of an excimer and subsequent dimerisation are unlikely. Extending the carbon chain could potentially overcome this problem by allowing the anthracenes to orientate themselves in an alignment that is favourable to the formation of an excimer.

5.8.1 Fluorescence spectra of bisanthracene duplexes

Fluorescence studies were carried out on all possible isomer combinations for *n* = 3 and 5. The normalized emission spectra are shown below (Fig. 184 *n* = 3 Fig. 184 *n* = 5).

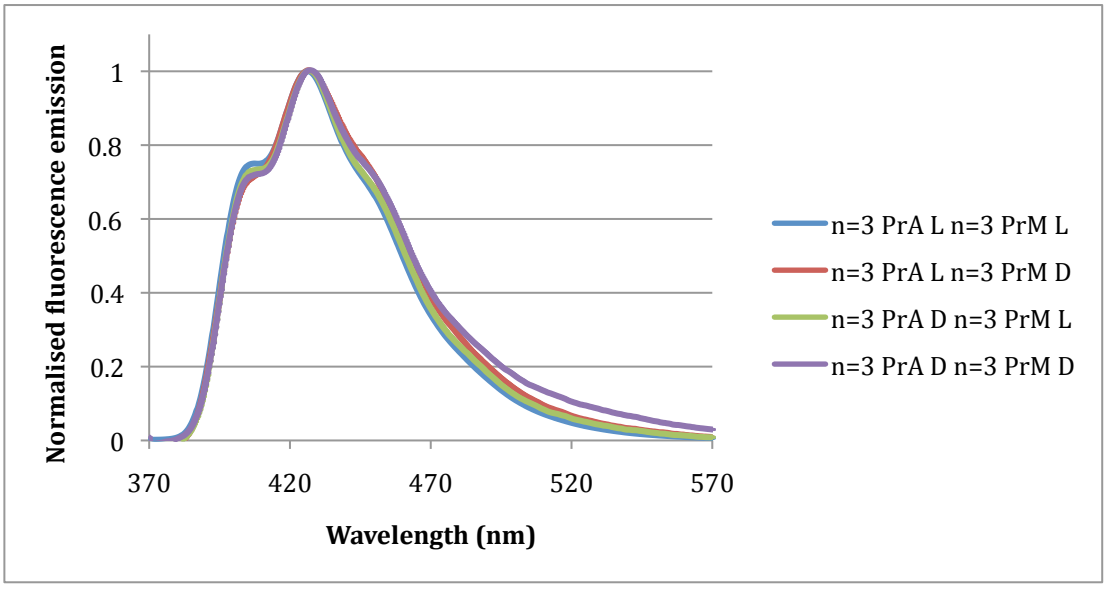

Fig. 184 Normalised fluorescence spectra of n = 3 bisanthracene duplexes 1μM concentration of oligo 10mM pH 7 phosphate buffer 100mM NaCl

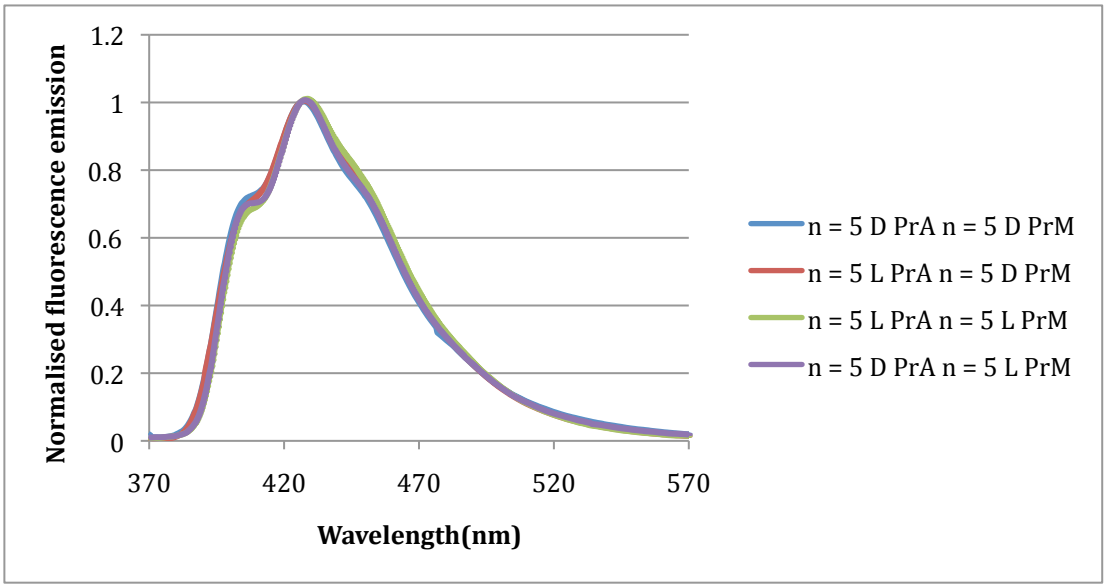

Fig. 185 Normalised fluorescence spectra of n = 3 bisanthracene duplexes 1µM concentration of oligo 10mM pH 7 phosphate buffer 100mM NaCl

As is the case for the *n* = 1 systems, there is again no sign of any excimer formation.

5.8.2 Melting Points of bisanthracene duplexes

Table 52 Melting points for bis anthracene tagged oligonucleotide duplexes of different carbon chain lengths 5µM concentration of oligo 10mM pH 7 phosphate buffer 100mM NaCl

	PrM							
PrA	(L) n=1	(D) n=1	(L) n=3	(D) n=3	(L) n=5	(D) n=5	(L) n=6	(D) n=6
Tm n=1 (L)	56	49.5	52	54		53	52	
Tm n=1 (D)	52.5	52	52	52.5		51.5		
Tm n=3 (L)	52.5	50	55.5	53		53.5		
Tm n=3 (D)	52	52	51	55.5		55		
Tm n=5 (L)	51.5		53		54	54		
Tm n=5 (D)	51.5	50	53	55	54	54.5		
Tm n=6 (L)	50.5						53.25	53.5
Tm n=6 (D)							53.5	53.5

With the exception of the *n* = 1 DD duplex, the melting points show a decrease in the matched isomer duplexes (e.g. LL and DD), and no real pattern for the LD and

DL duplexes. The table shows a general decrease in the difference in T_m between matching and mismatching isomers as the linker lengths increase. Interestingly, the trend with single anthracenes whereby the D gets more stable whilst the L gets less so does not seem to be replicated and indeed the overall trend is that the melting point becomes independent of the isomer combination. This could be expected given that the anthracenes are increasingly less rigidly held as the linker length is increased. This makes it likely that they will adopt the most energetically favourable conformation, as they are less constrained in the duplex.

5.8.3 CD spectra of bisanthracene duplexes

In continuation of the work whereby the exciton coupling between two n = 1 anthracenes in a duplex was studied, (see 3.19) the coupling between anthracenes with longer linker lengths was also examined in the same way, starting with anthracenes of the same carbon chain length.

5.8.3.1 CD of matched and mismatched longer tether length bisanthracene duplexes

The degree of exciton coupling was investigated for a wide range of duplexes consisting of different isomer/length combinations, a small selection of which are detailed below (Fig. 186).

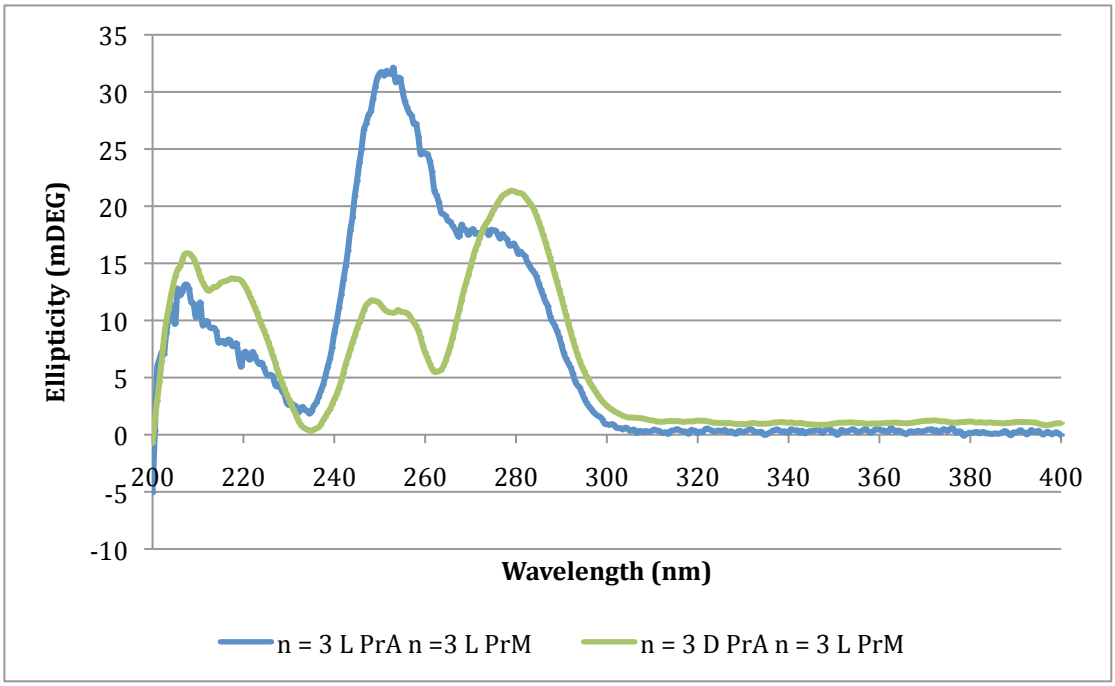

Fig. 186 CD spectra of *n* = 3 bis anthracene spectra 5µM concentration of oligo 10mM pH 7 phosphate buffer 100mM NaCl

The spectra for the *n* = 3 LL strands show an extremely strong peak at 254 nm. This implies particularly strong coupling of the anthracenes in this duplex compared with the other three possible combinations of isomer, and since the fluorescence spectra look identical (Fig. 184), this is most likely due to coupling between the anthracenes and the adjacent bases. Further studies of longer linker length spectra found a considerable increase in the broadness of the peaks, as found in the single strand forms. However, no combination gave any observable anthracene to anthracene exciton coupling, perhaps due to the aforementioned broadness of the peaks.

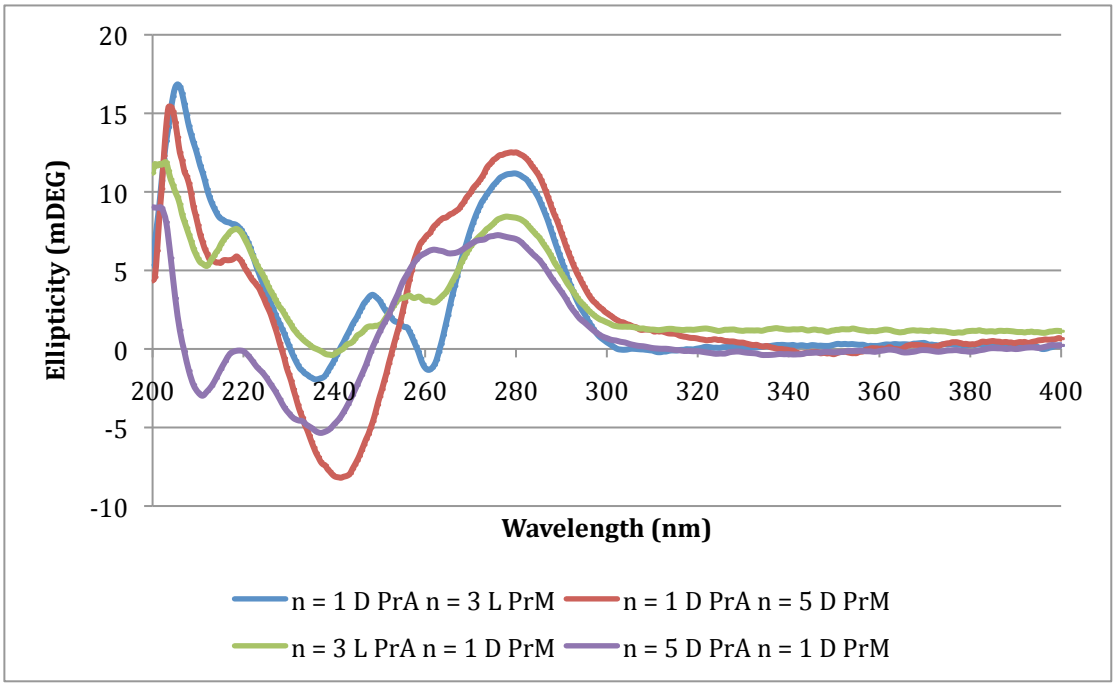

Fig. 187 CD spectra of mixed tether length duplexes 5μM concentration of oligo 10mM pH 7 phosphate buffer 100mM NaCl

As illustrated above, some combinations of linker and isomer gave markedly different spectra (Fig. 187 blue and green) whilst other combinations involving longer linkers gave more similar spectra (Fig. 187 red and purple). The existence of anthracene to anthracene exciton coupling may have been observed in some cases (Fig. 187 blue), however no patterns were observed and the instance of coupling may be a reflection of a unique combination. Furthermore, none of these differences were reflected in the fluorescence spectra whereby no excimer formation was observed.

5.9 Stacking conformation duplexes

Modelling studies show that an anthracene modification two (Probe MS) and three (Probe MG) base-pairs away on the 3' side would put the anthracene directly below the 7 position of a 15mer. Thus it was decided to try to form a bis-

anthracene duplex that could interact outside the duplex and potentially form an excimer.

Pr *A* ___ – 5' –*TGGACTCXCTCAATG* – 3'
Pr *M* __ – 3' –*ACCTGAGXGAGTTAC* – 3'
Pr *MS* _ – 3' –*ACCTGAGAGXGTTAC* – 3'
Pr *MG* _ – 3' –*ACCTGAGAGAXTTAC* – 3

Fig. 188 Table showing the different stacking conformation strands with the core sequence strand (*n* = 6 Probe A top), the standard complementary strand (*n* = 6 Probe M second from top), a complementary probe strand with the anthracene displaced by two bases (*n* = 6 Probe MS) and a complementary probe strand with the anthracene displaced by three bases (*n* = 6 Probe MG)

As the modelling studies also indicated that the short chain lengths stack into the duplex, it was decided to use the longest available isomer linkage, in this case *n* = 6, L and D.

5.9.1 Fluorescence studies of excimers in stacking duplexes

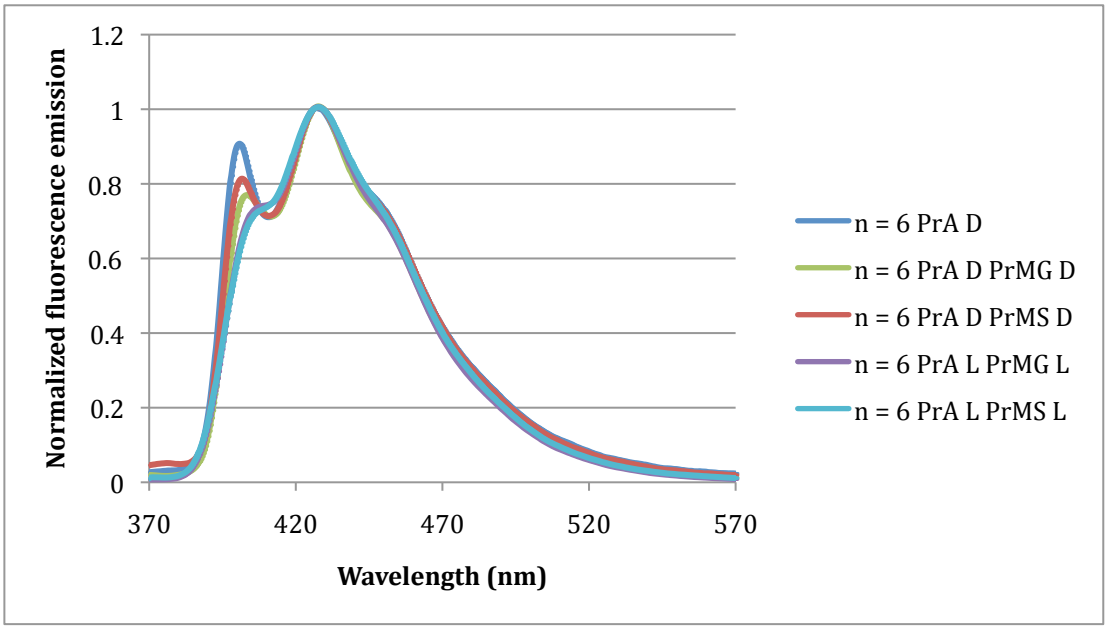

Fig. 189 Fluorescence spectra for bis anthracene tagged oligonucleotide duplexes with a non-opposite second anthracene tag 1µM concentration of oligo 10 mM pH 7 phosphate buffer 100mM NaCl

As can be seen from the graph there is no evidence of any excimer formation, possibly due to intercalation of the anthracenes.

5.9.2 Melting points

Table 53 Melting points (°C) for bis anthracene tagged oligonucleotide duplexes with a non-opposite second anthracene tag 5 μM concentration of oligo 10 mM pH 7 phosphate buffer 100 mM NaCl

Stacking Dimerisation Duplexes	*n* = 6 L PrM	*n* = 6 L PrMG	*n* = 6 L PrMS
n = 6 L PrA	53.3	42	43.5
	n = 6 D PrM	*n* = 6 D PrMG	*n* = 6 D PrMS
n = 6 D PrA	53.5	41.5	43

Initial melting point studies showed that the modified duplexes showed a considerable decrease in stability (*circa* 10 °C) compared to the analogous system (Probe M). This is in line with the observed results for a single mismatch and represents the loss of hydrogen bonding for one more base pair in the duplex compared to the Probe A-Probe M duplex. There does not appear to be either stabilization nor destabilization relative to the isomer combination.

5.10 Conclusions

The longer chain anthracene tethers have shown the potential to act as Base Discriminating Fluorophores (BDFs) through the sensing of the base directly opposite by a variable change of fluorescence emission upon hybridisation. The mode of this sensing has been studied using time-resolved fluorescence to resolve the different lifetimes. These studies have indicated that the change in the shortest lifetime correlates with the base selectivity. A trend in melting point was also observed for the different duplexes, and this can be explained through molecular modelling of the different.

5.11 References

1. Saito, Y.; Motegi, K.; Bag, S. S.; Saito, I., *Bioorg. Med. Chem.* **2008,** *16* (1), 107-113.
2. Fukui, K.; Tanaka, K., *Nucleic Acids Res.* **1996,** *24* (20), 3962-3967.
3. Hwang, G. T.; Seo, Y. J.; Kim, B. H., *J. Am. Chem. Soc.* **2004,** *126* (21), 6528-6529.
4. Hurley, D. J.; Seaman, S. E.; Mazura, J. C.; Tor, Y., *Org. Lett.* **2002,** *4* (14), 2305-2308.
5. Okamoto, A.; Tainaka, K.; Saito, I., *J. Am. Chem. Soc.* **2003,** *125* (17), 4972-4973.
6. Okamoto, A.; Kanatani, K.; Saito, I., *J. Am. Chem. Soc.* **2004,** *126* (15), 4820-4827.
7. Cekan, P.; Sigurdsson, S. T., *Chem. Commun.* **2008,** (29), 3393-3395.
8. Rehm, D.; Weller, A., *Isr. J. Chem.* **1970,** *8* (2), 259-&.
9. Manoharan, M.; Tivel, K. L.; Zhao, M.; Nafisi, K.; Netzel, T. L., *J. Phys. Chem.* **1995,** *99* (48), 17461-17472.
10. Heinlein, T.; Knemeyer, J. P.; Piestert, O.; Sauer, M., *J. Phys. Chem. B* **2003,** *107* (31), 7957-7964.
11. Seidel, C. A. M.; Schulz, A.; Sauer, M. H. M., *J. Phys. Chem.* **1996,** *100* (13), 5541-5553.
12. Asanuma, H.; Takarada, T.; Yoshida, T.; Tamaru, D.; Liang, X. G.; Komiyama, M., *Angew. Chem. Int. Ed.* **2001,** *40* (14), 2671-2673.
13. Kashida, H.; Liang, X. G.; Asanuma, H., *Curr. Org. Chem.* **2009,** *13* (11), 1065-1084.
14. Asanuma, H.; Liang, X.; Yoshida, T.; Komiyama, M., *ChemBioChem,* **2001,** *2*, 39 - 44.
15. Shi, Y.; Machida, K.; Kuzuya, A.; Komiyama, M., *Bioconjug. Chem.* **2005,** *16* (2), 306-311.

Chapter 6 NMR Studies of an anthracene tagged duplex

6.1 Introduction to NMR spectra of DNA

^{1}H NMR spectroscopy is a powerful method for studying the structure of modified oligonucleotides.[1] NMR spectroscopy as a whole can be used in numerous different ways to obtain many different kinds of information. As a result it can be considered to be a family of closely related methodologies as opposed to a single technique. In the field of modified DNA it has been successfully used to assign the unknown stereochemistry of a modified nucleoside and, more commonly, to determine the oligonucleotide structure.[2 3]

6.1.1 Proton shifts of bases, nucleotides and nucleosides

Nuclei that experience similar environments will have comparable resonance frequencies and will have ppm shifts that fall within a close range. However, these will vary systematically as a function of nucleotide sequence and overall DNA structure, since each local chemical environment will be slightly different. For instance the H8 of deoxyguanosine in the second G (G_2) of the sequence d(CGCAGAATTCGCG)$_2$ has δ = 7.95 ppm, whereas the H8 of the 11th base (G_{12}) has δ = 7.76 ppm. This means that it is often possible to distinguish different DNA residues.

The spectrum of the imino proton region reflecting the hydrogen bonding between base pairs is important in determining structure. However, for most NMR studies the solvent used is D_2O, which allows the dense region of sugar protons to be studied near the water peak, but as a result of rapid exchange of

the hydrogen atoms in hydrogen bonding groups with deuterium atoms, the hydrogen bonds cannot be observed in this solvent. In order to observe these hydrogen bonds, a sample must be dissolved in 10% D_2O and 90% H_2O, which provides a strong proton signal. This mixture allows 2D NOE experiments that can provide information on the proximity of the imino N-H to other protons in nearby bases and sugars.

Imino protons (Fig. 190) are usually sharp and relatively easy to analyze and this makes them particularly useful for assigning structural features. They are also in a region well away from any other peaks.

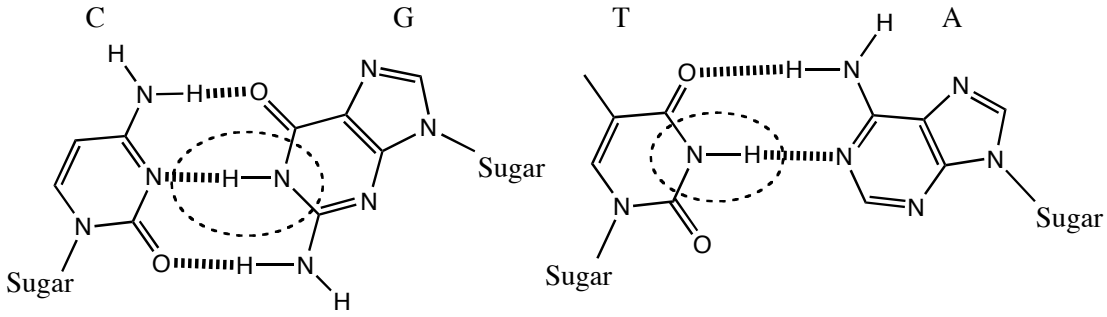

Fig. 190 Diagram of Watson-Crick base pairs showing imino protons

6.1.2 NMR experiments

6.1.2.1 TOCSY experiments

^1H-^1H TOCSY (TOtal Correlated SpectroscopY) is useful for dividing the proton signals into groups or coupling networks, especially when the multiplets overlap (have very similar chemical shifts) or there is extensive second order coupling. A TOCSY spectrum yields through bond correlations *via* spin-spin coupling. Correlations are seen throughout the coupling network and intensity is not related in a simple fashion to the number of bonds connecting the protons.

6.1.2.2 NOESY experiments

These experiments make use of the NOE effect, whereupon spin polarization is transferred from one spin population to another via cross relaxation. The NOE effect is observed through space, which makes it highly useful in determining the distances between non-bonded nuclei. This is because NOEs are quite strong when atoms are <2 Å apart but become very small when the atoms are separated by more than ~ 5 Å. This means that they can be used to observe NOEs between the imino protons and adjacent hydrogens.

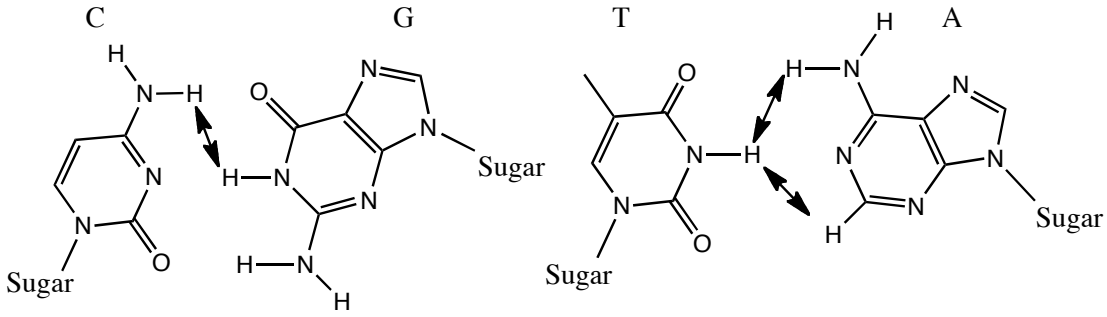

Fig. 191 Potential interbase NOEs between G-C and A-T base pairs

6.1.3 Preparation of sample for NMR studies

Although all samples were desalted using NAP-10 columns, it was found that the remaining TEAAc buffer gave rise to very strong peaks, therefore the oligonucleotides for NMR were further desalted by cold ethanol precipitation using 0.2 M NaOAc. The solution was then made up to a concentration of 950 μM with 10mM pH7 phosphate buffer and 100mM NaCl, both for a 100% D_20 sample and for a 5% D_2O in H_2O sample.

6.2 Analysis of the NMR spectrum of anthracene oligonucleotides

6.2.1 Previous work in identifying anthracene in oligonucleotides

Previous work in the group, by Dr. N Moran, involved the synthesis of trioligonucleotides containing an anthracene attached to a serinol non-nucleosidic backbone (Fig. 192).[4] The samples were dissolved in water with 10% D_2O using exciton sculpting for water suppression.

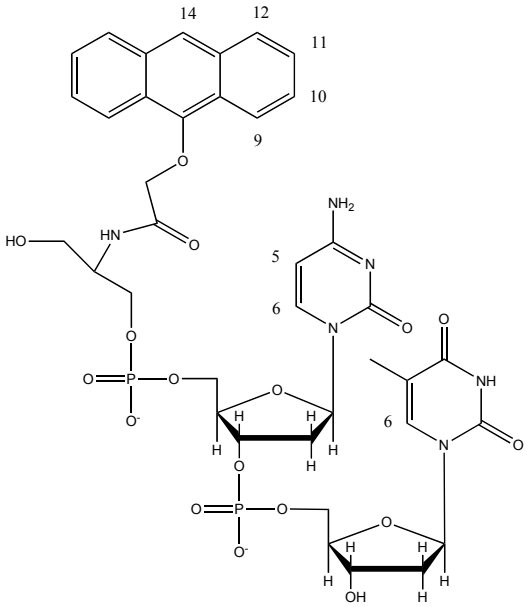

Fig. 192 Anthracene-CT Trioligonucleotides synthesized using a serinol linker[4]

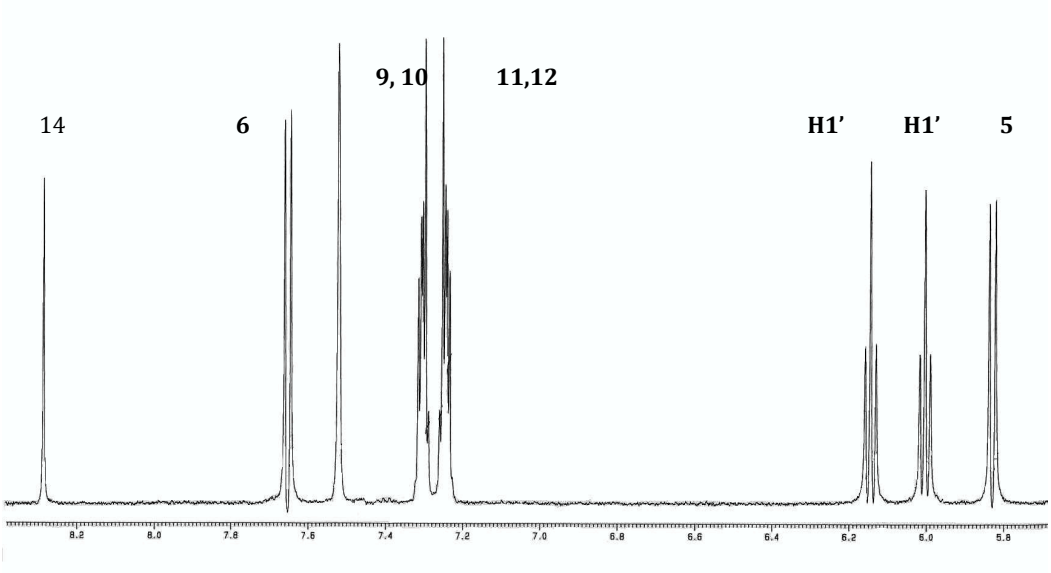

Fig. 193 500 ^{1}H MHz NMR spectrum of XCT trioligonucleotide chain in H_2O with 10% D_2O

Due to the smaller number of bases, and therefore protons, the spectrum was more easily assigned. The singlet at 8.29 ppm is assigned to the H14 proton, with multiplets at 7.25 ppm and 7.32 ppm corresponding to H11 and H12, and H9 and H10 respectively. The doublet at 7.65 ppm arises due to H6 of the cytosine, the doublet at 5.82 ppm from the H5 of cytosine, the peaks at 6.0 and 6.15 ppm correspond to the H1' sugar protons and the singlet at 7.53 ppm is due to the H6 of thymine.[5]

Further proof of these signals being from anthracene can be seen from ^{1}H NMR spectra of post-irradiation sample (Fig. 194) that show the loss of said signals, most likely due to photo-cleavage of the anthracene from the oligonucleotide strand.[4] It is noticeable that the integration of the peaks is not completely correct, but this may be as a consequence of the water suppression technique used.

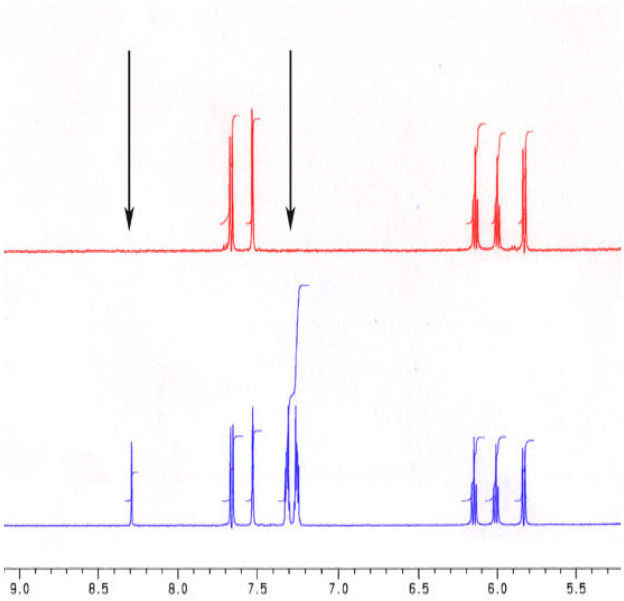

Fig. 194 ^{1}H NMR of anthracene tagged trioligonucleotide post (top) and pre (bottom) - irradiation

6.2.2 NMR studies on anthracene tagged DNA duplexes

An NMR analysis was undertaken on one of the anthracene duplex systems as part of a series of preliminary studies into the feasibility of using NMR to assign the location of anthracene within the modified duplex. The duplex chosen was the deletion version of the L isomer of Probe A, Probe A TarA2. There were a number of reasons for selecting this particular duplex but the most important factor was the high melting temperature that would ensure the greatest possible stability of the duplex through different temperature ranges that the NMR experiments were performed under. The high temperature also suggested a system where anthracene was intercalated within the duplex, making this system ideal for testing techniques to determine whether intercalated anthracene was present. Lastly, the system proved difficult to model computationally and it was hoped that NMR studies would provide some structural clues to help refine the structure, allowing successful molecular modelling to be undertaken.

6.2.3 Imino Protons 1D spectra

As described before, the imino protons can be very useful in base assignment of DNA. Generally, A-T imino protons appear at higher ppm values than G-C imino protons.

$$5' - TGGACTCXCTAATG - 3'$$
$$3' - ACCTAGGAGTTAC - 5'$$

Figure 1

Examination of the sequence shows that we would expect 14 proton signals, with 7 T imino protons and 7 G imino protons. However, only 12 peaks can be seen at

25.6 °C with 13 seen at lower temperatures (Fig. 195). This is due to fraying of the strands as the temperature increases. For bases at the end of the strand, fraying causes the imino proton to no longer appear in the NMR spectrum and this becomes more apparent as the temperature is raised. Lack of base stacking at the end of the strand, which occurs more for A-T than for G-C due to the greater number of hydrogen bonds in the latter. Hence, we see no imino protons for the A-T base pair at the 5' end and the G-C base pair at the 3' end at 25 °C, but only the 5' end A-T base pair imino proton is not visible at 15 °C. There is also the possibility of observing the melting of a base pair by taking NMR spectra at different temperatures. This is apparent in the spectra below where an imino peak at 12.8 ppm is observable at 15 °C but disappears at 26 °C. This would most likely correspond to the first G-C imino proton at the 3' end (with respect to the base).

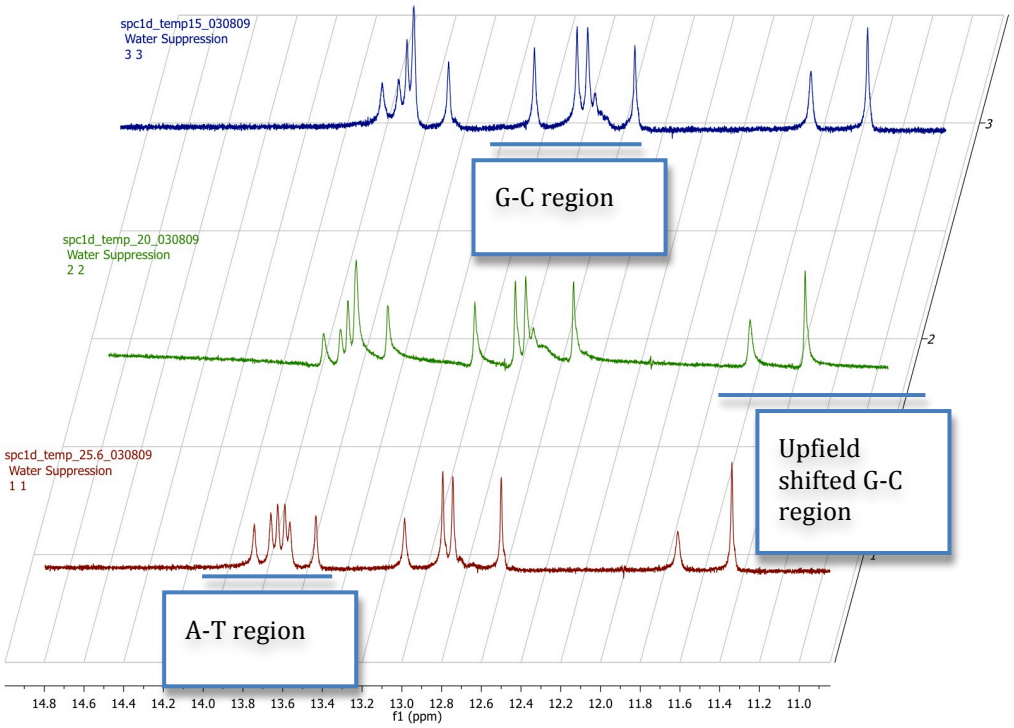

Fig. 195 900 MHz ^{1}H spectrum of the imino region of PrA L TarA2 at different temperatures (15 °C top, 20 °C middle, 25.6 °C bottom) in H_2O with 5%D_2O 950 µM DNA concentration 10 mM pH 7 phosphate buffer 100 mM NaCl

In the 1D spectrum of the oligonucleotide duplex we observe two peaks corresponding to two imino protons at 11.4 and 11.75 ppm that are significantly shifted upfield compared to the other G-C imino protons. It is tempting to assign these to the imino protons of the G-C base pairs adjacent to the anthracene, which are shifted due to the shielding effect of the aromatic rings. This shielding effect arises from the formation of ring currents in aromatic systems (Fig. 196) and a consequent magnetic field that causes upfield shifts when the hydrogen atom is above or below the ring and downfield shifts when it is alongside the ring.

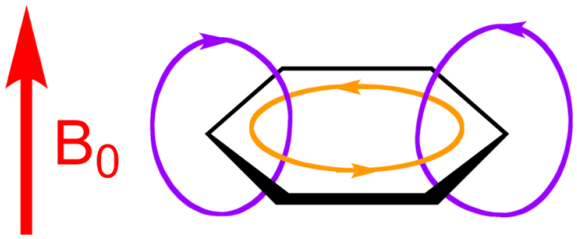

Fig. 196 Ring currents in aromatic systems

The large upfield shift observed in the spectrum is a characteristic of the anthracene binding close to the nucleobases where the moderate shielding effect of an adjacent base pair is replaced by the greater shielding from an aromatic system.[6] This has been observed in the NMR spectrum of DNA to which 9-amino acridine has been titrated,[7, 8] and would back up the observed melting point data.

6.2.4 2D NOESY spectrum of the imino region

Interestingly, the upfield GC imino protons (blue Fig. 197) mentioned earlier show 2D NOE cross peaks (red Fig. 197) to imino protons in the A-T region but do not show any NOE to each other or to any other imino hydrogens (green Fig. 197). This implies that they are either far from each other of there is some group in between that it blocking the NOE. This reinforces the hypothesis that they are from the central GC base pairs adjacent to AT base pairs and to anthracene.

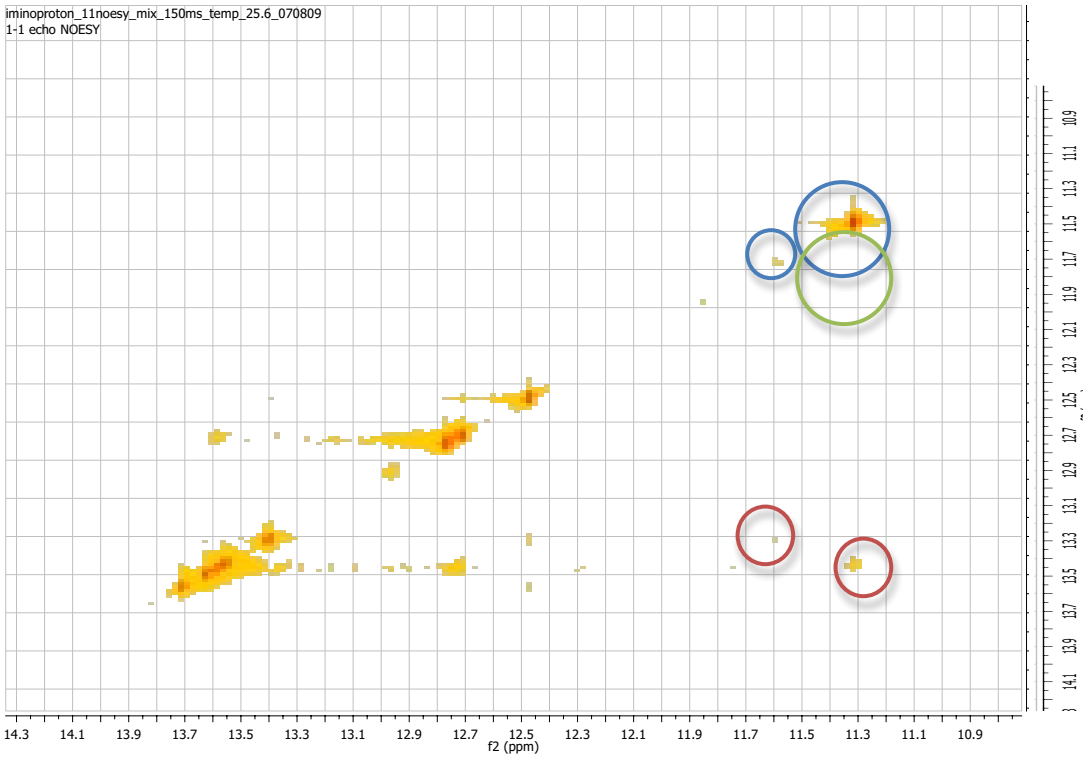

Fig. 197 900 MHz 2D NOESY spectrum of the imino region in H_2O with 10% D_2O 950 µM DNA concentration 10mM pH 7 phosphate buffer 100mM NaCl 25.6 °C mixing time 150 ms

However, expanding the ppm range of the 2D NOESY spectrum shows correlation between these upfield imino protons and protons in the aromatic region of the DNA around 8.1 ppm and 7.6 ppm which could be associated with anthracene (Fig. 198). This would imply a relatively close distance between the two protons and therefore would support the theory that anthracene may be intercalating between the groups.[1]

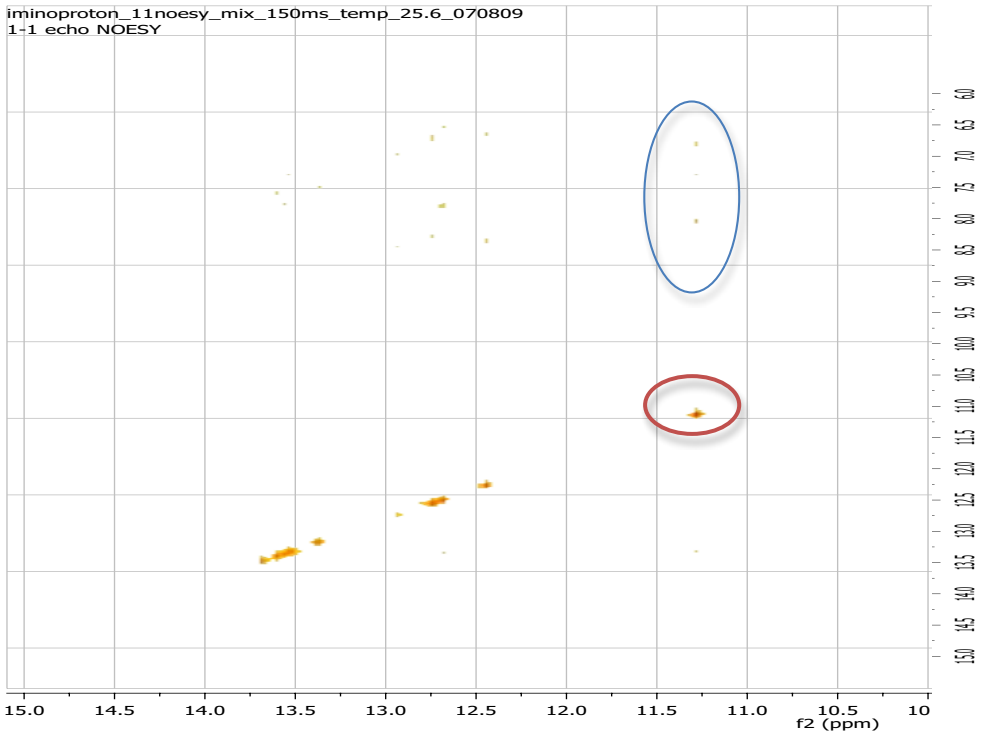

Fig. 198 900 MHz 2D NOESY spectrum of the imino and aromatic region of DNA in H_2O with 10% D_2O 950 µM DNA concentration 10mM pH 7 phosphate buffer 100mM NaCl

6.3 Analysis of the aromatic region of Probe A TarA2

6.3.1 TOCSY

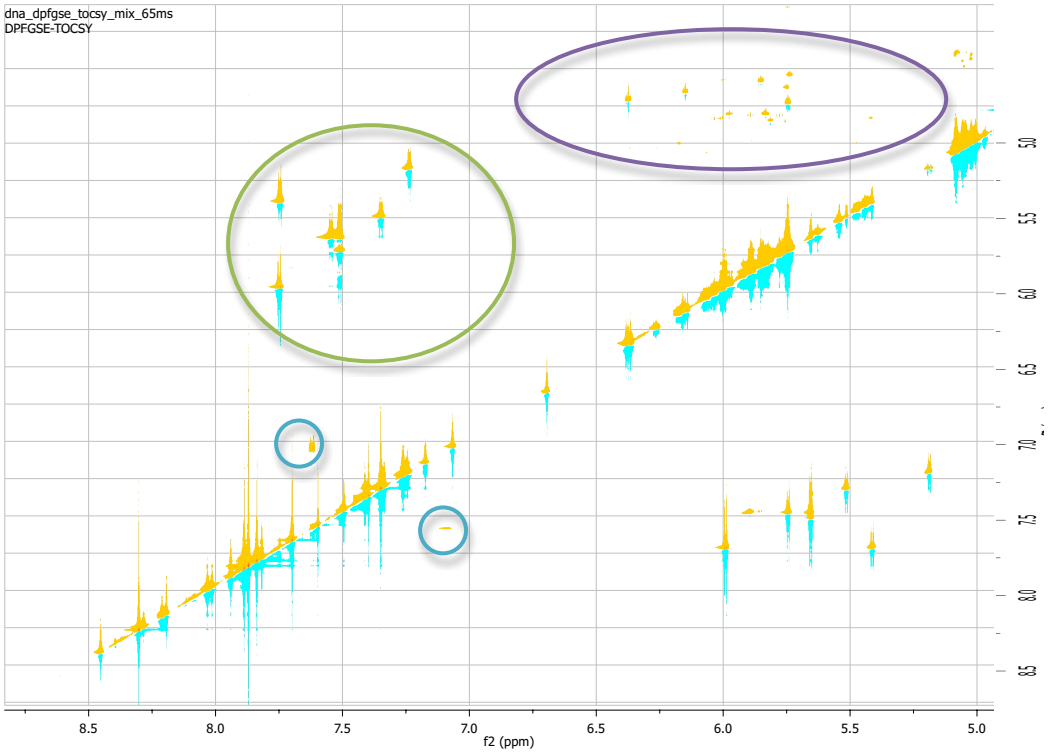

Fig. 199 900 MHz TOCSY spectrum of the sugar and aromatic region of modified DNA in D_2O 950 µM DNA concentration 10mM pH 7 phosphate buffer 100mM NaCl

TOCSY NMR experiments can identify cross peaks between protons that have characteristic shifts. These include the cross peaks between CyH5 and CyH6 (see Fig. 192 for diagram) and sugar H5 protons (Fig. 199 green and purple rings respectively). For the former, we observe 7 peaks corresponding to the expected number of C residues. Due to having multiple adjacent protons, anthracene provides a viable target for a TOCSY experiment. There is a specific cross peak between 7.0 ppm and 7.6 ppm (Fig. 199 blue) that is uncharacteristic of normal DNA and combined with its ppm values corresponding to the anthracene region, it is ascribed to two of the aromatic ring protons.

6.3.2 1D spectrum of the DNA aromatic region

As stated previously, NOE peaks were observed in the full DNA duplex spectra between G-C imino proton signals and the aromatic region of the spectrum. The peaks in the aromatic region with interactions (Fig. 200 red) have similar shifts to the peaks identified as being from anthracene in the trioligonucleotide. Although they do not have exactly the same ppm shift, this can be explained by considering that in the duplex form the anthracene would be in a more shielded environment and one would expect the peaks to be slightly shifted upfield. There is also the TOCSY peak that corresponds to the peaks circled in blue in Fig. 200. The coincidence of the blue and red circles below are a strong indication of the presence of an anthracene signal at 7.6 ppm. It should be noted that at the present time the identification of the exact anthracene peaks is not possible and thus only broad hypotheses may be possible.

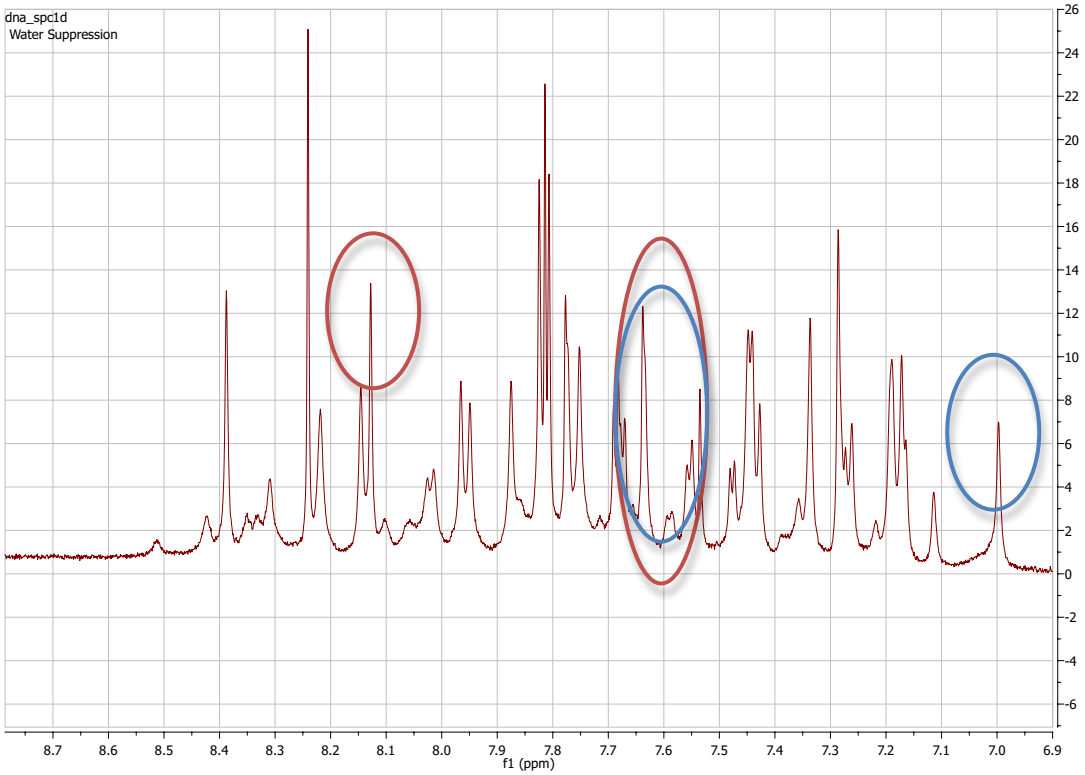

Fig. 200 900 MHz ^{1}H spectrum of the aromatic region of PrA L TarA2 at 15 °C in H_2O with 10%D_2O 950 µM 10mM pH 7 phosphate buffer 100mM NaCl

6.4 Conclusions

Further studies are ongoing, including a full NMR assignment of the duplex and samples of unmodified DNA have been synthesized in order to perform control studies. Preliminary results of the latter show that none of the GC protons are shifted upfield to the extent observed in the anthracene modified system. This would appear to confirm our conclusion that the observed shift in the anthracene tagged system was as a result of interactions between the flanking G imino protons and the anthracene aromatic rings.

In conclusion there are clear indications that the interactions between anthracene and the adjacent base pairs in the duplex may be monitored by NMR and, with more detailed analysis and assignment, could potentially be used to produce a model of the duplex.

6.5 References

1. Liang, X. G.; Asanuma, H.; Kashida, H.; Takasu, A.; Sakamoto, T.; Kawai, G.; Komiyama, M., *J. Am. Chem. Soc.* **2003,** *125* (52), 16408-16415.
2. Peyret, N.; Seneviratne, P. A.; Allawi, H. T.; SantaLucia, J., *Biochemistry* **1999,** *38* (12), 3468-3477.
3. Patel, D. J.; Kozlowski, S. A.; Ikuta, S.; Itakura, K., *Abs. Pap. Am. Chem. Soc.* **1983,** *186* (Aug), 93-BIOL.
4. Moran, N. Novel Anthracene-Tagged DNA Sensors. University of Exeter, **2006**.
5. Neumann, J. M.; Borrel, J.; Thiery, J. M.; Guschlbauer, W.; Trandinh, S., *Biochim. Biophys. Acta* **1977,** *479* (4), 427-440.
6. Nakamoto, K. T., M. and Strahan, G., *Drug-DNA Interactions*. Wiley: **2008**.
7. Assamunt, N.; Denny, W. A.; Leupin, W.; Kearns, D. R., *Biochemistry* **1985,** *24* (6), 1441-1449.
8. Assamunt, N.; Leupin, W.; Denny, W. A.; Kearns, D. R., *Biochemistry* **1985,** *24* (6), 1449-1460.

Chapter 7 Experimental

7.1 Synthesis and experimental details

7.1.1 Reagents and chemicals

Unless otherwise stated, solvents and reagents were obtained from commercial suppliers and used without further purification. Anhydrous solvents were dried by the usual procedures and used directly. Preparations of all target compounds were performed under an atmosphere of dry nitrogen, apart from the phosphytilation procedure which was performed under argon. Column chromatography was carried out using silica gel (Merck, grade 60) or alumina (basic, Brockman activity I).

^{1}H, ^{13}C and ^{31}P NMR spectra were recorded on Bruker AC 300, AV300, AV400 or AV 500. IR spectra were recorded on a Perkin Elmer Spectrum 100 FT-IR spectrometer. Elemental analyses were determined at the University of Birmingham. Electrospray Mass spectra were measured by a Waters micromass LCT Time of flight mass spectrometer. Melting points (M.p.) were determined using a Gallenkamp melting point apparatus and are uncorrected. All referenced compounds are previously known literature compounds that were compared to, and agreed with, the published assignments.

7.1.2 DNA synthesis and purification

Automated DNA synthesis of probe sequences was performed either at Queens University, Belfast on a Beckmann 1000M DNA synthesize or at the University of

Birmingham on an Applied Biosystems ABI 394 synthesizer. Millipore pure H_2O was used in all syntheses and studies of oligonucleotides. HPLC purification was carried out at Queen's University, Belfast using a Merck Hitachi Interface D-7000, pump L-7100, with a LaChrom diode array detector L-7455 or at the University of Birmingham using a Dionex system with Summit P580 pump and Summit UVD 170s UV/VIS Multi-Channel Detector with prep flow cell. MALDI-Tof mass spectra for oligonucleotides were obtained at the University of Birmingham using a Bruker Biflex IV Maldi time of flight mass spectrometer.

7.1.3 DNA analysis

7.1.3.1 UV Vis and CD

UV/Vis spectra were recorded at the University of Birmingham using a Varian Cary 5000 or Varian Cary 50 spectrometer. DNA melting temperatures were determined on a Varian Cary 5000 with a peltier heating accessory on a range of 15 to 85 °C with a heating rate of 0.5 °C /min. The value of the T_m was calculated from the first derivative of the melting curve using Varian software. Unless stated otherwise, all samples were monitored at 260 nm. Circular Dichroism spectra were taken on a Jasco J-810 spectropolarimeter scanning at a rate of 100nm/min, medium sensitivity.

7.1.3.3 Fluorescence and photochemistry

Quantum yields and fluorescence titrations were carried out on a Shimatzu RF-5301 PC spectrofluorimeter. Fluorescence decay profiles and lifetimes were taken using a Houriba Jobin Yvan Fluorolog 211 using a 371 nm pulsed LED excitation source operated at 1 MHz. The detection was accomplished with a cooled Hammamatsu 6158 single photon counting accessory. Alternatively a

pulsed frequency doubled Mirad 900 Ti sapphire laser with a 400-450 nm APD and 6 ps pulse was used at an excitation wavelength of 375 nm and the emission detected using an avalanche photodiode.

The decay profiles were fitted using a multiexponential decay function. Different exponential fitting functions were applied and the best fitting one was chosen by consideration of the X^2 parameter and Durbin-Watson test statistic.

The dimerisation irradiation at 365 nm was carried out on a 5 μM solution of DNA using medium pressure Mercury-Xenon lamps with a lead nitrate solution filter.

7.1.3.4 Cyclic voltammetry

Cyclic voltammetry experiments were carried out in dry, nitrogen purged CH_3CN on a BAS 100W electrochemical analyser with BAS 100 W software using tetrabutylammonium hexaflurophosphate (0.1M) as the supporting electrolyte, (Ag/AgCl) in 3M NaCl as the reference electrode (-35mV relative to SCE), and Pt wire as both the counter and working electrode. Prior to use, the platinum electrode was polished using 0.05μm alumina powder slurry and then washed with deionised water followed by methanol and dried with nitrogen. Decamethylferrocene was used as an internal reference.

7.1.3.5 Transient Absorption spectroscopy

This was performed at the University of Bordeaux 1 on a customized laser apparatus.

7.1.3.6 DNA NMR

This was performed at the Henry Wellcome Building NMR research centre at the University of Birmingham using a 900 MHz Oxford Instruments magnet. The oligonucleotide strands were additionally desalted by ethanol precipitation using 0.2 M NaOAc. Two samples were made up, firstly a water sample at 950 μM concentration of oligo with 10 mM pH 7 phosphate buffer, 100 mM NaCl solution and 5% D_2O and a 100% D_2O sample with the same concentrations. 1D spectra were obtained using excitation sculpting for water suppression using the procedure of Hwang and Shaka[1] and 2D NOESY spectra were obtained using the jump return procedure.[2]

7.2 Molecular modelling parameters

Structures were generated on a Silicon Graphics workstation using the InsightII modelling program. Energy minimization and molecular dynamics were performed on the University of Birmingham Bluebear computer cluster using the AMBER 8 modelling software. The input parameters for the energy minimization, equilibration and molecular dynamics were as follows:

Mdin for energy minimization

title

&cntrl

imin=1, maxcyc=1000000, NTB=0, cut=12.0

/

mdin for molecular dynamics

title NVT (canonical ensemble) dynamics: data gathering 2ns

&cntrl

imin=0, ntave=1000, ntwx=5000, ntwr=5000, ntf=2, NTB=0, cut=12.0

dt=0.002, nstlim=1000000, ntt=1, tempo0=300.0, tempi=300.0, ntc=2

ntx=5, irest=1

/

7.3 *n* = 1 synthesis

7.3.1 *n* = 1 Ester (2)

Ethyl 2-(anthracen-9-yloxy)acetate [3]

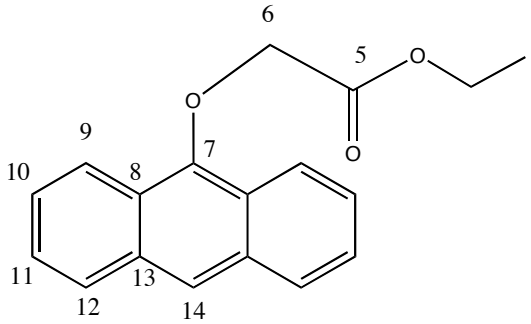

Anthrone (5.83 g, 0.03 mol) and K_2CO_3 (4.15 g, 0.03 mol) were dissolved in degassed acetone (200 mL) and stirred under N_2 at room temp. in the absence of light for 15 min. Ethyl bromoacetate (3.3 mL, 0.03 mol) was added and the

reaction mixture refluxed overnight. The solution was filtered to remove K_2CO_3 and dissolved in DCM (100 mL). The solution was washed with H_2O (1 x 50 mL) and dried over $MgSO_4$. The solvent was removed in *vacuo* to give an orange oil which solidified on standing. Column chromatography on silica (hexane with 10% EtOAc) yielded the desired product as a yellow solid (2.9 g, 30%). (R_f =0.58 in $CHCl_3$); M.p. 167-169 ˚C; δ_H (300 MHz, $CDCl_3$) 8.39 (2H, d, J = 7.7, H_9), 8.29 (1H, s, H_{14}), 8.03 (2H, d, J =7.5, H_{12}), 7.50-7.55 (4H, m, H_{10} and H_{11}), 4.83 (2H, s, OCH_2CO H_6), 4.41 (2H, q, J =7.2, CH_2CH$_3$), 1.41 (3H, t, J =7.2, CH$_2$CH_3); δ_C (100 MHz, $CDCl_3$) 169.1 (C_5=O), 149.5 (C_7), 132.6 (2xC_{13}), 128.9 (2xC_{12}), 126.3 (2xC_{10}), 126.1 (2xC_{11}), 124.5 (2xC_8), 123.6 (C_{14}), 121.9 (2xC_9), 74.0(C_6), 61.5 (CH$_2$CH$_3$), 14.2 (CH$_2$$CH_3$), *m/z* (ES+) calcd. for $C_{18}H_{16}O_3$ (M+Na$^+$) 303, found 303.

7.3.2 *n* = 1 Acid (3)

2-(Anthracen-9-yloxy)acetic acid [3]

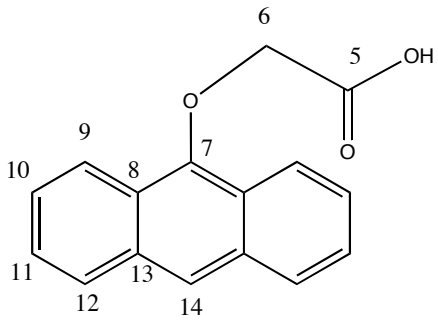

Ethyl 2-(anthracen-9-yloxy)acetate (2.9 g, 0.01 mol) was dissolved in a 1:1 soln. of 10 % NaOH (aq.) soln. and EtOH (200 mL) and refluxed overnight in the absence of light. The solution was concentrated under *vacuo* and dissolved in H_2O (500 mL). Conc. HCl was added dropwise to the solution to afford a precipitate, which was collected by suction filtration. The solid was washed with

H_2O and dried to give the desired product as a pearlescent, cream solid (2.64 g, 99% yield). M.p. 184-186 ˚C;

δ_H (300 MHz, $CDCl_3$) 8.31 (1H, s, H_{14}), 8.28 (2H, d, J = 7.7, H_9), 8.03 (2H, d, J = 7.6, H_{12}), 7.49-7.54 (4H, m, H_{10} and H_{11}), 4.88 (2H, s, OCH_2CO H_6); δ_C (75 MHz, $CDCl_3$) 172.1 (C_5=O), 149.5 (C_7), 132.6 (2xC_{13}), 128.9 (2xC_{12}), 127.2 (2xC_{10}), 126.1 (2xC_{11}), 125.7 (2xC_8), 123.6 (C_{14}), 121.6 (2xC_9), 71.2 (C_6); *m/z* (ES+) calcd for $C_{16}H_{11}O_3Na$ (M-H^++Na^+) 274.4, found 274.4.

7.3.3 *n* = 1 L Diol (4L)

2-(Anthracen-9-yloxy)-*N*-((2*R*,3*R*)-1,3-dihydroxybutan-2-yl)acetamide

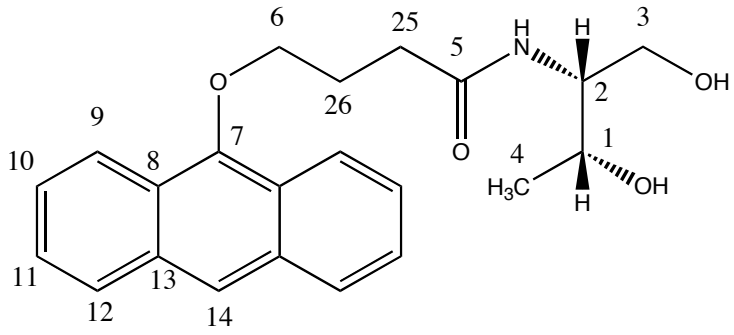

2-(Anthracen-9-yloxy)acetic acid (1.83 g, 7.3 mmol) was dissolved in anhydrous DMF (20 mL). HOBt (1.07 g, 7.9 mmol) was added to the soln. followed by DIPC (1.04 mL, 6.6 mmol) and the soln. was stirred under N_2 at room temp. in the absence of light for 15 mins. **L**- Threoninol (0.69 g, 6.6 mmol) and DIPEA (1.14 mL, 6.6 mmol) were added and the reaction left to stir at 40 ˚C for 40 hours. The soln. was diluted in MeOH/DCM (1:2 100mL) and washed with H_2O (3 x 50 mL) and dried over $MgSO_4$. The solvent was removed in *vacuo* and subsequent purification by silica column chromatography (DCM with 5% MeOH) gave the desired product as a pale yellow solid (0.72 g, 29%). (R_f =0.58 in DCM

with 10% MeOH); M.p. 179-185 ˚C (found: C, 69.81; H, 6.12; N, 4.41%. $C_{20}H_{21}NO_4$ + 0.25 eq. H_2O requires C, 69.85; H, 6.30; N, 4.07%); ν_{max}/cm^{-1} 3212 (OH), 2969 (N-H), 1651 (C=O); δ_H (300 MHz, $CDCl_3$) 8.29 (1H, s, *H14*), 8.13-8.27 (2H, m, *H9*), 8.00 (2H, dd, *J* = 6.5 and 3.2, *H12*), 7.99 (1H, s, N*H*), 7.49 (4H, m, *H10* and *H11*), 4.74 (2H, d, *J* = 5.8, OC*H*$_2$CO *H6*), 4.31-4.43 (1H, m, CH_3C*H*CH_2OH *H1*), 3.98-4.27 (3H, m, C*H*NH *H2,* CHC*H*$_2$OH *H3*), 1.41 (3H, d, *J* = 6.4, C*H*$_3$CHCH$_2$OH *H4*); δ_C (100 MHz, 1:1 CD_3CN:$CDCl_3$) 169.1 (*C5=O*), 149.5 (*C7*), 132.6 (2x*C13*), 128.9 (2x*C12*), 126.3 (2x*C10*), 126.1 (2x*C11*), 124.5 (2x*C8*), 123.6 (*C14*), 121.9 (2x*C9*), 74.0 (*C6*), 67.6 (*C1*), 63.8 (*C3*), 55.48 (*C2*), 20.7 (*C4*); *m/z* (ES+) calcd. for $C_{20}H_{21}NO_4Na$ (M+ Na^+) 362.1368, found 362.1357.

7.3.4 *n* = 1 D Diol (4D)

2-(Anthracen-9-yloxy)-*N*-((2*S*,3*S*)-1,3-dihydroxybutan-2-yl)acetamide

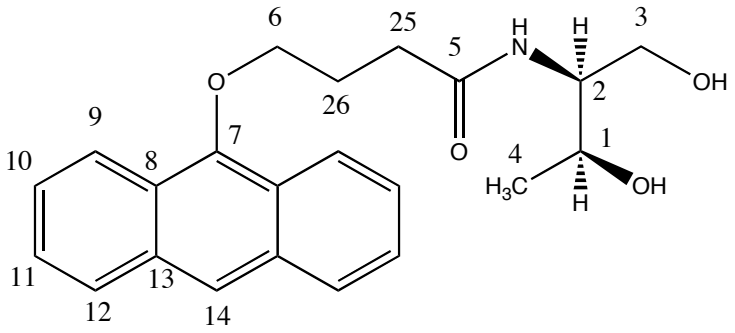

2-(Anthracen-9-yloxy)acetic acid (3.35 g, 13.0 mmol) was dissolved in anhydrous DMF (20 mL). HOBt (2.15 g, 13.0 mmol) was added to the soln. followed by DIPC (2.08 mL, 13.0 mmol) and the soln. stirred under N_2 at room temp.. in the absence of light for 15 mins. **D**- Threoninol (1.38 g, 13.0 mmol) and DIEA (2.28 mL, 13.0 mmol) were added and the reaction left to stir at 40 ˚C for 40 hours. The soln. was diluted in MeOH/DCM (1:2 100 mL) and washed with H_2O (3 x 50 mL) and dried over $MgSO_4$.The solvent was removed in *vacuo* and

subsequent purification by silica column chromatography (DCM with 5% MeOH) gave the desired product as a pale yellow solid (1.82 g, 41%). (R_f =0.58 in DCM with 10 % MeOH); M.p. 178-182 ˚C (found: C, 70.12; H, 6.30; N, 4.21%. $C_{20}H_{21}NO_4$ requires C, 70.78; H, 6.24; N, 4.13%); δ_H (300 MHz, CD_3CN) 8.33 (1H, s, *H14*), 8.23 (2H, dd, *J* = 8.3 and 1.6 *H9*), 8.04 (2H, dd, *J* = 6.5 and 3.3, *H12*), 7.65 (1H, s, N*H*), 7.33-7.62 (4H, m, *H10,* and *H11*), 4.66 (2H, d, *J* = 3.9, OC*H*$_2$CO *H6*), 4.16-4.36 (1H, m, CH_3CHCH_2OH *H1*), 3.95-4.02 (3H, m, C*H*NH *H2,* $CHCH_2OH$ *H3*), 3.82 (2H, t, *J* = 5.3, $CHCH_2OH$), 3.38 (1H, d, *J*= 4.0, CH_3CHCH_2OH), 3.26 (1H, t, *J*= 5.2, $CHCH_2OH$), 1.29 (3H, d, *J* = 6.3, CH_3CHCH_2OH *H4*); δ_C (100 MHz, 1:1 CD_3CN:$CDCl_3$) 169.1 (*C5*=*O*), 149.5 (*C7*), 132.7 (2x*C13*), 128.9 (2xC_{12}), 126.4 (2xC_{10}), 126.2 (2x*C11*), 124.5 (2xC_8), 123.6 (C_{14}), 121.7 (2x*C9*), 74.1 (*C6*), 67.5 (*C1*), 63.8 (*C3*), 55.6 (C_2), 20.7 (*C4*); *m/z* (ES+) calcd for $C_{20}H_{21}NO_4$ ($M+Na^+$) 362.1368, found 362.1357

7.3.5 *n* = 1 DMT L (5L)

2-(Anthracen-9-yloxy)-*N*-((2*R*,3*R*)-1-(bis(4-methoxyphenyl)(phenyl)methoxy)-3-hydroxybutan-2-yl)acetamide

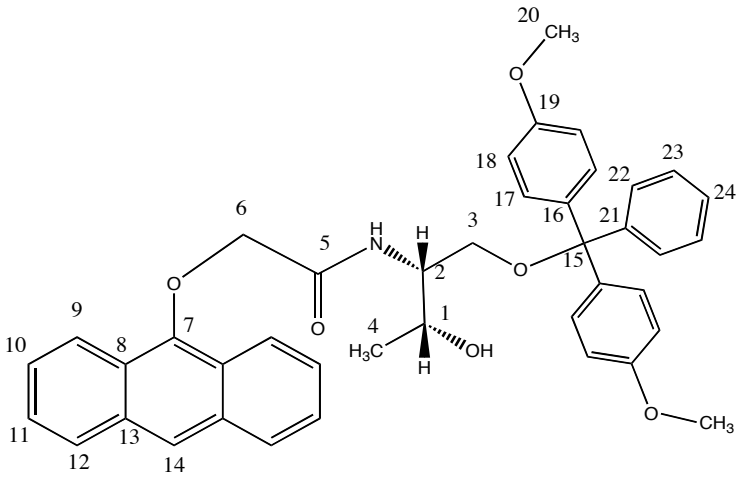

2-(Anthracen-9-yloxy)-*N*-((2*R*,3*R*)-1,3-dihydroxybutan-2-yl)acetamide) (0.73 g, 2.1 mmol) was dissolved in anhydrous pyridine (30 mL). Dimethoxytritylchloride (0.72 g, 2.1 mmol) was added to the soln. followed by DMAP (0.038 g, 0.3 mmol) and the reaction left to stir under N_2 at room temp.. in the absence of light for 24 hours. The reaction mixture was poured onto H_2O (50 mL), extracted with DCM (2 x 50 mL) and dried over $MgSO_4$. Column chromatography on silica (Hexane/EtOAc/TEA, 40:59:1) afforded the desired compound as a pale yellow crystalline solid (0.61 g, 44 %). (R_f =0.38 in DCM with 5% MeOH); M.p. 83-85 ˚C (found: C, 76.04; H, 6.75; N, 2.59 %. $C_{41}H_{39}O_6N$+0.33 eq TEA requires C, 76.46; H, 6.57; N, 2.76 %); ν_{max}/cm^{-1} 3414 (OH), 2933 (N-H), 1666 (C=O); δ_H (300 MHz, CD_3CN) 8.38 (1H, s, *H*$_{14}$), 8.25 (2H, d, *J* = 8.6, *H*$_9$), 8.08 (2H, d, *J* = 8.4, *H*$_{12}$), 7.53 (1H, d, *J* = 8.7, N*H*), 7.48-7.52 (4H, m, *H*$_{11}$ and *H*$_{22}$), 7.40-7.45 (2H, m, *H*$_{10}$), 7.35-7.40 (4H, m, *H*$_{17}$), 7.30 (2H, t, *J* = 7.4, *H*$_{23}$), 7.19-7.25 (1H,

m, H_{24}), 6.85 (4H, d, J = 8.7, H_{18}), 4.70 (2H, s, OCH_2CO H_6), 4.02-4.18 (1H, m, CHNH H_2), 4.11 (1H, m, CHCHOH H_1), 3.73 (6H, s, 2 x OCH_3 H_{20}), 3.03-3.43 (2H, m, CH_2ODMT H_3), 1.2 (3H, d, J = 6.2, CH_3CHCOH H_4); δ_C (125 MHz, CD_3CN) 169.3 (C_5=O), 159.7 (2xC_{19}), 150.2 (C_7), 146.2 (C_{21}), 137.2 (C_{16}), 137.0 (C_{16}), 13.4 (2xC_{13}), 131.0 (4xC_{17}), 129.5 (2xC_{12}), 129.0 (2xC_{22}), 128.8 (2xC_{23}), 127.8 (C_{24}), 126.9 (2xC_{10}), 126.8 (2xC_{11}), 125.1 (2xC_8), 124.2 (C_{14}), 122.6 (2xC_9), 114.1 (4xC_{18}), 87.0 (C_{15}), 74.7 (C_6), 67.3 (C_1), 64.4 (C_3), 55.8 (2xC_{20}), 55.3 (C_2), 20.8 (C_4); *m/z* (ES+) calcd for $C_{41}H_{39}O_6NNa$ ($M+Na^+$) 664.2675, found 664.2696.

7.3.6 *n* = 1 DMT D (5D)

2-(Anthracen-9-yloxy)-*N*-((2*S*,3*S*)-1-(bis(4-methoxyphenyl)(phenyl)methoxy)-3-hydroxybutan-2-yl)acetamide

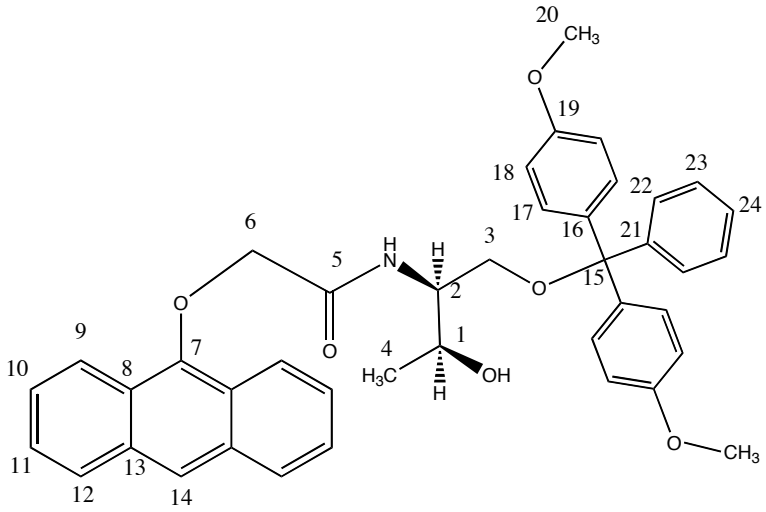

2-(Anthracen-9-yloxy)-*N*-((2*S*,3*S*)-1,3-dihydroxybutan-2-yl)acetamide) (0.73 g, 5.3 mmol) was dissolved in anhydrous pyridine (30 mL). Dimethoxytritylchloride (0.72 g, 5.3 mmol) was added to the soln. followed by

DMAP (0.038 g, 0.5 mmol) and the reaction left to stir under N_2 at room temp.. in the absence of light for 24 hours. The reaction mixture was poured onto H_2O (50 mL), extracted with DCM (2 x 50 mL) and dried over $MgSO_4$. Column chromatography on silica (Hex/EtOAc/TEA, 40:59:1) afforded the desired compound as a pale yellow crystalline solid (1.52 g, 54%). (R_f =0.38 in DCM with 5% MeOH); M.p. 82-85˚C (found: C, 75.9; H, 6.1; N, 2.1%. $C_{45}H_{47}NO_8$ + 0.25 eq EtOAc requires C, 76.0; H, 6.23; N, 2.11%); δ_H (500 MHz, CD_3CN) 8.37 (1H, s, *H_{14}*), 8.25 (2H, dt, *J* = 8.7 and 2.2, *H_9*), 8.06 (2H, d, *J* = 8.5, *H_{12}*), 7.53 (1H, d, *J* = 8.7, N*H*), 7.48-7.52 (4H, m, *H_{11}* and *H_{22}*), 7.42 (2H, m, *H_{10}*), 7.37 (4H, m, *H_{17}*), 7.30 (2H, dd, *J* = 10.5, and 4.8, *H_{23}*), 7.20-7.26 (1H, m, *H_{24}*), 6.84 (4H, dd, *J* = 1.8 and8.7, *H_{18}*), 4.69 (2H, d, *J* = 3.2, OC*H_2*CO *H_6*), 4.15 (1H, m, C*H*NH *H_2*), 4.11 (1H, m, CHC*H*OH *H_1*), 3.72 (6H, d, *J* = 2.3, 2 x OC*H_3*), 3.20-3.37 (2H, m, C*H_2*ODMT *H_3*), 1.2 (3H, d, *J* = 6.2, C*H_3*CHOH *H_4*); δ_C (125 MHz, CD_3CN) 169.3 (*C_5=O*), 159.7 (2x*C_{19}*), 150.2 (*C_7*), 146.2 (*C_{21}*), 137.2 (*C_{16}*), 137.0 (*C_{16}*), 13.4 (2x*C_{13}*), 131.0 (4x*C_{17}*), 129.5 (2x*C_{12}*), 129.0 (2x*C_{22}*), 128.8 (2x*C_{23}*), 127.8 (*C_{24}*), 126.9 (2x*C_{10}*), 126.8 (2x*C_{11}*), 125.1 (2x*C_8*), 124.2 (*C_{14}*), 122.6 (2x*C_9*), 114.1 (4x*C_{18}*), 87.0 (C_{15}), 74.7 (*C_6*), 67.3 (*C_1*), 64.4 (*C_3*), 55.8 (2x*C_{20}*), 55.3 (*C_2*), 20.8 (*C_4*); *m/z* (ES+) calcd. for $C_{41}H_{39}O_6NNa$ ($M+Na^+$) 664.2675, found 664.2696.

7.3.7 *n* = 1 L Phosphoramidite (6L)

(2*R*,3*R*)-3-(2-(Anthracen-9-yloxy)acetamido)-4-(bis(4-methoxyphenyl)(phenyl)methoxy)butan-2-yl 2-cyanoethyl diisopropylphosphoramidite

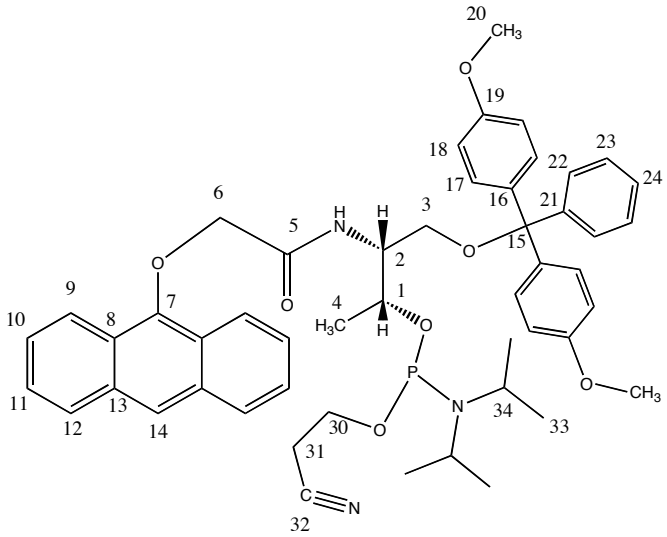

2-(Anthracen-9-yloxy)-*N*-((*R*,*R*)-1-(bis(4-methoxyphenyl)(phenyl)methoxy)-3-hydroxybutan-2-yl)acetamide (0.34g, 0.55mmol), pre-dried overnight over P_2O_5, was dissolved in dry DCM (15 mL) and stirred under argon. DIPEA (4 eq. 0.4 mL) was added followed by *2*-cyanoethyl-diisopropylchlorophosphoramidite (1.1 eq 0.12mL) *via* a disposable syringe dropwise and the reaction stirred for 30 mins. Solid supported BnOH was added (0.3g) and left to stir for 1 hour in the absence of light. The soln. was filtered, diluted with EtOAc (10 mL) and then washed with 2 M Na_2CO_3 (a.q.) soln. (2 x 50 mL), H_2O (1 x 50 mL) and brine (1 x 50 mL) and dried over Mg_2SO_4. The EtOAc was then removed in *vacuo* and the solid dissolved in 50:49:1 Hex:EtOAc.TEA The compound was then columned through activated alumina in 50:50 Hex:EtOAc. The desired fractions were collected and the solvent removed in *vacuo*. Co-evaporation in *vacuo* with acetonitrile three times removed final

traces of DIPEA to give the phosphoramidite as a yellow solid (0.35g 78%). (R_f =0.73 50:50 Hex:EtOAc); δ_H (300 MHz, CD_3CN) 8.39 (1H, s, *H14*), 8.22 (2H, d, *J* = 8.7, *H9*), 8.08 (2H, d, *J* = 8.5, *H12*), 7.45-7.56 (5H, m, *H11*, *H22* and N*H*), 7.36-7.45 (4H, m, *H10* and *H17*), 7.27-7.35 (2H, m, *H23*), 7.20-7.26 (1H, m, *H24*), 6.81-6.92 (4H, m, *H18*), 4.70 (2H, d, *J* = 2.6, OC*H*$_2$CO *H6*), 4.27-4.63 (2H, m, C*H*NH *H2* and CH_3C*H*OP *H1*), 3.73 (6H, s, OC*H*$_3$ *H20*), 3.33-3.58 (6H, m, C*H*$_2$ODMT *H3*, POC*H*$_2$ *H30* and PNC*H* *H34*), 2.44-2.62 (2H, m, C*H*$_2$CN *H31*), 0.98-1.07 (12H, m, C*H*$_3$ *H33*), 0.79 (3H, d, *J* = 6.8, C*H*$_3$CHOP *H4*); δ_P (121 MHz, CD_3CN) 148.4, 146.0; *m/z* (ES+) calcd. for $C_{50}H_{56}O_7N_3$ ($M+Na^+$) 864.3754, found 864.3769.

7.3.8 *n* = 1 D Phosphoramidite (6D)

(2*S*,3*S*)-3-(2-(Anthracen-9-yloxy)acetamido)-4-(bis(4-methoxyphenyl)(phenyl)methoxy)butan-2-yl 2-cyanoethyl diisopropylphosphoramidite

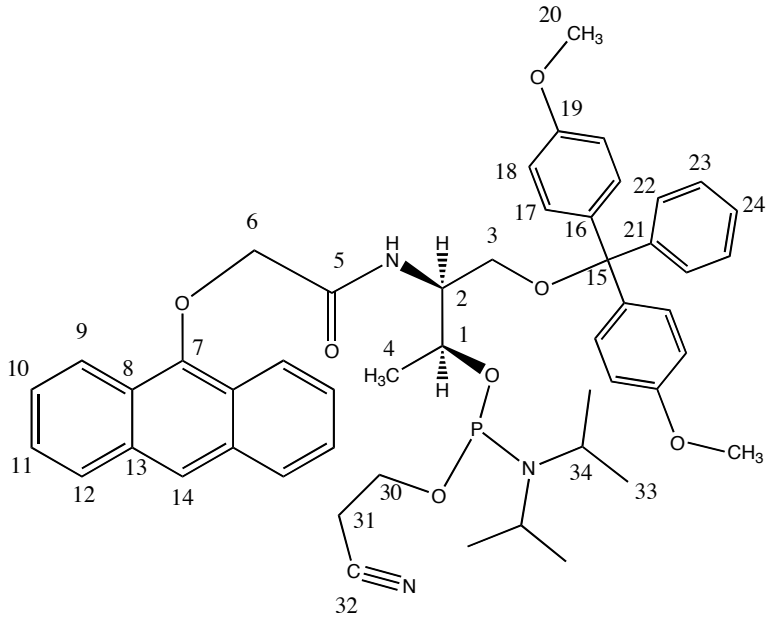

2-(Anthracen-9-yloxy)-N-((2*S*,3*S*)-1-(bis(4-methoxyphenyl)(phenyl)methoxy)-3-hydroxybutan-2-yl)acetamide (0.15g, 0.24mmol), pre-dried overnight over P_2O_5, was dissolved in dry DCM (10 mL)

and stirred under argon. DIPEA (4 eq., 0.17 mL) was added followed by *2*-cyanoethyl-diisopropylchlorophosphoramidite (1.1 eq, 0.05 mL) *via* a disposable syringe dropwise and the reaction stirred for 30 mins. Solid supported BnOH was added (0.3g) and left to stir for 1 hour in the absence of light. The soln. was filtered, diluted with EtOAc (10 mL) and then washed with 2 M Na_2CO_3 (a.q.) soln. (2 x 50 mL), H_2O (1 x 50 mL) and brine (1 x 50 mL) and dried over Mg_2SO_4. The EtOAc was then removed in *vacuo* and the solid dissolved in 50:50 Hex:EtOAc. The compound was then columned through activated alumina in 49:50:1 EtOAc:Hex:TEA. The desired fractions were collected and the solvent removed in *vacuo*. Co-evaporation in *vacuo* with acetonitrile three times gave the phosphoramidite as a yellow solid (0.05g, 27%); (R_f =0.6 50:50 Hex:EtOAc); δ_H (300 MHz, CD_3CN) 8.39 (1H, s, H_{14}), 8.22 (2H, d, J = 8.7, H_9), 8.08 (2H, d, J = 8.5, H_{12}), 7.45-7.56 (5H, m, H_{11}, H_{22} and N*H*), 7.36-7.45 (4H, m, H_{10} and H_{17}), 7.27-7.35 (2H, m, H_{23}), 7.20-7.26 (1H, m, H_{24}), 6.81-6.92 (4H, m, H_{18}), 4.70 (2H, d, J = 2.6, OCH_2CO H_6), 4.27-4.63 (2H, m, C*H*NH H_2 and CHC*H*OP H_1), 3.73 (6H, s, OCH_3 H_{20}), 3.33-3.58 (6H, m, CH_2ODMT H_3, POCH_2 H_{30} and PNC*H* H_{34}), 2.44-2.62 (2H, m, CH_2CN H_{31}), 0.98-1.07 (12H, m, CH_3 H_{33}), 0.79 (3H, d, J = 6.8, CH_3CHOP H_4); δ_P (121 MHz, CD_3CN) 148.3, 146.0; *m/z* (ES+) calcd. for $C_{50}H_{56}O_7N_3PNa$ ($M+Na^+$) 864.3754, found 864.3751.

7.4 *n* = 3 synthesis

7.4.1 *n* = 3 Ester (2b)

Ethyl 4-(anthracen-9-yloxy)butanoate [3]

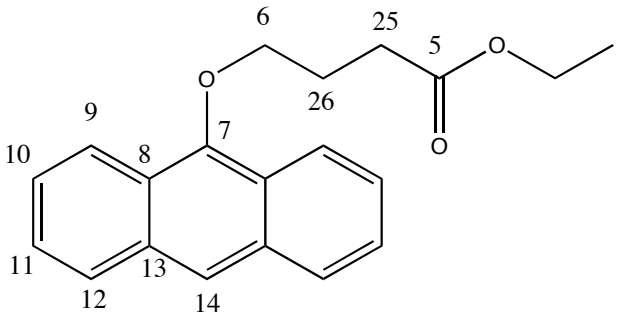

Anthrone (2.4 g, 12.5 mmol) and K_2CO_3 (1.8 g, 13 mmol) were dissolved in degassed acetone (200 mL) and stirred under N_2 at room temp. in the absence of light for 15 min. Ethyl *4* -bromobutyrate (1.8 mL, 12.5 mmol) was added and the reaction mixture refluxed overnight. The solution was filtered to remove K_2CO_3, evaporated *in vacuo* and redissolved in DCM (100 mL). The solution was washed with H_2O (1 x 50 mL) and dried over $MgSO_4$. The solvent was removed in *vacuo* to give an orange oil which solidified on standing. Column chromatography on silica (hexane with 10% EtOAc) yielded the desired product as a pale orange crystalline solid (1.9 g, 49%). (R_f =0.50 in hexane with 10% EtOAc); M.p. 73 ˚C δ_H (300 MHz, $CDCl_3$) 8.31 (2H, d, *J* = 9.0, H_9), 8.24 (1H, s, H_{14}), 8.01 (2H, d, *J* = 9.5, H_{12}), 7.45-7.53 (4H, m, H_{10} and H_{11}), 4.20-4.28 (4H, m, CH_2CH_3 and OCH_2CH_2 H_6), 2.82 (2H, t, *J* = 7.4, CH_2CH_2CO H_{25}), 2.42 (2H, m, $CH_2CH_2CH_2CO$ H_{26}), 1.34 (3H, t, *J* = 7.1, CH_2CH_3); δ_C (100 MHz, $CDCl_3$) 173.8 (C_5=O), 150.6 (C_7), 132.2 (2xC_{13}), 128.4 (2xC_{12}), 125.4 (2xC_{10}), 125.2 (2xC_{11}), 124.4 (2xC_8), 122.2 (C_{14}), 122.0 (2xC_9), 74.7 (C_6), 60.6 (CH_2CH_3), 31.2 (C_{25}), 26.0 (C_{26}),14.3 (CH_2CH_3); *m/z* (ES+) calcd. for $C_{20}H_{20}O_3Na$ ($M+Na^+$) 341.0, found 341.0.

7.4.2 *n* = 3 Acid (3b)

4-(Anthracen-9-yloxy)butanoic acid [3]

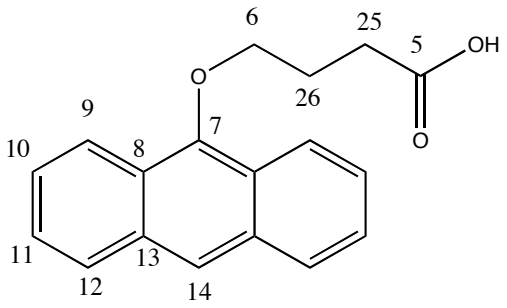

Ethyl 4-(anthracen-9-yloxy)butanoate (1.0 g, 3.3 mmol) was dissolved in a 1:1 soln. of 10 % NaOH (aq.) soln. and EtOH (200 ml) and refluxed overnight in the absence of light. The solution was concentrated under *vacuo* and dissolved in H_2O (500 mL). Conc. HCl was added dropwise to the solution to afford a precipitate which was collected by suction filtration. The solid was washed with H_2O and dried to give the desired product as a cream, crystalline solid (0.9 g, 95% yield). M.p. 117 ˚C; δ_H (300 MHz, $CDCl_3$) 8.29 (1H, s, H_{14}), 8.26 (2H, d, J = 9.9, H_9), 8.02 (2H, d, J = 9.6, H_{12}), 7.47-7.52 (4H, m, H_{10} and H_{11}), 4.27 (2H, t, J = 6.4, $OCH_2(CH_2)_2$ H_6), 2.90 (2H, t, J = 7.4, $(CH_2)_2CH_2CO$ H_{25}), 2.42-2.47 (2H, m, $CH_2CH_2CH_2CO$ H_{26}); δ_C (100 MHz, $CDCl_3/CD_3CN$) 173.8 (C_5=O), 150.6 (C_7), 132.2 (2xC_{13}), 128.4 (2xC_{12}), 125.4 (2xC_{10}), 125.2 (2xC_{11}), 124.4 (2xC_8), 122.2 (C_{14}), 122.0 (2xC_9), 74.7 (C_6), 30.2 (C_{25}), 25.7 (C_{26}); *m/z* (ES+) calcd. for $C_{18}H_{16}O_3Na$ (M-H^++Na^+) 302.1, found 302.1.

7.4.3 *n* = 3 L Diol (4bL)

4-(Anthracen-9-yloxy)-*N*-((2*R*,3*R*)-1,3-dihydroxybutan-2-yl)butanamide

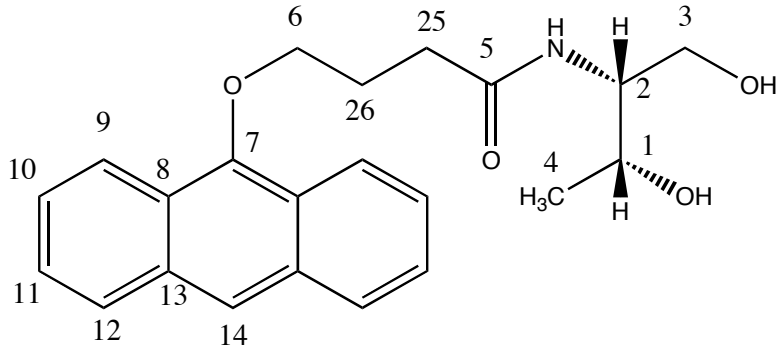

4-(Anthracen-9-yloxy)butanoic acid (1.28g, 4.5 mmol) was dissolved in anhydrous DMF (20 mL). HOBt (0.62 g, .0 mmol) was added to the soln. followed by DIPC (2.08 mL, 13.0 mmol) and the soln. stirred under N_2 at room temp. in the absence of light for 15 mins. **L**- Threoninol (1.38 g, 13.0 mmol) and DIPEA (2.28 mL, 13.0 mmol) were added and the reaction left to stir at 40 ˚C for 40 hours. The soln. was diluted in MeOH/DCM (1:2 100 mL) and washed with H_2O (3 x 50 mL) and dried over $MgSO_4$. The solvent was removed in *vacuo* and subsequent purification by silica column chromatography (DCM with 5% MeOH) gave the desired product as a pale yellow solid (1.24 g, 75%). (R_f =0.24 in DCM with 5% MeOH); M.p. 140-145 ˚C (found: C, 71.35; H, 6.72; N, 3.63%. $C_{22}H_{25}O_4N$ requires C, 71.91; H, 6.86; N, 3.81%); δ_H (400 MHz, $CDCl_3$) 8.18 (2H, dd, *J* = 11.6 and 4.5, *H*$_9$), 8.14 (1H, s, *H*$_{14}$), 7.98-7.96 (2H, m, *H*$_{12}$), 7.36-7.48 (4H, m, *H*$_{10}$ and *H*$_{11}$), 6.79 (1H, d, *J* = 8.6, N*H*), 4.10-4.20 (3H, m, OC*H*$_2$CH$_2$CH$_2$O *H*$_6$ and CH$_3$C*H*OH *H*$_1$), 3.87-3.94 (1H, m, C*H*NH *H*$_2$), 3.78 (2H, d, *J* = 4.7, CHC*H*$_2$OH *H*$_3$), 2.62-2.75 (2H, m, C*H*$_2$CO *H*$_{25}$), 2.27-2.40 (2H, m, C*H*$_2$CH$_2$CO *H*$_{26}$), 1.15 (3H, d, *J* = 6.4, C*H*$_3$CHCH$_2$OH *H*$_4$); δ_C (100 MHz, $CDCl_3$) 173.8 (*C*$_5$=*O*), 150.6 (*C*$_7$), 132.2 (2x*C*$_{13}$), 128.4 (2x*C*$_{12}$),

125.4 (2xC_{10}), 125.2 (2xC_{11}), 124.4 (2xC_8), 122.2 (C_{14}), 122.0 (2xC_9), 74.7 (C_6), 67.6 (C_1), 63.9 (C_3), 55.0 (C_2), 33.2 (C_{25}), 26.5(C_{26}), 20.3(C_4); *m/z* (ES+) calcd. for $C_{22}H_{25}O_4NNa$ ($M+Na^+$) 390.1681, found 390.1674.

7.4.4 *n* = 3 D Diol (4bD)

4-(Anthracen-9-yloxy)-*N*-((2*S*,3*S*)-1,3-dihydroxybutan-2-yl)butanamide

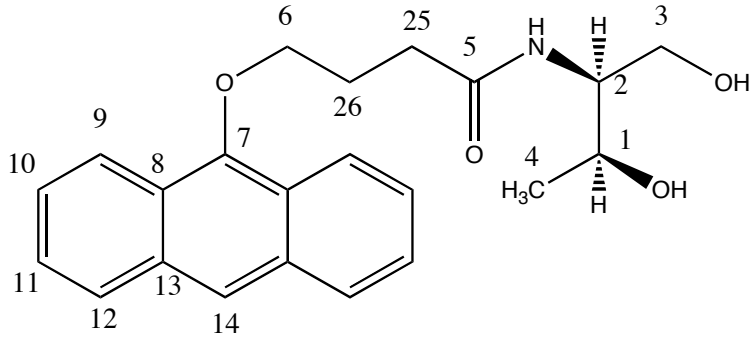

4-(Anthracen-9-yloxy)butanoic acid (2.28g, 8.1 mmol) was dissolved in anhydrous DMF (20 mL). HOBt (1.10 g, 8.1 mmol) was added to the soln. followed by DIPC (1.26 mL, 8.1 mmol) and the soln. stirred under N_2 at room temp. in the absence of light for 15 mins. **D-** Threoninol (0.86 g, 8.1 mmol) and DIPEA (1.26 mL, 8.1 mmol) were added and the reaction left to stir at 40 ˚C for 40 hours. The soln. was diluted in MeOH/DCM (1:2 100 mL) and washed with H_2O (3 x 50 mL) and dried over $MgSO_4$. The solvent was removed in *vacuo* and subsequent purification by silica column chromatography (DCM with 5% MeOH) gave the desired product as a pale yellow solid (2.43 g, 80%). (R_f =0.26 in DCM with 5% MeOH); M.p. 139-143 ˚C; δ_H (400 MHz, $CDCl_3$) 8.18 (2H, dd, *J* = 11.6 and 4.5, H_9), 8.14 (1H, s, H_{14}), 7.98-7.96 (2H, m, H_{12}), 7.36-7.47 (4H, m, H_{10} and H_{11}), 6.79 (1H, d, *J* = 8.6, N*H*), 4.09-4.20 (3H, m, OCH_2CH_2CH_2O H_6 and CH_3C*H*OH H_1), 3.87-3.94 (1H, m, C*H*NH H_2), 3.78 (2H, d, *J* = 4.7, CHCH_2OH H_3), 2.61-2.75 (2H, m,

CH_2CO H_{25}), 2.27-2.39 (2H, m, CH_2CH_2CO H_{26}), 1.15 (3H, d, J = 6.4, CH_3CHCH_2OH H_4); δ_C (75 MHz, $CDCl_3$) 173.6 (C_5=O), 150.8 (C_7), 132.3 (2xC_{13}), 128.5 (2xC_{12}), 125.4 (2xC_{10}), 125.3 (2xC_{11}), 124.5 (2xC_8), 122.3 (C_{14}), 122.0 (2xC_9), 74.8 (C_6), 68.3 (C_1), 64.5 (C_3), 54.8 (C_2), 33.4 (C_{25}), 26.7(C_{26}), 20.4(C_4); m/z (ES+) calcd. for $C_{22}H_{25}O_4NNa$ ($M+Na^+$), 390.1681 found 390.1681.

7.4.5 *n* = 3 L DMT (5bL)

2-(Anthracen-9-yloxy)-*N*-((2*R*,3*R*)-1-(bis(4-methoxyphenyl)(phenyl)methoxy)-3-hydroxybutan-2-yl)acetamide

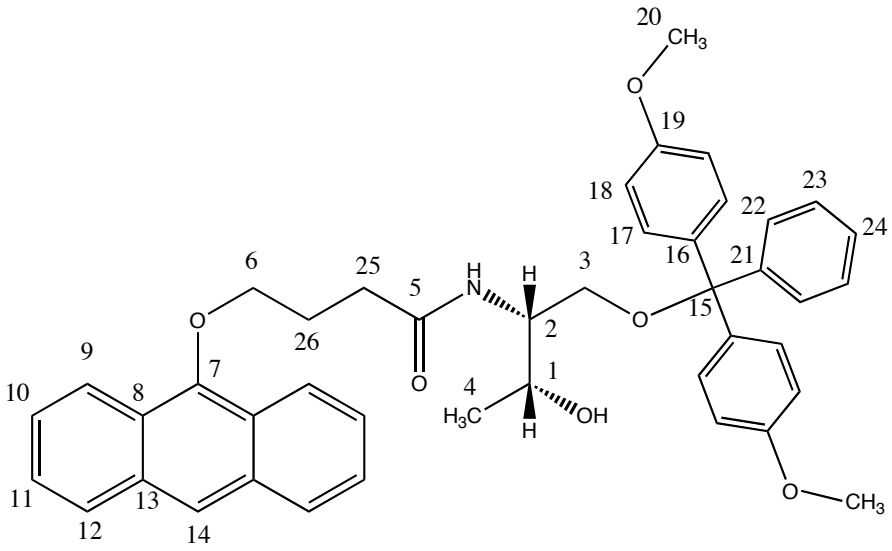

2-(Anthracen-9-yloxy)-*N*-((2*R*,3*R*)-1,3-dihydroxybutan-2-yl)acetamide) (2.35 g, 6.4 mmol) was dissolved in anhydrous pyridine (20 mL). Dimethoxytritylchloride (2.16 g, 6.4 mmol) was added to the soln. followed by DMAP (0.08 g, 0.6 mmol) and the reaction left to stir under N_2 at room temp. in the absence of light for 24 hours. The reaction mixture was poured onto H_2O (100 mL), extracted with DCM (4 x 50 mL) and dried over $MgSO_4$. The solvent was removed in *vacuo* and column chromatography on silica (Hex/EtOAc/TEA, 40:59:1) afforded the desired compound as a pale yellow crystalline solid (1.68

g, 39%). (R_f =0.47 in DCM with 5% MeOH); M.p. 88-90 ˚C, (found: C, 76.86; H, 6.35; N, 2.14%. $C_{43}H_{43}O_6N$ requires C, 77.11; H, 6.47; N, 2.09%); δ_H (400 MHz, CD_3CN) 8.30 (1H, s, *H14*), 8.25-8.29 (2H, m, *H9*), 8.03 (2H, dt, *J* = 3.7 and 2.7, *H12*), 7.43-7.49 (4H, m, *H11* and *H22*), 7.22-7.29 (6H, m, *H10* and *H17*), 7.13-7.21 (3H, m, *H23* and *H24*), 6.77-6.81 (4H, m, *H18*), 6.50 (1H, d, *J* = 8.9, N*H*), 4.15-4.23 (2H, m, O*C*$H_2$$CH_2CH_2$CO *H6*), 3.97-4.04 (1H, m, NHCHC*H*OH *H1*), 3.88-3.97 (1H, m, NHC*H*CHOH *H2*), 3.70 (6H, s, O*C*H_3), 3.09 (2H, tt, *J* = 13.7 and 5.2, CH_2ODMT *H3*), 3.00 (1H, d, *J* = 4.7, CH_2O*H*), 2.61 (2H, t, *J* = 7.3, OCH_2CH_2CH_2CO *H25*), 2.26-2.35 (2H, OCH_2C$H_2$$CH_2$CO *H26*), 1.05 (3H, d, *J* = 6.3, CH_3CHCH_2OH *H4*); δ_C (75 MHz, CD_3CN) 173.4 (*C5*=*O*), 159.5 (2x*C19*), 148.6 (*C7*), 146.1 (*C21*), 137.0 (2x*C16*), 133.4 (2x*C13*), 130.9 (4xC_{17}), 129.3 (2xC_{12}), 128.9 (2x*C22*), 128.7 (2x*C23*), 127.6 (*C24*), 126.6 (2xC_{10}), 126.3 (2x*C11*), 125.4 (2xC_8), 123.1 (2x*C9*), 122.9 (C_{14}), 113.9 (4xC_{18}), 86.7 (C_{15}), 76.1 (*C6*), 67.1 (*C1*), 64.4 (*C3*), 55.8 (2xC_{20}), 55.2 (C_2), 33.4 (C_{25}), 27.4 (*C26*), 20.5 (*C4*); *m/z* (ES+) calcd. for $C_{43}H_{43}O_6NNa$ ($M+Na^+$) 692.2988, found 692.2994.

7.4.6 *n* = 3 D DMT (5bD)

2-(Anthracen-9-yloxy)-*N*-((2*S*,3*S*)-1-(bis(4-methoxyphenyl)(phenyl)methoxy)-3-hydroxybutan-2-yl)acetamide

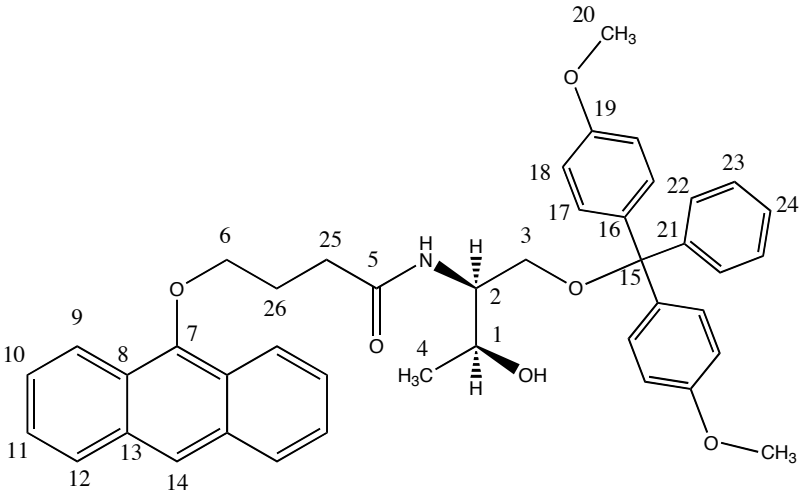

2-(Anthracen-9-yloxy)-*N*-((2*S*,3*S*)-1,3-dihydroxybutan-2-yl)acetamide) (2.4 g, 6.5 mmol) was dissolved in anhydrous pyridine (30 mL). Dimethoxytritylchloride (2.20 g, 3 mmol) was added to the soln. followed by DMAP (0.06 g, 0.3 mmol) and the reaction left to stir under N_2 at room temp. in the absence of light for 24 hours. The reaction mixture was poured onto H_2O (100 mL), extracted with DCM (4 x 50 mL) and dried over $MgSO_4$. The solvent was removed in *vacuo* and subsequent column chromatography on silica (Hex/EtOAc/TEA, 40:59:1) afforded the desired compound as a pale yellow crystalline solid (1.33 g, 30%). (R_f =0.55 in DCM with 5% MeOH); M.p. 78-81 ˚C, (found: C, 76.86; H, 6.35; N, 2.14%. $C_{43}H_{43}O_6N$ requires C, 77.11; H, 6.47; N, 2.09%); ν_{max}/cm^{-1} 3335 (OH), 1669 (C=O); δ_H (400 MHz, CD_3CN) 8.30 (1H, s, *H*$_{14}$), 8.25-8.29 (2H, m, *H*$_9$), 8.03 (2H, dt, *J* = 3.7 and 2.7, *H*$_{12}$), 7.43-7.49 (4H, m, *H*$_{11}$ and *H*$_{22}$), 7.22-7.29 (6H, m, *H*$_{10}$ and *H*$_{17}$), 7.13-7.21 (3H, m, *H*$_{23}$ and *H*$_{24}$), 6.77-6.81 (4H, m, *H*$_{18}$), 6.50 (1H, d, *J* = 8.9, N*H*), 4.15-4.23 (2H, m, OC*H*$_2$CH$_2$CH$_2$CO *H*$_6$), 3.97-

4.04 (1H, m, NHCHC*H*OH H_1), 3.88-3.97 (1H, m, NHC*H*CHOH H_2), 3.70 (6H, s, OCH_3), 3.09 (2H, tt, J = 13.7 and 5.2, CH_2ODMT H_3), 3.00 (1H, d, J = 4.7, CH_2OH), 2.61 (2H, t, J = 7.3, $OCH_2CH_2CH_2CO$ H_{25}), 2.26-2.35 (2H, $OCH_2CH_2CH_2CO$ H_{26}), 1.05 (3H, d, J = 6.3, CH_3CHOH H_4); δ_C (100 MHz, CD_3CN) 173.4 (C_5=O), 159.5 (2xC_{19}), 148.6 (C_7), 146.2 (C_{21}), 137.1 (2xC_{16}), 133.4 (2xC_{13}), 130.9 (4xC_{17}), 129.3 (2xC_{12}), 128.9 (2xC_{22}), 128.7 (2xC_{23}), 127.7 (C_{24}), 126.6 (2xC_{10}), 126.3 (2xC_{11}), 125.5 (2xC_8), 123.2 (2xC_9), 123.0 (C_{14}), 113.9 (4xC_{18}), 87.9 (C_{15}), 76.1 (C_6), 67.1 (C_1), 64.4 (C_3), 55.8 (2xC_{20}), 55.3 (C_2), 33.4 (C_{25}), 27.4 (C_{26}), 20.5 (C_4); *m/z* (ES+) calcd. for $C_{43}H_{43}O_6NNa$ 692.2988 ($M+Na^+$) found 692.2997.

7.4.7 *n* = 3 L Phosphoramidite (6bL)

(2*R*,3*R*)-3-(4-(Anthracen-9-yloxy)butanamido)-4-(bis(4-methoxyphenyl)(phenyl)methoxy)butan-2-yl (2-cyanoethyl) diisopropylphosphoramidite

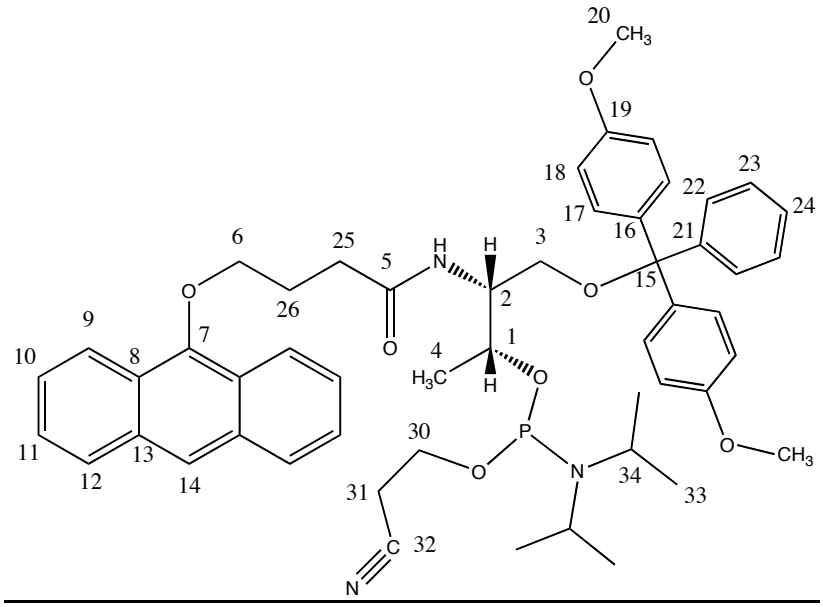

4-(Anthracen-9-yloxy)-*N*-((2*R*,3*R*)-1-(bis(4-methoxyphenyl)(phenyl)methoxy)-3-hydroxybutan-2-yl)butamide (0.60 g, 0.90 mmol) placed in a 25 mL round-bottomed flask with a stirrer bar and a septum. The flask was evacuated and filled with argon three times and the solid dissolved in anhydrous DCM (15 mL). DIPEA (0.7 mL, 3.8 mmol) was added and the solution stirred at room temp. in the absence of light. *2*-Cyanoethyl-diisopropylchlorophosphoramidite (0.20 mL, 0.98 mmol) was added *via* a disposable syringe dropwise and the reaction stirred for 1 hr. The soln. was then transferred to a 25 mL round-bottomed flask containing a stirrer bar and solid-supported BnOH (0.05 g, 0.13 mmol) and left to stir for 1 hr in the absence of light. The soln. was diluted with EtOAc (10 mL), filtered and then washed with 2 M Na_2CO_3 (a.q.) soln. (2 x 50 mL) and brine (1 x 50 mL) and dried over Mg_2SO_4. The soln. was then columned through activated basic alumina with EtOAC:Hex:TEA 49:50:1 and the filtrate evaporated in *vacuo* to give a yellow powdery solid (0.38g, 49%); (R_f = 0.63 50% pet ether 50% DCM); δ_H (300 MHz, CD_3CN) 8.31 (1H, s, *H*$_{14}$), 8.27 (2H, d, *J* = 9.3, *H*$_9$), 8.02-8.07 (2H, m, *H*$_{12}$), 7.37-7.52 (4H, m, *H*$_{11}$ and *H*$_{22}$), 7.22-7.30 (6H, m, *H*$_{10}$ and *H*$_{17}$), 7.13-7.22 (3H, m, *H*$_{23}$ and *H*$_{24}$), 6.75-6.83 (4H, m, *H*$_{18}$), 6.35 (1H, dd, *J* = 18.4 and 8.7, N*H*), 4.22 (2H, m, *J* = 2.9, OC*H*$_2$(CH$_2$)$_2$CO *H*$_6$), 3.71 (6H, s, OC*H*$_3$ *H*$_{20}$), 3.62-3.80 (2H, m, C*H*NH *H*$_2$ and CH$_3$C*H*OP *H*$_1$), 3.40-3.60 (6H, m, POC*H*$_2$ *H*$_{30}$ and PNC*H* *H*$_{34}$), 3.12 (2H, dd, *J* = 8.8 and 5.8, C*H*$_2$ODMT *H*$_3$), 2.39-2.66 (4H, m, OCH$_2$CH$_2$C*H*$_2$CO *H*$_{25}$ and C*H*$_2$CN *H*$_{31}$), 2.26-2.40 (2H, m, OCH$_2$C*H*$_2$CH$_2$CO *H*$_{26}$), 1.04-1.16 (12H, m, C*H*$_3$ *H*$_{33}$), 0.96 (3H, d, *J* = 6.8, C*H*$_3$CHOP *H*$_4$); δ_P (121 MHz, CD_3CN) 147.7, 147.0; (ES+) calcd. for $C_{52}H_{60}O_7N_3PNa$ ($M+Na^+$) 892.4067, found 892.4077.

3.4.8 *n* = 3 D Phosphoramidite (6bD)

(2*S*,3*S*)-3-(4-(Anthracen-9-yloxy)butanamido)-4-(bis(4-methoxyphenyl)(phenyl)methoxy)butan-2-yl (2-cyanoethyl) diisopropylphosphoramidite

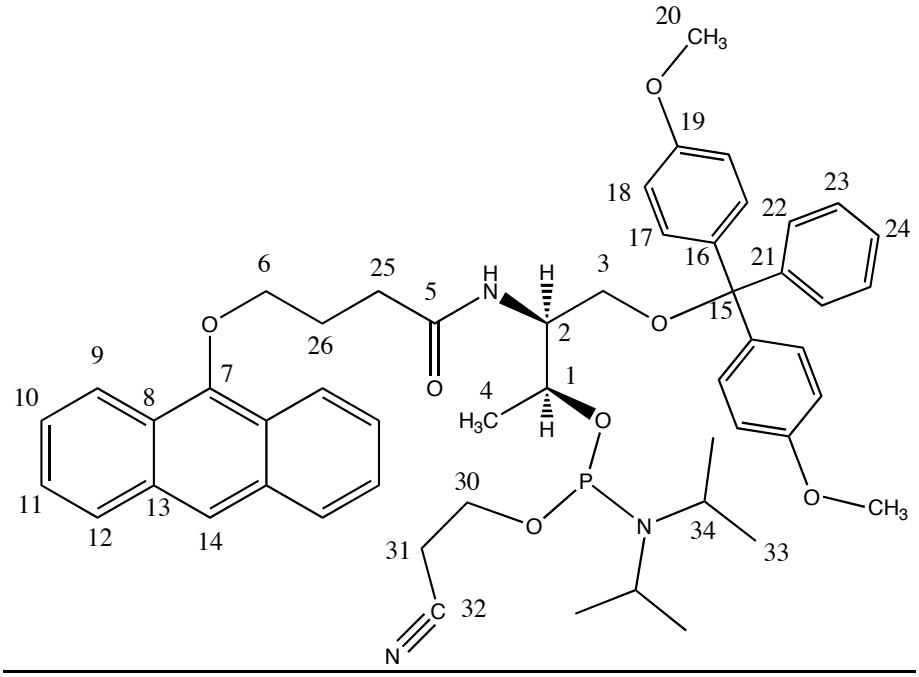

4-(Anthracen-9-yloxy)-*N*-((2*S*,3*S*)-1-(bis(4-methoxyphenyl)(phenyl)methoxy)-3-hydroxybutan-2-yl)butamide (0.60 g, 0.90 mmol) placed in a 25 mL round-bottomed flask with a stirrer bar and a septum. The flask was evacuated and filled with argon three times and the solid dissolved in anhydrous DCM (15 mL). DIPEA (0.7 mL, 3.8 mmol) was added and the solution stirred at room temp. in the absence of light. *2*-Cyanoethyl-diisopropylchlorophosphoramidite (0.20 mL, 0.98 mmol) was added *via* a disposable syringe dropwise and the reaction stirred for 1 hr. The soln. was then transferred to a 25 mL round-bottomed flask containing a stirrer bar and solid-supported BnOH (0.05 g, 0.13 mmol) and left to stir for 1 hr in the absence of

light. The soln. was diluted with EtOAc (10 mL), filtered and then washed with 2 M Na_2CO_3 (a.q.) soln. (2 x 50 mL) and brine (1 x 50 mL) and dried over Mg_2SO_4. The soln. was then columned through activated basic alumina with EtOAC:Hex:TEA 49:50:1 and the filtrate evaporated in *vacuo* to give a yellow powdery solid (0.36 g 46%); (R_f = 0.63 50% pet ether 50% DCM); δ_H (300 MHz, CD_3CN) 8.31 (1H, s, H_{14}), 8.27 (2H, d, J = 9.3, H_9), 8.02-8.07 (2H, m, H_{12}), 7.37-7.52 (4H, m, H_{11} and H_{22}), 7.22-7.30 (6H, m, H_{10} and H_{17}), 7.13-7.22 (3H, m, H_{23} and H_{24}), 6.75-6.83 (4H, m, H_{18}), 6.35 (1H, dd, J = 18.4 and 8.7, NH), 4.22 (2H, m, J = 2.9, OCH_2(CH_2)$_2$CO H_6), 3.71 (6H, s, OCH_3 H_{20}), 3.62-3.80 (2H, m, CHNH H_2 and CH_3CHOP H_1), 3.40-3.60 (6H, m, POCH_2 H_{30} and PNCH H_{34}), 3.12 (2H, dd, J = 8.8 and 5.8, CH_2ODMT H_3), 2.39-2.66 (4H, m, $OCH_2CH_2CH_2CO$ H_{25} and CH_2CN H_{31}), 2.26-2.40 (2H, m, $OCH_2CH_2CH_2CO$ H_{26}), 1.04-1.16 (12H, m, CH_3 H_{33}), 0.96 (3H, d, J = 6.8, CH_3CHOP H_4); δ_P (121 MHz, CD_3CN) 147.7, 147.0 *m/z* (ES+) calcd. for $C_{52}H_{60}O_7N_3PNa$ ($M+Na^+$) 892.4067, found 892.4054

7.5 *n* = 4 synthesis

7.5.1 *n* = 4 Ester (2c)

Ethyl 5-(anthracen-9-yloxy)pentanoate [3]

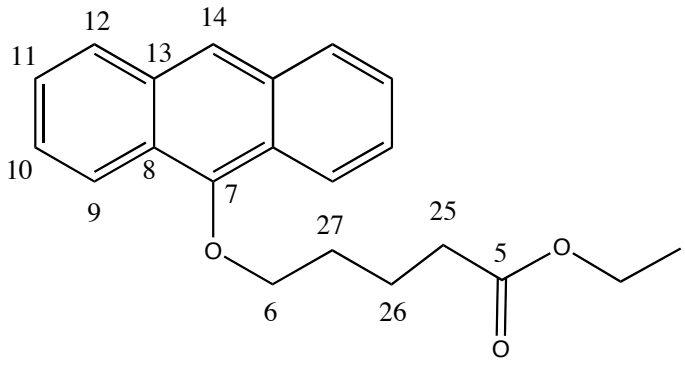

Anthrone (7.2 g, 37.5 mmol) and K_2CO_3 (5.4 g, 37.5 mmol) were dissolved in degassed acetone (200 mL) and stirred under N_2 at room temp. in the absence of light for 15 min. Ethyl *5*-bromovalerate (5.9 mL, 37.5 mmol) was added and the reaction mixture refluxed overnight. The solution was filtered to remove K_2CO_3, evaporated in *vacuo* and redissolved in DCM (100 mL). The solution was washed with H_2O (1 x 50 mL) and dried over $MgSO_4$. The solvent was removed in *vacuo* to give an orange oil which solidified on standing. Column chromatography on silica (hexane with 10% EtOAc) yielded the desired product as a white solid (5.6 g, 45%). (R_f =0.53 in $CHCl_3$); M.p. 70 ˚C; δ_H (300 MHz, $CDCl_3$) 8.30 (2H, d, J = 9.1, H_9), 8.24 (1H, s, H_{14}), 7.93 (2H, d, J = 9.7, H_{12}), 7.44-7.55 (4H, m, H_{10} and H_{11}), 4.17-4.26 (4H, m, CH_2CH$_3$ and OCH_2(CH$_2$)$_3$ H_6), 2.53 (2H, t, J = 7.5 (CH$_2$)$_3$CH_2CO H_{25}), 2.00-2.12 (4H, m, CH$_2$CH_2CH_2CH$_2$CO H_{26} and H_{27}), 1.31 (3H, t, J = 7.1, CH$_2$CH_3); δ_C (400 MHz, $CDCl_3$) 173.8 (C_5=O), 151.1 (C_7), 132.2 (2xC_{13}), 128.4 (2xC_{12}), 125.4 (2xC_{10}), 125.1 (2xC_{11}), 124.6 (2xC_8), 122.2 (2xC_9), 122.1 (C_{14}), 75.5

(C_6), 60.4 (CH_2CH_3), 58.5 (C_6), 34.3 (C_{25}), 30.1 (C_{26}), 14.3 (CH_2CH_3); *m/z* (ES+) calcd. for $C_{21}H_{22}O_3Na$ (M+Na) 355.2 found 355.2.

7.5.2 *n* = 4 Acid (3c)

5-(Anthracen-9-yloxy)pentanoic acid [3]

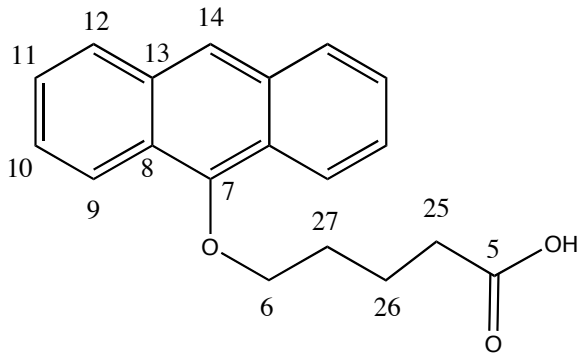

Ethyl 5-(anthracen-9-yloxy)pentanoate (5.6 g, 20.8 mmol) was dissolved in a 1:1 soln. of 10% NaOH (aq.) soln. and EtOH (200 mL) and refluxed overnight in the absence of light. The solution was concentrated in *vacuo* and dissolved in H_2O (500 mL). Conc. HCl was added drop wise to the solution to afford a precipitate which was collected by suction filtration. The solid was washed with H_2O and dried to give the desired product as a white solid (3.74 g, 76% yield). M.p. 117 ˚C; δ_H (300 MHz, $CDCl_3$) 8.29 (2H, d, J = 9.3, H_9), 8.24 (1H, s, H_{14}), 7.99 (2H, d, J = 9.4, H_{12}), 7.44-7.55 (4H, m, H_{10} and H_{11}), 4.25 (2H, t, J = 5.9, $OCH_2(CH_2)_3$ H_6), 2.62 (2H, t, J = 6.9, $(CH_2)_3CH_2CO$ H_{25}), 2.10-2.16 (4H, m, $CH_2CH_2CH_2CH_2CO$ $H_{26,}$ and H_{27}); δ_C (75 MHz, $CDCl_3$) 173.8 (C_5=O), 151.1 (C_7), 132.2 (2xC_{13}), 128.4 (2xC_{12}), 125.4 (2xC_{10}), 125.1 (2xC_{11}), 124.6 (2xC_8), 122.2 (2xC_9), 122.1 (C_{14}), 75.5 (C_6), 33.8 (C_{25}), 30.0 (C_{27}), 21.6 (C_{26}); *m/z* (ES+) calcd. for $C_{19}H_{18}O_3Na$ ($M\text{-}H^+ + Na^+$) 317.1 found 317.1.

7.5.3 *n* = 4 L Diol (4cL)

5-(Anthracen-9-yloxy)-*N*-((2*R*,3*R*)-1,3-dihydroxybutan-2-yl)pentanamide

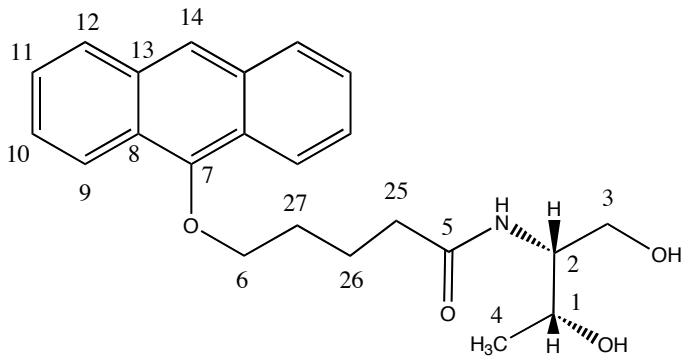

5-(Anthracen-9-yloxy)pentanoic acid (2.39g, 8.1 mmol) was dissolved in anhydrous DMF (20 mL). PyBOP (4.23 g, 8.1 mmol) was added to the soln. which was stirred under N_2 at room temp. in the absence of light for 15 mins. L-Threoninol (0.86 g, 8.1 mmol) and DIPEA (2.1 mL, 12.0 mmol) were added and the reaction left to stir at 40 ˚C for 40 hours. The soln. was diluted in MeOH/DCM (1:2 100 mL) and washed with H_2O (3 x 50 mL) and dried over $MgSO_4$. The solvent was removed in *vacuo* and subsequent purification by silica column chromatography (DCM with 5% MeOH) gave the desired product as an oily yellow solid (2.6 g, 83%). (R_f =0.47 in DCM with 5 % MeOH); M.p. 126-131 ˚C; δ_H (400 MHz, $CDCl_3$) 8.24 (2H, dd, *J* = 7.9 and 5.8, *H*$_9$), 8.18 (1H, s, *H*$_{14}$), 7.90-7.98 (2H, m, *H*$_{12}$), 7.42-7.51 (4H, m, *H*$_{10}$ and *H*$_{11}$), 6.57 (1H, d, *J* = 8.5, N*H*), 4.05-4.19 (3H, m, OC*H*$_2$CH$_2$CH$_2$O *H*$_6$ and NHCHC*H*OH *H*$_1$), 3.86 (1H, ddd, *J* = 16.9, 9.1 and 6.6, C*H*NH *H*$_2$), 3.72-3.81 (2H, m, CHC*H*$_2$OH *H*$_3$), 2.41 (2H, t, *J* = 6.6, C*H*$_2$CO *H*$_{25}$), 2.06 (4H, m, CH$_2$C*H*$_2$C*H*$_2$CH$_2$CO *H*$_{26}$ and *H*$_{27}$), 1.18 (3H, d, *J* = 6.4, C*H*$_3$CHOH *H*$_4$); δ_C (100 MHz, $CDCl_3$) 173.8 (*C*$_5$=*O*), 151.1 (*C*$_7$), 132.2 (2x*C*$_{13}$), 128.4 (2x*C*$_{12}$), 125.4 (2x*C*$_{10}$), 125.1 (2x*C*$_{11}$), 124.6 (2x*C*$_8$), 122.2 (2x*C*$_9$), 122.1 (*C*$_{14}$), 75.5 (*C*$_6$), 68.2 (*C*$_1$),

64.5 (C_3), 54.8 (C_2), 36.5 (C_{25}), 30.1 (C_{27}), 22.7 (C_{26}), 20.4 (C_4); *m/z* (ES+) calcd for $C_{23}H_{27}O_4NNa$ ($M+Na^+$) 404.1838, found 404.1832.

7.5.4 *n* = 4 D Diol (4cD)

5-(Anthracen-9-yloxy)-*N*-((2*S*,3*S*)-1,3-dihydroxybutan-2-yl)pentanamide

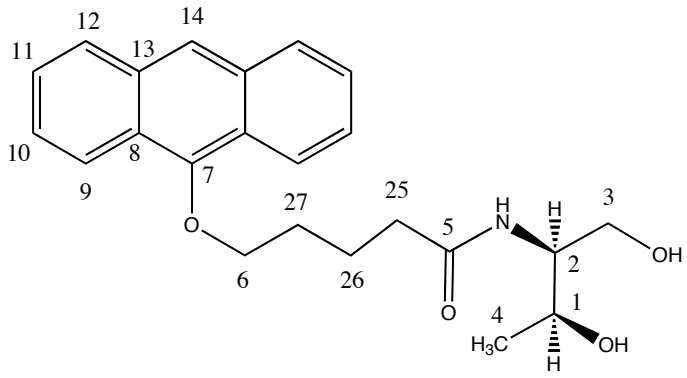

5-(Anthracen-9-yloxy) pentanoic acid (2.95g, 5.9 mmol) was dissolved in anhydrous DMF (20 mL). HBTU (3.08 g, 8.1 mmol) was added to the soln. which was stirred under N_2 at room temp. in the absence of light for 15 mins. D-Threoninol (0.846 g, 8.1 mmol) and DIPEA (2.0 mL, 14.0 mmol) were added and the reaction left to stir at 40 ˚C for 40 hours. The soln. was diluted in MeOH/DCM (1:2 100 mL) and washed with H_2O (3 x 50 mL) and dried over $MgSO_4$. The solvent was removed in *vacuo* and subsequent purification by silica column chromatography (DCM with 5% MeOH) gave the desired product as an oily yellow solid (2.2 g, 83%). (R_f =0.47 in DCM with 5% MeOH); M.p. 125-131 ˚C; δ_H (400 MHz, $CDCl_3$) 8.24 (2H, dd, *J* = 7.9 and 5.8, H_9), 8.18 (1H, s, H_{14}), 7.90-7.98 (2H, m, H_{12}), 7.42-7.51 (4H, m, H_{10} and H_{11}), 6.57 (1H, d, *J* = 8.5, N*H*), 4.05-4.19 (3H, m, O$CH_2$$CH_2$$CH_2$O H_6 and CH(CH_3)C*H*OH H_1), 3.86 (1H, ddd, *J* = 16.9, 9.1 and 6.6, C*H*NH H_2), 3.72-3.81 (2H, m, CHCH_2OH H_3), 2.41 (2H, t, *J* = 6.6, CH_2CO H_{25}), 2.06 (4H, m, CH_2CH_2C$H_2$$CH_2$CO H_{26} and H_{27}), 1.18 (3H, d, *J* = 6.4, CH_3CHOH H_4); δ_C

(100 MHz, $CDCl_3$) 173.7 (C_5=O), 151.1 (C_7), 132.2 (2xC_{13}), 128.4 (2xC_{12}), 125.4 (2xC_{10}), 125.1 (2xC_{11}), 124.6 (2xC_8), 122.2 (2xC_9), 122.1 (C_{14}), 75.6 (C_6), 68.6 (C_1), 64.9 (C_3), 54.6 (C_2), 36.6 (C_{25}), 30.1 (C_{27}), 22.7 (C_{26}), 20.5 (C_4); *m/z* (ES+) calcd. for $C_{23}H_{27}O_4NNa$ ($M+Na^+$) 404.1838, found 404.1835.

7.5.5 *n* = 4 L DMT (5cL)

5-(Anthracen-9-yloxy)-*N*-((2*R*,3*R*)-1-(bis(4-methoxyphenyl)(phenyl)methoxy)-3-hydroxybutan-2-yl)pentanamide

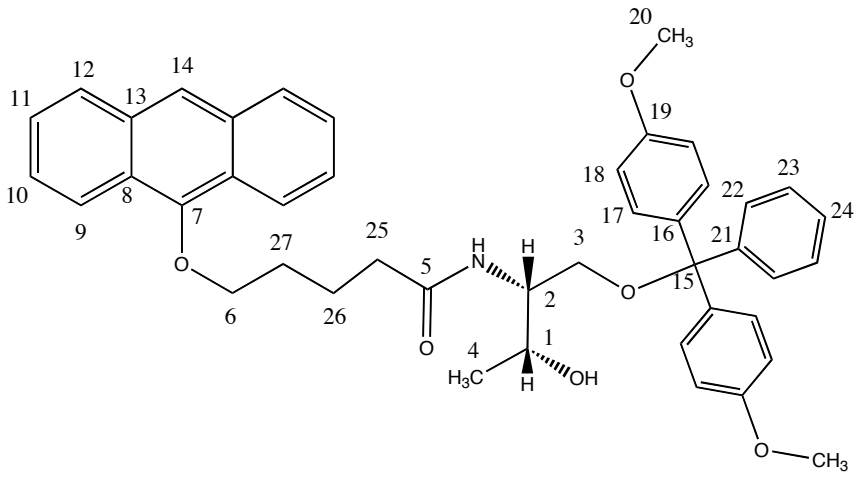

5-(Anthracen-9-yloxy)-*N*-((2*R*,3*R*)-1,3-dihydroxybutan-2-yl)pentanamide (2.6 g, 6.8 mmol) was dissolved in anhydrous pyridine (20 mL). Dimethoxytritylchloride (2.31 g, 6.8 mmol) was added to the soln. followed by DMAP (0.08 g, 0.7 mmol) and the reaction left to stir under N_2 at room temp. in the absence of light for 24 hours. The reaction mixture was poured onto H_2O (50 mL), extracted with DCM (2 x 50 mL) and dried over $MgSO_4$. The solvent was removed in *vacuo* and subsequent column chromatography on silica (Hex/EtOAc/TEA, 40:59:1) afforded the desired compound as a pale yellow crystalline solid (1.9 g, 41%). (R_f =0.48 in DCM with 5% MeOH); M.p. 78-79 °C, (found: C, 77.07; H, 7.05; N, 2.38%. $C_{44}H_{45}NO_6$ 0.25eq Et_3N requires C, 77.06; H,

6.93; N, 2.47%); ν_{max}/cm^{-1} 3338 (OH), 2942 (N-H), 1651 (C=O) δ_H (400 MHz, CD_3CN) 8.28 (1H, s, *H14*), 8.23-8.27 (2H, m, *H9*), 8.03 (2H, dd, *J* = 6.5 and 2.9, *H12*), 7.40-7.49 (6H, m, *H10*, *H11* and *H22*), 7.26-7.31 (6H, m, *H23* and *H17*), 7.18 (1H, t, *J* = 7.3, *H24*), 6.82 (4H, d, *J* = 8.8, *H18*), 6.48 (1H, d, *J* = 8.8, N*H*), 4.16 (2H, t, *J* = 6.1, OC*H*$_2$CO *H6*), 3.90-3.99 (2H, m, NHCHC*H*OH *H1* and NHC*H*CHOH *H2*), 3.69 (6H, s, OC*H*$_3$ *H20*), 3.05-3.19 (3H, m, C*H*$_2$ODMT *H3* and CH$_2$O*H*), 2.37 (2H, t, *J* = 7.1, OCH$_2$CH$_2$CH$_2$C*H*$_2$CO *H25*), 1.93-2.07 (4H, m, OCH$_2$C*H*$_2$C*H*$_2$CH$_2$CO *H26* and *H27*), 1.05 (3H, d, *J* = 6.2, C*H*$_3$CHOH *H4*); δ_C (75 MHz, CD_3CN) 173.8 (*C5=O*), 159.5 (2x*C19*), 152.2 (*C7*), 146.1 (*C21*), 137.0 (2x*C16*), 133.4 (2x*C13*), 130.9 (4x*C17*), 129.3 (2x*C12*), 129.0 (2x*C22*), 128.7 (2x*C23*), 127.7 (*C24*), 126.6 (2x*C10*), 126.3 (2x*C11*), 125.5 (2x*C8*), 123.1 (2x*C9*), 122.9 (*C14*), 113.9 (4x*C18*), 86.8 (C$_{15}$), 76.6 (*C6*), 67.3 (*C1*), 64.6 (*C3*), 55.7 (2x*C20*), 55.2 (*C2*), 36.7 (*C25*), 30.8 (*C27*), 23.4 (*C26*), 20.5 (*C4*); *m/z* (ES+) calcd. for $C_{44}H_{45}NO_6Na$ ($M+Na^+$) 706.3145, found 706.3148.

7.5.6 *n* = 4 D DMT (5cD)

5-(Anthracen-9-yloxy)-*N*-((2*S*,3*S*)-1-(bis(4-methoxyphenyl)(phenyl)methoxy)-3-hydroxybutan-2-yl)pentanamide

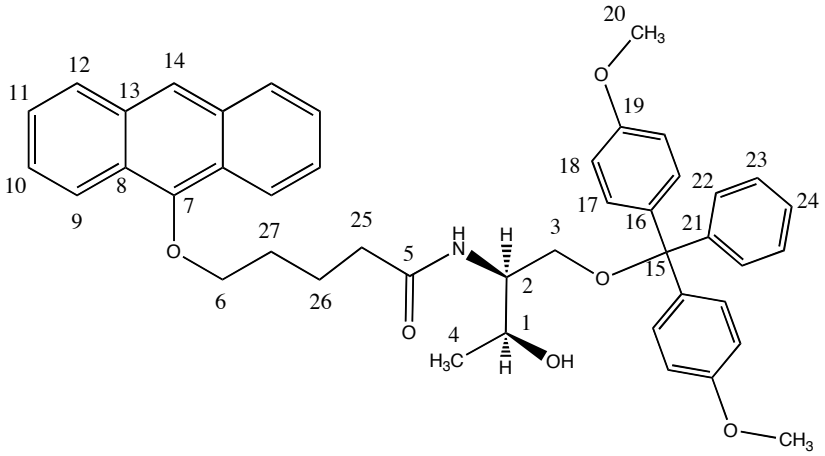

5-(Anthracen-9-yloxy)-*N*-((2*S*,3*S*)-1,3-dihydroxybutan-2-yl)pentanamide (2.2 g, 5.8 mmol) was dissolved in anhydrous pyridine (20 mL). Dimethoxytritylchloride (1.95 g, 5.8 mmol) was added to the soln. followed by DMAP (0.08 g, 0.6 mmol) and the reaction left to stir under N_2 at room temp. in the absence of light for 24 hours. The reaction mixture was poured onto H_2O (50 mL), extracted with DCM (2 x 50 mL) and dried over $MgSO_4$. The solvent was removed in *vacuo* and subsequent column chromatography on silica (Hex/EtOAc/TEA, 40:59:1) afforded the desired compound as a pale yellow crystalline solid (1.36 g, 35%). (R_f =0.48 in DCM with 5% MeOH); M.p. 77-79 ˚C; (found: C, 76.77; H, 6.55; N, 1.84%. $C_{44}H_{45}NO_6$ requires C, 77.28; H, 6.63; N, 2.05%); ν_{max}/cm^{-1} 3338 (OH), 2942 (N-H), 1651 (C=O) δ_H (400 MHz, CD_3CN) 8.28 (1H, s, H_{14}), 8.23-8.27 (2H, m, H_9), 8.03 (2H, dd, J = 6.5 and 2.9, H_{12}), 7.40-7.49 (6H, m, H_{10}, H_{11} and H_{22}), 7.26-7.31 (6H, m, H_{23} and H_{17}), 7.18 (1H, t, J = 7.3, H_{24}), 6.82 (4H, d, J = 8.8, H_{18}), 6.48 (1H, d, J = 8.8, N*H*), 4.16 (2H, t, J = 6.1, OCH_2 H_6),

3.90-3.99 (2H, m, NHCHC*H*OH H_1 and NHC*H*CHOH H_2), 3.69 (6H, s, OCH_3 H_{20}), 3.05-3.19 (3H, m, CH_2ODMT H_3 and CH$_2$O*H*), 2.37 (2H, t, J = 7.1, OCH$_2$CH$_2$CH$_2$CH_2CO H_{25}), 1.93-2.07 (4H, m, OCH$_2$CH_2CH_2CH$_2$CO H_{26} and H_{27}), 1.05 (3H, d, J = 6.2, CH_3CHOH H_4); δ_C (75 MHz, CD$_3$CN) 173.8 (C_5=O), 159.5 (2xC_{19}), 152.2 (C_7), 146.1 (C_{21}), 137.0 (2xC_{16}), 133.4 (2xC_{13}), 130.9 (4xC_{17}), 129.3 (2xC_{12}), 129.0 (2xC_{22}), 128.7 (2xC_{23}), 127.7 (C_{24}), 126.6 (2xC_{10}), 126.3 (2xC_{11}), 125.5 (2xC_8), 123.1 (2xC_9), 122.9 (C_{14}), 113.9 (4xC_{18}), 86.8 (C$_{15}$), 76.6 (C_6), 67.2 (C_1), 64.6 (C_3), 55.7 (2xC_{20}), 55.2 (C_2), 36.7 (C_{25}), 30.8 (C_{27}), 23.4 (C_{26}), 20.5 (C_4); *m/z* (ES+) calcd for $C_{44}H_{45}NO_6$ (M^++Na) 706.3145, found 706.3143.

7.5.7 *n* = 4 L Phosphoramidite (6cL)

(2*R*,3*R*)-3-(5-(Anthracen-9-yloxy)pentanamido)-4-(bis(4-methoxyphenyl)(phenyl)methoxy)butan-2-yl (2-cyanoethyl) diisopropylphosphoramidite

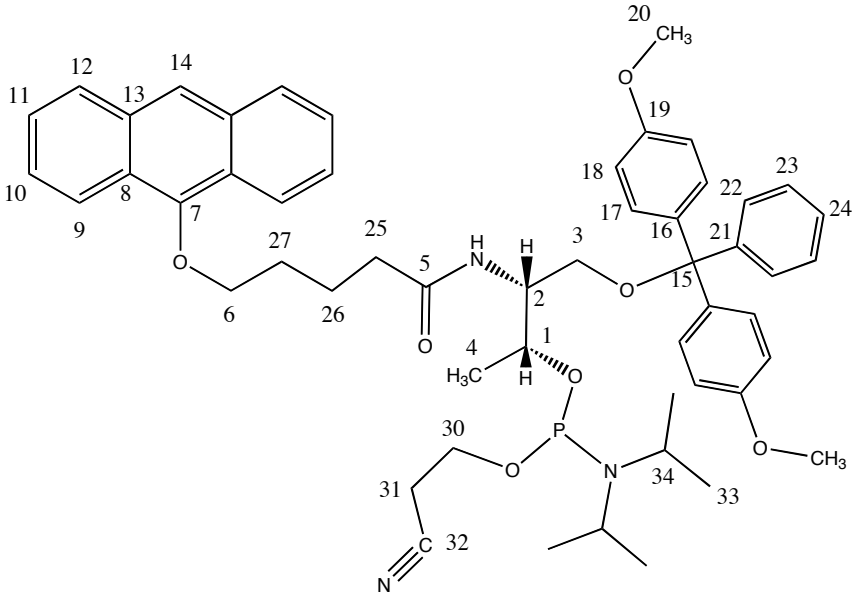

5-(Anthracen-9-yloxy)-*N*-((2*R*,3*R*)-1-(bis(4-methoxyphenyl)(phenyl)methoxy)-3-hydroxybutan-2-yl)pentamide (0.45 g, 0.66 mmol) placed in a 25 mL round-bottomed flask with a stirrer bar and a

septum. The flask was evacuated and filled with argon three times and the solid dissolved in anhydrous DCM (15 mL). DIPEA (0.47 mL, 2.6 mmol) was added and the solution stirred at room temp. in the absence of light. *2*-Cyanoethyl-diisopropylchlorophosphoramidite (0.15 mL, 0.66 mmol) was added *via* a disposable syringe dropwise and the reaction stirred for 1 hr. The soln. was then transferred to a 25 mL round-bottomed flask containing a stirrer bar and solid-supported BnOH (0.05 g, 0.13 mmol) and left to stir for 1 hr in the absence of light. The soln. was diluted with EtOAc (10 mL), filtered and then washed with 2 M Na_2CO_3 (a.q.) soln. (2 x 50 mL) and brine (1 x 50 mL) and dried over Mg_2SO_4. The soln. was then columned through activated basic alumina with EtOAC:Hex:TEA 49:50:1 and the filtrate evaporated in *vacuo* to give a yellow powdery solid (0.34g 58%) (R_f. =0.63 50% pet ether 50% DCM) δ_H (300 MHz, CD_3CN) 8.32 (1H, s, *H14*), 8.30-8.25 (2H, *m*, *H9*), 8.07 (2H, dd, *J* = 6.3 and 3.3, *H12*), 7.57-7.42 (4H, m, *H11* and *H22*), 7.39-7.26 (6H, m, *H10* and *H17*), 7.21 (3H, td, *J* = 7.2 and 5.0 *H23* and *H24*), 6.84 (4H, ddd, *J* = 6.9, 5.0 and 2.6, *H18*), 6.26 (1H, dd, *J* = 16.6 and 9.2, N*H*), 4.22 (2H, dt, *J* = 12.1 and 6.2, OC*H*$_2$CH$_2$CH$_2$ *H6*), 3.80-3.63 (2H, m, C*H*NH *H2* and CH$_3$C*H*OP *H1*), 3.73 (6H, s, OC*H*$_3$ *H20*), 3.43-3.60 (4H, m, POC*H*$_2$ *H30* and PNC*H* *H34*), 3.06-3.21 (2H, m, C*H*$_2$ODMT *H3*), 2.52 (2H, dt, *J* = 33.9 and 6.1, C*H*$_2$CN *H31*), 2.42 (2H, t, *J* = 6.0, OCH$_2$CH$_2$CH$_2$C*H*$_2$CO *H25*) 2.02-2.11 (4H, m, OCH$_2$C*H*$_2$C*H*$_2$CH$_2$CO *H26* and *H25*), 1.29-1.05 (12H, m, C*H*$_3$ *H33*), 0.98 (3H, d, *J* = 6.8, C*H*$_3$CHOP *H4*); δ_P (121 MHz, CD_3CN) 147.6, 147.0; *m/z* (ES+) calcd. for $C_{54}H_{64}O_7N_3NaP$ ($M+Na^+$) 906.4223, found 906.4233.

7.5.8 *n* = 4 D Phosphoramidite (6cD)

(2*S*,3*S*)-3-(5-(anthracen-9-yloxy)pentanamido)-4-(bis(4-methoxyphenyl) (phenyl)methoxy)butan-2-yl (2-cyanoethyl) diisopropylphosphoramidite

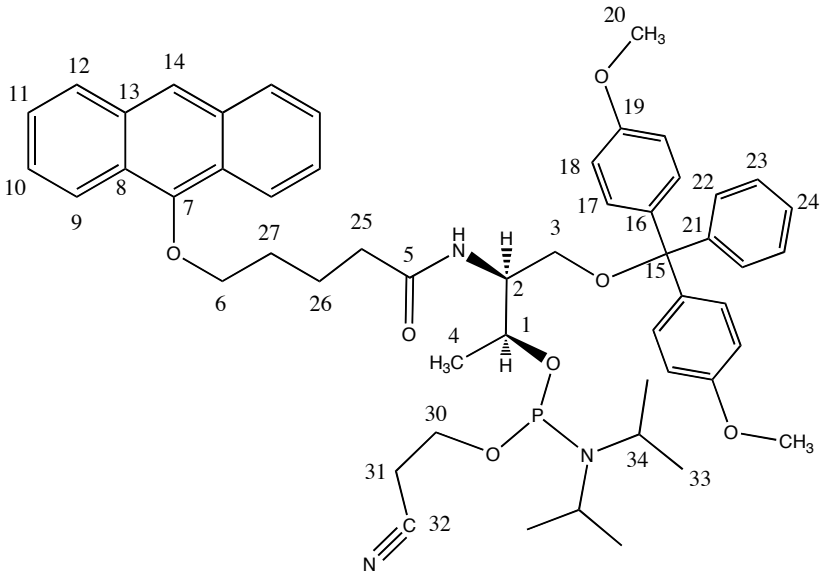

5-(Anthracen-9-yloxy)-*N*-((2*S*,3*S*)-1-(bis(4-methoxyphenyl)(phenyl)methoxy)-3-hydroxybutan-2-yl) pentamide (0.38 g, 0.56 mmol) placed in a 25 mL round-bottomed flask with a stirrer bar and a septum. The flask was evacuated and filled with argon three times and the solid dissolved in anhydrous DCM (15 mL). DIPEA (0.4 mL, 2.1 mmol) was added and the solution stirred at room temp. in the absence of light. *2*-Cyanoethyl-diisopropylchlorophosphoramidite (0.13 mL, 0.61 mmol) was added *via* a disposable syringe dropwise and the reaction stirred for 1 hr. The soln. was then transferred to a 25 mL round-bottomed flask containing a stirrer bar and solid-supported BnOH (0.05 g, 0.13 mmol) and left to stir for 1 hr in the absence of light. The soln. was diluted with EtOAc (10 mL), filtered and then washed with 2 M Na_2CO_3 (a.q.) soln. (2 x 50 mL) and brine (1 x 50 mL) and dried over Mg_2SO_4.

The soln. was then columned through activated basic alumina with EtOAC:Hex:TEA 49:50:1 and the filtrate evaporated in *vacuo* to give a yellow powdery solid (0.36g 59%); (R_f. =0.63 50% pet ether 50% DCM) δ_H (300 MHz, CD_3CN) 8.32 (1H, s, *H14*), 8.30-8.25 (2H, *m*, *H9*), 8.07 (2H, dd, *J* = 6.3 and 3.3, *H12*), 7.57-7.42 (4H, m, *H11* and *H22*), 7.39-7.26 (6H, m, *H10* and *H17*), 7.21 (3H, td, *J* = 7.2 and 5.0 *H23* and *H24*), 6.84 (4H, ddd, *J* = 6.9, 5.0 and 2.6, *H18*), 6.26 (1H, dd, *J* = 16.6 and 9.2, N*H*), 4.22 (2H, dt, *J* = 12.1 and 6.2, OC*H*$_2$CH$_2$CH$_2$ *H6*), 3.80-3.63 (3H, m, C*H*NH *H2* and CH(CH$_3$)C*H*OH *H1*), 3.73 (6H, s, OC*H*$_3$ *H20*), 3.43-3.60 (4H, m, POC*H*$_2$ *H30* and PNC*H* *H34*), 3.06-3.21 (2H, m, C*H*$_2$ODMT *H3*), 2.52 (2H, dt, *J* = 33.9, *J* = 6.1, C*H*$_2$CN *H31*), 2.41 (2H, t, *J* = 6.0, OCH$_2$CH$_2$CH$_2$C*H*$_2$CO *H25*), 2.02-2.11 (4H, m, OCH$_2$C*H*$_2$C*H*$_2$CH$_2$CO *H26* and *H27*), 1.29-1.05 (12H, m, C*H*$_3$ *H33*), 0.98 (3H, d, *J* = 6.8, C*H*$_3$CHOP *H4*); δ_P (121 MHz, CD_3CN) 147.6, 147.0; *m/z* (ES+) calcd. for $C_{54}H_{64}O_7N_3NaP$ ($M+Na^+$) 906.4223, found 906.4225.

7.6 *n* = 5 synthesis

7.6.1 *n* = 5 Ester (2d)

Ethyl 6-(anthracen-9-yloxy)hexanoate [3]

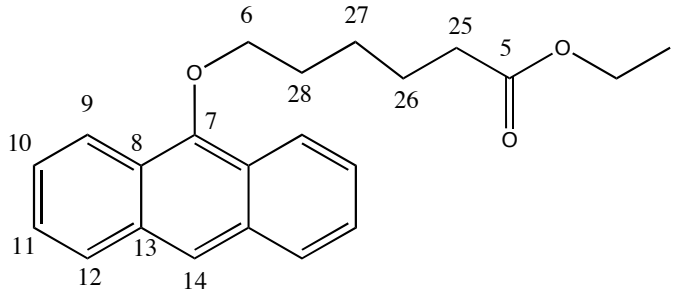

Anthrone (5.83 g, 0.03 mol) and K_2CO_3 (4.15 g, 0.03 mol) were dissolved in degassed acetone (200 mL) and stirred under N_2 at room temp. in the absence of light for 15 min. Ethyl *6*-bromohexanoate (5.3 mL, 0.03 mol) was added and the reaction mixture refluxed overnight. The solution was filtered to remove K_2CO_3 and dissolved in DCM (100 mL). The solution was washed with H_2O (1 x 50 mL) and dried over $MgSO_4$. The solvent was removed in *vacuo* to give an orange oil which solidified on standing. Column chromatography on silica (hexane with 10% EtOAc) yielded the desired product as a crystalline, cream solid (3.9 g, 39%). (R_f =0.23 in hexane with 10% EtOAc); M.p. 73 ˚C; δ_H (300 MHz, $CDCl_3$) 8.30 (2H, d, J = 9.1, H_9), 8.24 (1H, s, H_{14}), 7.91 (2H, d, J = 9.6, H_{12}), 7.47-7.53 (4H, m, H_{10} and H_{11}), 4.16-4.25 (4H, m, CH_2CH_3, $OCH_2(CH_2)_4$ H_6), 2.44 (2H, m, $(CH_2)_4CH_2CO$ H_{25}), 1.98-2.08 (2H, m, $CH_2CH_2(CH_2)_3CO$ H_{28}), 1.68-1.73 (4H, m, $(CH_2)_2CH_2CH_2CH_2CO$ H_{26} and H_{27}), 1.29 (3H, t, J = 7.2, CH_2CH_3 H_4); δ_C (100 MHz, $CDCl_3$) 178.5 (C_5=O), 151.1 (C_7), 132.4 (2xC_{13}), 128.4 (2xC_{12}), 125.5 (2xC_{10}), 125.1 (2xC_{11}), 124.7 (2xC_8), 122.4 (2xC_9), 122.1 (C_{14}), 75.5 (C_6), 60.3 (CH_2CH_3), 34.3 (C_{25}), 30.2 (C_{28}), 25.8 (C_{26}), 25.1 (C_{27}), 14.3 (CH_2CH_3); *m/z* (ES+) calcd. for $C_{21}H_{22}O_3Na$ ($M+Na^+$) 359.1 found 359.1.

7.6.2 *n* = 5 Acid (3d)

6-(Anthracen-9-yloxy)hexanoic acid [3]

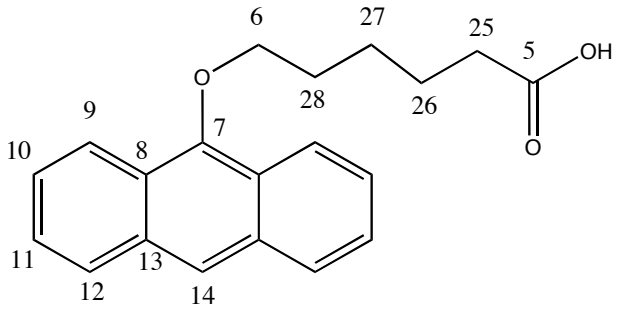

Ethyl 6-(anthracen-9-yloxy)hexanoate (3.9 g, 0.01 mol) was dissolved in a 1:1 soln. of 10% NaOH (aq.) soln. and EtOH (200 mL) and refluxed overnight in the absence of light. The solution was concentrated under *vacuo* and dissolved in H_2O (500 mL). Conc. HCl was added dropwise to the solution to afford a precipitate which was collected by suction filtration. The solid was washed with H_2O and dried to give the desired product as a cream solid (3.0 g, 97% yield). M.p. 143 ˚C; δ_H (400 MHz, $CDCl_3$) 8.28 (2H, d, J = 9.8, H_9), 8.25 (1H, s, H_{14}), 8.01 (2H, d, J = 9.6, H_{12}), 7.44-7.54 (4H, m, H_{10} and H_{11}), 4.21 (2H, t, J = 6.8, $OCH_2(CH_2)_4$ H_6), 2.50 (2H, t, J = 6.5, $O(CH_2)_4CH_2CO$ H_{25}), 2.11-2.13 (2H, m, OCH_2CH_2 H_{28}), 1.75-1.83 (4H, m, $O(CH_2)_2CH_2CH_2$ H_{26} and H_{27}); δ_C (100 MHz, $CDCl_3$) 178.5 (C_5=O), 151.1 (C_7), 132.4 (2xC_{13}), 128.4 (2xC_{12}), 125.5 (2xC_{10}), 125.1 (2xC_{11}), 124.7 (2xC_8), 122.4 (2xC_9), 122.1 (C_{14}), 75.5 (C_6), 33.8 (C_{25}), 30.4 (C_{28}), 25.8 (C_{26}), 24.7 (C_{27}); *m/z* (ES+) calcd. for $C_{20}H_{20}O_3Na$ ($M\text{-}H^+ + Na^+$) 331.1, found 331.1.

7.6.3 *n* = 5 L Diol (4dL)

6-(Anthracen-9-yloxy)-*N*-((2*R*,3*R*)-1,3-dihydroxybutan-2-yl)hexanamide

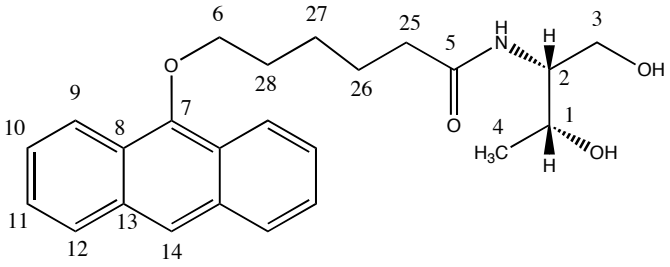

6-(Anthracen-9-yloxy) hexanoic acid (2.0g, 6 mmol) was dissolved in anhydrous DMF (40 mL). HBTU (3.08 g, 6 mmol) was added to the soln. which was stirred under N_2 at room temp. in the absence of light for 15 mins. L-Threoninol (0.68 g, 6 mmol) and DIPEA (1.7 mL, 10 mmol) were added and the reaction left to stir at 40 ˚C for 40 hours. The soln. was diluted in MeOH/DCM (1:2 100 mL) and washed with H_2O (3 x 50 mL) and dried over $MgSO_4$. The solvent was removed in *vacuo* and subsequent purification by silica column chromatography (DCM with 5% MeOH) gave the desired product as an oily yellow solid (2.6 g, 83%). (R_f =0.1 in DCM with 5% MeOH); M.p. 99-103 ˚C (found: C, 72.79; H, 7.57; N, 3.59%. $C_{24}H_{29}NO_4$ requires C, 72.89; H, 7.39; N, 3.54%); δ_H (300 MHz, CD_3CN) 8.23-8.28 (2H, m, *H*$_9$), 8.22 (1H, s, *H*$_{14}$), 7.97-8.02 (2H, d, *J* = 7.1, *H*$_{12}$), 7.42-7.51 (6H, m, *H*$_{10}$ and *H*$_{11}$), 6.39 (1H, d, *J* = 8.8, N*H*), 4.20 (2H, t, *J* = 6.5, OC*H*$_2$ *H*$_6$), 3.79-3.89 (2H, m, NHCH(CH_3)C*H*OH *H*$_1$ and NHC*H*(CH_3)CHOH *H*$_2$), 3.45-3.55 (3H, m, C*H*$_2$ODMT *H*$_3$ and CHCO*H)*, 2.90 (1H, s, CH_2CO*H*), 2.38 (2H, t, *J* = 7.2, C*H*$_2$CO *H*$_{25}$), 2.07 (2H, q, C*H*$_2CH_2CH_2CH_2CO$ *H*$_{28}$), 1.71-1.90 (4H, m, C*H*$_2CH_2CH_2CO$ *H*$_{27}$ and C*H*$_2CH_2CO$ *H*$_{26}$), 1.20 (3H, d, *J* = 6.4, C*H*$_3$CHOH *H*$_4$); δ_C (100 MHz, $CDCl_3$) 173.8 (*C*$_5$=*O*), 151.1 (*C*$_7$), 132.2 (2x*C*$_{13}$), 128.4 (2x*C*$_{12}$), 125.4 (2x*C*$_{10}$), 125.1 (2x*C*$_{11}$), 124.6 (2x*C*$_8$), 122.2 (2x*C*$_9$), 122.1 (*C*$_{14}$), 75.5

(C_6), 68.2 (C_1), 64.5 (C_3), 54.8 (C_2), 36.9 (C_{25}), 31.0 (C_{28}), 26.5 ($C_{26,27}$), 20.7 (C_4); *m/z* (ES+) calcd. for $C_{24}H_{29}O_4NNa$ (M+Na$^+$) 418.1994, found 418.1997.

7.6.4 *n* = 5 D Diol (4dD)

6-(Anthracen-9-yloxy)-*N*-((2*S*,3*S*)-1,3-dihydroxybutan-2-yl)hexanamide

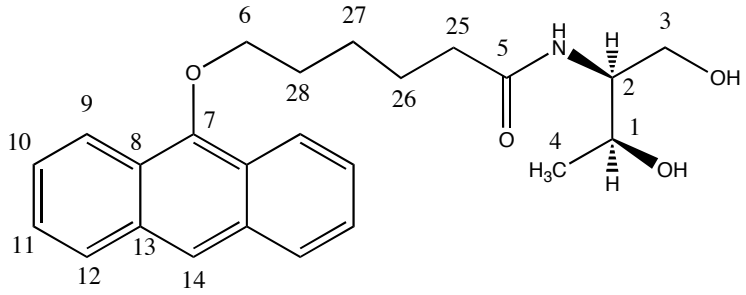

6-(Anthracen-9-yloxy) hexanoic acid (2.0g, 6 mmol) was dissolved in anhydrous DMF (40 mL). HBTU (3.08 g, 6 mmol) was added to the soln. which was stirred under N_2 at room temp. in the absence of light for 15 mins. D-Threoninol (0.68 g, 6 mmol) and DIPEA (1.7 mL, 10 mmol) were added and the reaction left to stir at 40 ˚C for 40 hours. The soln. was diluted in MeOH/DCM (1:2 100 mL) and washed with H_2O (3 x 50 mL) and dried over $MgSO_4$. The solvent was removed in *vacuo* and subsequent purification by silica column chromatography (DCM with 5% MeOH) gave the desired product as an oily yellow solid (2.6 g, 83%). (R_f =0.1 in DCM with 5 % MeOH); M.p. 100-102 ˚C; (found: C, 72.80; H, 7.57; N, 3.58%. $C_{54}H_{64}N_3O_7$ requires C, 72.89; H, 6.79; N, 2.01; O, 13.76%); δ_H (300 MHz, CD_3CN) 8.23-8.28 (2H, m, H_9), 8.22 (1H, s, H_{14}), 7.97-8.02 (2H, d, *J* = 7.1, H_{12}), 7.42-7.51 (6H, m, H_{10} and H_{11},), 6.39 (1H, d, *J* = 8.8, N*H*), 4.20 (2H, t, *J* = 6.5, OCH_2 H_6), 3.79-3.89 (2H, m, NHCH(CH_3)C*H*OH H_1 and

NHC*H*(CH_3)CHOH H_2), 3.45-3.55 (3H, m, CH_2ODMT H_3 and CHCO*H)*, 2.90 (1H, s, CH_2CO*H*), 2.38 (2H, t, *J* = 7.2 CH_2CO H_{25}), 2.07 (2H, q, C$H_2CH_2CH_2CH_2$CO H_{28}), 1.71-1.90 (4H, m, C$H_2CH_2CH_2$CO H_{27} and CH_2CH_2CO H_{26}), 1.20 (3H, d, *J* = 6.4, CH_3CHOH H_4); δ_C (75 MHz, CD_3CN) 174.1 (C_5=*O*), 159.4 (2xC_{19}), 152.1 (C_7), 146.1 (C_{21}), 137.0 (2xC_{16}), 133.3 (2xC_{13}), 130.9 (4xC_{17}), 129.2 (2xC_{12}), 128.9 (2xC_{22}), 128.7 (2xC_{23}), 127.6 (C_{24}), 126.5 (2xC_{10}), 126.2 (2xC_{11}), 125.4 (2xC_8), 123.1 (2xC_9), 122.8 (C_{14}), 113.9 (4xC_{18}), 86.7 (C_{15}), 76.6 (C_6), 67.2 (C_1), 64.5 (C_3), 55.7 (2xC_{20}), 55.3 (C_2), 36.9 (C_{25}), 31.0 (C_{28}), 26.5 ($C_{26,27}$), 20.7 (C_4); *m/z* (ES+) calcd. for $C_{24}H_{29}O_4NNa$ (M+Na^+)418.1994, found 418.1985.

7.6.5 *n* = 5 L DMT (5dL)

6-(Anthracen-9-yloxy)-*N*-((2*R*,3*R*)-1-(bis(4-methoxyphenyl)(phenyl)methoxy)-3-hydroxybutan-2-yl)hexanamide

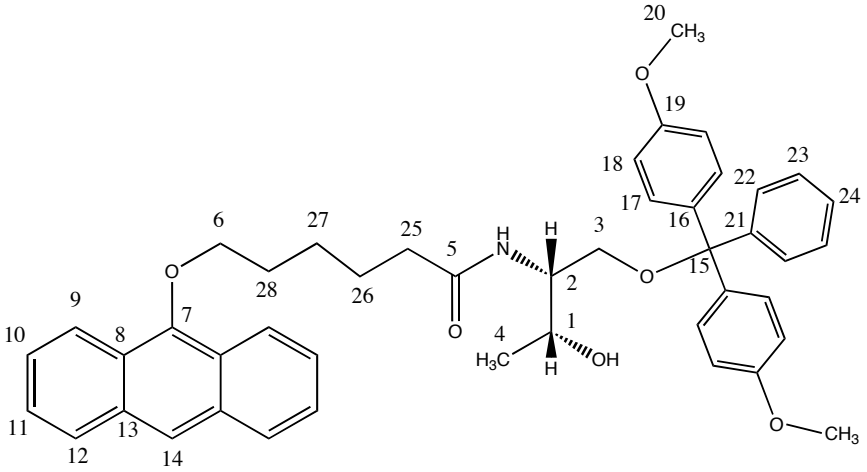

6-(Anthracen-9-yloxy)-*N*-((2*R*,3R)-1,3-dihydroxybutan-2-yl)hexanamide

(1.84g, 5.0 mmol) was dissolved in anhydrous pyridine (20 mL). Dimethoxytritylchloride (1.83 g, 5.0 mmol) was added to the soln. followed by DMAP (0.07 g, 0.5 mmol) and the reaction left to stir under N_2 at room temp. in the absence of light for 24 hours. The reaction mixture was poured onto H_2O (50 mL), extracted with DCM (2 x 50 mL) and dried over $MgSO_4$. The solvent was

removed in *vacuo* and subsequent column chromatography on silica (Hex/EtOAc/TEA, 40:59:1) afforded the desired compound as a pale yellow crystalline solid (1.45 g, 42%). (R_f =0.48 in DCM with 5% MeOH); M.p. 73-77 ˚C (found: C, 77.52; H, 6.89; N, 1.91%. $C_{45}H_{47}NO_6$ requires C, 77.45; H, 6.79; N, 2.01%); ν_{max}/cm^{-1} 3335 (OH), 2938 (N-H), 1642 (C=O); δ_H (300 MHz, CD_3CN) 8.29 (1H, s, H_{14}), 8.22-8.25 (2H, m, H_9), 8.01-8.03 (2H, m, H_{12}), 7.4-7.49 (6H, m, H_{10} H_{11} and H_{22}), 7.26-7.31 (6H, m, H_{23} and H_{17}), 7.17 (1H, m, H_{24}), 6.78-6.83 (4H, m, H_{18}), 6.33 (1H, d, J = 9.0, NH), 4.14 (2H, t, J = 6.0, OCH_2 H_6), 3.94 (2H, m, NHCH(CH_3)CHOH H_1 and NHCH(CH_3)CHOH H_2), 3.69 (6H, s, OCH_3 H_{20}), 2.94-3.19 (3H, m, CH_2ODMT H_3 CH_2COH), 2.30 (2H, t, J = 6.9, CH_2CO H_{25}), 1.98-2.14 (2H, m, C$H_2$$CH_2$$CH_2$$CH_2$$CH_2$CO H_{28}), 1.56-1.79 (4H, m, C$H_2$$CH_2$$CH_2$CO H_{27} and C$H_2$$CH_2$CO H_{26}), 1.04 (3H, d, J = 6.3, CH_3CHOH H_4); δ_C (75 MHz, CD_3CN) 173.7 (C_5=O), 159.5 (2xC_{19}), 152.2 (C_7), 146.1 (C_{21}), 137.1 (2xC_{16}), 133.4 (2xC_{13}), 130.9 (4xC_{17}), 129.3 (2xC_{12}), 129.0 (2xC_{22}), 128.7 (2xC_{23}), 127.7 (C_{24}), 126.6 (2xC_{10}), 126.2 (2xC_{11}), 125.5 (2xC_8), 123.2 (2xC_9), 122.9 (C_{14}), 113.9 (4xC_{18}), 86.7 (C_{15}), 76.8 (C_6), 67.3 (C_1), 64.6 (C_3), 55.8 (2xC_{20}), 55.2 (C_2), 36.9 (C_{25}), 29.8 (C_{28}), 26.6 ($C_{26,\ 27}$), 20.5 (C_4); *m/z* (ES+) calcd. for $C_{45}H_{47}O_6N$ ($M+Na^+$) 720.3301, found 720.3317.

7.6.6 *n* = 5 D DMT (5dD)

6-(Anthracen-9-yloxy)-*N*-((2*S*,3*S*)-1-(bis(4-methoxyphenyl)(phenyl)methoxy)-3-hydroxybutan-2-yl)hexanamide

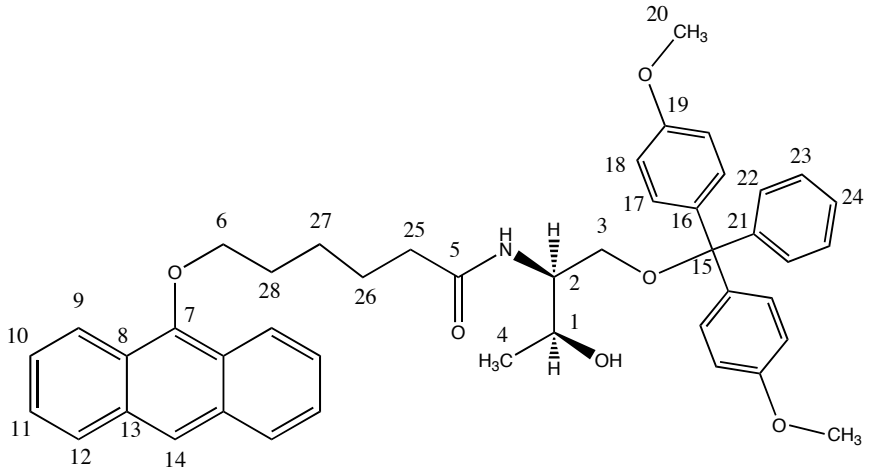

6-(Anthracen-9-yloxy)-*N*-((2*R*,3*R*)-1,3-dihydroxybutan-2-yl)hexanamide (1.84g, 5.0 mmol) was dissolved in anhydrous pyridine (20 mL). Dimethoxytritylchloride (1.83 g, 5.0 mmol) was added to the soln. followed by DMAP (0.07 g, 0.5 mmol) and the reaction left to stir under N_2 at room temp. in the absence of light for 24 hours. The reaction mixture was poured onto H_2O (50 mL), extracted with DCM (2 x 50 mL) and dried over $MgSO_4$. The solvent was removed in *vacuo* and subsequent column chromatography on silica (Hex/EtOAc/TEA, 40:59:1) afforded the desired compound as a pale yellow crystalline solid (1.10 g, 32%). (R_f =0.48 in DCM with 5% MeOH); M.p. 72-75 ˚C (found: C, 77.51; H, 6.93; N, 1.85%. $C_{45}H_{47}NO_6$ requires C, 77.45; H, 6.79; N, 2.01%); ν_{max}/cm^{-1} 3335 (OH), 2938 (N-H), 1642 (C=O); δ_H (300 MHz, CD_3CN) 8.29 (1H, s, *H*$_{14}$), 8.22-8.25 (2H, m, *H*$_9$), 8.01-8.03 (2H, m, *H*$_{12}$), 7.40-7.49 (6H, m, *H*$_{10}$, *H*$_{11}$ and *H*$_{22}$), 7.26-7.31 (6H, m, *H*$_{23}$ and *H*$_{17}$), 7.17 (1H, m, *H*$_{24}$), 6.78-6.83 (4H, m, *H*$_{18}$), 6.33 (1H, d, *J* = 9.0, N*H*), 4.14 (2H, t, *J* = 6.0, OC*H*$_2$ *H*$_6$), 3.94 (2H, m, NHCH(CH_3)C*H*OH *H*$_1$ and NHC*H*(CH_3)CHOH *H*$_2$), 3.69 (6H, s,OC*H*$_3$ *H*$_{20}$), 2.94-3.19

(3H, m, CH_2ODMT H_3 $CH_2CO$$H$), 2.30 (2H, t, J = 6.9, CH_2CO H_{25}), 1.98-2.14 (2H, m, C$H_2$$CH_2CH_2CH_2CH_2CO$ H_{28}), 1.56-1.79 (4H, m, C$H_2$$CH_2CH_2CO$ H_{27} and C$H_2$$CH_2CO$ H_{26}), 1.04 (3H, d, J = 6.3, CH_3CHOH H_4); δ_C (75 MHz, CD_3CN) 173.7 (C_5=O), 159.5 (2xC_{19}), 152.2 (C_7), 146.1 (C_{21}), 137.1 (2xC_{16}), 133.4 (2xC_{13}), 130.9 (4xC_{17}), 129.3 (2xC_{12}), 129.0 (2xC_{22}), 128.7 (2xC_{23}), 127.7 (C_{24}), 126.6 (2xC_{10}), 126.2 (2xC_{11}), 125.5 (2xC_8), 123.2 (2xC_9), 122.9 (C_{14}), 113.9 (4xC_{18}), 86.7 (C_{15}), 76.8 (C_6), 67.3 (C_1), 64.6 (C_3), 55.8 (2xC_{20}), 55.2 (C_2), 36.9 (C_{25}), 29.8 (C_{28}), 26.6 ($C_{26,\ 27}$), 20.5 (C_4); m/z (ES+) calcd. for $C_{45}H_{47}O_6N$ ($M+Na^+$) 720.3301, found 720.3300.

7.6.7 *n* = 5 L Phosphoramidite (6dL)

(2*R*,3*R*)-3-(6-(Anthracen-9-yloxy)hexanamido)-4-(bis(4-methoxyphenyl)(phenyl)methoxy)butan-2-yl (2-cyanoethyl) diisopropylphosphoramidite

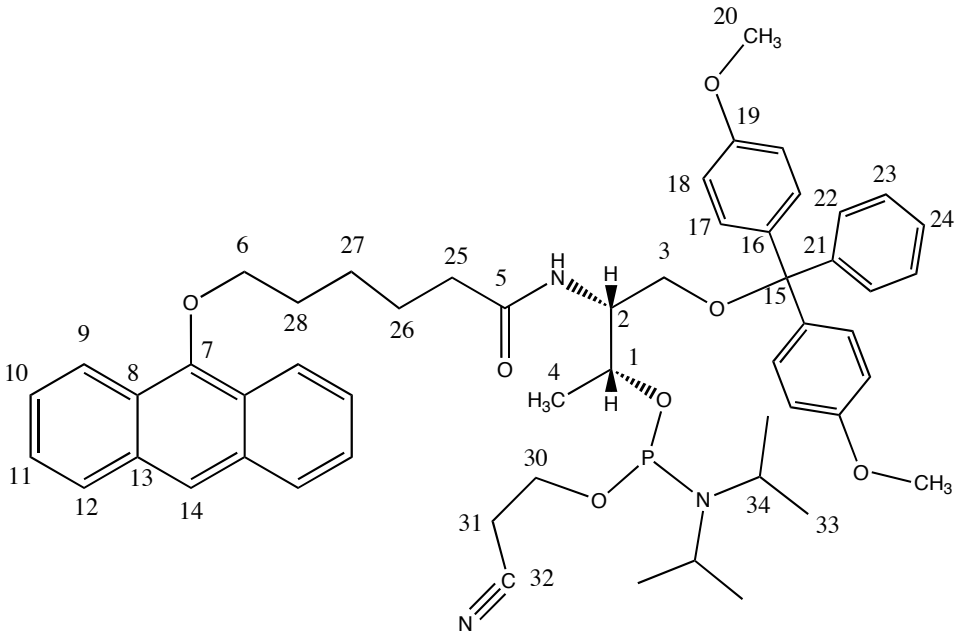

6-(Anthracen-9-yloxy)-*N*-((2*R*3*R*)-1-(bis(4-methoxyphenyl)(phenyl)methoxy)-3-hydroxybutan-2-yl)hexanamide (0.44

g, 0.63 mmol) placed in a 25 mL round-bottomed flask with a stirrer bar and a septum. The flask was evacuated and filled with argon three times and the solid dissolved in anhydrous DCM (15 mL). DIPEA (0.46 ml, 2.6 mmol) was added and the solution stirred at room temp. in the absence of light. *2*-Cyanoethyl-diisopropylchlorophosphoramidite (0.14 mL, 0.69 mmol) was added *via* a disposable syringe dropwise and the reaction stirred for 1 hr. The soln. was then transferred to a 25 mL round-bottomed flask containing a stirrer bar and solid-supported BnOH (0.05 g, 0.13 mmol) and left to stir for 1 hr in the absence of light. The soln. was diluted with EtOAc (10 mL), filtered and then washed with 2 M Na_2CO_3 (a.q.) soln. (2 x 50 mL) and brine (1 x 50 mL) and dried over Mg_2SO_4. The soln. was then columned through activated basic alumina with EtOAC:Hex:TEA 49:50:1 and the filtrate evaporated to give a yellow powdery solid (0.24g, 42%); (R_f. =0.65 50% pet ether 50% DCM); δ_H (300 MHz, CD_3CN) 8.29 (1H, s, *H14*), 8.25 (2H, d, *J* = 8.8, *H9*), 7.98-8.09 (2H, m, *H12*), 7.38-7.52 (4H, m, *H11* and *H22*), 7.22-7.32 (6H, m, *H10* and *H17*), 7.12-7.21 (3H, m, *H23* and *H24*), 6.81 (4H, dd, *J* = 8.7 and 4.4, *H18*), 6.35 (1H, m, N*H*), 4.05-4.24 (4H, m, OC*H*$_2$ *H6,* C*H*NH *H2* and (CH_3)C*H*OP *H1*), 3.73 (6H, s, OC*H*$_3$ *H20*), 3.49-3.63 (4H, m, POC*H*$_2$ *H30* and PNC*H* *H34*), 3.05-3.16 (2H, m, C*H*$_2$ODMT *H3*), 2.52 (2H, dt, *J* = 33.8 and 5.9, C*H*$_2$CN *H31*), 2.24-2.35 (2H, m, $OCH_2CH_2CH_2CO$ *H25*), 1.98-2.07 (2H, m, $CH_2CH_2CH_2CH_2CO$ *H28)*, 1.64-1.78 (4H, m, $CH_2CH_2CH_2CO$ *H27* and *H26*), 1.00-1.20 (12H, m, C*H*$_3$ *H33*), 0.96 (3H, d, *J* = 6.7, C*H*$_3$CHOP *H4*); δ_P (300 MHz, CD_3CN) 147.7, 147.0; *m/z* (ES+) calcd. for $C_{54}H_{64}O_7N_3NaP$ ($M+Na^+$) 920.4380, found 920.4400.

7.6.8 *n* = 5 D Phosphoramidite (6dD)

(2*S*,3*S*)-3-(6-(Anthracen-9-yloxy)hexanamido)-4-(bis(4-methoxyphenyl)(phenyl)methoxy)butan-2-yl (2-cyanoethyl) diisopropylphosphoramidite

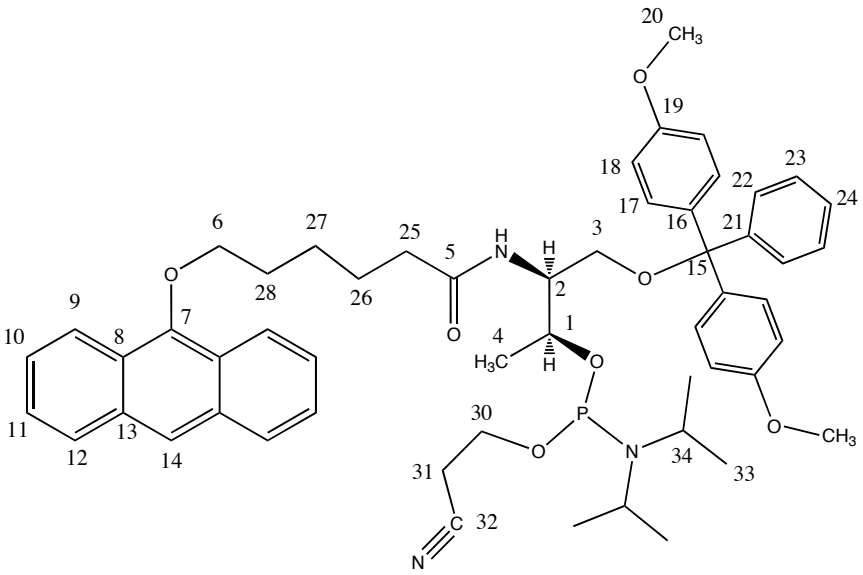

6-(Anthracen-9-yloxy)-*N*-((2*S*,3*S*)-1-(bis(4-methoxyphenyl)(phenyl)methoxy)-3-hydroxybutan-2-yl)hexanamide (0.87 g, 1.25 mmol) placed in a 25 mL round-bottomed flask with a stirrer bar and a septum. The flask was evacuated and filled with argon three times and the solid dissolved in anhydrous DCM (15 mL). DIPEA (0.91 mL, 5.13 mmol) was added and the solution stirred at room temp. in the absence of light. *2*-Cyanoethyl-diisopropylchlorophosphoramidite (0.28 mL, 1.37 mmol) was added *via* a disposable syringe dropwise and the reaction stirred for 1 hr. The soln. was then transferred to a 25 mL round-bottomed flask containing a stirrer bar and solid-supported BnOH (0.80 g, 0.25 mmol) and left to stir for 1 hr in the absence of light. The soln. was diluted with EtOAc (10 mL), filtered and then washed with 2 M Na_2CO_3 (a.q.) soln. (2 x 50 mL) and brine (1 x 50 mL) and dried over Mg_2SO_4.

The soln. was then columned through activated basic alumina with EtOAC:Hex:TEA 49:50:1 and the filtrate evaporated to give a yellow powdery solid (0.86 g, 78%). (R_f. = 0.63 50% pet ether 50% DCM); δ_H (300 MHz, CD_3CN) 8.29 (1H, s, *H14*), 8.25 (2H, d, *J* = 8.8, *H9*), 7.98-8.09 (2H, m, *H12*), 7.38-7.52 (4H, m, *H11* and *H22*), 7.22-7.32 (6H, m, *H10* and *H17*), 7.12-7.21 (3H, m, *H23* and *H24*), 6.81 (4H, dd, *J* = 8.7 and 4.4, *H18*), 6.35 (1H, m, N*H*), 4.05-4.24 (4H, m, OC*H*$_2$CO *H6,* C*H*NH *H2* and (CH$_3$)C*H*OH *H1*), 3.73 (6H, s, OC*H*$_3$ *H20*), 3.49-3.63 (4H, m, POC*H*$_2$ *H30* and PNC*H H34*), 3.05-3.16 (2H, m, C*H*$_2$ODMT *H3*), 2.52 (2H, dt, *J* = 33.8 and 5.9, C*H*$_2$CN *H31*), 2.24-2.35 (2H, m, OCH$_2$CH$_2$C*H*$_2$CO *H25*), 1.98-2.07 (2H, m, C*H*$_2$CH$_2$CH$_2$CH$_2$CO *H28)*, 1.64-1.78 (4H, m, C*H*$_2$C*H*$_2$CH$_2$CO *H27* and *H26*), 1.00-1.20 (12H, m, C*H*$_3$ *H33*), 0.96 (3H, d, *J* = 6.7, C*H*$_3$CHOP *H4*); δ_P (300 MHz, CD_3CN) 147.7, 147.0; *m/z* (ES+) calcd. for $C_{54}H_{64}O_7N_3NaP$ ($M+Na^+$) 920.4380, found 920.4388.

7.7 *n* = 6 synthesis

7.7.1 n = 6 Ester (2e)

Ethyl 7-(anthracen-9-yloxy)heptanoate [3]

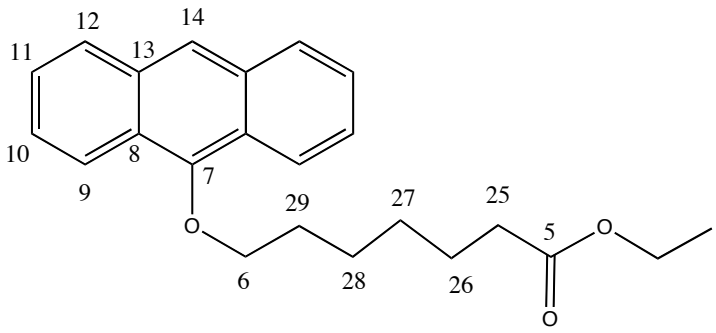

Anthrone (7.2 g, 37.5 mmol) and K_2CO_3 (5.4 g, 37.5 mmol) were dissolved in degassed acetone (200 mL) and stirred under N_2 at room temp. in the absence of light for 15 min. Ethyl *7*-bromoheptanoate (7.3 mL, 37.5 mmol) was added and the reaction mixture refluxed overnight. The solution was filtered to remove K_2CO_3 and dissolved in DCM (100 mL). The solution was washed with H_2O (1 x 50 mL) and dried over $MgSO_4$. The solvent was removed in *vacuo* to give an orange oil which solidified on standing. Column chromatography on silica (hexane with 10 % EtOAc) yielded the desired product as a cream solid (7.49 g, 55 %). (R_f =0.15 in Hexane with 5 % EtOAc); M.p. 69-70 ˚C; δ_H (300 MHz, $CDCl_3$) 8.18 (2H, d, *J* = 6.7, H_9), 8.11 (1H, s, H_{14}), 7.90 (2H, d, *J* = 6.7, H_{12}), 7.45-7.53 (4H, m, H_{10} and H_{11}), 4.13-4.23 (4H, m, CH_2CH_3, OCH_2 H_6), 2.27 (2H, t, *J* = 7.5, $O(CH_2)_5CH_2CO$), 1.75-1.80 (2H, m, OCH_2CH_2), 1.56-1.68 (4H, m, $O(CH_2)_2CH_2CH_2$), 1.42 (2H, m, $O(CH_2)_4CH_2$), 1.28 (3H, t, *J* = 7.1, CH_2CH_3); δ_C (400 MHz, $CDCl_3$) 174.2 (C_5=O), 151.3 (C_7), 132.4 (2xC_{13}), 128.4 (2xC_{12}), 125.4 (2xC_{10}), 125.1 (2xC_{11}), 124.7 (2xC_8), 122.3 (C_{14}), 122.0 (2xC_9), 75.9 (C_6), 60.2 (CH_2CH_3), 34.3 (C_{25}), 32.5 (C_{29}), 29.1 (C_{26}), 26.0 (C_{28}), 24.9 (C_{27}), 14.3 (CH_2CH_3). *m/z* (ES+) calcd for $C_{22}H_{24}O_3Na$ ($M+Na^+$) 373.1 found 373.1.

7.7.2 *n* = 6 Acid (3e)

7-(Anthracen-9-yloxy)heptanoic acid [3]

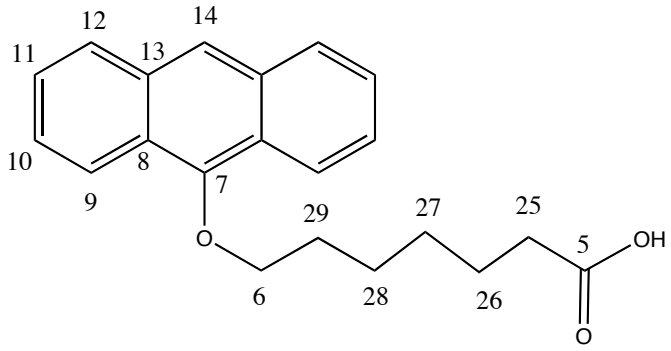

Ethyl 7-(anthracen-9-yloxy)heptanoate (7.49 g, 20.8 mmol) was dissolved in a 1:1 soln. of 10% NaOH (aq.) soln. and EtOH (200 mL) and refluxed overnight in the absence of light. The solution was concentrated in *vacuo* and dissolved in H_2O (500 mL). Conc. HCl was added drop wise to the solution to afford a precipitate, which was collected by suction filtration. The solid was washed with H_2O and dried to give the desired product as a cream, crystalline solid (5.66 g, 82% yield). M.p. 82-84 ˚C

δ_H (300 MHz, $CDCl_3$) 8.31 (2H, d, J = 9.1, H_9), 8.24 (1H, s, H_{14}), 8.20 (2H, d, J = 9.6, H_{12}), 7.44-7.55 (4H, m, H_{10} and H_{11}), 4.20 (2H, t, J = 6.6, $OCH_2(CH_2)_5CO$ H_6), 2.46 (2H, t, J = 7.4, $O(CH_2)_5CH_2CO$ H_{25}), 2.02-2.14 (2H, m, $OCH_2CH_2(CH_2)_3CO$ H_{29}), 1.68-1.85 (4H, m, $O(CH_2)_2CH_2CH_2CH_2CO$ H_{28}), 1.50-1.60 (2H, m, $O(CH_2)_4CH_2$ H_{27}); δ_C (100 MHz, $CDCl_3$) 178.2 (C_5=O), 151.5 (C_7), 132.4 (2xC_{13}), 128.4 (2xC_{12}), 125.4 (2xC_{10}), 125.1 (2xC_{11}), 124.7 (2xC_8), 122.3 (C_{14}), 122.0 (2xC_9), 75.9 (C_6), 33.9 (C_{25}), 30.5 (C_{29}), 29.0 (C_{26}) 26.0 (C_{28}), 24.7 (C_{27}); *m/z* (ES+) calcd for $C_{21}H_{22}O_3Na$ ($M\text{-}H^+ + Na^+$) 345.4, found 345.2.

7.7.3 *n* = 6 L Diol (4eL)

7-(Anthracen-9-yloxy)-*N*-((2*R*,3*R*)-1,3-dihydroxybutan-2-yl)heptanamide

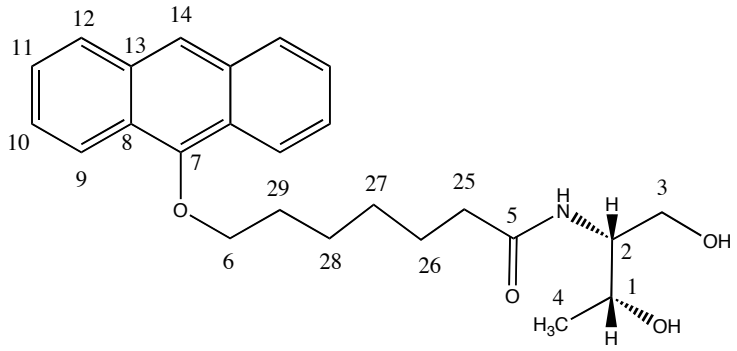

7-(Anthracen-9-yloxy)heptanoic acid (2.87g, 8.6 mmol) was dissolved in anhydrous DMF (20 mL). HBTU (3.5 g, 8.6 mmol) was added and the soln. stirred under N_2 at room temp. in the absence of light for 15 mins. L- Threoninol (0.89 g, 8.6 mmol) and DIPEA (2.38 mL, 8.6 mmol) were added and the reaction left to stir at 40 ˚C for 40 hours. The soln. was diluted in MeOH/DCM (1:2 100 mL) and washed with H_2O (3 x 50 mL) and dried over $MgSO_4$. The solvent was removed in *vacuo* and subsequent purification by silica column chromatography (DCM with 5% MeOH) gave the desired product as a pale yellow solid (2.74 g, 77%). (R_f =0.46 in DCM with 10% MeOH); M.p. 112-115 ˚C; δ_H (400 MHz, $CDCl_3$) 8.25 (2H, d, *J* = 7.6, *H*$_9$), 8.19 (1H, s, *H*$_{14}$), 7.96 (2H, d, *J* = 8.6, *H*$_{12}$), 7.45 (4H, m, *H*$_{10}$ and *H*$_{11}$), 6.33 (1H, d, *J* = 8.1, N*H*), 4.15-4.17 (3H, m, OC*H*$_2$CH$_2$ *H*$_6$ and CH$_3$C*H*OH *H*$_1$), 3.81-3.85 (1H, m, C*H*NH *H*$_2$), 3.76-3.79 (2H, m, CHC*H*$_2$OH *H*$_3$), 3.40 (1H, t, *J* = 5.1, CHO*H*), 3.31 (1H, d, *J* = 3.5, CH$_2$O*H*), 2.29 (2H, t, *J* = 7.6 C*H*$_2$CO *H*$_{25}$), 2.03 (2H, q, C*H*$_2$CH$_2$CH$_2$CH$_2$CH$_2$CO *H*$_{29}$), 1.75 (2H, q, C*H*$_2$CH$_2$CO *H*$_{26}$), 1.68 (2H, q, C*H*$_2$CH$_2$CH$_2$CH$_2$CO *H*$_{28}$), 1.48 (2H, q, C*H*$_2$CH$_2$CH$_2$CO *H*$_{27}$), 1.17 (3H, d, *J* = 6.1, C*H*$_3$CHOH *H*$_4$); δ_C (100 MHz, $CDCl_3$) 174.2 (*C*$_5$=*O*), 151.3 (*C*$_7$), 132.4 (2x*C*$_{13}$), 128.4

(2xC_{12}), 125.4 (2xC_{10}), 125.1 (2xC_{11}), 124.7 (2xC_8), 122.3 (C_{14}), 122.0 (2xC_9), 75.9 (C_6), 68.4 (C_1), 64.7(C_3), 54.7(C_2), 36.7(C_{25}), 30.5(C_{29}), 29.2(C_{28}), 26.0(C_{26}), 25.7(C_{27}), 20.5(C_4); *m/z* (ES+) calcd. for $C_{25}H_{31}O_4N$ ($M+Na^+$), 432.2151 found 432.2147.

7.7.3 *n* = 6 D Diol (4eD)

7-(anthracen-9-yloxy)-N-((2*S*,3*S*)-1,3-dihydroxybutan-2-yl)heptanamide

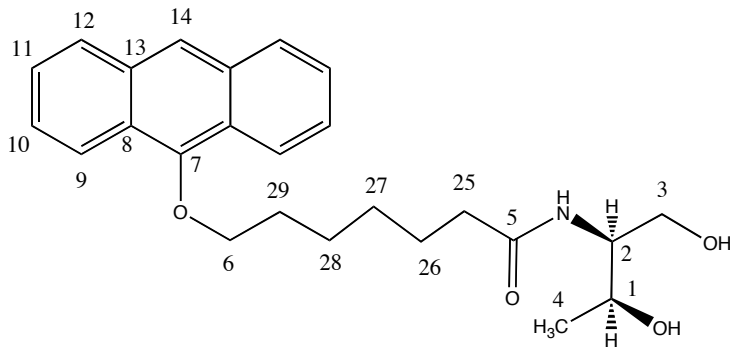

7-(Anthracen-9-yloxy)heptanoic acid (2.5g 7.5 mmol) was dissolved in anhydrous DMF (20 mL). PyBOP (3.91g, 7.5 mmol) was added and the soln. stirred under N_2 at room temp. in the absence of light for 15 mins. D- Threoninol (0.78 g, 7.5 mmol) and DIPEA (1.96 mL, 11.2 mmol) were added and the reaction left to stir at 40 ˚C for 40 hours. The soln. was diluted in MeOH/DCM (1:2 100 mL) and washed with H_2O (3 x 50 mL) and dried over $MgSO_4$. The solvent was removed in *vacuo* and subsequent purification by silica column chromatography (DCM with 5% MeOH) gave the desired product as a pale yellow solid (2.39 g, 79%). (R_f =0.46 in DCM with 10% MeOH); M.p. 113-115 ˚C; δ_H (400 MHz, $CDCl_3$) 8.25 (2H, d, *J* = 7.6, H_9), 8.19 (1H, s, H_{14}), 7.96 (2H, d, *J* = 8.6, H_{12}), 7.45 (4H, m, H_{10} and H_{11}), 6.33 (1H, d, *J* = 8.1, N*H*), 4.15-4.17 (3H, m, O$CH_2CH_2CH_2$O H_6 and

CH_3CHOH H_1), 3.81-3.85 (1H, m, $CHNH$ H_2), 3.76-3.79 (2H, m, $CHCH_2OH$ H_3), 3.40 (1H, t, J = 5.1, $CHOH$), 3.31 (1H, d, J = 3.5, CH_2OH), 2.29 (2H, t, J = 7.6 CH_2CO H_{25}), 2.03 (2H, q, $CH_2CH_2CH_2CH_2CH_2CO$ H_{29}), 1.75 (2H, q, CH_2CH_2CO H_{26}), 1.68 (2H, q, $CH_2CH_2CH_2CH_2CO$ H_{28}), 1.48 (2H, q, $CH_2CH_2CH_2CO$ H_{27}), 1.17 (3H, d, J = 6.1, CH_3CHOH H_4); δ_C (100 MHz, $CDCl_3$) 174.2 (C_5=O), 151.3 (C_7), 132.4 (2xC_{13}), 128.4 (2xC_{12}), 125.4 (2xC_{10}), 125.1 (2xC_{11}), 124.7 (2xC_8), 122.3 (C_{14}), 122.0 (2xC_9), 75.9 (C_6), 68.4 (C_1), 64.7 (C_3), 54.7 (C_2), 36.7 (C_{25}), 30.5 (C_{29}), 29.2 (C_{28}), 26.0 (C_{26}), 25.7 (C_{27}), 20.5 (C_4); m/z (ES+) calcd for $C_{25}H_{31}O_4NNa$ ($M+Na^+$), 432.2151 found 432.2147.

7.7.5 *n* = 6 L DMT (5eL)

7-(Anthracen-9-yloxy)-*N*-((2*R*,3*R*)-1-(bis(4-methoxyphenyl)(phenyl)methoxy)-3-hydroxybutan-2-yl)heptanamide

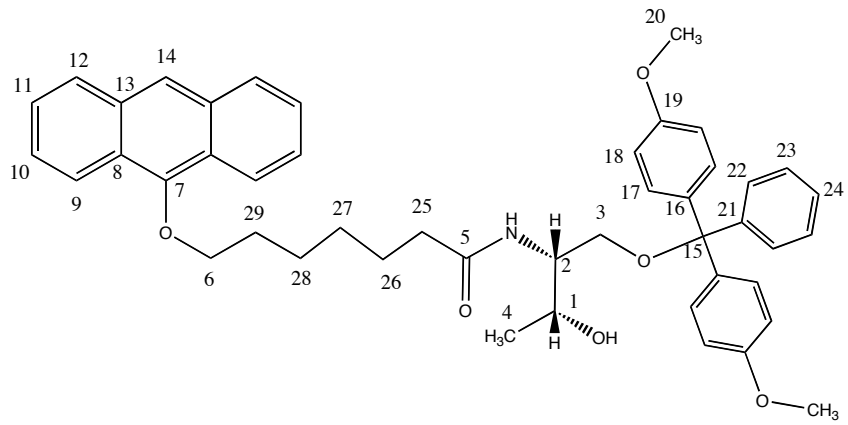

7-(Anthracen-9-yloxy)-*N*-((2*R*,3*R*)-1,3-dihydroxybutan-2-yl)heptanamide (2.92g, 7.2mmol) was dissolved in anhydrous pyridine (20 mL). Dimethoxytritylchloride (2.41 g, 7.2 mmol) was added to the soln. followed by DMAP (0.09 g, 0.7 mmol) and the reaction left to stir under N_2 at room temp. in the absence of light for 24 hours. The reaction mixture was poured onto H_2O (50

mL), extracted with DCM (2 x 50 mL) and dried over $MgSO_4$. The solvent was removed in *vacuo* and subsequent column chromatography on silica (Hex/EtOAc/TEA, 40:59:1) afforded the desired compound as a pale yellow crystalline solid (1.51 g, 30%). (R_f =0.63 in DCM with 5% MeOH); M.p. 88-90˚C (found: C, 76.78; H, 6.94; N, 1.78%. $C_{46}H_{49}NO_6$ +0.25 Eq. Et_3N requires C, 77.39; H, 7.21; N, 1.97%); ν_{max}/cm^{-1} 3335 (OH), 2938 (N-H), 1642 (C=O); δ_H (300 MHz, CD_3CN) 8.24-8.26 (2H, m, H_9), 8.24 (1H, s, H_{14}), 7.95-8.02 (2H, m, H_{12}), 7.40-7.51 (6H, m, H_{10} H_{11} and H_{22}), 7.25-7.32 (6H, m, H_{23} and H_{17}), 7.19 (1H, t, J = 7.2, H_{24}), 6.82 (4H, d, J = 8.8, H_{18}), 6.47 (1H, d, J = 8.8, N*H*), 4.04-4.13 (2H, m, O$CH_2(CH_2)_5$CO H_6), 3.93-4.03 (2H, m, NHC*H*CHOH H_2 and NHCHC*H*OH H_1), 3.70 (6H, s, OCH_3 H_{20}), 3.05-3.24 (3H, m, CH_2ODMT H_3 and CH_2CO*H*), 2.24 (2H, t, J = 7.3, CH_2CO H_{25}), 1.94 (2H, m, C$H_2CH_2CH_2CH_2CH_2$CO H_{29}), 1.65 (4H, m, C$H_2CH_2CH_2CH_2$CO H_{28} and CH_2CH_2CO H_{26}), 1.43 (2H, q, C$H_2CH_2CH_2$CO H_{27}), 1.06 (3H, d, J = 6.2, CH_3CHOH H_4); δ_C (100 MHz, CD_3CN) 174.1 (C_5=O), 159.5 (2xC_{19}), 152.2 (C_7), 146.1 (C_{21}), 137.0 (2xC_{16}), 133.4 (2xC_{13}), 130.9 (4xC_{17}), 129.3 (2xC_{12}), 129.0 (2xC_{22}), 128.7 (2xC_{23}), 127.6 (C_{24}), 126.5 (2xC_{10}), 126.2 (2xC_{11}), 125.5 (2xC_8), 123.1 (2xC_9), 122.8 (C_{14}), 113.9 (4xC_{18}), 86.8 (C_{15}), 76.8 (C_6), 67.3 (C_1), 64.6 (C_3), 55.8 (2xC_{20}), 55.2 (C_2), 36.9 (C_{25}), 31.1 (C_{29}), 29.8 (C_{28}), 26.7 (C_{26}), 26.6 (C_{27}), 20.5 (C_4); *m/z* (ES+) calcd for $C_{46}H_{49}O_6N$ ($M+Na^+$) 734.3458, found 734.3470.

7.7.6 *n* = 6 D DMT (5eD)

7-(Anthracen-9-yloxy)-*N*-((2*S*,3*S*)-1-(bis(4-methoxyphenyl)(phenyl)methoxy)-3-hydroxybutan-2-yl)heptanamide

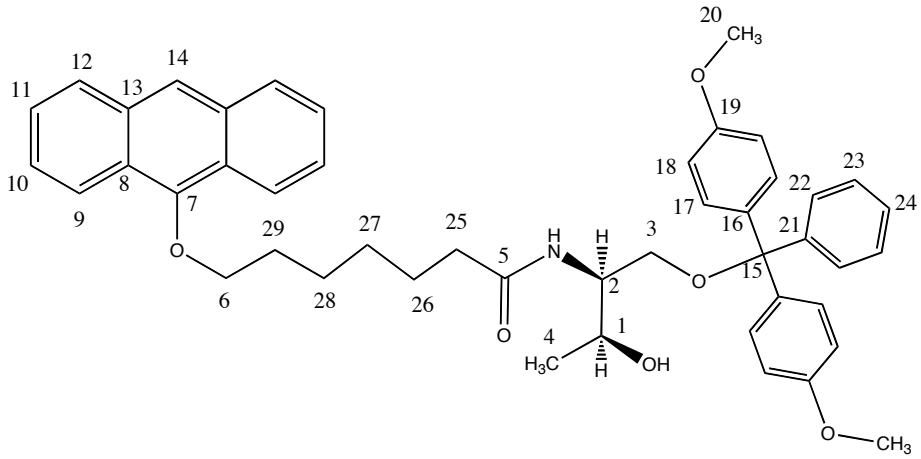

7-(Anthracen-9-yloxy)-*N*-((2*S*,3*S*)-1,3-dihydroxybutan-2-yl)heptanamide (3.51 g, 8.6 mmol) was dissolved in anhydrous pyridine (20 mL). Dimethoxytritylchloride (2.90 g, 8.6 mmol) was added to the soln. followed by DMAP (0.11 g, 0.9 mmol) and the reaction left to stir under N_2 at room temp. in the absence of light for 24 hours. The reaction mixture was poured onto H_2O (50 mL), extracted with DCM (2 x 50 mL) and dried over $MgSO_4$. The solvent was removed in *vacuo* and subsequent column chromatography on silica (Hex/EtOAc/TEA, 40:59:1) afforded the desired compound as a pale yellow crystalline solid (2.74 g, 45%). (R_f =0.48 in DCM with 5% MeOH); M.p. 87-90˚C (found: C, 77.63; H, 6.98; N, 2.10%. $C_{46}H_{49}NO_6$ requires C, 77.61; H, 6.94; N, 1.97%); ν_{max}/cm^{-1} 3335 (OH), 2938 (N-H), 1642 (C=O); δ_H (400 MHz, CD_3CN) 8.28 (1H, s, *H*$_{14}$), 8.25 (2H, d, *J* = 9.1, *H*$_9$), 8.03 (2H, d, *J* = 7.1, *H*$_{12}$), 7.40-7.49 (6H, m, *H*$_{10}$, *H*$_{11}$ and *H*$_{22}$), 7.26-7.31 (6H, m, *H*$_{23}$, and *H*$_{17}$), 7.20 (1H, m, *H*$_{24}$), 6.83 (4H, d, *J* = 8.6, *H*$_{18}$), 6.33 (1H, d, *J* = 8.6, N*H*), 4.14 (2H, t, *J* = 6, OC*H*$_2$CO *H*$_6$), 3.89-3.97 (2H,

m, NHC*H*CHOH H_2 and NHCHC*H*OH H_1), 3.72 (6H, s, OCH_3 H_{20}), 3.01-3.16 (3H, m, CH_2ODMT H_3 and CHCO*H*), 2.24 (2H, t, J = 7.6 CH_2CO H_{25}), 1.97 (2H, q, CH_2CH$_2$CH$_2$CH$_2$CH$_2$CO H_{29}), 1.66 (4H, m, CH_2CH$_2$CH$_2$CH$_2$CO H_{28} and CH_2CH$_2$CO H_{26}), 1.47 (2H, q, CH_2CH$_2$CH$_2$CO H_{27}), 1.04 (3H, d, J = 6.1, CH_3CHOH H_4); δ_C (75 MHz, CD$_3$CN) 174.0 (C_5=O), 159.5 (2xC_{19}), 152.2 (C_7), 146.1 (C_{21}), 137.1 (2xC_{16}), 133.4 (2xC_{13}), 130.9 (4xC_{17}), 129.3 (2xC_{12}), 129.0 (2xC_{22}), 128.7 (2xC_{23}), 127.7 (C_{24}), 126.6 (2xC_{10}), 126.2 (2xC_{11}), 125.5 (2xC_8), 123.2 (2xC_9), 122.9 (C_{14}), 113.9 (4xC_{18}), 86.7 (C_{15}), 76.8 (C_6), 67.3 (C_1), 64.6 (C_3), 55.8 (2xC_{20}), 55.2 (C_2), 36.9 (C_{25}), 31.1 (C_{29}), 29.8 (C_{28}), 26.7 (C_{26}), 26.6 (C_{27}), 20.5 (C_4); *m/z* (ES+) calcd for $C_{46}H_{49}O_6N$ (M+ Na^+) 734.3458, found 734.3469.

7.7.7 *n* = 6 L Phosphoramidite (6eL)

(2*R*,3*R*)-3-(7-(anthracen-9-yloxy)heptanamido)-4-(bis(4-methoxyphenyl)(phenyl)methoxy)butan-2-yl (2-cyanoethyl) diisopropylphosphoramidite

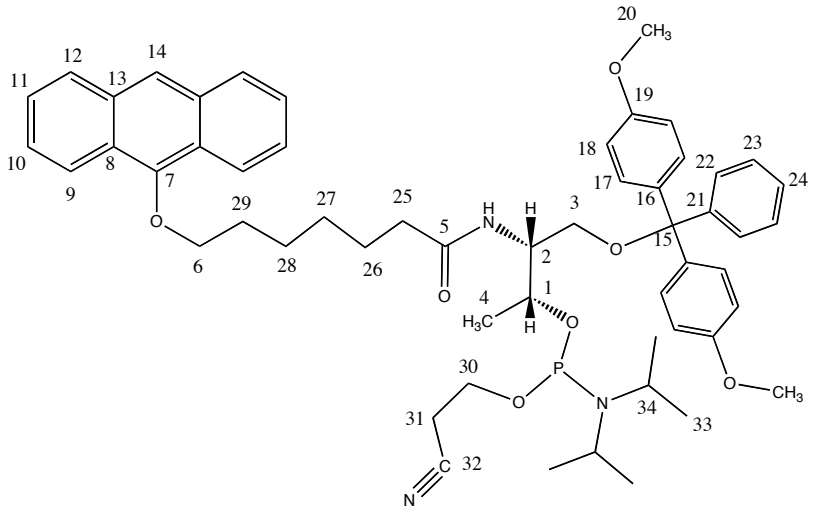

7-(Anthracen-9-yloxy)-*N*-((2*R*,3*R*)-1-(bis(4-methoxyphenyl)(phenyl)methoxy)-3-hydroxybutan-2-yl)heptanamide

(0.50 g, 0.42 mmol) placed in a 25 mL round-bottomed flask with a stirrer bar and a septum. The flask was evacuated and filled with argon three times and the solid dissolved in anhydrous DCM (15 mL). DIPEA (0.30 mL, 1.69 mmol) was added and the solution stirred at room temp. in the absence of light. *2*-Cyanoethyl-diisopropylchlorophosphoramidite (0.10 mL, 0.463 mmol) was added *via* a disposable syringe dropwise and the reaction stirred for 1 hr. The soln. was then transferred to a 25 mL round-bottomed flask containing a stirrer bar and solid-supported BnOH (0.80 g, 0.25 mmol) and left to stir for 1 hr in the absence of light. The soln. was diluted with EtOAc (10 mL), filtered and then washed with 2 M Na_2CO_3 (aq.) soln. (2 x 50 mL) and brine (1 x 50 mL) and dried over Mg_2SO_4. The soln. was then columned through activated basic alumina with EtOAC:Hex:TEA 49:50:1 and the filtrate evaporated in *vacuo* to give a yellow powdery solid (0.26g 60%); (R_f. =0.63 50% pet ether 50%); δ_H (300 MHz, CD_3CN) 8.29 (1H, s, *H14*), 8.23-8.28 (2H, m, *H9*), 8.01-8.08 (2H, m, *H12*), 7.39-7.53 (4H, m, *H11* and *H22*), 7.25-7.33 (6H, m, *H10* and *H17*), 7.22 (3H, m, *H23* and *H24*), 6.80-6.91 (4H, m, *H18*), 6.19 (1H, dd, *J* = 15.4 and 9.2, N*H*), 4.10-4.23 (4H, m, OC*H*$_2$CH$_2$CH$_2$ *H6*, C*H*NH *H2* and CHC*H*OP *H1*), 3.75 (6H, s, OC*H*$_3$ *H20*), 3.49-3.63 (4H, m, POC*H*$_2$ *H30* and PNC*H* *H34*), 3.12 (2H, m, C*H*$_2$ODMT *H3*), 2.52 (2H, dt, *J* = 34.7 and 6.0, C*H*$_2$CN *H31*), 2.28 (2H, t, *J* = 7.3 C*H*$_2$CO *H25*), 1.92-2.06 (2H, m, C*H*$_2$CH$_2$CH$_2$CH$_2$CH$_2$CO *H29*), 1.62-1.79 (4H, m, C*H*$_2$CH$_2$CH$_2$CH$_2$CO *H28* and C*H*$_2$CH$_2$CO *H26*), 1.51 (2H, dd, *J* = 15.2 and 8.1, C*H*$_2$CH$_2$CH$_2$CO *H27*), 1.13 (12H, m, C*H*$_3$ *H33*), 0.99 (3H, d, *J* = 6.8, C*H*$_3$CHOP *H4*); δ_P (121 MHz, CD_3CN) 147.7, 147.0; *m/z* (ES+) calcd. for $C_{55}H_{66}O_7N_3NaP$ ($M+Na^+$) 934.4536, found 934.4558.

7.7.8 *n* = 6 D Phosphoramidite (6eD)

(2*S*,3*S*)-3-(7-(anthracen-9-yloxy)heptanamido)-4-(bis(4-methoxyphenyl)(phenyl)methoxy)butan-2-yl (2-cyanoethyl) diisopropylphosphoramidite

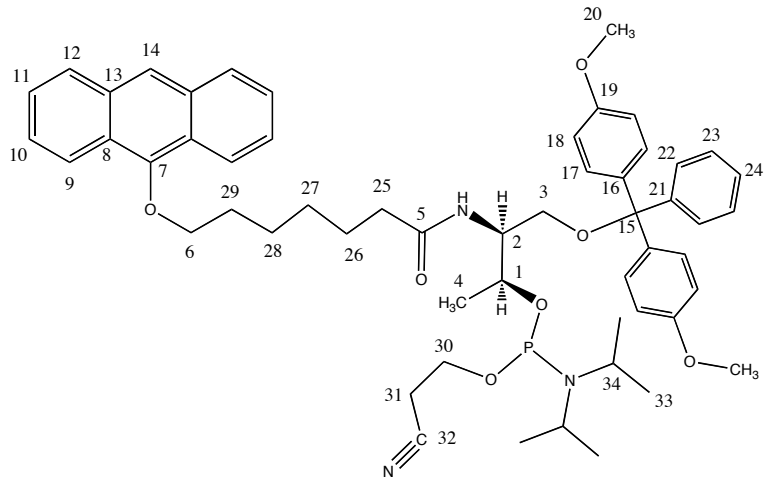

7-(Anthracen-9-yloxy)-*N*-((2*S*,3*S*)-1-(bis(4-methoxyphenyl)(phenyl)methoxy)-3-hydroxybutan-2-yl)heptanamide (0.3 g, 0.42 mmol) placed in a 25 mL round-bottomed flask with a stirrer bar and a septum. The flask was evacuated and filled with argon three times and the solid dissolved in anhydrous DCM (15 mL). DIPEA (0.21 mL, 1.3 mmol) was added and the solution stirred at room temp. in the absence of light. *2*-Cyanoethyl-diisopropylchlorophosphoramidite (0.1 mL, 0.45 mmol) was added *via* a disposable syringe dropwise and the reaction stirred for 1 hr. The soln. was then transferred to a 25 mL round-bottomed flask containing a stirrer bar and solid-supported BnOH (0.25 g) and left to stir for 1 hr in the absence of light. The soln. was diluted with EtOAc (10 mL), filtered and then washed with 2 M Na_2CO_3 (a.q.) soln. (2 x 50 mL) and brine (1 x 50 mL) and dried over Mg_2SO_4. The soln. was then columned through activated basic alumina with EtOAC:Hex:TEA 49:50:1 and the filtrate evaporated to give a yellow powdery solid (0.23 g, 59%); (R_f.

=0.63 50% pet ether 50%); δ_H (300 MHz, CD_3CN) 8.32 (1H, s, *H14*), 8.26-8.31 (2H, m, *H9*), 8.02-8.12 (2H, m, *H12*), 7.42-7.57 (4H, m, *H11* and *H22*), 7.26-7.38 (6H, m, *H10* and *H17*), 7.15-7.24 (3H, m, *H23* and *H24*), 6.80-6.91 (4H, m, *H18*), 6.19 (1H, dd, *J* = 15.4, and 9.2, N*H*), 4.10-4.23 (4H, m, OC*H*$_2$CH$_2$CH$_2$ *H6*, C*H*NH *H2* and CHC*H*OP *H1*), 3.75 (6H, s, OC*H*$_3$ *H20*), 3.49-3.63 (4H, m, POC*H*$_2$ *H30* and PNC*H* *H34*), 3.04-3.15 (2H, m, C*H*$_2$ODMT *H3*), 2.52 (2H, dt, *J* = 34.7 and 6.0, C*H*$_2$CN *H31*), 2.28 (2H, t, *J* = 7.3 C*H*$_2$CO *H25*), 1.99-2.06 (2H, m, C*H*$_2$CH$_2$CH$_2$CH$_2$CH$_2$CO *H29*), 1.62-1.79 (4H, m, C*H*$_2$CH$_2$CH$_2$CH$_2$CO *H28* and C*H*$_2$CH$_2$CO *H26*), 1.51 (2H, dd, *J* = 15.2 and 8.1, C*H*$_2$CH$_2$CH$_2$CO *H27*), 1.13 (12H, m, C*H*$_3$ *H33*), 0.99 (3H, d, *J* = 6.8, C*H*$_3$CHOP *H4*); δ_P (121 MHz, CD_3CN) 147.6, 146.9; *m/z* (ES+) calcd. for $C_{55}H_{66}O_7N_3NaP$ ($M+Na^+$) 934.4536, found 934.4573.

7.8 References

1. Hwang, T. L.; Shaka, A. J., *J. of Magnetic Resonance Series A* **1995,** *112* (2), 275-279.
2. Plateau, P.; Gueron, M., *J. Am. Chem. Soc.* **1982,** *104* (25), 7310-7311.
3. Molard, Y.; Bassani, D. M.; Desvergne, J. P.; Moran, N.; Tucker, J. H. R., *J. Org. Chem.* **2006,** *71* (22), 8523-8531.

Conclusions and further work

This project has encompassed the synthesis, characterization and study of a range of oligonucleotides that were modified by the inclusion of a non-nucleosidic anthracene unit.

This began with the synthesis of different stereoisomers of a non-nucleosidic backbone that were coupled to an anthracene unit *via* a short carbon chain linker (Fig. 201). This monomer was then coupled to DNA to synthesise a number of short (15-mer) oligonucleotide Probes using solid state DNA synthesis techniques which were then purified using RP-HPLC.

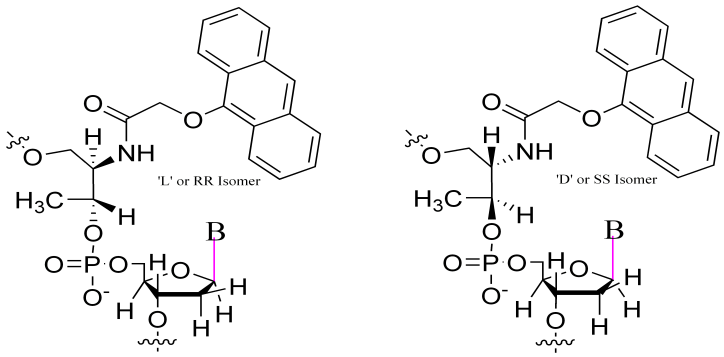

Fig. 201 Different diastereomers of anthracene tagged DNA

A range of complementary and mismatching DNA oligonucleotides were synthesized at the same time in order to create a library of duplexes.

Two systems were studied, the first a duplex with anthracene functioning as a non-bonding base opposite of a natural nucleobase and the second as a wedge type system.

These probes were studied using a variety of physical techniques that included variable temperature UV, fluorescence and CD spectroscopy in order to understand the effect of varying base pairs and introducing mismatches.

Fluorescence titrations were performed to analyse the response of the anthracene to different (i.e. matched and mismatched) environments (Fig. 202).

A dependence on the stereoconfiguration of the Probe and the location of the mismatch was found, such that only a mismatch upstream of the probe on the *RR* isomer probe strand (red) was found to sense mismatches.

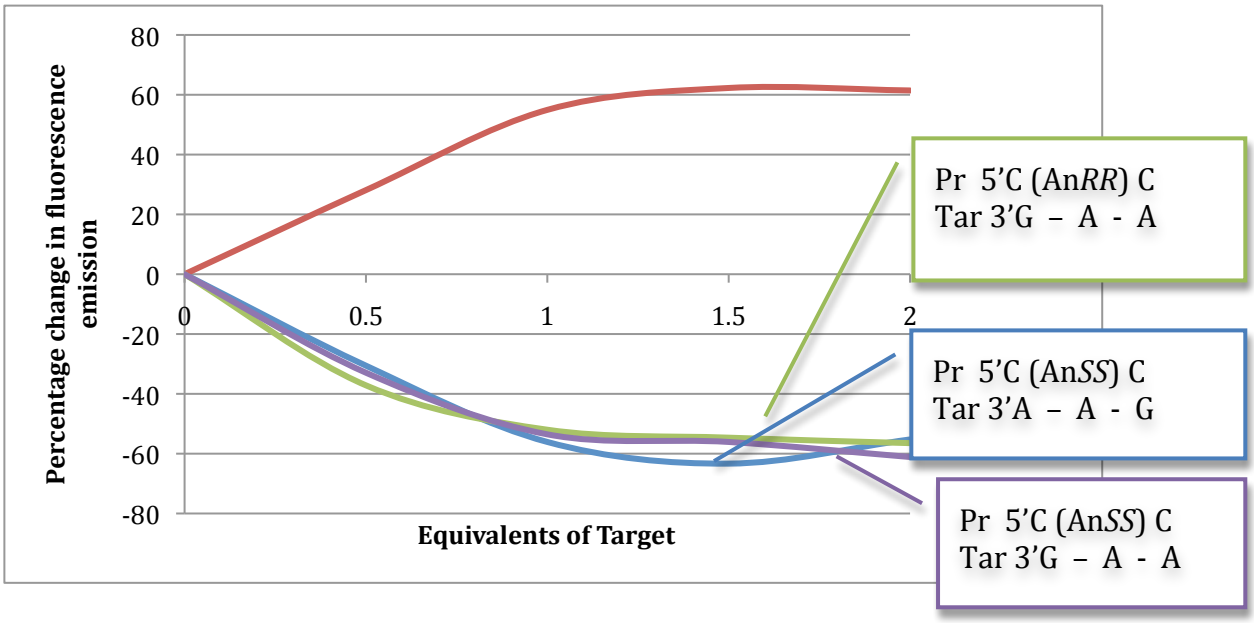

Fig. 202 Fluorescence titrations

This sensing ability and the studies on different matching and mismatching systems were used to synthesise a number of probes that were designed to detect SNPs involved in the onset of diabetes in humans.

Variable temperature UV spectroscopy was used to study and compare the stability of the different duplexes whilst CD spectroscopy was used to determine that the duplexes adopt the B form of DNA.

Based on the fluorescence titrations and lifetime measurements it was found that the anthracene is exposed to three different environments. Furthermore it was hypothesised that one of the lifetimes arose as a result of electron transfer processes. Simple thermodynamic calculations were performed to support this theory.

The PrA TarA1 and A2 fully matching duplexes (*RR* stereoisomer) were then studied in greater depth using transient absorption spectroscopy, to probe the

formation of electron transfer intermediates and by high field (900 MHz) NMR spectroscopy to look at the effect of intercalation of the anthracene between base pairs.

In order to rationalise the acquired data, molecular modelling studies of the system were undertaken using the AMBER modelling software in order to produce molecular dynamics optimised structures of the DNA duplex. The models proved to be very useful in establishing the structure of the duplex and the anthracene micro-environment. The models also helped to rationalise the upstream selectivity exhibited by the *RR* probe and the lack of sensing ability for the *SS* probe.

Further studies were undertaken by synthesising a full range of longer tether lengths and studying the effect of these changes on the properties of the duplex. These were shown to have the potential to discriminate between different bases directly opposite of the anthracene attachment through a variable fluorescence response upon hybridisation. Molecular modelling was used to explain the observed trends in melting point for the two stereoisomers as a consequence of increasing the carbon tether length.

Exciton coupling between anthracenes and formation of excimers in bis-anthracene systems of varying linker lengths was explored through the use of fluorescence and CD spectroscopy. This indicated that, in certain combinations of linker length and stereoisomer, there is some interaction between the anthracene moieties. However, in all cases there were no indications of the formation of anthracene excimers.

Further work will focus on the development of the n = 1 L nucleoside as a SNP sensor by targeting a number of known SNP sequences. As mentioned

previously, NMR studies are ongoing to further refine the structure of the duplex as well as transient absorption spectroscopy using shorter and stronger pulse lasers to try to visualise the quenching intermediates.

Work is also progressing on the creation of bisanthracene tagged oligonucleotides in which light can be used to control DNA hybridisation through the dimerisation of anthracene.

Appendix Table of Contents

Appendix 1 Synthesised DNA strands 4

A1.1 Unmodifed DNA Target strands 4
A1.1.1 Core sequence targets 4
A1.1.2 Modified Probe targets 4

A1.2 Anthracene Modified Strands *n* = 1 7
A1.2.1 Anthracene *n* = 1 L Isomer 7
A1.2.1.1 Core sequence 7
A1.2.1.2 Probe Modification – Downstream 7
A1.2.1.3 Probe Modification - Upstream 7
A1.2.1.4 Complementary modified strand 8
A1.2.2 Anthracene *n* = 1 D Isomer 8
A1.2.2.1 Core sequence 8
A1.2.2.2 Probe Modification – Downstream 8
A1.2.2.3 Probe Modification - Upstream 9
A1.2.2.4 Complementary modified strand 9

A1.3 *n* = 3 Linker 9
A1.3.1 Anthracene *n* = 3 L isomer 9
A1.3.1.1 Core sequence 9
A1.3.1.2 Probe Modification – Downstream 9
A1.3.1.3 Probe Modification - Upstream 10
A1.3.1.4 Complementary modified strand 10
A1.3.2 Anthracene *n* = 3 D isomer 11
A1.3.2.1 Core sequence 11
A1.3.2.2 Probe Modification – Downstream 11
A1.3.2.3 Probe Modification - Upstream 11
A1.3.2.4 Complementary modified strand 12

A1.4 *n* = 4 Linker 12
A1.4.1 Anthracene *n* = 4 L isomer 12
A1.4.1.1 Core sequence 12
A1.4.1.2 Complementary modified strand 12
A1.4.2 Anthracene *n* = 4 D isomer 12
A1.4.2.1 Core sequence 12

A1.5 *n* = 5 Linker 13
A1.5.1 Anthracene *n* = 5 L 13
A1.5.1.1 Core Sequence 13
A1.5.1.2 Probe Modification – Downstream 13
A1.5.1.3 Probe Modification - Upstream 13
A1.5.1.4 Complementary modified strand 14
A1.5.2 Anthracence *n* = 5 D 14
A1.5.2.1 Core sequence 14
A1.5.2.2 Probe Modification – Downstream 14
A1.5.2.3 Probe Modification - Upstream 14
A1.5.2.4 Complementary modified strand 15

A1.6 *n* = 6 Linker **15**
A1.6.1 Anthracene *n* = 6 L **15**
A1.6.1.1 Core Sequence 15
A1.6.1.2 Probe Modification – Downstream 15
A1.6.1.3 Probe Modification - Upstream 16
A1.6.1.4 Complementary modified strand 16
A1.6.2 Anthracene *n* = 6 D **17**
A1.6.2.1 Core sequence 17
A1.6.2.2 Probe Modification – Downstream 17
A1.6.2.3 Probe Modification - Upstream 17
A1.6.2.4 Complementary modified strand 18
A1.7 SNP Probes **18**
Appendix 2 Fluorescence Measurements **20**
A2.1 Quantum yields **20**
A2.1.1 Single strand quantum yields **20**
A2.1.1.1 *n* = 1 single strand quantum yields 20
A2.1.1.2 *n* = x single strand quantum yields 21
A2.1.2 Hybridised quantum yields **21**
A2.1.2.1 Hybridised quantum yields *n* = 1 21
A2.1.2.2 Hybridised quantum yields *n* = x 23
A2.2 Fluorescence titrations **24**
A2.2.1 *n* = 1 ..... **24**
A2.2.2 *n* = x **26**
A2.3 Fluorescence lifetimes **28**
A2.3.1 Fluorescence lifetimes for *n* = 1 single strands **28**
A2.3.2 *n* = x single strand fluorescence lifetimes **29**
A2.3.3 *n* = 1 hybridised fluorescence lifetimes **29**
A2.3.3.1 Base opposite matching 29
A2.3.3.2 *n* = 1 Base opposite Probe A mismatching 30
A2.3.3.3 *n* = 1 Base opposite mismatching – L isomer Probe varied target fixed 30
A2.3.3.3 *n* = 1 deletion matching and mismatching 31
A2.3.4 Fluorescent Lifetimes *n* = x hybridized **31**
A2.3.4.1 *n* = x Base opposite matching adenine only 31
A2.3.4.2 *n* = 3 and 6 Base opposite varied 32
A2.3.4.3 *n* = x deletion matching 32
A2.3.6 *n* = x mismatch **33**
A2.3.7 Degassed samples **33**
A2.3.8 Bisanthracene duplexes **33**
A2.3.8 SNP Probes **33**
Appendix 3 Melting Points **34**
A3.1 Single anthracene systems **34**
A3.1.1 Unmodified DNA **34**
A3.1.1.1 Base opposite system 34
A3.1.1.2 Deletion system 34
A3.1.2 Matching base opposite duplex melting temperatures **35**
A3.1.3 Matching deletion duplex melting temperatures **35**
A3.1.4 Mismatching base opposite duplex melting temperatures **35**
A3.1.5 Mismatching deletion duplex melting points **36**
A3.1.6 SNP Probes **36**

A3.2 Bisanthracene systems **37**
A3.2.1 Facing bis anthracene systems **37**
A3.2.2 Stacking bisanthracene systems **37**
Appendix 4 ..... **38**
A4.1 Application of the Rehm-Weller Equation **38**
A4.1.1 Pyrimidines **38**
A4.1.2 Purines **38**

Appendix 1 Synthesised DNA strands

A1.1 Unmodified DNA Target strands

A1.1.1 Core sequence targets

Target A1 5'-CATTGAG(A)GAGTCCA – 3'
m/z Calculated for $C_{147}H_{185}N_{60}O_{86}P_{14}^{+}$ (M + H^+) 4602 Found (MALDI-Tof) 4605
Ret. Time 15.24 min
ε value (M-1) 153900 M^{-1}
Yield: 0.46 µmol 46%

Target A2 5'-CATTGAG__GAGTCCA-3'
m/z Calculated for $C_{137}H_{160}N_{55}O_{81}P_{13}^{+}$ (M + H^+) 4275.7 Found (MALDI-Tof)4276
Ret. Time 15.07
ε value 140700 M^{-1}
Yield: 0.40 µmol 40%

Target A3 5'-CATTGAG(T)GAGTCCA-3'
m/z Calculated for $C_{147}H_{186}N_{57}O_{88}P_{14}^{+}$ (M + H^+) 4593 Found (MALDI-Tof) 4597
Ret. Time 15.41 min
ε value 149400 M^{-1}
Yield: 0.43 µmol 43%

Target A4 5'-CATTGAG(C)GAGTCCA-3'
m/z Calculated for $C_{146}H_{185}N_{58}O_{87}P_{14}^{+}$ (M + H^+) 4578 Found (MALDI-Tof) 4581
Ret. Time 15.45 min
ε value 147300 M^{-1}
Yield: 0.30 µmol 30%

Target A5 5'-CATTGAG(G)GAGTCCA-3'
m/z Calculated for $C_{146}H_{185}N_{58}O_{88}P_{14}Na^{+}$ (M + H^+ +Na^+) 4617 Found (MALDI-Tof) 4622
Ret. Time 15.22 min
ε value 150800 M^{-1}
Yield: 0.40 µmol 40%

A1.1.2 Modified Probe targets

Target B1 CATTGAC(A)GAGTCCA – 3'
m/z Calculated for $C_{146}H_{185}N_{58}O_{86}P_{14}^{+}$ (M + H^+) 4562 Found (MALDI-Tof) 4565
Ret. Time 15.00 min
ε value 150200 M^{-1}
Yield: 0.31 µmol 31%

Target B2 5'CATTGAC__GAGTCCA – 3'
m/z Calculated for $C_{136}H_{172}N_{53}O_{81}P_{13}^-$ (M -H$^+$) 4247 Found (MALDI-Tof) 4239
Ret. Time 15.62 min
ε value 137400 M^{-1}
Yield: 0.42 µmol 42%

Target C1 5'CATTGAT(A)GAGTCCA – 3'
m/z Calculated for $C_{147}H_{186}N_{57}O_{87}P_{14}^+$ (M + H$^+$) 4577 Found (MALDI-Tof) 4579
Ret. Time 15.54 min
ε value 152700 M^{-1}
Yield: 0.35 µmol 35%

Target C2 5'CATTGAT__GAGTCCA – 3'
m/z Calculated for $C_{137}H_{167}N_{52}O_{82}P_{13}^-$ (M - H$^+$) 4262 Found (MALDI-Tof) 4255
Ret. Time 15.49 min
ε value 138700 M^{-1}
Yield: 0.44 µmol 44%

Target D1 5'CATTGAA(A)GAGTCCA – 3'
m/z Calculated for $C_{147}H_{185}N_{60}O_{85}P_{14}^+$ (M + H$^+$) 4586 Found (MALDI-Tof) 4588
Ret. Time 15.32 min
ε value 154600 M^{-1}
Yield: 0.41 µmol 41%

Target D2 5'CATTGAA__GAGTCCA – 3'
m/z Calculated for $C_{137}H_{172}N_{55}O_{80}P_{13}^+$ (M + H$^+$) 4273 Found (MALDI-Tof) 4263
Ret. Time 15.09 min
ε value 142600 M^{-1}
Yield: 0.39 µmol 39%

Target E1 CATTGAG(A)CAGTCCA – 3'
m/z Calculated for $C_{146}H_{185}N_{58}O_{86}P_{14}^+$ (M + H$^+$) 4562 Found (MALDI-Tof) 4565
Ret. Time 15.03 min
ε value 150200 M^{-1}
Yield: 0.49 µmol 49%

Target E2 CATTGAG__CAGTCCA – 3'
m/z Calculated for $C_{136}H_{172}N_{53}O_{81}P_{13}^-$ (M -H$^+$) 4247 Found (MALDI-Tof) 4242
Ret. Time 15.59 min
ε value 136800 M^{-1}
Yield: 0.44 µmol 44%

Target F1 5'CATTGAG(A)TAGTCCA – 3'
m/z Calculated for $C_{147}H_{186}N_{57}O_{87}P_{14}^+$ (M + H$^+$) 4577 Found (MALDI-Tof) 4579
Ret. Time 15.47 min
ε value 152700 M^{-1}
Yield: 0.39 µmol 39%

Target F2 5'CATTGAG___TAGTCCA – 3'
m/z Calculated for $C_{137}H_{167}N_{52}O_{82}P_{13}^-$ (M - H^+) 4262 Found (MALDI-Tof) 4252
Ret. Time 15.43 min
ε value 140100 M^{-1}
Yield: 0.43 µmol 43%

Target G1 5'CATTGAG(A)AAGTCCA – 3'
m/z Calculated for $C_{147}H_{185}N_{60}O_{85}P_{14}^+$ (M + H^+) 4586 Found (MALDI-Tof) 4588
Ret. Time 15.31 min
ε value 154600 M^{-1}
Yield: 0.38 µmol 38%

Target G2 5'CATTGAG___AAGTCCA – 3'
m/z Calculated for $C_{137}H_{172}N_{55}O_{80}P_{13}^+$ (M + H^+) 4273 Found (MALDI-Tof) 4264
Ret. Time 15.01 min
ε value 142600 M^{-1}
Yield: 0.36 µmol 36%

Target MT 5'-TGGACTCTCTCAATG -3'
m/z Calculated for $C_{147}H_{184}N_{57}O_{88}P_{14}^-$ (M - H^+) 4591 Found (ES-) 4592
Ret. Time 15.31 min
ε value 154600 M^{-1}
Yield: 0.11 µmol 11%

Target MA 5'-TGGACTCACTCAATG -3'
m/z Calculated for $C_{147}H_{183}N_{60}O_{86}P_{14}^-$ (M - H^+) 4600 Found (ES-) 4602
Ret. Time 15.31 min
ε value 142300 M^{-1}
Yield: 0.19 µmol 19%

Target 2MM 5'CATTGAG(A)AAATCCA – 3'
m/z Calculated for $C_{147}H_{184}N_{57}O_{87}P_{14}^-$ (M - H^+) 4575 Found (ES-) 4577
Ret. Time 15.31 min
ε value 155900 M^{-1}
Yield: 0.10 µmol 10%

A1.2 Anthracene Modified Strands *n* = 1

A1.2.1 Anthracene *n* = 1 L Isomer

A1.2.1.1 Core sequence

n = 1 L Probe A: 5'-TGGACTC(X)CTCAATG -3'
m/z Calculated for $C_{156}H_{192}N_{51}O_{89}P_{14}^{1+}$ $(M + H)^+$ 4638.8 Found (MALDI-Tof) 4639
Ret. Time 23.86 min
ε value 181344 M^{-1}
Yield: 6.96 µmol 58%

A1.2.1.2 Probe Modification – Downstream

n = 1 L Probe B: 5'-TGGACTC(X)GTCAATG -3'
m/z Calculated for $C_{155}H_{194}N_{51}O_{89}P_{14}^{1+}$ $(M + H^+)$ 4681.1 Found (MALDI-Tof) 4681
Ret. Time 24.38 min
ε value 185444 M^{-1}
Yield: 0.49 µmol 49%

n = 1 L Probe C: 5'-TGGACTC(X)ATCAATG -3'
m/z Calculated for $C_{155}H_{193}N_{51}O_{88}P_{14}$ (M) 4664.1 Found (MALDI-Tof) 4662
Ret. Time 23.24 min
ε value 187544 M^{-1}
Yield: 0.47 µmol 47%

n = 1 L Probe D: 5'-TGGACTC(X)TTCAATG -3' – T instead of C next to X 3' end
m/z Calculated for $C_{157}H_{193}N_{50}O_{90}P_{14}^{-}$ $(M - H^+)$ 4653.7 Found (MALDI-Tof) 4654
Ret. Time 24.10 min
ε value 182244 M^{-1}
Yield: 0.41 µmol 41%

A1.2.1.3 Probe Modification - Upstream

n = 1 L Probe E: 5'-TGGACTG(X)CTCAATG -3'
m/z Calculated for $C_{155}H_{192}N_{51}O_{89}P_{14}^{-}$ $(M - H^+)$ 4679.1 Found (MALDI-Tof) 4679
Ret. Time 23.11 min
ε value 183044 M^{-1}
Yield: 0.42 µmol 42%

n = 1 L Probe F: 5'-TGGACTA(X)CTCAATG -3'
m/z Calculated for $C_{157}H_{192}N_{53}O_{88}P_{14}$ $(M - H^+)$ 4663.0 Found (MALDI-Tof) 4663
Ret. Time 22.91 min
ε value 187144 M^{-1}
Yield: 0.45 µmol 45%

n = 1 L Probe G: 5'-TGGACTT(X)CTCAATG -3'
m/z Calculated for $C_{157}H_{192}N_{50}O_{90}P_{14}^-$ (M -H^+) 4653.7 Found (MALDI-Tof) 4654
Ret. Time 23.30 min
ε value 182244 M^{-1}
Yield: 0.40 µmol 40%

A1.2.1.4 Complementary modified strand

n = 1 L Probe M: 5' 5' CATTGAGXGAGTCCA -3'
m/z Calculated for $C_{157}H_{194}N_{56}O_{87}P_{14}^{2+}$ (M) 4689 Found (MALDI-Tof) 4689
Ret. Time 21.27 min
ε value 192144 M^{-1}
Yield: 0.33 µmol 33%

A1.2.2 Anthracene *n* = 1 D Isomer

A1.2.2.1 Core sequence

n = 1 D Probe A: 5'-TGGACTC(X)CTCAATG -3'
m/z Calculated for $C_{156}H_{192}N_{51}O_{89}P_{14}^-$ (M –H^+) 4639 Found (ES-) 4640
Ret. Time 21.92
ε value 181344 M^{-1}
Yield: 0.12 µmol 12%

A1.2.2.2 Probe Modification – Downstream

n = 1 D Probe B: 5'-TGGACTC(X)GTCAATG -3'
m/z Calculated for $C_{155}H_{192}N_{51}O_{89}P_{14}^-$ (M - H^+) 4679.1 Found (MALDI-Tof)/(ES -) 4681
Ret. Time 22.65 min
ε value 185444 M^{-1}
Yield: 0.07 µmol 7%

n = 1 D Probe C: 5'-TGGACTC(X)ATCAATG -3'
m/z Calculated for $C_{155}H_{193}N_{51}O_{88}P_{14}$ (M) 4664.1 Found (MALDI-Tof) 4664 (ES-)4665
Ret. Time 23.40 min
ε value 187544 M^{-1}
Yield: 0.04 µmol 4%

n = 1 D Probe D: 5'-TGGACTC(X)TTCAATG -3'
m/z Calculated for $C_{157}H_{193}N_{50}O_{90}P_{14}^-$ (M -H^+) 4653.7 Found (MALDI-Tof) 4655
Ret. Time 23.10 min
ε value 182244 M^{-1}
Yield: 0.02 µmol 2%

A1.2.2.3 Probe Modification - Upstream

n = 1 D Probe E: 5'-TGGACTG(X)CTCAATG -3'
m/z Calculated for $C_{155}H_{194}N_{51}O_{89}P_{14}^-$ (M + H^+) 4681.1 Found (MALDI-Tof) 4681
Ret. Time 22.58 min
ε value 183044 M^{-1}
Yield: 0.10 µmol 10%

n = 1 D Probe F: 5'-TGGACTA(X)CTCAATG -3'
m/z Calculated for $C_{157}H_{194}N_{53}O_{88}P_{14}$ (M + H^+) 4665.1 Found (MALDI-Tof) 4665
Ret. Time 23.30 min
ε value 187144 M^{-1}
Yield: 0.11 µmol 11%

n = 1 D Probe G: 5'-TGGACTT(X)CTCAATG -3'
m/z Calculated for $C_{157}H_{195}N_{50}O_{90}P_{14}^+$ (M + H^+) 4655.7 Found (MALDI-Tof) 4657
Ret. Time 23.03 min
ε value 182244 M^{-1}
Yield: 0.03 µmol 3%

A1.2.2.4 Complementary modified strand

n = 1 D Probe M: 5' CATTGAG(X)GAGTCCA -3'
m/z Calculated for $C_{157}H_{195}N_{56}O_{87}P_{14}^+$(M +$H^+$) 4690 Found (MALDI-Tof) 4689
Ret. Time 21.02 min
ε value 192144 M^{-1}
Yield: 0.05 µmol 5%

A1.3 *n* = 3 Linker

A1.3.1 Anthracene *n* = 3 L isomer

A1.3.1.1 Core sequence

n = 3 L Probe A: 5'-TGGACTC(X)CTCAATG -3'
m/z Calculated for $C_{158}H_{196}N_{51}O_{89}P_{14}^-$ (M – H^+) 4667 Found (ES-) 4668
Ret. Time 25.46 min
ε value 181344 M^{-1}
Yield: 0.65 µmol 65%

A1.3.1.2 Probe Modification – Downstream

n = 3 L Probe B: 5'-TGGACTC(X)GTCAATG -3'
m/z Calculated for $C_{159}H_{196}N_{53}O_{89}P_{14}^-$ (M - H^+) 4707 Found (ES-) 4707
Ret. Time 26.54 min

ε value 185444 M^{-1}
Yield: 0.28 µmol 28%

n = 3 L Probe C: 5'-TGGACTC(X)ATCAATG -3'
m/z Calculated for $C_{159}H_{196}N_{53}O_{88}P_{14}^-$ (M -H^+) 4691 Found (ES-) 4692
Ret. Time 25.71 min
ε value 187544 M^{-1}
Yield: 0.61 µmol 61%

n = 3 L Probe D: 5'-TGGACTC(X)TTCAATG -3'
m/z Calculated for $C_{159}H_{197}N_{50}O_{90}P_{14}^-$ (M - H^+) 4682 Found (ES-) 4684
Ret. Time 25.95 min
ε value 182244 M^{-1}
Yield: 0.42 µmol 42%

A1.3.1.3 Probe Modification - Upstream

n = 3 L Probe E: 5'-TGGACTG(X)CTCAATG -3'
m/z Calculated for $C_{159}H_{196}N_{53}O_{89}P_{14}^-$ (M - H^+) 4707 Found (ES-) 4709
Ret. Time 25.41 min
ε value 183044 M^{-1}
Yield: 0.72 µmol 72%

n = 3 L Probe F: 5'-TGGACTA(X)CTCAATG -3'
m/z Calculated for $C_{159}H_{196}N_{53}O_{88}P_{14}^-$ (M -H^+) 4691 Found (ES-) 4693
Ret. Time 25.44 min
ε value 187144 M^{-1}
Yield: 0.68 µmol 68%

n = 3 L Probe G: 5'-TGGACTT(X)CTCAATG -3'
m/z Calculated for $C_{159}H_{197}N_{50}O_{90}P_{14}^-$ (M - H^+) 4682 Found (ES-) 4684
Ret. Time 25.67 min
ε value 182244 M^{-1}
Yield: 0.73 µmol 73%

A1.3.1.4 Complementary modified strand

n = 3 L Probe M: 5' 5' CATTGAG(X)GAGTCCA -3'
m/z Calculated for $C_{159}H_{195}N_{56}O_{87}P_{14}^-$(M – H^+) 4716 Found (ES-) 4718
Ret. Time 25.30 min
ε value 192144 M^{-1}
Yield: 0.48 µmol 48%

A1.3.2 Anthracene *n* = 3 D isomer

A1.3.2.1 Core sequence

n = 3 D Probe A: 5'-TGGACTC(X)CTCAATG -3'
m/z Calculated for $C_{158}H_{196}N_{51}O_{89}P_{14}^-$ (M – H^+) 4667 Found (ES-) 4668
Ret. Time 25.63
ε value 181344 M^{-1}
Yield: 0.73 µmol 73%

A1.3.2.2 Probe Modification – Downstream

n = 3 D Probe B: 5'-TGGACTC(X)GTCAATG -3'
m/z Calculated for $C_{159}H_{196}N_{53}O_{89}P_{14}^-$ (M - H^+) 4707 Found (ES-) 4708
Ret. Time 25.82 min
ε value 185444 M^{-1}
Yield: 0.92 µmol 92%

n = 3 D Probe C: 5'-TGGACTC(X)ATCAATG -3'
m/z Calculated for $C_{159}H_{196}N_{53}O_{88}P_{14}^-$ (M -H^+) 4691 Found (ES-) 4693
Ret. Time 25.79 min
ε value 187544 M^{-1}
Yield: 0.69 µmol 69%

n = 3 D Probe D: 5'-TGGACTC(X)TTCAATG -3'
m/z Calculated for $C_{159}H_{197}N_{50}O_{90}P_{14}^-$ (M - H^+) 4682 Found (ES-) 4683
Ret. Time 25.92 min
ε value 182244 M^{-1}
Yield: 0.95 µmol 95%

A1.3.2.3 Probe Modification - Upstream

n = 3 D Probe E: 5'-TGGACTG(X)CTCAATG -3'
m/z Calculated for $C_{159}H_{196}N_{53}O_{89}P_{14}^-$ (M - H^+) 4707 Found (ES-) 4709
Ret. Time 25.63 min
ε value 183044 M^{-1}
Yield: 0.90 µmol 90%

n = 3 D Probe F: 5'-TGGACTA(X)CTCAATG -3'
m/z Calculated for $C_{159}H_{196}N_{53}O_{88}P_{14}^-$ (M -H^+) 4691 Found (ES-) 4693
Ret. Time 25.75 min
ε value 187144 M^{-1}
Yield: 0.84 µmol 84%

n = 3 D Probe G: 5'-TGGACTT(X)CTCAATG -3'
m/z Calculated for $C_{159}H_{197}N_{50}O_{90}P_{14}^-$ (M - H^+) 4682 Found (ES-) 4694
Ret. Time 25.80 min
ε value 182244 M^{-1}
Yield: 0.82 µmol 82%

A1.3.2.4 Complementary modified strand

n = 3 D Probe M: 5’ 5' CATTGAG(X)GAGTCCA -3’
m/z Calculated for $C_{159}H_{195}N_{56}O_{87}P_{14}^-$(M – H^+) 4716 Found (ES-) 4717
Ret. Time 25.62 min
ε value 192144 M^{-1}
Yield: 0.46 µmol 46%

A1.4 *n* = 4 Linker

A1.4.1 Anthracene *n* = 4 L isomer

A1.4.1.1 Core sequence

n = 4 L Probe A: 5’-TGGACTC(X)CTCAATG -3’
m/z Calculated for $C_{159}H_{198}N_{51}O_{89}P_{14}^-$ (M – H^+) 4681 Found (ES-) 4682
Ret. Time 26.57 min
ε value 181344 M^{-1}
Yield: 0.46 µmol 46%

A1.4.1.2 Complementary modified strand

n = 4 L Probe M: 5’ 5' CATTGAGXGAGTCCA -3’
m/z Calculated for $C_{160}H_{197}N_{57}O_{87}P_{14}^-$(M -$H^+$) 4717 Found (ES-) 4717
Ret. Time 25.30 min
ε value 192144 M^{-1}
Yield: 0.24 µmol 24%

A1.4.2 Anthracene *n* = 4 D isomer

A1.4.2.1 Core sequence

n = 4 D Probe A: 5’-TGGACTC(X)CTCAATG -3’
m/z Calculated for $C_{159}H_{198}N_{51}O_{89}P_{14}^-$ (M – H^+) 4681 Found (ES-) 4682
Ret. Time 25.1
ε value 181344 M^{-1}
Yield: 0.48 µmol 48%

A1.5 *n* = 5 Linker

A1.5.1 Anthracene *n* = 5 L

A1.5.1.1 Core Sequence

n = 5 L Probe A: 5'-TGGACTC(X)CTCAATG -3'
m/z Calculated for $C_{160}H_{200}N_{51}O_{89}P_{14}^-$ (M – H^+) 4695 Found (ES-) 4696
Ret. Time 26.4 min
ε value 181344 M^{-1}
Yield: 0.44 µmol 44%

A1.5.1.2 Probe Modification – Downstream

n = 5 L Probe B: 5'-TGGACTC(X)GTCAATG -3'
m/z Calculated for $C_{161}H_{200}N_{53}O_{89}P_{14}^-$ (M – H^+) 4733 Found (ES-) 4737
Ret. Time 28.17 min
ε value 185444 M^{-1}

n = 5 L Probe C: 5'-TGGACTC(X)ATCAATG -3'
m/z Calculated for $C_{161}H_{200}N_{53}O_{88}P_{14}^-$ (M –H^+) 4719 Found (ES-) 4721
Ret. Time 27.26 min
ε value 187544 M^{-1}

n = 5 L Probe D: 5'-TGGACTC(X)TTCAATG -3'
m/z Calculated for $C_{161}H_{201}N_{50}O_{90}P_{14}^-$(M – H^+) 4710 Found (ES-) 4712
Ret. Time 27.26 min
ε value 182244 M^{-1}

A1.5.1.3 Probe Modification - Upstream

n = 5 L Probe E: 5'-TGGACTG(X)CTCAATG -3'
m/z Calculated for $C_{161}H_{200}N_{53}O_{89}P_{14}^-$(M – H^+) 4735 Found (ES-) 4735
Ret. Time 27.24 min
ε value 183044 M^{-1}
Yield: 0.39 µmol 39%

A1.5.1.4 Complementary modified strand

n = 5 L Probe M: 5’ 5' CATTGAGXGAGTCCA -3’
m/z Calculated for $C_{161}H_{199}N_{56}O_{87}P_{14}^-$(M – H^+) 4745 Found (ES -) 4746
Ret. Time 26.79 min
ε value 192144 M^{-1}
Yield: 0.24 µmol 24%

A1.5.2 Anthracene *n* = 5 D

A1.5.2.1 Core sequence

n = 5 D Probe A: 5’-TGGACTC(X)CTCAATG -3’
m/z Calculated for $C_{160}H_{200}N_{51}O_{89}P_{14}^-$ (M – H^+) 4695 Found (ES-) 4697
Ret. Time 26.94 min
ε value 181344 M^{-1}
Yield: 0.53 µmol 53%

A1.5.2.2 Probe Modification – Downstream

n = 5 D Probe B: 5’-TGGACTC(X)GTCAATG -3’
m/z Calculated for $C_{161}H_{200}N_{53}O_{89}P_{14}^-$ (M – H^+) 4733 Found (ES-) 4737
Ret. Time 27.22 min
ε value 185444 M^{-1}
Yield: 0.72 µmol 72%

n = 5 D Probe C: 5’-TGGACTC(X)ATCAATG -3’
m/z Calculated for $C_{161}H_{199}N_{53}O_{88}P_{14}Na^-$ (M –H^++Na^+) 4741 Found (ES-) 4742
Ret. Time 27.00 min
ε value 187544 M^{-1}
Yield: 0.45 µmol 45%

n = 5 D Probe D: 5’-TGGACTC(X)TTCAATG -3’
m/z Calculated for $C_{161}H_{201}N_{50}O_{90}P_{14}^-$ (M – H^+) 4710 Found (ES-) 4712
Ret. Time 27.06 min
ε value 182244 M^{-1}
Yield: 0.83 µmol 83%

A1.5.2.3 Probe Modification - Upstream

n = 5 D Probe E: 5’-TGGACTG(X)CTCAATG -3’
m/z Calculated for $C_{161}H_{200}N_{53}O_{89}P_{14}^-$(M – H^+) 4735 Found (ES-) 4736
Ret. Time 27.05 min
ε value 183044 M^{-1}
Yield: 0.53 µmol 53%

n = 5 D Probe F: 5'-TGGACTA(X)CTCAATG -3'
m/z Calculated for $C_{161}H_{200}N_{53}O_{88}P_{14}^-$ (M – H^+) 4719 Found (ES-) 4720
Ret. Time 27.07 min
ε value 187144 M^{-1}
Yield: 0.60 µmol 60%

n = 5 D Probe G: 5'-TGGACTT(X)CTCAATG -3'
m/z Calculated for $C_{161}H_{201}N_{50}O_{90}P_{14}^-$ (M – H^+) 4711 Found (ES-) 4712
Ret. Time 27.04 min
ε value 182244 M^{-1}
Yield: 0.60 µmol 60%

A1.5.2.4 Complementary modified strand

n = 5 D Probe M: 5' 5' CATTGAG(X)GAGTCCA -3'
m/z Calculated for $C_{161}H_{199}N_{56}O_{87}P_{14}^-$ (M – H^+) 4745 Found (ES-) 4746
Ret. Time 26.85 min
ε value 192144 M^{-1}
Yield: 0.74 µmol 74%

A1.6 *n* = 6 Linker

A1.6.1 Anthracene *n* = 6 L

A1.6.1.1 Core Sequence

n = 6 L Probe A: 5'-TGGACTC(X)CTCAATG -3'
m/z Calculated for $C_{161}H_{202}N_{51}O_{89}P_{14}^-$ (M – H^+) 4709 Found (ES-) 4710
Ret. Time 28.08 min
ε value 181344 M^{-1}
Yield: 0.40 µmol 40%

A1.6.1.2 Probe Modification – Downstream

n = 6 L Probe B: 5'-TGGACTC(X)GTCAATG -3'
m/z Calculated for $C_{162}H_{202}N_{53}O_{89}P_{14}^-$(M -$H^+$) 4749 Found (ES-) 4750
Ret. Time 28.46 min
ε value 185444 M^{-1}
Yield: 0.47 µmol 47%

n = 6 L Probe C: 5'-TGGACTC(X)ATCAATG -3'
m/z Calculated for $C_{162}H_{202}N_{53}O_{88}P_{14}^-$(M -$H^+$) 4733 Found (ES-) 4734
Ret. Time 28.08 min
ε value 187544 M^{-1}

Yield: 0.54 µmol 54%

n = 6 L Probe D: 5'-TGGACTC(X)TTCAATG -3'
m/z Calculated for $C_{162}H_{203}N_{50}O_{90}P_{14}^-$ (M -H^+) 4724 Found (ES-) 4724
Ret. Time 28.15 min
ε value 182244 M^{-1}
Yield: 0.47 µmol 47%

A1.6.1.3 Probe Modification - Upstream

n = 6 L Probe E: 5'-TGGACTG(X)CTCAATG -3'
m/z Calculated for $C_{162}H_{202}N_{53}O_{89}P_{14}^-$ (M -H^+) 4749 Found (ES-) 4749
Ret. Time 28.15 min
ε value 183044 M^{-1}
Yield: 0.50 µmol 50%

n = 6 L Probe F: 5'-TGGACTA(X)CTCAATG -3'
m/z Calculated for $C_{162}H_{202}N_{53}O_{88}P_{14}^-$ (M -H^+) 4733 Found (ES-) 4733
Ret. Time 28.21min
ε value 187144 M^{-1}
Yield: 0.43 µmol 43%

n = 6 L Probe G: 5'-TGGACTT(X)CTCAATG -3'
m/z Calculated for $C_{162}H_{203}N_{50}O_{90}P_{14}^-$ (M -H^+) 4724 Found (ES-)4724
Ret. Time 28.34 min
ε value 182244 M^{-1}
Yield: 0.32 µmol 32%

A1.6.1.4 Complementary modified strand

n = 6 L Probe M: 5' 5' CATTGAG(X)GAGTCCA -3'
m/z Calculated for $C_{161}H_{203}N_{56}O_{87}P_{14}^-$(M -$H^+$) 4745.8 Found (ES-) 4747
Ret. Time 28.32 min
ε value 192144 M^{-1}
Yield: 0.38 µmol 38%

n = 6 L Probe MG: 5' 5' CATTGAGA(X)AGTCCA -3'
m/z Calculated for $C_{162}H_{201}N_{56}O_{86}P_{14}^-$(M -$H^+$) 4742 Found (ES-) 4742
Ret. Time 28.13
ε value 142600 M^{-1}
Yield: 0.43 µmol 43%

n = 6 L Probe MS: 5' 5' CATTGAGAG(X)GTCCA -3'
m/z Calculated for $C_{162}H_{201}N_{56}O_{87}P_{14}^-$ (M -H^+) 4745 Found (ES-) 4747
Ret. Time 28.13 min
ε value 140700 M^{-1}
Yield: 0.40 µmol 40%

A1.6.2 Anthracene *n* = 6 D

A1.6.2.1 Core sequence

n = 6 D Probe A: 5'-TGGACTC(X)CTCAATG -3'
m/z Calculated for $C_{161}H_{202}N_{51}O_{89}P_{14}^-$ (M -H^+) 4709 Found (ES-) 4711
Ret. Time 28.02 min
ε value 181344 M^{-1}
Yield: 0.35 µmol 35%

A1.6.2.2 Probe Modification – Downstream

n = 6 D Probe B: 5'-TGGACTC(X)GTCAATG -3'
m/z Calculated for $C_{162}H_{202}N_{53}O_{89}P_{14}^-$(M -$H^+$) 4749 Found (ES-) 4751
Ret. Time 28.48 min
ε value 185444 M^{-1}
Yield: 0.22 µmol 22%

n = 6 D Probe C: 5'-TGGACTC(X)ATCAATG -3'
m/z Calculated for $C_{162}H_{202}N_{53}O_{88}P_{14}^-$(M -$H^+$) 4733 Found (ES-) 4735
Ret. Time 28.13 min
ε value 187544 M^{-1}
Yield: 0.33 µmol 33%

n = 6 D Probe D: 5'-TGGACTC(X)TTCAATG -3'
m/z Calculated for $C_{162}H_{203}N_{50}O_{90}P_{14}^-$ (M -H^+) 4724 Found (ES-) 4726
Ret. Time 28.16 min
ε value 182244 M^{-1}
Yield: 0.21 µmol 21%

A1.6.2.3 Probe Modification - Upstream

n = 6 D Probe E: 5'-TGGACTG(X)CTCAATG -3'
m/z Calculated for $C_{162}H_{202}N_{53}O_{89}P_{14}^-$ (M -H^+) 4749 Found (ES-) 4751
Ret. Time 28.17 min
ε value 183044 M^{-1}
Yield: 0.23 µmol 23%

n = 6 D Probe F: 5'-TGGACTA(X)CTCAATG -3'
m/z Calculated for $C_{162}H_{202}N_{53}O_{88}P_{14}^-$ (M -H^+) 4733 Found (ES-) 4735
Ret. Time 28.25 min
ε value 187144 M^{-1}
Yield: 0.10 µmol 10%

n = 6 D Probe G: 5'-TGGACTT(X)CTCAATG -3'
m/z Calculated for $C_{162}H_{203}N_{50}O_{90}P_{14}^-$ (M -H^+) 4724 Found (ES-) 4726
Ret. Time 28.33 min

ε value 182244 M^{-1}
Yield: 0.29 µmol 29%

A1.6.2.4 Complementary modified strand

n = 6 D Probe M: 5' CATTGAG(X)GAGTCCA -3'
m/z Calculated for $C_{161}H_{203}N_{56}O_{87}P_{14}^-$(M -$H^+$) 4745.8 Found (ES-) 4746
Ret. Time 28.13
ε value 192144 M^{-1}
Yield: 0.14 µmol 14%

n = 6 D Probe MG: 5' CATTGAGAGA(X)TCCA -3'
m/z Calculated for $C_{162}H_{201}N_{56}O_{86}P_{14}^-$(M -$H^+$) 4742 Found (ES-) 4742
Ret. Time
ε value 142600 M^{-1}
Yield: 0.35 µmol 35%

n = 6 D Probe MS: 5' CATTGAGAG(X)GTCCA -3'
m/z Calculated for $C_{162}H_{201}N_{56}O_{87}P_{14}^-$(M -$H^+$) 4758 Found (ES-) 4758
Ret. Time
ε value 140700 M^{-1}
Yield: 0.44 µmol 44%

A1.7 SNP Probes

SNP Tar T 5' TAACTAGAAGGTGC - 3'
m/z Calculated for $C_{138}H_{151}N_{57}O_{83}P_{13}^-$(M -$H^+$) 4392 Found (ES-) 4394
Ret. Time
ε value 144000 M^{-1}
Yield: 0.28 µmol 28%

SNP Tar G 5' TAACTAGCAGGTGC-3'
m/z Calculated for $C_{137}H_{186}N_{55}O_{84}P_{13}^-$(M -$H^+$) 4368 Found (ES-) 4369
Ret. Time
ε value 138800 M^{-1}
Yield: 0.24 µmol 24%

n = 1 L SNP Probe T 5' GCACCTT(X)CTAGTTA- 3'
m/z Calculated for $C_{156}H_{193}N_{48}O_{90}P_{14}^-$(M -$H^+$) 4614 Found (ES-) 4616
Ret. Time 28.13
ε value 182644 M^{-1}
Yield: 0.43 µmol 43%

n = 1 L SNP Probe G 5’ GCACCTG(X) CTAGTTA- 3’
m/z Calculated for $C_{156}H_{192}N_{51}O_{89}P_{14}^{-}$(M -$H^{+}$) 4639 Found (ES-) 4640
Ret. Time 28.13
ε value 183444 M^{-1}
Yield: 0.79 µmol 79%

Appendix 2 Fluorescence Measurements

Different colours are used to provide a visual reference to the type of sequence

	Fully Matched
	Downstream Single Mismatch
	Upstream Single Mismatch
	Double Mismatch
	Double Upstream Mismatch
	Triple Mismatch
	Missing Mismatch

A2.1 Quantum yields

A2.1.1 Single strand quantum yields

A2.1.1.1 *n* = 1 single strand quantum yields

Table 54 Quantum Yields of single strand Probes recorded at room temperature λex 350 nm λem 426 nm 1 µM oligonucleotide concentration 10 mM pH 7 phosphate buffer 100 mM NaCl excitation slit width 3 nm emission slit width 5 nm

Probe	Core Sequence	QY
L Pr A	5' CLC	0.0181
L Pr B	5' CLG	0.0149
L Pr C	5' CLA	0.0152
L Pr D	5' CLT	0.0206
L Pr E	5' GLC	0.0227
L Pr F	5' ALC	0.0259
L Pr G	5' TLC	0.0294
D Pr A	5' CDC	0.0527
D Pr B	5' CDG	0.0066
D Pr C	5' CDA	0.0416
D Pr D	5' CDT	0.1106
D Pr E	5' GDC	0.0456
D Pr F	5' ADC	0.0682
D Pr G	5' TDC	0.0237

A2.1.1.2 *n* = x single strand quantum yields

Table 55 Quantum Yields of single strand Probes of different linker lengths recorded at room temperature λex 350 nm λem 426 nm 1 µM oligonucleotide concentration 10 mM pH 7 phosphate buffer 100 mM NaCl excitation slit width 3 nm emission slit width 5 nm

Different linker lengths Single strand		
Isomer	*n*	QY
L RR	1	0.020
D SS	1	0.061
L RR	3	0.007
D SS	3	0.010
L RR	4	0.011
D SS	4	0.011
L RR	5	0.005
D SS	5	0.012
L RR	6	0.013
D SS	6	0.006

A2.1.2 Hybridised quantum yields

A2.1.2.1 Hybridised quantum yields *n* = 1

Table 56 Quantum Yields of single strand and hybridised Probes recorded at room temperature λex 350 nm λem 426 nm 1 µM oligonucleotide concentration 10 mM pH 7 phosphate buffer 100 mM NaCl excitation slit width 3 nm emission slit width 5 nm

Fluorescence Quantum Yields			A1	A2
		Single Strand	3'GAG	3'G_G
n=1 Pr A L	5' CLC	0.0181	0.0078	0.0097
n=1 Pr B L	5' CLG	0.0149	0.0076	0.0096
n=1 Pr C L	5' CLA	0.0152	0.0205	0.0127
n=1 Pr D L	5' CLT	0.0206	0.0155	
n=1 Pr E L	5' GLC	0.0227	0.0304	0.0511
n=1 Pr F L	5' ALC	0.0259		0.0408
n=1 Pr G L	5' TLC	0.0294		0.0063
n=1 Pr A D	5' CDC	0.0527	0.0181	0.0211
n=1 Pr B D	5' CDG	0.0066		
n=1 Pr C D	5' CDA	0.0416		
n=1 Pr D D	5' CDT	0.1106		
n=1 Pr E D	5' GDC	0.0456		
n=1 Pr F D	5' ADC	0.0682		
n=1 Pr G D	5' TDC	0.0237		

Table 57 Quantum Yields of Probes hybridized with downstream modified targets recorded at room temperature λex 350 nm λem 426 nm 1 µM oligonucleotide concentration 10 mM pH 7 phosphate buffer 100 mM NaCl excitation slit width 3 nm emission slit width 5 nm

		B1	B2	C1	C2	D1	D2
		GAC	G_C	GAT	G_T	GAA	G_A
n=1 Pr A L	5' CLC	0.0087	0.0034	0.0080	0.0082	0.0099	0.0084
n=1 Pr B L	5' CLG	0.0063	0.0117	0.0055			
n=1 Pr C L	5' CLA		0.0072	0.0074	0.0111		
n=1 Pr D L	5' CLT		0.0126			0.0121	0.0138
n=1 Pr E L	5' GLC	0.0173	0.0261				
n=1 Pr F L	5' ALC		0.0161				
n=1 Pr G L	5' TLC		0.0075				
n=1 Pr A D	5' CDC	0.0315	0.0117				
n=1 Pr B D	5' CDG	0.0127	0.0143				
n=1 Pr C D	5' CDA			0.0128	0.0137		
n=1 Pr D D	5' CDT					0.0184	0.0127
n=1 Pr E D	5' GDC						
n=1 Pr F D	5' ADC						
n=1 Pr G D	5' TDC						

Table 58 Quantum Yields of Probes hybridized with upstream modified targets recorded at room temperature λex 350 nm λem 426 nm 1 µM oligonucleotide concentration 10 mM pH 7 phosphate buffer 100 mM NaCl excitation slit width 3 nm emission slit width 5 nm

		E1	E2	F1	F2	G1	G2
		CAG	C_G	TAG	T_G	AAG	A_G
n=1 Pr A L	5' CLC	0.0375	0.0145	0.0286	0.0197	0.0304	0.0210
n=1 Pr B L	5' CLG	0.0338		0.0336		0.0330	0.0277
n=1 Pr C L	5' CLA	0.0622		0.0406		0.0466	0.0322
n=1 Pr D L	5' CLT	0.0476	0.0234		0.0290	0.0594	0.0502
n=1 Pr E L	5' GLC	0.0212	0.0205			0.0465	0.0439
n=1 Pr F L	5' ALC	0.0283	0.0225	0.0233	0.0112		0.0343
n=1 Pr G L	5' TLC	0.0291		0.0234	0.0047	0.0464	0.0275

n=1 Pr A D	5' CDC	0.0290	0.0259			0.0285	0.0374
n=1 Pr B D	5' CDG						
n=1 Pr C D	5' CDA						
n=1 Pr D D	5' CDT						
n=1 Pr E D	5' GDC	0.0271	0.0265				
n=1 Pr F D	5' ADC			0.0144	0.0131		
n=1 Pr G D	5' TDC					0.0281	0.0379

A2.1.2.2 Hybridised quantum yields *n* = x

Table 59 Quantum Yields of Probes hybridized with adenine opposite matching targets recorded at room temperature λex 350 nm λem 426 nm 1 μM oligonucleotide concentration 10 mM pH 7 phosphate buffer 100 mM NaCl excitation slit width 3 nm emission slit width 5 nm

Different linker lengths duplex base opposite (A1)		
Isomer	*n*	QY
L RR	1	0.007
D SS	1	0.018
L RR	3	0.011
D SS	3	0.024
L RR	4	0.017
D SS	4	0.027
L RR	5	0.017
D SS	5	0.031
L RR	6	0.033
D SS	6	0.017

A2.2 Fluorescence titrations

A2.2.1 *n* = 1

Table 60 Percentage change in fluorescence at 426 nm of matched duplexes with different bases opposite anthracene and double mismatches. Recorded at room temperature λex 350 nm λem 426 nm 1 µM oligonucleotide concentration 10 mM pH 7 phosphate buffer 100 mM NaCl excitation slit width 3 nm emission slit width 5 nm

		A1	A2	A3	A4	A5	2MM
		3'GAG	3'G_G	GTG	GCG	GGG	GAAT
n=1 Pr A L	5' CLC	-75	-50	-76	-75	-78	61
n=1 Pr B L	5' CLG	-73	-27	-72	-52	-68	143
n=1 Pr C L	5' CLA	-63	-62	-56	-67	-71	124
n=1 Pr D L	5' CLT	-52	-80	-81	-62	-71	172
n=1 Pr E L	5' GLC	123	124	64	70	125	72
n=1 Pr F L	5' ALC	57	47	13	64	64	13
n=1 Pr G L	5' TLC	-65	-79	-81	-80	-75	29
n=1 Pr A D	5' CDC	-72	-77	-86	-81	-79	-24
n=1 Pr B D	5' CDG	335	235	69	135	182	82
n=1 Pr C D	5' CDA	23	-57	-42	-64	0	-18
n=1 Pr D D	5' CDT	-80	-85	-89			-51
n=1 Pr E D	5' GDC						25
n=1 Pr F D	5' ADC						-31
n=1 Pr G D	5' TDC						28

Table 61 Percentage change in fluorescence at 426 nm of matched duplexes with different bases downstream of anthracene for base opposite system and deletion system. Recorded at room temperature λex 350 nm λem 426 nm 1 µM oligonucleotide concentration 10 mM pH 7 phosphate buffer 100 mM NaCl excitation slit width 3 nm emission slit width 5 nm

		B1	B2	C1	C2	D1	D2
		GAC	G_C	GAT	G_T	GAA	G_A
n=1 Pr A L	5' CLC	-75	-98	-75	-74	-55	-72
n=1 Pr B L	5' CLG	-72	-52	-70	-77	-50	-37
n=1 Pr C L	5' CLA	-73	-87	-65	-51	-68	-60
n=1 Pr D L	5' CLT	-50	-65	-58	-77	-51	-10
n=1 Pr E L	5' GLC	-23	-21	178	102	100	120
n=1 Pr F L	5' ALC	-8	-58	45	36	35	57
n=1 Pr G L	5' TLC	-67	-92	-55	-76	-44	-67

n=1 Pr A D	5' CDC	-54	-91	-73	-82	-56	-57
n=1 Pr B D	5' CDG	72	146	-51	20	364	256
n=1 Pr C D	5' CDA	-60	-84	-74	-65	-19	-39
n=1 Pr D D	5' CDT		-77			-83	-86
n=1 Pr E D	5' GDC						
n=1 Pr F D	5' ADC						
n=1 Pr G D	5' TDC						

Table 62 Percentage change in fluorescence at 426 nm of mismatched duplexes with different bases upstream of anthracene for base opposite system and deletion system. Recorded at room temperature λex 350 nm λem 426 nm 1 μM oligonucleotide concentration 10 mM pH 7 phosphate buffer 100 mM NaCl excitation slit width 3 nm emission slit width 5 nm

		E1	E2	F1	F2	G1	G2
		CAG	C_G	TAG	T_G	AAG	A_G
n=1 Pr A L	5' CLC	86	-52	45	-15	70	25
n=1 Pr B L	5' CLG	131	57	144	33	137	164
n=1 Pr C L	5' CLA	255	-11	94	122	120	92
n=1 Pr D L	5' CLT	144	-11	89	17	154	192
n=1 Pr E L	5' GLC	-21	-11	12	-50	102	109
n=1 Pr F L	5' ALC	13	-41	-30	-64	33	22
n=1 Pr G L	5' TLC	0	-51	-38	-87	58	18
n=1 Pr A D	5' CDC	-68	-66	-52	-40	-61	-6
n=1 Pr B D	5' CDG	247		82		120	219
n=1 Pr C D	5' CDA						
n=1 Pr D D	5' CDT						
n=1 Pr E D	5' GDC	-50	-44	-51	-70		
n=1 Pr F D	5' ADC			-81	-81	-19	-15
n=1 Pr G D	5' TDC			-50	-76	18	36

A2.2.2 *n* = x

Table 63 Percentage change in fluorescence at 426 nm of matched duplexes with different bases opposite of anthracene and different tether lengths for base opposite system. Recorded at room temperature λex 350 nm λem 426 nm 1 μM oligonucleotide concentration 10 mM pH 7 phosphate buffer 100 mM NaCl excitation slit width 3 nm emission slit width 5nm for *n* = 1, 10 nm otherwise

		A1	A3	A4	A5
		3'GAG	GTG	GCG	GGG
Probe A n=1 L	5' CLC	-75	-76	-75	-78
Probe A n=1 D	5' CDC	-72	-86	-81	-79
Probe A n=3 L	5' CLC	52	-52	-43	10
Probe A n=3 D	5' CDC	166	-53	-27	43
Probe A n=4 L	5' CLC	70	-57	-26	29
Probe A n=4 D	5' CDC	161	-43	22	98
Probe A n=5 L	5' CLC	230	-25	-10	130
Probe A n=5 D	5' CDC	205	-35	20	107
Probe A n=6 L	5' CDC	139	-34	35	88
Probe A n=6 D	5' CDC	170	-41	31	111

Table 64 Percentage change in fluorescence at 426 nm of matched duplexes with different bases downstream of anthracene on the opposite strand for base opposite system recorded at room temperature λex 350 nm λem 426 nm 1 μM oligonucleotide concentration 10 mM pH 7 phosphate buffer 100 mM NaCl excitation slit width 3 nm emission slit width 5 nm for *n* = 1, 10 nm otherwise

		B1	C1	D1
		GAC	GAT	GAA
Probe A n=1 L	5' CLC	-75	-75	-55
Probe A n=1 D	5' CDC	-54	-73	-56
Probe A n=3 L	5' CLC	-14	-1	-6
Probe A n=3 D	5' CDC	-42	-4	27
Probe A n=4 L	5' CLC	-28	-6	-14
Probe A n=4 D	5' CDC	-26	-2	24
Probe A n=5 L	5' CLC	-18	-13	0
Probe A n=5 D	5' CDC	-21	-21	25
Probe A n=6 L	5' CDC	4	9	30
Probe A n=6 D	5' CDC	5	19	45

Table 65 Percentage change in fluorescence at 426 nm of matched duplexes with different bases upstream of anthracene on the opposite strand for base opposite system recorded at room temperature λex 350 nm λem 426 nm 1 μM oligonucleotide concentration 10 mM pH 7 phosphate buffer 100 mM NaCl excitation slit width 3 nm emission slit width 5 nm for *n* = 1, 10 nm otherwise

		E1	F1	G1
		CAG	TAG	AAG
Probe A n=1 L	5' CLC	86	45	70
Probe A n=1 D	5' CDC	-68	-52	-61
Probe A n=3 L	5' CLC	43	10	32
Probe A n=3 D	5' CDC	19	24	42
Probe A n=4 L	5' CLC	29	24	86
Probe A n=4 D	5' CDC	168	7	25
Probe A n=5 L	5' CLC	18	6	42
Probe A n=5 D	5' CDC	55	27	78
Probe A n=6 L	5' CDC	39	11	48
Probe A n=6 D	5' CDC	38	11	43

Table 66 Percentage change in fluorescence at 426 nm of matched duplexes for the deletion system recorded at room temperature λex 350 nm λem 426 nm 1 μM oligonucleotide concentration 10 mM pH 7 phosphate buffer 100 mM NaCl excitation slit width 3 nm emission slit width 5 nm for *n* = 1, 10 nm otherwise

		A2
		3'G_G
Probe A n=1 L	5' CLC	-50
Probe A n=1 D	5' CDC	-77
Probe A n=3 L	5' CLC	-68
Probe A n=3 D	5' CDC	-37
Probe A n=4 L	5' CLC	-54
Probe A n=4 D	5' CDC	24
Probe A n=5 L	5' CLC	-26
Probe A n=5 D	5' CDC	-20
Probe A n=6 L	5' CDC	-10
Probe A n=6 D	5' CDC	-37

A2.3 Fluorescence lifetimes

A2.3.1 Fluorescence lifetimes for *n* = 1 single strands

Table 67 Lifetimes of single strand form oligonucleotides. Recorded at room temperature λex 375 nm λem 426 nm 1 μM oligonucleotide concentration 10 mM pH 7 phosphate buffer 100 mM NaCl

SS Oligo		τ 1 (ns)	τ 1 Weighted (%)	τ 2 (ns)	τ 2 Weighted (%)	τ 3 (ns)	τ 3 Weighted (%)	χ^2
n=1 L PrA	5' CLC	0.92	11	3.50	33	11.95	56	1.021
n=1 L PrB	5' CLG	0.80	18	3.41	35	9.34	47	1.086
n=1 L PrC	5' CLA	0.93	10	3.86	36	8.81	54	0.99
n=1 L PrD	5' CLT	0.68	20	2.77	37	10.11	43	0.981
n=1 L PrE	5' GLC	1.39	13	5.08	53	12.84	34	1.022
n=1 L PrF	5' ALC	1.50	12	5.40	58	12.55	29	0.997
n=1 L PrG	5' TLC	0.88	12	3.57	33	11.56	54	1.005
n=1 D PrA	5' CDC	1.19	8	4.47	20	13.87	73	0.98
n=1 D PrB	5' CDG	0.92	16	3.73	33	9.57	51	0.999
n=1 D PrC	5' CDA	1.27	8	5.06	47	14.58	45	0.957
n=1 D PrD	5' CDT	0.94	5	4.06	15	16.69	80	1.01
n=1 D PrE	5' GDC	1.06	6	5.23	38	13.42	56	1.028
n=1 D PrF	5' ADC	1.58	5	5.68	41	16.13	54	1.036
n=1 D PrG	5' TDC	0.99	9	4.28	34	16.21	57	0.96

A2.3.2 *n* = x single strand fluorescence lifetimes

Table 68 Fluorescent lifetimes of single stranded anthracene modified oligonucleotides of differing chain lengths. Recorded at room temperature λex 375 nm λem 426 nm 1 μM oligonucleotide concentration 10 mM pH 7 phosphate buffer 100 mM NaCl

n	Probe	Isomer	τ 1 (ns)	τ 1 Weighted (%)	τ 2 (ns)	τ 2 Weighted (%)	τ 3 (ns)	τ 3 Weighted %	χ^2
1	A	L	0.92	11	3.5	33	11.95	56	1.021
1	A	D	1.19	8	4.47	20	13.87	73	0.98
3	A	L	0.589	37	2.96	40	9.76	23	1.05
3	A	D	0.795	34	3	41	9.33	26	1.021
4	A	L	0.532	31	2.52	44	8.35	25	1.04
4	A	D	0.621	35	2.56	42	8.26	24	0.97
5	A	L	0.559	31	2.59	42	9.04	27	1.011
5	A	D	0.76	42	3.23	37	10.9	21	1.24
6	A	L	0.706	32	2.82	40	8.65	28	0.987
6	A	D	0.567	28	2.61	41	8.29	31	0.95

A2.3.3 *n* = 1 hybridised fluorescence lifetimes

A2.3.3.1 Base opposite matching

Table 69 Fluorescence lifetimes of Probes L isomer double-stranded matching. Recorded at room temperature λex 350 nm λem 426 nm 1 μM oligonucleotide concentration 10 mM pH 7 phosphate buffer 100 mM NaCl

n	Probe	Isomer	Target	τ 1 (ns)	τ 1 Weighted (%)	τ 2 (ns)	τ 2 Weighted (%)	τ 3 (ns)	τ 3 Weighted (%)	χ^2
1	A	L	A1	0.92	39	3.9	33	13	28	1.013
1	A	D	A1	1.5	33	3.68	41	9.08	25	0.999
1	B	L	B1	0.87	60	2.89	21	15.7	18	1.021
1	C	L	C1	0.98	46	3.61	39	14.8	15	0.996
1	D	L	D1	1.2	54	3.07	35	14.7	11	1.046
1	E	L	E1	1.79	12	4.43	80	15.9	8	0.991
1	F	L	F1	1.46	22	5.16	60	10.9	18	1.012
1	G	L	G1	0	0	3.21	7.63	13.6	92.4	1.006

A2.3.3.2 *n* = 1 Base opposite Probe A mismatching

Table 70 Fluorescence lifetimes of Probe A double-stranded mismatching. Recorded at room temperature λex 350 nm λem 426 nm 1 μM oligonucleotide concentration 10 mM pH 7 phosphate buffer 100 mM NaCl

n		Probe	Target	τ 1 (ns)	τ 1 Weighted (%)	τ 2 (ns)	τ 2 Weighted (%)	τ 3 (ns)	τ 3 Weighted (%)	χ^2
1	A	L	A1	1.05	38	4.28	36	12.4	26	1.044
1	A	D	A1	1.5	33	3.68	41	9.08	25	0.999
1	A	L	B1	0.78	39	3.9	33	12.9	27	1.018
1	A	L	D1	0.94	32	4.08	40	12.9	28	1.011
1	A	L	E1	0	0	5.13	20	13.27	80	1.017
1	A	L	F1	0	0	5.91	29	13.45	71	0.97
1	A	L	G1	0.88	2	4.6	21	14.41	77	0.969
1	A	D	B1	1.47	9	5.93	55	12.6	35	1.056
1	A	D	D1	1.41	11	5.57	55	12.1	34	1.15
1	A	D	E1	1.23	10	5.14	42	12.6	47	1.11
1	A	D	G1	1.02	12	4.53	48	13.3	40	1.037

A2.3.3.3 *n* = 1 Base opposite mismatching – L isomer Probe varied target fixed

Table 71 Fluorescence lifetimes of Probe A double-stranded mismatching for the base opposite system. Recorded at room temperature λex 350 nm λem 426 nm 1 μM oligonucleotide concentration 10 mM pH 7 phosphate buffer 100 mM NaCl

Probe	Target	τ 1 (ns)	τ 1 Weighted (%)	τ 2 (ns)	τ 2 Weighted (%)	τ 3 (ns)	τ 3 Weighted (%)	χ^2
n=1 L Pr	E1	0	0	5.13	20	13.27	80	1.02
n=1 L PrB	E1	0	0	2.86	16	16.63	84	1.02
n=1 L PrC	E1	0	0	3.024	5	16.81	95	0.97
n=1 L PrD	E1	0	0	2.31	9	14.95	91	1.04
n=1 L PrE	E1	1	0.02	5.03	77	11.14	21	0.98
n=1 L PrF	E1	0	0	2.86	16	12.12	84	1.05
n=1 L PrG	E1	0	0	2.94	17	10.54	83	0.96

A2.3.3.3 *n* = 1 deletion matching and mismatching

Table 72 Fluorescence lifetimes of Probe A double-stranded mismatching for the deletion system. Recorded at room temperature λex 350 nm λem 426 nm 1 μM oligonucleotide concentration 10 mM pH 7 phosphate buffer 100 mM NaCl

n	Isomer	Probe	Target	τ 1 (ns)	τ 1 Weighted (%)	τ 2 (ns)	τ 2 Weighted (%)	τ 3 (ns)	τ 3 Weighted (%)	χ^2
1	L	A	A2	1.14	50	2.79	32	11.3	18	0.993
1	L	A	B2	1.21	27	5.61	40	14.6	33	0.99
1	L	A	C2	0.96	45	4.24	28	13	27	1.006
1	L	A	D2	0.84	40	4.19	32	13.1	27	0.999
1	L	A	E2	1.09	27	4.79	39	13.9	34	1.032
1	L	A	F2	1.25	26	3.90	55	10.8	19	1.002
1	L	A	G2	0.97	10	4.06	27	9.94	62	0.982
1	D	A	A2	1.19	27	2.1	66	11.9	7	1.034
1	D	A	B2	0.85	36	3.23	40	11.8	24	1.005
1	D	A	C2	1.02	52	3.43	32	10.5	16	0.993
1	D	A	D2	0.98	17	4.75	63	9.87	20	1.049
1	D	A	E2	1.16	8	5.78	27	14.4	65	1.021
1	D	A	F2	1.21	22	5.01	42	12.3	36	0.997
1	D	A	G2	0.62	10	4.47	31	13.87	59	1.094

A2.3.4 Fluorescent Lifetimes *n* = x hybridized

A2.3.4.1 *n* = x Base opposite matching adenine only

Table 73 Fluorescence lifetimes of Probe A double-stranded longer tether lengths for the base opposite system Recorded at room temperature λex 350 nm λem 426 nm 1 μM oligonucleotide concentration 10 mM pH 7 phosphate buffer 100 mM NaCl

n		Probe	Target	τ 1 (ns)	τ 1 Weighted (%)	τ 2 (ns)	τ 2 Weighted (%)	τ 3 (ns)	τ 3 Weighted (%)	χ^2
1	L	A	A1	1.05	38	4.28	36	12.4	26	1.044
1	D	A	A1	1.5	33	3.68	41	9.08	25	0.999
3	L	A	A1	0.82	13	3.97	54	8.76	33	1.053
3	D	A	A1	0.99	14	4.43	31	7.67	55.4	1.037
4	D	A	A1	1.27	10	4.44	34	7.2	55	1.007
5	L	A	A1	1.29	9	8.42	60	19.2	31	1.086
5	D	A	A1	1.31	15	3.48	39	7.9	45	0.946
6	L	A	A1	1.51	13	4.89	30	8.2	57	1.027
6	D	A	A1	1.49	16	5.75	58	9.75	26	1.017

A2.3.4.2 *n* = 3 and 6 Base opposite varied

Table 74 Fluorescence lifetimes of Probe A double-stranded selected longer tether lengths for the base opposite system with varied bases. Recorded at room temperature λex 350 nm λem 426 nm 1 μM oligonucleotide concentration 10 mM pH 7 phosphate buffer 100 mM NaCl

n	Isomer	Probe	Target	τ 1 (ns)	τ 1 Weighted (%)	τ 2 (ns)	τ 2 Weighted (%)	τ 3 (ns)	τ 3 Weighted (%)	χ^2
3	L	A	A1	0.817	13	3.97	54	8.76	33	1.053
3	L	A	A3	0.572	60	1.65	27	10.4	13	0.96
3	L	A	A4	0.64	55	1.97	35	9.92	11	0.962
3	L	A	A5	0.81	25	3.51	56	8.45	19	1
3	D	A	A1	0.987	14	4.43	31	7.67	55	1.037
3	D	A	A3	0.55	56	1.72	36	8.15	8	1.04
3	D	A	A4	0.796	47	2.57	40	7.71	13	0.93
3	D	A	A5	1.11	24	3.57	58	7.68	18	0.964
6	L	A	A1	1.51	13	4.89	30	8.2	57	1.027
6	L	A	A3	0.821	46	2.21	43	8.18	11	0.931
6	L	A	A4	1.03	16	2.4	78	7.79	6	0.963
6	L	A	A5	1.38	18	4.54	55	8.34	27	0.769
6	D	A	A1	1.49	16	5.75	58	9.75	26	1.017
6	D	A	A3	0.89	47	2.53	37	8.98	16	0.99
6	D	A	A4	1.36	29	2.65	64	8.47	7	1.064
6	D	A	A5	1.49	22	5.37	66	14.06	12	1.073

A2.3.4.3 *n* = x deletion matching

Table 75 Fluorescence lifetimes of Probe A double-stranded selected longer tether lengths for the deletion system. Recorded at room temperature λex 350 nm λem 426 nm 1 μM oligonucleotide concentration 10 mM pH 7 phosphate buffer 100 mM NaCl

n		Probe	Target	τ 1 (ns)	τ 1 Weighted (%)	τ 2 (ns)	τ 2 Weighted (%)	τ 3 (ns)	τ 3 Weighted (%)	χ^2
1	L	A	A2	1.14	50	2.79	32	11.3	18	0.993
1	D	A	A2	1.19	27	2.1	66	11.9	7	1.034
3	L	A	A2	0.525	64	2.26	19	10.1	17	0.985
3	D	A	A2	0.783	65	1.77	30	9.55	4	0.969
4	D	A	A2	1.6	58	2.4	39	9.53	4	1.011
5	D	A	A2	0.907	56	2.16	34	8.81	11	1.016
6	L	A	A2	1.02	45	2.11	46	8.15	9	0.992
6	D	A	A2	0.9	46	2.22	43	9.24	11	0.996

A2.3.6 *n* = x mismatch

A2.3.7 Degassed samples

Table 76 Fluorescence lifetimes of Probe A L isomersingle stranded. Recorded at room temperature λex 350 nm λem 426 nm 1 μM oligonucleotide concentration 10 mM pH 7 phosphate buffer 100 mM NaCl sample was degassed with nitrogen for ½ hour

n		Probe	O_2 content	τ 1 (ns)	τ 1 Weighted (%)	τ 2 (ns)	τ 2 Weighted (%)	τ 3 (ns)	τ 3 Weighted (%)	χ^2
1	L	A	Degassed	0.726	29	3.43	41	11.4	31	1.028
1	L	A		0.778	30	3.49	41	11.3	29	1.007

A2.3.8 Bisanthracene duplexes

Table 77 Fluorescence lifetimes of Probes A and M L and D isomers single stranded and double stranded. Recorded at room temperature λex 350 nm λem 405 and 500 nm 1 μM oligonucleotide concentration 10 mM pH 7 phosphate buffer 100 mM NaCl

Probe(s) n = 1	Monitored Wavelength (nm)	τ 1 (ns)	τ 1 Weighted (%)	τ 2 (ns)	τ 2 Weighted (%)	T 3 (ns)	τ 3 Weighted (%)	τ Av(ns)	χ^2
PrM L	405	1.54	12	7.06	27	20.05	61	18.08	1.02
	500	2.01	15	8.54	24	20.82	62	18.83	0.95
PrA L	405	0.98	59	3.33	32	11.85	9	6.10	0.90
	500	0.94	62	3.39	30	11.98	8	6.13	1.01
PrA L PrM L	405	0.64	51	3.12	36	11.74	13	7.30	0.97
	500	0.51	64	2.28	28	8.78	8	4.68	1.03
PrA D	405	1.16	38	4.41	29	13.79	34	11.07	1.02
	500	1.18	48	4.88	29	14.03	23	10.12	1.02
PrA D PrM L	405	0.76	67	3.26	25	10.96	8	5.80	0.98
	500	0.51	64	2.28	28	8.78	8	4.68	1.03

A2.3.8 SNP Probes

Table 78 Fluorescence lifetimes of SNP Probes G and T L isomer double stranded. Recorded at room temperature λex 350 nm λem 405 and 500 nm 1 μM oligonucleotide concentration 10 mM pH 7 phosphate buffer 100 mM NaCl

		τ 1 (ns)	τ 1 Weighted (%)	τ 2 (ns)	τ 2 Weighted (%)	τ 3 (ns)	τ 3 Weighted (%)	χ^2
SNP Probe G	SNP Tar G	2.37	7	5.04	68	8.88	28	1.047
SNP Probe T	SNP TarT	2.11	9	8.85	70	15.7	20	1.005

Appendix 3 Melting Points

A3.1 Single anthracene systems

All melting points were recorded on a Varian Cary 5000 with a multisample peltier heating block. at 5 µM concentration in Millipore water with 10 mM pH 7 phosphate buffer and 100 mM NaCl. Three temperature ramps were performed on each sample, one ramp from 15 °C to 85 °C at the rate of 0.5 °C/min, followed by a cooling ramp back to 15 °C at the same rate and finally a third ramp up to 85 °C. The melting point was calculated as the average of the first derivative of the first and third melting curves.

A3.1.1 Unmodified DNA

A3.1.1.1 Base opposite system

Table 79 Melting points of unmodified DNA oligonucleotides (°C) 5 µM with 10 mM pH 7 phosphate buffer and 100 mM NaCl

Target Strand	A1	B1	C1	D1	E1	F1	G1
	3'GAG	GAC	GAT	GAA	CAG	TAG	AAG
Tar MT 5'CTC	55	36	41	42.5	41.5	42.5	42
Tar MA 5'CAC	54	34.5	41	40.5	40	41.5	46

A3.1.1.2 Deletion system

Table 80 Melting points of unmodified DNA oligonucleotides (°C) deletion system 5 µM with 10 mM pH 7 phosphate buffer and 100 mM NaCl

Target Strand	A2	B2	C2	D2	E2	F2	G2
	3'G_G	G_C	G_T	G_A	C_G	T_G	A_G
Tar MA 5'CAC	49.5	33	33.5	36.5	35.5	34.5	38

A3.1.2 Matching base opposite duplex melting temperatures

Table 81 Melting points of different matching Probes base opposite system (°C) 5 µM with 10 mM pH 7 phosphate buffer and 100 mM NaCl

	n=1 L	n=1 D	n=3 L	n=3 D	n=4 L	n=4 D	n=5 L	n=5 D	n=6 L	n=6 D
PrATarA1	53.5	48	49.5	50.5	49	50	49	48	48	52.5
PrBTarB1	57	56	53	51				50.5		50
PrCTarC1	55	51	51	51				47		49
PrDTarD1	52	50	48	48				46		46
PrETarE1	52	47	50.5	51			50.5	51	51	51
PrFTarF1	49	43	46.5	45.5				47	46.5	47
PrGTarG1	51	44	47	47				47		46.5

A3.1.3 Matching deletion duplex melting temperatures

Table 82 Melting points of different matching Probes deletion system (°C) 5 µM with 10 mM pH 7 phosphate buffer and 100 mM NaCl

	n=1 L	n=1 D	n=3 L	n=3 D	n=4 L	n=4 D	n=5 L	n=5 D	n=6 L	n=6 D
PrATarA2	61	53.5	57	57	53.5	57	51	54	53.5	58.5
PrBTarB2	63	58	62	60				58.5		57
PrCTarC2	61	59	60	58				54		56
PrDTarD2	59	51	55	54				51		50
PrETarE2	61	52	59	56.5			55.5	46	55.5	56.5
PrFTarF2	54	48	54	52.5				53	52.5	53
PrGTarG2	55	49.5	56	52.5				49	52	51

A3.1.4 Mismatching base opposite duplex melting temperatures

Table 83 Melting points of Probes of different tether lengths for the base opposite system (°C) 5 µM with 10 mM pH 7 phosphate buffer and 100 mM NaCl

Target Strand	A1	A3	A4	A5	B1	C1	D1	E1	F1	G1
	3'GAG	GTG	GCG	GGG	GAC	GAT	GAA	CAG	TAG	AAG
Tm n=1 (L)	53.4	55	55	55	39.8	44.4	44.6	44.3	44.6	46
Tm n=1 (D)	48	48	46	48	35.5	39.5	37.5	36.5	35	35
Tm n=3 (L)	49.5	50	50	52	37.5	40	40	43	40	41
Tm n=3 (D)	50.5	47	46.5	48	37	41	38	40.5	40	42
Tm n=4 (L)	49	48	50	49.5	29	37	36.5	42.5	39.5	39
Tm n=4 (D)	50	51	51	51.5	35	41	37.5	41	40	41
Tm n=5 (L)	49	49	49.5	48	35.5	39	38.5	43	40	40
Tm n=5	48	51	50.5	51	33.5	39	37	42.5	40.5	41

(D)										
Tm n=6 (L)	49	50	50.5	50.5	34	39	38	36	36.5	39.5
Tm n=6 (D)	48.5	50.5	46	50	34	40.5	41	44	40.5	41

A3.1.5 Mismatching deletion duplex melting points

Table 84 Melting points of Probes of different tether lengths for the deletion system (°C) 5 µM with 10 mM pH 7 phosphate buffer and 100 mM NaCl

Target Strand	A2	B2	C2	D2	E2	F2	G2
	3'G_G	G_C	G_T	G_A	C_G	T_G	A_G
Tm n=1 L	61	52	49.1	46.2	45.7	46	46.7
Tm n=1 D	53.5	43	44.5	43.5	39	38.5	39.5
Tm n=3 L	57	46.5	46	45	43	43	47.5
Tm n=3 D	57	42.5	42	43	42	42.5	44.5
Tm n=4 L	52	41.5	43.5	43	42.5	42.5	43.5
Tm n=4 D	57	42	43	39	44	43	45.5
Tm n=5 L	51	42	42	42.5	44	42.5	44.5
Tm n=5 D	54	40.5	42	41.5	43	43.5	45.5
Tm n=6 L	53.5	40	41	38	43	41	44.5
Tm n=6 D	58.5	40.5	43	43	44.5	43.5	43.5

A3.1.6 SNP Probes

Table 85 Melting points of SNP Probes (°C) 5 µM with 10 mM pH 7 phosphate buffer and 100 mM NaCl

SNP	TarG	TarT
PrG	55	34
PrT	37.5	41

A3.2 Bisanthracene systems

A3.2.1 Facing bis anthracene systems

Table 86 Melting points of bis anthracene duplexes of Probes of different tether lengths (°C) 5 µM with 10 mM pH 7 phosphate buffer and 100 mM NaCl

	PrM							
PrA	(L) n=1	(D) n=1	(L) n=3	(D) n=3	(L) n=5	(D) n=5	(L) n=6	(D) n=6
Tm n=1 (L)	56	49.5	52	54		53	52	
Tm n=1 (D)	52.5	52	52	52.5		51.5		
Tm n=3 (L)	52.5	50	55.5	53		53.5		
Tm n=3 (D)	52	52	51	55.5		55		
Tm n=5 (L)	51.5		53		54	54		
Tm n=5 (D)	51.5	50	53	55	54	54.5		
Tm n=6 (L)	50.5						53.25	53.5
Tm n=6 (D)							53.5	53.5

A3.2.2 Stacking bisanthracene systems

Table 87 Melting points of bis anthracene duplexes of n = 6 Probes of the base stacking system(°C) 5 µM with 10 mM pH 7 phosphate buffer and 100 mM NaCl

Stacking Dimerisation Duplexes	n = 6 L PrM	n = 6 L PrMG	n = 6 L PrMS
n = 6 L PrA	53	42	43.5
	n = 6 D PrM	n = 6 D PrMG	C071PrMS
n = 6 D PrA	53.5	41.5	43

Appendix 4

A4.1 Application of the Rehm-Weller Equation

Nucleobase reduction:

$$\Delta G^{\circ}_{ET} = E^{\circ}(An^{\bullet+}/An) - E^{\circ}(N/N^{\bullet-}) - E_{\infty}(An) + \Delta G^{\circ}_{(\varepsilon)}$$

Equation 18

Nucleobase oxidation:

$$\Delta G^{\circ}_{ET} = E^{\circ}(N^{\bullet+}/N) - E^{\circ}(An/An^{\bullet-}) - E_{\infty}(An) + \Delta G^{\circ}_{(\varepsilon)}$$

Equation 19

A4.1.1 Pyrimidines

If we consider the reduction of Cytosine by anthracene (Equation 1)

Anthracene E°_{ox} =1.2145 V (vs SCE) Cytosine E°_{red}=-1.45 V (vs SCE)

ΔG°_{ET} = 1.2145 - -1.45-3.01 -0.1 ΔG°_{ET} = -0.45 eV

If we consider the oxidation of Cytosine by anthracene (Equation 2)

Anthracene E°_{red} =-2.2885 V Cytosine E°_{ox}= 0.769 V

ΔG°_{ET} = 0.769 - -2.29-3.01 -0.1 ΔG°_{ET} = -0.05 eV

Hence, we can see that the reduction of cytosine is more favourable than oxidation.

A4.1.2 Purines

If we consider the oxidation of Guanine by anthracene

Anthracene E°_{red} =-2.2885 V Guanine E°_{ox}= 0.83 V

ΔG°_{ET} = 0.83 - -2.29-3.01 -0.1 ΔG°_{ET} = 0.0085 eV

Index of oligonucleotide sequences

Anthracene tagged Probes X = L or D

Probe A: 5'-TGGACTC(X)CTCAATG -3'
Probe B: 5'-TGGACTC(X)GTCAATG -3'
Probe C: 5'-TGGACTC(X)ATCAATG -3'
Probe D: 5'-TGGACTC(X)TTCAATG -3'
Probe E: 5'-TGGACTG(X)CTCAATG -3'
Probe F: 5'-TGGACTA(X)CTCAATG -3'
Probe G: 5'-TGGACTT(X)CTCAATG -3'

Complementary Probe

Probe M: 5' 5' CATTGAGXGAGTCCA -3'

Complementary base opposite strands

Target A1 5'-CATTGAG(A)GAGTCCA – 3'
Target A3 5'-CATTGAG(T)GAGTCCA-3'
Target A4 5'-CATTGAG(C)GAGTCCA-3'
Target A5 5'-CATTGAG(G)GAGTCCA-3'
Target B1 5'-CATTGAC(A)GAGTCCA–3'
Target C1 5'-CATTGAT(A)GAGTCCA – 3'
Target D1 5'-CATTGAA(A)GAGTCCA – 3'
Target E1 5'-CATTGAG(A)CAGTCCA – 3'
Target F1 5'-CATTGAG(A)TAGTCCA – 3'
Target G1 5'-CATTGAG(A)AAGTCCA – 3'

Complementary deletion strands

Target A2 5'-CATTGAG__GAGTCCA-3'
Target B2 5'-CATTGAC__GAGTCCA – 3'
Target C2 5'-CATTGAT__GAGTCCA – 3'
Target D2 5'-CATTGAA__GAGTCCA – 3'
Target E2 5'-CATTGAG__CAGTCCA – 3'
Target F2 5'-CATTGAG__TAGTCCA – 3'
Target G2 5'CATTGAG__AAGTCCA – 3'

Unmodified Probe strands

Target MT 5'-TGGACTC(T)CTCAATG -3'
Target MA 5'-TGGACTC(A)CTCAATG -3'